
**Tephrostratigraphy, petrography, geochemistry, age
and fossil record of the Ganigobis Shale Member and
associated glaciomarine deposits of the Dwyka Group,
Late Carboniferous, southern Africa.**

Dissertation zur Erlangung des
naturwissenschaftlichen Doktorgrades
der Bayerischen Julius-Maximilians-Universität Würzburg

vorgelegt von

Berthold Bangert

aus
Freiburg im Breisgau

Würzburg 2000

Preface

Thin, bentonitic tuff beds were initially recognised by Harald Stollhofen in the Dwyka Group of the Aranos Basin (southern Namibia) in 1994 and were described to greater detail by Hermann Grill in 1997. The following study concentrates on the volcanology, petrography, tephro-stratigraphy and tephrochronology as well as geochemistry of these ashfall tuff beds.

The most detailed studied area was situated in the vicinity of Ganigobis within the Aranos Basin of southern Namibia where the tuff beds are preserved in a more than 40 m thick, marine silty mudstone-unit (Ganigobis Shale Member). Extensive field study of the Ganigobis Shale Member triggered the need for a comprehensive examination of all preserved features within the mudstone unit e.g. including the preserved fossils.

Thicker and better preserved ashfall tuff beds of the Dwyka Group were sampled in cut banks of the Orange River near Zwartbas in the Karasburg Basin (southern Namibia). They were initially discovered by Volker Lorenz. The sedimentology, mineralogy and geochemistry of these ashfall tuff beds and the surrounding mudstones of the Dwyka Group were studied to greater detail by Markus Geiger. Own results but also parts of his results are incorporated in this study.

A third study area is located in the Western Cape Province (South Africa) where ashfall tuff beds of the Dwyka Group and the overlying Prince Albert Formation (Ecca Group) were sampled in outcrops and cores of SOEKOR drill holes. Samples were used to study the petrology and geochemistry of the tuff beds while juvenile zircons of the beds were used for SHRIMP-based age determinations. Two tuffaceous beds, sampled in the Dwyka Group of KwaZulu-Natal (South Africa), were additionally included in this study.

Würzburg, 29 July 2000

BANGERT, B. (2000): Tephrostratigraphy, petrography, geochemistry, age and fossil record of the Ganigobis Shale Member and associated glaciomarine deposits of the Dwyka Group, Late Carboniferous, southern Africa.- Dissertation (Dr.rer.nat.) Universität Würzburg, Germany; 260 pp., 154 Figures, 31 Tables, 8 Plates.
--

Abstract

Thin pyroclastic marker beds are preserved in argillaceous units of the Dwyka Group in southern Namibia and South Africa which are the earliest witnesses of volcanism in Karoo-equivalent strata of southern Africa. The aim of this study is to present the field appearance of these marker beds, to characterise their mineralogy, geochemistry and heavy mineral contents and to present new radiometric age data from their juvenile zircons.

Carboniferous-Permian Karoo deposits in the Aranos Basin of southern Namibia include the glacially dominated, Carboniferous Dwyka Group and the shelf sediments of the overlying Permian Ecca Group totaling approximately 400 m in sediment thickness. The Dwyka Group can be subdivided into four upward-fining deglaciation sequences, each capped by relatively fine-grained glaciolacustrine or glaciomarine deposits. The uppermost part of the second deglaciation sequence comprises a thick fossiliferous mudstone unit, referred to as the "Ganigobis Shale Member". An abundance of marine macro- and ichnofossils as well as extrabasinally derived ashfall tuff beds characterise the more than 40 m thick mudstones and provide the basis for an integrated high-resolution biostratigraphic and tephrostratigraphic framework. The uppermost part of the third deglaciation sequence of the Dwyka Group consists of approximately 75 m thick siltstones and mudstones referred to as the "Hardap Shale Member" which contain fossils such as the bivalve *Eurydesma mytiloides*. The Hardap Shale Member is apparently devoid of tuff beds.

The Ganigobis Shale Member contains remains of paleoniscoid fishes (e.g. *Namaichthys schroederi*), bivalves (e.g. *Nuculopsis*), gastropods (e.g. *Peruvispira*), scyphozoa (e.g. *Conularia*), crinoid stalks, sponges and sponge spicules, radiolaria, coprolites and permineralised wood. These mostly marine body and trace fossils record the extent of the first of a series of marine incursions into the disintegrating Gondwanan interior as early as the Carboniferous.

Within the Ganigobis Shale Member 21 bentonitic tuff beds were determined which in

part can be traced laterally over tens of kilometres indicating an ashfall derivation. The thickness of the white to yellow and brownish tuff beds varies between 0.1 and 2.0 cm. Further bentonitic tuff beds of the Dwyka Group were detected in cut banks of the Orange River near Zwartbas in the Karasburg Basin (southern Namibia). The clay matrix of the 65 tuff beds is less frequently replaced by secondary gypsum minerals than in the tuff beds near Ganigobis. The tuff beds vary between 0.1 and 4.0 cm in thickness. Due to a similar fossil content and age of the background deposits, the tuff beds are thought to have originated from the same source area as those from the Aranos Basin.

Tuff beds from the Western Cape Province of South Africa were sampled from SOEKOR cores and in roadcuts. The yellow tuff beds sampled from the cores in the uppermost parts of DS II and III (Dwyka Group) display a thickness between 0.1 and 2.0. Samples were especially used for the preparation of thin-sections and geochemistry. Apart from a tuffaceous bed in the uppermost part of DS III, tuff beds in roadcuts originated from the base of the Prince Albert Formation (Ecca Group). The numerous, bentonitic tuff beds are 0.2-8 cm thick and light green to white. They do not show any internal bedding structures and could not be traced into the field due to the lack of exposure.

Thin-sections reveal the derivation of the tuff beds as distal fallout ashes produced by explosive volcanic eruptions. The matrix consists of a micro- to cryptocrystalline quartz-clay mineral mixture. Most obvious are secondarily grown kaolinite booklets. Rare fragments of splinter quartz, completely recrystallized ash-sized particles of former volcanic glass and few apatite and zircon grains are the only juvenile components which are determined with confidence.

The tuff beds contain as non-opaque, juvenile heavy minerals mostly zircon, apatite, monazite and sphene but also biotite, garnet, hornblende and tourmaline. The 100 to 220 μm large zircons are mostly euhedral and elongated prismatic to needlelike. Some of zircons show inclusions of

apatite or glassy material. The apatites are clear and euhedral to subhedral. Few euhedral sphenes and monazites show distinct and unrounded crystal faces. Biotite flakes only occur in certain tuff beds in higher amounts whereas garnet, hornblende and tourmaline only turn up in tuff bed VIIIa.

Geochemical analyses point to an original, intermediate to acid composition of the tuff samples. Al_2O_3 and K_2O are significantly enriched whereas all other major elements show lesser values than comparable igneous rocks. LREE enrichment and Eu-anomalies show that the parent magma of the tuff beds was a highly evolved calc-alkaline magma. La enrichment supports the involvement of a dominantly crustal source. Tectonomagmatic discrimination diagrams point to a volcanic arc setting. Bedding characteristics and the lack of any Carboniferous-Permian volcanic successions onshore Namibia makes an aeolian transport of the ash particles over larger distances likely. Siliceous, arc-related magmatism of Carboniferous-Permian age is known from South America (Patagonia). Siliceous ashes could thus have been transported by prevailing south-westerly winds to South Africa and Namibia. The thickness and frequency of the tuff beds is highest in South Africa and generally decreases towards the north (Namibia). A second, more local source area could have been located in an intracontinental rift zone along the western margin of southern Africa which is indicated by north-south directed ice-flow directions in the Late Carboniferous and which hosted a marine seaway during Permian times (Whitehill sea). Especially the large size of juvenile components within the ashes (e.g. zircons) contradicts an aeolian transport from

South America.

SHRIMP-based age determinations of juvenile magmatic zircons separated from the tuff beds allow a new time calibration of Dwyka Group deglaciation sequences II - IV and the Dwyka/Ecca boundary. The start of the deposition of the Dwyka Group will stay uncertain as basal deposits of DS I are not preserved. If sediment structures in the Waaiport Formation (Witteberg Group) are of glacial origin, glaciation started at 342 Ma and DS I may have lasted for 36 Ma. Zircons of the Ganigobis Shale Member yield SHRIMP-ages of 302-300 Ma. This dates the uppermost part of the second deglaciation sequence in southern Namibia to the Late Carboniferous (Gzelian) and provides a minimum age for the onset of Karoo-equivalent marine deposition. The age of the uppermost argillaceous part of the third deglaciation sequence (297 Ma) was determined from zircons of a tuffaceous bed sampled in a roadcut in the Western Cape Province, South Africa. The deposits correlate with the Hardap Shale Member in the Aranos Basin of southern Namibia which are part of the much more widespread Eurydesma transgression. The age of the Dwyka/Ecca boundary was determined by SHRIMP-measurements of juvenile zircons from two tuff beds of the basal Prince Albert Formation sampled in the Western Cape Province (South Africa). The zircons revealed ages of 289 - 288 Ma which date the Dwyka/Ecca boundary at about 290 Ma. According to these ages, deglaciation sequences II-IV lasted for 5 Ma on average. Deposition of Dwyka Group-sediments in southern Namibia started by latest at about 306 Ma and ended at about 290 Ma before present.

Zusammenfassung

Geringmächtige, bentonitische Tuffe treten in Tonsteinabschnitten der karbonen Dwyka Gruppe im südlichen Namibia und Südafrika auf. Sie repräsentieren die ersten Hinweise auf eine vulkanische Tätigkeit innerhalb der Karoosedimente im südlichen Afrika.

Die vorliegende Dissertation faßt die Geländebeschreibung der Tuffe, ihre

Petrographie, Mineralogie und Geochemie zusammen. Im Rahmen einer Schwermineralanalyse wurden juvenile Zirkone abgetrennt, deren radiometrisches Alter mittels SHRIMP-Analyse ermittelt wurde. Sie stellen die ersten radiometrisch exakt ermittelten Altersdaten innerhalb der Dwyka Gruppe dar.

Permokarbone Karoosedimente des Aranos Beckens in Südnamibia setzen sich aus der glazigenen Dwyka Gruppe des Karbons und den Schelfsedimenten der folgenden Ecca Gruppe des Perms zusammen. Sie erreichen eine maximale Gesamtmächtigkeit von 400 m.

Die Dwyka-Gruppe kann dabei in vier Entgletscherungssequenzen (DS) unterteilt werden. Die Korngröße der Gesteine nimmt in jeder dieser Entgletscherungssequenzen zum Hangenden hin ab. Der oberste Bereich jeder Entgletscherungssequenz ist durch glaziolakustrine oder glaziomarine Ablagerungen gekennzeichnet. Im Fall der zweiten Entgletscherungssequenz handelt es sich um einen mehr als 40 m mächtigen, fossilführenden Tonsteinabschnitt, der als 'Ganigobis Shale Member' bekannt ist. Eine Vielzahl von meist marinen Makro- und Spurenfossilien sowie distale Aschentuffe bilden die Grundlage für eine hochauflösende, biostratigraphische und tephrostratigraphische Gliederung des 'Ganigobis Shale Members'.

Der oberste Bereich der dritten Entgletscherungssequenz innerhalb der Dwyka-Gruppe im Aranos Becken Südnamibias besteht aus ca. 75 m mächtigen Ton- und Siltsteinen, die das 'Hardap Shale Member' bilden. Das 'Hardap Shale Member' enthält Makrofossilien wie die weltweit biostratigraphisch wichtige Muschel *Eurydesma mytiloides*, enthält jedoch nach den vorliegenden Untersuchungen keine Tuffe.

Das 'Ganigobis Shale Member' beinhaltet fossile Überreste von palaeoniskoiden Fischen wie *Namaichthys schroederi*, Muscheln wie *Nuculopsis*, Gastropoden wie *Peruvispira*, Scyphozoen wie *Conularia*, Crinoideenstielglieder, Schwämme und Schwammnadeln, Radiolarien, Koprolithen und versteinertes Holz. Die marinen Makro- und Spurenfossilien dokumentieren die Ausmaße einer ersten, marinen Transgression auf den bereits im Karbon langsam zerfallenen Superkontinent Gondwana.

21 bentonitische Aschentuffe wurden innerhalb des 'Ganigobis Shale Member' bestimmt, die teilweise über mehrere Kilometer hinweg lateral verfolgt werden können und somit eine Aschenfallablagerung dokumentieren. Die Mächtigkeiten der weiß-gelben bis bräunlichen

Tuffhorizonte beträgt zwischen 0.1 und 2.0 cm. Weitere, mächtigere Aschentuffe der Dwyka Gruppe wurden in Uferbänken des Orange Rivers in der Nähe von Zwartbas im Karasburg Becken Südnamibias entdeckt. Die Tonmineralmatrix der 65 Aschentuffe ist weniger durch sekundäre Gipsminerale ersetzt als in den Tuffen in der Umgebung von Ganigobis. Die Mächtigkeit dieser Tuffe beträgt zwischen 0.1 und 4.0 cm. Aufgrund eines ähnlichen Fossilinhaltes der Hintergrundsedimente und eines ähnlichen Alters der Tuffe kann von dem gleichen Herkunftsgebiet der Aschen ausgegangen werden.

In Südafrika wurden in der Provinz Westkap sowohl Tuffe in Bohrkernen der Ölfirma SOEKOR als auch in Straßenaufschlüssen beprobt. In den Bohrkernen sind gelbliche Tuffe im obersten Bereich der Entgletscherungssequenzen II und III vorhanden, die in der Mächtigkeit zwischen 0.1 und 2.0 cm variieren. Die Proben waren besonders für die Bestimmung der Petrographie der Tuffe mittels Dünnschliffen und für die geochemischen Analysen wichtig.

Außer einem 8 cm mächtigen, tuffitischen Horizont im obersten Bereich der Entgletscherungssequenz III, stammen die in Straßenaufschlüssen beprobten Tuffe ausschließlich aus dem Basisbereich der Prince Albert Formation (Ecca Gruppe). Die leicht grünlich-weißlichen Tuffe sind zwischen 0.2 und 8 cm mächtig. Sie sind intern nicht geschichtet und konnten aufgrund der schlechten Aufschlußverhältnisse nicht ins Gelände verfolgt werden.

Dünnschliffe der Tuffe zeigen, daß es sich bei den Horizonten um distale Aschenfallablagerungen handelt, die durch explosiven Vulkanismus gefördert wurden. Die Matrix besteht aus einer mikro- bis kryptokristallinem Quarz-Tonmineral - Mischung. Sehr auffällig sind sekundär gesprossene Kaolinitgrauen mit einer Größe von maximal 232 x 104 µm. Idiomorpher, hexagonaler Quarz, Splitterquarze und Quarzfragmente, vollständig rekristallisierte Aschenkörner (Größe: 220 µm) und vereinzelt Schwerminerale wie Apatit und Zirkon sind weitere juvenile Komponenten. Folgende transparente, juvenile Schwerminerale wurden bei der Schwermineralanalyse festgestellt: Zirkon,

Apatit, Monazit, Titanit, Biotit, Granat, Hornblende und Turmalin. Die bis zu 264 μm großen Zirkone sind meist idiomorph und prismatisch bis nadelförmig. Einige besitzen Apatiteinschlüsse oder Einschlüsse glasigen Materials. Die klaren Apatite besitzen eine Größe von bis zu 280 μm und sind meist idiomorph bis hypidiomorph. Sporadisch auftretende Monazite und Titanite (maximale Größe bis zu 180 bzw. 160 μm) zeigen scharfe und ungerundete Kanten. Bis zu 200 μm großer Biotit tritt nur in im Tuffhorizont IVb des Aranos Beckens und in zwei Tuffen der Dwyka Gruppe Südafrikas (Bohrung OL 1/69) in größeren Mengen auf. Granat, Hornblende und Turmalin wurden nur im Tuffhorizont VIIIa (Aranos Becken) bestimmt.

Geochemische Analysen weisen auf eine intermediäre bis saure Ausgangszusammensetzung der Tuffe hin. Al_2O_3 und K_2O sind stark angereichert, während alle anderen Hauptelemente geringere Konzentrationen als vergleichbare magmatische Gesteine aufweisen. Die Anreicherung der leichten Seltenen Erdelemente (LREE) und die Eu-Anomalien zeigen, daß die Zusammensetzung des Ausgangsmagma der Tuffe kalk-alkalisch und auch sehr differenziert war. Die Anreicherung von Lanthan (La) läßt ebenfalls auf eine hohe Differentiation des Ausgangsmagmas schließen. Tektonomagmatische Diskriminationsdiagramme deuten eine Subduktionszone als Herkunftsgebiet der Tuffe an. Die Korngröße der Tuffe und das Fehlen jeglicher permokarboner, vulkanischer Abfolgen in Namibia läßt auf einen Transport der Aschen über größere Distanzen schließen. Saurer Inselbogenmagmatismus ist während des Permokarbons aus Südamerika (Patagonien) bekannt. Saure Aschen könnten bei vorherrschenden südwestlichen Windrichtungen von Südamerika nach Südafrika und Namibia transportiert worden sein. Die Mächtigkeit und Häufigkeit der Aschentuffe in der Dwyka Gruppe ist in der südwestlichen Kapregion Südafrikas am höchsten und nimmt Richtung Namibia und auch innerhalb Namibias ab.

Ein zweites, lokaleres Herkunftsgebiet der Aschentuffe könnte innerhalb einer kontinentalen Riftzone gelegen haben, die am Westrand des südlichen Afrikas gelegen war. Sie ist im

Oberkarbon durch allgemein nord-südgerichtete Eisstromrichtungen im Aranos und Karasburg Becken in Namibia und im Perm durch die marinen Ablagerungen der Whitehill Formation (Ecca Gruppe) angedeutet. Gegen einen weiteren Transportweg der Tuffe aus Südamerika spricht vor allem die Größe der juvenilen Komponenten.

Altersbestimmungen an juvenilen Zirkonen mittels SHRIMP ermöglichen sowohl eine neue Zeiteinschätzung der Entgletscherungssequenzen II - IV innerhalb der Dwyka Gruppe als auch eine zeitliche Neukalibrierung der Dwyka-/Ecca Grenze. Der genaue Sedimentationsbeginn der Dwyka-Gruppe wird unbekannt bleiben, da basale Einheiten von DS I nicht erhalten sind. Wenn Sedimentstrukturen in der die Dwyka Gruppe direkt unterlagernden Waaiport Formation (Witteberg Gruppe, Cape Supergruppe) glazigenen Ursprungs sind, begann die erste Entgletscherungssequenz in Südafrika frühestens bei 342 Ma, dauerte circa 36 Ma und endete spätestens bei 306 Ma. Datierte Zirkone aus Tuffen des Ganigobis Shale Members ergeben SHRIMP-Alter von 302 - 300 Ma. Damit fallen der oberste Bereich der zweiten Entgletscherungssequenz und die in den marinen Ablagerungen enthaltenen Fossilien in das Oberkarbon (Gzelian). Das Alter des Topbereichs der dritten Entgletscherungssequenz (297 Ma) wurde an Zirkonen einer tuffitischen Schicht bestimmt, die in einem Straßenaufschluß an der N 12 in der Provinz Westkap in Südafrika beprobt wurde. Die dort aufgeschlossenen Ablagerungen korrelieren mit dem Hardap Shale Member im Aranos Becken Südnamibias und sind Teil der weltweit bekannten Eurydesma - Transgression. Das Alter der Dwyka / Ecca-Grenze wurde durch SHRIMP-Messungen an juvenilen Zirkonen von Tuffen der basalen Prince Albert Formation (Ecca Gruppe) in der Provinz Westkap (Südafrika) bestimmt. Die U-Pb - Messungen an den Zirkonen ergaben Alter von 289 - 288 Ma, die die Dwyka / Ecca-Grenze bei circa 290 Ma festlegen. Diesen Altersbestimmungen zufolge dauerten die Entgletscherungssequenzen II - IV im Durchschnitt 5 Ma. Die Ablagerung der Dwyka-Gruppe in Südnamibia begann somit spätestens bei 306 Ma und endete bei 290 Ma.

Acknowledgements

I am grateful to a number of people who have contributed to the success of this dissertation.

In the first place I would like to mention my supervisor Volker Lorenz (Würzburg) for the opportunity to carry out this study, for his help and good co-operation in the field (concerning especially the fossils) and his constructive criticism of a previous draft of this study.

Harald Stollhofen (Würzburg) is thanked for introducing me to the field area near Ganigobis, for the help in the recognition of characteristic features of the tuff beds and in numerous sedimentological and geological questions. He was the initiator of our international publications which would not have been realised without him.

Markus Geiger (Würzburg) is acknowledged for his assistance during two field seasons and his inexhaustible endeavour sampling the thin tuff beds, for numerous hours in the labs of the Institut für Geologie at Würzburg and countless discussions and suggestions concerning most topics presented in this study. Axel Frey, Joachim Lehmann and Peter Schultheiß (all Würzburg) assisted in sample preparation, separation and further laboratory work.

Special thanks to Hermann Grill (now Aachen) whose studies laid the foundation for further research in the Dwyka Group of southern Namibia. He taught me how to "survive" in the field and helped in questions regarding the stratigraphy and the depositional history of the Dwyka Group. Frank Holzförster (Würzburg, now Grahamstown) is thanked for inspiring discussions about the general stratigraphy of the Karoo Supergroup in southern Africa as well as for help in general geological questions. Stephan Königer (Würzburg) is acknowledged for his help and fruitful discussions about tuff beds in general, about heavy minerals and their separation techniques.

I wish to thank Hans-Peter Schultze (Berlin), Franz Fürsich, Gerd Geyer, Markus Wilmsen, Michael Schlirf and Bettina von Rützen (all Würzburg) concerning help in the determination of fossils and ichnofossils and related questions. I am indebted to Michael Streng (Bremen) who

took SEM photomicrographs of the heavy minerals.

Peter Richter and Rosemarie Baur (Würzburg) are thanked for undertaking XRF-analyses and LOI-determinations, Rainer Hock (Würzburg) introduced me into X-ray diffractometry and Barabara Sponholz (Würzburg) helped in questions concerning clay mineralogy and the separation of the clay fraction from the tuff beds and mudstones. Dieter Bühmann (Pretoria) is thanked for general advice in X-ray diffractometry and the quantitative XRD-analyses. Wolfgang Schubert (Würzburg) is acknowledged for the assistance in thin-section petrography of the volcanic clasts.

Juliane Hauck, Hildegard Schönig and Emilie Keck (all Würzburg) are thanked for taking photographs of rock samples, fossils, thin-sections and heavy minerals. Emilie Keck assisted in preparing slides for talks. Rupert Wassermann (Würzburg) did a hard job in the preparation most of the thin-sections from the tuff beds. Karin Stuis-Pfeuffer and Maike Dörnemann (Würzburg) supported in administrative matters mostly concerning the management of our Federal Research Foundation (DFG) project.

I wish to thank Hans Ruppert and his team in Göttingen for XRF-analyses and the determination of trace and rare earth elements by ICP-MS. I appreciate his advice concerning sampling techniques for geochemistry, his general help in questions concerning geochemistry and his constructive criticism of a previous draft of the geochemistry chapter.

Special thanks to Winfried Zimmerle (Celle) for his lectures on the petrography of argillaceous rocks and especially the determination of heavy minerals.

Michael Greller and Jost Haneke (Mainz) are acknowledged for their help in carrying-out XRD analyses at the Geologisches Landesamt Rheinland-Pfalz.

Jochen Röhl und Annette Schmid-Röhl (Tübingen) are thanked for TOC and nitrogen-determinations of mudstones samples from the Dwyka Group in southern Namibia.

We all are indebted to Richard Armstrong (Canberra) who did the SHRIMP-based age determinations on zircons of the tuff beds which led to the first radiometrically precise age dates of the Dwyka Group in southern Africa.

I wish to say thanks to Vic von Brunn (Pietermaritzburg) and Johan Visser (Bloemfontein) for their help concerning Dwyka Group exposures in South Africa. I benefited a lot from Vic von Brunn's experience concerning publishing in international journals. Jurie Viljoen, Doug Cole and Bob Thomas (all Bellville) supplied analytical data, geological maps and scientific exchange with them were of considerable benefit.

We all wish to thank Marion Bamford (Johannesburg) for the determination of fossil wood from the Lower Karoo Supergroup and the excellent scientific exchange between BPI Paleontology and the Institut für Geologie at Würzburg.

I want to thank my friends and colleagues Christoph Arz, Bernd Frommherz, Gary Hampson, Dougal Jerram, Michael Seyferth, Ansgar Wanke and Stephen White for helpful comments and discussions related and unrelated to science.

Research was funded by the German Research Foundation (DFG) for two and a half years. The Postgraduate Research Program "Interdisciplinary Geoscience research in Africa" of the Faculty of Geosciences in Würzburg with Martin Okrusch as leader is thanked for the possibility of scientific exchange as well as for logistic support in Namibia. Further logistic support by the Geological Survey of Namibia (Gabi Schneider, Wulf Hegenberger, Mimi Dunaiski) is gratefully acknowledged. The Council of National Monuments is acknowledged for the determination of fossils outside Namibia. The Council for Geoscience in Pretoria kindly gave access to geological maps and to SOEKOR boreholes cores OL1/69, SA 1/66, KL 1/65, QU 1/65 and Enkelde Wilgenboom. Carlos Peres at Zwartbas, Andrew Codd (Cape Town) and Stephan Kurszlaukis (Johannesburg) are thanked for their hospitality.

Finally, I would like to thank my parents for their widespread and generous support. I am indebted to my wife Petra for her patience and encouragement since the start of this dissertation. She had to struggle with my little sons Julius and Lorenz when I stayed at the Institut für Geologie.

Table of Contents

Preface	1
Abstract	2
Zusammenfassung	3
Acknowledgements	6
Table of Contents	8
1 Introduction	13
1.1 Glacial history of Gondwana	13
1.2 Palaeogeographic reconstructions and tectonic setting of the Aranos Basin, southern Namibia	15
1.3 The principal framework of Dwyka Group deglaciation sequences	17
1.4 The distribution of Dwyka Group deglaciation sequences in southern Namibia	22
2 The Ganigobis Shale Member	25
2.1 The tuff beds of the Ganigobis Shale Member	25
2.2 The threefold subdivision of the Ganigobis Shale Member	27
2.3 The base of the Ganigobis Shale Member	27
Cut banks of the Fish River: Locality #2	30
Cut banks of the Tses River: Locality #23	33
Roadcut of the D98: Locality #45	35
Cut banks of the Asab River: Locality #31	35
Cut banks near Farm Aretitis: Localities #32 and 30	36
2.4 The middle part of the Ganigobis Shale Member	37
Cut banks near Haams: Localities #15 and 16	38
Cut banks of the Brukkaros River: Locality 20	40
Cut banks of the Haams River: Locality 13	40
Cut banks of the Brukkaros River: Locality 44	40
2.5 The upper part of the Ganigobis Shale Member	41
Cut banks of the Ganigobes River: Locality 40	41
Cut banks of the Ganigobes River: Locality 43	41
Cut banks of the Brukkaros River: Locality 27	42
Cut banks of the Brukkaros River: Locality 9	44
2.6 The Ganigobis Shale Member in the southern part of the Aranos Basin	45
2.6.1.1 Farm Tsaraxa: Locality 25	45
2.6.1.2 South of Farm Snyfontein: Locality 24	46
2.7 Thickness, basin topography and tectonic framework of the Ganigobis Shale Member	46
3 Life in an ice-age: The fossils of the Ganigobis Shale Member	48
3.1 Palaeoniscoid fish remains	48
3.1.1 Previous work	48
3.1.2 New observations	49
3.1.3 Discussion	50
3.1.4 Palaeoenvironmental significance	50
3.2 Coprolites	52
3.3 Permineralised wood	54
3.4 Gastropods	57
3.5 Bivalves	58

3.6 Conularia and sponges	59
3.7 Other fossils of the Ganigobis Shale Member	60
4 The mudstones of the Ganigobis Shale Member	60
4.1 Mineralogy of the mudstones	60
4.2 Geochemistry of the mudstones	61
4.2.1 Major elements.....	61
4.2.2 Trace elements	63
4.2.3 Organic matter and nitrogen contents of the mudstones	63
4.2.4 Sulphur and pyrite content of the mudstones.	64
4.2.5 Chemical Index of Alteration (CIA)	65
4.3 Gamma-ray spectrometry of the mudstones	67
4.3.1 Theory and methodology of Gamma-ray spectrometry:	67
4.3.2 Absolute U and Th-values and Th/K and Th/U ratios of the Ganigobis Shale Member	67
4.3.3 Correlation of outcrops within the Ganigobis Shale Member.....	68
4.3.4 The threefold subdivision of the Ganigobis Shale Member from the perspective of gamma ray spectrometry.....	72
4.4 Conclusions: The depositional history of the Ganigobis Shale Member	72
4.4.1 The base and the lower part of the Ganigobis Shale Member up to tuff beds VI.....	72
4.4.2 The middle part of the Ganigobis Shale Member between tuff beds VI and VIIIa.....	73
4.4.3 The upper part of the Ganigobis Shale Member above tuff bed VIIIa.....	74
5 Ganigobis Shale Member-equivalents at Zwartbas (Karasburg Basin, southern Namibia)	74
5.1 Geological setting	74
5.2 The tuff beds of the Dwyka Group at Zwartbas	75
5.3 The base of the Dwyka Group at Zwartbas	76
5.4 Marine, periglacial deposits at Zwartbas	76
5.5 The occurrence of fossils within the glaciomarine deposits at Zwartbas	78
5.5.1 Palaeoniscoid fish remains	78
5.5.2 Spiral coprolites	78
5.5.3 Gastropods.....	78
5.5.4 Bivalves.....	78
5.5.5 Radiolaria	78
5.5.6 Permineralised wood	78
5.5.7 Trace fossils	78
5.6 Comparison between the glaciomarine deposits at Zwartbas and near Ganigobis.	79
6 The Hardap Shale Member	82
6.1 Locality #1 southeast of Hardap Dam	82
6.2 Cut banks of the Fish River: Locality #6	83
6.3 Localities #4 and 5 along the B 1	83
6.4 Cut banks of the Wasser River: Locality #26	84
6.5 Locality #3 in the vicinity of Schlip	85
6.5.1 Gamma-ray measurements of the siltstones	86
6.5.2 Petrography of the calcrete beds	87
6.5.3 Geochemistry of the calcrete beds.....	87
7 The Dwyka Group in the main Karoo Basin (South Africa)	87
7.1 Eastern Cape Province	87
7.2 Western Cape Province	88

7.2.1 Roadcuts of the N12 about 30 km north of Klaarstroom	88
7.2.2 Roadcuts south of Laingsburg	90
7.2.3 Outcrops east of Elandsvlei	92
7.3 Northern Cape Province	92
7.3.1 Niewoudtville.....	92
7.3.2 Slagberg	92
7.3.3 Outcrop along the road Niewoudtville - Louriesfontein	92
7.4 KwaZulu-Natal	92
7.5 SOEKOR boreholes	94
7.5.1 Enkelde Wilgenboom	94
7.5.2 KL 1/65.....	94
7.5.3 QU 1/65	95
7.5.4 SA 1/66.....	95
7.5.5 OL 1/69.....	96
7.6 Stratigraphic comparison of the deglaciation sequences recorded in the boreholes.....	97
8 Petrography of the tephrostratigraphic marker beds.....	100
8.1 Terminology and classification.....	100
8.2 General petrographic description of the marker beds.....	100
8.2.1 Matrix	101
8.2.2 Primary volcanic components	102
8.2.2.1 Relic structures of volcanic glass particles	101
8.2.2.2 Quartz.....	104
8.2.2.3 Apatite and zircon	105
8.2.2.4 Feldspar.....	105
8.2.2.5 Biotite.....	105
8.2.3 Secondary minerals.....	105
8.2.3.1 Kaolinite.....	105
8.2.3.2 Muscovite.....	107
8.2.3.3 Opaque minerals.....	107
8.2.3.4 Carbonates.....	108
8.3 Mineralogy of all examined marker beds deduced from XRD-analysis.....	108
8.3.1 Clay minerals	110
8.3.1.1 Illite.....	110
8.3.1.2 Interstratified illite / smectite clay minerals	110
8.3.1.3 Smectite.....	111
8.3.1.4 Kaolinite.....	111
8.3.1.5 Palygorskite.....	111
8.3.1.6 Clinochlore.....	111
8.3.2 Quartz	111
8.3.3 Feldspars	111
8.3.4 Mica	116
8.3.5 Other minerals.....	116
8.3.6 Quantitative analysis of the XRD-measurements	116
8.4 Mineralogical evolution of marker beds.....	117
9 Heavy minerals	118
9.1 Heavy minerals of the analysed tuff beds.....	119
9.1.1 Primary volcanic heavy minerals	119
9.1.1.1 Apatite.....	119
Shape, elongation and size	119
Colour, inclusions and growth obstruction.....	121
9.1.1.2 Zircon.....	121
Shape, elongation and size	122
Colour and inclusions	124
Magmatic zoning and growth obstruction.....	125
9.1.1.3 Monazite.....	125
9.1.1.4 Sphene (titanite)	126

9.1.1.5 Rutile.....	127
9.1.1.6 Biotite	127
9.1.1.7 Hornblende.....	129
9.1.1.8 Garnet Group	129
9.1.1.9 Tourmaline.....	130
9.1.2 Authigenic heavy minerals.....	130
9.1.2.1 Barite.....	130
9.1.2.2 Opaque minerals	131
9.1.2.3 Leucoxene.....	132
9.2 Heavy-mineral suites of the tuff beds from the Aranos Basin.....	132
9.2.1 Tuff bed Ib.....	132
9.2.2 Tuff bed IIb	132
9.2.3 Tuff bed IIIb.....	133
9.2.4 Tuff bed IVa.....	135
9.2.5 Tuff bed IVb.....	135
9.2.6 Tuff bed IVc.....	137
9.2.7 Tuff bed V	137
9.2.8 Tuff bed VI.....	138
9.2.9 Tuff bed VII	138
9.2.10 Tuff bed VIIIa	138
9.3 Analysed tuff beds from Zwartbas, southern Namibia.....	139
9.3.1 Tuff bed IIIb.....	139
9.3.2 Tuff bed XXIVa	140
9.4 Analysed tuff beds from the Western Cape Province (South Africa).....	140
9.4.1 OL 1/69: 378.00 m	140
9.4.2 OL 1/69: 396.36 m.....	140
9.4.3 Tuffaceous bed from the Dwyka Group about 30 km north of Klaarstroom.....	142
9.4.4 Tuff bed from the Eccca Group about 30 km north of Klaarstroom	142
9.4.5 Tuff bed from the Eccca Group north of Ladismith.....	143
9.4.6 Tuffaceous bed from the Dwyka Group of KwaZulu-Natal about 2 km east of Nondweni.....	143
9.5 Quantitative analysis of the main tuff beds.....	145
9.6 Heavy minerals in the adjacent mudstones.....	145
9.6.1 Qualitative analysis	146
9.7 Discussion of the heavy-mineral suite.....	146
10 Geochemistry of the bentonitic tuff beds, Dwyka Group, southern Africa	147
10.1 Introduction	147
10.2 The geochemistry of the present-day tuff beds: Major elements.....	148
10.2.1 SiO ₂	148
10.2.2 TiO ₂	149
10.2.3 Al ₂ O ₃	150
10.2.4 Fe ₂ O ₃	150
10.2.5 MnO	150
10.2.6 MgO	151
10.2.7 CaO	151
10.2.8 Na ₂ O.....	152
10.2.9 K ₂ O.....	152
10.2.10 P ₂ O ₅	153
10.2.11 LOI.....	153
10.3 The geochemistry of the present-day tuff beds: Trace elements.....	154
10.3.1 Niobium (Nb)	155
10.3.2 Zirconium (Zr)	155
10.3.3 Strontium (Sr).....	155
10.3.4 Barium (Ba).....	156
10.3.5 Rubidium (Rb)	156
10.3.6 Lead (Pb).....	157

10.3.7 Gallium (Ga)	157
10.3.8 Zinc (Zn)	157
10.3.9 Copper (Cu)	158
10.3.10 Nickel (Ni)	158
10.3.11 Cobalt (Co)	158
10.3.12 Chromium (Cr)	159
10.3.13 Vanadium (V)	159
10.3.14 Conclusions.....	159
10.4 Major and trace element variations of the tuff beds	160
10.5 Rare earth elements (REE).....	163
10.6 The geochemical origin of the volcanic ash.....	167
10.6.1 TiO ₂ /Al ₂ O ₃	167
10.6.2 Zr/Ti-Nb/Y	168
10.7 The geotectonic origin of the tuff beds	170
10.8 Potential source areas of the tuff beds.....	172
10.8.1 Previous studies and opinions.....	172
10.8.2 Own considerations.....	172
10.9 Volcanic clasts.....	176
10.9.1 Thin-section petrography.....	176
10.9.2 Geochemical rock classification of the volcanic clasts	178
10.9.3 REE - discrimination of the volcanic clasts	180
10.9.4 Radiometric age of the volcanic clasts.....	180
11 New radiometric age determinations of tuff beds from the Dwyka and Ecca Groups, southern Africa	181
11.1 Sample selection.....	182
11.2 Analytical procedures	182
11.3 Dating results	183
11.3.1 Dwyka Group (top DS II) of the Aranos Basin (southern Namibia): tuff bed #23 IIb.....	183
11.3.2 Dwyka Group (top DS II) of the Aranos Basin (Namibia): tuff bed #45 IIb	185
11.3.3 Dwyka Group (DS II) near Zwartbas, Karasburg Basin (southern Namibia): tuff bed IIIb.....	185
11.3.4 Dwyka Group (DS II) near Zwartbas, Karasburg Basin (southern Namibia): tuff bed XXXIV.....	185
11.3.5 Dwyka Group (top DS III), 30 km north of Klaarstroom, Western Cape Province, South Africa.....	187
11.3.6 Dwyka Group, 2 km east of Nondweni, KwaZulu-Natal, South Africa	187
11.3.7 Ecca Group (basal Prince Albert Formation), 30 km north of Klaarstroom, Western Cape Province, South Africa: tuff bed VIb.....	189
11.3.8 Ecca Group (basal Prince Albert Formation), south of Laingsburg, Western Cape Province, South Africa.....	189
11.4 Discussion of the new dating results	191
11.4.1 Aranos Basin (Namibia)	191
11.4.2 Karasburg Basin (Namibia)	191
11.4.3 Western Cape Province (South Africa).....	191
11.4.4 KwaZulu-Natal (South Africa)	192
11.5 The duration of the Ganigobis Shale Member.....	193
11.6 The duration of the deglaciation sequences of the Dwyka Group.....	194
11.7 Eustatic sea-level changes within the lower Karoo Supergroup of southern Africa	194
References	198
Appendices	209

1 Introduction

1.1 Glacial history of Gondwana

The Carboniferous-Permian history of Gondwana represents a period of dramatic climatic amelioration from an ice-house to a green-house stage. In the Late Carboniferous, parts of southern Gondwana (South America, Africa, Antarctica, Australia and India) were subjected to glaciation with major continental ice sheets (e.g. Veevers and McA Powell, 1987), glaciers and marine ice-sheets. Glacial deposits are known from the Paraná Basin (South America) of southern Brazil and northern Argentina (Itararé Subgroup: Dos Santos *et al.*, 1996), southern Africa (Dwyka Group; e.g. Von Brunn, 1996), Antarctica (Victoria Land, Central Transantarctic Mountains, Pensacola and Ellsworth Mountains: Collinson *et al.*, 1994; south-eastern Australia (New South Wales: Dickins, 1996), western Australia and India: Mishra, 1996. In Africa, Dwyka Group- and Dwyka Group-equivalent deposits are known from South Africa, Namibia, Botswana (Martin, 1981a), Zimbabwe (Oesterlen, 1990), Malawi (Ring, 1995), Madagascar (Wopfner, 1998), Tanzania (Diekmann, 1993) and Zaire (Crowell and Frakes, 1975). Based on the distribution of glacial deposits, striated pavements and incised glacial valleys, the reconstruction of the ice cover suggests that a continental ice sheet existed in the south-central parts of southern Africa (e.g. Zambia, Zimbabwe, Botswana). This continental ice sheet sent its lobes to the west (Kaokoveld lobe heading towards the north-eastern Paraná Basin), to the south-west (Botswana lobe heading towards the Aranos Basin (the Namibian part of the Kalahari Basin, (Johnson *et al.*, 1996), to the south and then to west (Transvaal lobe, main Karoo Basin) and to the south-east (KwaZulu-Natal) (cf. Crowell and Frakes, 1975). The glacial Dwyka Group in southern Africa constitutes the lowermost stratigraphic unit of the Karoo Supergroup (Visser, 1989) which includes mostly continental Carboniferous-Permian to Jurassic deposits of about 10 km thickness (Visser, 1996). Deposits of

the whole Karoo Supergroup cover an area of about 300 000 km² (Smith *et al.*, 1993).

In South Africa, Dwyka Group-sediments crop out at the outer margin of the main Karoo Basin but are also reported from drill holes in the Western Cape Province towards the centre of the main Karoo Basin (Viljoen, 1994; Fig. 1). In southern Namibia, Dwyka Group-deposits are known from the Karasburg Basin (Haughton and Frommurze, 1927; Visser, 1983b), which originally continue to the east into South Africa, and in the Aranos Basin situated between Mariental and Keetmanshoop (Grill, 1997; Fig. 1). In northern Namibia sediments of the Dwyka Group occur in the Huab Basin (Reunig and Martin, 1957; Holzförster and Stollhofen, in press), in the Waterberg Basin (Gunthorpe, 1987) and in the Kaokoveld where remnants of glacial sediments are found in modern valleys draining towards the Atlantic ocean (Martin, 1981a).

The correlation of these rather isolated occurrences of Dwyka Group deposits in South Africa and southern Namibia is complicated because of their variable thickness and heterolithic facies architecture. This emphasises the need of reliable chronostratigraphic markers such as widespread fallout tuff beds which would also provide the possibility of radiometric dating. Such tuff beds are only rarely documented from the Dwyka Group of southern Africa (Viljoen, 1995) but are well known from the overlying Permian Ecca- and Beaufort Groups and are listed in Veevers *et al.* (1994). Until 1994 unknown ashfall tuff beds were recognised in the Aranos Basin of southern Namibia on which this study will focus in the following. Further ashfall tuff beds from the Karasburg Basin in southern Namibia which were detected in 1997, and tuff beds from the Dwyka Group and lower Ecca Group of the Western Cape Province were used for comparison. The determination of their age by radiometric dating of juvenile zircons separated from the tuff beds of the three mentioned basin areas and the subdivision of the Dwyka Group in deglaciation sequences will improve the correlation of Dwyka Group-deposits between single basin areas of southern Africa.

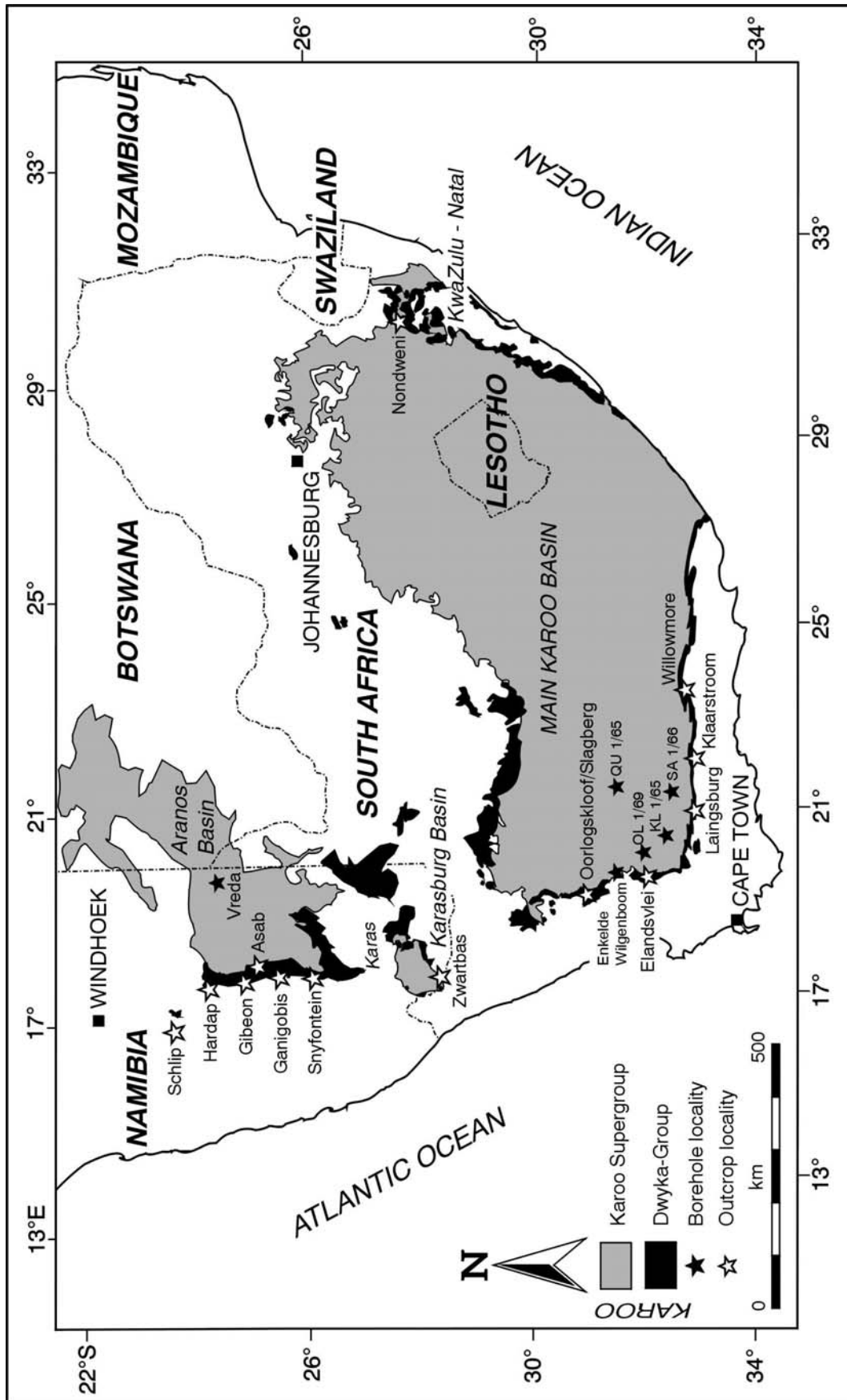


Fig. 1: Simplified map of southern Africa showing the distribution of Dwyka Group outcrops (black), the distribution of Karoo basins (grey) as well as borehole and outcrop localities mentioned in this study.

1.2 Palaeogeographic reconstructions and tectonic setting of the Aranos Basin, southern Namibia

The Aranos Basin of southern Namibia developed within one of the intra-continental rifts which predate the opening of the South Atlantic in Middle Cretaceous times. Within the Aranos Basin of southern Namibia Carboniferous-Permian Karoo deposits are preserved which include the glacially dominated Dwyka Group and the shelf-sediments of the overlying Ecca Group totaling approximately 400 m in sediment thickness. The uppermost part of Ecca Group-equivalent deposits is formed by the Whitehill Formation which locally crops out in the vicinity of Keetmanshoop. Younger sedimentary Karoo strata are missing in the Aranos Basin apart from few occurrences of conglomeratic sediments north-east of Mariental to which Stollhofen

(1999) attributed a possible Triassic age by comparing the occurrences to deposits of the Stormberg Group in the main Karoo Basin of South Africa. Outcrops of the Carboniferous - Permian Dwyka and Ecca Groups are limited to the east by overlying calcretes and conglomerates of the Cretaceous/Cenozoic Kalahari Group and to the north and north-west by flood basalts and interlayered sediments of the Kalkrand Formation (Gerschütz, 1996) which belongs stratigraphically to the Jurassic Drakensberg Group.

Intracontinental rift-development in the Aranos Basin of southern Namibia is indicated by sediment thickness variations and by ice-flow directions within the Dwyka Group and by progradation directions of deltaic systems in the lower Ecca Group. Sediment thicknesses of the Dwyka Group generally diminish from east to west.

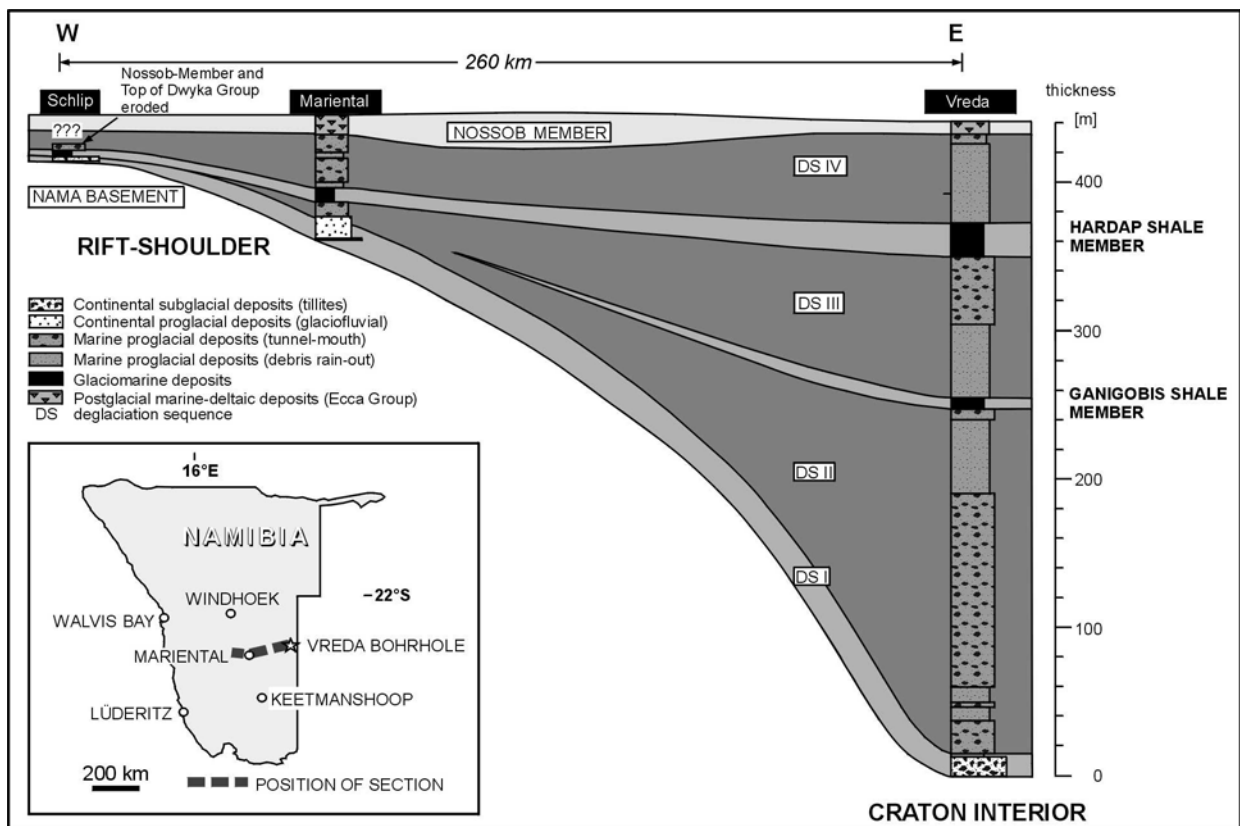


Fig. 2: E-W stratigraphic profile of the Dwyka Group in southern Namibia illustrating significant reductions in stratigraphic thicknesses and facies architecture towards the suggested rift shoulder (DS: deglaciation sequences; modified after Stollhofen *et al.* (in press).

Boreholes in eastern Botswana record a thickness of Dwyka Group-deposits of 415 and more than 448 m (Key *et al.*, 1998) which corresponds to the reported thickness of the Dwyka Group in the Vreda borehole in eastern Namibia (440 m; Grill, 1997). This seems to be the maximum thickness of the Dwyka Group east of the rift-zone towards the craton-interior. Outcrops in the Aranos Basin show a gradual thickness decrease to the north and also to the west due to the formation and uplift of the western part of the rift-shoulder. They record condensed Dwyka Group-sections of 150 m thickness in the vicinity of Ganigobis, 80 m south-west of Mariental (Grill, 1997) and 20-30 m in the vicinity of Schlip (Fig. 2).

Westerly directed ice-flow is reported from the eastern part of the Aranos Basin (Visser, 1983b) which belongs to the cratonic interior whereas south and south-westerly directed ice-flow in the western part of the Aranos Basin seems to be parallel to the rift-zone (Fig. 4).

South to south-westerly directed progradation of fluvial (Nossob Member) and wave-dominated (Auob Member) deltaic systems in the post-glacial Ecca Group trace this overall direction (Grill, 1997, Fig. 4). In northern Namibia the intra-continental rift-zone must have been active in Late Palaeozoic times when westerly directed deeply incised palaeovalleys developed due to retrograde erosion. Through Dwyka times they were further excavated by wet-based, temperate glaciers which also transported debris towards the centre of the rift zone (Fig. 4; Martin (1975), Stollhofen *et al.* (in press).

Several palaeogeographic reconstructions show the Karasburg Basin separated from the Aranos Basin by an elevated area coinciding with the Karas Mountains in southern Namibia (e.g. Visser, 1983b; Fig. 1 and Fig. 4). Consideration is given to the possibility that this "basin configuration" is really a Carboniferous-Permian structure or that it could be much younger and probably caused by post-Karoo tectonism. The reasons for the doubts are, that glacial striations (cf. Martin and Wilczewski, 1970); (Grill, 1997)

in both basins are generally N-S directed, at a considerable angle to the present-day "basin" outlines.

On the basis of equivalent southerly directed transport directions, Stratten (1977) suggested the occurrence of the Namaqualand ice lobe. During the deposition of the lower part of the Dwyka Group in southern Namibia, glaciers of the Namaqualand lobe could have reached as far south as Zwartbas (Karasburg Basin, Fig. 1 and Fig. 4) where 1.5 m thick lodgement tillites are preserved at the base of the sequence which were deposited in a subglacial environment.

About 250 km to the north in the Aranos Basin, outcrops of the Dwyka Group south of Snyfontein (Fig. 1) show 3-4 m thick basal lodgement tillites. Another 80 km further north these deposits reach thicknesses up to 20 m in the vicinity of Ganigobis (cf. Grill, 1997), Fig. 1 and Fig. 4).

In a broader context, the north-south trending axis of the Namaland ice lobe was located centrally in between the converging westwardly directed Transvaal (Stratten, 1977) and eastwardly directed Asunción (Santos *et al.*, 1996) ice sheets (Fig. 3).

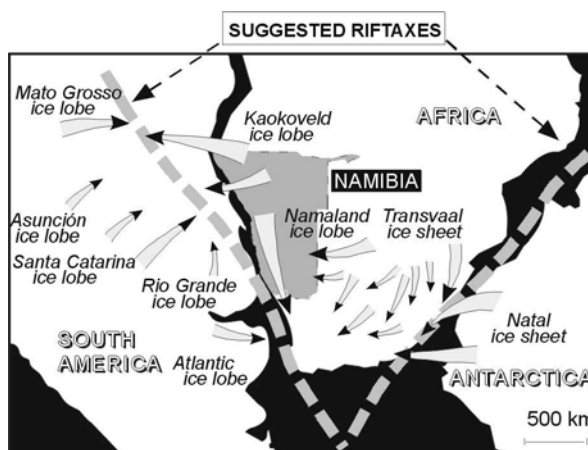


Fig. 3: Compilation of palaeo-ice flow directions in southern Gondwana during the Dwyka glaciation suggesting an early rift valley depression (based on Stratten (1967); Stratten, (1977); Frakes and Crowell (1969); França and Potter (1988); Visser (1993) and Santos *et al.*, (1996), from Stollhofen *et al.*, in press).

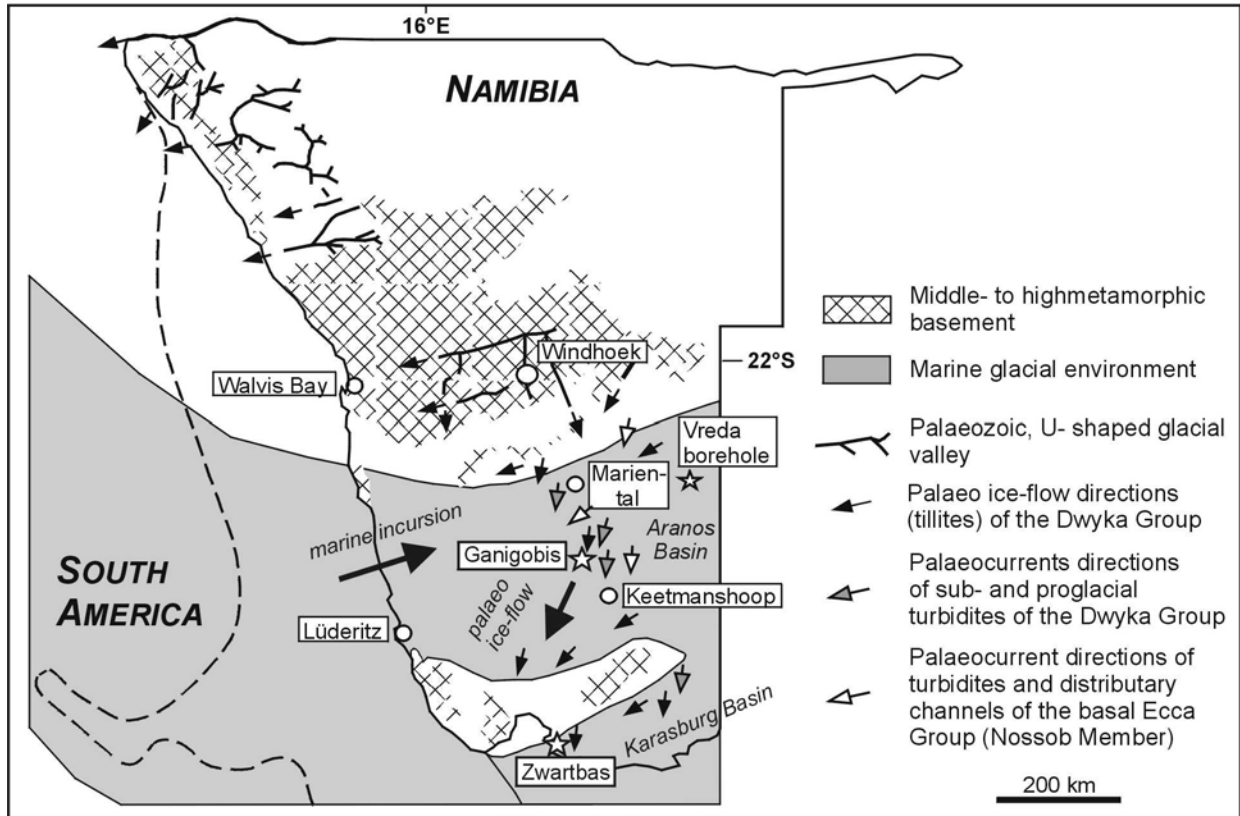


Fig. 4: Compilation of directions of glacially shaped valleys (Martin, 1975), palaeocurrent and palaeo-ice-flow directions involving data of Grill, 1997 and the suggested distribution of marine sedimentary facies of the Late Palaeozoic Dwyka Group and Ecca Groups in Namibia (data from Horsthemke *et al.*, 1990; Visser, 1993 and Williams, 1995; modified from Stollhofen *et al.*, in press).

An equivalent orientation of incised glacial valleys on both sides of the present-day Atlantic Ocean suggests the existence of an elongate, N-S trending basin. This has been interpreted to reflect the axis of an early southern South Atlantic rift-valley depression which favoured the incursion of a shallow intracontinental seaway facilitating the deposition of the Ganigobis Shale Member. It might also indicate the future line of disintegration between Africa and South America as early as during the Carboniferous-Permian (Stollhofen *et al.*, in press; Fig. 3).

1.3 The principal framework of Dwyka Group deglaciation sequences

In the main Karoo Basin Visser (1983a, 1986) distinguishes between two major lithofacies associations developed within the Dwyka Group: (1) A platform association consisting of a more homogeneous diamictite sequence which attains a

thickness of 300 - 800 m and (2) a valley/inlet association with a more variable thickness and lithofacies. However, no sharp boundary exists between the two associations.

The **platform association** mainly prevails in the southern and western parts of the main Karoo Basin and is characterised by multiple clast-poor and clast-rich diamictite units mainly deposited in a marine glacial to periglacial setting (Visser, 1993). They developed by diamicton during continuous suspension rain-out of fine particles and release of ice-rafted debris onto the basin floor in an overall low-energy setting (cf. Eyles and Eyles, 1993). The diamictite units are separated by shale beds up to 30 m thick, especially in the western part of the basin (Elandsvlei, South Africa; Visser, 1983a). The complex resulting stratigraphy can be attributed to diachronous ice advances and retreats resulting in stacked diamictite sequences (Visser, 1983a).

The **valley/inlet association** attains smaller thicknesses (< 300 m), shows rapid facies changes and mostly late-stage glacial deposits. It is characteristic for the northern part of the main Karoo Basin, for the Dwyka Group in KwaZulu-Natal and in the Karoo basins of southern Namibia. In addition to the diamictite-facies of the platform association, subglacially formed lodgement tillites as well as clast- and matrix-supported conglomerates and breccias of fluvio-glacial origin characterise the valley/inlet association. Further typical facies associations of the valley/inlet association are (1) varved silt- and mudstones inferring glaciolacustrine deposits, (2) thin horizontally-bedded silt- and mudstone units without dropstones originating from suspension settling of clay and silt in a marine environment and (3) ripple-cross laminated sandstones deposited by turbidites.

Theron and Blignault (1975) recognised that the stratigraphic framework of the Dwyka Group in the Western Cape Province (South Africa) is reflected by 3-4 parallel, topographic ridges north of the Cape Fold Belt where the beds are tilted.

The basal diamictites are usually resistant to erosion and form ridges whereas the softer and fine-grained, upper parts of the sequences are easily eroded and tend to crop out in narrow valleys (Fig. 5)

This internal arrangement of the glacial deposits can be traced for about 400 km in width to the west and east where the ridges amalgamate to a single ridge. Based on the cyclic sedimentation of the glacial deposits, Visser (1997) interpreted these four successions as deglaciation sequences (DS). A complete sequence consists of a massive basal diamictite overlain by a combination of bedded diamictites, diamictites containing sandstone bodies, siltstones and mudstones with or without ice-rafted material. Each sequence rests on either an erosional contact or on a sharp, non-depositional contact between succeeding lithofacies. However, the sequences are commonly incomplete so that the thickness of the individual sequences varies between 20 and 350 m (Visser, 1997).

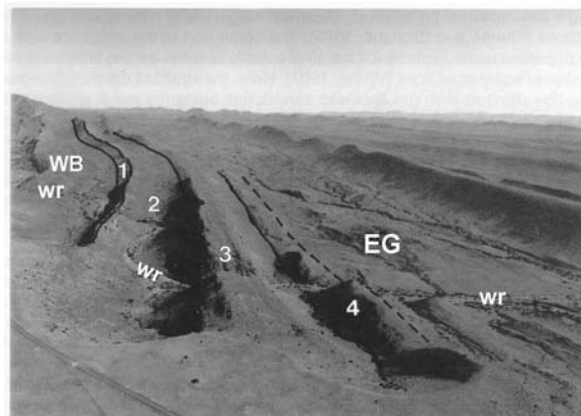


Fig. 5: Aerial photograph of the steeply dipping (75°) Lower Karoo sequence south of Laingsburg (South Africa). The basal contacts of Dwyka Group deglaciation sequences (1-4) are shown by solid lines and the top of the Dwyka Group by a broken line. WB: Carboniferous Witteberg Group; EG: Permian Ecca Group; wr: Witbergs River (Cole and Wickens, 1998)

A deglaciation sequence is thought to have formed at an active ice margin with the basal diamictite zone representing dense rain-out of glacial debris and suspension settling of mud followed by resedimentation (Visser, 1994). The basal zone was probably deposited during a slow retreat of the relatively stable ice margin under polar to subpolar climatic conditions (Theron and Blignault, 1975). Bedded diamictites represent debris-flow deposits with the enclosed sandstones being a result of deposition in subaqueous channels and outwash fans (Visser *et al.*, 1987). The upper parts were deposited under more unstable ice marginal conditions within a more temperate setting and deeper water conditions (Visser, 1997). Mudstones in the upper part of the sequences were primarily derived from flocculation and settling out from suspension of fine particles which were transported seaward by overflow plumes. These plumes originated from sediment-charged subglacial freshwater streams emanating from the melting base along the seaward margin of a retreating ice sheet (Von Brunn, 1996).

Visser (1997) suggested that the duration of the deglaciation sequences is between 9 and 11 Ma implying major global tectono-eustatic events.

Deposition of DS I should have begun at about 306 Ma (Moscovian) and DS IV should have lasted until about 277 Ma (Artinskian, (Menning *et al.*, 1997). The end of the Dwyka Group has been indirectly determined by the Swartberg folding event of the Cape Fold Belt at 278 ± 2 Ma ($^{40}\text{Ar}/^{39}\text{Ar}$ age) which affected the Dwyka Group-deposits but not the overlying Ecca Group-sediments (Hälbich *et al.*, 1983).

Bangert *et al.* (1999) applied the concept of deglaciation sequences to the Aranos Basin in southern Namibia where deglaciation sequences I-IV are completely documented in the Vreda test drill (cf. Grill, 1997). Outcrops of the Tses-Ganigobis area only document DS I-III. DS III and IV are recorded towards the north in the Mariental area (Fig. 8). Occurrences of the Dwyka Group in the Aranos Basin of southern Namibia are characterised by up to 200 m thick deposits of strongly varying lithologies such as subglacially formed tillites; continental, fluvio-glacial conglomerates and marine glacial to periglacial, clast-poor diamictites, bedded diamictites, silt- and mudstones with and without dropstones (Grill, 1997).

Dwyka Group-deposits unconformably overly interlayered red shales and quartzites of the Precambrian to lower Cambrian Nama Group (Gresse and Germs, 1993). If overlain by Dwyka Group-sediments, the uppermost 2 m of Nama beds commonly show severe impact by glacially induced shear stress of the overriding, grounded glaciers. This is recorded by vertical wedge-shaped cracks which are up to 1 m deep, 20 cm wide and up to several meters long. Glacial striation directly on Nama Group-sediments (Heath, 1972) and large fragments of Nama quartzite within the lowermost local tillites provide further evidence (Grill, 1997).

The Dwyka Group in the Aranos Basin starts with lodgement tillites of deglaciation sequence I (**DS I**) reaching a maximum thickness of 10 - 25 m in the Mariental-Ganigobis area (Fig. 6). They are overlain by varved siltstones and fine-grained sandstones which formed in glaciolacustrine settings and which are only preserved as lenses and striated surfaces. Fluvio-glacial deposits like medium to coarse-grained, trough cross-stratified sandstones and clast-supported conglomerates

follow on top of the glaciolacustrine deposits. The continental subglacial, glaciolacustrine and fluvio-glacial facies association at the base of the Dwyka Group is only found in the northern part of the Aranos Basin between Schlip and Tses and pinches out southwards (cf. Grill, 1997).

DS II comprises a strongly heterolithic upward-fining unit which was formed in a predominantly marine or a least subaquatic environment (Grill, 1997). The unit comprises a thickness of 95 m north-west of Ganigobis whereas a maximum thickness of about 240 m is recorded in the Vreda borehole (Fig. 6). DS II begins with a distinctly glacially-scoured, clast-poor, massive diamictite succeeded by stratified, clast-supported to matrix-supported diamictite containing sandy and silty streaks and lenses forming a distinct parallel stratification (Grill, 1997). In this stratigraphic interval they dominate the sediments north of Ganigobis whereas to the south (e.g. south of Farm Snyfontein) the sediments are almost entirely dominated of dropstone-bearing mudstones. To the top they are overlain by about 30 m (Ganigobis locality) of clast-poor diamictites with a fine-grained sandy to silty matrix changing gradually into massive or laminated mudstones with lonestones. The lonestones are well rounded to subrounded, often faceted and striated with an average clast size of about 1 cm (Grill, 1997). Lithologies mainly comprise red quartzites, less frequently granitic and undeformed volcanic dropstones. Clasts embedded in these mudstones were released from debris-laden floating ice in a glaciomarine environment. In the uppermost part of DS II an essentially dropstone-free, silty mudstone unit (Ganigobis Shale Member; Martin and Wilczewski, 1970; Tab. 1) suggests that fully marine conditions were finally established. It originated mainly from offshore suspension load settling and comprises a thickness of more than 40 m at Ganigobis. The silty mudstones contain bentonitic ashfall tuffs and concretionary nodules bearing remains of palaeoniscoid fishes, gastropods and bilvalves which confirm the marine character.

DS III has a maximum thickness of about 120 m recorded in the Vreda borehole whereas its thickness diminishes to 60 m in the vicinity of Ganigobis (Fig. 6). In the Vreda borehole, DS III is mainly composed of periglacial tunnel mouth and debris rain-out diamictites and thick massive or cross-bedded sandstones, representing sediment gravity flows (Heath, 1972; Grill, 1997). Small outcrops in the vicinity of Tses only show silty mudstones with sparse granitic or gneissic dropstones. The uppermost part of DS III is formed by a 75 m thick succession of dropstone-rich sandy mudstones. As sand and dropstone contents decrease upwards, these dropstone-rich mudstones gradually grade up-section into plane bedded mudstones (Hardap Shale Member, (South African Committee for Stratigraphy, 1980) in which dropstones are completely absent. The latter are characterised by occurrences of the marine bivalve *Eurydesma mytiloides* (Heath, 1972), Bryozoa and Asteroidea (Martin and Wilczewski, 1970) and were correlated to the Gondwana-wide *Eurydesma* transgression (Dickins, 1984). Sediments of DS III are more widespread preserved in the northern part of the Aranos Basin between Mariental and Anis Kubub (Heath, 1972) where massive or cross-bedded, turbiditic sandstones showing Bouma B, C, and D subdivisions are intercalated and locally make up to 40 % of the sediment thickness (Grill, 1997).

DS IV is 60 m thick in the Vreda borehole (Fig. 6) but is only poorly exposed in outcrops east of Asab. It consists of sandstones followed by dropstone-bearing mudstones. This sequence is capped by greenish, dropstone-free mudstones containing thin sand horizons that represent distal turbidite beds which define the base of the overlying, fluviially dominated delta complex of the Nossob Member (Prince Albert Formation).

The thinning of the subglacial facies association to the south and the contemporaneous thickening of marine glacial and periglacial facies associations in the same direction is explained by a general southward deepening of the basin and an increasing distance from the ice margin which was presumably located farther north. As the deglaciation sequences of the Dwyka Group formed during successive periods of glacial retreat and accelerating melt-water flux, glaciers of the Namaqualand ice lobe decoupled from the substratum. Deposits originated mainly from the undermelting of the glacial ice forming diamictites by debris rain-out (cf. Brodzikowski and van Loon, 1991; Fig. 7).

The process of decoupling was enhanced by contemporaneous marine transgressions which proceeded from the south and south-west into the area. Major marine transgressions are indicated by the dark, essentially dropstone-free mudstones of the Ganigobis Shale Member in the uppermost part of DS II and the Hardap Shale Member at the top of DS III. In the north of the Aranos Basin between Asab and Mariental, deposits of DS II are only rarely preserved at the eroded banks of the Fish River whereas deposits of DS III and IV predominate. Glaciers or lobes of ice sheets were thus still grounded in this area of the basin leading to the non-preservation of glacial deposits of DS I and most of DS II. With the further retreat of the Namaqualand ice lobe and its associated glaciers, deposits of DS III and IV could be preserved in front of the disintegrating glacial ice.

Palaeocurrent analyses of turbiditic sandstones of DS III and IV reveal the same trend of southerly directed sediment transport (Grill, 1997) as the glacial striations do.

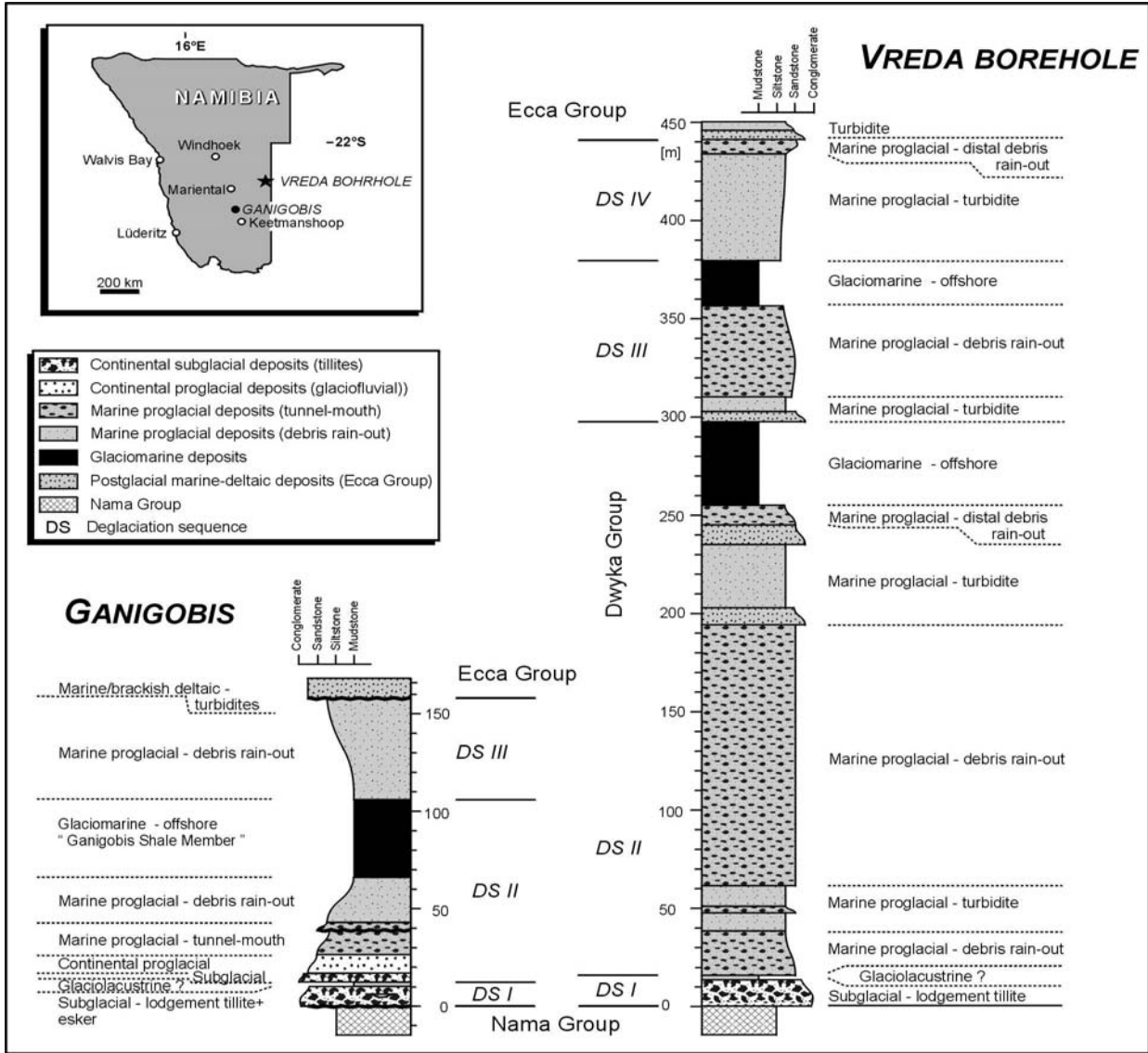


Fig. 6: Comparison between sections of the Dwyka Group near Ganigobis (outcrops) and in the Vreda borehole (compiled from Grill, 1997).

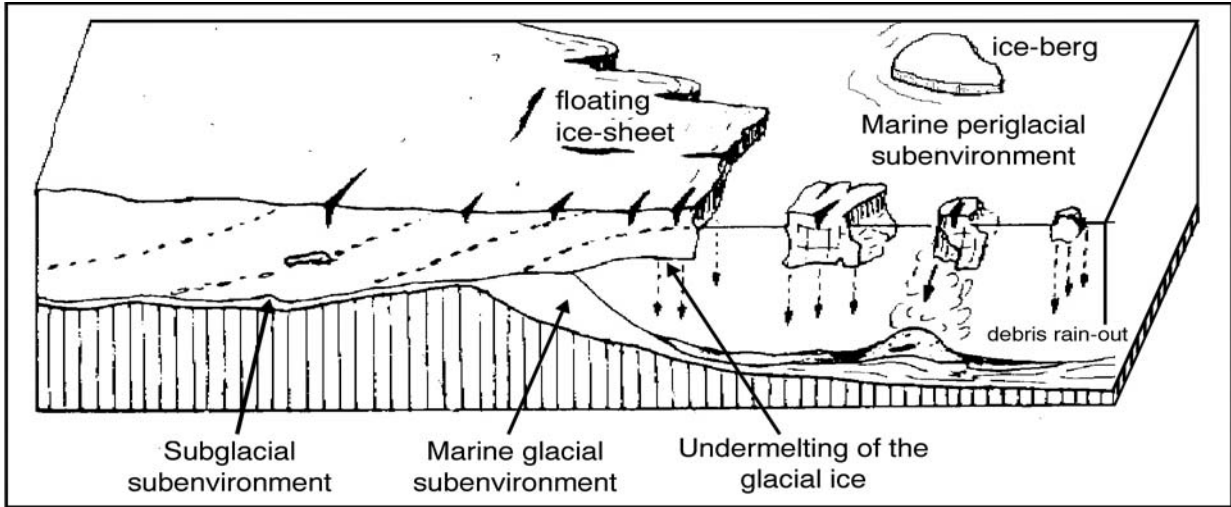


Fig. 7: Schematic model of Dwyka Group depositional environments preserved in the study area. Modified from Brodzikowski and van Loon (1991).

1.4 The distribution of Dwyka Group deglaciation sequences in southern Namibia

Sediments of the Dwyka Group are generally flat lying and dip less than 5° to the east. Deposits of DS I are therefore located on the western side of the basin conformably overlying rocks of the Nama Group to the west. Outcrops of lodgement tillites are found along the river banks of the Fish River, on mesas west of Fish River and in the lowermost part of the escarpments west and north-west of Keetmanshoop (south of Farm Snyfontein). The type locality for the Dwyka Group-deposits of DS I and II within the Aranos Basin is located north-west of Ganigobis along the Fish River. Further exposures of glaciomarine sediments of the basal DS II are found east of Farm 12 Anis Kubub and Gibeon as well as in the south as part of the escarpments west and north-west of Keetmanshoop where DS II is completely dominated by dropstone-bearing mudstones. The Ganigobis Shale Member forming the uppermost part of DS II can be traced from Farm Tsaraxa in the south to Farm 12 Aretitis in the north (Fig. 8). Dropstone-bearing shales with very thin bentonitic tuff beds and concretions with fish remains (*Namaichthys schroederi*) also occur in the south (south of Farm Snyfontein). The mostly dropstone-free Ganigobis Shale Member changes into silty green shales without bentonitic beds northward of Farm 12 Aretitis and finally pinches out north of Farm 96 Anis Kubub (37 km south-south-west of Mariental (Heath, 1972). Exposures of Dwyka Group-sediments assigned to DS III are primarily found in the eastern part of the Aranos Basin (Fig. 8). Outcrops of the Hardap Shale Member which forms the top of DS III are found for example 4 km south-east of Hardap dam (cf. Chapter 6.1). They also occur below the escarpment formed by the overlying Nossob Sandstone Member which runs N-S east of the B 1 and also as part of the escarpments west and north-west of Keetmanshoop. The highest part of the Dwyka Group (DS IV) is found east of Asab where the Nossob Sandstone pinches out. In this area the Karoo strata are not overlain by the

Cretaceous/Cenozoic calcretes and conglomerates (Heath, 1972).

The comparison between the lithological units introduced by Heath (1972, Tab. 1) and the overall subdivision of Dwyka Group deposits in deglaciation sequences is difficult as lithologies and facies associations change rapidly over short distances. Heath concentrated on the area between Mariental and Asab where sediments of the upper part of the Dwyka Group (DS III and IV) are more widespread than deposits of the lower part which are mainly found near the banks of the Fish River. His subdivisions of the Dwyka Group thus focus more on the upper part of the Dwyka Group whereas the subdivision of the lower part of the Dwyka Group (DS I and II) is rather incomplete.

Heath (1972)	this study
upper boulder mudstone	DS IV
lower boulder mudstone	DS IV
alternating sandstone and green mudstone	DS III: Hardap Shale Member
tilloid and pebbly mudstone	DS III
lower pebbly mudstone	DS II: Ganigobis Shale Member
basal tillite	DS I/II

Tab. 1: Comparison between the lithological units of the Dwyka Group within the Aranos Basin suggested by Heath (1972) and the deglaciation sequences mentioned in this study.

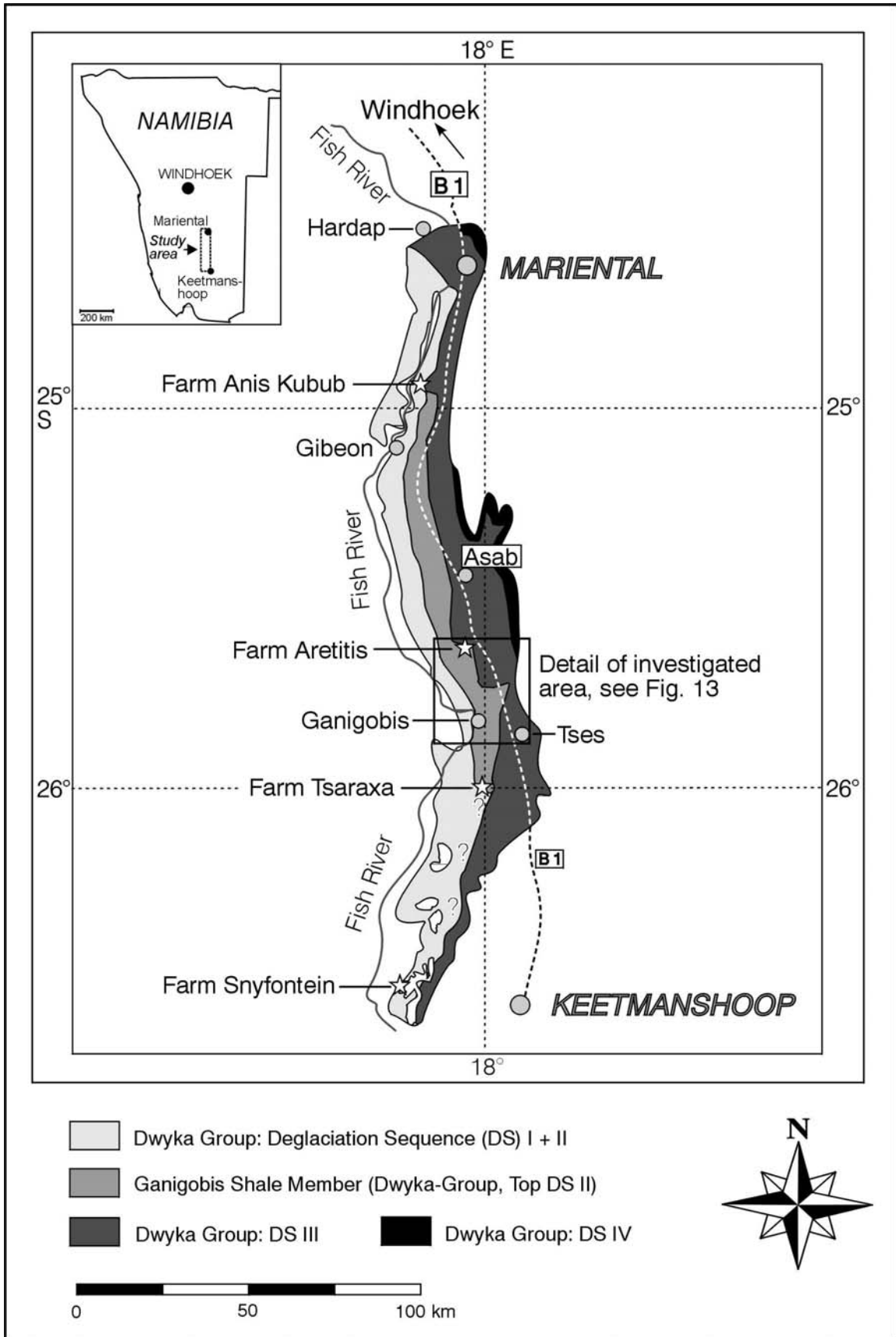


Fig. 8: Simplified geological map of the area between Mariental and Keetmanshoop in southern Namibia showing the distribution of Dwyka Group deglaciation sequences (DS I-IV) and the Ganigobis Shale Member forming the uppermost part of DS II (Bangert *et al.*, in press).

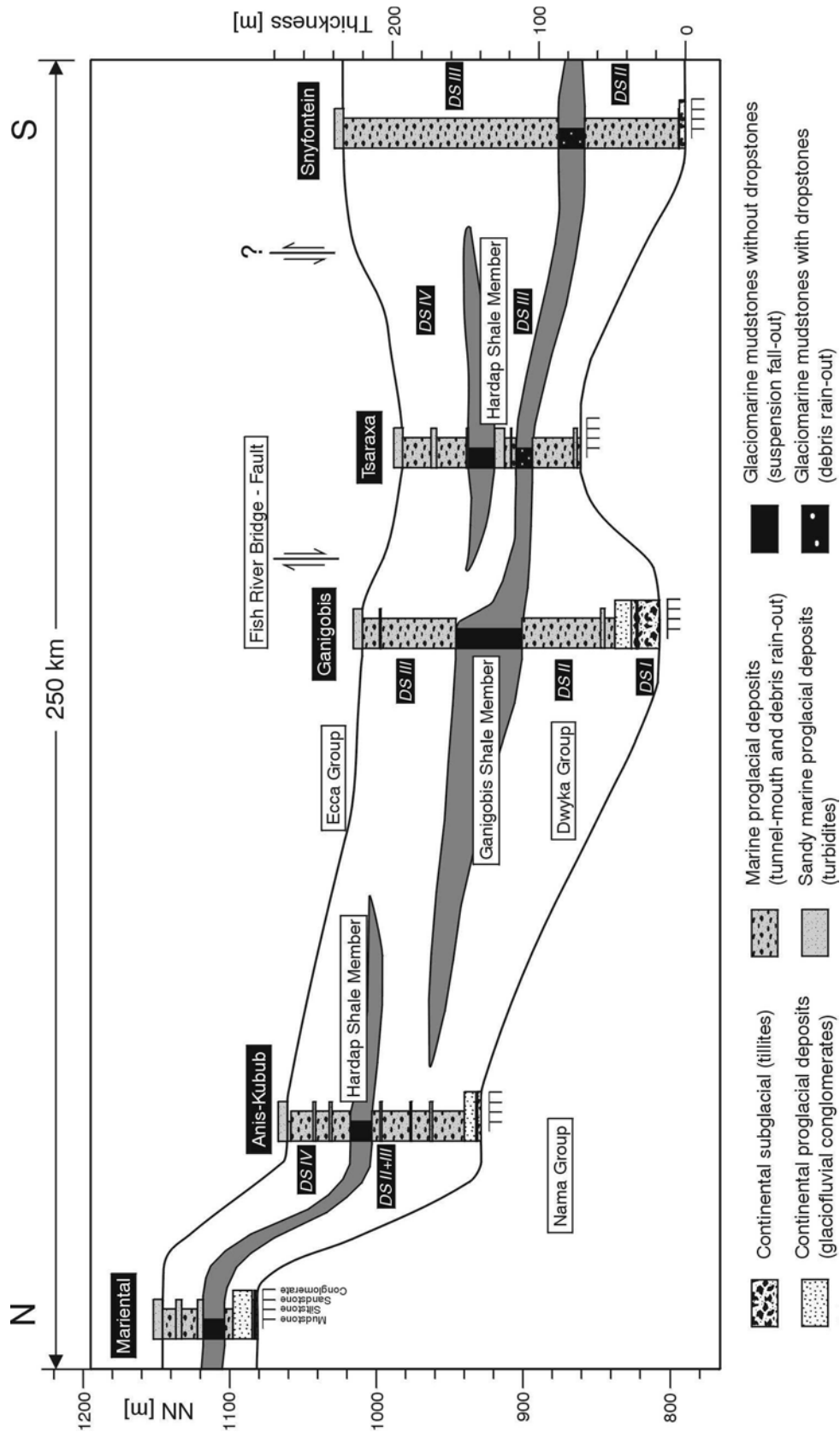


Fig. 9: Schematic N-S cross-section between Mariental and Keetmanshoop illustrating important shale members, deglaciation sequences and the facies architecture of the Dwyka Group in southern Namibia (Bangert *et al.*, in press). See Fig. 1 for location of individual sections.

2 The Ganigobis Shale Member

The more than 40 m thick Ganigobis Shale Member (Martin and Wilczewski, 1970) situated in the uppermost part of DS II is unique since no other shale unit with an equivalent thickness, marine fossils and contents of bentonitic tuff beds is known in the Dwyka Group of southern Africa. Occurrences of marine fossils are known since the beginning of the 20th century (Schroeder, 1908). Extensive investigations on the geology and geography of the "German" Namaland were done by Paul Range (1912, 1920, 1928) and Wagner (1915). Gürich (1923) studied the palaeoniscoid fish remains preserved in siliceous-phosphatic concretions within the Ganigobis Shale Member comprehensively. Gardiner (1962) and Jubb and Gardiner (1975) revised his work but did not add much new information. Modern geological studies about the lithology and fossil contents in this area started with Henno Martin (1953, 1975, 1981a); Martin and Wilczewski, (1970); Martin *et al.* (1970). Further contributions were added by Heath (1972); Visser (1983a, 1983b, 1997); Grill (1997); Bangert *et al.* (1998, 1999, in press); Bangert and Bamford (in press).

In its type area, in the vicinity of Tses and Ganigobis, the Ganigobis Shale Member is mainly exposed in eroded river banks of the Fish River and its tributaries from the east and north (Tses, Ganigobes and Asab Rivers). The type area is located between Farm Waterval in the

south (Tses River) and Farm 12 Aretitis in the north (Asab River). Dimensions of the area give a maximum north-south extension of 30 km and a maximum east-west extension of 10 km (Fig. 9).

2.1 The tuff beds of the Ganigobis Shale Member

The Ganigobis Shale Member in the vicinity of Ganigobis embodies 21 fine-grained ash-fall derived tuff beds which occur in 8 groups and which will be comprehensively described in Chapter 8 and following chapters. All tuff beds, their thickness and the vertical distance to the underlying tuff bed are summarised in Tab. 20 in Appendix A-3. They are essentially undeformed and flat lying with dips less than 2°. The thickness of the tuff beds (0.1-2.0 cm) and the vertical distances between them remain constant over distances of up to 15 km. All tuff beds are bentonites which are relatively soft and greasy, especially if the beds get into contact with water as the smectitic portion of the clay minerals swell rapidly. Their colour is overall white-yellow-beige to slightly grey but can also be red, when oxidised (e.g. tuff bed #30 IVb) or dark grey, when reduced (e.g. tuff bed #2 IVa). Especially in the upper part of the Ganigobis Shale Member the pyroclastic material is partly replaced by fibrous gypsum and blocky calcite, which increases thicknesses to up to 10 cm (e.g. tuff IVa in Fig. 10).

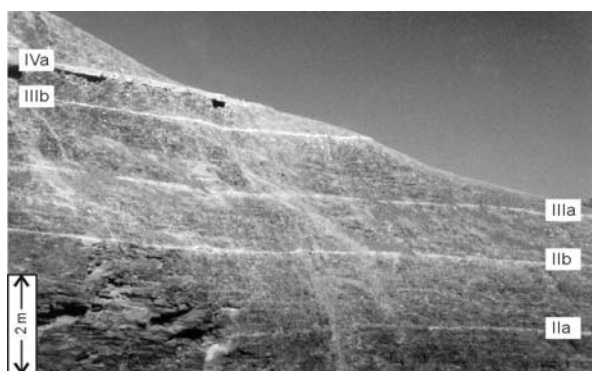


Fig. 10: Left: Field occurrence of cm-thick, bentonitic tuff beds IIa to IVa (Ganigobis Shale Member) in outcrop #32, 26 km north-west of Tses (see Fig. 13 for location); right: Field occurrence of tuff bed Vc in outcrop #2, 2.5 km north of Ganigobis (see Fig. 13 for location), note the sharp base and the wavy and blurred upper part of the tuff bed.

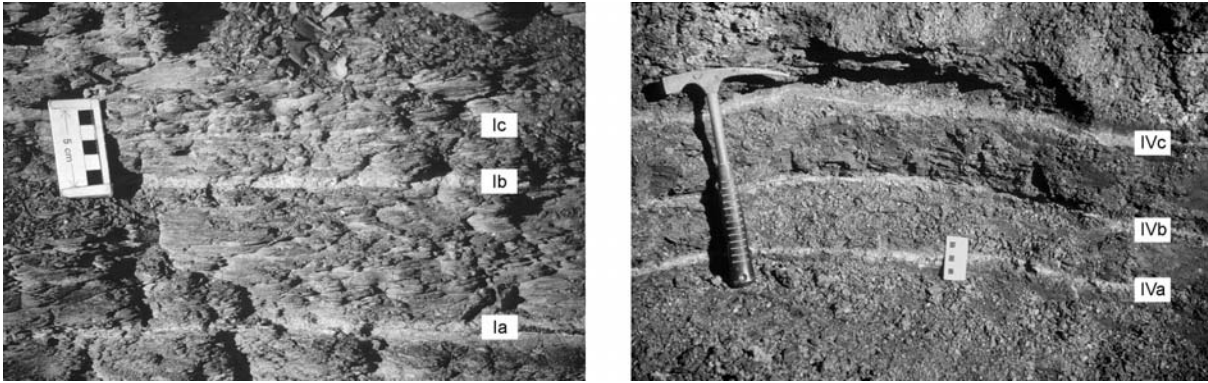


Fig. 11: Left: Field occurrence of tuff beds Ia to Ic in outcrop #2, 2.5 km north of Ganigobis (see Fig. 13 for location); right: Field occurrence of tuff beds IVa to IVc in outcrop #22, 9.5 km west of Tses (see Fig. 13 for location). Especially tuff beds IVa to IVc (called the ‘triplet’ by Grill, 1997) are excellent stratigraphic markers and can be traced about a distance of at least 30 km.

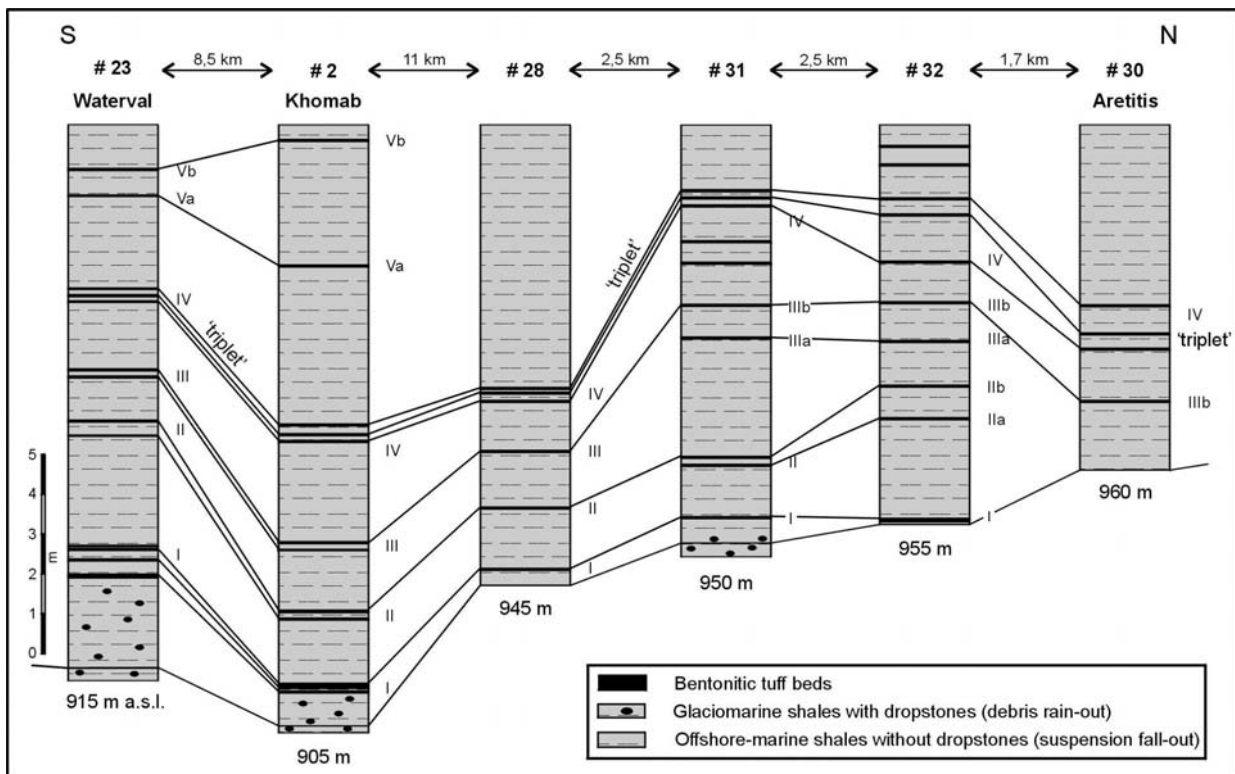


Fig. 12: Correlation of tuff bed groups I to V of the Ganigobis Shale Member in six major outcrops along a north-south directed section between Farm Waterval and Farm Aretitis. The correlation is based on field observations which mainly rely on tuff beds IVa to IVc (Fig. 11), mudstone intervals between single tuff beds change due to different sedimentation rates and syndepositional faulting. See Fig. 13 for location of the single sections; a.s.l.: above sea level.

Some tuff beds consist of a mixture of mud material and pyroclastic material which might be reinforced by bioturbation. The bases of the tuff beds are mostly sharp, whereas the tops are sometimes wavy probably due to weak bottom-currents during deposition (Fig. 10). Due to the similar appearance of the tuff beds, the field-

based correlation of the tuff beds between single outcrops was difficult. As mudstone intervals between the tuff beds IVa, IVb and IVc (called the ‘triplet’ by Grill (1997) remain constant in most of the studied area (except the northernmost part), these tuff beds served as good marker beds.

Correlation of tuff beds I to V in the southern part of the study area (localities #45, #22, #23 and #2) was easier than in the northern part (localities #28, #31, #32 and #30) as intervals remain more constant (for location of the outcrops see Fig. 13). In outcrop #30 the mudstone intervals between the tuff beds IV a, b, c are exactly three times the intervals measured in outcrop #2 (cf. Chapter 2.3). Tuff beds can be correlated from this outcrop to the south into outcrops #32 and #31.

The 21 tuff beds have permitted the establishment of a detailed tephrostratigraphy. Consequently, the Ganigobis Shale Member can be subdivided into three parts. The lower part of the succession (up to 1.5 m above tuff bed VIb) consists of blue-black massive, silty mudstones from the base up to tuff bed Vc. Medium grey silty mudstones, which display a distinct lamination with an average laminae thickness of < 1 mm, occur from close above tuff bed Vc up to 1.5 m above tuff bed VIb. The middle part of the Ganigobis Shale Member (from 1.5 m above tuff bed VIb to tuff bed VIIIa) mainly consists of black mudstones and commonly contains normally graded, calcareous, less than 1 m thick sandstone interbeds which are interpreted as distal turbidite deposits. The upper part (from tuff bed VIIIa to the top of the Ganigobis Shale Member) is again comprised of black mudstones with sporadic sandstone interbeds.

2.2 The threefold subdivision of the Ganigobis Shale Member

The base and the lowermost 20 m of the Ganigobis Shale Member are exposed in more outcrops than the middle and upper parts. The largest and most important outcrop (#2) of the base and the following mudstone dominated strata is situated at the river banks of the Fish River north of Ganigobis. They provide three-dimensional impressions due to cut banks of the E-W directed Ganigobes (#38) and Khomab Rivers displaying the base and the lowermost 20 m of the Ganigobis Shale Member. Cliffs which reach a maximum height of 18 m with an average of 3-10 m stretch around the bend of the Fish

River creating continuous outcrops of the Ganigobis Shale Member over a length of 2.5 km. Outcrop #2 is continued to the north in outcrop #41 at the river banks of the Asab River where mudstones, which contain dropstones, underlie the Ganigobis Shales. For comparison of the lowermost part of the Ganigobis Shale Member outcrops #23 near Farm Waterval in the south and outcrops #32 and 30 at the river banks of the Asab River should be mentioned. Another important outcrop (#45) including the base and the lowermost part of the Ganigobis Shale Member is located in a roadcut (D98 Tses - Berseba) 20 km west of Tses just directly east of the bridge crossing the Fish River.

The middle part of the Ganigobis Shale Member is rather poorly exposed and the best outcrops are located at the river banks of the Asab and Huam Rivers in the vicinity of Haams (#13, 15, 16, 19 and 20).

The upper part of the Ganigobis Shale Member crops out in two areas – one next to the B1 at the river banks of the Brukkaros River (#9 and 27), the other is located north-east of Ganigobis at the Ganigobes River (#40 and 43). All outcrops including type of outcrop, exposed features and co-ordinates are listed in Tab. 18 in Appendix A-1.

2.3 The base of the Ganigobis Shale Member

The lowermost part of the Ganigobis Shale Member is characterised by a rapid transition from dropstone-bearing mudstones to mainly dropstone-free mudstones with interbedded phosphatic-siliceous concretions enclosing remains of palaeoniscoid fishes. 16 of the 21 recognised tuff beds are present in this part. The base itself is demarcated by the virtual boundary between mudstones with abundant dropstones and mudstones containing only solitary dropstones which occur about 1 m below tuff bed Ia. From the north to south the base of the Ganigobis Shale Member crops out at localities #31, 2, 23, and 45.

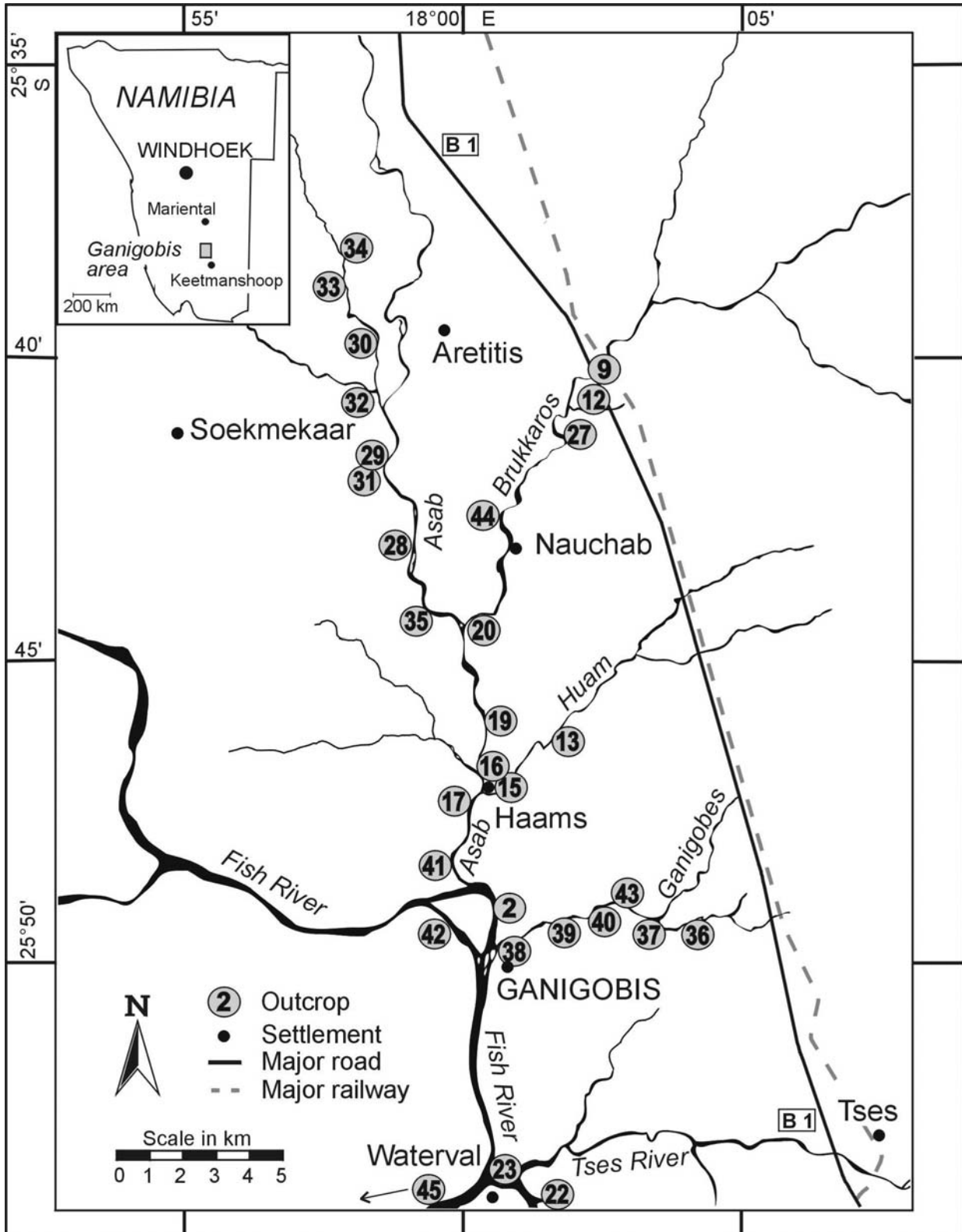


Fig. 13: Detailed location map of the type area of the Ganigobis Shale Member in the vicinity of Ganigobis, southern Namibia.

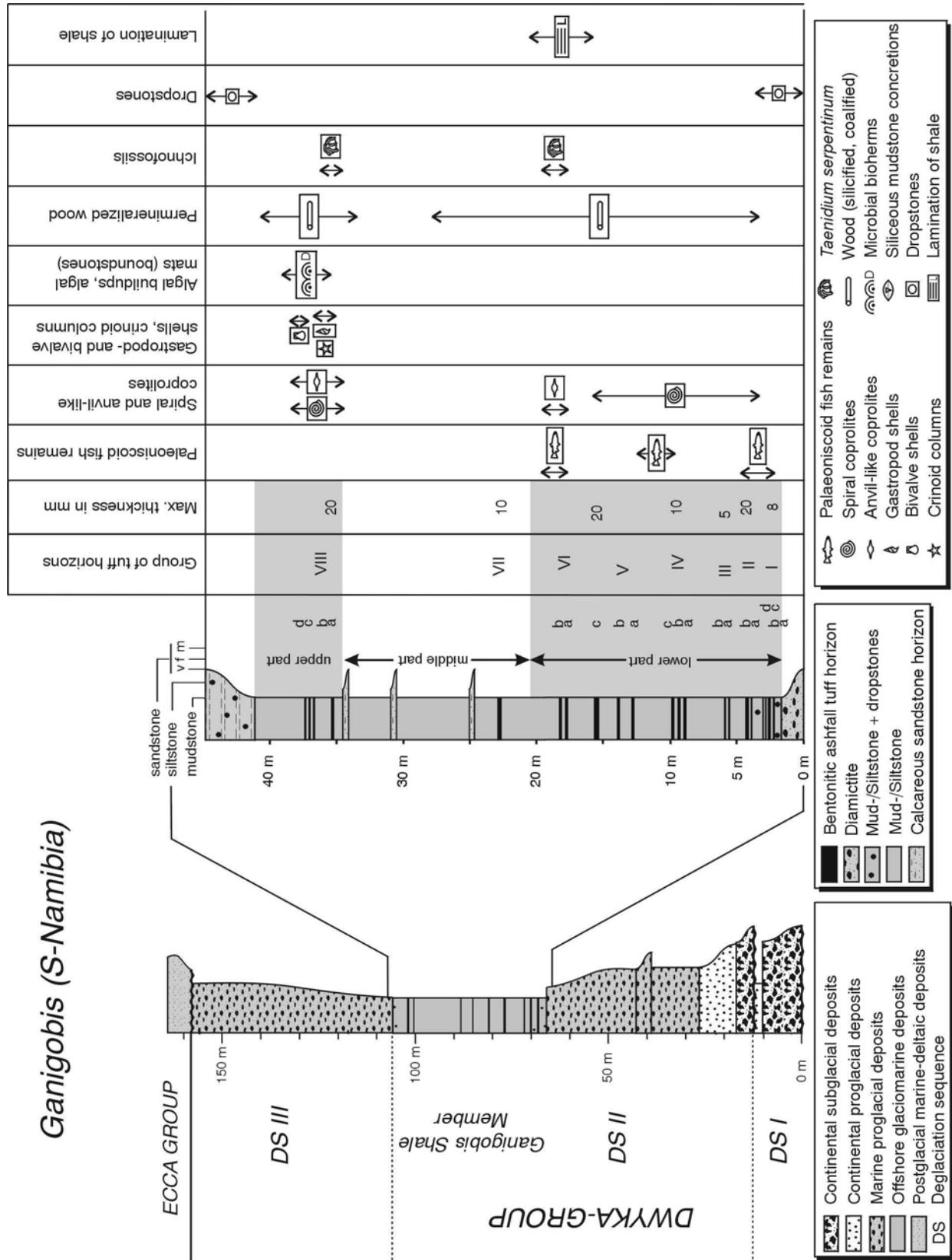


Fig. 14: Logged section of the Dwyka Group in the vicinity of Ganigobis (southern Namibia) with proposed deglaciation sequences. Detailed tephrostratigraphy and fossil record of the glaciomarine Ganigobis Shale Member at Ganigobis is shown in the right column (Bangert *et al.*, in press).

Cut banks of the Fish River: Locality #2

The base of the Ganigobis Shale Member is best exposed by the northernmost mudstone cliffs eroded by the Fish River about 2.5 km north of Ganigobis (#2: 25°48'52" S, 18°00'40" E, Fig. 15).

Occasionally huge, rounded blocks of more than 1 m in diameter occur below the base of the Ganigobis Shale Member within the dropstone-bearing mudstones but do not appear in the dropstone-free mudstones up-section. They consist of very clast-poor diamictite with a fine-grained sandy matrix and mostly quartzitic dropstones of an estimated average clast size (EACS; Visser, 1986) of 2 cm. These blocks were probably deposited as a whole in frozen state.

The occurrence of mostly quartzitic dropstones extends up to 0.7 m below tuff bed Ia. The greatest, measured diameter of a quartzitic dropstone reaches 60 cm, the EACS is about 1 cm.

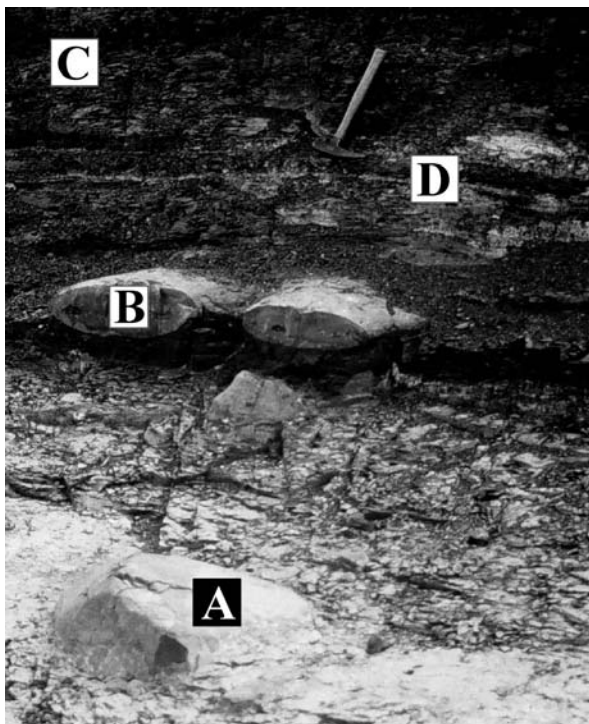


Fig. 15: The base of the Ganigobis Shale Member in outcrop #2 north of Ganigobis displaying dropstone-bearing mudstones (A), amalgamating mudstone concretions (B) and mainly dropstone-free mudstones (C) including tuff bed Ib just below the hammer (D).

Smaller dropstones of quartzitic, doleritic and metamorphic lithologies are well-rounded to rounded whereas the bigger ones are mostly angular to subangular (Fig. 15). As an exception a single, angular, grey quartzitic dropstone with a size of 20 x 16 x 8 cm was discovered about 20 cm above tuff bed Ic. Yellow-orange weathered pyritic concretions with a maximum diameter of 5 cm occur about 1 – 1.5 m below tuff bed Ia within the uppermost part of the dropstone-bearing mudstones. They were at first thought to have been volcanic in origin equivalent to the tuff beds above. Just above these small pyritic concretions and 25 respectively 45 cm below tuff bed Ia two laterally extensive concretionary mudstone beds occur (Fig. 15). These mudstone concretions amalgamate, forming laterally intermittent layers up to 0.2 m thick and several tens of meters wide. They contain up to 5 cm large, well-rounded to rounded, mostly quartzitic and plutonic dropstones. Further solitary, angular to subangular dropstones (mostly quartzites) were discovered by Volker Lorenz below tuff beds IIIb, IVa and Vc which are the highest occurring dropstones within the Ganigobis Shale Member (cf. Tab. 19 in Appendix A-2).

Above the tuff beds I phosphatic-siliceous mudstone concretions with a maximum diameter of 12 cm and maximum thickness of 5 cm occur which contain scales, fins and skull fragments of palaeoniscoid fishes. The fish fossils will be described in more detail in Chapter 3.1. The fossiliferous concretions appear up-section up to tuff bed IIb. Above this tuff bed and further up to the tuff beds IV only few concretions without fish remains are present within the silty mudstones. Further up-section, above tuff bed group IV and especially below tuff beds group V more fossiliferous concretions with palaeoniscoid fish remains appear in the Ganigobis Shale Member which were already mentioned by Grill (1997). Aside from the preserved fish fossils, other phosphatic-siliceous mudstone concretions bear up to 5 cm long, mostly spiral coprolites which occur from below tuff bed Ib up to 0.4 m above tuff Vc. A further description and interpretation follows in chapter 3.2.

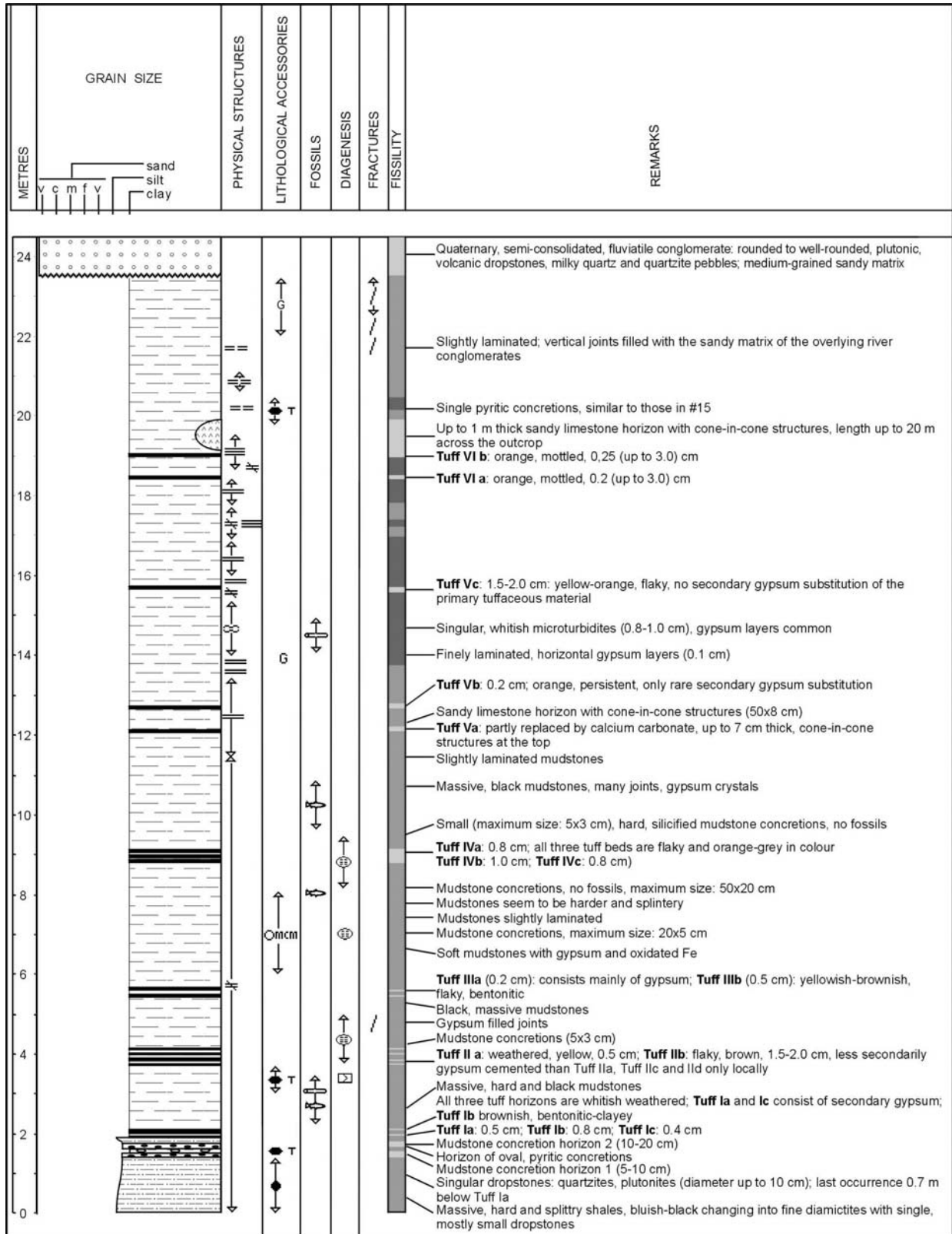


Fig. 16: Measured section of outcrop #2 displaying lithology, fossil contents and tuff beds of the lower part of the Ganigobis Shale Member. For symbols see Fig. 17.

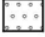








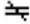

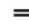
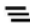












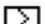
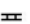





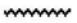






<h1>LEGEND</h1>									
<h2>LITHOLOGY</h2>									
	CONGLOMERATE		SILTSTONE		LIMESTONE				
	SANDSTONE		SILTY SHALE		SANDY LIMESTONE with cone-in-cone- concretions				
	SILTY SANDSTONE		SHALE / MUDSTONE		ASHFALL TUFF				
<h2>PHYSICAL STRUCTURES</h2>									
	structureless/massive		Continuous parallel lamination		parallel lamination				
	planar tabular bedding		Discontinuous parallel lamination		non-parallel wavy lamination				
	wave ripple		Discontinuous flaser lamination		micro turbidites				
<h2>LITHOLOGICAL ACCESSORIES</h2>									
	mudstone intraclast		organic matter		gypsum crystals				
	limestone intraclast		muscovite flakes		dropstones				
<h2>DIAGENESIS</h2>									
	mudstone concretion		gypsum cement		calcareous cement				
	nodule / concretion		cone-in-cone structure						
<h2>FOSSILS</h2>									
	fish remains		bivalves (Myonia and Nuculopsis)						
<h2>OTHERS</h2>									
	fracture, general		scoured contact		inverse grading / coarsening upwards				
<h2>FISSILITY</h2>									
	Extreme		Strong		Moderate		Poor		Non-fissile

Fig. 17: Legend for measured sections of the Ganigobis Shale Member (Fig. 16, Fig. 19, Fig. 23, Fig. 26, Fig. 34, Fig. 35)

Permineralised wood was found in situ from 0.75 m above tuff bed Ic up to 1.1 m below tuff bed Vc. Two samples were passed to Dr. Marion Bamford at the BPI Palaeontology, University of the Witwatersrand in Johannesburg who determined the samples as *Araucarioxylon sp.* The sample which crops out 0.75 m above tuff bed Ic is flattened, slightly coalified and shows glassy spheres on the surface. It has a maximum size of 1.90 x 0.38 x 0.03 m (Fig. 18). A detailed description follows in Chapter 3.3. Other permineralised wood exposed in situ from below tuff IIIb to the top of the Ganigobis Shale Member is oval to spherical and not coalified. Between tuff bed groups I and II permineralised wood often forms the nucleus of siliceous mudstone concretions. The orientation of the wood found in situ varies between 80 and 130° (Tab. 19 in Appendix A-2).

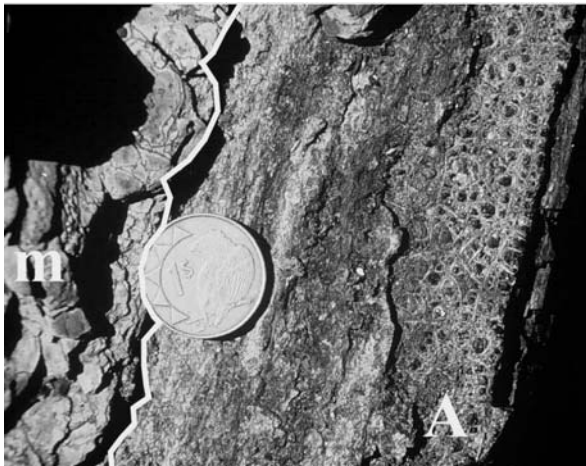


Fig. 18: Flattened, slightly coalified sample of *Araucarioxylon sp.* displaying glassy spheres (A) on the surface; m: adjacent mudstones.

Cut banks of the Tses River: Locality #23

The single outcrop is located about 300 m east of Farm Waterval (25°53'35" S, 18°00'51" E) at the Tses River and has a length of 120 m and a height of 20 m. It essentially comprises the same section found 5 km to the north at locality #2, starting off from below tuff beds I and ending

above tuff bed VI (Fig. 19). The overall thickness, however, is condensed which is pinpointed by an overall smaller distance between the single tuff beds. The tuff beds within the outcrop are several times offset by normal faults dipping to the east with a displacement of about 10-30 cm.

Yellow-orange weathered pyritic concretions with a maximum size of 20 x 5 cm occur about 2.5 m below the tuff bed Ia within the uppermost part of the dropstone-bearing mudstones. About 2 m below tuff Ia a further tuff bed was discovered, termed tuff bed '0'. It was fully replaced by secondary sulphates displaying a thickness of 1.5 cm over 1 m length. About 1 to 1.5 m below tuff bed Ia red to yellow plant debris with a size of less than 2 mm is frequently found on bedding and joint planes. The occurrence of mostly quartzitic dropstones extends up to 0.9 m below tuff bed Ia (Fig. 19).

In addition to outcrop #2 a thin, 0.5 cm tuff bed Id is added which was also found at outcrop #38 directly north of Ganigobis. Siliceous concretions with spiral coprolites were discovered between tuffs I and II and below and above tuff IVa whereas siliceous-phosphatic concretions with palaeoniscoid fish remains appear to concentrate between tuff beds III and IV and below and above tuff bed Va. Permineralised wood was not found in situ in the outcrop. Again, the colour of the mudstones varies between medium grey to dark grey and black. They are mostly massive between the base and about 0.5 m above tuff bed Vb. Especially between tuffs Vb and VI distinctly laminated mudstones alternate with massive mudstones. Mm-thick fine-grained sandy layers, probably representing distal turbidite, start about 2 m above tuff bed Vb. A lenticular, grey, partly micritic bed which is located 3.5 m above tuff bed Vb possesses a thickness of 3 - 50 cm and shows cone-in-cone structures at the base and the upper limit. Tuff bed VI passes into a 2 - 60 cm grey, micritic bed and also shows cone-in-cone structures at the base and the top.

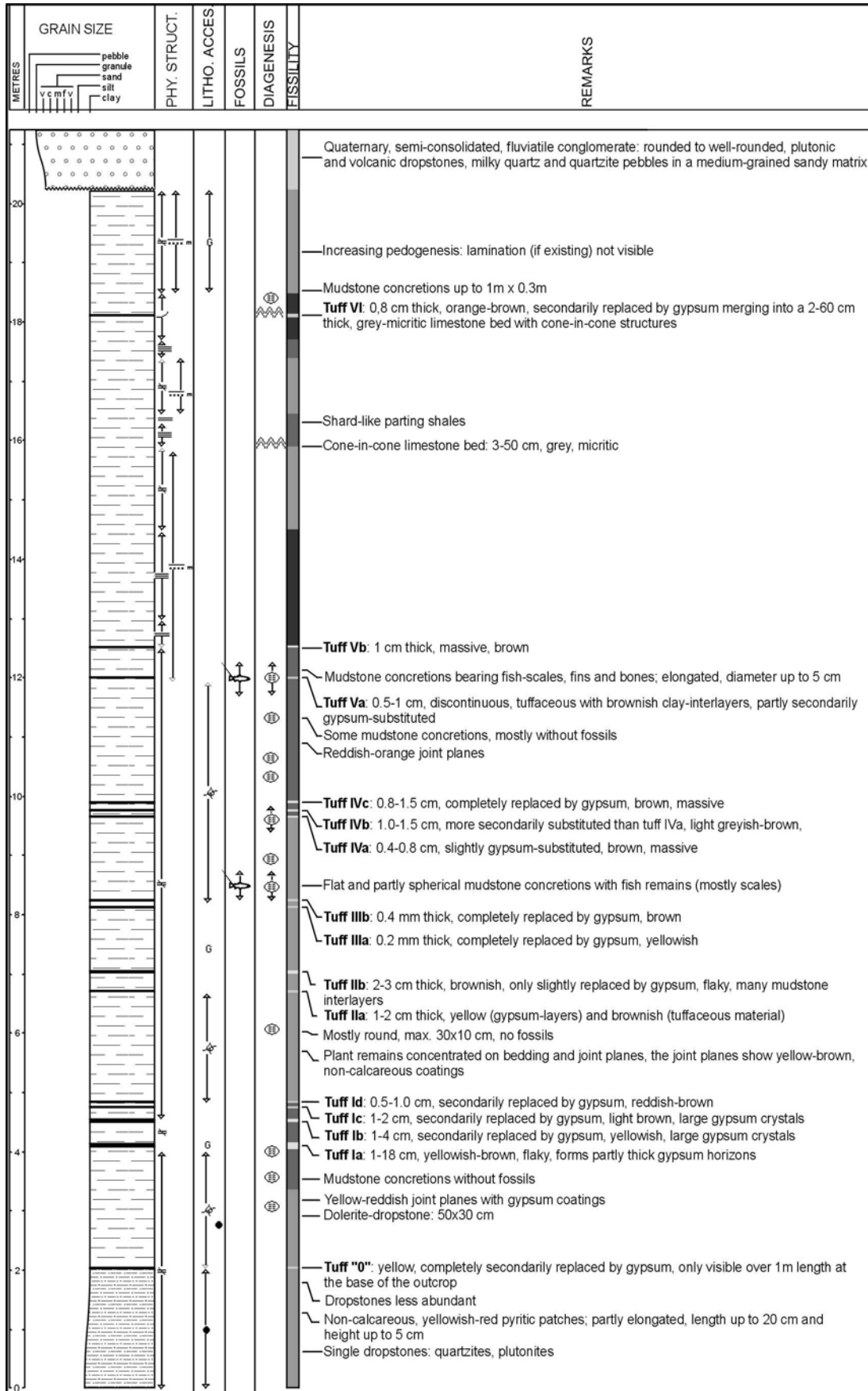


Fig. 19: Measured section of the cut banks east of Farm Waterval (locality #23) displaying lithology, fossil contents and tuff beds of the lower part of the Ganigobis Shale Member. For symbols see Fig. 17.

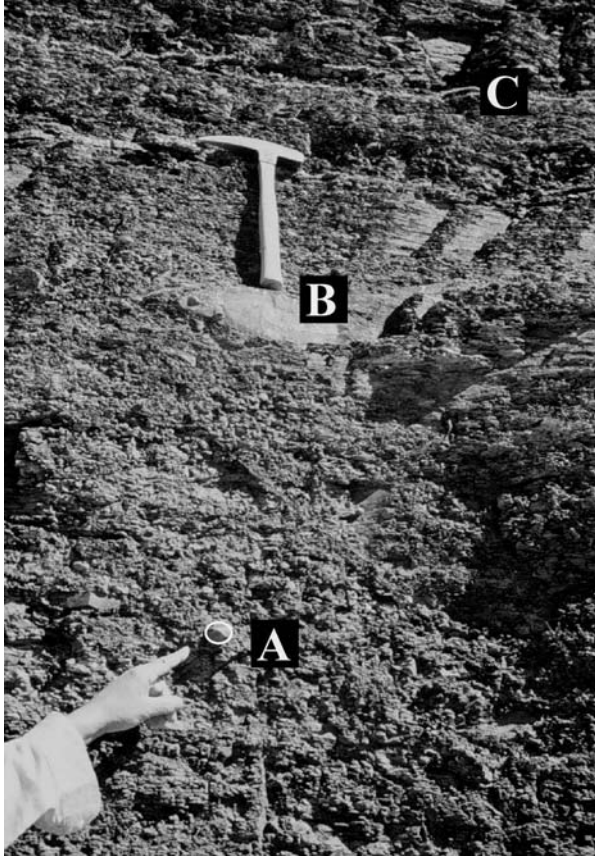


Fig. 20: Detail of outcrop #23 showing uppermost, cm-large, quartzitic dropstone (A: encircled) 0.9 m below tuff bed Ia (C) as well as massive mudstone concretion (B, below the hammer).

Roadcut of the D98: Locality #45

Further to the south-west, the base of the Ganigobis Shale Member crops out in a roadcut (D98 Tses- Berseba) 20 km west of Tses (# 45: 25°53'22" S, 17°56'48" E). The outcrop is situated directly east of the bridge which crosses the Fish River in a gully north of the gravel road. Tuff bed groups I to IV are exposed within the outcrop and are several times offset by normal faults dipping to the east with displacements of about 5 - 20 cm.

The exposed section starts off with 5 - 6 m thick, fine-grained diamictites with clasts of a maximum size of 60 x 45 x 40 cm. Dropstone-bearing mudstones begin about 0.9 m below tuff beds I. Close to the base of the Ganigobis Shale Member mostly plutonic and quartzitic dropstones (EACS: 5 cm) are found about 1.6 m below tuff beds I concentrated in a 20 - 50 cm thick bed. A subangular to subrounded block of

grey quartzite with a size of 70 x 50 x 40 cm is exposed 1.4 m below tuff beds I. As an exception a grey, subrounded quartzitic dropstone with a size of 12 x 10 x 7 cm was found 0.7 m above tuff beds I. Flat and elongated mudstone concretions are exposed 1.2 m below tuff beds I with a maximum size of 100 x 50 x 20 cm well comparable with the lower of the amalgamated, concretionary mudstone beds of locality #2. 0.8 m below tuff beds I a second concretionary mudstone bed with a maximum thickness of 15 cm was recognised which appears to correlate with the second, concretionary mudstone bed of locality #2. Next to the gully permineralised wood with a size of 50x5 cm was found between tuff beds IV and V. Previous to the fieldwork of this study, Roy Miller detected a large mudstone concretion containing a fully preserved palaeoniscoid fish which is stored in the collection of the museum of the Geological Survey of Namibia in Windhoek.

Cut banks of the Asab River: Locality #31

The fourth outcrop of the base of the Ganigobis Shale Member is located about 15 km NNW of Ganigobis (#31: 25°41'48" S, 17°58'18" E). The three cut banks are located at a westerly tributary of the Asab River. They stretch over a length of 200 m and reach a height of 6 - 7 m.

The outcrop is especially important for the correlation of the tuff beds from Ganigobis to Aretitis in the north as the base of the Ganigobis Shale Member is found at the bottom of the middle cut bank. The base is characterised by blue dropstone-bearing mudstones and by large merged mudstone concretions comparable to ones at locality #2. The angular quartzitic and plutonic dropstones possess a maximum size of 10 cm with an EACS in the mm-range. Permineralised wood which forms the nucleus of mudstone concretions, fish scales of palaeoniscoid fishes and spiral coprolites preserved in siliceous-phosphatic mudstone concretions are also characteristic for the outcrop but could not be fitted to the overall tephrostratigraphy as they were mostly not found in situ. The outcrop comprises tuff bed groups I - V.

Cut banks near Farm Aretitis: Localities #32 and 30

The cut banks (localities #32 and 30) are the northernmost outcrops within the study area. The eroded riverbanks are located at a tributary of the Asab River which runs in N-S direction parallel to the Asab River. Locality #32 (25°40'33" S, 17°58'24" E) encompasses tuff bed groups I – V. However, the base of the Ganigobis Shale Member with the transition from dropstone-bearing mudstones to mainly dropstone-free mudstones is not exposed. Locality #30 (25°39'42" S, 17°58'21" E) shows tuff bed groups III and IV. Intervals between the tuff beds at both outcrops vary and are generally larger than at localities #2 and 23.

Locality 32: Similar to locality #23, yellow-red plant debris was recognised below tuff bed IIa. Reef-like build-ups of microbial limestone with a size less than 1 m are exposed above tuff bed I. Round, elongate, siliceous mudstone concretions with a maximum diameter of 5 cm and with one or two spherical holes in the centre (diameter about 1 cm) represent permineralised trace fossils (*Tisoo* isp.; Frey and Cowles, 1969) and are also found above tuff bed I (Fig. 21).

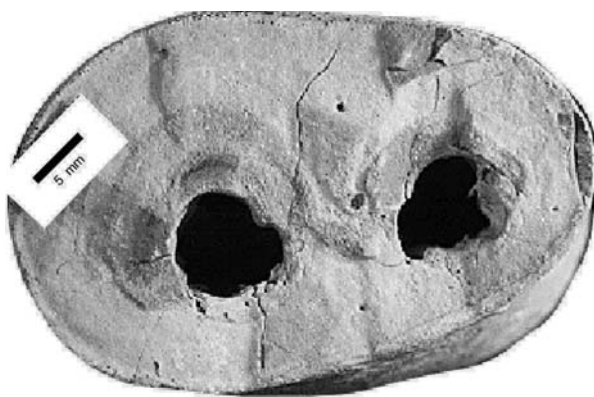


Fig. 21: Permineralised trace fossil *Tisoo* isp. with two holes probably generated by a burrowing arthropod.

This type of trace fossil is a burrow probably generated by an arthropod (Frey and Cowles, 1969). The mudstones between tuff beds IIa and IIIa are massive with cm-large mudstone intraclasts which also occur above tuff IVa. Spiral coprolites in siliceous concretions are found e.g. below tuff bed IVa (Fig. 23).



Fig. 22: General view of outcrop #32 displaying the lower part of the Ganigobis Shale Member between tuff beds I and V. This photograph shows the typical type of outcrop (eroded river banks) within the study area.

Locality #30: Elongated mudstone concretions devoid of fossils are found above and below tuff bed IIIb and up to tuff bed IVa. Merged mudstone concretions with a thickness of about 5 cm occur 0.4 m above tuff bed IVc. About 2 m above tuff bed IVc gypsum crystals appear within the mostly black and massive mudstones. The top of the outcrop is capped by a fine-grained, calcareous sandstone bed with cone-in-cone structures at the top (Fig. 24). It is important for the correlation of the tuff beds that the mudstone intervals between the tuff beds IV (42 cm between IVa and IVb and 74 cm between IVb and IVc) is three times the intervals between the tuff beds IV at locality #2 (16 cm between IVa and IVb and 24 cm between IVb and IVc; cf. Chapter 2.1).

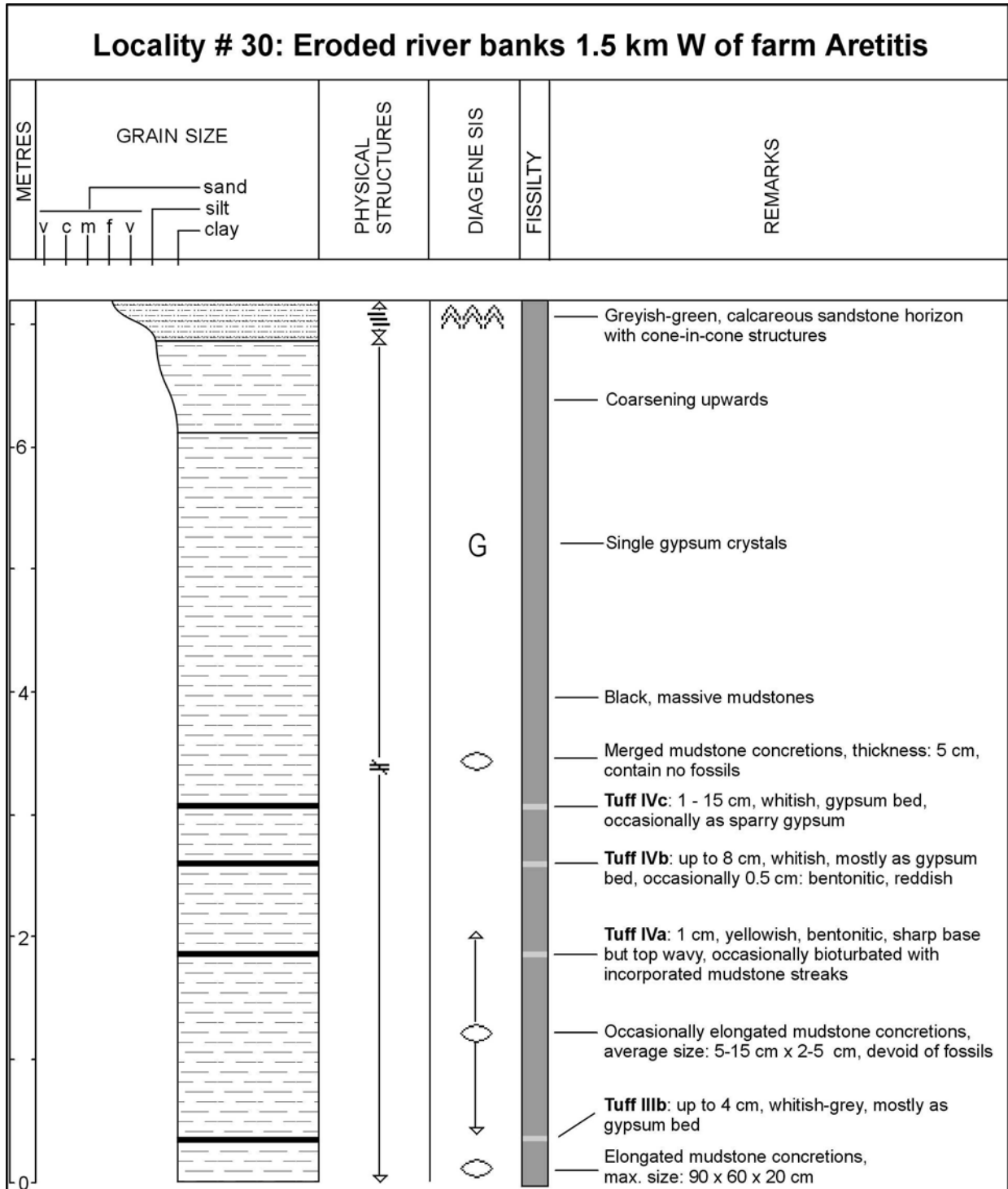


Fig. 23: Measured section of outcrop #30 displaying lithology, diagenetic structures and tuff beds of the lower part of the Ganigobis Shale Member. For symbols see Fig. 17.

2.4 The middle part of the Ganigobis Shale Member

The middle part of the Ganigobis Shale Member consists of more monotonous black mudstones

with less fossiliferous concretions and only one tuff bed preserved compared to the lower and upper part of the Ganigobis Shale Member. The middle part is characterised by normally graded, calcareous sandstone interbeds which are interpreted as distal turbidite deposits (Fig. 24).



Fig. 24: Normally graded, calcareous sandstone interbeds displaying cone-in-cone structures mostly at top and bottom are interpreted as distal turbidite deposits. Note the lateral interfingering between sandstone and mudstone.

Outcrops are located at the river banks of the Asab and Huam Rivers in the vicinity of the homesteads Haams and Nauchas. Outcrops at localities #15, 16 and 19 represent the lower segment of the middle part of the Ganigobis Shale Member.

Cut banks near Haams: Localities #15 and 16

Outcrop #15 is a eroded cut bank of the Huam River (25°47'11" S, 18°00'37" E) which is an easterly tributary of the Asab River. It is located 20 m west of the track towards the northerly located Haams. Outcrop #16 is an eroded cut bank of the Asab River (25°46'56" S, 18°00'21" E) which is located about 150 m west of Haams. The eroded cut bank of the Asab River is continued to the north with outcrops about 1.5 km north of Haams (locality #19: 25°45'47" S, 18°00'23" E).

The outcrop at locality #16 displays the strata from 1.6 m below tuff bed VIb up to 1.4 m below tuff bed VII. In outcrop #15 sediments of the Ganigobis Shale Member are exposed from 2.8 m below tuff bed VII up to 0.8 m above tuff bed VII (Fig. 26).

Outcrop #16 starts off with a 30 - 50 cm thick concretionary-like, calcareous, fine-grained sandstone bed displaying cone-in-cone structures. Black massive mudstones follow up-section to another 30 cm thick, calcareous, fine-grained

sandstone bed which displays cone-in-cone structures. It is overlain by the mostly gypsum-substituted, up to 3 mm thick tuff bed VIb. Small and oval, siliceous mudstone concretions with an average size of less than 12 cm occur below and above tuff bed VIb which internally show rings of intimately disseminated pyrite. They occasionally contain remains of palaeoniscoid fish such as scales and jaws which show rows of 1 mm-sized teeth. They will be described in more detail in Chapter 3.1.

Single, yellow weathered pyritic mudstone concretions with a maximum size of 30 x 8 cm and some up to 50 cm large calcareous sandstone concretions with cone-in-cone structures at the bottom and upper limit occur at the top of the outcrop (Fig. 26).

Outcrop #16 ends and outcrop #15 starts off with two horizons of thin elongated pyritic concretions interbedded in black, massive mudstones. After a break of 0.7 m eight lines of mostly horizontally oriented oval pyritic concretions with sizes between 3 - 8 cm are exposed. They are followed by the up to 5 mm thick, flaky, bentonitic tuff bed VII and further two rows of mostly horizontally oriented oval pyritic concretions with sizes between 2 - 6 cm. The outcrop is capped by a 5 - 40 cm thick, concretionary, calcareous sandstone bed displaying cone-in-cone structures (Fig. 26 and Fig. 25).

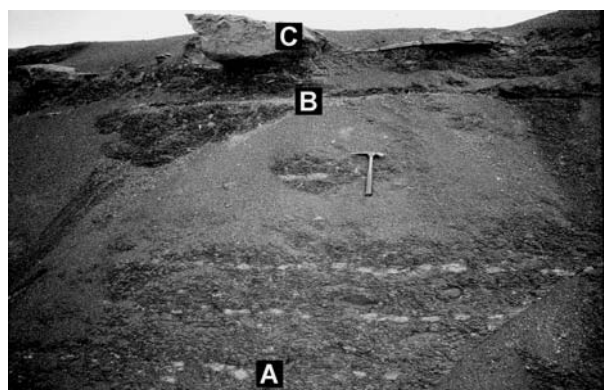


Fig. 25: Photograph of outcrop #15 showing pyritic concretions (A) aligned horizontally, tuff bed VII (B) and calcareous sandstone beds with cone-in-cone structures (C).

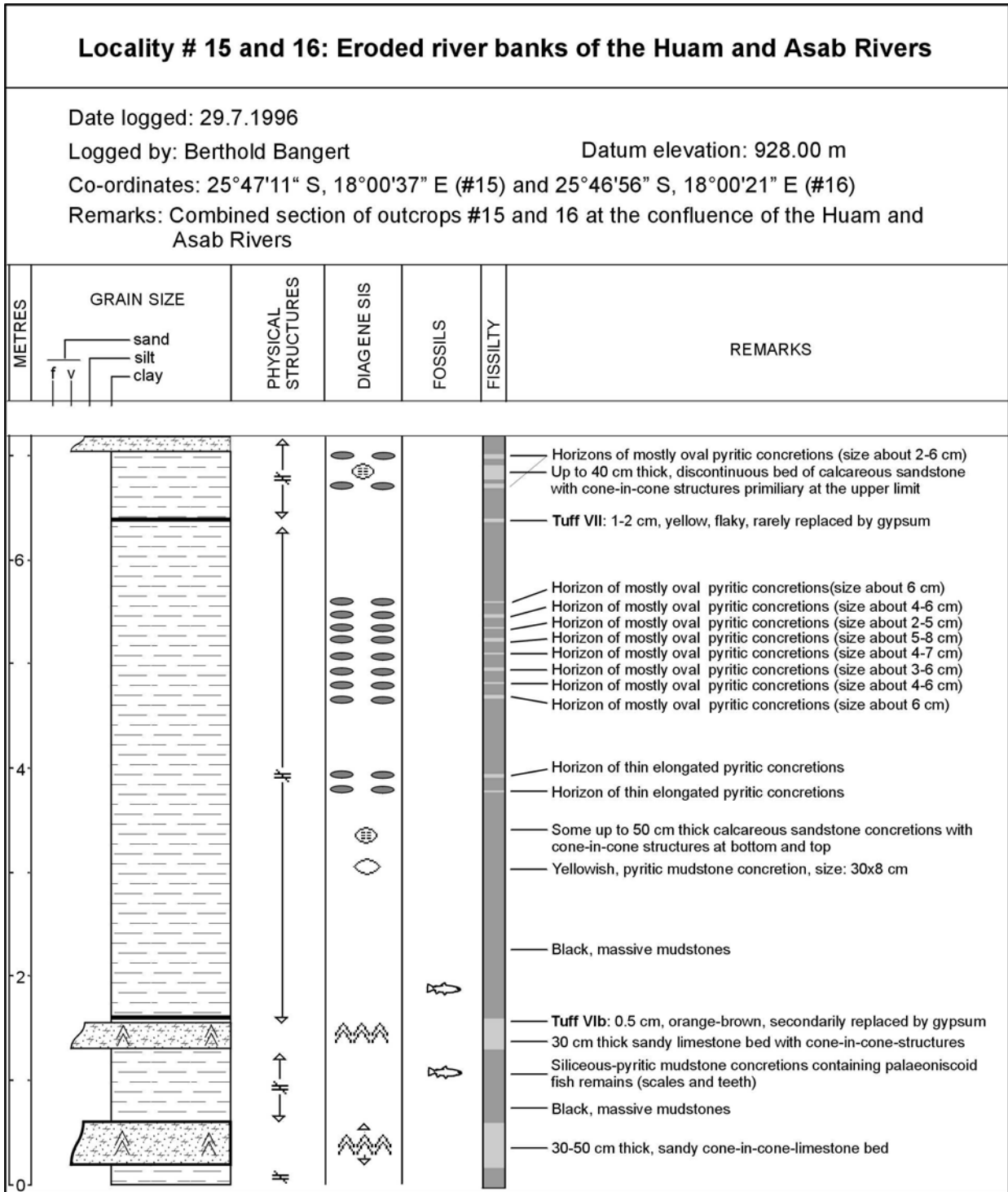


Fig. 26: Combined section of outcrops #15 and 16 displaying lithology, diagenetic structures, fossil contents and tuff beds of the middle part of the Ganigobis Shale Member. For symbols see Fig. 17.

Outcrop #19 starts off just above tuff bed VIb and ends below tuff bed VII including 10 beds of pyritic concretions. No additional features were recognised.

The outcrops at localities #20, 35, 13 and 44 comprise the mudstone interval between tuff beds VII and VIIIa and represent the upper segment of the middle part of the Ganigobis Shale Member.

Cut banks of the Brukkaros River: Locality 20

The eroded river bank of locality #20 is situated at the Brukkaros River (25°44'15" S, 18°00'10" E) east of the confluence with the Asab River and west of the track between Tses and Aretitis. It displays a flaky, bentonitic tuff bed VII in the lowermost part which has a thickness of 4 mm in this particular outcrop and is rarely substituted by secondary sulphates. Pyritic concretions occur below the tuff bed which have a maximum size of 6 x 2.5 cm and are, like in locality #15, aligned in horizons. Two beds of concretionary, calcareous sandstones with cone-in-cone structures appear about 0.7 m and 2.0 m above the tuff bed enclosed in black, massive mudstones. Trace fossils such as *Taenidium* isp. displaying a length of 10 cm and a width of 0.5 cm were found on a fine-grained, turbiditic sandstone bed showing beautifully preserved menisci. The most striking features in this outcrop are up to 0.2 m high, reef-like build-ups of grey, microbial limestone which rest on 5 cm thick microbial limestone mats, located below tuff bed VII. The limestone is more resistant to erosion and forms mounds with a height of up to 0.6 m within the Brukkaros River. As an exception within the Ganigobis Shale Member an up to 11.60 m long permineralised tree log was discovered within the outcrop a little further downstream. The measured diameter of the root was 26 cm and the top measured 8-10 cm. Beautifully knotholes with a maximum diameter of 5 cm are preserved (Fig. 27).

Tuff bed VII, concretionary, calcareous sandstone beds and small pyritic concretions interbedded in black, massive mudstones are also found in outcrop #35 about 1.5 km west of #20 at the Asab River.



Fig. 27: 11.60 m long permineralised tree log in outcrop #20 detected above tuff bed VII. The diameter of the root is 26 cm decreasing to 8-10 cm at the end of the tree.

Cut banks of the Haams River: Locality 13

Outcrop #13 (25°48'17" S, 18°01'43" E) is found at the Huam River about 2.5 km upstream of locality #15. The mudstones are massive, show up to 5 mm large mudstone intraclasts and are speckled with orange-red pyritic concretions reaching a maximum size of 14 x 5 cm. The centre of these concretions is occasionally made up of cm-large funnel-shaped coprolites which have apparently been the nucleus of these concretions. There are two zones exposed in the outcrop where the concretions form up to 20 cm thick beds. The beds display colours from light grey to orange and dark-red. Brown, calcareous, fine-grained sandstone beds with cone-in-cone structures are found all over the outcrop which reach a maximum height of 1 m. They internally show discontinuous bedding and deform the underlying mudstones. These sandstone beds occasionally continue in cm-thick calcareous sandstone beds.

Cut banks of the Brukkaros River: Locality 44

The eroded riverbank of outcrop #44 (25°42'32" S, 18°00'45" E) is situated at the Brukkaros River about 0.5 km west of Nauchas and 4 km upstream from outcrop #20. As in outcrop #13 no tuff beds were discovered. A yellow, mm-thick bed of calcareous sandstone passes into a up to 22 cm thick, concretionary limestone bed with cone-in-cone structures and stylolithes. Orange pyritic concretions reaching a maximum size of 10 x 5 cm are again abundant within the black, massive mudstones.

As in locality #13 the concretions occasionally show cm-large funnel-shaped coprolites in their centres.

2.5 The upper part of the Ganigobis Shale Member

The upper part of the Ganigobis Shale Member is characterised by black mudstones with abundant fossils and group VIII tuff beds. Outcrops are located at the riverbanks of the Ganigobes River (#40 and 43) north-east of Ganigobis and at the river banks of the Brukkaros River (#9 and 27) next to the main road to Windhoek (B1). To the top the dropstone-free mudstones of the Ganigobis Shale Member pass up-section into mudstones with quartzitic and plutonic dropstones.

Cut banks of the Ganigobes River: Locality 40

Outcrop #40 (25°48'56" S, 18°02'36" E) is a eroded river bank of the Ganigobes River which passes to the east into outcrop #43 (25°48'55" S, 18°02'45" E). Round, siliceous, partly amalgamating concretions which are devoid of fossils are conspicuous in outcrop #40. They reach a maximum length of 70 cm. The most striking features in this outcrop are up to 0.3 m high bioherms of grey, microbial limestone. They rest on a non-continuous, 2 mm thick tuff bed. As the outcrop is continuously passing into outcrop #43, the tuff bed is denominated as tuff bed VIIIA.

Cut banks of the Ganigobes River: Locality 43

Outcrop #43 displays four poorly preserved tuff beds and columnar, microbial limestone bioherms reaching a height of up to 2.5 m and a maximum width of 1.5 m embedded in black massive mudstones and in grey calcareous nodular siltstones. The bioherms were already described to detail by Grill (1997). Apart from normal mudstones, Grill identified four different facies types which mainly compose the bioherms within the outcrop. An "algal mat facies" is characterised by relatively thin boundstone beds which reach thicknesses of about 5 - 20 cm and are mostly found about 1 m above tuff bed VIIIA. These algal mats were also identified in localities #20, 32 and 40. Apart from a micritic limestone

portion they are mostly made up of mm-thick layers of blue-green algae (Cyanophycean algae) interbedded with thin mudstone layers (Grill, 1997). The "algal-serpulid build-up facies" forms the major vertical structures which are mainly comprised of boundstones made up of Dasycladacean algae as well as less frequent serpulids, ostracod shells and sponge spicules (Grill, 1997). Up to 40 cm long tubes with a diameter of about 1 cm which consist of micritic limestone are conspicuous on these build-ups and probably represent burrowing structures (Fig. 28).

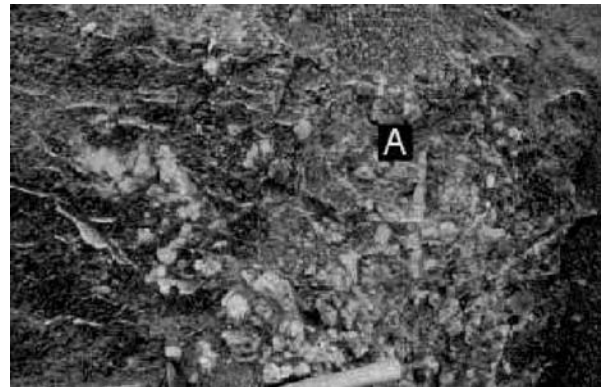


Fig. 28: Surface of the bioherms displaying micritic limestone tubes, up to 40 cm long and with a diameter of about 1 cm (A) and brown-grey massive micrite nodules.

Nodules of brown-grey massive micrite with a maximum size of 5 x 3 cm are the main constituents of Grill's third facies type which form parts of these vertical build-ups. In between these bioherms grey calcareous nodular siltstones predominate containing white weathered, up to 30 x 6 cm large limestone nodules (Grill, 1997).

Within the outcrop four poorly preserved tuff beds are exposed which are denoted as tuff beds VIIIA to VIIId. They mostly possess a thickness within the mm-range whereas tuff bed VIIIC reaches a thickness of up to 1 cm. The thickness of all tuff beds is enlarged by secondary sulphates. The "algal mat facies" tends to be based on tuff bed VIIIA whereas the vertical growth of the build-ups seems to start in a later phase from these microbial limestone mats. Contrary to Grill's opinion, the tuff beds do not affect the bioherm growth as they are incorporated in the vertical build-ups (Fig. 30).

The growth of the bioherms is only interrupted and is continued after the deposition of the volcanic ash. Tuff bed VIIIc (Grill's tuff B-IIb) is continuous within the outcrop whereas tuff bed VIII d is only preserved in the vicinity of the central and highest build-ups (Fig. 31).

Cut banks of the Brukkaros River: Locality 27

Outcrop #27 (25°41'24" S, 18°01'54" E) is situated at the Brukkaros River about 1.3 km south-west of the B1 to Windhoek. Black massive mudstones with interbedded sandy and calcareous, concretionary beds are intruded by five parallel aligned carbonatite dykes. Tuff bed VIIIa is exposed at the top of the eroded riverbanks and is almost completely replaced by secondary sulphates. Below the tuff bed up to 3 m long and 60 cm high concretionary, calcareous sandstone beds are frequently exposed which rapidly pinch out to the sides.

Many of them show cone-in-cone structures at the base and top, others which apparently contain less calcium carbonate resemble more like ordinary channel-fill sandstones. They reveal four types of trace fossils: (1) small, up to 1-2 cm long and up to 3 mm wide structures, (2) U- and S-shaped, meandering trails with a width of 1 mm and a length of 5 mm, (3) U-shaped, about 8 mm

wide, meandering, cylindrical traces showing menisci-like fillings and (4) up to 15 cm long, mudstone-filled tubes with a diameter of up to 2 cm are preserved within the sandstones. Type one is interpreted as *Planolites isp.* whereas type two may depict *Planolites montanus*. Types three and four were probably produced by burrowing organisms (Fig. 29).

The high degree of bioturbation may indicate a marine rather than non-marine palaeo-environment.

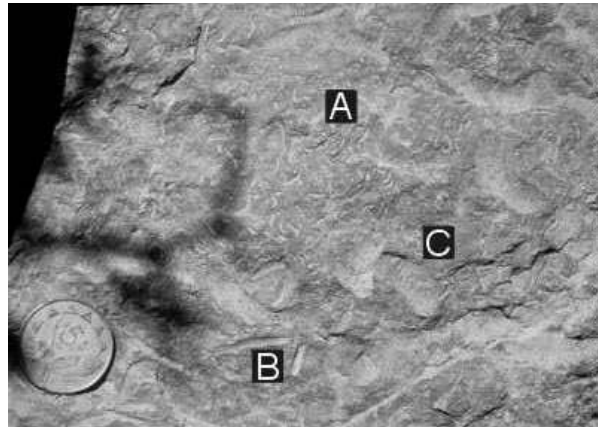


Fig. 29: Trace fossils on channel-fill sandstones: (A) *Planolites montanus*; (B) *Planolites isp.* and (C) Indeterminable traces showing menisci-like fillings, for further descriptions see text below.

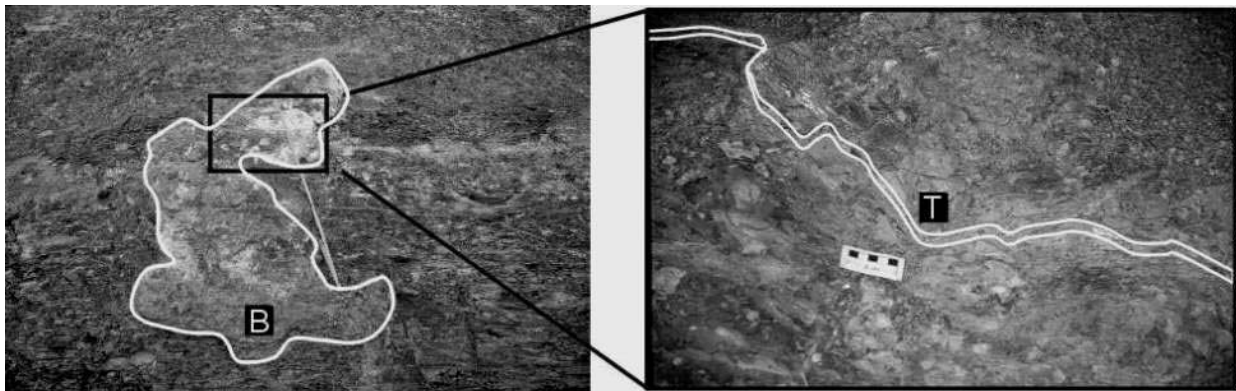


Fig. 30: Left: Bioherm (B) mainly made up of brown-grey massive micrite nodules, scale is 1 m; Right: tuff bed VIIIc (T) is incorporated within the bioherm and does not affect the bioherm growth (locality #43).

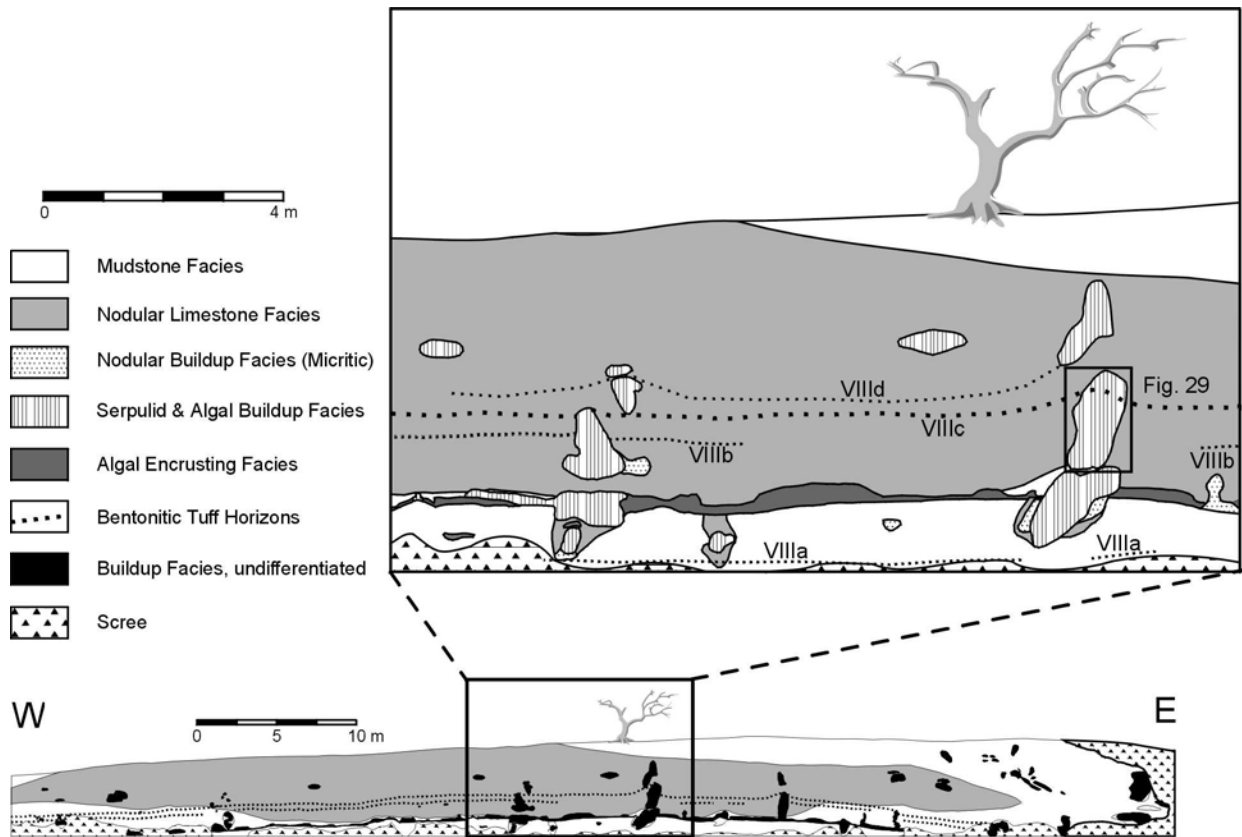


Fig. 31: Sketch of outcrop #43 showing the complete outcrop in the lower part and the centre of the outcrop detailed in the upper part (from Grill, 1997). Note that the position, lateral extent and denominations of the tuff beds were completely revised.

Anvil-like structures which are made up of brownish ferrous, coarse sparite form the nuclei of smaller mudstone concretions. These up to 15 cm long structures are quadratic (side lengths up to 2 cm) in the middle part and end to both sides peaked (Fig. 32).



Fig. 32: Anvil-like coprolite found in outcrops of the middle and upper parts of the Ganigobis Shale Member. Left tip is broken off; found in locality #15.

They are mostly found without the surrounding mudstone matrix of the concretions sticking sub-vertical to vertical in the mudstone exposures.

These structures of a larger, unknown animal which may represent permineralized coprolites are also found in localities #13 and 15 in the middle part of the Ganigobis Shale Member. Like in several outcrops of the lower part of the Ganigobis Shale Member spiral coprolites with diameters of up to 1 cm were occasionally found in the siliceous mudstone concretions. Single examples of the scyphozoan *Conularia sp.* (Schroeder, 1908) will be described in more detail in Chapter 3.6. Up to 80 x 12 cm large microbial boundstone biostroms are found in the rivercuts below tuff horizon VIIIa.

Important for the correlation with localities #40 and 43 are about ten shallow mounds to the east of the river banks (25°41'39" S, 18°01'88" E). They probably represent the top surfaces of bioherms as exposed in outcrop #43 where the third dimension of the bioherms is not exposed.

The mounds possess a maximum diameter of 4-5 m and a maximum height of 1.5 m and are covered by round to elongate nodules of

brownish-grey massive micrite with a maximum size of 6 x 2 cm, thin calcareous tubes with central conduits and dendritic, micritic nodules. Permineralised fossil wood mostly found in situ and crinoid columns were further detected on the mounds or next to the mounds. One especially well preserved sample of fossilised wood displays 1 - 7 mm thick annual growth rings. The genus seems to be very similar to *Megaporoxylon scherzi* Kräusel (Bangert and Bamford, in press) and will be described in more detail in Chapter 3.3. Two disrupted boundstone samples containing crinoids stalks were found next to the mounds by Markus Geiger (Institut für Geologie, Würzburg). The samples are angular to subrounded clasts of grey micrite embedded in a brownish, sparitic matrix. The stalks are 0.2 - 1.0 cm long with a diameter ranging from 0.1 to 0.5 cm, single ossicles are less than 0.1 - 0.2 cm long. Sponge spicules (up to 1 cm in length and 0.1 cm in width) are also preserved on the surface of one of the samples. The crinoid columns oriented in all directions and thus not preserved in their original position indicating reworking of the crinoid stalks. Numerous gastropod shells of a single species (*Peruvispira vipersdorfensis*, (Dickins, 1961) are found concentrated in irregular, partly branching mudstone concretions between the mudstone banks of the Brukkaros River and the mounds. The up to 1 cm high shells will be described in more detail in Chapter 3.4.

Five parallel running, vertical, 35 - 80 cm thick carbonatite dykes striking about 64° penetrate the black mudstones in a distance of 60 - 250 cm. They are eroded by the Brukkaros River and form vertical walls as they are more resistant against erosion than the mudstones. Some of these yellowish weathered, otherwise greyish carbonatite dykes are vesicular in the centre or in discrete zones parallel to the rim. 2 - 3 mm large quartz grains and probably corroded olivine were detected with the hand lens whereas mica or xenoliths were not recognized. The carbonatite dykes can be followed in the field for about 1 km and are exposed 500 m and 800 m to the ENE in two small outcrops. Two almost vertical carbonatite dykes were further registered in locality #28.

Cut banks of the Brukkaros River: Locality 9

Outcrop #9 (25°40'16" S, 18°02'36" E, Fig. 34) is situated at the Brukkaros River about 0.3 km east of the B1. It is characterised by massive black mudstones with two interbedded bentonitic tuff beds. A 2 cm thick bentonitic tuff bed which reaches a maximum thickness of up to 8 cm due to the secondary replacement of the tuff bed by calcite, is correlated with tuff bed VIIIa. The calcite in tuff bed VIIIa may have originated from an up to 15 cm thick, brown-grey microbial limestone bed which rests directly upon the tuff bed. The occurrence of this limestone bed are comparable with outcrop #40.

Another 0.2 - 0.5 cm, red and sulphate-substituted tuff bed occurs about 1.55 m above the lower tuff bed VIIIa and is correlated with tuff bed VIIIb in outcrop #40. Flattened, permineralised wood with a size of >40 x 4.5 x 2 cm was found in situ 2 m below tuff bed VIIIa. In the same tephrostratigraphic position a single gastropod shell of the genus *Omphalonema* was discovered which will be described to detail in chapter 3.4.



Fig. 33: This small bioherm with a size of 95x75 cm is exposed in outcrop #9 just above tuff bed VIIIa, for further descriptions see text below.

A bioherm with the size of 95x75 cm is exposed just below the bridge of the railway line Keetmanshoop - Windhoek which appears to be similar to the ones exposed in outcrop #43 (Fig. 33). The bioherm obviously started its growth on tuff bed VIIIa. It is characterised by elongate to cauliflower-shaped nodules of brown-grey massive micrite with a maximum size of 4 x 1.5 cm. These nodules are especially found in the upper parts of the bioherm. Larger calcareous, knoblike mudstone concretions occur on top of the build-up which contain finely dispersed sulphides (e.g. pyrite) in their interior. They correlate with other conspicuous, oval shaped, up to 80 x 22 cm large mudstone concretions which form a discontinuous bed about 60 - 70 cm above tuff bed VIIIa. These concretions were generally non-fossiliferous with two important exceptions. Thin bivalve shells, probably of the genus *Myonia*, were discovered in a large mudstone concretion 55 cm above tuff bed VIIIa. They will be described to detail in chapter 3.5.

Another of these large mudstone concretion contained permineralised wood with a size of 35 x 15 x 8 cm striking 171°. The wood was surrounded by a thin layer (3 - 4 mm) of pyritic mudstone. Towards the uppermost top of the outcrops the overall black mudstones pass into green siltstones with single quartzitic and plutonic dropstones (Fig. 34).

All mentioned features of the Ganigobis Shale Member are summarised in Tab. 19 in Appendix A-2.

2.6 The Ganigobis Shale Member in the southern part of the Aranos Basin

South of the type area described above, the Ganigobis Shale Member is only sporadically exposed. To the south the thickness decreases and the facies changes from black, dropstone-free to dropstone-bearing shales. Two major outcrop areas are described in the following: *i*, eroded river banks in the vicinity of Farm Tsaraxa and *ii*, a large escarpment exposed south of Farm Snyfontein.

2.6.1.1 Farm Tsaraxa: Locality 25

Up to 3 m high river banks of the Wasser River form the southernmost outcrops of the Ganigobis Shale Member in its type facies (cf. Chapter 2.3) south of Farm Tsaraxa which is situated 22 km south-west of Tses (Fig. 8; 26°04'16" S, 17°57'29" E). Black silty mudstones which generally lack dropstones contain the typical flat, up to 15 x 5 cm large siliceous mudstone concretions which are devoid of fossils.

Two, sometimes three, thin (< 3 mm) bentonitic tuff beds were found within the outcrops. They were

denominated as tuff beds IVa-c by Grill (1997) which is, however, doubted by the author.

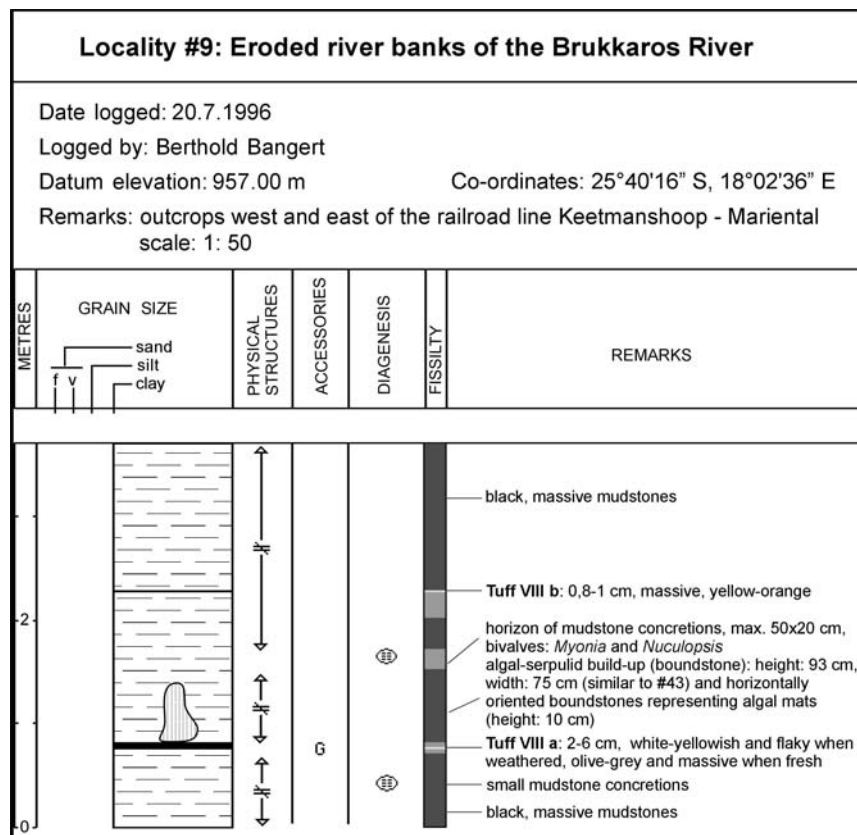


Fig. 34: Measured section of outcrop #9 displaying lithology, diagenetic structures and tuff beds of the upper part of the Ganigobis Shale Member. For symbols see Fig. 17

Undeformed volcanic dropstones (cf. Chapter 10.9) and pieces of permineralised wood were found on flat hills north of the Wasser River (26°03'00" S, 17°57'15" E).

2.6.1.2 South of Farm Snyfontein: Locality 24

A large escarpment is exposed about 14 km south-west of Farm Snyfontein or 33 km WNW of Keetmanshoop (26°33'49" S, 17°47'03" E). It displays strata of the upper parts of the Nama Group, a complete section of the Dwyka Group (DS I-IV) and sediments of the Nossob Member (Prince Albert Formation) which form the topmost part of the outcrops.

Sediments of the Dwyka Group start with 3 - 4 m thick basal lodgement tillites and change rapidly into shales containing varying amounts of dropstones. These shales, up to 250 m thick, are occasionally intercalated by brown, fine- to middle-grained, calcareous sandstones which show the typical cone-in-cone structures. About 70 m above the base of the Dwyka Group four mm-thin, slided tuff beds and a mudstone concretion containing remains of the palaeoniscoid fish *Namaichthys schroederi* (Chapter 3.1) were discovered. This part of the outcrop was logged in greater detail (Fig. 35) as it is determined to be located in the uppermost part of DS II and correlates with the Ganigobis Shale Member further north. The tuff beds are up to 0.5 m thick, mostly replaced by gypsum but also occasionally flaky and bentonitic. They cannot be traced all over the escarpment as they only crop out in the most vertical sections. The fish remains bearing concretion was found between tuff beds I and II.

Gamma-ray values in this part of the outcrop were measured in intervals of 0.5 m. 25 measurements thus cover 12.0 m sediment thickness. Values of uranium vary between 175 and 281 ppm and average 225 ppm which is generally lower than in outcrop # 2 north of Ganigobis where U averages 270 ppm (cf. chapter 4.3.2). Thorium values are also lower and lie between 128 and 202 ppm averaging 171 ppm (cf. outcrop #2: 212 ppm Th on average). In contrary Th/K-ratios range between 4.91 (4.46 in

outcrop #2) and 7.16 (8.62 in outcrop #2). The average of the Th/K-ratio is 6.16 in both outcrops which suggests a potential correlation independent from the detected tuff beds and the fish fossil-bearing concretion. Th/U-ratios are also similar between the compared outcrops #2 and 24 and vary between 3.03 (2.43 in outcrop #2) and 7.16 (9.94 in outcrop #2) and average 4.42 (4.88 in outcrop #2; chapter 4.3.2).

2.7 Thickness, basin topography and tectonic framework of the Ganigobis Shale Member

In the detailed study area the sediment thickness of the Ganigobis Shale Member decreases from the central outcrops at the Fish River north of Ganigobis (locality #2) towards the south and the north. In the following the sediment thickness between tuff beds IIIb and IVc is compared as they are found in all comparable outcrops.

Outcrop #2 displays a sediment thickness of 3.4 m between tuff beds IIIb and IVc. Towards the south, the sediment thickness between the tuff beds and the overall thickness of the Ganigobis Shale Member decreases rapidly. In outcrop #23, 5 km south of locality #2, a sediment thickness between tuff beds IIIb and IVc of only 1.6 m is found. Outcrop #45 at the Fish River bridge, 11.3 km south-west of locality #2, displays only few metres of sediment thickness between tuff beds I and IV which cannot be quoted quantitatively due to the restricted exposure and the normal faults displacing the tuff beds. Further southwards in the vicinity of Farm Tsaraxa (26°04'16" S, 17°57'29" E, 27.5 km south-west of locality #2) the whole Ganigobis Shale Member possesses a thickness of 3-4 m with three poorly preserved tuff beds and dropstone-bearing shales. South of these outcrops dropstones are always embedded within the Dwyka shales, recognisable in large escarpments south of Snyfontein and WNW of Keetmanshoop (26°33'49" S, 17°47'03" E), about 80 km south-west of locality #2.

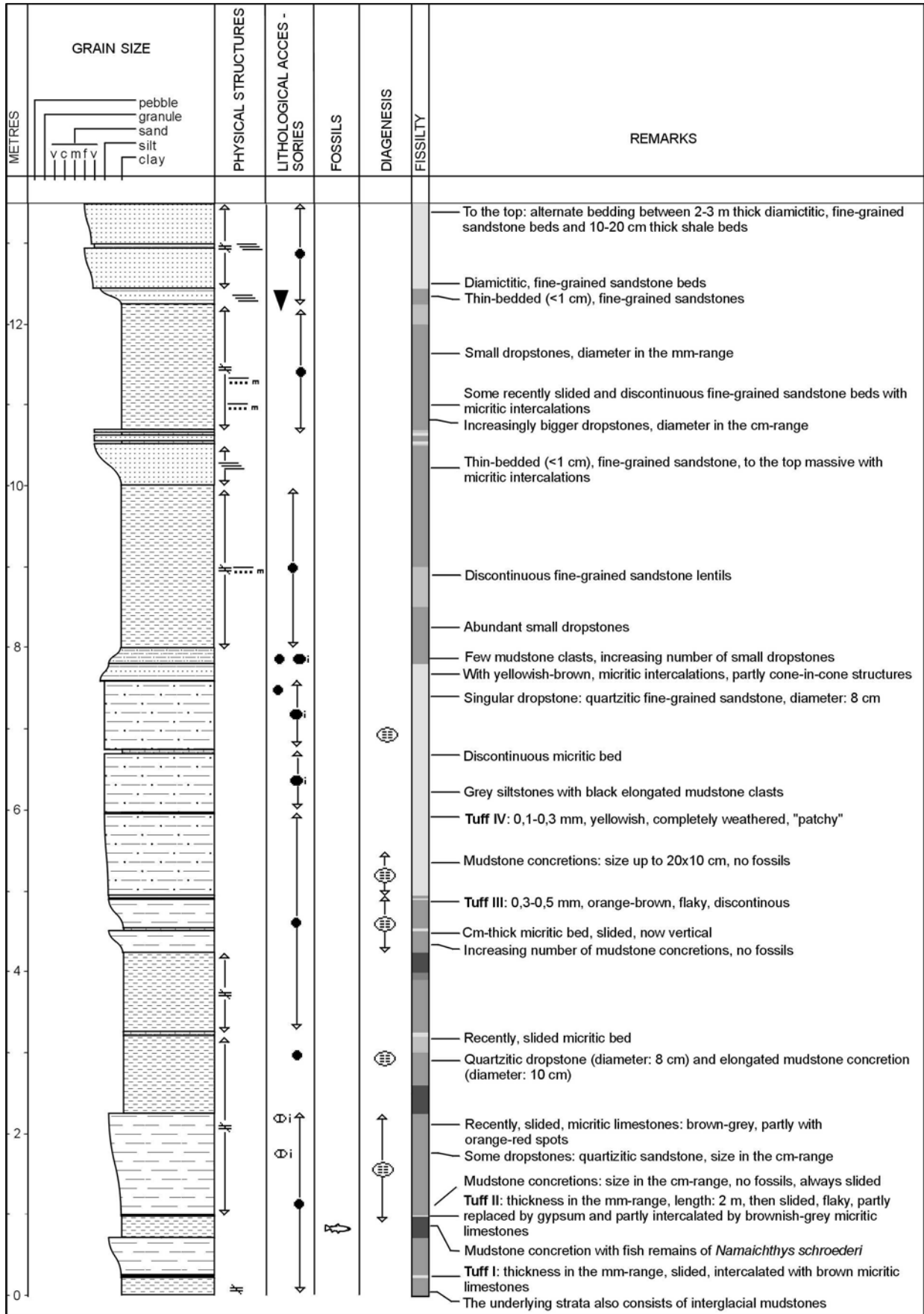


Fig. 35: Measured section of outcrop #24 displaying lithology, fossil contents and tuff beds of Ganigobis Shale Member-equivalent rocks south of Snyfontein. For symbols see Fig. 17

Towards the north of outcrop #2 the thickness between tuff beds IIIb and IVc diminishes to 2.5 m in outcrop #31 which is located 13 km north of locality #2. In localities #32 and 30 located 15.5 and 17.5 km north of outcrop #2 the thickness between these tuff beds remains constant with 2.4 m. The overall thickness of the Ganigobis Shale Member decreases in these outcrops to about 15 m.

Implying that the silty mudstones of the Ganigobis Shale Member dip less than 2° the greatest thickness of the Ganigobis Shale Member in outcrop #2 is also indirectly expressed in the altitude above sea-level (#2: 905 m a.s.l.). The basin floor on which the Ganigobis Shales were deposited was obviously the deepest at locality #2, respectively the water column was the highest within the whole basin giving rise to the deposition of the thickest sediment packages in this area. To the south the shales at locality #23 start off at 915 m a.s.l. whereas the outcrops at localities #31, 32 and 30 begin at 950, 955 and 960 m.

A major, post-Dwyka aged fault zone is exposed in outcrop #28 at the Asab River running NE-SW (135°/85°) which has to be taken into account when discussing the small-scaled basin topography. Although correlated with each other, outcrops #27 and 9 have an altitude between 950 and 960 m a.s.l. whereas localities #40 and 43 are situated 933 m a.s.l. To explain the difference in altitude, the fault zone is expected to continue about 6 km to the north-east passing south of outcrop # 27. If the hanging wall block is located on the southern side of the fault zone leading to the lower geographical height of localities #40 and 43, a maximum displacement of 30 m would be likely. Applying this to outcrops # 31, 32 and 30, which are found north of the faultzone, they should have been located at 920, 925 and 930 m a.s.l. after the subtraction of 30 m.

Tuff beds and concretionary horizons were used by Grill (1997) and Stollhofen (1999) to document synsedimentary faulting within the Ganigobis Shale Member at locality #2. Activity of these faults is for example displayed in synsedimentary thickness differences of the silty mudstones between tuff beds I and III as well as between IVc and V at the Fish and the Khomab

River.

The normal faults strike NE-SW and NW-SE to NNW-SSE. Both fault groups form horst and graben structures with displacements mostly ranging below 1 m. These extensional features are of the same orientation as larger listric faults which are important for the documentation of early pre-South Atlantic rifting (Chapter 1.2, Stollhofen, 1999).

3 Life in an ice-age: The fossils of the Ganigobis Shale Member

The following fossils were found in the Ganigobis Shale Member (GSM) in the vicinity of Ganigobis:

In the lower and middle part of the GSM:

- remains of palaeoniscoid fishes preserved in siliceous, small mudstone concretions
- mostly spiral coprolites preserved in siliceous, small mudstone concretions
- permineralised wood

In the upper part of the GSM:

- gastropods (*Peruvispira vipersdorfensis*, Dickins, 1961 and *Omphalonema*)
- bivalves (*Nuculopsis* sp., McLachlan and Anderson, 1973 and *Myonia*-like bivalves)
- scyphozoa (*Conularia* sp., Schroeder, 1908)
- crinoid stalks
- sponges and sponge spicules
- foraminifers, radiolaria
- permineralised wood
- funnel-shaped and anvil-like coprolites

3.1 Palaeoniscoid fish remains

3.1.1 Previous work

Gürich (1923) summarised as much as five genera from locality #2 north of Ganigobis which were revised by Gardiner (1962). Two genera were described extensively whereas the description of genera III to V is rather obscure:

a, *Namaichthys schroederi* Gürich

The main body of the fish is fusiform and the skull itself could reach a maximum length of up

to 10 cm. The bones of the skull show a coarse ornamentation (Plate 1, Figs. 1 and 4: 1), the operculars show growth lines and are twice as long as wide. The lower and upper jaws show series of 1.0 - 1.5 mm large, curved teeth arranged in intervals of 0.5 - 2.0 mm which are anteriorly directed backwards and posteriorly directed forwards (Plate 1, Figs. 2 and 3: 1). The pectoral fin has at least sixteen lepidotrichia, the principal rays are unarticulated for over a third of their length, but bifurcate distally. The pelvic fin is formed of fifteen lepidotrichia and like the pectoral fin it shows numerous small fulcra. The rays are articulated along the whole of their length. The unpaired, dorsal (25 rays) and anal fins (23 rays) are triangular and possess the same size. The caudal fin is deeply cleft, inequilateral and rather small (Plate 1: Figs. 1 and 4: 3).

The scales are thick, rhomboidal and deeply imbricating. Posteriorly they are denticulate, the first two or three scale rows show tooth-like projections posteriorly (Plate 1: Figs. 1 and 3: 2). If there is a weak ornamentation of the scales, it consists of fine transverse ridges with a thin layer of blue enamel.

b, *Watsonichthys lotzi* Gürich (*Acrolepis lotzi*, Gürich, 1923)

Few fish fossils belong to species *Watsonichthys lotzi* Gürich (Gardiner, 1962) or *Acrolepis lotzi* (Gürich, 1923).

In contrast to *Namaichthys schroederi* Gürich, *Watsonichthys lotzi* Gürich shows strong ornamented scales with 7-10 ridges of enamel. Some of the ridges do not extend the whole length of the scale. The lepidotrichia of the pectoral fins are unarticulated and the size and the shape of the operculars and the rostrum differ considerably from *Namaichthys schroederi* Gürich.

c, Third genus (*Rhadinichthys?*) of Gürich (1923)

Gürich described this genus from a single concretion with a diameter of 5 cm which preserved a lower jaw and scales. The lower jaw shows a simple ornamentation displaying fine

ribs which do not bifurcate. The teeth are slender and up to 0.75 mm long. The scales are weakly sculptured showing concentric ribs and partly a diagonal subdivision into two fields.

d, Fourth genus (*Elonichthys?*) of Gürich (1923)

Gürich described this genus from another single concretion with a diameter of 5 cm which preserved a head and two rows of 6 lepidotrichia with a length of 8 mm and a width of 1.5 mm. The straight ornamentation of the lower jaw of this species differs from *Namaichthys schroederi* Gürich which shows a rather curved ornamentation.

e, Fifth genus of Gürich (1923)

Scales with growth lines parallel to the rims of the rhombic outline of the scales were different to all other described fossil fish remains.

3.1.2 New observations

Most of the fossiliferous mudstone concretions display impressions of scales which are found centred in the middle of the concretions. The fish remains are mostly oriented perpendicular to the c-axis of the concretions, in cases they are preserved oblique or dorso-ventral (Evans, 1998). Except one well preserved example found in outcrop #45 the fishes were never found articulated. Entire skulls are commonly preserved isolated within the mudstone concretions, other concretions only show the caudal areas of the fish which are preserved in an articulated and splayed state, with no anterior trunk (Plate 1, Figs. 5 and 6).

All of the fish remain impressions found in the Ganigobis Shale Member in localities #2, 16, 22, 23 and 45 belong to the palaeoniscoid fishes (order: Palaeoniscoidea; family: Acrolepidae).

25 concretions with fish remains were described which is summarised in Tab. 2. 14 of them probably belong to *Namaichthys schroederi* Gürich whereas the other 7 probably belong to *Watsonichthys lotzi* Gürich. Four remaining concretions with fish remains were not determinable (Tab. 2). Grill (1997) described 6

pieces of concretions with palaeoniscoid fish remains of *Namaichthys schroederi* G. (Tab. 2).

As the fossilised bones of the fishes are mostly disrupted, generic names were mainly assigned on analyses of the mostly coherently preserved scales which are preserved in 14 concretions. In co-operation with Hans-Peter Schultze of the Museum für Naturkunde in Berlin, two major types of fish scales were recognised:

i, rhombic to rectangular scales: not imbricating, slight or no ornamentation, partly blue enamel size: 2-4 x 1-4 mm (9 concretions): *Namaichthys schroederi* Gürich (Plate 1, Fig. 7)

ii, rhombic scales: mostly imbricating, partly rounded, strongly ornamented, about 8 ridges parallel to the long axis of the rhombohedran, no blue enamel, size: 5-7 x 3-5 mm (5 concretions): *Watsonichthys lotzi* Gürich (Plate 1, Fig. 8)

3.1.3 Discussion

Fish remains of *Watsonichthys lotzi* Gürich seem to be concentrated between tuff beds I and II whereas fish remains of *Namaichthys schroederi* Gürich are found between tuff beds I and III and IV and V. Caudal fins of *Namaichthys schroederi* Gürich are especially found between tuff beds IV and V in outcrops #2 and 22. The outer shape of the concretions resemble the curvature of the caudal area of the fishes.

The tephrostratigraphic occurrence of both genera seems to coincide with the trend to develop simpler scales. *Namaichthys* with its mostly plain scales seems to be more modern than *Watsonichthys* with its strongly ornamented scales. Gardiner (1962) therefore concluded that *Elonichthys*, *Watsonichthys* or *Acrolepis* have been common within the Lower Carboniferous whereas *Namaichthys* obviously developed later, in the Upper Carboniferous. The genera *Namaichthys* and *Elonichthys* are closely related due to their similar body shape, structure and ornamentation of the scales, dentition and disposition and should have arisen from the same ancestral stock in different times whereas *Watsonichthys* or *Acrolepis* separated a little earlier in time than the former two genera (Fig. 36).

Gürich (1923) and Gardiner (1962) both discussed the value of fish scale-determinations

in order to distinguish between single fish genera. Gürich addressed some value to the description of scales whereas Gardiner stated that there is little value in distinguishing between single fish genera by the determination of fish scales. Especially the assignment of isolated scales to individual species can be very dubious. He pointed out that the genus *Elonichthys* for example possesses all the types of scale ornamentation which occur in the genera *Namaichthys*, *Acrolepis* and *Watsonichthys*.

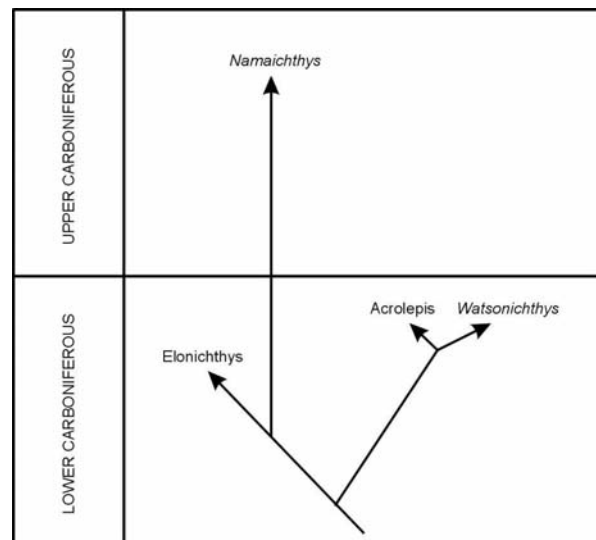


Fig. 36: Evolutionary tree of *Namaichthys* and its relatives (Gardiner, 1962)

3.1.4 Palaeoenvironmental significance

The palaeoenvironmental significance of the fishes is not very high as they are nektonic. They might have been deposited in the shales but lived somewhere else. Martin and Wilczewski (1970) and McLachlan and Anderson (1973) concluded from finds of other marine fossils such as bivalves, of scyphozoans (*Conularia*), sponge spicules and crinoid stalks that the palaeoniscoid fishes lived in a marine palaeoenvironment. In contrast; Bender *et al.* (1991) reported the discovery of specimens of *Namaichthys digita* from the fluviially deposited Beaufort Group and the non-marine deposited Upper Ecca Group indicating an overall non-marine environment.

#	Condition of the concretion	Size of the concretion	Tephrostratigraphy	Description	Genus
1	concretion incomplete	width: 7.5 cm and thickness: >5.5 cm	#2: below tuffs I	scales coherent: max. 7x5 mm, not imbricating, rounded rhombohedrans, ornamented: 7- 10 ridges	<i>Watsonichthys lotzi</i>
2	concretion incomplete	thickness: >4.5 cm	#2: between tuffs I+II	scales coherent: max. 7x4 mm, not imbricating, rounded rhombohedrans, ornamented: 7- 10 ridges (Plate 1, Fig. 8)	<i>Watsonichthys lotzi</i> (Schultze, written comm.)
3	almost complete	18x13x7 cm	#2: between tuffs I+II	scales coherent: max. 4x2 mm, not imbricating, rectangles, no ornamentation, partly bluish enamel	<i>Namaichthys schoederi</i>
4	concretion incomplete	>14x>10x8 cm	#2: 100 cm above tuff Ic	scales coherent: max. 4x2 mm, not imbricating, rectangles, no ornamentation, partly bluish enamel, lower jaw (3x0.8 cm)	<i>Namaichthys schoederi</i>
5	concretion incomplete	thickness: 5.5 cm	#2: 70 cm above tuff Ib	scales coherent: rhombic, strongly ornamented, 8 ridges, to the rims of the concretion imbricating, not in the centre, size: max 7x5 mm	<i>Watsonichthys lotzi</i>
6	concretion incomplete	thickness: 5.0 cm	#2: between tuffs I+II	single scales, not coherent, scales similar to 5, size: max. 7x4 mm	<i>Watsonichthys lotzi</i>
7	half concretion	8x7x5.5 cm	#2: between tuffs I+II	coherent scales: rhombic, ornamented, ridges bifurcate, bluish enamel, size: 6x3 mm, different to 2 (Schultze)	<i>Namaichthys schoederi</i> (Schultze, written comm.)
8	concretion incomplete	thickness: 5.0 cm	#2: 50 cm above tuff IIb	scales mostly coherent: angular rhombic, ornamented, 7-10 ridges, imbricating, size: max 5x3 mm	<i>Namaichthys schoederi</i>
9	concretion incomplete	width: 6.5 cm and thickness: 3.0 cm	#2: between tuffs II+III	bones: up to 2 cm long and 0.5 cm wide, fin with 3-4 lepidotrichia	<i>Namaichthys schoederi</i> (Schultze, written comm.)
10	concretion complete	width: 10.0 cm and thickness: 4.5 cm	#2: between tuffs II+III	bones: up to 3.5 cm long and 0.5 cm wide, fin with 4-5 lepidotrichia, tail fin (1x0.3 cm)	<i>Namaichthys schoederi</i> (Schultze, written comm.)
11	concretion incomplete	width: 4.0 cm and thickness: 2.0 cm	#2: between tuffs II+III	scales coherent: max. 2x1 mm, slightly imbricating, rhombohedrans, no ornamentation, 2 tail fins (2x1 cm), (Plate 1, Fig. 6)	<i>Namaichthys schoederi</i>
12	pieces		#2: between tuffs II+III	scales coherent: max. 4x3 mm, not imbricating, rhombohedrans, no ornamentation	<i>Namaichthys schoederi</i>
13	concretion incomplete	width: 5.0 cm and thickness: 2.2 cm	#23: between tuffs II+III	scales coherent: max. 3x2.5 mm, not imbricating, rhombohedrans, no ornamentation (Plate 1, Fig. 7)	<i>Namaichthys schoederi</i>
14	concretion incomplete	width: 11.0 cm and thickness: >3.5 cm	#23: above tuffs III	scales partly coherent: angular rhombic, strongly ornamented, 7-10 ridges, imbricating, size: max 6.5x4 mm	<i>Watsonichthys lotzi</i>
15	pieces		#2: 55 cm above tuff IIIb	grey-whitish, rectangular, calcareous particles (pieces of bones?), size: 3x3 mm	?
16	concretion complete	8.0x6.3x2.7 cm	#2: 400 cm above tuff IVc	bones, caudal fin, tail fin with 7 lepidotrichia, lower jaw (2.5x0.3 cm), few, small scales (rhombic, no ornamentation)	<i>Namaichthys schoederi</i>
17	half concretion	>7.0x4.5x2.0 cm	#2: 400 cm below tuff Vc	bones of the skull, tail fin with 5-6 lepidotrichia	?
18	concretion complete	8.0x5.0x2.5 cm	#2: below tuff Vc	single bones, lower jaw (2.5x0.3 cm)	?
19	concretion incomplete	width: 3.8 cm and thickness: 2.2 cm	#22: between tuffs IV+V	caudal fin (max. 2.4x1.7 cm), deeply cleft, inequilateral	<i>Namaichthys schoederi</i>
20	concretion incomplete	width: 3.3 cm and thickness: 1.4 cm	#22: between tuffs IV+V	caudal fin (max. 3.2x1.4 cm), deeply cleft, inequilateral (Plate 1, Fig. 5)	<i>Namaichthys schoederi</i>
21	concretion incomplete	width: 4.5 cm and thickness: 2.5 cm	#22: between tuffs IV+V	bones, lower jaw (3.0x0.4 cm)	<i>Namaichthys schoederi</i> (Schultze, written comm.)
22	concretion incomplete	width: 5.0 cm and thickness: 2.5 cm	#22: between tuffs IV+V	bones of the skull, pointed snout	<i>Namaichthys schoederi</i> ?
23	concretion complete	9.0x8.0x3.0 cm	#16: 35 cm below tuff VI	disrupted but complete fossilised fish: scales: not ornamented, size: 2x1.5 mm, rhombic to rectangular, not imbricating; lower jaw (3.2x0.3 cm), (Plate 1, Fig. 3)	<i>Namaichthys schoederi</i> (Schultze, written comm.)
24	concretion complete	11.0x11.0x4.5 cm	#16: 15 cm above tuff VI	few bones, lower jaw (5.0x0.6 cm), small (1 mm), white, elongate particles (teeth?)	?
25	concretion complete	13.0x10.0x5.5 cm	#24: Snyfontein	disrupted but complete fossilised fish: scales: not ornamented, size: max. 4x4 mm, rhombic to quadratic, not imbricating, bluish enamel; lower jaw (2.0x0.2 cm) with row of teeth (size: < 1 mm); bones of skull disrupted; caudal fin (1.5x1 cm); fossil remains are rusty-brown (Plate 1, Fig. 4)	<i>Namaichthys schoederi</i>
26	6 pieces collected by H. Grill (stored in the collection of the Institut für Paläontologie, University Würzburg)		#2: between tuffs IV+V	4 pieces with small, rhombic scales, size max. 3x1.5 mm (Fig. 1 of Plate 1, Grill (1997)); 1 piece with scull plates, denticulate scales, normal scales and fin (Fig. 2 of Plate 1, Grill (1997)); 1 piece with lower jaw and up to 1 mm large teeth (Fig. 3 of Plate 1, Grill (1997))	<i>Namaichthys schoederi</i>

Tab. 2: Description of fish fossil-bearing concretions contained in the lower part of the Ganigobis Shale Member (Aranos Basin, southern Namibia).

3.2 Coprolites

Coprolites are fossilised excrements of animals. Three different types were distinguished within the Ganigobis Shale Member.

Spiral coprolites are frequently found in the lower part of the Ganigobis Shale Member in outcrops #2, 23, 29, 31 and 32 but were also recognised in locality #27. The up to 5 cm long coprolites form the nucleus of siliceous mudstone concretions. The coprolites possess a maximum diameter of 2.0 cm and mostly show a spiral-like enrolment with up to 5 whorls in cross-section (Fig. 37).

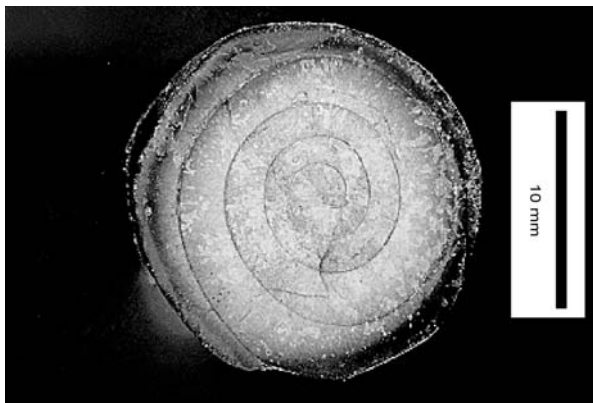


Fig. 37: Cross section of a spiral coprolite showing an enrolment with 5 whorls, found in outcrop locality #2 just below tuff bed IIb.

In longitudinal sections they occasionally show a flattened conical shape displaying small hooks

at the turning points. They are made up of light grey massive mudstone which occasionally shows traces of pyrite but do not display other features such as scales of fishes for example (Fig. 38).

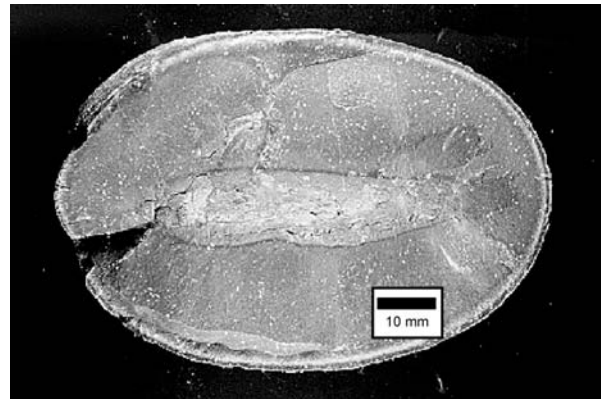


Fig. 38: Longitudinal section of a coprolite showing a flattened conical form; from outcrop locality #2, between tuff beds IIb and IIIb.

They are believed to be the fossilised contents of an intestinal spiral valve of a larger unknown animal, probably of a shark. McLachlan and Anderson (1973) mentioned the class Chondrichthyes being responsible for spiral coprolites of the Lower Permian Prince Albert Formation (Ecca Group) in the north-western part of the main Karoo Basin in South Africa.

Plate 1: Figure captions

Fig. 1: Skull plates (1), normal scales, denticulate scales with tooth-like projections (2) and pectoral (?) fin of *Namaichthys schroederi* (3); #2: between tuff beds IV and V; from Grill (1997).

Fig. 2: Lower jaw (1) with several teeth of *Namaichthys schroederi*; #2: between tuff beds IV and V; from Grill (1997)

Fig. 3: Skull plates (1) and normal scales, denticulate scales with tooth-like projections (2) of *Namaichthys schroederi*, #16: 35 cm below tuff bed VI.

Fig. 4: Disrupted but complete fossilised fish with lower jaw and row of teeth (1); not ornamented scales (2) and caudal fin (3) of *Namaichthys schroederi*, #24: Snyfontein.

Fig. 5: Caudal fin: deeply cleft, inequilateral; *Namaichthys schroederi*, #22: between tuff beds IV and V.

Fig. 6: Coherent scales and 2 tail fins of *Namaichthys schroederi*, #2: between tuff beds II and III.

Fig. 7: Coherent scales of *Namaichthys schroederi*: not imbricating, rhombohedrans, no ornamentation, #23: between tuff beds II and III.

Fig. 8: Coherent scales of *Watsonichthys lotzi*: not imbricating, rounded rhombohedrans, ornamented: 7- 10 ridges, #2: between tuff beds I and II.

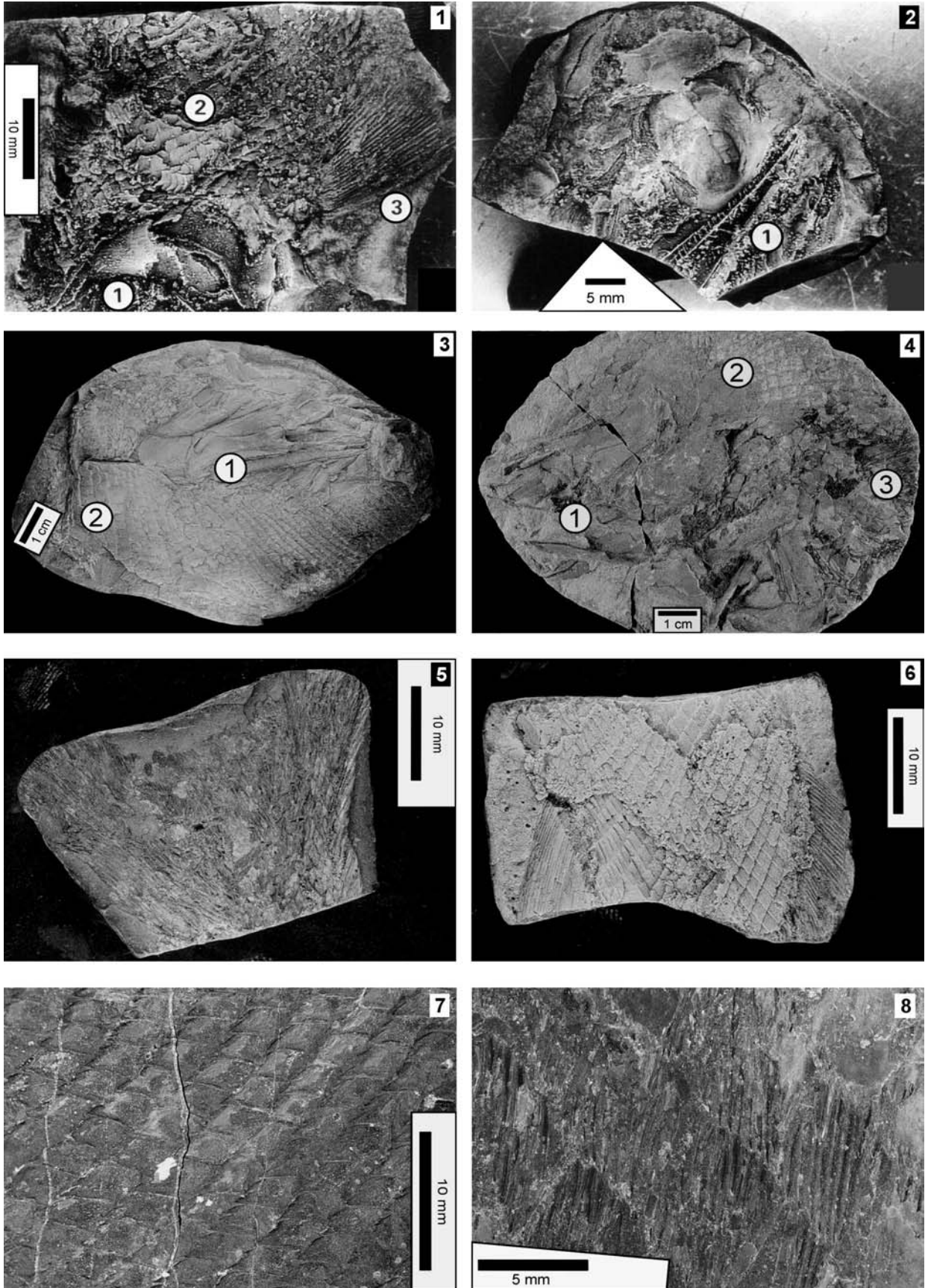


Plate 1: Palaeoniscoid fish remains contained in siliceous-phosphatic concretions within the lower part of the Ganigobis Shale Member (Aranos Basin, southern Namibia). Figure captions are found on the following page.

Type two are 2 - 4 cm large funnel-shaped coprolites forming the nucleus of orange-red pyritic concretions were especially recognised in the middle part of the Ganigobis Shale Member in outcrops #13 and 44 but were also found on top of the tuff beds VI in outcrop #2. The "funnels" were mostly oriented upside down with the peak of the funnel directed downwards. (Fig. 39)

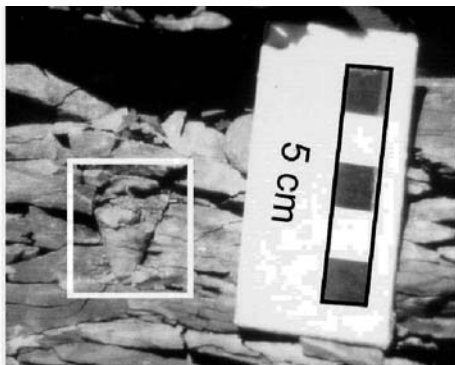


Fig. 39: Funnel-shaped coprolite in mudstones of outcrop #13.

The third type of coprolites are up to 15 cm long, anvil-like coprolites made up of a brown ferruginous, coarse sparitic material. They form the nuclei of smaller mudstone concretions and are found in localities #13 and 15 in the middle part and in locality #27 in the upper part of the Ganigobis Shale Member. They were already described in chapter 2.4 and 2.5.

3.3 Permineralised wood

Permineralised wood was found *in situ* in all three parts of the Ganigobis Shale Member. In the lower part permineralised wood was detected in outcrops #2, 29, 31 and 45, in the middle part in locality 20 and in the upper part in localities #9 and 27.

Four samples of permineralised wood from this study were described by Marion Bamford (BPI Palaeontology, University of Witwatersrand, Johannesburg).

The first sample described by M. Bamford is a flattened, slightly coalified wood with glassy spheres on the surface which was found 0.75 m above tuff bed Ic in outcrop #2 (cf. Fig. 18).

"This 8 x 5 x 2 cm large piece of wood, is

black, carbonaceous and poorly preserved. No growth rings are visible. The earlywood tracheids are squarish in outline and have a mean tangential diameter of 28 μm (range 25 - 37 μm) and mean radial diameter of 34 μm (range 27 - 40 μm). The rays are low, 4-8-12 cells high and uniseriate. The walls are thin and smooth. No pitting was preserved."

The second specimen also originated from the lower part of the Ganigobis Shale Member (locality #28):

"The specimen is grey, longitudinally compressed with longitudinal grooves, but has surprisingly well preserved secondary xylem. The central pith, of unknown extent, consists of a mass of large parenchyma cells in a variety of shapes. The primary xylem is in lobes extending into the pith and adjacent to the secondary xylem, i.e. endarch. In longitudinal section these protoxylem tracheids have close spiral thickening. The metaxylem tracheids have alternate biseriate pitting. In the secondary xylem the tracheids are squarish in outline. The earlywood tracheid mean tangential diameter is 35 μm (range 25 - 45 μm) and mean radial diameter is 33 μm (range 27 - 45 μm). The growth rings are close together near the pith, less than 1mm wide. The latewood is made up of 2 - 3 rows of radially compressed tracheids. The latewood tracheid mean tangential diameter is 33 μm (range 20 - 40 μm) and mean radial diameter is 12 μm (range 10 - 18 μm). Adjacent cell walls are 7 - 10 μm thick. The rays are low, 1-5-12 cells high, exclusively uniseriate and relatively rare. No cross-field pits were seen but tracheid bordered pitting is clear in some areas. These pits are uniseriate or biseriate and alternate, contiguous and slightly oblique. Their diameter is 12 - 15 μm . This wood with the araucarian secondary xylem and central pith is typical of the Dwyka woods of Namibia described by Kräusel (1956a and b)."

Both woods belong to the araucarian conifers and are denoted as *Araucarioxylon sp.* (class: Gymnospermopsida, order: Coniferales). Conifers are forest trees and are known since the Westphalian (Carboniferous). Coniferales are evergreen and their needles or scales function for more than a single season.

The wood is dense and characterised by circular-bordered pits. The reproductive organs consist of simple pollen cones which produce saccate pollen (Frommherz, 1998).

A third specimen from the Ganigobis Shale Member, which was collected by Hermann Grill in 1995 near locality #25 (cf. Chapter 2.6.1.1), was described as follows:

"The piece of wood measures 9.0 x 9.0 x 4.5 cm and is grey-black and very hard. Growth rings are 1 - 2 mm wide and obviously from a trunk with a diameter more than 50 cm. The tracheids are square to rectangular in transverse section and the earlywood tracheids have a mean tangential diameter of 26 μm (range 20 - 30 μm), and a mean radial diameter of 24 μm (range 20 - 30 μm). The latewood tracheids have a mean tangential diameter of 25 μm (range 23 - 27 μm), and a mean radial diameter of 13 μm (range 10 - 15 μm). The bordered pits on the radial walls of the tracheids are 1-2 seriate, alternate to subopposite and separate. Their diameter is 10 μm . The rays are uniseriate and have an average height of 5 cells (range 2 - 8 μm). The crossfield pits were not preserved."

The wood is denoted as *Megaporoxylon kaokense* Kräusel and probably belongs to the family Cordaitaceae (class: Gymnospermopsida, order: Cordaitales). The size of the Cordaitaceae varied between shrubs and large trees depending on their palaeoenvironment (Frommherz, 1998). The order Cordaitales is world-wide known from the Namurian (Carboniferous) to the Lower Permian.

The woods *Araucarioxylon* and *Protophyllocladoxylon* are closely related and are also reported from the Permian of Antarctica (Neish *et al.*, 1993) and India (Jeyasingh and Kumarasamy, 1995).

The fourth specimen originated from the upper part of the Ganigobis Shale Member from locality #27:

"The growth rings are very clearly seen, varying in width from 1-7 mm, with an average of 4.6 mm. Latewood comprises one tenth to one quarter of each ring and ends abruptly at the beginning of the earlywood. The transition from earlywood to latewood is gradual (Fig. 40: 1). There are usually 20-30 rows of latewood cells. The pith is only a few centimetres in diameter and the parenchyma is heterocellular. The primary xylem lobes are very small and endarch (Fig. 40: 2). The tracheids of the secondary xylem are square to polygonal and thin walled (wall between two adjacent cells is 5 μm wide) in the earlywood, and only slightly thicker in the latewood (7.5 μm). The earlywood mean tangential diameter is 35 μm (range 25 - 42 μm) and mean radial diameter is 36 μm (range 25 - 47 μm). The latewood mean tangential diameter is 29 μm (range 25 - 35 μm) and mean radial diameter is 12 μm (range 7 - 22 μm). Bordered pitting on the radial walls of the tracheids is mixed, predominantly uniseriate and contiguous (90%) but also biseriate and alternate, and uniseriate and separate (Fig. 40: 3). In the earlywood the mean diameter of the pits is 12.5 μm , and 10 μm in the latewood. The pit apertures are mostly 5 μm wide and round but some areas show the cross-like structure of elongated pits of adjacent cells overlapping at right angles, particularly in the narrow latewood tracheids. The rays are uniseriate and low, 2-10-15 cells high, with thin, unpitted walls. The cross-field pits are large, simple, oval to fusiform and obliquely orientated, the single pit (very rarely two) filling most of the field (Fig. 40: 4). In the earlywood they are on average 37 μm long and 15 μm wide, orientated in the same direction. The latewood cross-field pits are orientated in the opposite direction and are smaller, but because the field is also smaller, they too occupy most of the field. These pits are 20 μm long and 5 μm wide, and also without a border. No resin canals, resin or axial parenchyma were seen."

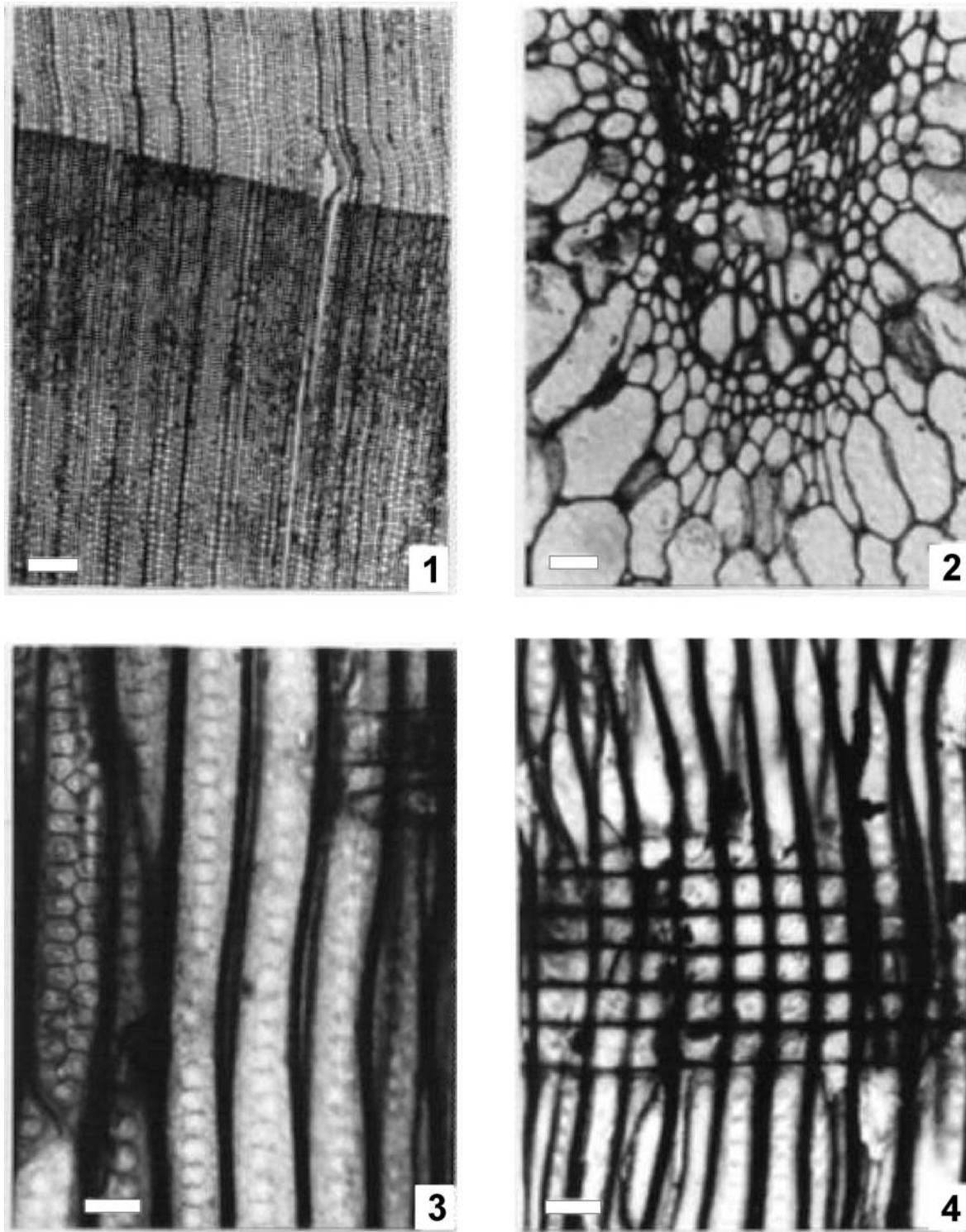


Fig. 40: Details of the excellently preserved wood specimen found at locality #27: *Megaporoxylon scherzi* Kräusel (Bangert and Bamford, in press)

- 1, Earlywood tracheids with thin walls in upper part and thicker walled latewood tracheids below. Scale bar = 350 μm .
- 2, Transverse section showing the primary xylem at the top, pith with secretory cells (dark deposit) and metaxylem (large central cells). Scale bar = 60 μm .
- 3, Radial longitudinal section: Uni- and biseriate bordered pitting on radial walls of earlywood tracheids. Scale bar = 20 μm .
- 4, Radial longitudinal section: Crossfield pitting; oopores in the earlywood are oval oblique. Scale bar = 40 μm

The wood is very similar to *Megaporoxylon scherzi* described by Kräusel from the upper Dwyka beds of the Karoo formation, near Mariental (Kräusel, 1956a and b). Kräusel gave no measurements but observed that the cross-field pits of *Megaporoxylon kaokense* are up to three times larger than the tracheid pits (Kräusel, 1956a). *Megaporoxylon scherzi* is very similar but has oval slanting (obliquely orientated) pits, whereas *Megaporoxylon kaokense* has more rounded pits. The wood is therefore identified as *Megaporoxylon scherzi* Kräusel (Fig. 41).

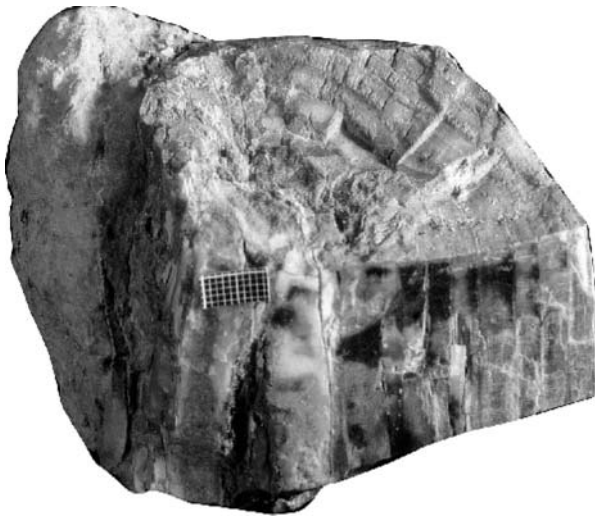


Fig. 41: Hand specimen of *Megaporoxylon scherzi*, note the 1-7 mm wide growth rings to the right; locality #27.

It is much better preserved than the other specimens which could only be identified as *Araucarioxylon sp.* These woods do not have the distinct growth rings that this sample has. Sample two has pith, endarch primary xylem but distinctly lobed and the tracheid cross-field pits are larger.

Megaporoxylon scherzi has very clear growth rings and abundant latewood whereas *Megaporoxylon kaokense* has narrower latewood. In both cases the wood nearest to the pith has been studied, in other words the wood of the very young tree. The specimens originate from different localities as *M. scherzi* was found in the upper part and *M. kaokense* was detected in the lower part of the Ganigobis Shale Member and are therefore very unlikely to be exactly contemporaneous. The growth rings imply a

seasonal environment which is reasonable due to the high latitude position of southern Gondwana during the Carboniferous and Early Permian. With the apparently restricted occurrence of *Megaporoxylon* through time, the wood can be considered as a biostratigraphic tool. This is because Gondwanan woods with piths seem to be confined to the Carboniferous and Lower Permian deposits and are then replaced by woods with no piths.

The plant groups occurring in Gondwana at this time comprise the Cordaitales, Glossopteridales and early conifers. The Cordaitales occurred from the Late Carboniferous to the Early Permian (Trivett and Rothwell, 1991) and many organ genera have been assigned to this group. The glossopterids are predominantly a Permian group; leaves have also been found in Dwyka Group deposits of the south-western main Karoo Basin (Anderson and McLachlan, 1976). *Araucarioxylon* is supposed to be the wood type of the glossopterids (Gould and Delevoryas, 1977) but this wood type may well belong to more than one plant group. The cordaitalean woods *Mesoxylon* and *Cordaioxylon* have large piths and *Araucarioxylon* a secondary xylem (Trivett and Rothwell, 1991). It is therefore not possible to determine to which group these woods with pith belonged. More detailed collecting may eventually shed some light on the whole plants in these groups (Bangert and Bamford, in press).

3.4 Gastropods

Two different species of gastropods were discovered in the upper part of the Ganigobis Shale Member:

Numerous gastropod shells of a single species (*Peruvispira vipersdorfensis*, Dickins, 1961) were discovered in outcrop #27 (Fig. 42). The shells are restricted to a relatively narrow stratigraphic interval marked by tuff bed VIIIa. They are concentrated in irregular, partly branching mudstone concretions which appear to represent fossilised burrows with widths of up to 10 cm. The height of the gastropods averages 5 mm with a maximum of 10 mm and a width of about 6 mm. Most of the shells are poorly preserved and show three, but in some cases also four or five whorls. The upper whorl surface is almost

straight with the slit-band at the outer edge. Below the slit-band the outline of the shell is concave, the apical angle ranges from 38° to 46° (Dickins, 1961). Dickins reports occurrences of *Peruvispira vipersdorfensis* from Farm 63 Viperstorf east of Asab and from near the main road B1 about 8 miles (12 km) north of Tses which probably corresponds to outcrop #27. *Peruvispira delicata* is known from the Itararé Subgroup of Brazil and from the middle to upper Carboniferous Santa Elena Formation of Argentina (*Peruvispira* sp., Rocha-Campos, 1970). *Peruvispira* was also found in the Permian of New Zealand (Johnston and Stevens, 1985).



Fig. 42: Gastropod shell of *Peruvispira vipersdorfensis* (Dickins, 1961) detected in outcrop #27. Shells mainly display three whorls, only few show four or five whorls.

A single, weakly trochospiral, gastropod shell with a maximum diameter of 4.3 x 3.2 cm and a height of 2.5 cm was found 2 m below tuff bed VIIIa in locality #9. The turbiniform shape and the spiral-like ornament suggest a relation to the genus *Omphalonema* (superfamily Platyceratacea; family: Holopeidae: L. Ord.-M. Perm). *Omphalonema* has no shoulders and the umbilicus is narrow (not seen in the illustrated sample, Fig. 43). This genus was not mentioned yet from the Dwyka Group of southern Africa but has been described from the Early Permian of north-east Asia (Grabau, 1936).



Fig. 43: Gastropod shell of the genus *Omphalonema* (apical view) detected in outcrop #9 shows a turbiniform shape, a spiral-like ornamentation, a narrow umbilicus and no shoulder.

3.5 Bivalves

Two types of bivalve shells have been found associated with tuff beds VIIIa-VIIIc in the vicinity of Ganigobis (outcrops #9 and 27). Two small bivalve shells were collected in outcrop #9. The shell has a subtrigonal shape and is equivalved, the anterior side is elongated and the posterior side is truncated without any ornamentation. The anterior-posterior diameter ranges between 5 and 6 mm and the dorso-ventral diameter totals 3 mm. It is further characterised by a taxodont hinge; the teeth cannot be seen. These shells relate to the family Nuculidae (Fig. 44).

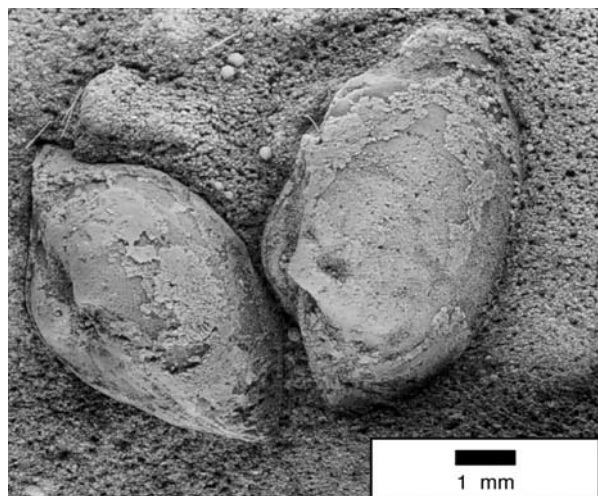


Fig. 44: Bivalve shells (Nuculidae) detected in outcrop #9 display a subtrigonal form and a taxodont hinge (apical view).

Nuculanid bivalves of the genus *Paleyoldia* sp. (Nuculanidae) were also identified by Grill (1997) in outcrop #43 (Fig. 45).

Nuculopsis sp. was found within the Prince Albert Formation (Ecca Group) at Farm Blaauw Krantz in the north-western part of the main Karoo Basin (McLachlan and Anderson, 1973).

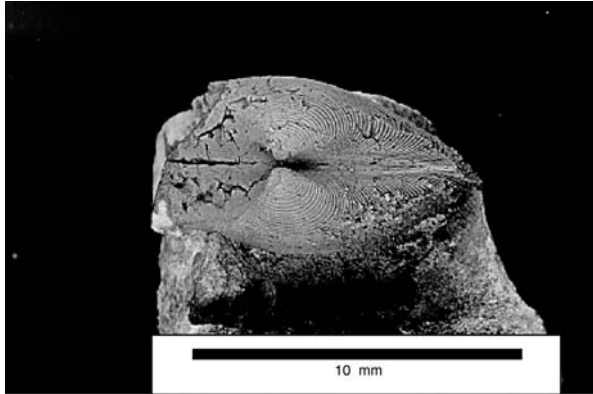


Fig. 45: Dorsal view of a nuculanid bivalve (genus *Paleyoldia*, family Nuculanidae) showing a subtrigonal shell with concentric ornamentation and a palaeotaxodont hinge (collected by Hermann Grill in outcrop #43)

The second type of bivalve is thin-shelled, elongate, the anterior-posterior diameter reaches 1 cm and the dorso-ventral diameter totals 4 mm (Fig. 46). Furthermore, the shells are characterised by prominent growth lines. Hinge and teeth cannot be seen. The bivalves probably belong to the genus *Myonia* (subclass: Anomalodesmata; order: Pholadomyoidea). *Myonia* is well known from Carboniferous and Permian strata in Australia, India, Brazil and Argentina (Rocha-Campos, 1970). The bivalves in the Aranos Basin of southern Namibia were discovered in a large mudstone concretion 55 cm above tuff bed VIIIa in outcrop #9. All detected bivalves indicate a marine environment.

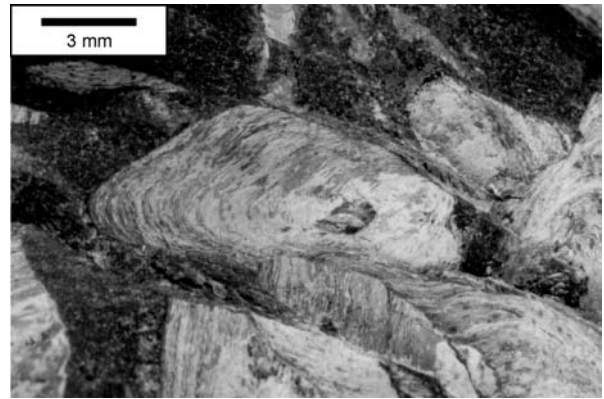


Fig. 46: Bivalve shells probably of the genus *Myonia* with thin, elongate shells; note the prominent growth lines; found in outcrop #9.

3.6 Conularia and sponges

The presence of *Conularia* sp. (class: Scyphozoa, subclass: Conulata) near Ganigobis has been reported by Schroeder (1908) and later illustrated by Range (1912). *Conularia* are partly sessile and partly migrating, marine fossils and occurred from the Late Cambrian to Permian ages. A sample of *Conularia* sp. collected at locality #27 was found at the stratigraphic level of tuff marker bed VIIIa. It is characterised by a conical shape and a maximum length of 3 cm with a diameter of 1.5 cm. The upper end is rectangular in cross-section and the outer surface is covered by a grid of fine lines (Fig. 47). The sample stuck sub-vertically to vertically within the mudstone exposures.

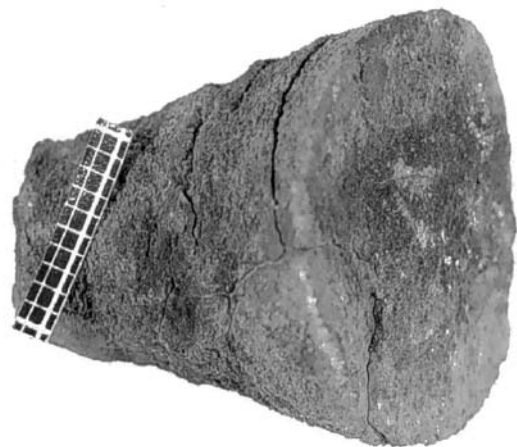


Fig. 47: *Conularia*. sp. found in outcrop # 27.

Also sticking sub-vertically to vertically within the mudstone exposures of outcrop #27 are single, sessile living sponges which partly branch. They display irregular shapes and possess a 1 mm thick, calcareous peel.

3.7 Other fossils of the Ganigobis Shale Member

Crinoid stalks and sponge spicules were already described in chapter 2.5 (outcrop #27).

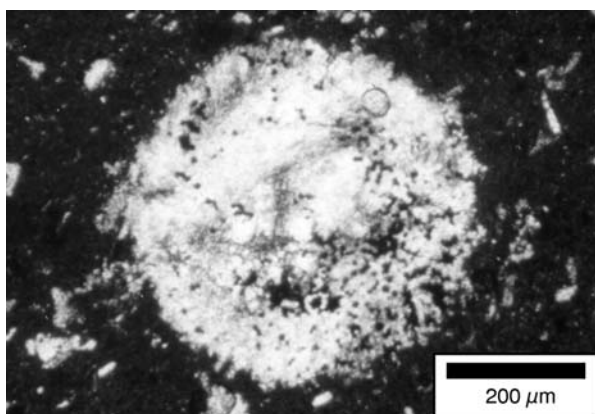


Fig. 48: Photo-micrograph of a calcareous globule displaying a rather fibrous and incomplete limit which suggests that the globule was initially a radiolaria; sample from locality #2, just below tuff bed Ib.

White, up to 1 mm in diameter, calcareous globules are concentrated close to the rims of most of the mudstone concretions.

The rather fibrous and incomplete limit of the globules leads to the conclusion that silica was leached away and replaced by calcite. Originally, the globules were most likely radiolaria as calcispheres normally show distinct outer boundaries (Fig. 48).

Radiolaria, foraminifers (*Hyperammina*, *Ammodiscus*, *Glomospira*, *Ammobacculites* and *Spiroplectammina*), echinoid spines and scolecodonts are mentioned from the Ganigobis Shale Member by Martin and Wilczewski (1970) and confirm a marine environment. A specimen of the goniatite *Eosianites* was described by Martin *et al.* (1970) from shales of the Dwyka Group near Schlip. The Hardap Shales of deglaciation sequence III bear shells of *Eurydesma mytiloides* (Dickins, 1961, Grill, 1997), bryozoa (Wass, 1970) and a single arm of a starfish (Lane and Frakes, 1970). A helpful overview of the fossil contents of the Dwyka Group in Namibia is given by Pickford (1995) who summarised the literature until the early 1990's.

4 The mudstones of the Ganigobis Shale Member

About 99 % of the Ganigobis Shale Member is made up of mostly silty mudstones. Their colour varies between medium grey to dark grey and black. The lower part of the succession (up to 1.5 m above tuff horizon VIb, Fig. 5) consists of blue-black massive, silty mudstones from the base up to tuff horizon Vc. Medium grey silty mudstones, which display a distinct lamination with an average laminae thickness of < 1mm, occur from close above tuff horizon Vc up to 1.5 m above tuff horizon VIb. Such a distinct lamination was not recognised in the mudstones of the middle and upper part of the Ganigobis Shale Member as the middle part of the Ganigobis Shale Member (from 1.5 m above tuff horizon VIb to tuff horizon VIIIa) and the upper

part (from tuff horizon VIIIa to the top of the Ganigobis Shale Member) mainly consists of black, massive mudstones.

4.1 Mineralogy of the mudstones

In order to determine the mineralogy of the mudstones, 15 powder samples were analysed by XRD at the Geologisches Landesamt Rheinland-Pfalz in Mainz, Germany. These samples cover the whole sequence of the Ganigobis Shale Member and were taken at vertical distances of roughly every 4 metres.

Mudstones of the lower part of the Ganigobis Shale Member were sampled in outcrop #2, samples of the middle part originate from outcrops #15 and 13 and samples were taken from localities #27 and 9 representing the upper part of the Ganigobis Shale Member. An overview of all measurements is given in Fig. 49, single analyses are listed in Appendix D-1.

The mineralogy of all 15 samples does not vary significantly and is dominated by quartz making up about two thirds of the samples. Feldspars include albite and anorthite and as well as orthoclase, anorthoclase and sanidine. Plagioclases occur more frequently than K-feldspars.

The clay mineral suite consists of illite, kaolinite and clinocllore. Clinocllore contents reach 20 % in places. Muscovite and the zeolite gismodine is also present in almost all samples. Further, rather sporadically identified minerals comprise the Ti-oxide anatase, paragonite (Namica), the sulphates gypsum and celestine ((Sr,Ba) SO₄) and hausmannite (Mn₃O₄).

4.2 Geochemistry of the mudstones

XRF-analyses were carried out on 25 mudstone samples of outcrop #2 at the Institut für Mineralogie, University of Würzburg in 1996. As the mudstone samples were taken in intervals of 1

m, only the lower half of the Ganigobis Shale Member (24 m) is covered; results are presented in Appendix Tab. 23 in Appendix F-1.

The geochemistry of the mudstones of the upper half of the Ganigobis Shale Member was not investigated as the topic of this dissertation was focused on the tuff beds.

4.2.1 Major elements

The major element geochemistry of the investigated mudstone samples does not differ a lot from average published values. The adequacy of average values is generally questioned as there are substantial differences in the chemical and mineralogical composition of different mudstones (Blatt *et al.*, 1980).

The investigated mudstones of the Ganigobis Shale Member show relative high SiO₂- values (62%) which is explained by a high proportion of silt in the mudstones (Tab. 3). This is probably due to a near-shore position of the sample site within the basin and high detrital runoff of rivers. Al₂O₃-values (18%) are higher than the values from Wedepohl (1978: 15 %) which accounts for a secondary enrichment of Al₂O₃ within the clay minerals (kaolinite, illite). Al₂O₃ might also be derived from finely disseminated glass shards within the mudstones which altered into smectites and illites.

weight %	SiO ₂	TiO ₂	Al ₂ O ₃	Fe ₂ O ₃	MnO	MgO	CaO	Na ₂ O	K ₂ O	P ₂ O ₅	S	LOI
mean: mudstones (Ganigobis Shale Member)	60.03	0.72	18.08	6.20	0.05	2.51	0.87	1.33	4.02	0.21	0.64	6.18
mean: mudstones (in Wedepohl, 1978)	53-60	0.87	~15	2.5	0.1	1.5	4.8	0.8	2.45	0.15	n.v.	n.v.

ppm	V	Cr	Co	Ni	Zn	Rb	Sr	Y	Zr	Nb	Ba
mean: mudstones (Ganigobis Shale Member)	129	93	14	43	153	198	153	55	192	31	493
mean: mudstones (in Wedepohl, 1978)	98	83	11	71	90	164	20-360	34	164	16	546

Tab. 3: Comparison between XRF-data (mean values) derived from mudstones of the Ganigobis Shale Member (25 samples) and values from Wedepohl (1978: varying number of samples); n.v.: no values.

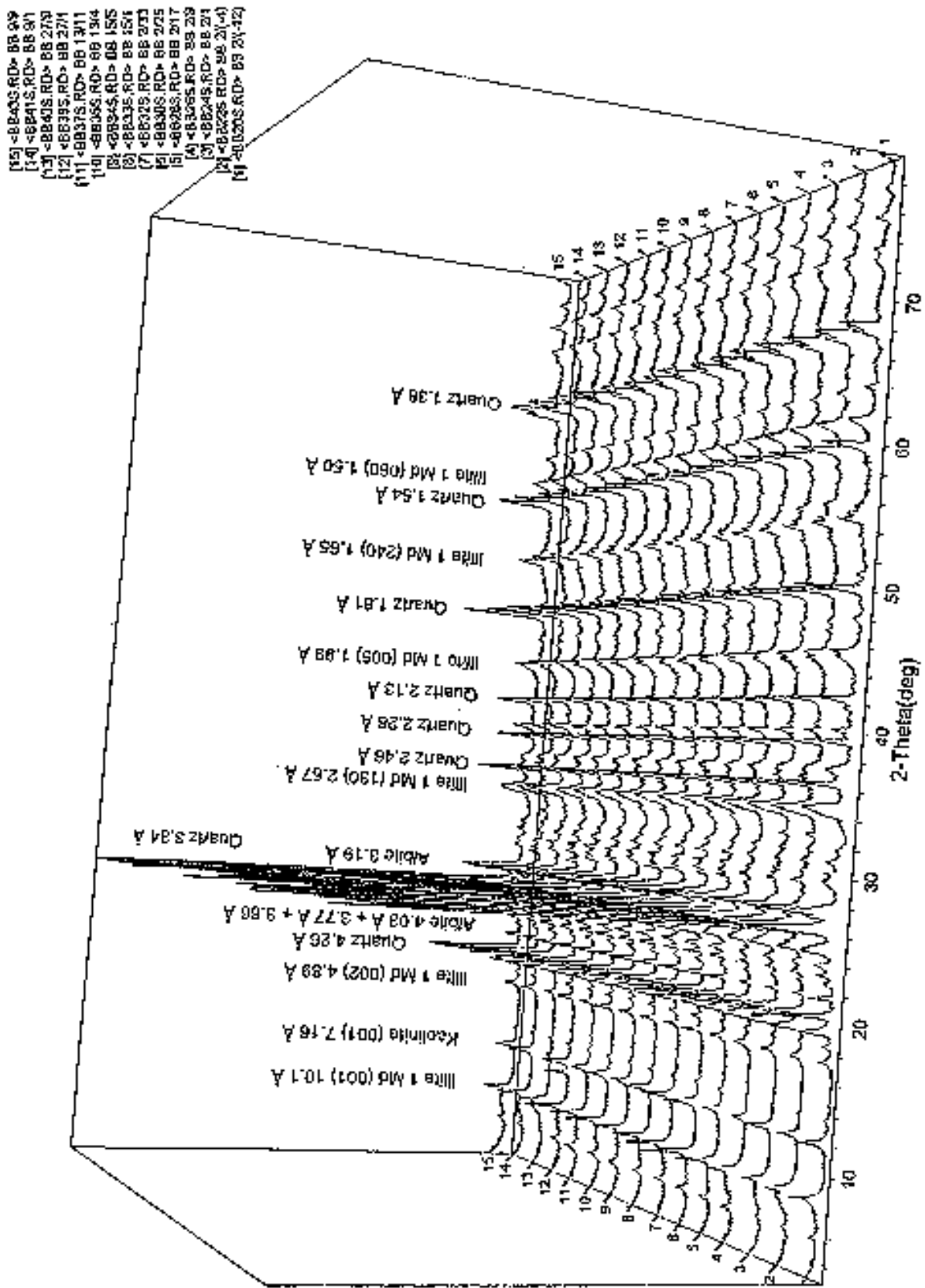


Fig. 49: X-ray powder diffraction patterns for all measured mudstone samples of the Ganigobis Shale Member showing major mineral phases with hkl-indices and d – spaces (Å).

Higher Fe_2O_3 - and MgO - values than in Wedepohl (1978) probably originate from chlorites such as clinocllore. CaO is depleted within the mudstones whereas Na_2O is slightly enriched probably due to mica such as paragonite (cf. Chapter 4.1). K_2O (4.1%) is kept in clay minerals and feldspars and is significantly higher than on average mudstones which is probably due to admixture of pyroclastic material within the mudstones. The existence of former glass within the mudstones adjacent to the tuff beds was supposed by Dr. W. Zimmerle, Celle, Germany during the analysis of thin-sections of the mudstones.

4.2.2 Trace elements

V, Cr, Co and Ni are mobile and mostly incorporated into clay minerals. Zn possesses only restricted mobility and is thus concentrated in hydroxides. Rb-values in the investigated mudstones are higher than in shale averages as Rb is strongly associated with K. Sr corresponds closely with Ca. However, it is less mobile and therefore less depleted. Zr has a large ionic radius and is only incorporated into heavy minerals such as zircon. Ash-fall derived zircons may enrich the Zr-values in the adjacent mudstones. Nb and Y are also incorporated into heavy minerals whereas Ba is found in K-mica and K-feldspars and is highly mobile (Tab. 3).

4.2.3 Organic matter and nitrogen contents of the mudstones

The total organic content (TOC) and the nitrogen content were measured with the element analyser "vario EL" at the Institut für Geologie und Paläontologie, University of Tübingen. The total carbon content of rocks is made up by organic carbon and inorganic carbon which is associated with the carbonate content of the rock. As the carbonate content of the rock is mostly less than 1 % (confirmed by the XRF-data, cf. Appendix F-1), the total carbon content equals almost the organic content.

The TOC varies between 0.7 and 2.4 % (average: 1.2 %) in the measured samples which originate from outcrops #2, 15, 13 and 9 (cf.

Chapter 4.2.3) and cover the whole Ganigobis Shale Member in intervals of 2 m (Fig. 51).

In the lower part of the Ganigobis Shale Member (cf. Chapter 2.3) two peaks are conspicuous which are situated between tuff beds I and II (1.82 % TOC) and above IV (1.75 % TOC, Tab. 4). These sections of the Ganigobis Shale Member contain most of the discovered fish fossils and coprolites and are interpreted as marine condensed sequences with starved sedimentation and high input of organic matter during sea-level high-stands (cf. Chapter 4.4). Below tuff beds V and further to the top, the TOC-content decreases to values of about 0.8 %. This section consists of laminated, silty mudstones which suggest higher sedimentation rates and thus a lower input of organic matter. A third peak with values of 1.87 % and 2.40 % TOC is found in the tephrostratigraphic level of group VIII tuff beds. This part of the section contains bilvalves, gastropods and crinoid stalks.

The organic matter is predominantly inertinite, made up of semifusinite and fusinite. The vitrinite reflectance is rather constant and ranges from 0.97 % to 1.10 % (Grill, 1997).

Among petroleum geologists a basic criterion for source rock quality is the content of organic carbon (TOC). The mudstones of the Ganigobis Shale Member have a fair to good source quality according to a classification of North (1985; Fig. 51). The type of the organic matter is the second critical parameter for hydrocarbon yield of a source rock.

Macerals in the studied samples consist mostly of inertinite which is typical for organic matter of type IV (Grill, 1997). Organic matter of type IV is only capable of forming gas (North, 1985). Nitrogen in the marine environment is mainly derived from the discharge of rivers. The nitrogen contents in the analysed samples of the Ganigobis Shale Member ranges from 0.09 to 0.17 % with an average of 0.13 %. The nitrogen-graph correlates very well with the TOC-graph (Fig. 51) which indicates that almost all nitrogen is fixed within the organic matter.

Sample	m	TOC (%)	N (%)	TOC/N
#2/(-11)	0	0.6914	0.0921	7.51
#2/(-8)	2	1.4202	0.1406	10.10
#2/(-4)	4	1.8195	0.1668	10.91
#2/(-2)	6	1.5754	0.1321	11.93
#2/1	8	1.4974	0.1498	10.00
#2/5	10	1.4941	0.1497	9.98
#2/9	12	1.7541	0.1548	11.33
#2/13	14	1.3592	0.1221	11.13
#2/17	16	1.0147	0.111	9.14
#2/21	18	0.831	0.1003	8.29
#2/25	20	0.7094	0.0954	7.44
#2/29	22	0.6962	0.1004	6.93
#2/33	24	0.6658	0.1257	5.30
#15/1	26	0.9849	0.1081	9.11
#15/5	28	0.6969	0.1076	6.48
#13/4	30	1.0557	0.1208	8.74
#13/8	32	0.8727	0.1177	7.41
#13/11	34	0.7741	0.1098	7.05
#9/1	36	1.8745	0.143	13.11
#9/5	38	1.3396	0.1357	9.87
#9/9	39	2.4023	0.153	15.70
#9/13	41	1.0869	0.1348	8.06

Tab. 4: TOC and N-content (weight %) and TOC/N covering the whole Ganigobis Shale Member beginning 1.5 m below tuff beds I (#2/(-11) and ending 2.0 m above tuff bed VIIIa (#9/13). For sample denominations see Appendix B-1.3.

The TOC/N – ratio is used to determine the type and origin of organic matter. The ratio varies between 5.30 and 15.70 averaging 9.34 (Tab. 4). Such values between 4 and 10 are characteristic for marine phytoplankton (cf. Schmidt-Röhl, 1999).

4.2.4 Sulphur and pyrite content of the mudstones.

Sulphur contents were determined by XRF from mudstone samples of outcrop #2 (cf. Chapter 4.2). Sulphur varies between less than 0.2 and 1.2%. The graph of sulphur in Fig. 51 (third column) shows that sulphur contents are remarkably high between the tephrostratigraphic levels of tuff beds I and IV. Values vary between 0.31 and 1.16 %. Above tuff beds IV (and also below tuff beds I) values rapidly decrease and fall below the detection limit of 0.02 % (Tab. 5). This suggests that the oxygenation regime was probably most of the time anoxic between tuff beds I and IV whereas above group IV tuff beds

more oxidizing conditions prevailed during the deposition of the mudstones (Fig. 51).

Pyrite forms under anoxic conditions and contains about 90 % of the existing sulphur (Fisher and Hudson, 1987). The pyrite content is therefore 1.7 times the sulphur content (cf. Schmidt-Röhl, 1999) and makes up 0.03 and 1.97 % of the analysed mudstones of outcrop #2 (Tab. 5). Highest values were again found between tuff beds I and III and above IV which coincides with the appearance of macroscopic pyrite within the siliceous-phosphatic concretions which were already described in Chapter 2.3. Pyrite mostly occurs finely disseminated as framboids but also appears in larger spheres with sizes up to 500 µm.

The TOC/S ratio can be used to distinguish ancient marine from freshwater or brackish sedimentary rocks. Organic-rich freshwater sediments exhibit much less diagenetic pyrite than marine sediments because fresh water contains less dissolved sulphate than seawater.

Sample	m	S	Pyrite	TOC/S	CIA
# 2(-12)	0	0.04	0.07	n.a.	73.77
# 2(-10)	1	< 0.02	< 0.03	n.a.	64.47
# 2(-8)	2	0.95	1.62	1.49	75.08
# 2(-6)	3	0.56	0.95	n.a.	77.34
# 2(-4)	4	1.00	1.70	1.82	77.33
# 2(-2)	5	0.52	0.88	3.03	77.63
# 2(-1)	6	0.93	1.58	n.a.	78.02
# 2(1)	7	1.16	1.97	1.29	76.74
# 2(3)	8	0.56	0.95	n.a.	77.42
# 2(5)	9	0.74	1.26	2.02	76.77
# 2(7)	10	0.31	0.53	n.a.	76.54
# 2(9)	11	0.51	0.87	3.44	78.05
# 2(11)	12	0.68	1.16	n.a.	75.42
# 2(13)	13	0.58	0.99	2.34	73.05
# 2(15)	14	0.41	0.70	n.a.	74.06
# 2(17)	15	< 0.02	< 0.03	50.74	73.43
# 2(21)	17	< 0.02	< 0.03	41.55	73.36
# 2(23)	18	< 0.02	< 0.03	n.a.	73.26
# 2(25)	19	< 0.02	< 0.03	35.47	73.28
# 2(27)	20	< 0.02	< 0.03	n.a.	70.68
# 2(29)	21	< 0.02	< 0.03	34.81	72.96
# 2(31)	22	< 0.02	< 0.03	n.a.	73.21
# 2(33)	23	< 0.02	< 0.03	33.29	71.22
# 2(35)	24	< 0.02	< 0.03	n.a.	72.93

Tab. 5: Sulphur and pyrite content (weight %) and TOC/S and CIA covering the lower half of the Ganigobis Shale Member; n.a.: not analysed.

Sulphate reacts with H_2S to sulphide which finally reacts with iron to pyrite. As a result, organic-rich freshwater sediments display a much higher TOC/S ratio than marine sediments with similar organic contents. Freshwater rocks are characterised by TOC/S values of more than 10 whereas marine, sedimentary rocks exhibit ratios commonly between 0.5 and 5 (Berner and Raiswell, 1984). The analysed mudstones of the Ganigobis Shale Member display a dramatic change in this ratio taking place just above tuff beds group IV. Below this tephrostratigraphic level values vary between 1.29 and 3.44 indicating a marine environment. Above tuff beds IV values range from 34.81 to 50.74 suggesting a freshwater to brackish environment (Tab. 5 and Fig. 51).

4.2.5 Chemical Index of Alteration (CIA)

The Chemical Index of Alteration (CIA) is a good measure of the degree of chemical weathering which is based on the ratio between alumina and alkalis (Nesbitt and Young, 1982).

$$CIA = Al_2O_3 * 100 / (Al_2O_3 + CaO + Na_2O + K_2O)$$

As chemical weathering is minimal under glacial conditions, CIA values are low. The matrix of diamictites from the Dwyka Group of the main Karoo Basin for example reveals values averaging 60 but rises to 70 in interbedded mudstones (Visser and Young, 1990).

Analysed mudstone samples from the Ganigobis Shale Member show an average CIA of 74.42 (24 samples, Tab. 5 and Fig. 51). Sample #2/19 was excluded as it shows an unusual high

CaO-value of 13.68. Calcium, sodium and potassium were generally removed from feldspars, which are a major component of the mudstones, by aggressive solutions. Aluminous clay minerals such as kaolinite and illite were concentrated. The proportion of alumina to alkalis is thus increased within the mudstones (Fig. 50). As chemical weathering mostly occurs in warm climates, the mudstones were most probably formed under warmer climatic conditions.

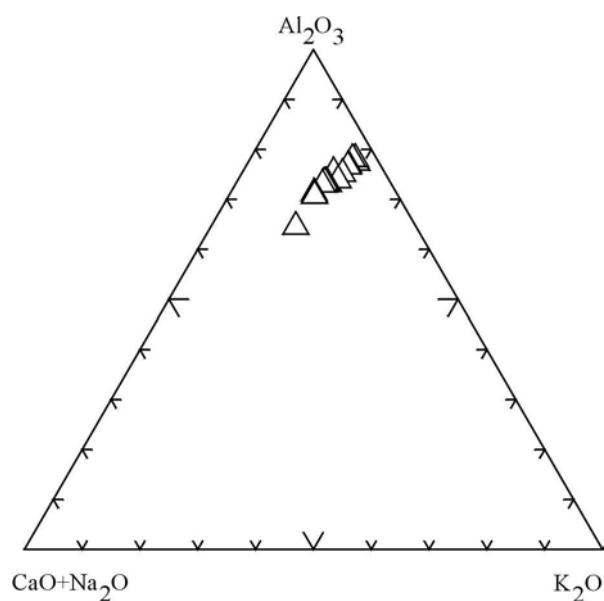


Fig. 50: Ternary diagram of alumina and alkalis of mudstones originating from the Ganigobis Shale Member (after Visser and Young, 1990). Chemical Index of Alteration (CIA) values may be read along a vertical axis drawn upward from the centre of the base of the diagram revealing values which range between 70 and 80 for the mudstones of the Ganigobis Shale Member.

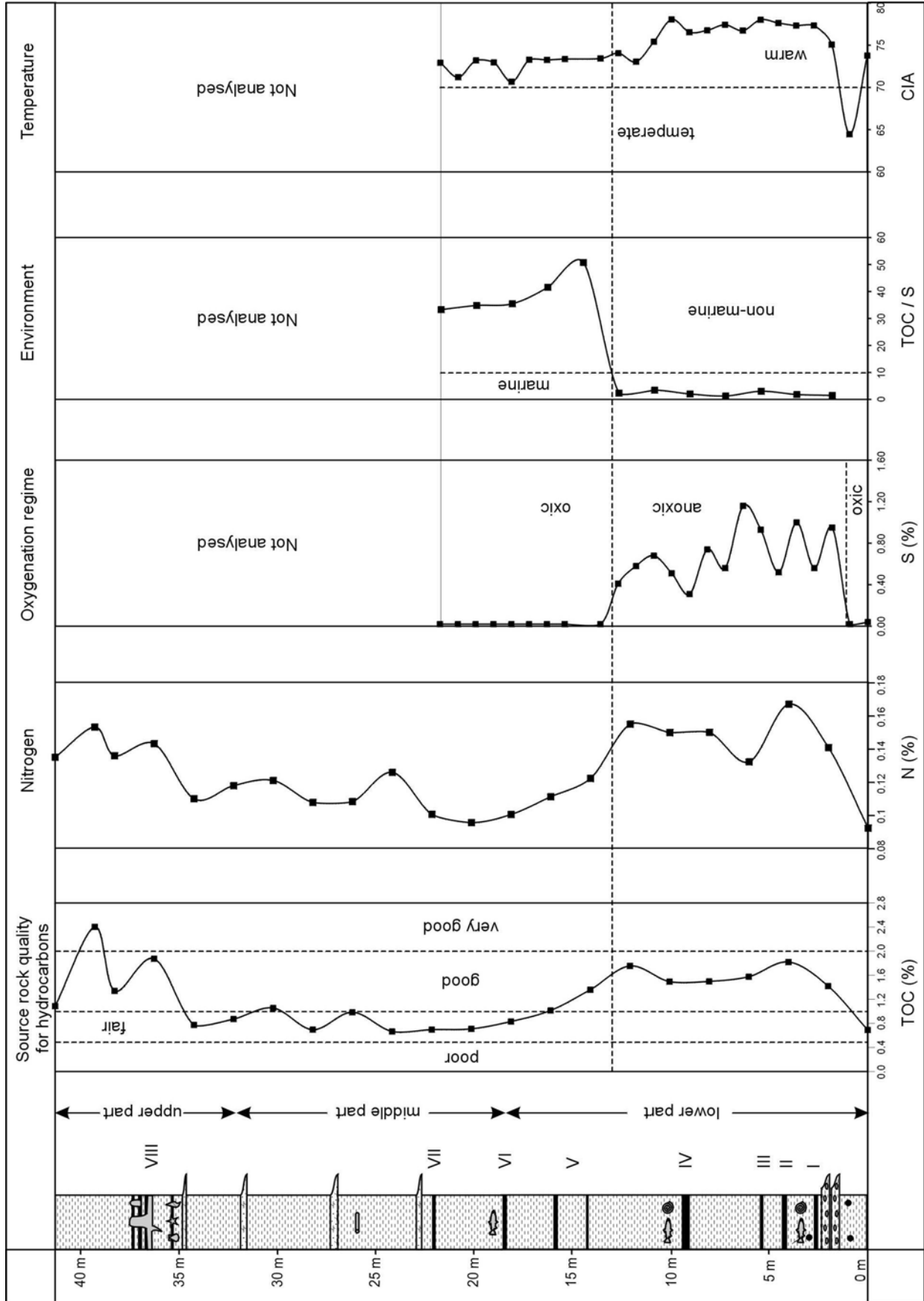


Fig. 51: Combined diagram of the Ganigobis Shale Member including tephrostratigraphy and major fossil appearances combined with charts of TOC, N, S, TOC/S and CIA. See text for explanation.

4.3 Gamma-ray spectrometry of the mudstones

Gamma ray logs provide a measure of the natural radioactivity of rocks which are used extensively in the hydrocarbon industry to interpret the lithology of rocks in the sub-surface. The logs record changes in mineralogy as opposed to simply changes in grain-size. In order to correlate outcrops within the Ganigobis Shale Member independently from the tuff beds, a portable Exploranium gamma-ray spectrometer was used in the field to measure radioactive potassium (^{40}K), uranium (^{238}U) and thorium (^{232}Th)-contents in 27 outcrops. All measurements are listed in Tab. 21 in Appendix C.

4.3.1 Theory and methodology of Gamma-ray spectrometry:

Theory: Almost all natural gamma radiation originates from the decay of the three radionuclides ^{40}K , ^{238}U and ^{232}Th . During radioactive decay these elements emit high-energy electromagnetic radiation (gamma-rays). By measuring the intensity and the energy of these gamma-rays at a particular location, the abundance of K, U and Th can be determined. K only emits a single gamma ray, whereas both U and Th emit a number of gamma rays of different energies but only one is usually measured by the detector of the spectrometer. The Exploranium Gr-320 gamma ray spectrometer used in this study is able to detect gamma rays emitted from rock surfaces and to divide them into four channels: (1) total gamma rays of all energies; (2) ^{40}K gamma rays; (3) ^{214}Bi gamma rays from the uranium series; (4) ^{208}Tl gamma rays from the thorium series (Myers and Wignall, 1987).

In marine mudstones K and Th is mainly embodied in clay minerals, detrital K-feldspar and mica. Illite, for example, carries between 3.4 and 8.3 % K (Myers and Wignall, 1987). Quartz contains an average of 2 ppm Th whereas illite has 10-25 ppm Th. Unlike Th, uranium can also be partly dissolved in the oceans as uranyl carbonate complex which might lead to an enrichment of the sediment by non-detrital U. U

and Th are mainly contained in the accessory minerals such as zircon (up to 6000 ppm U and up to 4000 ppm Th) or monazite (up to 3000 ppm U and up to 200000 ppm Th). The latter two are particularly concentrated in acidic ashfall tuffs.

Methodology: The detector measures the natural radioactivity in a diameter of 2 m, the main contribution occurs within a diameter of 0.5 m. Measurements were carried out at intervals of approximately 0.5 m; single, cm-thick tuff beds were unfortunately not detectable. Sections should be as unweathered as possible since leaching of K and U may occur in deeply weathered rocks (Myers and Wignall, 1987). As a rock sample was taken with each measurement, the measurement was carried out within the cavity produced by the rock-sampling procedure. Measurements in cavities generally increase gamma-ray counts unrelated to lithology (Myers and Bristow, 1989) but as it was performed for all measurements, the ratios of K, U and Th should not be effected. The overall strong radioactivity of the mudstones allowed a short counting time of 60 s averaging 10000-11000 ppm of total gamma ray radiation.

4.3.2 Absolute U and Th-values and Th/K and Th/U ratios of the Ganigobis Shale Member

Gamma-ray measurements of outcrops #2, 15, 13, 18, 27 and 9 were combined as they represent the whole Ganigobis Shale Member (Fig. 54).

U-values range from 175 to 320 ppm U. Lowest values are found at the base of the Ganigobis Shale Member and in the middle part where silt- and sandrich, turbiditic horizons are more frequent. Major peaks of a high concentration of U mainly coincide with the occurrences of groups of tuff beds. With a higher percentage of heavy minerals such as zircon, monazite and apatite than in the surrounding mudstones, the tuff beds generally contain more radioactive uranium.

Th-values vary between 150 and 200 ppm Th between the base of the Ganigobis Shale Member and tuff beds IV. Above tuff beds group IV and further to the top of outcrop #2 Th-values rise and vary between 200 and 250 ppm Th. This trend might be due to mineralogical differences of the

mudstones such as different amounts of heavy minerals. Th-values remain high in most of the middle part of the Ganigobis Shale Member. They start to decrease in outcrop #18 and shrink to values of 150 to 200 ppm in the upper part of the Ganigobis Shale Member (Fig. 52).

Th/K ratio: Between tuff beds I and IV the Th/K-ratio varies between 5 - 6 whereas about 2 m above tuff beds IV the ratio increases significantly up to values of more than 8 and remains high further to the top of outcrop #2. In the middle and upper parts of the Ganigobis Shale Member ratios remain between 6 and 8 but tend to decrease slightly in the uppermost part. The increase in Th/K-values from below 6 up to more than 8 is in agreement with the onset of lamination within the mudstones starting close above tuff beds Vc. Increased clastic input leads to higher Th-values as thorium is mainly fixed in sand- and silt-sized heavy minerals such as the monazite and zircon groups (Davies and Elliott, 1996).

Th/U-ratio: Between tuff beds I and IV the Th/U-ratios vary between 2.5 - 6 averaging 3.5. Below and above tuff beds IV, ratios increase subsequently leading to an average of 5.3: They climax between tuff beds Vb and c with values of almost 10. Further peaks still reach 8.5 in the highest parts of outcrop #2. The middle part of the Ganigobis Shale Member shows values averaging 6.2 whereas values decrease to an average of 4.3 in the upper part of the Ganigobis Shale Member.

Adams and Weaver (1958) considered three geochemical facies in sedimentary rocks on the basis of 319 thorium and uranium determinations. Low Th/U-ratios below 2 are indicative of conditions where extraction from sea or fresh water is the major mechanism for the fixation of uranium in the sediment. This is mostly the case in marine black shales and phosphatic rocks but can also occur in pure carbonates, cherts and anhydrites. Intermediate Th/U-ratios between 2 and 7 are thought to reflect poorly weathered and rapidly deposited igneous rock detritus admixed with mud- and siltstones or greywackes. High Th/U-ratios above 7 may develop in two ways: (i) by the concentration of heavy minerals such as monazites and (ii) by the removal of uranium

during weathering and leaching leaving the relative insoluble thorium behind in high concentrations. Such a high concentration of Th is often found in placers, bauxites or deeply weathered paleosoils.

The marine mudstones of the Ganigobis and also the Hardap Shale Members of DS III never show Th/U ratios below 2 leading to the conclusion that the siltstones of the Hardap Shale Member (Th/U-ratios between 2 and 8) are admixed with terrestrial detritus whereas the silty mudstones of the Ganigobis Shale Member are blended with pyroclastic and detrital material. Low Th/U-ratios between tuff beds I and IV coincide with high TOC and sulphur contents of the mudstones in this stratigraphic interval which suggests anoxic depositional conditions (Fig. 51). Sediments deposited under anoxic conditions tend to fix uranium and allow the preservation of organic matter (Myers and Wignall, 1987). The highest peaks between tuff beds V and VI are associated with a mostly well defined lamination of the shales in this part of the Ganigobis Shale Member leading to the removal of uranium by the input of heavily weathered detritus from the land. The middle part of the Ganigobis Shale Member still shows high Th/U-ratios although obviously less pyroclastic substrate was deposited and the shales are not laminated. The upper part of the Ganigobis Shale Member shows high deviations of the Th/U-ratios implying an increased input of pyroclastic material with the group VIII tuff beds climaxing in a Th/U-ratio of almost 8 just below tuff bed VIIIa in outcrop locality #27.

4.3.3 *Correlation of outcrops within the Ganigobis Shale Member*

The two largest outcrops of the lower part of the Ganigobis Shale Member at localities #2 and 23 can be correlated on the basis of Th/K and Th/U-ratios obtained by gamma ray measurements. Both outcrops exhibit very similar curves, especially when considering the Th/K-ratios. The rapid increase in the Th/K-ratios documented earlier in the study (cf. Chapter 4.3.2) is documented in both outcrops. The Th/U-ratios show similar patterns but the correlation is not as easy as with the Th/K-ratio. (Fig. 52 and Fig. 53).

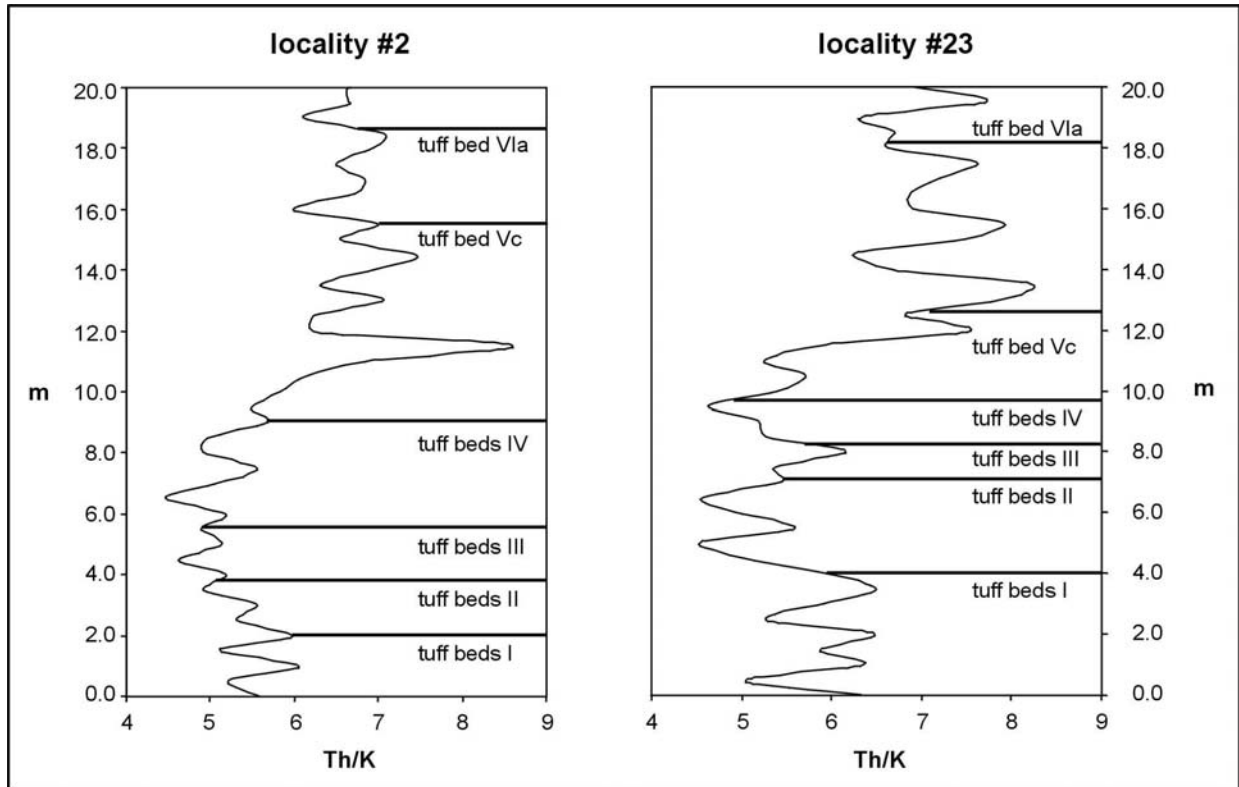


Fig. 52: Th/K-ratios of the lower half of the Ganigobis Shale Member in outcrops # 2 and 23 based on gamma-ray spectrometry. Peaks are mostly associated with the occurrence of the tuff beds, see text for discussion.

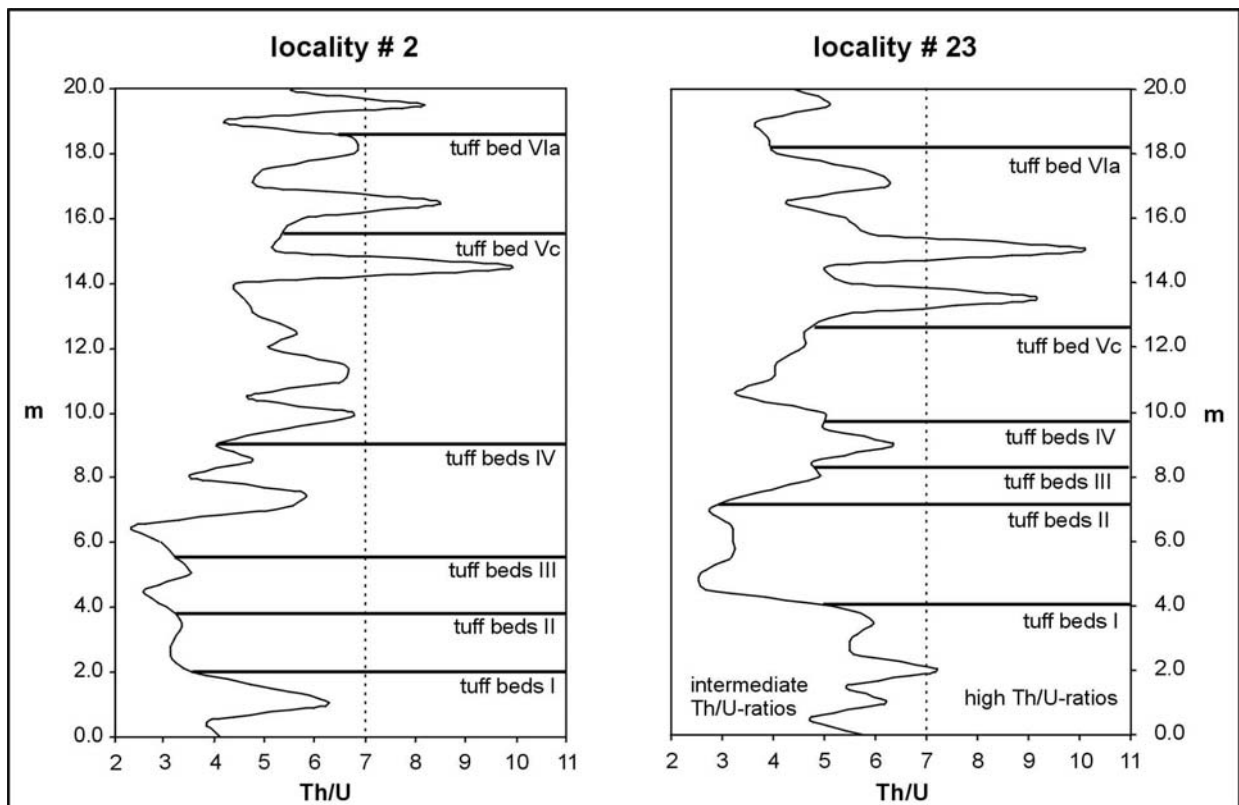


Fig. 53: Th/U-ratios of the lower half of the Ganigobis Shale Member in outcrops # 2 and 23 based on gamma-ray spectrometry; subdivision of the Th/U-ratios according to Adams and Weaver (1958); see text for discussion.

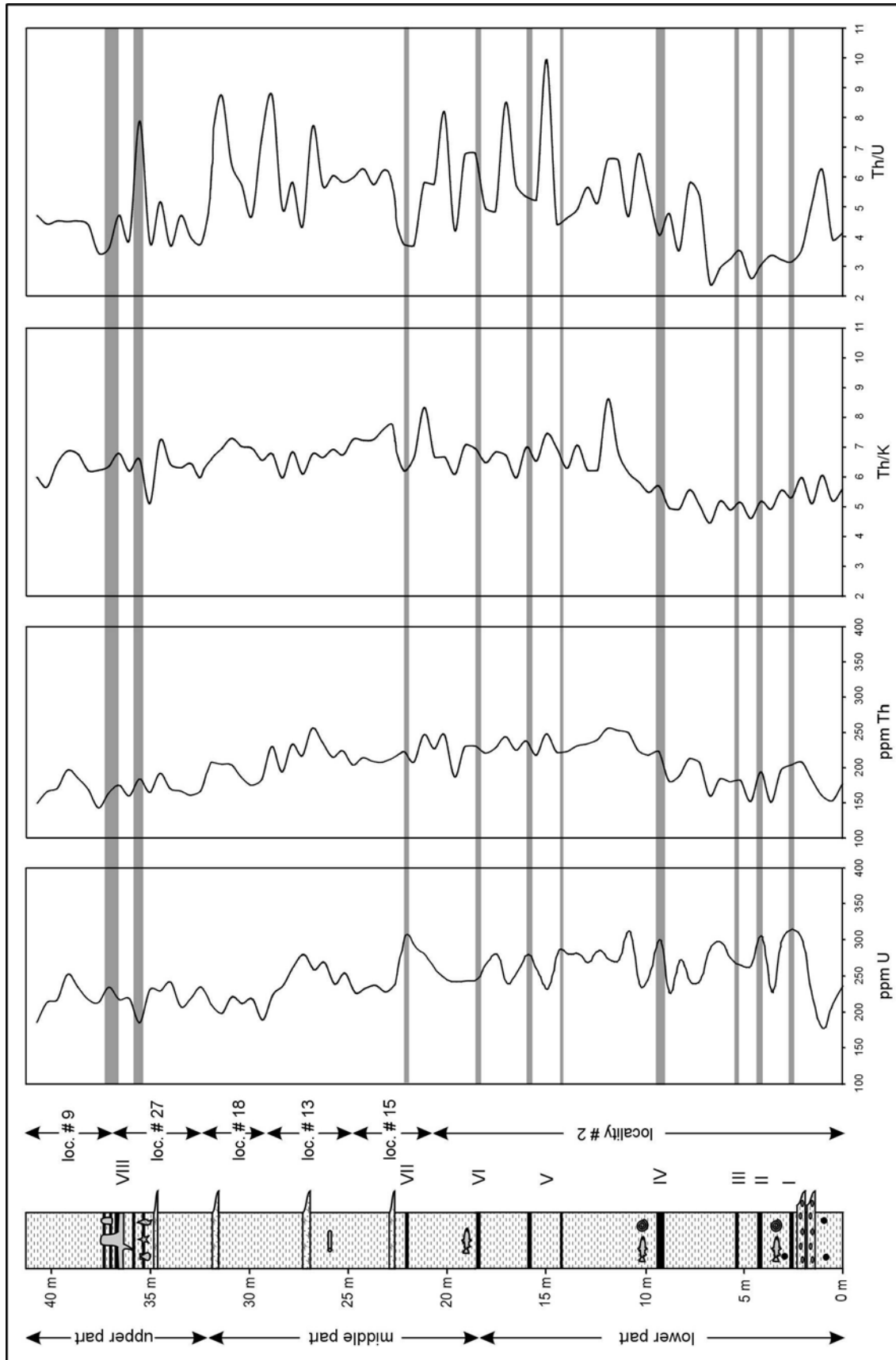


Fig. 54: Combined diagram of the Ganigobis Shale Member including tephrostratigraphy and major fossil appearances combined with gamma ray spectrometry-based charts of U and Th (ppm) and ratios of Th/K and Th/U. See text for explanation.

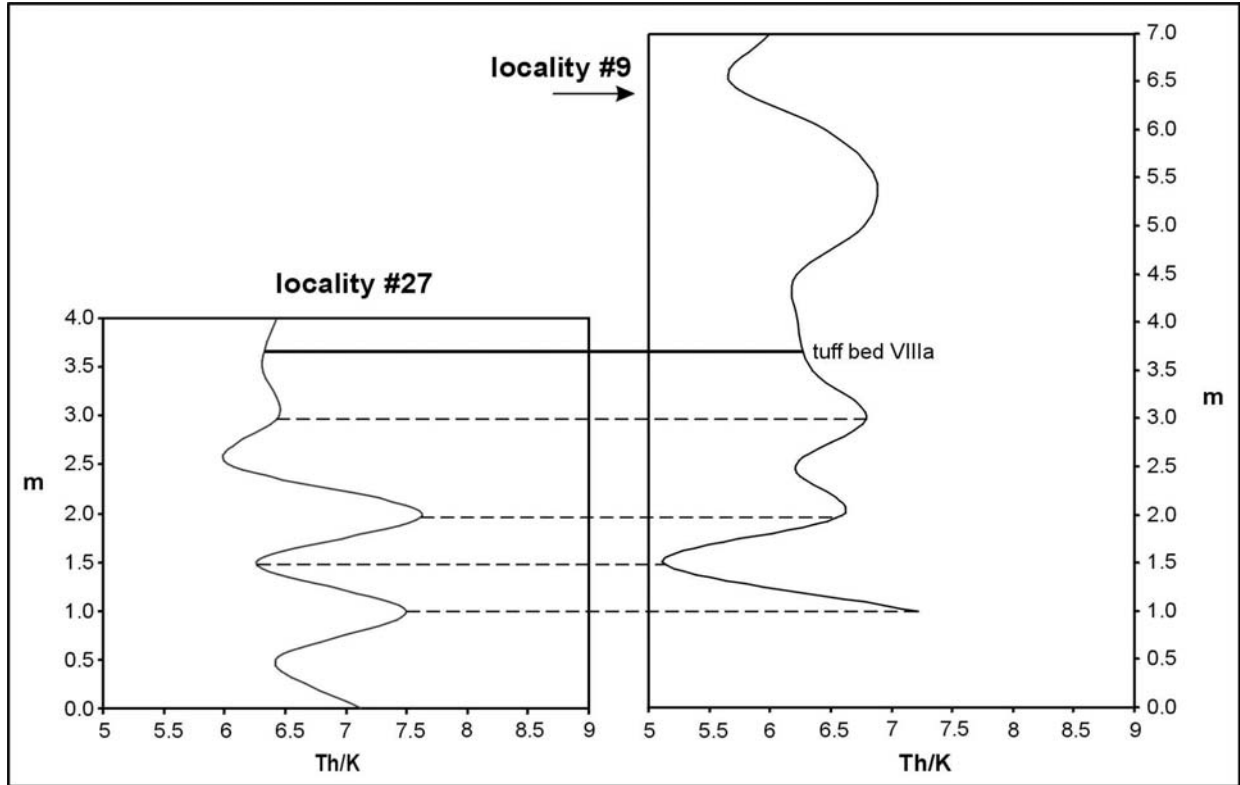


Fig. 55: Th/K-ratios of the upper part of the Ganigobis Shale Member in outcrops # 27 and 9 based on gamma-ray spectrometry, see text for discussion.

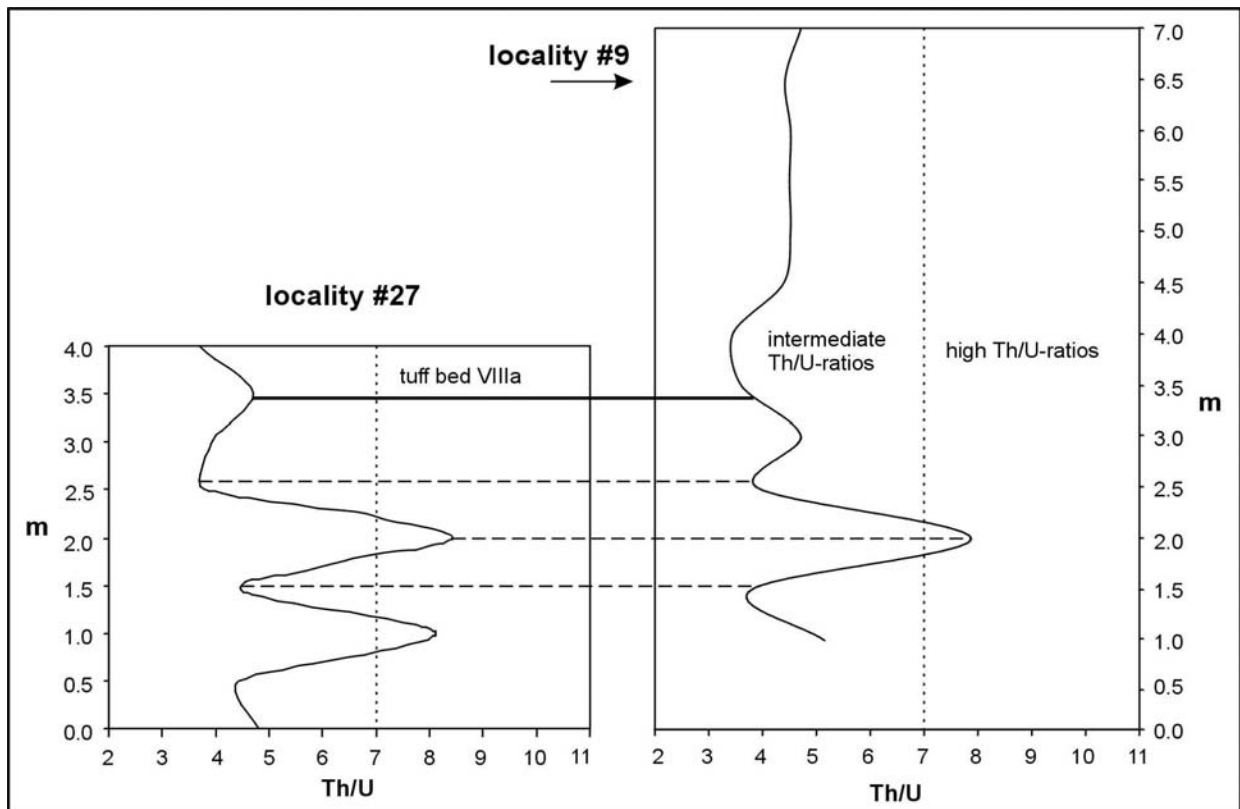


Fig. 56: Th/U-ratios of the upper part of the Ganigobis Shale Member in outcrops # 27 and 9 based on gamma-ray spectrometry; subdivision of the Th/U-ratios according to Adams and Weaver (1958); see text for discussion.

Outcrops in the middle part of the Ganigobis Shale Member were too small (3-4 measurements) to be correlated with each other. Two outcrops in the upper part at localities #9 and 27 can also be perfectly correlated. Based on tuff bed VIIIa existing in both outcrops, the whole outcrop of locality #27 can be correlated to the lower part of the outcrop at locality #9. In outcrop locality #27 Th/K-ratios vary between 6 and 7.5 and Th/U between 3.5 and 8.5 whereas in outcrop locality #9 the ratios diverge between 5 and 7.5 for Th/K respectively 3.5 and 8 (Fig. 55 and Fig. 56).

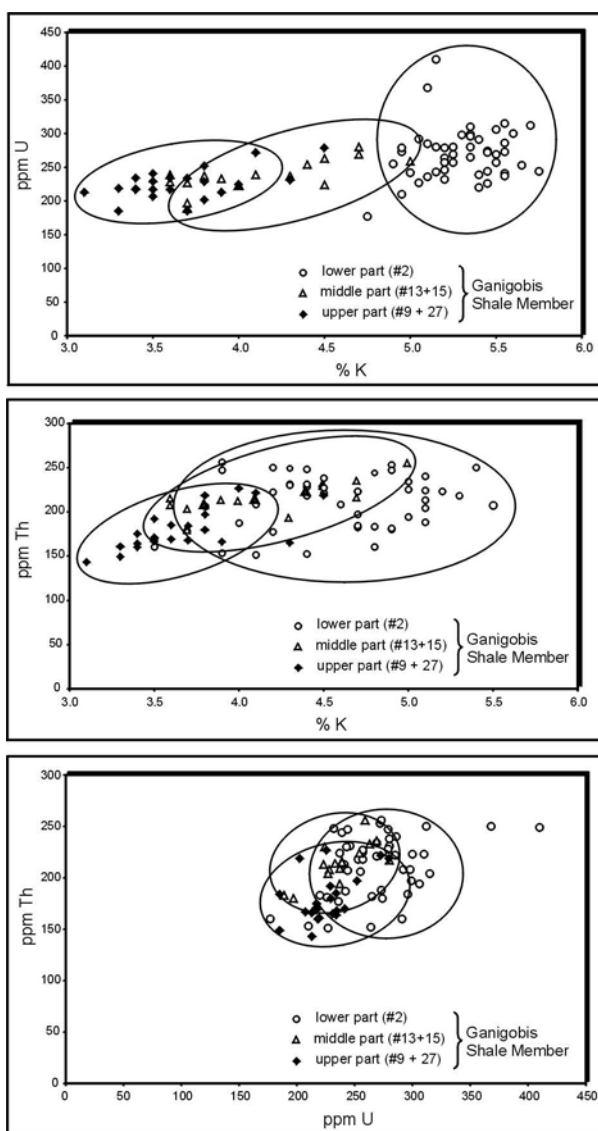


Fig. 57: K(%) vs. U (ppm), K (%) vs. Th (ppm) and U (ppm) vs. Th (ppm) – plots confirming the threefold subdivision of the Ganigobis Shale Member by gamma-ray spectrometry.

4.3.4 *The threefold subdivision of the Ganigobis Shale Member from the perspective of gamma ray spectrometry*

The threefold subdivision of the Ganigobis Shale Member in a lower, middle and upper part can be deduced from the results of the gamma ray measurements. K, Th and U values of outcrop localities # 2, 13 and 15, 9 and 27 were plotted against each other. The K vs. U-plot shows that there are significant differences between the lower, middle and upper parts of the Ganigobis Shale Member. Mudstones of the lower part (locality #2) have 5-6 % ^{40}K and 200-350 ppm ^{238}U whereas mudstones of the middle part contain 3.5-5 % ^{40}K and 200-300 ppm ^{238}U . Most measured mudstones of the upper part carry only 3-4 % ^{40}K and 200-250 ppm ^{238}U .

This threefold subdivision is less obvious within the K vs. Th and U vs. Th-plots but can still be maintained. Th-values vary between 150 and 250 ppm (Fig. 57).

4.4 Conclusions: The depositional history of the Ganigobis Shale Member

The Ganigobis Shale Member forms the uppermost part of deglaciation sequence II within the Dwyka Group of southern Namibia. It has a thickness of more than 40 m and consists mainly of argillaceous rocks with interbedded but inconsistent sandstone horizons which reach thicknesses of up to 1 m.

4.4.1 *The base and the lower part of the Ganigobis Shale Member up to tuff beds VI.*

The Ganigobis Shale Member is underlain by a clast-poor, up to 30 m thick diamictite unit. It is characterised by a fine-grained sandy to silty matrix which formed by debris-rain out in a marine setting and changes gradually up-section into massive or laminated mudstones with lonestones. Within the Ganigobis Shale Member dropstones occur in decreasing numbers towards a level 0.7 m below tuff bed Ia. Between groups of tuff beds II and V isolated dropstones were found whereas dropstones are completely absent higher up in the succession. The majority of the

dropstones are well rounded to subrounded, a few are also faceted and striated. A maximum clast size of 0.6 m was determined, with an average of about 1 cm. Clasts mainly comprise red and grey quartzites, less frequently also granitic and undeformed gabbroid, trachytic, andesitic and basaltic dropstones occur, the latter two being frequently amygdaloidal. The Ganigobis Shale Member is followed by massive mudstones with limestones which mark the onset of deglaciation sequence III.

The dropstones were generally released from debris-laden floating ice in a glaciomarine environment. Due to the rather uniform lithology of the Ganigobis Shale Member, the mudstones seem to have been deposited rather distally with respect to the ice-margin. As deglaciation became stronger in the course of DS II, glaciers started to produce more debris-laden floating ice. Rain-out of this debris formed the partly clast-rich diamictites underlying the Ganigobis Shale Member. With the successive retreat of the ice-margin less debris-laden ice reached the area of Ganigobis resulting in mudstones with less frequent dropstones. The deposition of dropstones was rather rapidly stopped at a tephrostratigraphic level about 0.7 m below tuff bed Ia.

The contemporaneous marine transgression proceeding from the south and south-west produced water depths of probably up to 600 m. Martin and Wilczewski (1970) deduced from radiolarians and from a goniatite found at Schlip (Fig. 1) in combination with the sloping of the Dwyka Group-deposits. Only argillaceous material reached this part of the basin forming the mudstones of the Ganigobis Shale Member. The marine transgressions climaxed between tuff beds I and II, between IV and V and above VI. These parts of the Ganigobis Shale Member contain the discovered fish fossils and coprolites and are interpreted as marine condensed sequences with starved sedimentation and accumulation of organic matter during sea-level high stand (cf. Chapter 4.2.3). Sulphur contents within the mudstones are also high between tuff beds I and IV leading to the conclusion that the depositional environment at the bottom of the basin was anoxic (Fig. 54). Ground-living fossils were therefore not discovered in this part of the

section. Ratios of TOC/S and TOC/N confirm an overall marine environment (cf. Chapter 4.2.3 and 4.2.4).

Between the tephrostratigraphic levels I and IV 11 of the 21 recognised tuff beds are interbedded. This pronounced phase of volcanism and the sudden change in climate and rise in sea-level may have depended on each other. Eldholm and Thomas (1993) have speculated that the generation of voluminous fine-grained volcanic ash, the ascent of eruption columns into the Earth's stratosphere and associated volcanically released CO₂ may have pronounced effects on solar insolation. Resultant climatic changes through the greenhouse effect may be the prime cause of eustatic sea-level changes.

Detailed geochemical analysis of the mudstones of the Ganigobis Shale Member (cf. Chapter 4.2) revealed a dramatic change in the sulphur values, but also TOC and nitrogen decreased at about 1 m below tuff bed Va. As sulphur values fall below the detection limit of 0.02 %, the depositional conditions at the bottom of the basin changed to a more oxidised state. Both, TOC and N-values decrease to about 50 % which is probably due to an increased sediment supply. Increased sediment supply is defined by a distinct lamination of the mudstones starting close above tuff bed Vc. Low sulphur contents lead to high TOC/S ratios averaging about 40 which indicate rather brackish or more likely non-marine conditions (Berner and Raiswell, 1984). CIA-values are always higher than 70 (with one exception) indicating a relatively warm climate. Values below tuff beds IV average almost 77 whereas above tuff beds IV values decrease to 73 on average indicating a climate deterioration (Visser and Young, 1990; Fig. 51).

4.4.2 The middle part of the Ganigobis Shale Member between tuff beds VI and VIIIa.

The middle part is characterised by monotonous black mudstones which contain normally graded, calcareous sandstone interbeds (cf. Chapter 2.4). Tuff bed VII is the only tuff bed which is preserved within the mudstones.

The calcareous sandstone interbeds interpreted as distal turbidite deposits and abundant permineralised fossil wood imply a smaller

distance to the shoreline compared to the basal part of the Ganigobis Shale Member. Water depth probably decreased and oxidizing conditions prevailed at the bottom of the basin. The salinity of the water remained still low favouring at least brackish conditions probably due to a high discharge of melt water. TOC-values remained below 1 % and N-values below 0.12 %. They correlate positively with each other as all nitrogen is fixed within the organic matter. Sulphur contents of the mudstones are concentrated in single, yellow weathered pyritic mudstone concretions with maximum sizes of 30 x 8 cm and in smaller, pyritic concretions which are horizontally aligned within the mudstones (cf. Chapter 2.4). Up to 0.2 m high, reef-like build-ups of grey, microbial limestone which rest on 5 cm thick microbial limestone mats are found higher up in the middle part of the Ganigobis Shale Member indicating rather low water depths.

4.4.3 *The upper part of the Ganigobis Shale Member above tuff bed VIIIa.*

The upper part of the Ganigobis Shale Member is marked by abundant fossils which differ considerably from the basal part. TOC and N-values rise significantly and peak in values of 2.4 and 0.15 %. These might coincide with another marine condensed sequence in which four tuff beds, microbial bioherms and sessile-living fossils are preserved. Interestingly, no palaeoniscoid fish remains were discovered. Water depths remain very low as indicated from the occurrence of microbial bioherms. Sessile-living fossils such as the bivalves, gastropods, scyphozoans and crinoidea point to oxidizing conditions at the bottom floor of the basin. The observation that abundant fossils of only one particular species (e.g. the gastropod *Peruvispira vipersdorfensis*) are concentrated at certain stratigraphic levels within strictly confined horizons most probably indicates a temporarily stressed environment. The latter was probably caused by short-term changes in sea water salinity, presumably during peaks of freshwater discharge.

About 3 to 5 m of dropstone-free mudstones of the Ganigobis Shale Member are exposed above the uppermost tuff bed VIIIId. The shales tend to

change their colour from black to green indicating an admixture of silt. Mostly granitic or gneissic dropstones within green siltstones witness the existence of debris-laden ice-rafts and a successive progradation of the ice-margin respectively of single glaciers leading to a climate deterioration.

5 Ganigobis Shale Member-equivalents at Zwartbas (Karasburg Basin, southern Namibia)

5.1 Geological setting

Equivalents of the Ganigobis Shale Member are well exposed over a distance of about 1 km along the northern banks of the Orange River at Zwartbas (28°41'43" S / 17°33'26"E to 28°41'19" S / 17°33'62" E) which is located about 10 km west of Noordoewer just north of the international boundary between Namibia and South Africa (Fig. 1).

Sediments of the Karoo Supergroup rest discontinuously on deposits of the folded Late Precambrian to Early Cambrian Nama Group (Gresse and Germs, 1993). Polished surfaces with parallel NNE-SSW oriented grooves, furrows and scratches are witnesses of glacial erosion prior to the sedimentation of the glacial Dwyka Group (Geiger, 2000a). Generally, Karoo deposits at Zwartbas yield Late Carboniferous glacio-marine shales containing abundant dropstones which are overlain by non-glacial shales of the Permian Prince Albert-Formation. The distinctive feature to discriminate between both units is the dropstone content, which marks a glacially to non-glacially controlled sedimentary environment. The Prince Albert-Formation is cut off by an intrusive body of the Jurassic Tandjesberg Dolerite Complex which penetrated the shale units. The tectonic setting and palaeogeographic reconstructions of the outcrops located within the Karasburg Basin of southern Namibia were already elaborated in Chapter 1.2.

Deposits of the Dwyka Group mainly consist of dropstone-bearing mudstones which are about 145 m thick (Fig. 58). Lodgement tillites, dropstone-rich diamictites and coarse grained

clastic deposits occur especially at the base, intercalated calcareous mudstone concretions and calcareous sandstone horizons are found throughout the whole sequence. The Dwyka Group-sediments at Zwartbas contain a greater number of bentonitic ash beds than equivalent strata in the Aranos Basin further north. 65 distinct ash tuff beds, 0.1-3.5 cm thick, occur in 38 groups within the lower 95 m of the succession. All significant features which are dealt with in this contribution appear up to the level of tuff bed group XXX (55 tuff beds) which comprises the lowermost 70 m of the Dwyka Group.

The dip of Dwyka Group sediments changes over a distance of about 500 m from flat lying strata in the east to steeply dipping strata in the west along the banks of the Orange River. The change of dips is attributed to deformation caused by overriding glaciers. Minor displacements by WNW-ESE running normal faults are considered to be of post-Permian age.



Fig. 58: River banks of the Orange River banks near Zwartbas consisting of the glaciomarine Dwyka Shales (Geiger, 2000a: locality #1: S 28°41.432' / E 017°33.256'). The river banks are up to 30 m high.

5.2 The tuff beds of the Dwyka Group at Zwartbas

Altogether 65 tuff beds were discovered at the cut banks along the Orange River which are less altered than the tuff beds exposed in the Aranos Basin further north. Successive tuff beds, which occur in small, mostly cm-thick intervals, were combined into tuff groups which led to the subdivision into 38 tuff groups. The colour of the

beds is generally yellow, in cases they appear white and their thickness is occasionally enlarged due to secondary gypsum. The tuff beds are less than 1 mm to a few mm thick, tuff beds such as X, XIX and XXIVa reach thicknesses up to 4 cm (Fig. 59).



Fig. 59: Bentonitic tuff beds XVIIIId (maximum thickness: 15 mm), XIX (maximum thickness: 35 mm; at head of hammer) and XXa (maximum thickness: 2 mm) at Zwartbas, note that tuff bed XXa is totally replaced by gypsum (S 28°41.432' / E 017°33.256').

The highest frequency of tuff beds are found from below 50 to 70 m above the base of DS II, where 30 ash layers could be detected within 20 m. The tuff beds are laterally continuous and can be excellently traced along the river banks. They are relatively soft and swell in contact with water due to their high amount of illitic-smectitic clay minerals. Signs of bioturbation could not be detected, the tuff beds are macroscopically not graded and are compact. They apparently do not contain material of the background sedimentation which points to rapid deposition of the tuff beds and a insignificant background sedimentation. As an exception tuff beds IIIb and c are separated by a darker bed of tuffaceous shale (Fig. 60).



Fig. 60: Tuff bed IIIb passes to the top into darker, tuffaceous shale and is overlain by tuff bed IIIc (S 28°41.103' / E 017°33.551').

5.3 The base of the Dwyka Group at Zwartbas

Either fissile black shales or yellow to red calcareous lodgement tillites with cone-in-cone structures superpose the unconformity at the base of the Dwyka Group. If the lodgement tillite does not rest directly on the unconformity, it overlies an up to 70 cm thick shale unit which might belong to DS I. The lodgement tillite representing the base of DS II is mainly found in morphological depressions and in cavities (Fig. 61).



Fig. 61: Calcareous lodgement tillite resting directly on Nama Group rocks which show NNE-SSW oriented glacial striations (S 28°41.432' / E 017°33.256') at lower left.

Lithology and average size of the clasts in the tillite and in the shale are similar. Quartzites, gneiss, granites and cherts rarely exceed 5 cm in the basal shale and 10 cm in the lodgement till. Near the road to Rosh Pinah (S 28°40.927' / E

017°32.380'), the tillite itself shows glacial striations which indicate a second ice advance. Additionally patches of trough cross-bedded sandstone overly the tillite. The red, moderately sorted, graded, but mature sandstone carries sporadically coarser clasts. The sandstone is interpreted as a fluviually deposited sandy drift of an esker. The coincidence of fluvial and subglacial facies associations in the lowermost 2 m of the Dwyka Group-deposits at Zwartbas suggests a continental environment especially when the red colour of the tillite and the sandstones is taken into account.

Laminated mudstones with a thickness of 50 cm appear about 2.5 m above the unconformity. The lamination consists of alternating green clay and brown silt layers. A few dropstones are found within them. A 74 mm thick section contains 14 couplets of clay and silt; a single layer therefore averages 2.64 mm (Geiger, 2000a).

5.4 Marine, periglacial deposits at Zwartbas

From 2 m above the base of the Dwyka Group to the top of the Dwyka Group silty shales and diamictitic shales grade into each other and are hard to distinguish from each other as the appearance of dropstones is accidental (Geiger, 2000a). Diamictitic shales are units with an increased content of dropstones.



Fig. 62: Dropstone-bearing shale with hammer-sized dropstone just above the hammer. Markus Geiger is pointing at tuff beds IIIb + c (right arm) and IIIc (left arm); (S 28°41.103' / E 017°33.551').

Dropstone-bearing horizons varying between 0.2 and 1.5 m in thickness were found between tuff markers IIIb and IIIe, above Vb and XIb, below XXXIV and 3.5 m above XXXVIII (Fig. 62). The majority of the dropstones are well rounded to subrounded, a few are also faceted and striated. A maximum clast size of 1.5 m diameter was determined. Dropstones mainly comprise subangular plates of grey to green schist and quartzite, less frequently pebbles of granite, pegmatite, gneiss, and amygdaloidal basalts occur (Bangert *et al.*, in press). The whole sequence is believed to have been deposited in a periglacial marine environment and probably belongs to DS II as major incisions could not be detected throughout the succession.

About 40 m from the base of the Dwyka Group a bed of clast-poor diamictite is present (“Hippo Diamictite”; Geiger, 2000a). It is an unsorted, non-graded, matrix-supported diamictite with a grey calcareous silty matrix without any sedimentary structures. Its thickness varies laterally from 30 cm to 80 cm (Fig. 63).

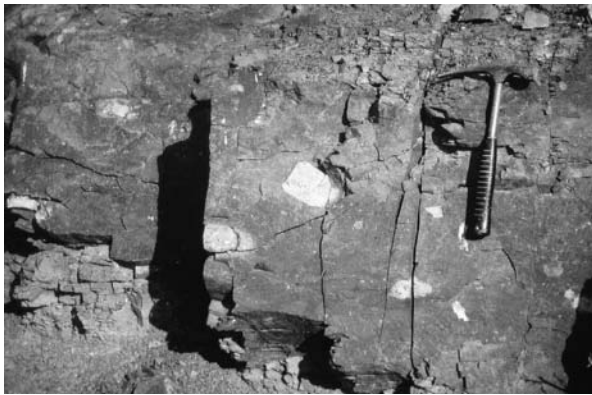


Fig. 63: 30 - 60 cm thick, massive bed of clast-poor diamictite with up to 15 cm large, mostly quartzitic or gneissic, rounded dropstones (“Hippo Diamictite”; Geiger, 2000a) probably formed by Heinrich events (S 28°41.432' / E 017°33.256').

This coarse diamictite bed is interpreted to represent a phase of increased terrigenous input due to the onset of deglaciation. Withdrawing and melting glaciers tend to more frequent calving. The more icebergs get detached and drift off, the more material is carried off and discharged, leading to the abundance of clasts within the diamictitic layer. Similar surpassing temporary

discharge of coarse grained iceberg-rafted debris (Heinrich layers) in the North Atlantic was discovered by Heinrich (1988). He ascribed them to instabilities of the ice-stream flow within the Laurentide Ice Sheet (Heinrich, 1988; Seidov and Maslin, 1999).

A convolute bedded marlstone with increased clast content turns up about 100 m above the base of the Dwyka Group (“Goats Cliff Diamictite”, Geiger, 2000a). Quartzite and gneiss constitute the clast lithology with a typical EACS of 4 to 6 cm and a clast packing density (CPD) of 40 to 50. The sediment is contorted, suggesting either gravity induced sliding of the unlithified material or glacially induced shear movements in the lithified state.

The shales display two types of concretions which are frequently found throughout the complete succession.

i, Black, perfectly rounded or oval nodules and larger bodies with sinuously rounded bodies, occasionally fossil-bearing, are the first type of concretions. They consist of carbonate-cemented mudstone. The nodules occur either isolated or are enriched in horizons. They normally vary from 5 to 20 cm in horizontal and from 10 to 40 cm in vertical diameter.

ii; Pervasive bodies of black concretions occur between tuff bed groups XI and XII and above XXXIII. They are up to 30 cm thick, but extend laterally several metres. Yellow and brown laterally persistent concretionary layers up to 60 cm in thickness are also found throughout the whole succession.



Fig. 64: Tuff bed IIIb on the right passes into an up to 20 cm thick, massive, brown, calcareous bed (S 28°41.103' / E 017°33.521')

In cases, they pass into tuff beds. It is thus possible that they developed from altered ash layers (Fig. 64). Cone-in-cone structures indicate a certain carbonate content. The dark brown colour probably originates from higher iron content (Geiger, 2000a).

5.5 The occurrence of fossils within the glaciomarine deposits at Zwartbas

Similar to the Ganigobis Shale Member in the Aranos Basin, fossils were found concentrated in certain stratigraphic intervals. The highest frequency of fossils occurs between tuff beds VI and X, the second major interval with abundant fossils is located between tuff beds XIV and XVI.

5.5.1 *Palaeoniscoid fish remains*

Several concretions which contain remnants of fish fossils occur from 2 m below tuff beds VI to 1.5 m below tuff beds XI (about 30 m to 33 m from the base of the Dwyka Group) and between tuff beds XIV to XVIa (about 48 m to 51 m from the base of the Dwyka Group). These fish remains are mainly found within siliceous-phosphatic nodules. Single bones, scales or sometimes moulds of more or less complete, but deformed bodies, about 25 cm long, are present. Pyrite veins occasionally stretch across these fossiliferous concretions. The fishes correspond with the findings near Ganigobis in the Aranos Basin and are determined as *Namaichthys schroederi*.

5.5.2 *Spiral coprolites*

Spiral coprolites are the most abundant fossils at Zwartbas. They have been determined at four stratigraphic levels, coinciding with tuff beds VIa-VIIIb, 2 m below XIb, and immediately below XV and XXIX. The coprolites are up to 10 cm long and have a radial diameter of about 2 cm. They are similar to the ones found near Ganigobis.

5.5.3 *Gastropods*

Only one evolute, trochospiral gastropod shell, measuring 0.6 cm in length, was found between tuff beds XXIV and XXV but could not be

specified accurately.

5.5.4 *Bivalves*

An external shell mould was detected between tuff beds IX and X. Only a part of one valve could be excavated. The body is crescent-shaped with a bending ridge extending from the shorter wing to the middle of the convex side. Dendritic structures cover the shell. The shape suggests a bivalve but it could not be determined to further detail. McLachlan and Anderson (1973) report the find of a bivalve classified as *Phestia* sp., whose contour and shape is similar to the new finding (Geiger, 2000a).

5.5.5 *Radiolaria*

Between 0.5 and 1.0 mm large calcispheres occur from tuff group VIa to XXV. The spheres are only found within concretions. The SiO₂ of the radiolaria was replaced by carbonate which destroyed the former internal structures. They are similar to the ones from the Ganigobis Shale Member in the Aranos Basin (cf. Chapter 3.7).

5.5.6 *Permineralised wood*

Permineralised wood is found as small branches with a diameter of 2 or 3 cm and as logs with diameters up to 30 cm. Cross-sections generally show an oval shape as the logs are flattened by the load of the overlying rocks. Growth rings are usually well preserved and vary from 2 to 10 mm. Coalified wood sometimes shows pyrite concentrated on growth ring boundaries. Samples were found to concentrate at four stratigraphic levels, either enclosed in concretions or dispersed in the sediment. Logs associated with tuff group VI record an E-W to ESE-WNW trending alignment; about 3 m up section (tuff groups IX and X) wood fragments are oriented NE-SW. Further 15 m higher up in the section (tuff XVI) permineralised wood logs vary considerably in their orientation over the following 16 m but are then oriented in a preferred ESE-WNW direction immediately below tuff group XXVIII.

5.5.7 *Trace fossils*

Traces of *Helminthopsis* isp. occur only 1.1-1.6 m above the base of deglaciation sequence II

within the varved horizon. The highest degree of bioturbation, however, is developed in the central part of the section. At the level of tuff beds X to XI, horizontally or vertically oriented, isolated burrows are present showing a length of 2-3 cm. The 0.5 cm thick hollow tubes with 0.1 cm thick walls are often filled with calcite. Conspicuous worm-shaped traces identified as *Taenidium serpentinum* were observed at the stratigraphic levels of tuff group X, 2 m to 3 m above beds XI and below tuff group XV. These traces cover black, fossiliferous concretions occurring within the mudstones. Fracture planes in the rocks display transverse sections of the bioturbated sediment, as sediment-filled burrows wind their way through the mud without apparent orientation. The traces were probably produced by an infaunal deposit feeder.

Between tuff groups IX up to 3 m above XI intrafaunal burrows are regarded as *Chondrites intricatus*. A main burrow diverges downward into a number of branches similar to an upside-down tree. The trace fossil was frequently observed on fractured surfaces of concretions. *Chondrites* isp. generally suggests marine conditions and is often associated with low-oxygen substrates.

Two or even three, subparallel, cylindrical tubes constituting the long axis of conical or cylindrical siliceous mudstone concretions, up to 5 cm in diameter, represent the trace fossil *Tisooa* isp.; it was found between tuff beds XXVIII and XXXI. This type of trace fossil is a burrow generated either by an arthropod (Frey and Cowles, 1969) or suspension-feeding bivalves (Wang, 1997).

A simple, tube-like, up to 3 cm long and 0.8 cm wide, vertically oriented burrow is the most abundant and pervasive fossil. *Skolithos* isp. appears with only few interruptions from tuff group II to XXX (Geiger, 2000a). Photographs of most of the fossils are found in Geiger (2000a).

5.6 Comparison between the glaciomarine deposits at Zwartbas and near Ganigobis.

Both sequences are stratigraphically located within DS II and, comparing the ages (cf. Chapter 11.3) of SHRIMP-based analyses of zircons from

the tuff beds, both sequences possess a similar age of about 302 Ma. However, the glaciomarine deposits at Zwartbas are about 145 m thick whereas the whole Ganigobis Shale Member near Ganigobis has a thickness of more than 40 m. It is difficult to tell to which part of the sequence at Zwartbas the deposits near Ganigobis belong to. The lithology of the rocks is similar (silty mudstones), the dropstone content of the shales at Zwartbas is higher and more continuous than at Ganigobis where dropstones mostly occur in the lowermost 0.7 m. The correlation on the basis of tuff beds revealed as not possible. Equidistant plotting of the tuff beds of both localities unfortunately showed no convincing similarities (Fig. 65).

The maximum thickness of the tuff beds at Zwartbas is about twice the thickness of the tuff beds near Ganigobis, the outcrops at Zwartbas show 65 tuff beds altogether whereas outcrops near Ganigobis only contain 21 tuff beds.

The mudstone intervals between the tuff beds of both localities also do not resemble each other. TOC-values of the mudstones near Ganigobis are higher than in equivalents from Zwartbas (between 0.7 and 2.4 % averaging 1.2 % at Ganigobis and between 0.2 and 1.5 % averaging 0.7 % at Zwartbas).

Sulphur contents are relatively low in the mudstones from Zwartbas (cf. Geiger, 2000b), but change a lot in the mudstones from Ganigobis (cf. Chapter 4.2.4). CIA-values (Ganigobis: 74 vs. 74 at Zwartbas; Geiger, 2000b) and nitrogen contents in the analysed mudstone samples of both sequences are quite similar (Ganigobis: 0.09 to 0.17 % averaging 0.13 %; Zwartbas: 0.03-0.16 % averaging 0.13).

In both sequences, however, TOC and N-values correlate positively in combination with major occurrences of vertebrate and invertebrate fossils.

The Ganigobis Shale Member near Ganigobis revealed three major peaks probably coinciding with marine condensed sequences with starved sedimentation and high input of organic matter (cf. Chapter 4.2.3).

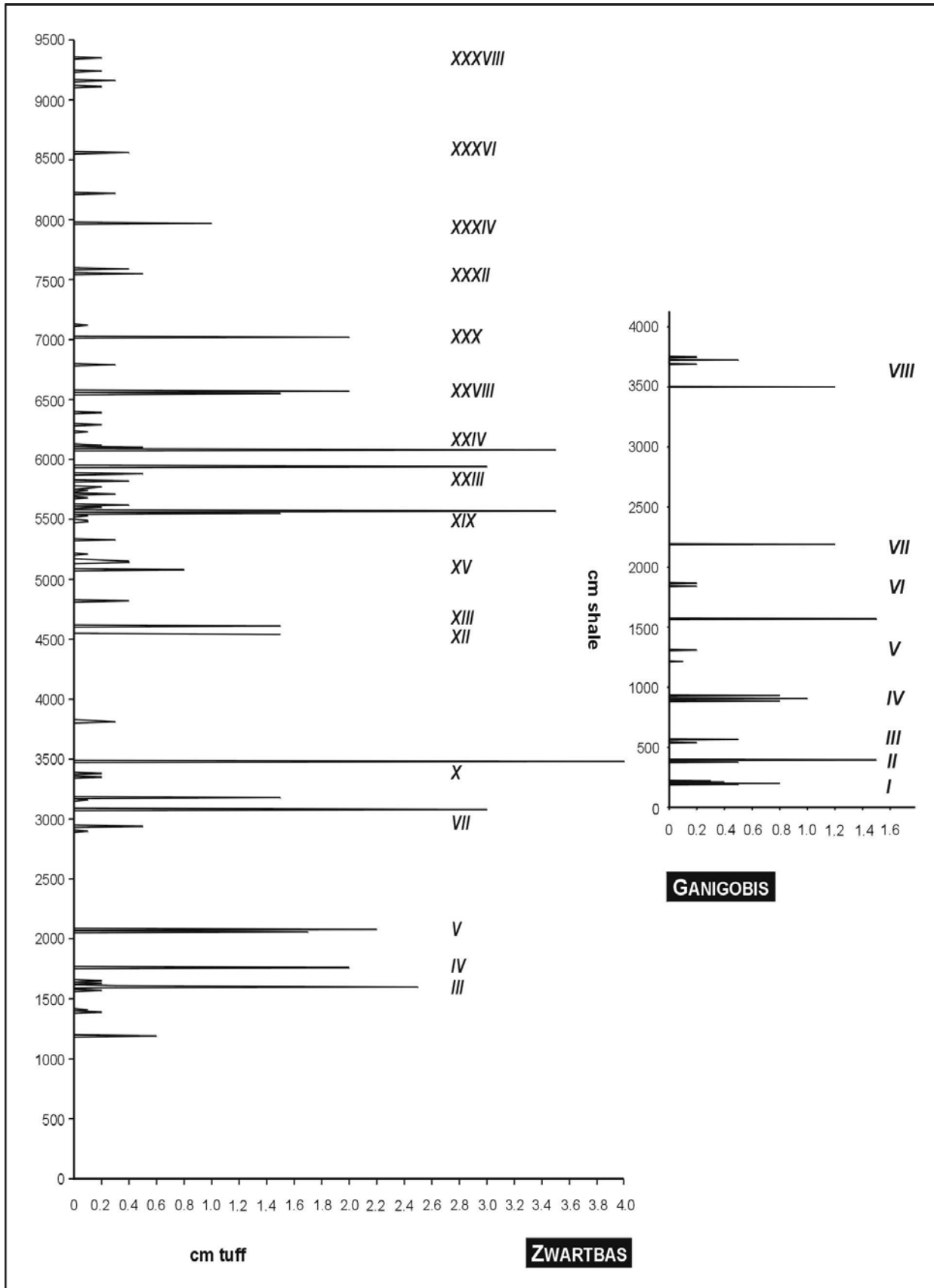


Fig. 65: Equidistant plotting of the thickness of tuff beds exposed at Zwartbas and in the vicinity of Ganigobis displaying no convincing similarities

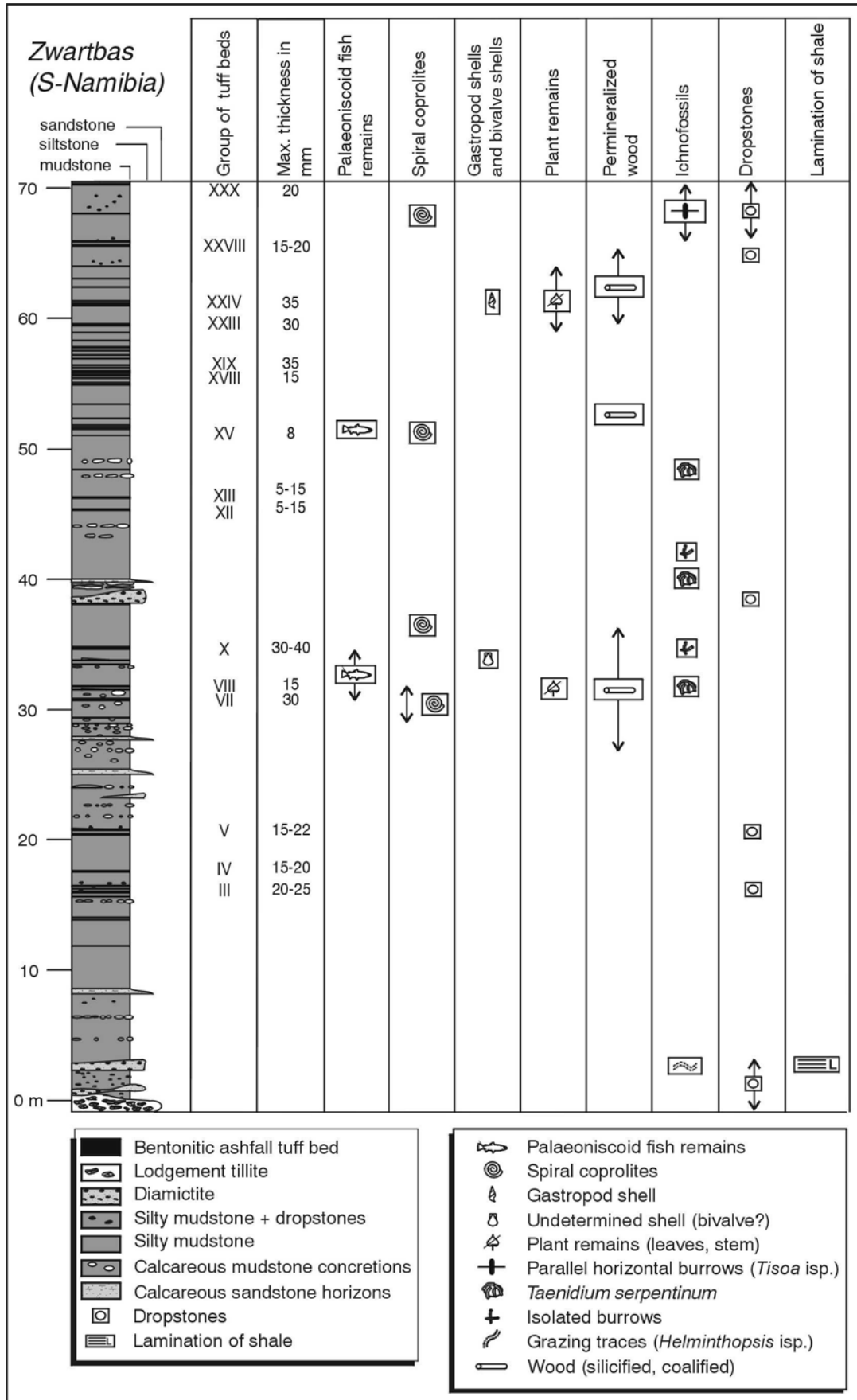


Fig. 66: Logged section of the basal part of the Dwyka Group in the vicinity of Zwartbas combined with detailed tephrostratigraphy and the fossil record (Bangert et al., in press)

The sequence at Zwartbas also exhibits three peaks of TOC and N coinciding with major occurrences of fossils. The lowermost is tephrostratigraphically located between tuff beds VI and X where TOC-values reach 0.9 % and where fish fossils, spiral coprolites, plant remains and permineralised wood are abundant. The second major peak is found between tuff beds XIV and XVI where TOC-values reach up to 1.1 % and where the above mentioned fossils are also frequent. A third peak is detected above tuff beds XXIV with TOC-values reaching the maximum value of almost 1.5 %. In this part of the section spiral coprolites, a gastropod shell, plant remains and permineralised wood were found whereas fish fossils did not appear.

Based on the fossil finds and peaks of TOC, the more than 40 m thick Ganigobis Shale Member can be placed in between tuff beds VI and XXX within the 145 m thick section exposed at Zwartbas. As tuff beds VI are located about 30 m and tuff bed XXX is found about 70 m above the base of the sequence, the thickness of roughly 40 m is maintained (Fig. 66).

6 The Hardap Shale Member

Plane bedded dropstone-free, offshore marine mudstones displaying a maximum thickness of 75 m are exposed in the uppermost part of deglaciation sequence III. Due to its type locality which is located 4 km south-east of Hardap dam and 12 km NNW of Mariental, it is called the Hardap Shale Member (South African Committee for Stratigraphy, 1980). The Hardap Shale Member corresponds to Heath's unit of "alternating sandstone and green mudstone" (Tab. 1; Heath, 1972).

Outcrops of the Hardap Shale Member are especially found north-west of Mariental near Hardap in its type locality (#1), south-west of Mariental (#6), and south-west of the former railway station "Falkenhorst" north of Gibeon (#4 and 5). Hardap Shale Member equivalents are also exposed in locality #26 along the Wasser River south of Tses.

6.1 Locality #1 southeast of Hardap Dam

The most important outcrop is an escarpment

located 4 km southeast of Hardap Dam (#1: 24°31'35" S, 17°54'20" E) and west of the Fish River. It displays about 20 m thick green-grey shales with interbedded thin sandstone horizons which wedge out laterally. The frequency and thickness of these sandstone beds increase to the top of the outcrop. Tuff beds were not detected within the whole outcrop. In the uppermost part of the outcrop single volcanic dropstones occur which are overlain by 30 – 40 cm thick sandstone beds which contain the bivalve *Eurydesma mytiloides* Reed and further *Inoceramus*-like pelecypods (Range, 1912; Grill, 1997). The surfaces of these sandstone beds are covered by trace fossils such as *Rhizocorallium irregulare*, *Rosselia* isp. and *Planolites* isp. (Grill, 1997). A more detailed description of the fossils including photographs is found in Grill (1997). *Eurydesma* is described from all other Gondwanan continents except Antarctica. It is considered to be characteristic of a major transgression in the Sakmarian, the *Eurydesma* transgression, which is indicative of the widespread final deglaciation of Gondwanaland at the end of the Carboniferous- Permian glacial period (Dickins, 1984). The age of this widespread transgression has to be reconsidered due to the *Eurydesma* occurrences within the Hardap Shale Member described above and new radiometric age determinations presented in this study (cf. Chapter 11.3). The correlation of the Hardap Shale Member with shale units in the uppermost part of DS III in South Africa, in which radiometrically dated tuff beds occur, reveals an age of the Hardap Shale Member of approximately 297 Ma which is regarded as Late Carboniferous (Gzelian) considering the numerical time scale of Menning *et al.* (1997).

Gamma-ray values of the silty mudstones were measured in intervals of 0.5 m. Values of uranium vary between 170 and 296 ppm and average 234 ppm; values are generally higher than in outcrop #3 near Schlip (cf. Chapter 6.5.1) but are lower than in outcrop # 2 north of Ganigobis where U averages 270 ppm mainly depending on the grain size of the measured rocks (cf. Chapter 4.3.2). Thorium values and Th/K-ratios are also lower and lie between 132 and 234 ppm averaging 187 ppm (cf. outcrop #3: 153 and

#2: 212 ppm Th on average) respectively between 4.31 and 7.39 averaging 5.59 (Fig. 67; average Th/K ratio in outcrop #2 is 6.16 and in outcrop #3 is 5.11). Th/U-ratios vary between 4.05 and 8.41 and average 4.94 (Fig. 67). High ratios above 8

are only locally found in the uppermost part of the outcrop and point to the removal of uranium by weathering and leaching, leaving the relative insoluble thorium behind in high concentrations.

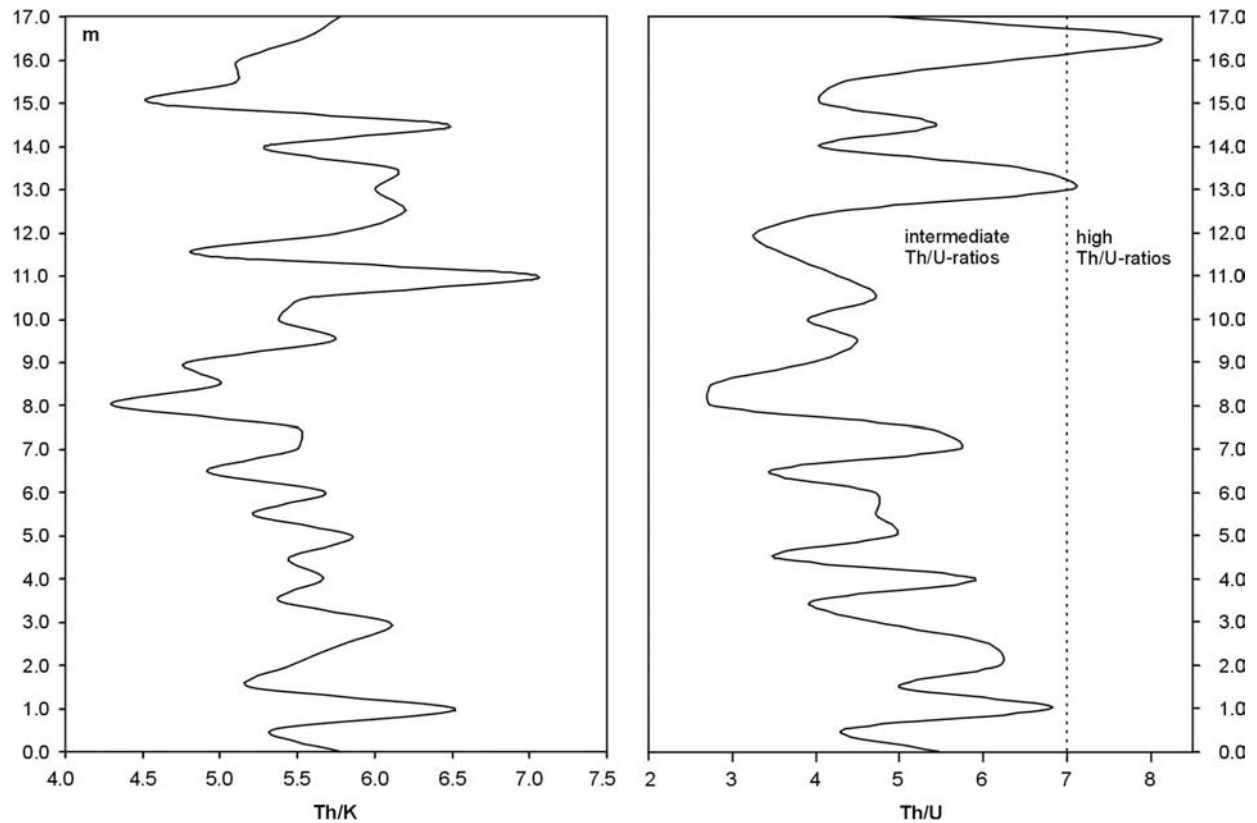


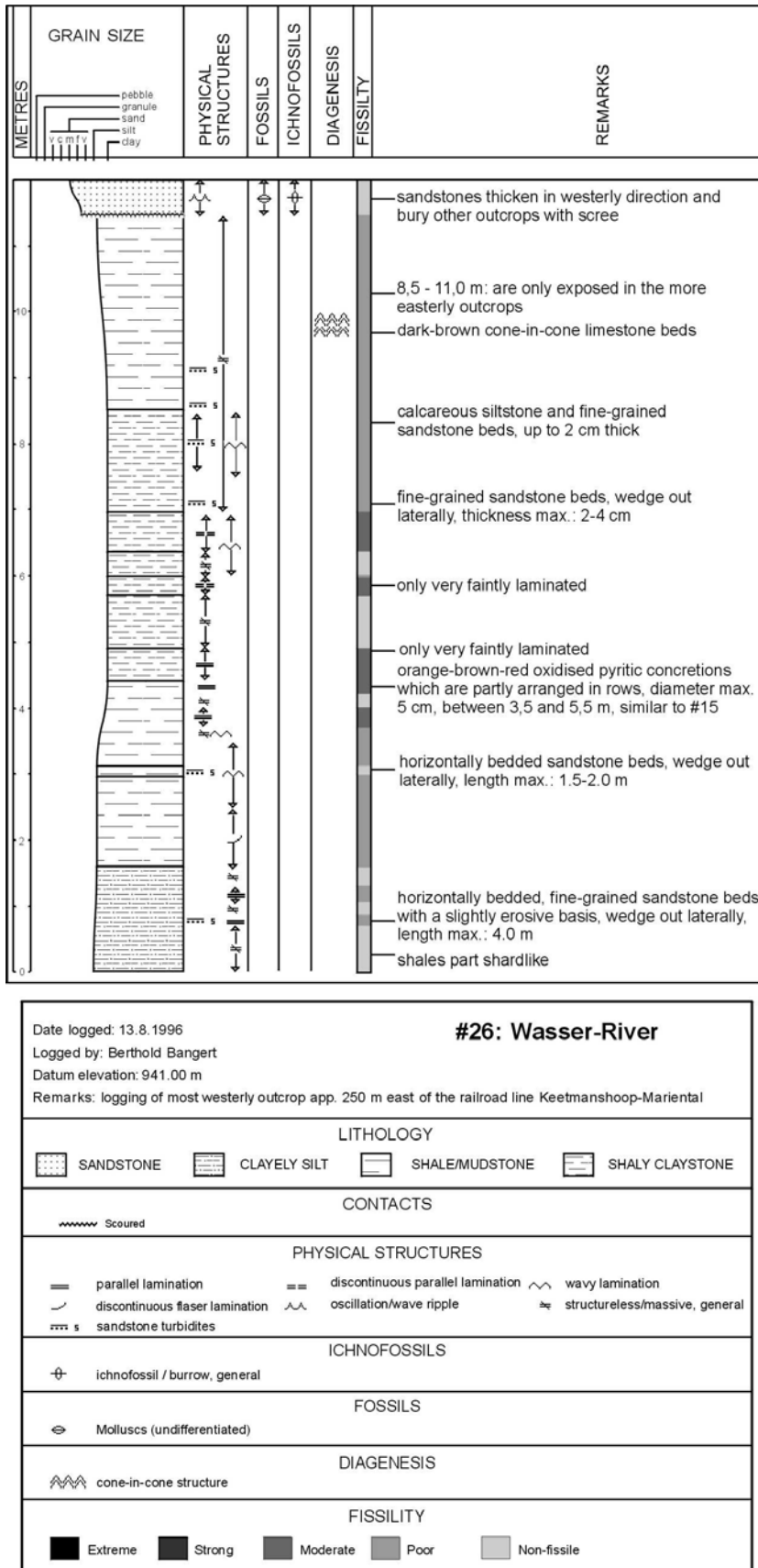
Fig. 67: Th/K and Th/U-ratios of outcrop # 1 near Hardap based on gamma-ray spectrometry; subdivision of the Th/U-ratios after Adams and Weaver, 1958; see text for discussion.

6.2 Cut banks of the Fish River: Locality #6

This outcrop is a river bank of the Fish River located 200 m south of the C19 Mariental-Maltahöhe (24°39'32" S, 17°55'59" E). It displays about 3 m green-grey shales of the Hardap Shale Member and a 30 cm thick fine-grained, ripple-laminated sandstone-horizon in the uppermost part. Tuff beds or fossils were not detected. Uranium values of the shales are quite high and vary between 208 and 301 ppm whereas Th-values lie between 189 and 232 ppm (6 measurements).

6.3 Localities #4 and 5 along the B 1

Outcrops #4 and 5 show green-grey shales of the Hardap Shale Member (DS III) lacking any tuff beds or fossils. Outcrop #4 is an eroded riverbank located about 2.5 km west of Falkenhorst (25°03'02" S, 17°51'02" E) which displays 2 m of green-grey shales with interbedded sandstone beds showing cone-in-cone structures. Shales near the base contain cm-sized quartzitic dropstones. Outcrop #5 is formed by a deeply incised creek and is located south of Falkenhorst station, about 50 m west of the B1 to Windhoek (25°05'41" S, 17°51'47" E). It exhibits up to 3 m of green-grey shales which contain thin, white gypsum beds.



Uranium values of these shales are similar to the ones in outcrop #6 and vary between 187 and 286 ppm whereas Th-values are lower compared to outcrop #6 and lie between 158 and 204 ppm.

6.4 Cut banks of the Wasser River: Locality #26

Following the Wasser River upstream from Farm Tsaraxa (Chapter 2.6.1.1) to the east, clast-poor diamictites and shales with mainly quartzitic and plutonic dropstones, which are assigned to DS III, are intercalated with thick sandstone beds.

Farther east, about 250 m east of the railroad line Keetmanshoop-Mariental and west of the B1, three large river banks are conspicuous which are located about 19 km south of Tses (26°05'03" S, 18°08'07" E). They mainly show green shales lacking any dropstones and tuff beds and are correlated with the Hardap Shale Member (DS III) in the north near Mariental. These sediments are obviously younger than the black to green shales of the Ganigobis Shale Member (DS II) which are exposed near Tses. A major normal fault dislocates both sediment packages which is excellently exposed near outcrop #45 (Fig. 13).

Fig. 68: Measured section of outcrop #26 displaying the lithology, fossil content and diagenetic features of mainly green shales correlated with the Hardap Shale Member (DS III).

The fault can be easily traced a few kilometres to the south-east and probably runs through just north of outcrop #26 (cf. Geological Map of Namibia; 1: 1 000 000, Miller and Schalk, 1980). The green shales are well laminated at the base and grade into massive siltstones with interlayered fine-grained sandstone beds towards the tops of the outcrops. The tops of the outcrops are covered by up to 4 m thick, horizontally bedded sandstones which display slump folding, bioturbation and undetermined trace fossils (Fig. 68). Calcareous, brown, fine- and middle-grained sandstone beds showing excellently developed cone-in-cone structures and micritic limestone are found above the outcrops on the plateau.

Up to dm-sized dropstones set in at this level which comprise garnet-bearing mica slates, pegmatites and volcanic clasts with an amygdaloidal texture. They mark the onset of DS IV.

Gamma-ray values of these shales were again measured at intervals of 0.5 m covering 8.5 m

sediment thickness and 18 measurements. Uranium values vary between 204 and 270 ppm and average 234 ppm; the average value is identical to the U-value in outcrop #1 south-east of Hardap (cf. Chapter 6.1) but is generally lower than in outcrop # 2 north of Ganigobis where U averages 270 ppm. Thorium values and Th/K-ratios are lower and lie between 145 and 195 ppm averaging 164 ppm (cf. outcrop #1: 187 and #2: 212 ppm Th on average) respectively between 4.39 (4.31 in outcrop #1) and 7.00 (7.39 in outcrop #1) averaging 5.96 (5.59 in outcrop #1). (Fig. 69; average Th/K ratio in outcrop #2 is 6.16). Th/U-ratios are completely different compared to outcrop #1 and vary between 2.14 (4.05 in outcrop #1) and 5.81 (8.41 in outcrop #1) averaging 3.75 (4.94 in outcrop #1; Fig. 69). These low Th/U-ratios are often associated with marine conditions where extraction from sea or fresh water is the major mechanism for the fixation of uranium in the sediment.

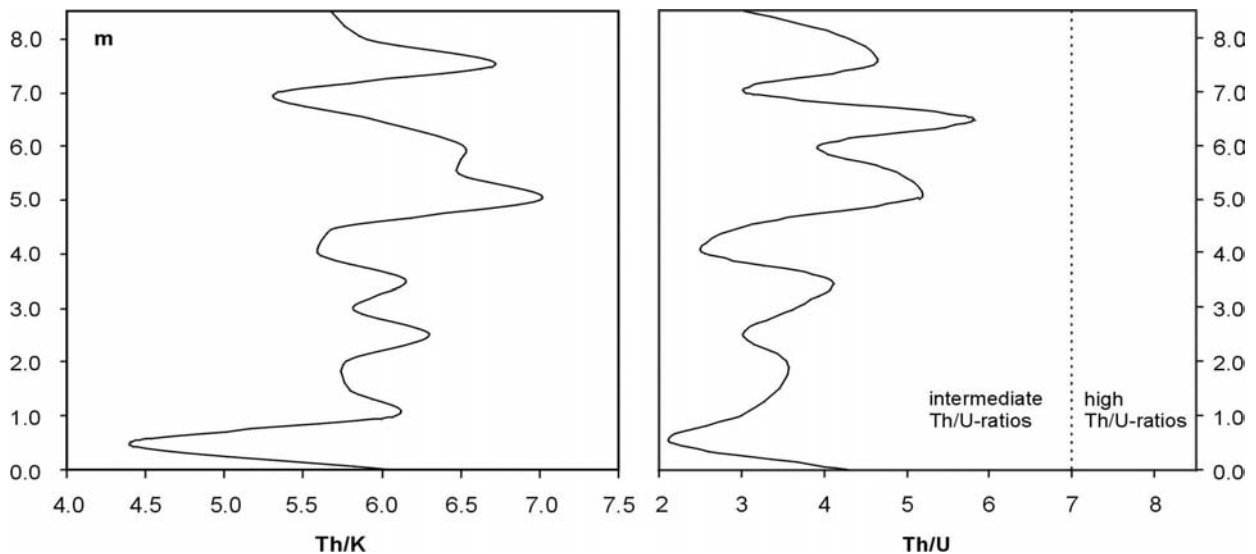


Fig. 69: Th/K and Th/U-ratios of outcrop # 26 at the Wasser River based on gamma-ray spectrometry, note the similar values of the Th/K-ratio compared to outcrop #1 south-east of Hardap about 170 km further north; subdivision of the Th/U-ratios after Adams and Weaver, 1958.

6.5 Locality #3 in the vicinity of Schlip

The northernmost exposures of the Dwyka Group which belong to the Aranos Basin are located in south-central Namibia south and west of Schlip (Fig. 1). Outcrops are mainly found at

cut banks of the Sand River and the Schlip River. The outcrop specified here is located 150 m south-east of the main church at the Sand River (24°02'49" S, 17°07'05" E). It generally shows Dwyka Group-aged green siltstones which conformably overly Proterozoic quartzites of the Damara sequence. The approximately 7 m thick

siltstones could neither be correlated with the silty mudstones of the Ganigobis Shale Member nor with the siltstones of the Hardap Shale Member. In Fig. 2 of Martin & Wilczewski (1970), these siltstones are located 3 m above the Nama / Dwyka Group unconformity and above a “basal moraine” which might locate them into the

lowermost part of DS I. The siltstones are interbedded with up to 10 cm thick, fine-grained sandstone horizons which are interpreted as distal turbidites. The uppermost 2.7 m of the outcrop contain 10 distinct, white, up to 1.2 cm thick calcrete beds which were initially interpreted as tuff beds (Fig. 70).

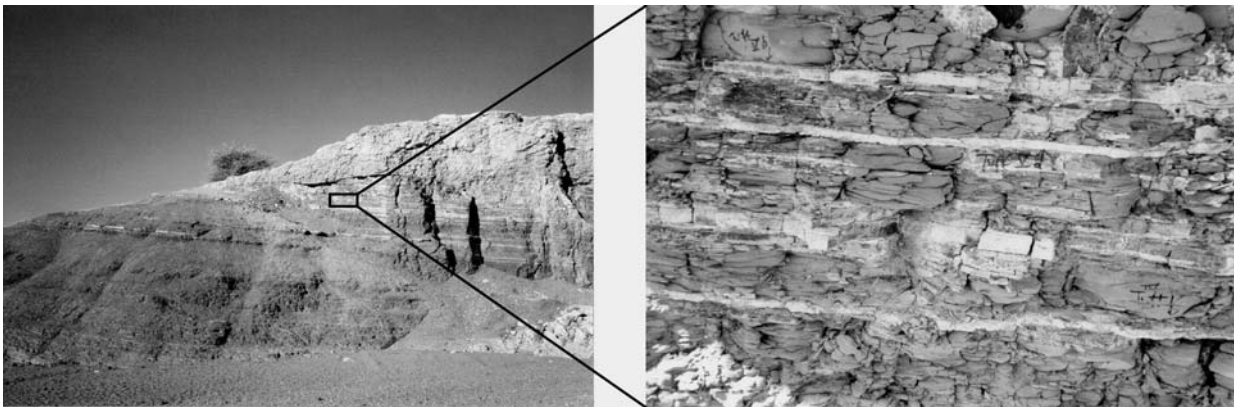


Fig. 70: River banks of the Sand River near Schlip showing mainly green, silty shales of Dwyka Group-age (left) with interbedded white, thin calcrete beds initially interpreted as tuff beds (right).

6.5.1 Gamma-ray measurements of the siltstones

Gamma-ray values of the siltstones were measured at intervals of 0.5 m. Values of uranium vary between 157 and 262 ppm and average 187 ppm; values are generally lower than in, for example, outcrop # 2 north of Ganigobis where U averages 270 ppm. This is attributed to a larger grain size of the measured rocks as gamma-ray values generally decrease with larger grain sizes of rocks. Thorium values and Th/K-ratios are also lower and lie between 119 and 196 ppm

averaging 153 ppm (cf. outcrop #2: 212 ppm Th on average) respectively between 4.02 and 6.08 averaging 5.11 (Fig. 71; average Th/K ratio in outcrop #2 is 6.16). Missing tuff beds probably lead to lower ratios as Th is mainly fixed in heavy minerals such as monazite and zircon (Davies & Elliot, 1996). Th/U-ratios vary much between 3.35 and 9.15 and average 5.24 (Fig. 71). Locally high ratios above 7 point to the removal of uranium by weathering and leaching which leaves the relative insoluble thorium behind in high concentrations.

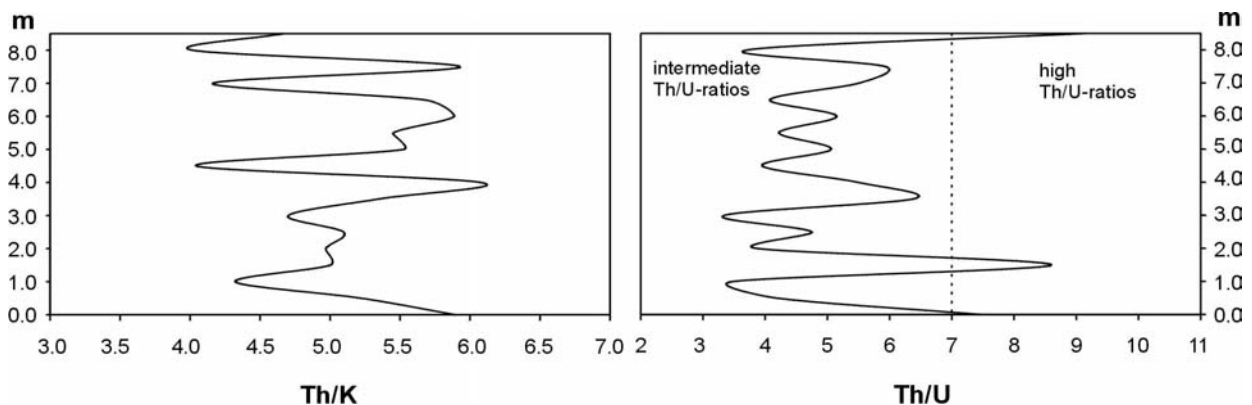


Fig. 71: Th/K and Th/U-ratios of outcrop # 3 near Schlip based on gamma-ray spectrometry, subdivision of the Th/U-ratios after Adams and Weaver, 1958; see text for discussion

6.5.2 Petrography of the calccrete beds

Thin-sections of these beds mainly show 1 - 30 μm large, rounded calcite grains which form the completely calcified and partly chloritised matrix. A varying number of dark mudstone clasts are embedded within the white matrix. The mudstone clasts are up to 2 mm long and show internal bedding planes. In one case brown clasts, which internally display two subunits, form a disrupted, about 0.6 mm thick bed. Further detected features are up to 0.75 mm large pseudomorphs after feldspar which are completely calcified and few

rounded quartz grains (size up to 0.5 mm).

6.5.3 Geochemistry of the calccrete beds

The geochemistry of 8 calccrete beds was analysed by XRF at the Institut für Mineralogie, University of Würzburg. The bulk rock samples are characterised by an average of 41.7 % CaO and 14.6 % SiO_2 with an extremely high loss on ignition of 34.6 % which is attributed to a high amount of organic matter within the beds. The trace element concentrations are partly very low except Yttrium which shows unexceptional high values of 61 ppm on average (Tab. 6).

sample	% SiO_2	TiO_2	Al_2O_3	Fe_2O_3	MnO	MgO	CaO	Na_2O	K_2O	P_2O_5	S	LOI	Total
3/13 Cc I	17.27	0.16	3.30	1.57	0.01	1.92	40.20	0.10	0.63	0.02	<0.02	31.63	96.81
3/14 Cc IIb	11.73	0.15	3.99	1.71	0.01	1.05	43.72	0.03	0.83	0.02	<0.02	35.78	99.02
3/15 Cc III	14.61	0.18	3.49	1.81	0.02	1.18	42.00	0.10	0.71	0.01	<0.02	34.64	98.75
3/16 Cc IV	12.36	0.13	2.83	1.01	0.01	1.54	44.30	0.07	0.60	0.01	<0.02	36.40	99.26
3/17 Cc Va	11.02	0.11	2.95	0.78	0.04	1.30	45.30	0.06	0.67	0.01	<0.02	36.94	99.18
3/18 Cc VI	19.40	0.24	4.45	2.29	0.02	1.67	37.54	0.20	0.88	0.02	0.03	31.81	98.55
3/19 Cc VII	12.09	0.17	3.10	2.68	0.08	1.38	43.69	0.10	0.53	0.04	<0.02	35.72	99.58
3/20 Cc VIII	18.39	0.22	6.11	2.22	0.03	1.59	37.05	0.08	1.24	0.01	<0.02	33.82	100.76
mean	14.61	0.17	3.78	1.76	0.03	1.45	41.73	0.09	0.76	0.02	0.03	34.59	98.99

sample	ppm V	Cr	Co	Ni	Zn	Rb	Sr	Y	Zr	Nb	Ba
3/13 Cc I	37	24	<10	<10	25	42	188	55	79	18	71
3/14 Cc IIb	47	18	10	<10	29	51	116	75	51	19	58
3/15 Cc III	45	16	<10	<10	19	44	103	81	73	18	46
3/16 Cc IV	31	14	<10	<10	16	40	179	57	51	16	55
3/17 Cc Va	34	19	<10	<10	22	44	179	54	56	17	68
3/18 Cc VI	54	26	<10	12	50	54	237	43	75	20	86
3/19 Cc VII	43	15	<10	10	31	35	201	86	686	16	82
3/20 Cc VIII	50	46	<10	12	41	70	99	36	68	20	146
mean	43	22	<10	<10	29	48	163	61	142	18	77

Tab. 6: Major and trace elements of calccrete beds interbedded in silty mudstones of the Dwyka Group near Schlip determined by XRF at the Institut für Mineralogie, University of Würzburg. The calccrete beds were initially interpreted as tuff beds.

7 The Dwyka Group in the main Karoo Basin (South Africa)

Exposures of the Dwyka Group are mainly found at the margin of the main Karoo Basin in South Africa (Fig. 1). Relevant outcrops for this study are located at the southern border of the main Karoo Basin (Eastern and Western Cape Province) as well as at the western border in the Western and Northern Cape Province. A third study area is located in KwaZulu-Natal where two tuffaceous beds were detected in an outcrop

east of Nondweni.

7.1 Eastern Cape Province

A roadcut along the N9 Willowmore – Aberdeen was investigated north of Beervleidam (33°04'10" S, 23°29'33" E; Fig. 1) in the Eastern Cape Province. Deposits of the Dwyka Group are exposed as follows:

The base of the outcrop consists of about 20 m dark-grey, clast-rich, steeply dipping diamictites. Dropstones are up to 3-4 (8) cm large, granitic and quartzitic clasts which are subrounded to rounded, the EACS is about 0.3 cm. The basal unit is followed by about 2 m thick, bedded, olive-grey diamictites which is richer in clasts including few generally subrounded granitic clasts of up to 3 cm with an EACS of < 0.1 cm. These are succeeded by 10 m of middle-grey, clast-rich diamictites which contain up to 5 cm large angular to subrounded gneissic, granitic and quartzitic clasts with an EACS of 0.5 cm and by about 1.5 m intercalated, bedded diamictites and green siltstones without dropstones. The shales contain three mm-thin, white tuff beds which were not sampled as they are heavily altered. The thin siltstone sequence is overlain by 3 m thick, olive-grey, clast-rich diamictites which display subangular to subrounded quartzitic and granitic clasts up to 3 cm in size with an EACS of approximately 0.2 cm. Further to the top follow dropstone-free shales of the Prince Albert Formation (Ecca Group).

7.2 Western Cape Province

7.2.1 Roadcuts of the N12 about 30 km north of Klaarstroom

The two specified outcrops are located along the N12 Oudtshoorn - Beaufort West, about 30 km north of Klaarstroom (Fig. 1). Deposits of the Karoo Supergroup were affected by successive phases of folding in this area which is located directly north of the Cape Fold Belt. The outcrops of the Dwyka Group and the Prince Albert Formation (Ecca Group) are located in a local syncline with the synclinal axis dipping to the west. The overall structure is an anticline with the strata younging towards the north and south (Fig. 72).

i, Outcrop within the Dwyka Group (33°08'35" S, 22°32'49" E)

A 3 m thick shale-unit is interbedded within the diamictite-dominated Dwyka Group. The diamictites are dark-grey and clast-rich to the

footwall and clast-poorer to the hanging wall. A 8-9 cm thick bentonitic zone is located about 2 m above the base of the shale-unit (Fig. 73). Its base is flat and the bentonitic clay material has a green colour with dark hematitic intercalations. The middle of the zone shows intercalations with black organic-rich matter. In the uppermost part of the zone the yellow bentonitic clay material displays an increasing percentage of silt and passes gradually into siltstones of the background sedimentation.

In comparison with other outcrops of the Dwyka Group in the Western Cape Province and with analysed boreholes, the shale unit probably correlates with the top of DS III. In order to determine the age of this shale unit, juvenile, magmatic zircons were separated from samples of this tuffaceous zone. Ion-microprobe (SHRIMP) analyses reveal a weighted mean $^{206}\text{Pb}/^{238}\text{U}$ age of 297.1 ± 1.8 Ma (cf. Chapter 11.3.5). The heavy mineral content (cf. Chapter 9.4.3) and the geochemistry of the clay mineral-dominated bentonitic material was also determined (cf. Chapter 10).

ii, Outcrop within the Prince Albert Formation (Ecca Group; 33°08'39" S, 22°32'51" E)

This sample locality is a roadcut only 200 m north of the sample locality described above. The single outcrop displays about 15 m of steeply dipping diamictites and dropstone-bearing mudstones of the Dwyka Group as well as 30 m of silty mudstones intercalated with bentonitic tuff beds of the lower Prince Albert Formation (Ecca Group). Sediments in the footwall of the shales comprise clast-poor diamictites showing a green, fine-grained sandy matrix in which up to 15 cm large, plutonic and quartzitic dropstones (EACS: 0.5 cm) are found. The basal part (8 m) of the following deposits consists of pencil-like weathered mudstones interbedded with more silty and sandier beds which show rip-up clasts and few, up to 5 x 3 cm large dropstones. Tuff beds were not detected in this part of the outcrop except a 2 - 3 cm thick, white tuffaceous bed.

The Ecca Group starts off with 10 m of thin siltstone and sandstone beds intercalated with mudstones and bentonitic tuff beds (tuff bed

groups II-V in Fig. 75). To the hanging wall uniform splintery mudstones are increasingly interbedded with bentonitic tuff beds (tuff bed groups VI-VIII in Fig. 75).

This facies association continues to the top of the outcrop and displays numerous more tuff beds (Fig. 74) which were not logged to greater detail. The 1-8 cm thick bentonitic tuff beds are light

green to white depending on the state of weathering. They do not display any internal bedding structures. Strong post-depositional deformation led to a pronounced foliation. They show beautifully preserved slickensides preferentially developed in their bentonitic clay minerals.

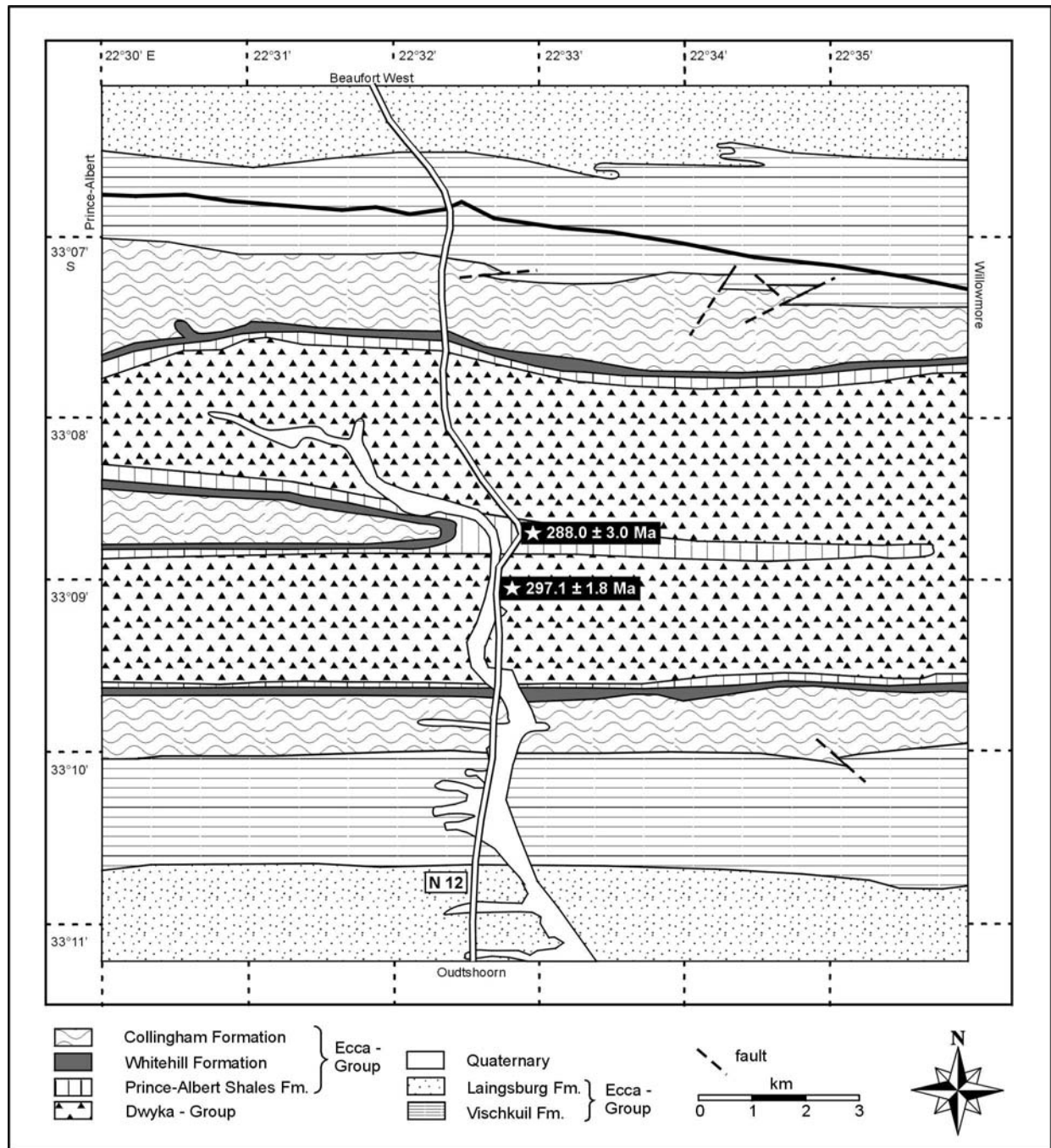


Fig. 72: Geological map of an area about 30 km north of Klararoom, asterisks mark sample locations of tuff beds including SHRIMP-based radiometric ages determined from their juvenile zircons. The map is thankfully reproduced from an unpublished map of the Council for Geoscience in Bellville, South Africa.

The tuff beds were only discovered in the described outcrops and could not be traced in the field due to the lack of exposure. Tuff bed VIb with a thickness of about 8 cm was chosen for sampling. Juvenile, magmatic zircons were separated from this tuff bed which is located only 15 m above the lithological Dwyka / Ecca boundary. Fifteen different zircons of this sample were analysed for their U-Th-Pb isotope

compositions by ion-microprobe (SHRIMP) and gave a weighted mean $^{206}\text{Pb} / ^{238}\text{U}$ age of 288.0 ± 3.0 Ma (cf. Chapter 11.3.7). The petrography (cf. Chapter 8.2), the mineralogy (cf. Chapter 8.3), the heavy mineral content (cf. Chapter 9.4.4) and the geochemistry of the bentonitic material was additionally determined; three other tuff beds were sampled for geochemical comparison (cf. Chapter 10).

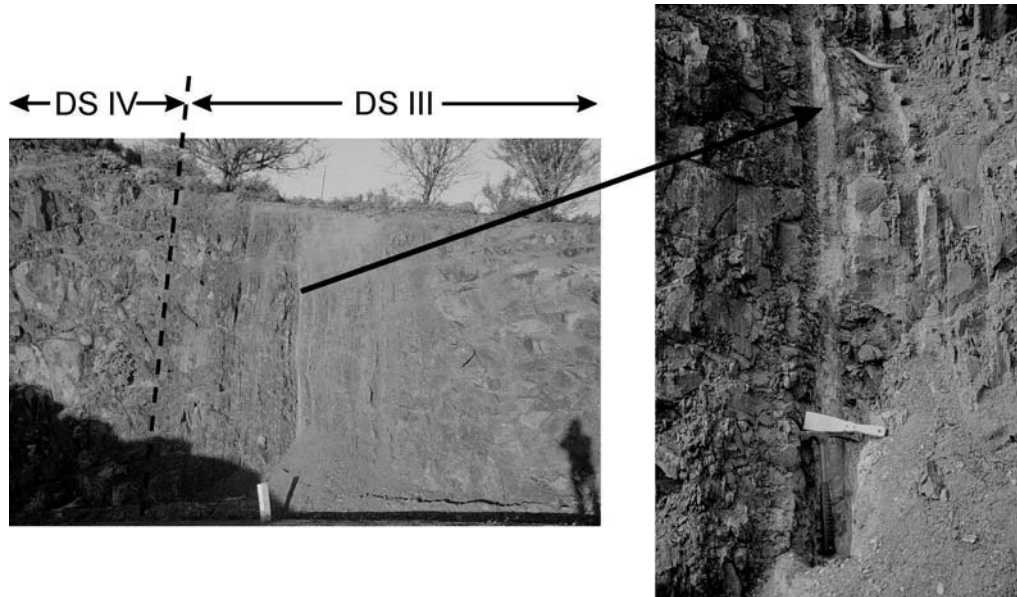


Fig. 73: **Left:** 3 m thick shale-unit probably located on top of DS III (Dwyka Group) is underlain by dark-grey, clast-rich diamictites to the right and followed by clast-poorer diamictites to the left. **Right:** A 8-9 cm thick bentonitic zone is located 2 m above the base of this shale-unit which was extensively sampled for radiometric age determinations.



Fig. 74: Field occurrence of cm-thick, bentonitic tuff beds (Prince Albert Formation, Ecca Group) about 30 km north of Klaarstroom, Western Cape Province, South Africa

7.2.2 Roadcuts south of Laingsburg

Equivalent shales of the Prince Albert Formation are exposed in a roadcut 13.2 km south of Laingsburg heading towards Ladismith ($33^{\circ}16'41''$ S, $21^{\circ}54'46''$ E; Fig. 1 and Fig. 77). The shales are heavily folded and partly overturned, the entire thickness of the shale unit was therefore hard to determine. It is thought to be similar to the one described above from Klaarstroom. Numerous bentonitic tuff beds are intercalated within blue-grey splintery mudstones. Their field appearance and thickness is similar to the ones described from Klaarstroom, however, they are less well preserved which is probably due to the period the tuff beds were exposed to weathering (Fig. 76).

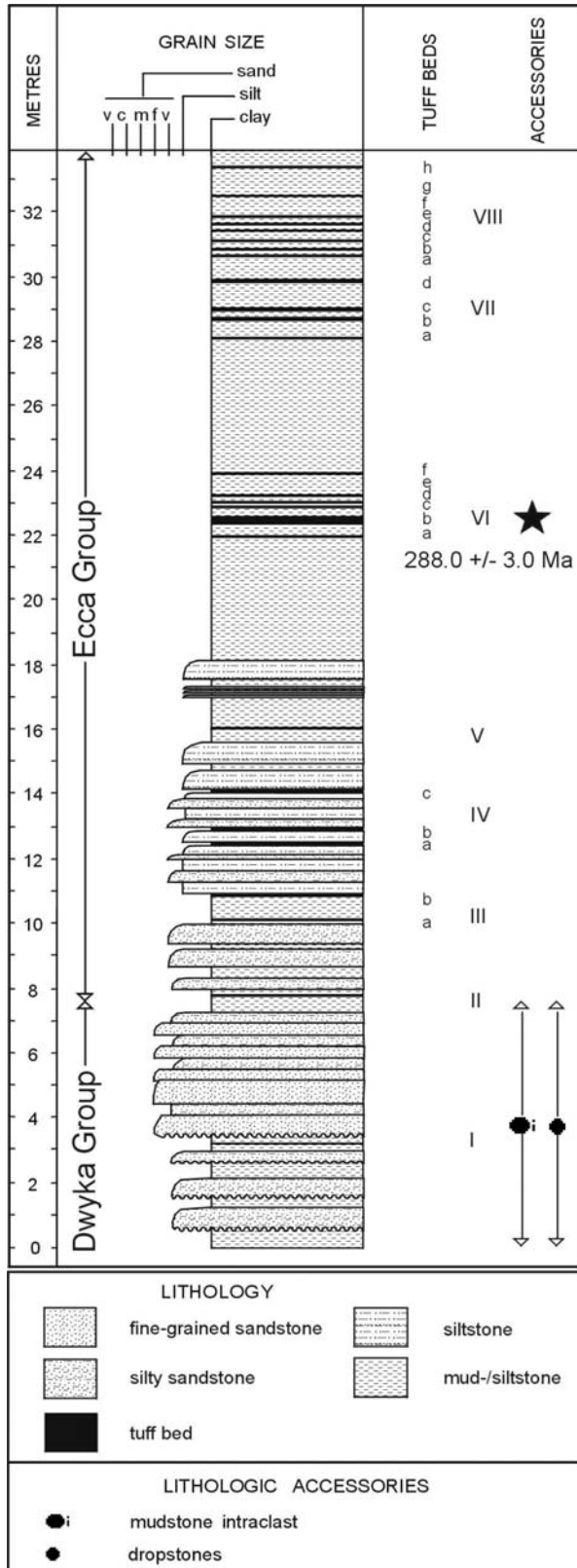


Fig. 75: Measured section of the uppermost Dwyka Group and lowermost Ecca Group (Prince Albert Formation) in roadcuts of the N12 north of Klaarstroom indicating the lithology, the tuff beds and lithological accessories as well as the radiometrically determined age date.



Fig. 76: Field occurrence of cm-thick, bentonitic tuff beds (Prince Albert Formation, Ecca Group) 13.2 km south of Laingsburg, Western Cape Province, South Africa.

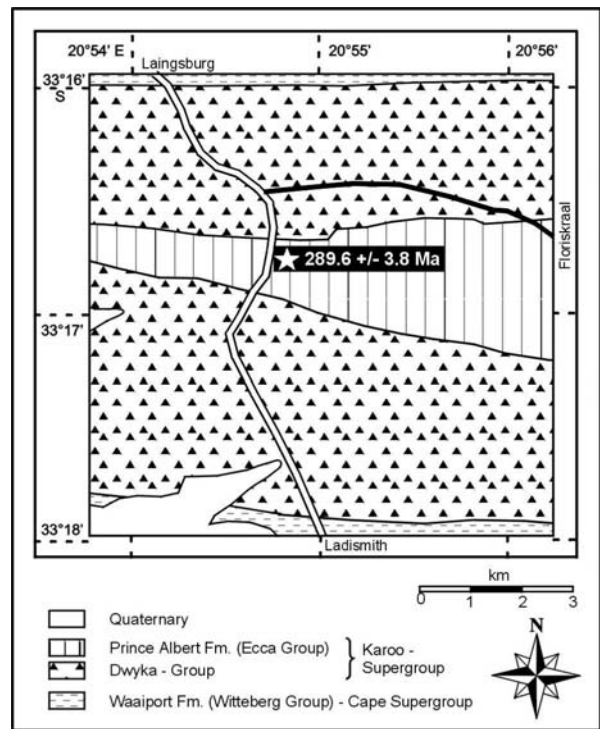


Fig. 77: Geological map of the area about 13 km south of Laingsburg, the asterisk marks the sample location of the Ecca-equivalent tuff beds including the SHRIMP-based radiometric age determined from juvenile zircons. The map is thankfully reproduced from an unpublished map of the Council for Geoscience in Bellville, South Africa.

In order to compare the radiometric age obtained from juvenile zircons of the Ecca-equivalent tuff bed from north of Klaarstroom, juvenile zircons were sampled from of a tuff bed close above the Dwyka/Ecca boundary which

reveal a $^{206}\text{Pb}/^{238}\text{U}$ age of 289.6 ± 3.8 Ma (cf. Chapter 11.3.8).

Both ages ascertain that the Prince Albert Formation has an Early Sakmarian age according to the numerical time scale of Menning et al. (1997).

The petrography (thin-sections, cf. Chapter 8.2), the mineralogy (XRD, cf. Chapter 8.3), the heavy mineral content (cf. Chapter 9.4.5) and the geochemistry of this age-dated tuff bed were additionally determined and three other tuff beds were sampled for geochemical comparison (cf. Chapter 10).

7.2.3 Outcrops east of Elandsvlei

Elandsvlei is located about 260 km NNE of Cape Town ($32^{\circ}20'00''$ S, $19^{\circ}38'43''$ E, Fig. 1). Dwyka Group exposures, up to 600 m thick (Visser, 1992), are found about 200 m west of the gravel road to Calvinia (R 355) on the track to Elandsvlei. The highest parts of the Dwyka Group are represented by fine-grained, bedded diamictites and dark grey siltstones containing single, cm-scaled dropstones. These shales are interbedded with about 10 persistent, horizontally bedded gypsum horizons of 1-10 cm thickness which might represent former tuff beds (Fig. 78).



Fig. 78: Up to 5 cm thick gypsum horizons which might represent former tuff beds are interbedded with dark grey, dropstone-bearing siltstones of the uppermost Dwyka Group east of Elandsvlei, South Africa.

7.3 Northern Cape Province

7.3.1 Niewoudtville

Glacial floors of the Dwyka Group are excellently exposed south of Niewoudtville on Farm Oorlogskloof (Fig. 1). Due to the delicate glacial structures (bulbous bedforms, long ridges and small grooves) preserved, the outcrops are protected by the Geological Society of South Africa (Site C6).

2 km south of this site and east of the road to Matjesfontein ($31^{\circ}27'09''$ S, $19^{\circ}09'51''$ E), river banks of the Oorlogskloofriver expose shales of the Dwyka Group which contain dropstones and, in the uppermost part, discrete yellow fine-grained calcrete beds which could be easily mixed up with tuff beds.

7.3.2 Slagberg

Slagberg is located north-east of Niewoudtville ($31^{\circ}10'12''$ S, $19^{\circ}18'42''$ E, Fig. 1) and displays an almost complete stratigraphic section of the Dwyka Group with a thickness of 250 m (Visser, 1992). A basal diamictite unit is overlain by ripple-cross laminated or massive sandstones, conglomerates, horizontally bedded siltstones and clast-poor diamictites which do not yield any tuff beds. The middle and upper parts are mainly dominated by clast-poor diamictites which are interbedded with clast-rich diamictites and dropstone-bearing siltstones not investigated for tuff beds so far.

7.3.3 Outcrop along the road Niewoudtville - Louriesfontein

North-east of the waterfall of the Willems River along the road Niewoudtville – Louriesfontein ($31^{\circ}18'34''$ S, $19^{\circ}07'31''$ E) massive, clast-poor diamictites cut into bedded diamictites and siltstones with dropstones but expose no tuff beds.

7.4 KwaZulu-Natal

Grey-green shales are exposed 2 km east of Nondweni in a small creek next to the Vryheid-Nqutu road ($28^{\circ}10'50''$ S; $30^{\circ}50'72''$ E, Fig. 1).

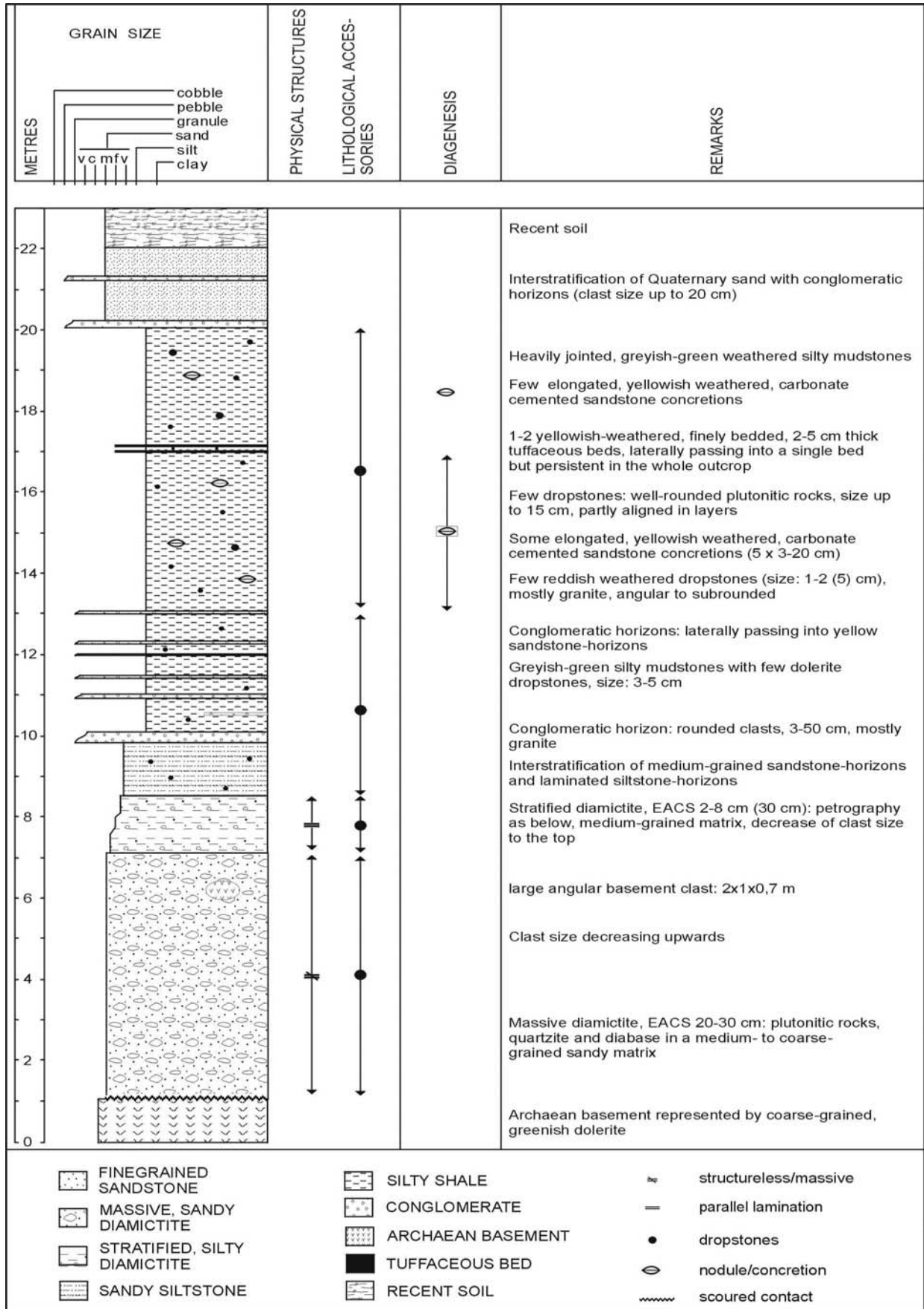


Fig. 79: Measured section of the basal part of the Dwyka Group 2 km east of Nondweni showing the lithology, diagenetic features and the stratigraphic occurrence of the tuffaceous beds.

The Dwyka Group in this area has a minimum thickness of 180 m (von Brunn, 1977) and is capped by Jurassic dolerite forming the summits of isolated hills in this locality.

The true thickness of the Dwyka Group is difficult to ascertain owing to the affect of the pronounced palaeorelief differences, which vary as much as 130 m over distances of 1 km (Versfeld, 1988).

The 22 m-thick sedimentary sequence of the Dwyka Group unconformably rests on green-blue Archaean dolerite and begins with massive and stratified diamictite. The diamictites are followed by sandstone, siltstone and mudstone containing dropstones. Two partly-laminated, cm-thick tuffaceous beds which show a pale-yellow colour, occur 3 m below the top of the section with dropstone-bearing siltstones (Fig. 79).

The grey-green to light yellow weathered tuffaceous beds are not persistent in quantity and thickness. The vertical distance between the two beds gradually diminishes from 12 to 3 cm downstream in the Nondweni creek, where they merge into a single horizon which might have originated from turbiditic redeposition. The 1.5 and 6.0 cm thick beds occasionally possess a lenticular shape. The base of each bed is mostly undulatory whereas the upper boundary is flat and well-defined (Fig. 80). The grain size of the beds is of the order of fine-grained sand. Thin (0.5 to 2.0 mm) laminae of the same rock material appear a few mm to cm above the main tuffaceous bed in similar intervals (Fig. 80).



Fig. 80: Close-up photograph displaying the tuffaceous beds in the outcrop. Note the undulatory base and the well-defined upper limit of the major bed located below the scale.

The petrography (thin-sections, cf. Chapter 8.2), the mineralogy (XRD, cf. Chapter 8.3), the heavy mineral content (cf. Chapter 9.4.6) and the geochemistry (cf. Chapter 10) of the tuffaceous material was determined. Two obviously juvenile zircons were separated from of these tuffaceous beds which reveal a $^{204}\text{Pb}/^{206}\text{Pb}$ age of 2054 ± 31 Ma (cf. Chapter 11.3.6).

7.5 SOEKOR boreholes

In order to sample relative recently exposed and therefore less altered tuff beds for thin-section preparation, heavy mineral separation and geochemistry, deposits of the Dwyka Group of the main Karoo Basin were investigated in boreholes Enkelde Wilgenboom (near Calvinia; Northern Cape Province: $31^{\circ}29'40''$ S, $19^{\circ}53'50''$ E), KL 1/65, QU 1/65, SA 1/66 and OL 1/69 (Fig. 1). In the short amount of time available before the start of the Gondwana 10 – Conference in Cape Town, sediments of the borehole Enkelde Wilgenboom could not be assigned to the concept of deglaciation sequences. The other boreholes were logged in the week following the Conference which allowed a more precise logging and sampling. As it was not a main topic of this study, the existing facies were not further defined; such facies interpretations can be found for example in Visser (1983b) or Grill (1997).

7.5.1 Enkelde Wilgenboom

The core of borehole Enkelde Wilgenboom revealed tuff beds interbedded in two thin shale units found at the depths 880.10 - 879.30 m and at 798.79 – 798.36 m which is succeeded by intercalations of mudstones and bedded diamictites up to a depth of 793.50 m.

In the first unit yellow tuff beds were detected and sampled at 879.95 m (thickness: 2 cm) and 879.75 m (1 cm). Further tuff beds occur at 879.84 and 879.86 m (0.5 cm).

The second shale unit contained sampled tuff beds at 798.79 m (1 cm) and 798.39 m (2 cm). A further tuff bed was recognised at 798.84 (0.5 cm).

7.5.2 KL 1/65

The Dwyka Group has a thickness of 536 m in

borehole KL 1/65. DS I possesses a thickness of 146 m and is dominated in the lower part by clast-rich diamictites with mostly subangular, up to 6 cm large clasts (sandstone, quartzite, granite). Further up section the clast-rich diamictites grade into clast-poor and bedded diamictites which contain subangular to subrounded, up to 3 cm large clasts (sandstone, granite). DS II starts off with clast-rich diamictites (subangular to rounded clasts with sizes of up to 7 cm) and has an overall thickness of 72 m. The uppermost 5 m of this unit consist of bedded diamictites which are intercalated with partly laminated siltstones and clast-rich diamictites. A 0.2 cm thick tuff bed was recognised at the depth of 1819.63 m. DS III is the thickest unit and displays 220 m of mainly clast-rich diamictites with subangular to subrounded, granitic clasts with sizes of up to 10 (30) cm. Between the depths 1619 and 1596 m bedded diamictites are followed by finely bedded or laminated siltstones which form the uppermost part of DS III. Two, very thin (0.2 cm) tuff beds were recognised and sampled at the depths 1616.50 and 1612.54 m. DS IV begins with clast-poor diamictites with subangular to subrounded clasts which mainly consist of granite. The Prince Albert Shales begin at 1503 m giving DS IV a thickness of 93 m.

7.5.3 QU 1/65

The Dwyka Group has a thickness of 400 m in this borehole and begins at the depth of 2413 m. DS I is rather incomplete and ends at 2382.30 m. It displays clast-poor diamictites which are interbedded with sandy siltstones showing reworked horizons and slumping structures. Thin clast-rich diamictites with subrounded clasts of up to 7 cm in size are intercalated with nicely laminated siltstone beds containing dropstones and with bedded, silty diamictites. DS II starts off with very clast-rich diamictites with rounded to subrounded, sandstone or granitic clasts reaching 8 cm in size. The EACS is about 1 cm with many clasts ranging between 1 and 4 cm in size. This facies generally continues upwards to a depth of 2333.25 m but is more frequently intercalated by fine-grained, horizontally bedded sandstone horizons which show slumping structures. DS II

has an overall thickness of 49 m. DS III begins with clast-rich diamictites with up to 6 cm large, mainly rounded and smaller, partly subangular granitic clasts with an EACS of about 0.5 cm. Exceptional large clasts reach 40 cm in size and consist of quartzitic sandstones or olive-green, amygdaloidal volcanic clasts. Between the depths 2257 and 2226 m flaser-bedded diamictites and clast-poor diamictites alternate with sandy siltstones and black muddy siltstones which part shard-like. Two, thin, yellow tuff beds were sampled at 2244.80 and 2239.31 m. DS III comprises a thickness of 107 m. DS IV can be subdivided in two parts, the lower part consists of clast-poor diamictites with up to 5 cm large subrounded to subangular clasts which decrease upwardly in size and number. Faintly bedded, fine-grained, light grey-brown sandstones containing few small dropstones occur from 2031.30 m to the top of the Dwyka Group at 2013.00 m leaving DS IV an overall thickness of 113 m.

7.5.4 SA 1/66

The Dwyka Group begins at 3591 m in this borehole and comprises an overall thickness of 669 m. The subdivision in sequences is complicated as clast-rich diamictites dominate the spectrum of the deposits and fine-grained sediments are mainly missing. DS I is recorded with a thickness of 94 m and mainly shows clast-rich diamictites with subangular to subrounded, granitic and quartzitic clasts of up to 12 cm in size. The EACS varies from more than 1 mm to below 1 cm. The uppermost 6 m are dominated by clast-poorer, flaser-bedded diamictites. DS II begins at 3497 m with 141 m of clast-rich diamictites (EACS: 0.3 cm and clast sizes up to 5 cm) which are followed by 74 m of clast-poor diamictites up to a depth of 3282 m (EACS: 0.3 cm and clast sizes up to 8 cm), the diamictites are slightly bedded at the depths of 3355 and 3312 m. Partly flaser-bedded diamictites occur between the depths 3287 and 3282 m. They are again overlain by 55 m of clast-poor diamictites of which the uppermost 7 m show horizontal, partly flaser-bedding with few up to 4 cm large, angular dropstones (granites, gneiss) which probably represent the uppermost part of DS II. Taking

these boundaries into account, DS II comprises an overall thickness of 270 m. DS III is mainly comprised by clast-rich diamictites with subangular to subrounded clasts which are mainly plutonic in origin and are occasionally up to 30 cm in size. The clast-rich diamictites have a thickness of 116 m and are followed by 5 m of bedded diamictites which are intercalated with siltstones containing dropstones which both mark the topmost part of DS III. DS IV consists of 184 m thick clast-poor diamictites with subrounded

clasts up to 5 cm in size. The Prince Albert Shales set in at 2922 m.

7.5.5 OL 1/69

The core of borehole OL 1/69 was studied with greater detail as it contains many tuff beds in the uppermost part of DS III. Lithologies and all other preserved structures of the diamictites are found in Fig. 81 and will not be denominated here to greater detail.

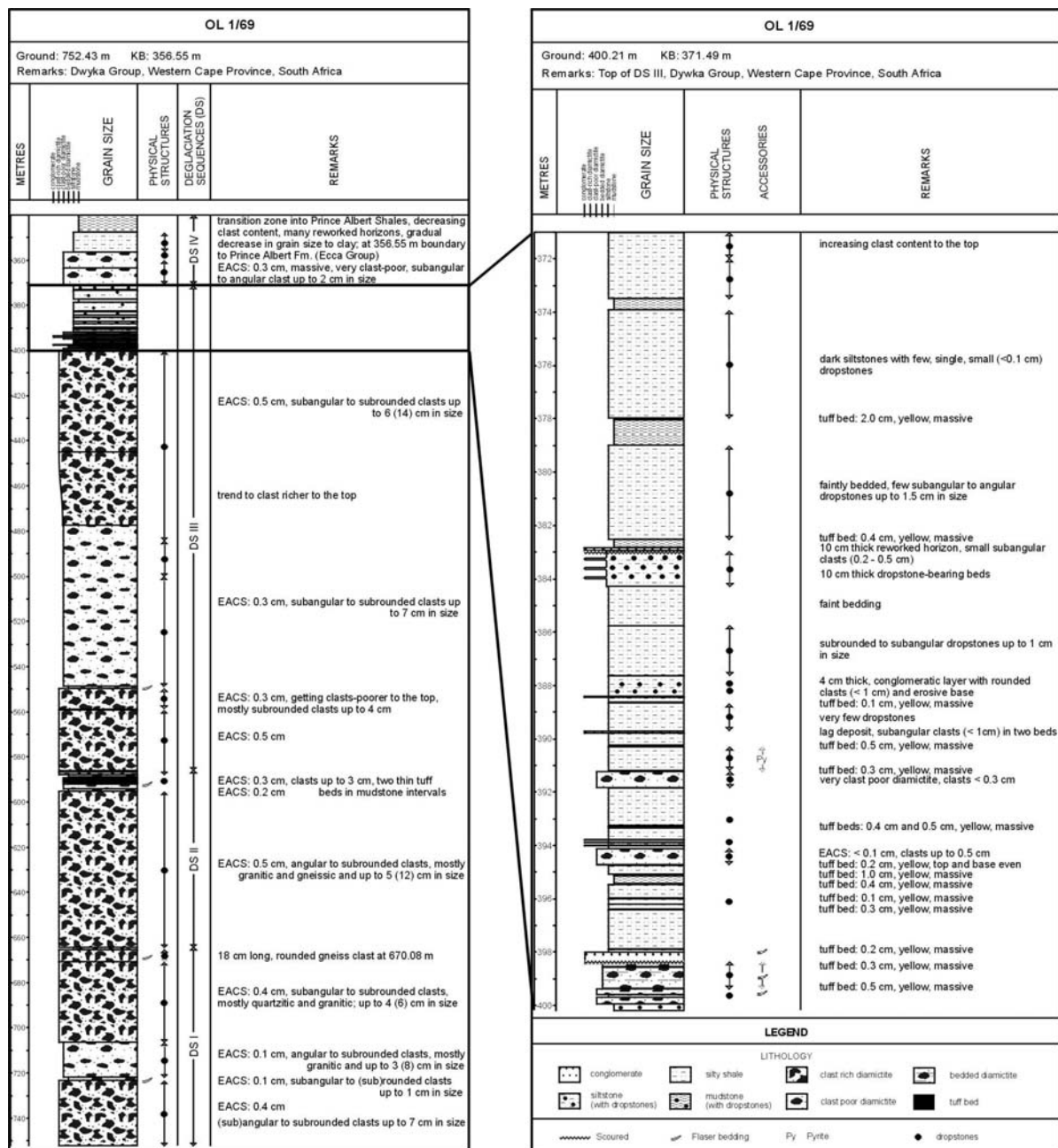


Fig. 81: Left: measured section of borehole OL 1/69 displaying the lithology and physical structures of the core and recorded deglaciation sequences; right: detailed section of the uppermost part of DS III showing the general lithology of the core including the detected tuff beds.

The Dwyka Group has an overall thickness of 383 m in this borehole and begins at the depth of 752 m. DS I comprises 87 m of sediment thickness and consists of 65 m clast-rich diamictites, 16 m of clast-poorer diamictites, 5 m of bedded diamictites and 1 m of finely bedded siltstones at the top of DS I.

DS II starts off with 70 m of clast-rich diamictites followed by 8 m of interbedded clast-poor diamictites, bedded diamictites and mudstones containing varying amounts of dropstones. Two thin (<0.2 mm) tuff beds were recognised and sampled in this part. DS III is very thick and comprises 188 m of clast-rich diamictites and clast-poor diamictites which grade into each other. Faintly bedded diamictites are subordinate. The uppermost 29 m of DS III are mainly comprised of silty mudstones with varying amounts of dropstones. The lowermost part of the sequence consists of clast-poor and bedded diamictites as well as by very clast-rich diamictitic layers (400 – 398 m). 15 tuff beds were altogether recognised in this part, 8 of them occur between 400 and 394 m (Fig. 82).



Fig. 82: Silty mudstones in the uppermost part of DS III of diamictite-dominated borehole OL1/69 contain thin tuff beds (white arrows) and few dropstones.

The tuff beds are yellow, massive, bentonitic and between 0.1 and 2.0 cm thick. Macroscopically they do not show any internal structures and the bases and uppermost parts of the tuff beds are mostly sharp. In order to obtain an adequate amount of sample material, only tuff beds with a thickness exceeding 0.3 cm were sampled.

DS IV is only 15 m thick and consists of massive, very clast poor diamictites which grade into the Prince Albert Shales. The clast content decreases and the grain size is reduced to clay; the boundary to Prince Albert Formation (Ecca Group) is at 356.55 m.

7.6 Stratigraphic comparison of the deglaciation sequences recorded in the boreholes

DS I is poorly preserved within the whole main Karoo Basin and only found to a greater extent in the southwesternmost part of the basin where glaciomarine conditions prevailed throughout the whole deposition of the Dwyka Group. Sediments of DS I reach the greatest thickness in borehole KL 1/65 with 145 m and diminish to 90 m in boreholes OL 1/65 and SA 1/66 and to 30 m in borehole QU 1/65 (Fig. 83). DS I is not exposed near Niewoudtville and Loeriesfontein to the north and near Klarstroom to east where glacial erosion took place (Visser *et al.*, 1997). Ice flow patterns reveal that sediment was transported from the north (“Northern Cape Source”), from the east and directly from the south (Cape Fold Belt; Visser *et al.*, 1997; Fig. 84). During the sedimentation of DS II, the depocentre was located in the southwesternmost part of the basin where thicknesses of more than 400 m are reported (cf. Visser *et al.*, 1997), Fig. 5). In boreholes OL 1/69 and KL 1/65 DS II has a thickness of about 75 m which increases to the south-east to about 220 m (SA 1/66 and north of Klarstroom, Fig. 83). Ice flow patterns still show a subordinate northerly direction but the main ice flow occurred from the east (Fig. 84). The thickness of the glaciomarine sediments of DS III remains constant with more than 200 m in the boreholes and north of Klarstroom (Fig. 83). Visser *et al.*, 1997 report a sediment thickness of DS III of about 300 m to the west at Elandsvlei (Fig. 1) indicating that the depocentre of the basin was still located to the west. According to Visser *et al.* (1997), ice flow from the north ceased whereas easterly directions predominate (Fig. 84). DS IV thickens to the east with 15 m in OL1/69, 93 m in KL 1/65, 184 m in SA 1/66 and about 240 m north of Klarstroom (Fig. 83).

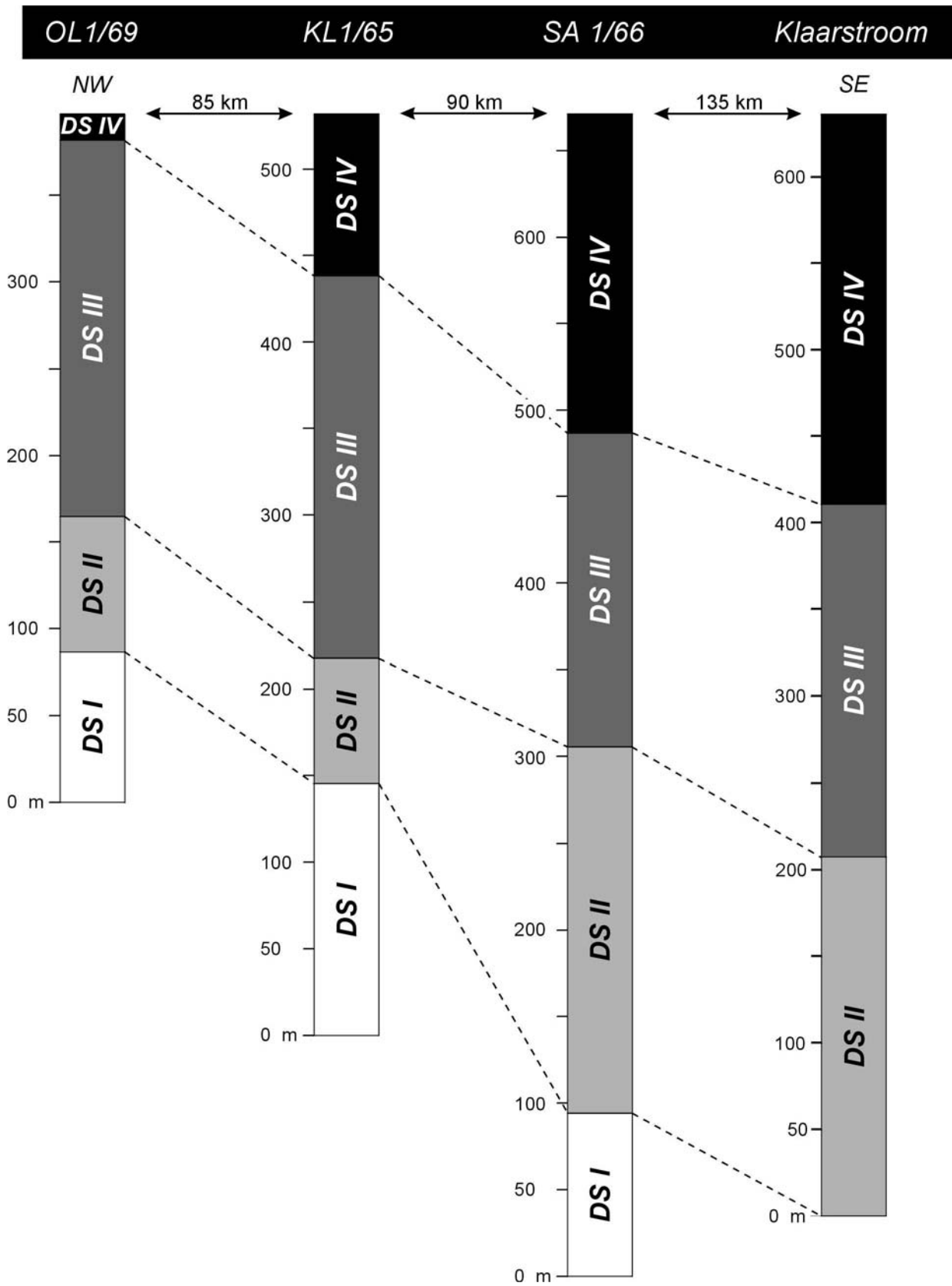


Fig. 83: Correlation of deglaciation sequences (DS) of boreholes OL 1/69, KL 1/65, SA 1/66 and outcrops north of Klaarstroom (section of Klaarstroom is modified from Visser, 1997), for location of the boreholes and the outcrops see Fig. 1.

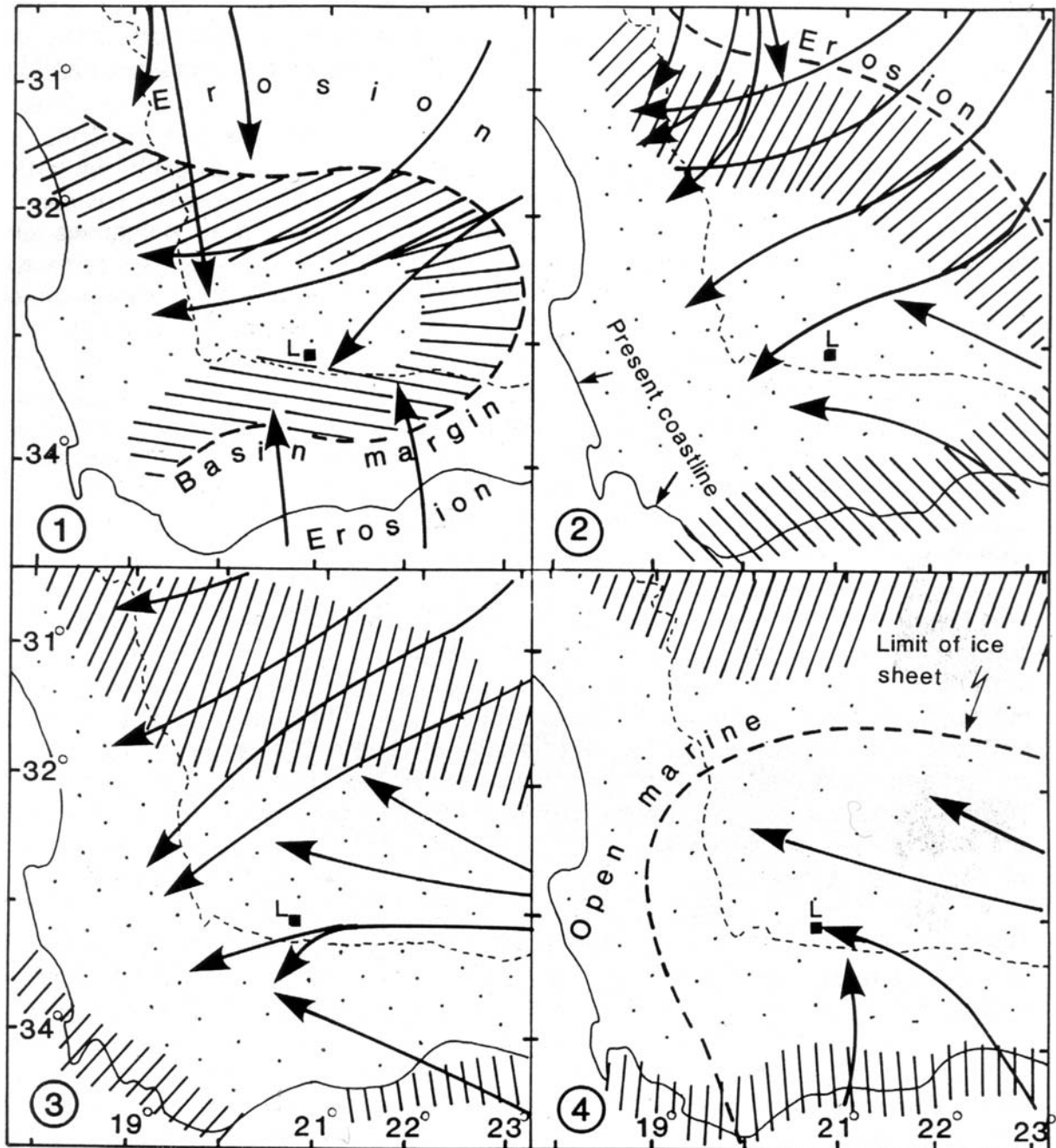


Fig. 84: Reconstruction of ice-flow patterns during deposition of deglaciation sequences I (1) to IV (4) (Visser *et al.*, 1997). Outline of the Karoo Basin is shown by a dashed line; palaeoslope trends within the basin are hatched. L = Laingsburg.

The decrease in thickness of deposits of DS IV is due to the fact that open marine conditions prevailed towards the west where post-glacial muds were already deposited simultaneously with

the diamictites of DS IV. Ice streams from the south-east and south-southeast were the major input sources of debris forming the deposits of DS IV (Visser *et al.*, 1997; Fig. 84).

8 Petrography of the tephrostratigraphic marker beds

The petrography of the examined tuff beds of the Dwyka Group in southern Africa is similar to most other Palaeozoic bentonites on earth (e.g. Kolata *et al.*, 1996).

The most distinctive mineralogical feature of the tuff beds is the high proportion of clay minerals and clay-sized particles accounting for between 80 and 90 % of the total rock volume. The remaining portion is made up of primary and secondary minerals, detrital grains and rock fragments. Clay minerals mainly result from the devitrification of acid to intermediate volcanic glass. Accompanying juvenile minerals include fragments and splinters of quartz as well as heavy minerals such as zircon, apatite, monazite, sphene, rutile, biotite, garnet, hornblende and tourmaline. Secondarily formed minerals mostly comprise barite and opaque minerals as well as leucoxene.

This chapter contains a description of the matrix, phenocryst content and ash relic structures, grain-size characteristics and the mineralogical composition detected by XRD analysis.

The following sampled tuff beds were used for the descriptions:

- tuff beds from the Ganigobis Shale Member (DS II, Dwyka Group) of the Aranos Basin (southern Namibia) including tuff beds I to VIIIa
- tuff beds from the Dwyka Group (DS II) near Zwartbas (southern Namibia) especially tuff beds IIIb, VIIIb and XXIVa
- tuff beds from the Dwyka Group (DS III) of borehole OL1/69 (Western Cape Province, South Africa)
- a tuffaceous bed from the Dwyka Group (DS III), north of Klaarstroom, South Africa
- tuffaceous beds from the Dwyka Group east of Nondweni, KwaZulu-Natal, South Africa
- tuff beds from the Ecca Group of two localities in Western Cape Province, South Africa

Note, that not all listed tuff beds were included

into all descriptions due to the subsequent sampling and analysis of the three successive field seasons 1996-1998.

8.1 Terminology and classification

Volcanic ash includes the finest grained tephra and is composed of various proportions of vitric, crystal, or lithic particles of juvenile, cognate or accidental origin forming >75 vol % of an aggregate (Fisher and Schmincke, 1984). Tuff is the consolidated equivalent of ash, and is subdivided into fine- and coarse-grained varieties according to the size of component particles. Tuffs can be further classified according to (1) the depositional environment (e.g. lacustrine tuff), (2) the manner of transport (e.g. fallout tuff), or (3) their petrographic composition (e.g. vitric, crystal, or lithic tuff (Schmid, 1981). Tuffaceous deposits are mixed pyroclastic-epiclastic sediments that contain 25-75 vol % pyroclasts (Schmid, 1981).

“Bentonite” was originally used for deposits of smectite-dominated clays derived from tephra deposits by alteration. This definition is based on the clay mineral species and not on the precursor material. However, the term bentonite has for many decades been used to describe thin, widespread, clay-altered ash layers that are commonly, but not necessarily, dominated by smectite (Fisher and Schmincke, 1984).

8.2 General petrographic description of the marker beds

Macroscopically the tuff beds are mostly homogenous beds showing horizontally aligned clay minerals which easily swell after the contact with water. The grain size of the tuff beds is generally that of fine ash and only the phenocrysts and glass relics are generally larger than 62.5 μm (coarse ash). The main primary components such as quartz, glass relics, biotite, apatite, zircon and feldspar constitute 5 - 20 (35) Vol.% of the total rock content.

In other words 80 - 95 Vol.% of the total rock is made up of the matrix which mainly represents altered glassy volcanic ash. The tuff beds are therefore denoted as vitric tuffs (cf. Schmid, 1981). They are normally graded, showing a fining upward of crystal particles and glass relic structures. Two or more graded units were only rarely discovered in thin-sections (e.g. in the tuff bed from depth 399.25 m of OL 1/69) which mostly suggests single ash-fall events. Partly blocky gypsum or also calcite can substitute the clay mineral matrix. Fragments of the adjacent silty mudstones are occasionally visible (e.g. tuff bed # 30 IVa).

Apart from the tuffaceous beds of the Dwyka Group north of Klaarstroom and east of Nondweni, all sampled tuff beds are regarded to be tuff beds. Only in #30 tuff bed IVb silty rip up clasts are admixed which suggest post-depositional redeposition by turbidites. The tuffaceous character of the two mentioned beds will be described later to detail (c.f. Chapter 8.3).

The following petrographic description is mainly based on the analysis of the thin-sections. The microscopic study, however, is impeded as all examined tuff beds are very fine-grained. Microscopes used and the methods of thin-section preparation is summarised in Appendix B-2. To support the microscopic study, results from XRD-analysis were added.

8.2.1 *Matrix*

The colourless to brown or grey matrix of all tuff beds consists of micro- to cryptocrystalline clay minerals (mixed layered illite-montmorillonite as indicated by XRD-analysis) with minor contents of microcrystalline quartz and occasionally albite. The matrix contains variable amounts of secondarily formed and finely disseminated opaque minerals which causes the brown colours of the heavily weathered tuff beds.

8.2.2 *Primary volcanic components*

8.2.2.1 *Relic structures of volcanic glass particles*

The preservation of glass relic structures mainly depends on the degree of alteration of the single

tuff beds. Thin-sections of the heavily weathered tuff beds from the Aranos Basin of southern Namibia mostly show up to 220 x 56 μm large (especially tuff bed IIb), round to elongate flattened, decomposed ash grains which are completely recrystallized into fine-grained quartz or kaolinite. Their average length and width totals 70 μm (median: 56 μm) respectively 39 μm (13 measurements); their colour is generally lighter than the surrounding matrix. Some of the ash grains are certainly transformed into stacks of kaolinite or vermicules. Others contain euhedral to anhedral quartz grains in their centres or show a rather concentric structure. The illitic-smectitic dominated clay minerals surround the ash grains. Thin-sections of tuff beds V and VIIIa show normal grading which is displayed in the frequency and size decrease of quartz fragments and splinters as well as of coarser ash grains. Irregularly formed, round to elongate flattened, partly coupled ash particles reaching a maximum length of 700 μm are especially concentrated near the base of tuff bed VIIIa (#9; Plate 2, Fig. 3). Their size diminishes towards the top of the tuff bed. The elongate flattened particles probably represent collapsed pumice grains. In an exceptional well preserved thin-section of tuff bed Ic (#2) very small, pointed shards with smooth and conchoidal fracture surfaces occur which probably represent broken vesicles walls pointing to an andesitic to dacitic parent magma (cf. Heiken, 1974). Only one delicate example of a y-shaped glass shard was detected in tuff bed Ic (#2, Plate 2, Fig. 7).

Thin-sections of the tuff beds from Zwartbas in southern Namibia show a normal gradation with coarser quartz fragments and splinters (up to 112 x 56 μm) and further, mostly kaolinised pyroclasts with a maximum size of 120 x 88 μm at the base. The uppermost part of the tuff beds contains only few quartz grains, smaller pyroclasts and ash grains with a size of up to 20 μm and finely dispersed opaque minerals.

Tuff beds from the borehole OL 1/69 are only in part normally graded, others show no grain size trends. Pyroclasts including coarser ash grains and collapsed pumice are embedded in a cryptocrystalline clay mineral dominated matrix.

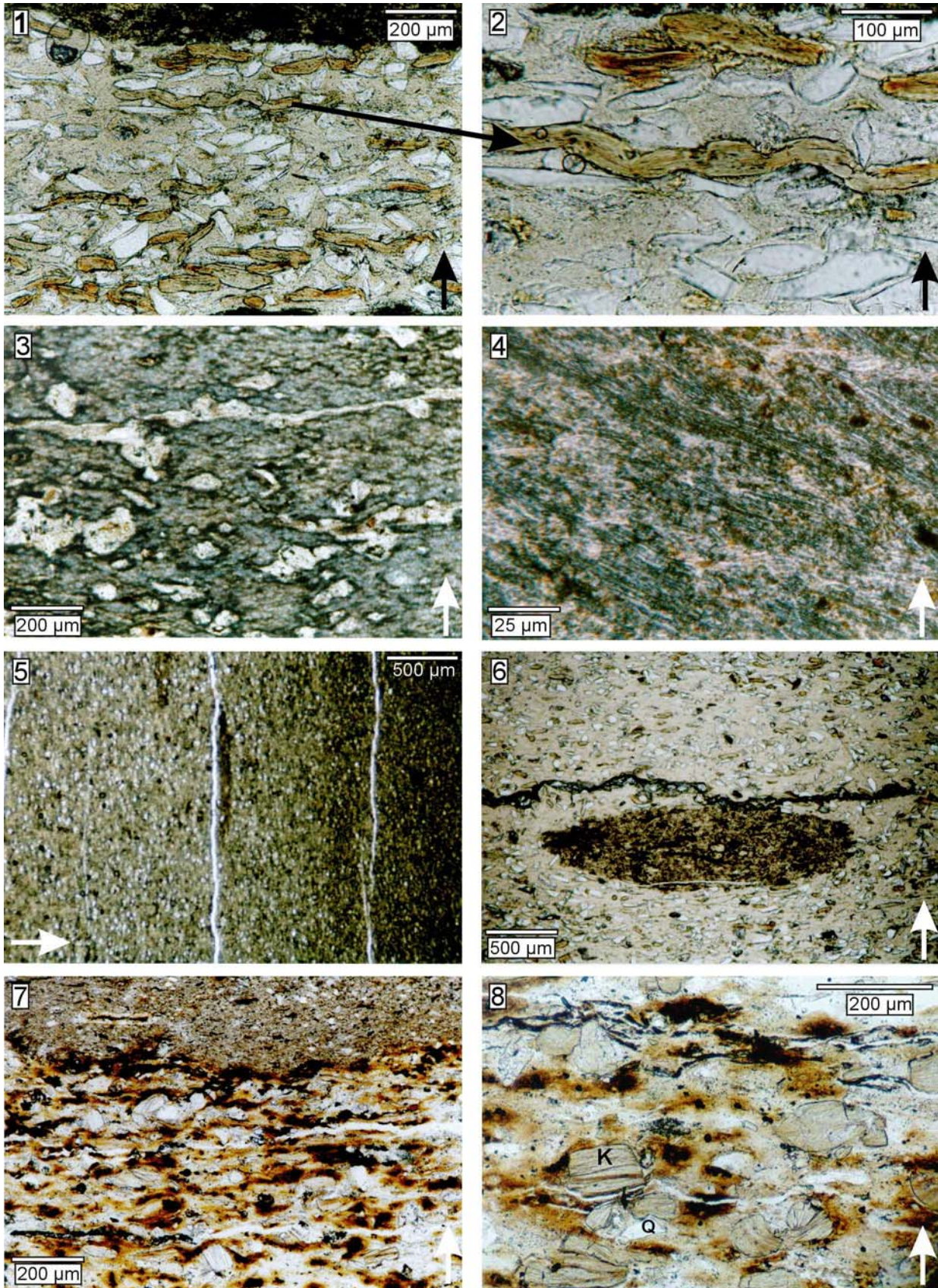


Plate 2: Selected photo-micrographs displaying the texture and relic structures of former volcanic glass within the examined tuff beds.

Plate 2: Selected photo-micrographs displaying the texture and relic structures of former volcanic glass.

- Fig. 1:** Photo-micrograph of tuff bed OL 1/69: 396.36 m displaying many quartz fragments, quartz splinters as well as thin and elongated, collapsed pumice which are mostly transformed into kaolinite. Larger, elongate, rectangular fragments of siltstones are located at the top and bottom of the photomicrograph (II Nic, 63 x).
- Fig. 2:** Same section of tuff bed OL 1/69: 396.36 m with larger magnification (163 x, II Nic) showing sinuous, elongated, collapsed pumice as well as quartz fragments and splinters embedded in a cryptocrystalline clay mineral matrix.
- Fig. 3:** Photo-micrograph of tuff bed VIIIa (#9) displaying irregularly formed, round to elongate flattened, partly coupled ash particles reaching a maximum length of 700 μm embedded in a crypto- to microcrystalline clay mineral matrix (63 x, II Nic).
- Fig. 4:** Photo-micrograph of tuff bed OL 1/69: 378.00 m mainly indicating compacted remnants of glass walls of flattened vesicles as well as collapsed pumice (500 x, II Nic).
- Fig. 5:** Photo-micrograph of the 9 mm thick, normally graded tuff bed OL 1/69: 390.59 m showing larger pyroclasts and quartz splinters at the base which decrease in size to the top (25 x, II Nic).
- Fig. 6:** Photo-micrograph of tuff bed OL 1/69: 396.36 m displaying a large fragment of siltstone (rip-up clast) within the crystal-rich tuff bed (25 x, II Nic).
- Fig. 7:** Photo-micrograph of tuff bed Ib (#2) showing the undulating but sharp contact between the tuff bed and the underlying siltstone, the heavily altered tuff bed is composed of singular quartz grains, large, secondary kaolinite booklets and secondary opaque minerals embedded in a cryptocrystalline, brown clay mineral matrix (63 x, II Nic).
- Fig. 8:** Photo-micrograph of tuff bed IVb (#2) revealing the typical texture of a heavily altered tuff bed sampled directly from the outcrop. Note the quartz fragments (Q), the secondary, partly fibrous kaolinite booklets (K) and the secondary, mostly clustered opaque minerals which are all embedded in the cryptocrystalline matrix (100 x, II Nic).

Collapsed pumice is conspicuous and reaches a maximum size of 160 x 20 μm . Another thin-section shows compacted remains of glass walls of flattened vesicles (Plate 2, Fig. 4, cf. Fisher and Schmincke, 1984). The tuff bed from the depth of 390.59 m is a 9 mm thick, normally graded tuff bed which displays up to 100 μm large pyroclasts and up to 70 μm large quartz splinters at the base. To the top the average size decreases to 20 μm (Plate 2, Fig. 5). The tuff bed from the depth of 396.36 m comes close to a crystal tuff as it has an exceptionally high portion of quartz fragments and splinters. Collapsed pumice grains are very thin and elongated and mostly transformed into kaolinite (Plate 2, Figs. 1 and 2).

Larger, elongate rectangular fragments of siltstones with a size of up to 2.0 x 0.5 mm probably represent rip-up clasts suggesting turbiditic action. They are found near the base of the tuff bed. Quartz splinters are particularly imbricated close to the siltstone fragments (Plate 2, Fig. 6). Finally the tuff bed from the depth 399.25 m probably shows multiple grading (three

layers) with pyroclasts reaching a maximum size of 200 x 60 μm .

Thin-sections of the tuff beds from the Ecca Group of the Western Cape Province of South Africa are similar to the ones of the borehole OL 1/69 but show a higher degree of kaolinisation of the ash as they were sampled from surface outcrops.

Thin-sections of the tuffaceous beds of east of Nondweni, KwaZulu/Natal (South Africa) occasionally reveal multiple normal grading units with a sharp but non-erosive contact to the underlying graded sequence. The base of each unit begins with angular, undeformed splinters of quartz 100 μm in size and relics of devitrified platy to cusped glass shards. The size and number of recognisable minerals decreases towards the top of each unit which is composed of a more monotonous matrix containing single devitrified glass shards relics about 10 μm in size (Fig. 85). All glass shards have irregular shapes due to their pyroclastic origin with the surfaces being slightly rounded probably by redepositional processes or by abrasion.

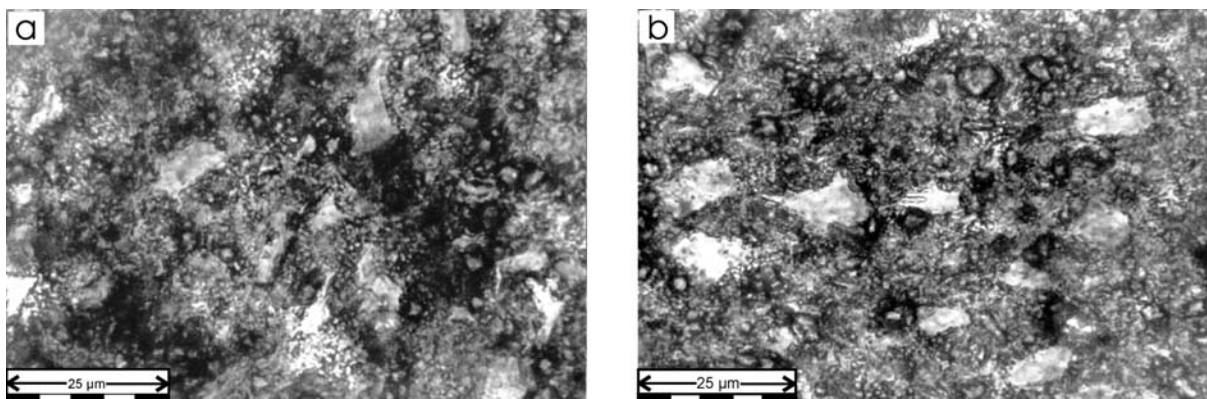


Fig. 85: Photo-micrographs of thin-sections of the Dwyka Group- aged tuffaceous beds east of Nondweni, KwaZulu-Natal, South Africa displaying mostly platy, about 10 μm large glass shards; enlargement 500x, II Nic.

Possibly juvenile, lithic fragments were very rarely detected within the thin-sections. A fine example is shown in Plate 2, Fig. 8 (left grain located above the scale) displaying a rounded, light green, granular grain with a length of 65 μm .

8.2.2.2 Quartz

Volcanically derived quartz is the most common juvenile mineral present in the analysed tuff beds.

Quartz phenocrysts generally occur in three different configurations - as fragments, splinters or complete, euhedral quartz grains. Quartz fragments are the most frequent displaying clear, subhedral to anhedral portions of euhedral phenocrysts (Plate 2, Figs. 2 and 8; Plate 3, Fig. 8). They are mostly triangular or rectangular but are also polygonal. Measurements of 70 fragments show that their lengths vary between 24 and 112 μm (average: 59 μm , standard deviation: 19.11 μm) and their width is between 12 and 96 μm (average: 35 μm , standard deviation: 15.26 μm).

Colourless, elongated, and inclusion-free quartz splinters display angular to cusped or thorn-shaped forms which indicate their volcanic / pyroclastic origin. They are occasionally aligned parallel to the bedding of tuff beds (Plate 2, Fig. 2; Plate 3, Fig. 8). 43 measurements show that they are between 24 and 120 (340) μm long (average: 58 μm , median: 48 μm , standard deviation: 48.78 μm) and between 3 and 40 μm wide (average: 16 μm , standard deviation: 7.23 μm).

Euhedral, hexagonal quartz phenocrysts are the least frequent (Plate 3, Fig. 4). They are characteristically 'water-clear' and crystallise as phenocrysts from silicic magmas in the high-temperature (beta) form, inverting to the low-temperature phase (alpha paramorph) when temperatures fall below 573° C within the magma (Deer et al., 1992). Their lengths range between 32 and 152 μm (average: 71 μm , median: 64 μm , standard deviation: 29.40 μm) and their width varies between 24 and 72 μm (average: 43 μm , standard deviation: 11.96 μm).

Mosaic-like extinction which is most likely caused by explosive eruption processes rarely occurs under polarised light. Quartz phenocrysts are occasionally marginally corroded probably due to the resorption of the edges within the magma (Donaldson and Henderson, 1980). Others show embayments similar to those recognised in zircons pointing to growth obstruction within the parent magma. However, some marginal corrosion of the quartz phenocrysts or rounding of their edges might have originated from post-depositional alteration or transport. Minute fluid inclusions or opaque substances were rarely observed within the quartz grains.

Visual estimates of quartz phenocryst contents within the tuffs reach 30 Vol.% (tuff bed at 396.36 m from OL 1/69), but principally contents of 1 - 5 Vol. % were determined (e.g. tuff bed Ib from the Aranos Basin). An upward decrease in grain size and number of quartz splinters within single tuff layers was locally observed.

8.2.2.3 *Apatite and zircon*

Juvenile, euhedral apatites and zircons were occasionally detected within the thin-sections of the tuff beds. The length of the apatites varies between 16 and 56 μm (average: 43 μm , standard deviation: 12.91 μm) and the width is between 6 and 40 μm (average: 49 μm , standard deviation: 16.47 μm ; 11 measurements) (Plate 3, Fig. 3). Zircons are between 30 and 88 μm long (average: 49 μm , standard deviation: 16.47 μm) and between 12 and 40 μm wide (average: 22 μm , standard deviation: 7.58 μm ; 19 measurements) (Plate 3, Figs. 1 and 2). Zircons occasionally show euhedral apatite inclusions whereas apatites display inclusions of zircon and elongate, tubular inclusions of volcanic glass. Both, apatites and zircons generally show a smaller grain size than in the heavy mineral separates. This is due to the different positions the heavy minerals are bisected in the thin-sections.

8.2.2.4 *Feldspar*

Euhedral to subhedral crystals of plagioclase with lamellar (polysynthetic) twinning were only detected in a thin-section of the borehole OL 1/69 from depth 396.36 m. They show maximum sizes of 96 x 56 μm (Plate 3, Fig. 6). Former feldspar also exists as relic structures within the tuff beds but is mainly replaced by kaolinite aggregates and vermicules. XRD analysis proved the presence of finely disseminated plagioclase (albite and anorthite) in the examined tuff beds whereas sanidine and microcline only occur in minor amounts. Due to the high susceptibility to alteration, feldspar contents within the tuff beds may not reflect their original abundance in the parent volcanic ash. Moreover, the relative amounts of different kinds of feldspar in tuffs may be modified from those of the parent ash because plagioclase, particularly Ca-rich varieties, is apparently much more altered or dissolved during weathering than K-feldspar (Banfield and Eggleton, 1990).

8.2.2.5 *Biotite*

In contrast to the examined heavy mineral separates biotite occurs in thin-sections of almost all tuff beds as euhedral but mostly subhedral to

anhedral flakes which are mostly altered to a certain degree into kaolinite. As kaolinite has a specific gravity of 2.61 - 2.68 g/cm^3 (Deer *et al.*, 1992), it is likely that most of the minerals were not separated by the heavy liquid which has a density of approximately 2.90 g/cm^3 . When detected, biotites are principally the largest phenocrysts in the tuff beds reaching an average length of 100 μm (40 - 240 μm , with a high standard deviation of 47.29 μm) and an average width of 62 μm (24 - 120 μm , with a high standard deviation of 29.14 μm ; overall 52 measurements). The principally thin, normally bleached, yellow-green to light brown flakes reach greatest sizes in tuff beds Ib and IVb from southern Namibia (Plate 3, Fig. 5) and in the tuff bed from 396.36 m of OL 1/69 in which biotites show an internal mesh of small apatite inclusions (see Chapter 9.4.2). Biotites are occasionally slightly pleochroitic and opaque at the crystals' rims. Some show lateral embayments due to resorption processes in the parent magma chamber (cf. Donaldson and Henderson, 1980); others possess minute opaque inclusions. Alteration of the biotites often proceeds from the edges inward (Bohor and Triplehorn, 1993) which finally leads to expansion and the formation of a kaolinite vermicule (Chapter 8.2.3.1).

8.2.3 *Secondary minerals*

8.2.3.1 *Kaolinite*

Slightly pleochroitic, yellow to light brown kaolinite appears in three different varieties within the examined tuff beds in varying amounts: (1) very fine-grained crystals with only a few microns in size mostly occurring as pore-filling clay or dispersed in the microcrystalline matrix, (2) mostly large platy or fibrous stacks of crystals varying in length between 40 and 232 μm (average: 99 μm , standard deviation: 39.20 μm) and in width between 16 and 104 μm (average: 53 μm , standard deviation: 19.77 μm ; 108 measurements) and (3) rarely vertical columnar and vermicular stacks of kaolinite crystals displaying a length of up to 128 μm (average: 68 μm) and a width of up to 136 μm (average: 93 μm ; 8 measurements).

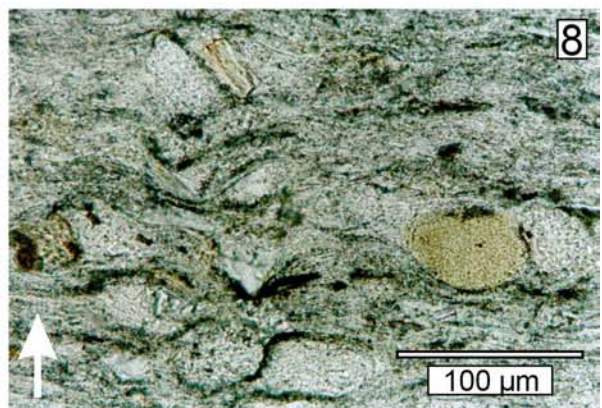
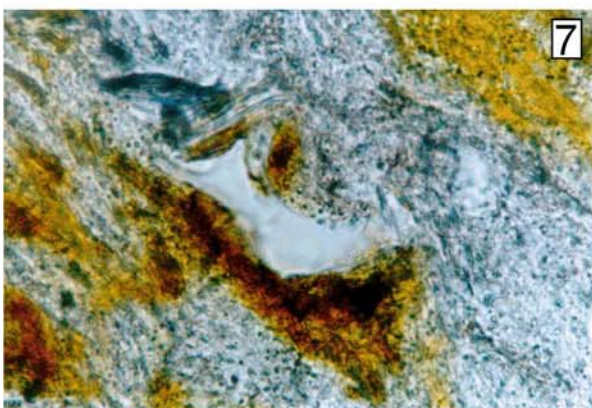
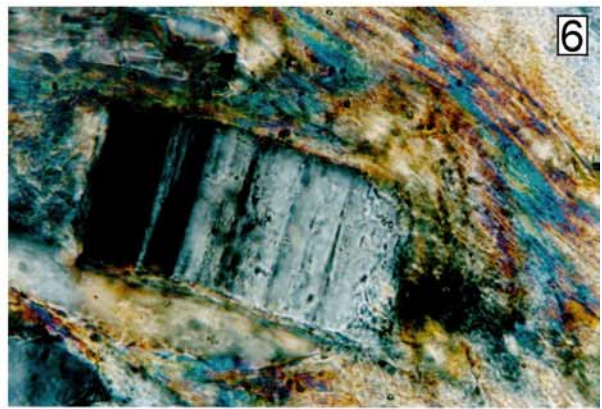
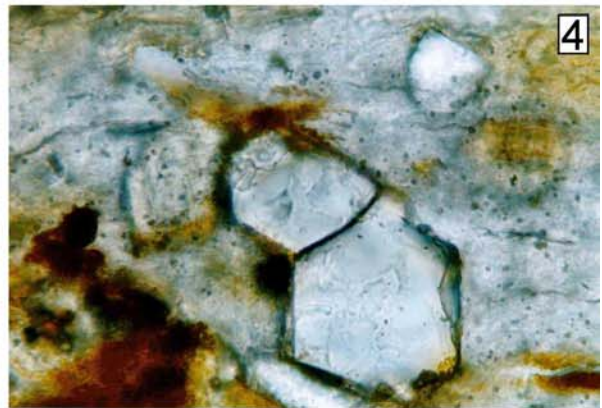
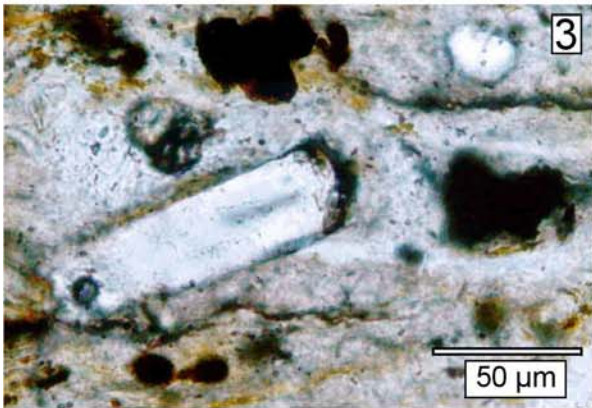
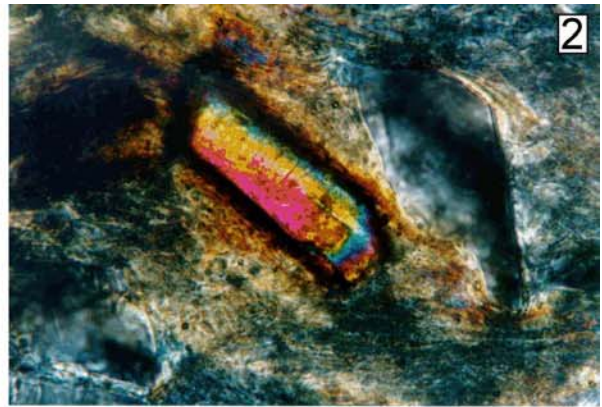
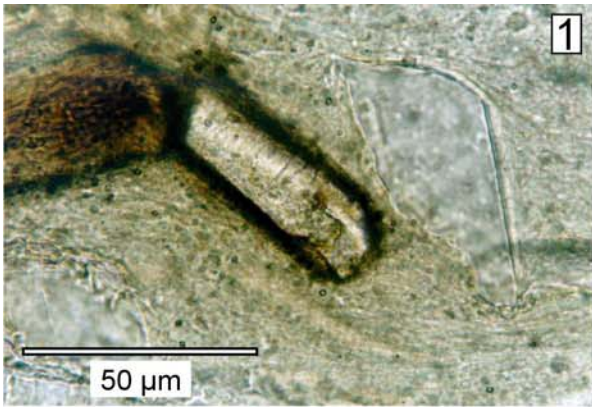


Plate 3: Selected photo-micrographs displaying typical phenocrysts contained within the examined tuff beds.

Plate 3: Selected photo-micrographs displaying typical phenocrysts contained within the examined tuff beds.

Fig. 1: euhedral zircon, quartz fragments and an unidentified mineral in tuff bed OL 1/69: 396.36 m, II Nic, 630 x.

Fig. 2: same as Fig. 1 but X Nic.

Fig. 3: euhedral apatite displaying an elongate and a darker, globular inclusion, quartz crystal and opaque ore minerals, #2 tuff IVb, II Nic, 400 x.

Fig. 4: euhedral β -quartz, #2 tuff IVb, II Nic, 630 x.

Fig. 5: slightly fractured and altered, subhedral biotite, #2 tuff IVb, II Nic, 630 x.

Fig. 6: euhedral crystal of plagioclase with lamellar (polysynthetic) twinning, OL 1/69: 396.36 m, X Nic, 630 x.

Fig. 7: single y-shard in tuff bed #23 Ib (II Nic, 630 x).

Fig. 8: typical texture of a tuff bed of OL 1/69: 390.59 m, note the quartz crystals and fragments and the green, lithic fragment embedded in a clay mineral-dominated matrix (II Nic, 250 x).

The internal arrangement of single kaolinite plates within the vermicules is mostly horizontal and aligned parallel to bedding of the tuff beds but may also attain oblique to vertical positions. A fan-shaped arrangement in curved vermicules is especially found in tuff bed IVc from the Aranos Basin. Kaolinite vermicules are especially conspicuous within heavily weathered tuff beds from surface outcrops (e.g. tuff IVb from the Aranos Basin, Plate 2, Fig. 8) and less frequent in thin-sections from boreholes such as OL 1/69.

Within the examined tuff beds, kaolinite formed mainly from the alteration of glass, biotites and feldspar and can also be pseudomorphic after these minerals (cf. Bohor and Triplehorn, 1993). The characteristic vermicules probably crystallised *in situ*- (cf. Heim, 1970) and were not formed from a gel (Eberl *et al.*, 1990).

8.2.3.2 Muscovite

Muscovite occurs in tuff beds Ib, Ic, IIb, IVb, IVc, VI of the Aranos Basin in minor contents up to 2 Vol. %. The thin, colourless flakes measure up to 160 μm in length (average: 77 μm) and up to 24 μm in width (average: 12 μm , 9 measurements). The flakes are mostly aligned parallel to bedding but occasionally also oblique. Small stacks of several individual muscovite crystals were occasionally found stacking together with intercalated kaolinite vermicules.

Muscovite often occurs as a secondary product of altered feldspar and biotite. Bohor and Triplehorn (1993) classified muscovite as a non-

volcanic mineral and therefore as a detritally derived. As abundant muscovite flakes are present in the mudstones adjacent to the examined tuff beds, muscovite is thought to be mainly a detrital component within the tuff beds. Highest amounts of muscovite were especially detected in the tuff bed VI from the Aranos Basin. Nevertheless, muscovite is being reported as a primary component in tuff beds from the Lower Rotliegend of the Saar-Nahe-Basin (Königer, 1999) as well as in a tuff bed from the Upper Rotliegend of the Saar-Nahe-Basin (Schleicher and Lippolt, 1981; Stollhofen, 1991).

8.2.3.3 Opaque minerals

Black or occasionally brown-red opaque minerals such as goethite occur finely dispersed in nests or in streaks (Plate 2, Fig. 8). Grains are mostly round(ed) but sporadically angular to subangular. The size of the grains varies but is mostly below 5 μm . Finely dispersed opaque minerals trace the structure of the original glassy matrix occasionally appearing as a net-like structure. XRD analysis reveals that the main opaque minerals consist of goethite, ulvospinel and iwakiite (see Chapter 8.3.5). In tuff bed Ib from the Aranos Basin of southern Namibia up to 160 μm large, secondary hematite crystals were detected which are red-brown, pseudo-hexagonal and radially fibrous.

8.2.3.4 Carbonates

Some tuff beds contain varying amounts of finely dispersed carbonate. Carbonate most likely formed by precipitation from groundwater that seeped through the porous tephra deposit before they were compacted. Especially tuff bed VIIIa Ib from the Aranos Basin of southern Namibia contains considerable amounts of calcite.

8.3 Mineralogy of all examined marker beds deduced from XRD-analysis

In order to confirm the results of the mineralogical investigations of the thin-sections, extensive X-ray based measurements were carried out on 15 samples of 8 different tuff beds of the Ganigobis Shale Member (Dwyka Group, southern Namibia). Additional XRD-measurements were done on samples of the tuffaceous beds from Nondweni, KwaZulu-Natal and of two tuff beds from the Ecca Group of the Western Cape Province (South Africa).

Measurements were carried out in three different ways (all methodologies and equipment used are listed in Appendix B-3.1):

- 1, on whole rock powder samples (at the Geologisches Landesamt Rheinland-Pfalz in Mainz, Germany) (Appendix D-2)
- 2a, on non treated textured specimens of the separated clay fraction on a smear slide (at the Mineralogisches Institut, University of Würzburg, Germany; cf. Figs. 87-90)
- 2b, on textured specimens of the separated clay fraction on a smear slide, treated with glycerol (at the Mineralogisches Institut, University of Würzburg, Germany; cf. Figs. 87-90)

The reflections of the clay minerals are mainly superposed by reflections of quartz in powder samples. Quartz was mainly removed during clay mineral separation. The separated clay fraction of the bentonitic tuff beds (untreated and treated with Glycerol) was used to specify the clay mineral content. Measurements of the separated clay fraction were analysed by hand with tables listed in Heim (1970). Quartz and feldspars in the clay fractions were partly determined by hand whereas all other minerals were determined with the help of the software Winjade 3.1 (powder diffraction files from 1996). In the following the mineralogical content of the measured tuff beds will be described.

Summary: The tuff beds mainly consist of clay minerals such as illite and randomly interstratified illite-montmorillonite clay minerals with minor kaolinite, palygorskite or chlorite, quartz and feldspars. Minor components are muscovites, pyroxenes, Fe- and Ti-oxides, hydroxides, sulphates, phosphates, carbonates and borates (Tab. 7). A quantitative analysis is elaborated in Chapter 8.3.6.

Tuff	clay minerals							zeolites
	quartz	illite	illite/smectite-ML	smectite-group	kaolinite-group	palygorskite	chlinochlore	
# 2 T Ib	x	x	IM-ML :76% illite	x				x
# 2 T IIb	x	x	IM-ML :74% illite	x	x			
# 23 T IIb	x	x	IM-ML :73% illite	x		x		
# 28 T IIb	x	x	IM-ML :72% illite	x	x	x		
# 32 T IIb	x	x	IM-ML :90% illite	x	x			x
# 45 T IIb	x	x	IM-ML :71% illite	x				
# 30 T IVa	x	x	IM-ML :72% illite	x	x	x		x
# 32 T IVa	x	x	IM-ML :70% illite	x		x		
# 2 T IVb	x	x	IM-ML :78% illite	x	x	x	x	
# 2 T V	x	x	IM-ML :76% illite	x	x		x	x
# 23 T V	x	x	IM-ML :70% illite	x	x			x
# 15 T VII	x	x	IM-ML :73% illite	x	x		x	x
# 27 T VIIIa	x	x	not analysed	not analysed	not analysed	not analysed		x
# 9 T VIIIa	x	x	IM-ML :78% illite	x	x			
# 31 Tuff	x	x	not analysed	not analysed	not analysed	not analysed		x
# 13 Tz B	x	x	not analysed	x		x		x
Ecca N Klarstroom/RSA	x	x	IM-ML :90% illite	x		x		x
Ecca N Ladismith/RSA	x	x	IM-ML :90% illite		x	x		x
Dwyka Nondweni/RSA	x	x	not analysed	x	x	x	x	x

Tuff	mica				feldspar		other silicates	
	muscovites	Li-mica	Na-mica	V-mica	plagioclase	K-feldspar	pyroxenes	garnet
# 2 T Ib	x				x			
# 2 T IIb	x	x						
# 23 T IIb	x	x					x	
# 28 T IIb	x	x	x					
# 32 T IIb	x	x				x		
# 45 T IIb	x	x						
# 30 T IVa	x				x	x	x	
# 32 T IVa	x				x			
# 2 T IVb	x		x		x			
# 2 T V	x	x	x	x				
# 23 T V	x	x						
# 15 T VII	x				x			
# 27 T VIIIa					x			
# 9 T VIIIa	x				x			x
# 31 Tuff	x	x			x	x		
# 13 Tz B	x				x	x		
Ecca N Klarstroom/RSA	x							
Ecca N Ladismith/RSA	x	x						
Dwyka Nondweni/RSA					x	x		

Tuff	zircon	oxides			phosphates	sulphates	carbonates	borates	hydroxides
		Ti-oxides	Fe-oxides						
# 2 T Ib			x						
# 2 T IIb	x	x	x			x			
# 23 T IIb		x	x			x			
# 28 T IIb		x	x	x	x	x			
# 32 T IIb			x	x	x	x			
# 45 T IIb	x	x	x						
# 30 T IVa		x					x		
# 32 T IVa			x		x				
# 2 T IVb		x	x	x	x				
# 2 T V		x	x						
# 23 T V		x	x	x	x			x	
# 15 T VII			x	x					
# 27 T VIIIa				x	x		x	x	
# 9 T VIIIa			x	x		x			
# 31 Tuff			x		x				
# 13 Tz B			x	x	x				
Ecca N Klarstroom/RSA			x	x	x				
Ecca N Ladismith/RSA			x	x			x		
Dwyka Nondweni/RSA			x		x				

Tab. 7: Overview of the mineralogical composition of the examined tuff beds by XRD analysis (x: detected).

8.3.1 Clay minerals

8.3.1.1 Illite

Illite is the main clay mineral in the analysed tuff beds. Illites are fine-grained, dioctahedral mica-like clays that usually contain less K, more water and less tetrahedral Al compared to the coarser grained muscovite micas (Wilson, 1987). Polytypes of illites 1 Md show rather broad reflections which are often asymmetrical towards the low-angle side due to marginal swelling (Wilson, 1987). In the analyses of the clay fraction the 10 Å-peak is hidden by the (001) illite / (002) smectite peak whereas other prominent peaks are characteristic at 4.90 Å (002), 4.49 Å (020) and 2.00 Å (005). Other peaks which mostly occur in the glycerol-treated clay fraction are found at 3.33 Å (003), 2.88 Å (023), 2.57 Å (130), 2.38 Å (220) and 2.13 Å (202).

Illite 2 M1 and 2 M2, which has usually more narrow and sharper reflections (Wilson, 1987), was additionally analysed in the diagrams of the powder samples but not in the diagrams of the clay fraction.

8.3.1.2 Interstratified illite / smectite clay minerals

Randomly interstratified illite / smectite clay minerals were detected in almost all samples of the separated clay fraction. They are represented by a very characteristic reflection of 001 illite / 002 smectite which is mostly found at 11.36 Å (cf. Heim, 1971) and which reaches up to 9920 counts in #23 tuff V. Two important peaks of these illite / smectite mixed layered clay minerals (IS-ML) are at 4.94 Å (002 I / 004 S) which may interfere with the reflection of illite 1 Md (002) at 4.89 Å and at 3.38 Å (003 I / 005 S) which may interfere with the reflection of (003) illite 1 Md at 3.33 Å. Measurements of the clay fraction treated with glycerol revealed a reflection of (001 I / 001 S) at an average of 13.45 Å varying between 12.93 Å and 14.39 Å. The characteristic reflection of 001 I / 002 S shifts to lower Å-values ranging between 9.55 and 9.98 Å with an average of 9.72 Å. Using the peak-migration

curve of Reynolds (1980) (Fig. 86), the percentage of illite within the mixed layered illite / smectite clay minerals can be determined. Values vary between 70 and 78 % (90 %) averaging 73.6 % illite for the tuff beds from the Aranos Basin of southern Namibia (Tab. 8).

Tuff bed	% Illite of IS-ML
#2 T Ib	76
#2 T IIb	74
#45 T IIb	71
#2 T IVb	78
#2 T V	76
#23 T IIb	73
#23 T V	70
#28 T IIb	72
#30 T IVa	72
#32 T IVa	70
#9 T VIIa	78
#15 T VII	73
Mean	73.58
Ecca N Ladismith	90
Ecca N Klarstroom	90
E Nondweni, RSA	90

Tab. 8: Percentage of illite within the mixed layered illite / smectite clay minerals of the examined tuff beds.

Subsequently 22 - 30 % (10 %) smectite remains which is still enough to allow the bentonitic material to swell after contact with water. Glycerol-treated samples occasionally reveal peaks of (002 I / 003 S) at 5.25 Å (#23 tuff V, Fig. 89: 6) and (003 I / 006 S) at 3.17 Å (#2 tuff Ib, Fig. 87: 2).

Regular interstratified illite / smectite clay minerals called rectorite were additionally detected in the measured powder samples. The main reflection of 26.6 Å could not be detected due to insufficiencies of the diffractometers both in Mainz and Würzburg, the 13.3 Å peak may interfere with the (001 I / 001 S) reflection of randomly interstratified illite/smectite in the measured clay fraction.

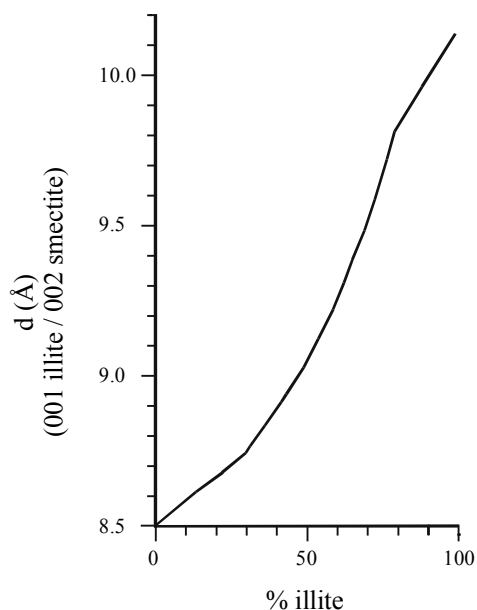


Fig. 86: Peak-migration curve for randomly interstratified 001 illite – 002 smectite (Reynolds, 1980)

8.3.1.3 Smectite

A rather unusual peak of smectite appears at 18.26 Å in the glycerol-treated clay fraction of the tuffaceous beds east of Nondweni in South Africa (Fig. 90: 8).

8.3.1.4 Kaolinite

The dioctahedral clay mineral kaolinite appears only in minor amounts in the analysed tuff beds and is easily recognised with the (001) reflection at 7.16 Å and the (002) reflection at 3.57 Å (e.g.: Fig. 88: 5).

8.3.1.5 Palygorskite

Palygorskite has a fibrous morphology and a chain structure and differs therefore from all other clay minerals which are layer-silicate minerals. It was only pinpointed in the analyses of the clay fractions with its reflection at 6.37 Å (200), other reflections of palygorskite were not found. However, palygorskite was also detected in tuff beds of the Ecca Group by Viljoen (1995) (e.g.: Fig. 87: 7 and Fig. 90: 3 and 5).

8.3.1.6 Clinochlore

Trioctahedral clinochlore is a Mg-rich chlorite. The most prominent reflection in the measured clay fraction of the tuffaceous beds east of Nondweni in South Africa is the (001) peak of clinochlore with 7022 counts. Further peaks occur at 4.75 Å (003), at 2.87 Å (005) which interferes with illite 1 Md (023), 2.70 Å and 2.63 Å (Fig. 90: 7). Clinochlore was also identified in #2 tuff IVb with its (002) peak at 7.07 Å (Fig. 89: 1) and in #2 tuff Vc (Fig. 89: 3) respectively # 15 tuff VII (Fig. 89: 7) with its (004) peak at 3.51 Å.

8.3.2 Quartz

Quartz occurs in all analysed bentonitic tuff beds to varying amounts (cf. chapter 8.2.2.2). With the separation of the clay fraction, quartz was mostly eliminated from these samples and occurred only in few samples such as #32 tuff IIb, #2 tuff Vc, #23 tuff V, #15 tuff VII and the analysed tuff beds from South Africa. Prominent peaks are mostly found at 3.34 Å and 4.26 Å, others include 2.46 Å, 2.24 Å, 2.13 Å and 1.83 Å (e.g.: Fig. 90: 7).

8.3.3 Feldspars

Albite is the most important feldspar found in almost all the analysed tuff beds. The characteristic reflection is at 3.19 Å, another important peak is found at 3.79 Å (especially in #23 tuff V, Fig. 89: 5), others include 4.04 Å and 3.68 Å. Next frequently analysed in the powder samples is anorthite. Most of the feldspars are therefore plagioclases.

K-feldspars such as sanidine, orthoclase, anorthoclase and microcline were only sporadically identified and only in the tuffaceous beds from east of Nondweni, South Africa, K-feldspar becomes more important (Fig. 90: 7). Feldspars were not detected in the analysed tuff beds from the Ecca Group of South Africa.

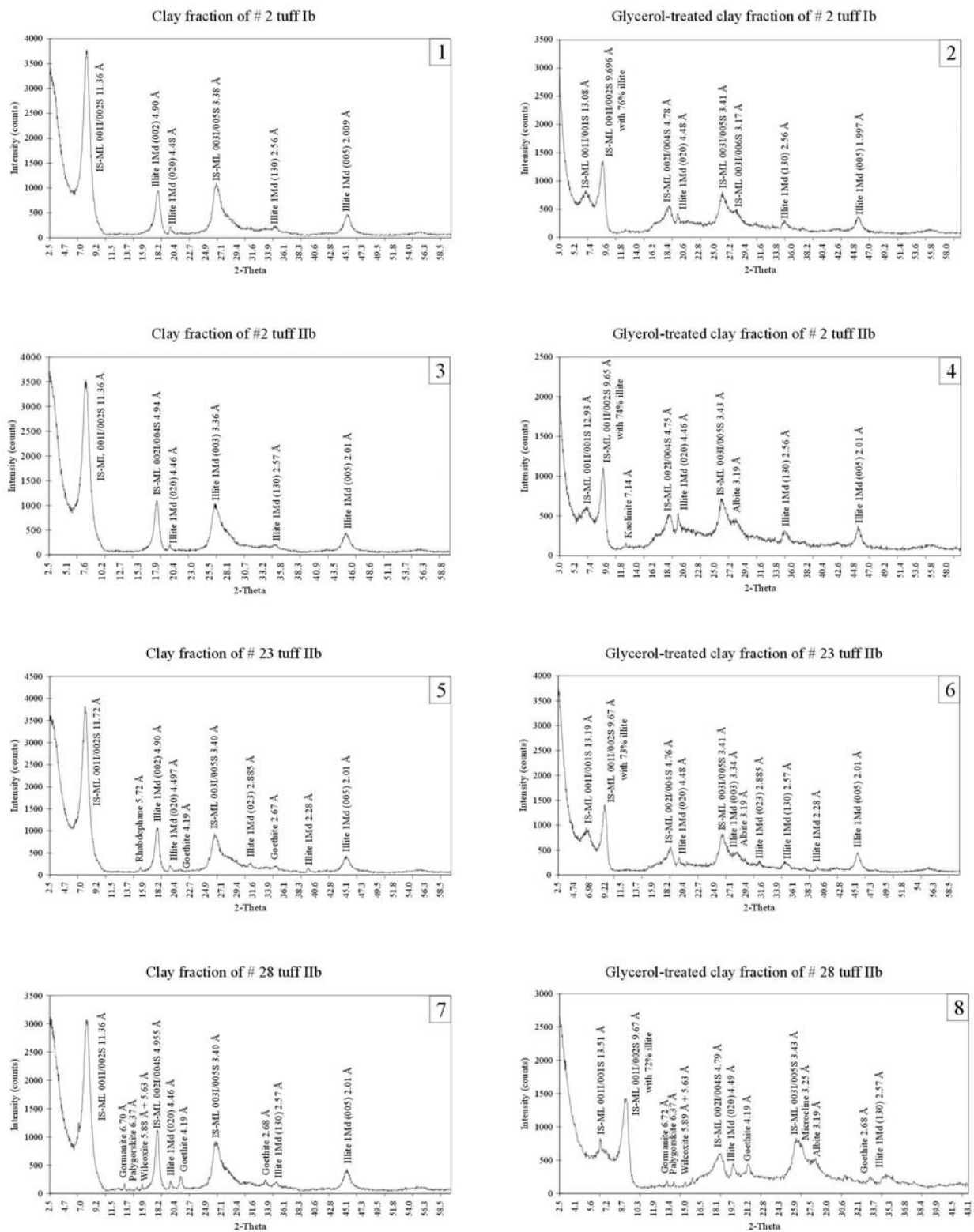


Fig. 87: X-ray diffractometer traces of the non-treated clay fraction (left) and of the glycerol-treated clay fraction (right) of #2 tuff Ib (1, 2) and IIb (3, 4) from 2 km north of Ganigobis as well as well as of #23 tuff IIb (5, 6) from 5 km south of Ganigobis and of #28 tuff IIb (7, 8) from 13 km north of Ganigobis (DS II, Dwyka Group, Aranos Basin, southern Namibia).

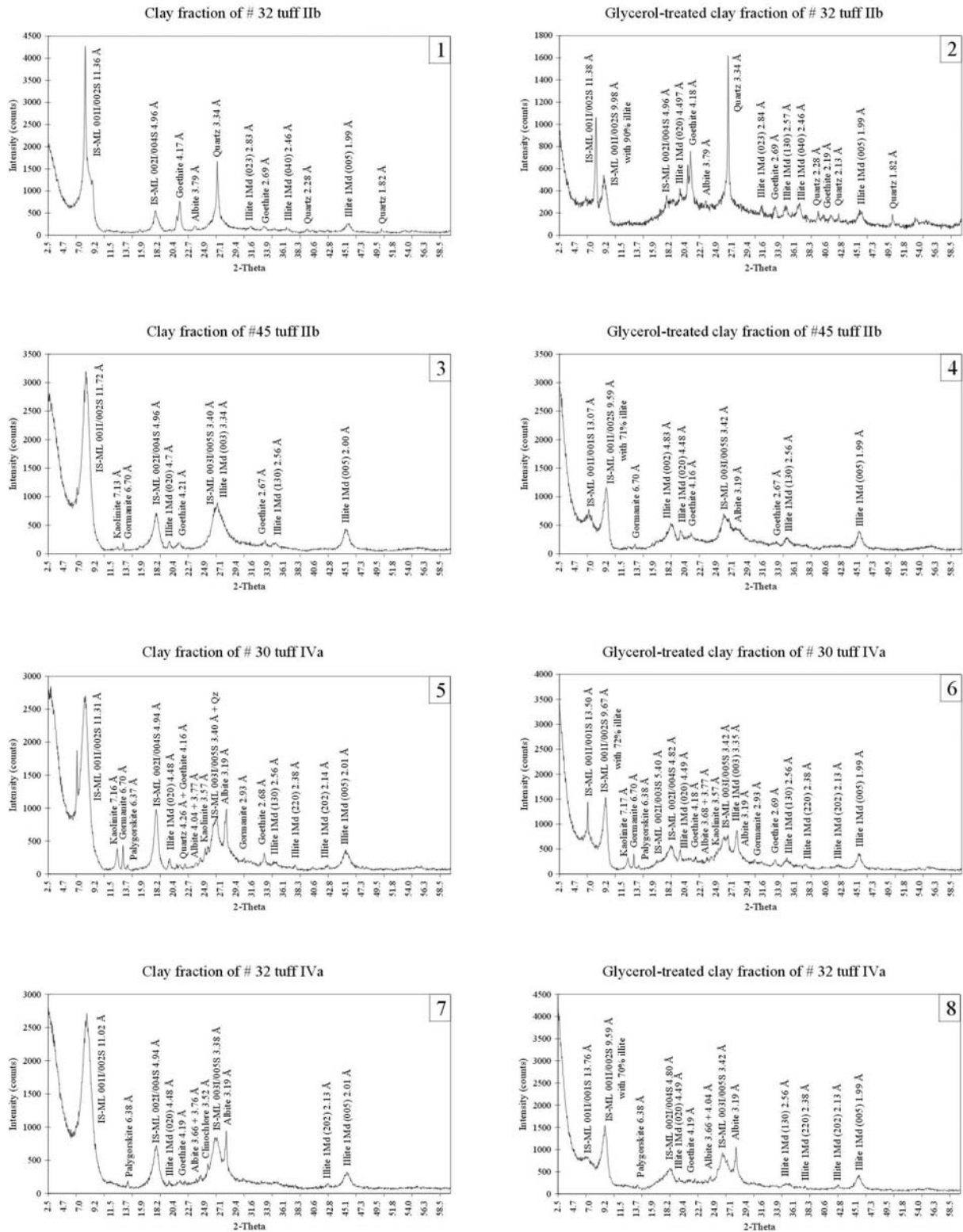


Fig. 88: X-ray diffractometer traces of the non-treated clay fraction (left) and of the glycerol-treated clay fraction (right) of #32 tuff IIB (1, 2) from 18 km north of Ganigobis, #45 tuff IIB (3, 4) from 12 km southwest of Ganigobis, #30 tuff IVa (5, 6) from 19 km north of Ganigobis and of #32 tuff IVa (7, 8) from 18 km north of Ganigobis (DS II, Dwyka Group, Aranos Basin, southern Namibia).

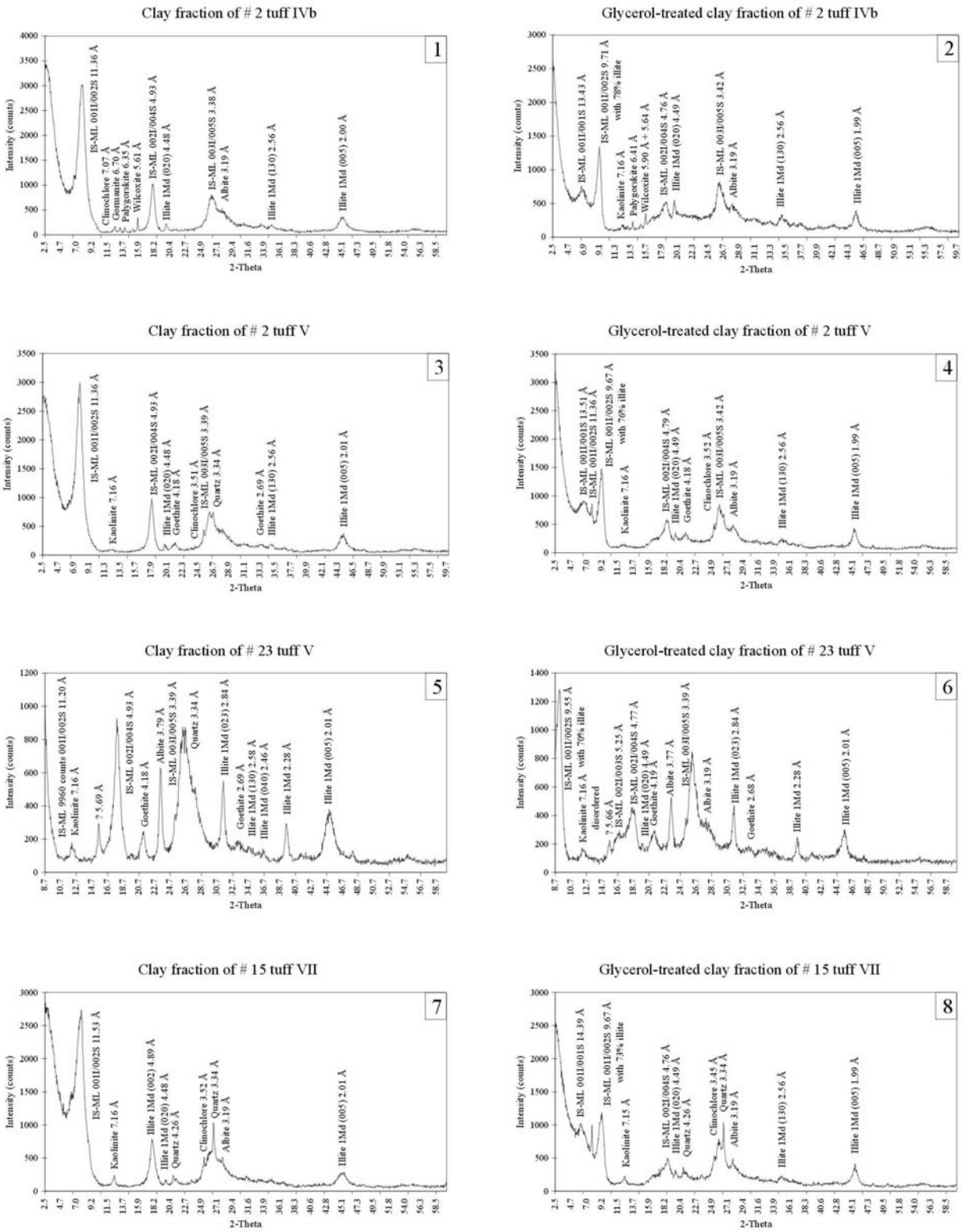


Fig. 89: X-ray diffractometer traces of the non-treated clay fraction (left) and of the glycerol-treated clay fraction (right) of #2 tuff IVb (1, 2) and #2 tuff Vc (3, 4) from 2 km north of Ganigobis, #23 tuff V (5, 6) from 5 km south of Ganigobis and of #15 tuff VII (7, 8) from 5 km north of Ganigobis (DS II, Dwyka Group, Aranos Basin, southern Namibia).

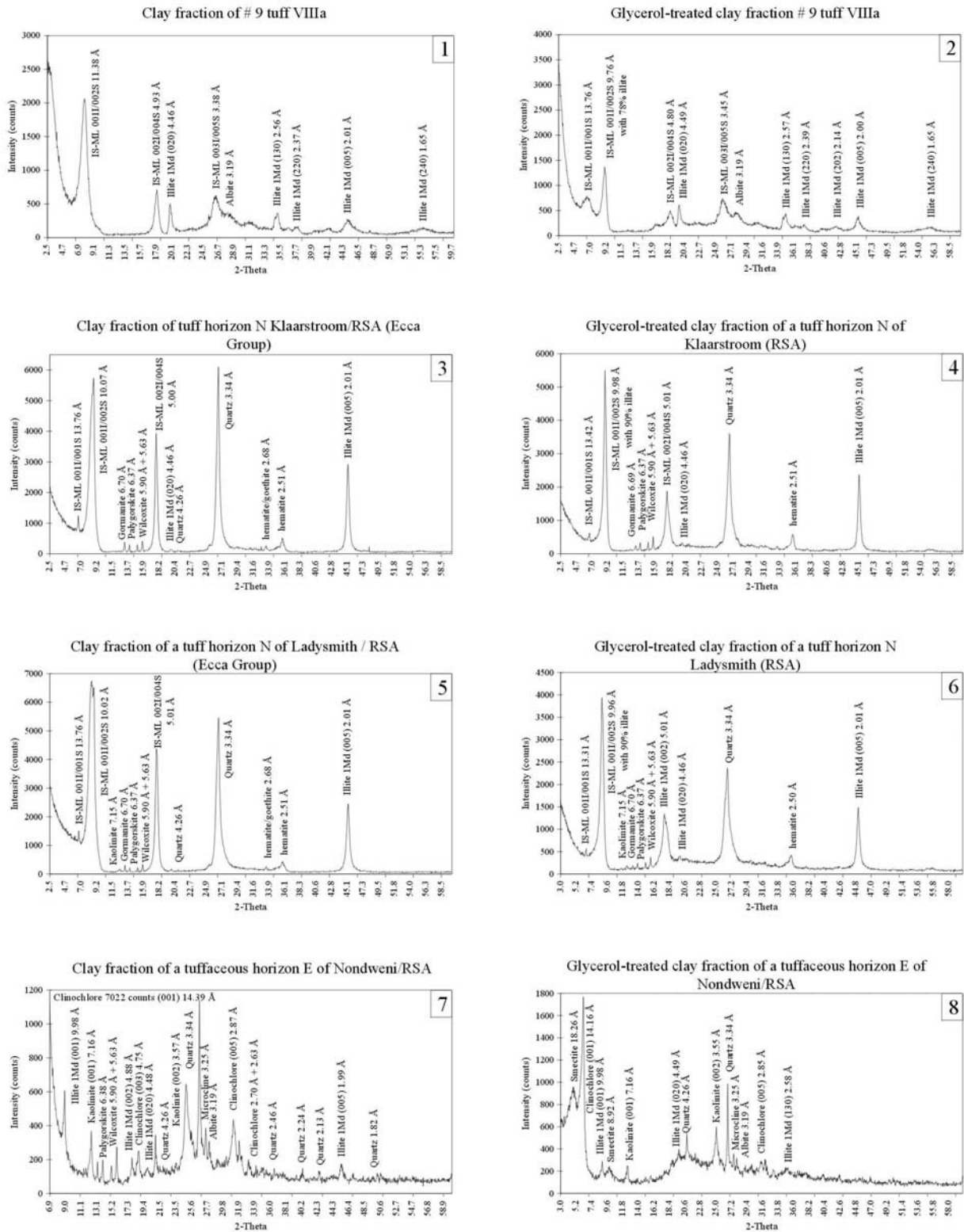


Fig. 90: X-ray diffractometer traces of the non-treated clay fraction (left) and of the glycerol-treated clay fraction (right) of #9 tuff VIIIa (1, 2) from 18 km NNW of Ganigobis (DS II, Dwyka Group, Aranos Basin, southern Namibia), of tuff beds from north of Klaarstroom (3, 4) and north of Ladysmith (5, 6; Ecca Group, main Karoo Basin, South Africa) and of tuffaceous beds from east of Nondweni (Dwyka Group, main Karoo Basin, South Africa).

8.3.4 Mica

In almost all measured powder samples micas were analysed with the help of the software Winjade 3.1. Due to the similar position of their reflections 5 different polytypes of muscovites and 4 different polytypes of lepidolite (Li-mica) were listed, paragonite (Na-muscovite), roscoelite (V-mica) and montdorite (biotite) were only sporadically identified.

8.3.5 Other minerals

Other minerals were mostly recognised in the powder samples and analysed with the software Winjade 3.1:

A zeolite (gismodine) was frequently identified within the analysed tuff beds. Minor peaks of Ti-oxides such as rutile, anatase and brookite were in cases detected in powder samples. Occurrences of these Ti-oxides approximately coincide with the heavy mineral contents of the tuff beds.

Pyroxenes, tourmaline (schörl), zircon, garnet (pyrope) occasionally occur. The high content of zircon in tuff bed IIB detected in the heavy mineral samples was confirmed by the XRD-analysis. Pyrope was found both in the heavy mineral samples and in the XRD-analysis in #9 tuff VIIa. However, tourmaline occurred in different tuff beds.

Fe-oxides comprise goethite, ulvospinel (Fe_2TiO_4), iwakiite (MnFe_2O_4) and jacobsonite (MnFe_2O_4), gibbsite ($\text{Al}(\text{OH})_3$) and boehmite ($\text{Al}(\text{OOH})$) are hydroxides. Quite frequent are sulphates such as barite, anhydrite, wilcoxite ($\text{MgAlSO}_4 \cdot 2\text{H}_2\text{O}$), jarosite ($\text{KFe}_3(\text{SO}_4)_2(\text{OH})_6$) and bassanite ($\text{CaSO}_4 \cdot 0.5\text{H}_2\text{O}$). Minor amounts of phosphates comprise celestine ($(\text{Sr},\text{Ba})\text{SO}_4$), rhabdophane ($\text{CePO}_4 \cdot \text{H}_2\text{O}$), gormanite ($\text{Fe}_3\text{Al}_4(\text{PO}_4)_4(\text{OH})_6 \cdot 2\text{H}_2\text{O}$), sidorenkite ($\text{Na}_3\text{Mn}(\text{PO}_4)(\text{CO}_3)$) and collinsite ($\text{Ca}_2\text{Mg}(\text{PO}_4)_2 \cdot 2\text{H}_2\text{O}$). Carbonates such as calcite, aragonite and strontianite (SrCO_3) and borates such as warwickite ($(\text{Mg},\text{Fe})_3\text{Ti}(\text{BO}_3)_2\text{O}_2$) and inyoite ($\text{CaB}_3\text{O}_3(\text{OH})_5 \cdot 4\text{H}_2\text{O}$) occasionally occur. Goethite, hematite, rhabdophane, gormanite and wilcoxite were also analysed in the measured clay fractions.

8.3.6 Quantitative analysis of the XRD-measurements

The (semi-)quantitative interpretation of the XRD-measurements is attained by the comparison between relative peak heights (cf. Brime, 1985). In this type of approach, no account is taken of the variable diffracting powder of individual mineral species which results from differences in composition, degree of crystallinity, etc. (Wilson, 1987). Other, more accurate but also more time-consuming methods are for example described in Chung (1974a and b). The quantitative analysis of the powder samples was carried out by D. Bühmann (Council for Geoscience) in Pretoria (South Africa).

Methodology: Following the identification of all existing mineral phases, the background radiation is determined and subtracted from the analysed peak heights. The heights of the most prominent peaks are determined and added. The results are converted into percent. The peak heights of certain minerals are corrected by factors (listed in (JCPDS, 1974). Quartz and calcite, for example, are reduced by a factor 3. The peak height of the clay minerals are determined by the first, strong reflection (smectite 14.5 Å, illite 10 Å, kaolinite and chlorite each 7.1 Å). If kaolinite and chlorite are both present, the 7.1 Å reflection is the sum of both minerals; the ratio between kaolinite and chlorite is determined by the ratio of the peaks at 3.58 Å (kaolinite) and 3.54 Å (chlorite).

Results: Illite and illite / smectite mixed layered clay minerals mostly dominate the mineral suite and vary between 45 and 87 %. Tuff beds from outcrop localities #30 and 32 show contents of only 15-18 % illite / smectite due to the high percentages of plagioclase. Generally, illite shows a ratio between the peak heights of 10 Å and 4.45 Å of 1:1 (#31 tuff) and 1:4 (#32 tuffs IIB and IVa) which might be due to the different proportions of sanidine in the tuff bed from #31 and plagioclase in the tuff beds from #32. The tuffaceous beds east of Nondweni in South Africa apparently contain no illite. Tuff bed IVb from outcrop locality #2 is dominated by illite (49 %) and chlorite (34 %); kaolinite was not analysed in any

sample.

Quartz shows the highest proportions (71 %) in the beds east of Nondweni suggesting that these beds are tuffaceous in nature. Tuff beds from the area of Ganigobis (Aranos Basin, southern Namibia) display proportions between 3 % (tuff beds IVb and VIIIa) and 26 % (tuff beds V).

Albite is present in most samples and varies between 0 and 19 %. However, tuff bed IVa from outcrop localities #30 and 32 contains up to 75 % albite. K-feldspars such as *sanidine* and *microcline* occur in four tuff beds with contents less than 10 %. The distinction between peaks of

different K-feldspars is rather complicated as they interfere with each other.

The Ti-oxide *anatase* occurs in tuff beds IIb, V and VIIIa from southern Namibia in proportions between 7 and 19 %. Tuff bed VIIIa from outcrop locality #9 additionally contains 36 % *calcite* probably due to the directly overlying boundstones. However, tuff bed VIIIa from the top of outcrop locality #27 consists of up to 76 % (water-saturated) *gypsum* whereas tuff bed V from locality #23 shows 13 % *barite* and 40 % *rhabdophane* (Ce-phosphate; Tab. 9).

Tuff horizon	Illite/Smectite	Chlorite	Quartz	Albite	Sanidin	Microcline	Anatase	Calcite	Gypsum	Bassanite	Barite	Rhabdophane
#2 T Ib	68	0	18	12	3	0	0	0	0	0	0	0
#2 T IIb	87	0	7	7	0	0	0	0	0	0	0	0
#23 T IIb	71	0	9	8	0	0	12	0	0	0	0	0
#28 T IIb	70	0	11	19	0	0	0	0	0	0	0	0
#32 T IIb	15	0	10	75	0	0	0	0	0	0	0	0
#45 T IIb	82	0	9	0	0	0	9	0	0	0	0	0
#30 T IVa	18	0	11	71	0	0	0	0	0	0	0	0
#32 T IVa	15	0	10	75	0	0	0	0	0	0	0	0
#2 T IVb	49	34	3	12	2	0	0	0	0	0	0	0
#2 T V	45	0	26	10	0	0	19	0	0	0	0	0
#23 T V	20	0	24	3	0	0	0	0	0	0	13	40
#15 T VII	78	0	11	3	0	0	9	0	0	0	0	0
#9 T VIIIa	47	0	3	8	0	0	7	36	0	0	0	0
#27 T VIIIa	10	0	12	2	0	0	0	0	4	72	0	0
#31 Tuff	61	0	23	9	7	0	0	0	0	0	0	0
Ecca N Ladismith	76	0	24	0	0	0	0	0	0	0	0	0
Ecca N Klaarstroom	48	0	52	0	0	0	0	0	0	0	0	0
E Nondweni, RSA	0	0	71	19	0	10	0	0	0	0	0	0

Tab. 9: Quantitative analysis of the examined tuff beds

8.4 Mineralogical evolution of marker beds

Originally the marine deposited and ash-fall derived tuff beds consisted of vitric, crystal and lithic grains. Vitric grains are colourless glass shards and ash-sized pumice. Crystal grains

comprise euhedral quartz, splinters and fragments of quartz, feldspar. Lithic grains are for example sedimentary xenoliths. Pumice, quartz, feldspar and lithic fragments can still be detected in the tuff beds whereas the glass was completely transformed into clay minerals. Generally the

glass was altered into smectites which were later transformed into randomly interstratified illite/smectite clay minerals and pure illite. The randomly interstratified clay minerals are characteristic for bentonitic tuff beds indicating the incomplete transformation of smectite to illite.

The chain of reaction could have happened as proposed by Iijima (1978):

Volcanic glass + H₂O → montmorillonite + silica (opal - A) +/- ions in solution → montmorillonite + alkali zeolites + silica (opal - CT) → montmorillonite/illite mixed layered clay minerals + analcime + quartz (chert) → illite + albite + quartz

9 Heavy minerals

Heavy minerals are accessory minerals of rocks (< 1 %) with a specific gravity higher than 2.90 (Boenigk, 1983). Acidic igneous rocks may contain apatite, biotite, brookite, hornblende, monazite, muscovite, rutile, sphene, pink tourmaline and zircon whereas in basic igneous rocks augite, chromite, diopside, hypersthene, ilmenite, magnetite, olivine, picotite and pleonast can occur. Heavy minerals are more frequent in acidic crystalline rocks than in basic rocks and zircon, tourmaline and rutile are more widespread than others (Zimmerle, 1995).

Most acidic to intermediate ash fall derived tuff beds contain heavy-minerals such as biotite, zircon, apatite, and occasionally sphene (Weaver, 1963). Fisher and Schmincke (1984) added allanite and rutile, but also mentioned sanidine and high-temperature quartz as primary magmatic non-heavy minerals. Additionally monazite, garnet, hornblende and tourmaline have to be quoted (cf. Königer, 1999).

Ash deposits and their heavy-mineral content can be contaminated with admixed non-volcanic components

- (1) by the assimilation of country rock material into the parent magma.
- (2) by the penetration of ejecting magma through adjacent country rocks during explosive eruptions leading to entrainment of xenocrysts and xenoliths (cf. Königer, 1999).
- (3) by turbiditic redeposition of subaqueously

The illitization of smectites can take place in burial depths of 2-3 km and already with less than 100° C (Pearson and Small, 1988). However, fundamental for the process of illitization is the K-supply (cf. Singer and Stoffers, 1980) which might have originated in this case from decaying K-feldspars within the tuff beds. With sufficient K-supply illitization may even take place under surface conditions, for example in soils (Niederbudde, 1975). The analysed tuff beds have therefore not necessarily been buried at depths of 2-3 km, especially if considered that not all smectite is completely transformed into illite.

deposited ash.

- (4) by reworking caused by bioturbation within the unconsolidated tuff beds. This may lead to the contamination of the heavy mineral suite by rounded tourmaline and zircon, rutile and leucoxene (alteration product of Ti-bearing minerals).
- (5) by secondary formation of authigenic heavy minerals (e.g. barite and opaque heavy minerals such as goethite) during diagenesis and weathering. Goethite may also precipitate directly from both marine and meteoric waters (Deer *et al.*, 1992).

An important aspect considering heavy mineral studies is the *aeolian fractionation* of distally derived fallout beds which may lead to downwind changes in mineralogical and chemical composition (Fisher and Schmincke, 1984). Fractionation within a travelling ash cloud results from settling velocity differences of minerals, crystals, pumice particles, glass shards and rock fragments. An ash fall deposit of a homogeneous magma becomes therefore increasingly silicic with distance from the vent because of a progressive loss of crystals (plagioclase, hornblende, pyroxene, apatite, magnetite) which contain less silica than the glass shards (Fisher and Schmincke, 1984).

Concerning the heavy mineral suite of the studied bentonitic tuff beds, the stability of heavy minerals against acidic leaching processes, alkaline fluids or deep burial has to be considered. Sphene and apatite are for example unstable within a highly acidic milieu (Morton, 1985).

9.1 Heavy minerals of the analysed tuff beds

Juvenile heavy minerals of the ash-fall derived tuff beds were used to support the petrographic investigation of the tuff beds, to support the correlation of single tuff beds between outcrops in the study area and to deduce the geochemical character of the original airborne ash material by recognising the primary volcanic heavy minerals.

The heavy mineral content of tuff beds from the Dwyka Group of southern Namibia (Aranos Basin) and the Western Cape Province (South Africa) were determined in grain mounts under the microscope. Heavy minerals of Dwyka-equivalent tuff beds from the Karasburg Basin near Zwartbas (Namibia) were determined in two samples but will be elaborated to further detail in the diploma thesis of Markus Geiger (Geiger, 2000b).

Of the 21 tuff beds from the Dwyka Group of southern Namibia near Ganigobis ten tuff beds, mainly the thicker ones, were chosen for heavy mineral separation. Only eight of the beds revealed the possibility of quantitative analysis of their transparent heavy minerals. Five different tuff beds contained sufficiently enough zircons to analyse them statistically.

The methodology of heavy mineral separation is described in Appendix B-4.

The following juvenile, non-opaque heavy minerals (density more than 2.9 g/cm³) were observed within the grain mounts of the tuff beds in the order of decreasing frequency and will be described in the following:

Apatite and zircon are ubiquitous, monazite, sphene (titanite) and rutile occur in many separates whereas biotite, hornblende, garnet and pink tourmaline turn up only occasionally.

9.1.1 Primary volcanic heavy minerals

9.1.1.1 Apatite

Apatite (Ca₅(PO₄)₃(F,OH,Cl), Greek: to deceive) with a specific gravity of 3.1-3.3 g/cm³ is a common juvenile accessory component in all magmatic rocks, unweathered fresh silicic volcanic ashes and also commonly in marine deposited bentonites (Weaver, 1963). However, in most tonsteins which are nonmarine kaolinitic claystones of pyroclastic origin usually in combination with coal-bearing sequences, apatite is not present due to its susceptibility to dissolution by acids (Bohor and Triplehorn, 1993). Almost all analysed tuff beds contain apatites of varying amounts between 0 % and 92 % averaging 57 % (Tab. 11).

Shape, elongation and size

Within the heavy mineral separates of the investigated tuff beds, apatite occurs as euhedral to anhedral and broken, hexagonal prisms. Crystal faces of euhedral apatites are well developed but mostly show a certain degree of corrosion varying between rough faces with etching pits, saw-tooth-like rims and grooves and hollows giving the crystals an irregular form (Plate 4, Fig. 10). Terminations of euhedral apatites are mostly simple pyramidal or show a combination between a pyramid and a basal face (Plate 4, Fig. 1). Some apatites are only terminated with crystal faces at one end whereas the other side is straight (Plate 4, Figs. 2 and 5). Hexagonal basal faces were occasionally observed (Plate 4, Fig. 4). Irregular broken crystals with rounded faces are quite frequent indicating a certain degree of reworking whereas totally rounded, egg-shaped crystals (Mange and Maurer, 1991) were not detected. Of 71 measured euhedral apatite crystals from the Ganigobis area 44 % are normal-prismatic and 27 % are long-prismatic whereas only 14 % are stubby and 15 % are needle-like taking the zircon habit classification (cf. Chapter 9.1.1.2). The elongation of all measured apatites varies between 1.10 and 7.38 with an average elongation of 3.40 and a standard deviation of 1.54 (Fig. 91).

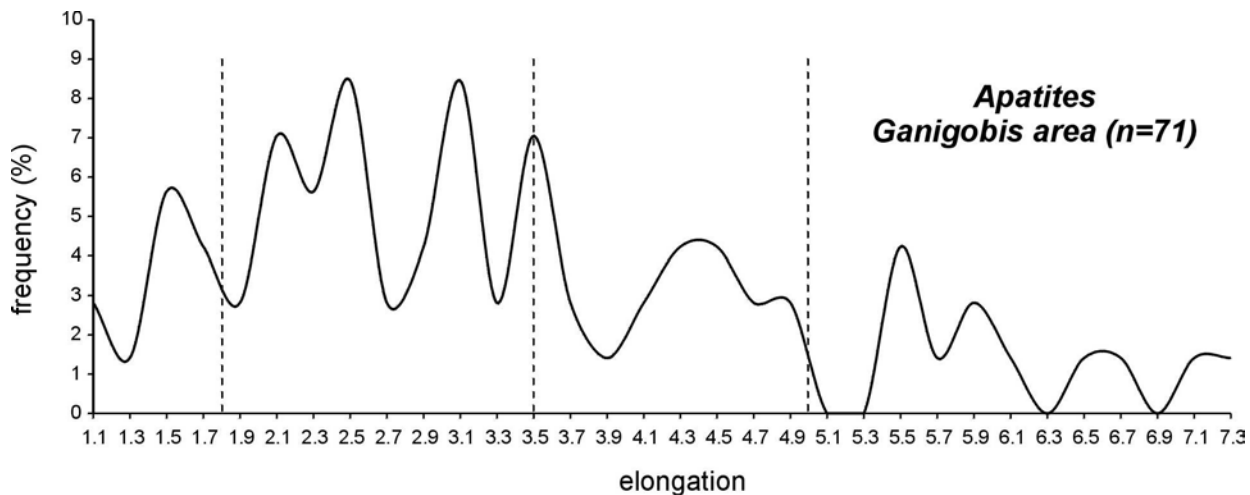


Fig. 91: Elongation-frequency graph of 71 selected apatites contained in tuff beds of the Ganigobis Shale Member near Ganigobis (Aranos Basin). Note the almost homogenous distribution of elongation values; the subdivision of elongation values is adopted from the zircon measurements and indicated by the vertical, dashed lines.

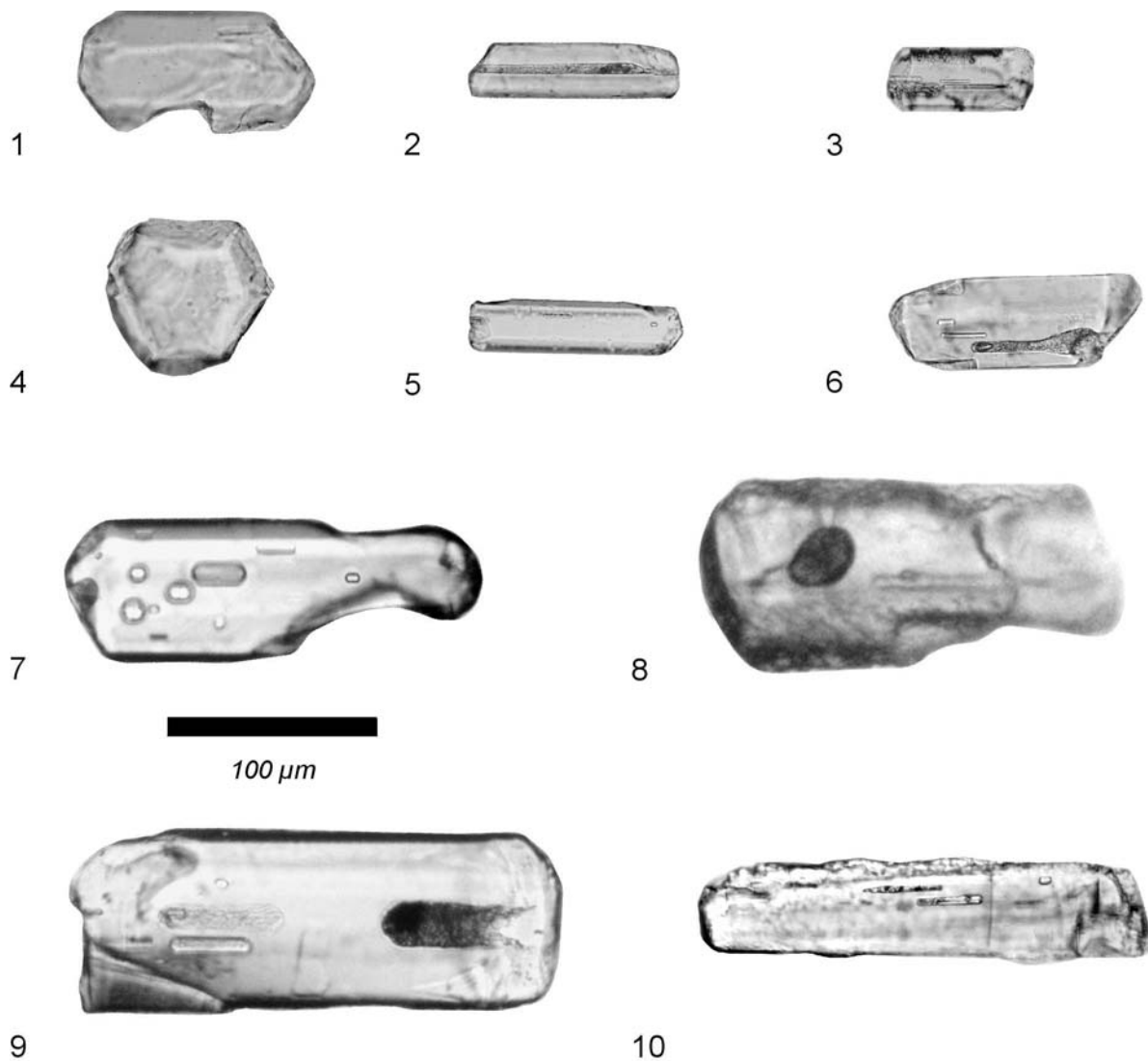


Plate 4: Juvenile apatites separated from the analysed tuff beds.

Plate 4: Juvenile apatites separated from the analysed tuff beds.

Fig. 1: normal-prismatic apatite with growth obstruction at its lower side, #2 tuff Vc

Fig. 2: long-prismatic apatite displaying elongate, axial, tubular cavity filled with brown-grey magmatic material, #27 tuff VIIIa

Fig. 3: normal-prismatic apatite showing elongate, colourless inclusions oriented parallel to the c-axis probably being early crystallised gas or fluid inclusions, #2 tuff IVb

Fig. 4: basal face of an euhedral apatite, note the distinct crystal faces, OL 1/69: 396.36 m

Fig. 5: long-prismatic apatite with minute to small, globular and elongate inclusions oriented parallel to the c-axis, #2 tuff IIb

Fig. 6: normal-prismatic apatite displaying elongate gas/fluid inclusions oriented parallel to the c-axis and elongate, axial, tubular cavities filled with brown-grey magmatic material, #30 tuff IVb

Fig. 7: large, normal-prismatic, euhedral apatite with growth obstruction at its lower side; note the small, elongate gas / fluid inclusions oriented parallel to the c-axis, #45 tuff IIb

Fig. 8: large, normal-prismatic apatite showing large, globular inclusion probably consisting of dark, magmatic material, Ecça Group, north of Klaarstroom, South Africa

Fig. 9: very large, normal-prismatic apatite with slightly corroded edges; note the large elongate, axial, tubular cavity filled with brown-grey magmatic material and the smaller inclusion of an euhedral apatite, #45 tuff IIb.

Fig. 10: long-prismatic apatite with corroded edges, note the small elongate fluid inclusions, Ecça Group, north of Klaarstroom, South Africa (all figures: II Nic, 500 x)

The length of all measured apatite grains varies between 36 and 280 μm (average: 157 μm , standard deviation: 54.49 μm) whereas their width varies between 24 and 80 μm (average: 49 μm , standard deviation: 12.92 μm). Generally apatite is little larger than zircon and thus occurred more often in the 90-180 μm fraction (e.g. #45 IIb). This can be explained by the lower gravity of apatite compared to zircon which led to a greater transport distance of larger apatite crystals within ash clouds (cf. Königer, 1999).

Colour, inclusions and growth obstruction

Apatite crystals are generally colourless and clear in the tuff beds. The apatites show a medium-high relief and a low-order grey interference colour.

They contain the following types of inclusions:

- (1) colourless long-prismatic inclusions with an orientation parallel to the c-axis which reach a length of 60 μm and a width of 20 μm (Plate 4, Figs. 3 and 6) as well as minute to small (1-10 μm) globular inclusions oriented randomly or aligned in rows which are probably early crystallised gas / fluid inclusions (Plate 4, Fig. 7).
- (2) axial elongated tubular cavities or occasional larger globular inclusions (Plate 4, Fig. 8), often filled with light grey to altered brown,

magmatic material (Zimmerle, 1976); the tubes cover either the whole length of the apatite crystal (Plate 4, Fig. 2) or only parts, always starting from one side of the crystal and reaching a width of 12 μm (Plate 4, Fig. 6). Using the optical refraction (Becke line) of the light grey, magmatic material against the permanent mount with $n=1.54$, it appeared that the filling has an acidic to intermediate character.

- (3) occasionally small, euhedral apatite or zircon crystals are found as inclusions within larger apatite crystals, which reach a length of 60 respectively 80 μm and width of 5 respectively 10 μm (Plate 4, Fig. 9).

Some crystals show indentations probably developed by growth obstruction within the magma which is typical of volcanically derived apatites (Plate 4, Fig. 1).

9.1.1.2 Zircon

Crystals of zircon (ZrSiO_4 ; specific gravity 4.7-4.8 g/cm^3 ; Persian: of golden colour) are extremely resistant to alteration and are almost always present in bentonites and tonsteins (Bohor and Triplehorn, 1993). All analysed tuff beds contain zircons of varying amounts between 8 % and 97 % averaging 39 % (Tab. 11).

Shape, elongation and size

Most of the zircons are euhedral to subhedral, their crystal faces are mostly well developed and not abraded. In few cases minor rounding at the edges of euhedral crystals or fragments was observed which indicates either minor reworking of the ash or slight corrosion within the parent magma.

Perfect crystals show the typical bipyramidal shape with both ends perfectly preserved. Ditetragonal-dipyramidal terminations can be distinguished from tetragonal-bipyramidal terminations which are either simple or complex. Most of the zircons show a simple arrangement of their crystal faces (e.g. Plate 5, Fig. 1). Some zircons are only terminated with crystal faces at one end whereas the other side is straight and even zircons being simply rectangular exist which exhibit no terminations with crystal faces (Plate 5, Fig. 5). A higher percentage of zircons are broken and fragmented. Fragmentation may originate from crushing of the rock. But especially smaller zircons can be imperfect and may have been damaged during the ejection of the parent magma, thus representing juvenile phases of rocks (cf. Poldervaart, 1956). In each tuff bed rounded zircons of non-juvenile origin are present indicating minor reworking of the tuff bed most likely due to bottom currents or

bioturbation of the unconsolidated ash.

For comparisons among single tuff beds, the following features of zircon grains were measured: (1) maximum and minimum length (longest and shortest extent of a crystal, commonly parallel to c-axis); (2) maximum and minimum width (largest and smallest extent perpendicular to the maximum length); and (3) length/width ratio (l/w ratio) which is commonly expressed by the term elongation (cf. Winter, 1981).

The length and width of 717 zircons of 12 different tuff beds were determined disregarding further measurements of several inclusions. Several tuff beds produced hundreds of euhedral zircons. Others, however, yielded less than 15 zircons which was insufficient to include them into statistics. If possible, 50 zircons of each bed and outcrop were measured (Tab. 10). In accordance with Taylor (1937), Winter (1981) and Königer (1999) the habit of the zircons was classified into four groups based on their elongation:

- (1) *Stubby* with an elongation <1.8 (e.g. Plate 5, Fig. 8)
- (2) *Normal-prismatic*, 1.8-3.5 (e.g. Plate 5, Fig. 10)
- (3) *Long-prismatic*, 3.5-5.0 (e.g. Plate 5, Fig. 6)
- (4) *Needle-prismatic*, >5.0 (e.g. Plate 5, Fig. 2)

Plate 5: Juvenile zircons separated from the analysed tuff beds.

- Fig. 1:** large, euhedral, needle-prismatic, bi-pyramidal zircon with simple, acicular terminations, #2 tuff IIB.
- Fig. 2:** euhedral, needle-prismatic, bi-pyramidal zircon with more complex, acicular terminations, note the dark globular inclusion on the left, the small globular inclusion in the middle of the crystal and the 65 µm long, elongate inclusion on the right, probably a fluid inclusion, #2 tuff IIB.
- Fig. 3:** long-prismatic, euhedral, bi-pyramidal zircon showing straight terminations, note the dark, globular inclusions probably of ore minerals and the small, clear inclusions probably consisting of apatite, #45 tuff IIB.
- Fig. 4:** normal-prismatic, euhedral, bi-pyramidal malacon displaying simple terminations, #23 tuff IIB.
- Fig. 5:** normal-prismatic, one-sided zircon showing 100 µm long, elongate inclusion probably of magmatic material, #2 tuff IVb.
- Fig. 6:** needle-prismatic, euhedral, bi-pyramidal zircon, note growth obstruction on its upper side, the elongate apatite inclusion and the darker, globular inclusions, #2 tuff IIB.
- Fig. 7:** stubby, euhedral zircon displaying severe growth obstruction on its left and lower side, #2 tuff IIB.
- Fig. 8:** stubby, euhedral zircon, note the distinct crystal faces, #23 tuff IIB.
- Fig. 9:** stubby, six-sided zircon with nice magmatic zoning and darker, globular inclusions, Dwyka Group, north of Klaarstroom, South Africa.
- Fig. 10:** euhedral, bi-pyramidal zircon showing a large inclusion of apatite, Ecce Group, north of Klaarstroom, South Africa (all figures: II Nic, 500 x).

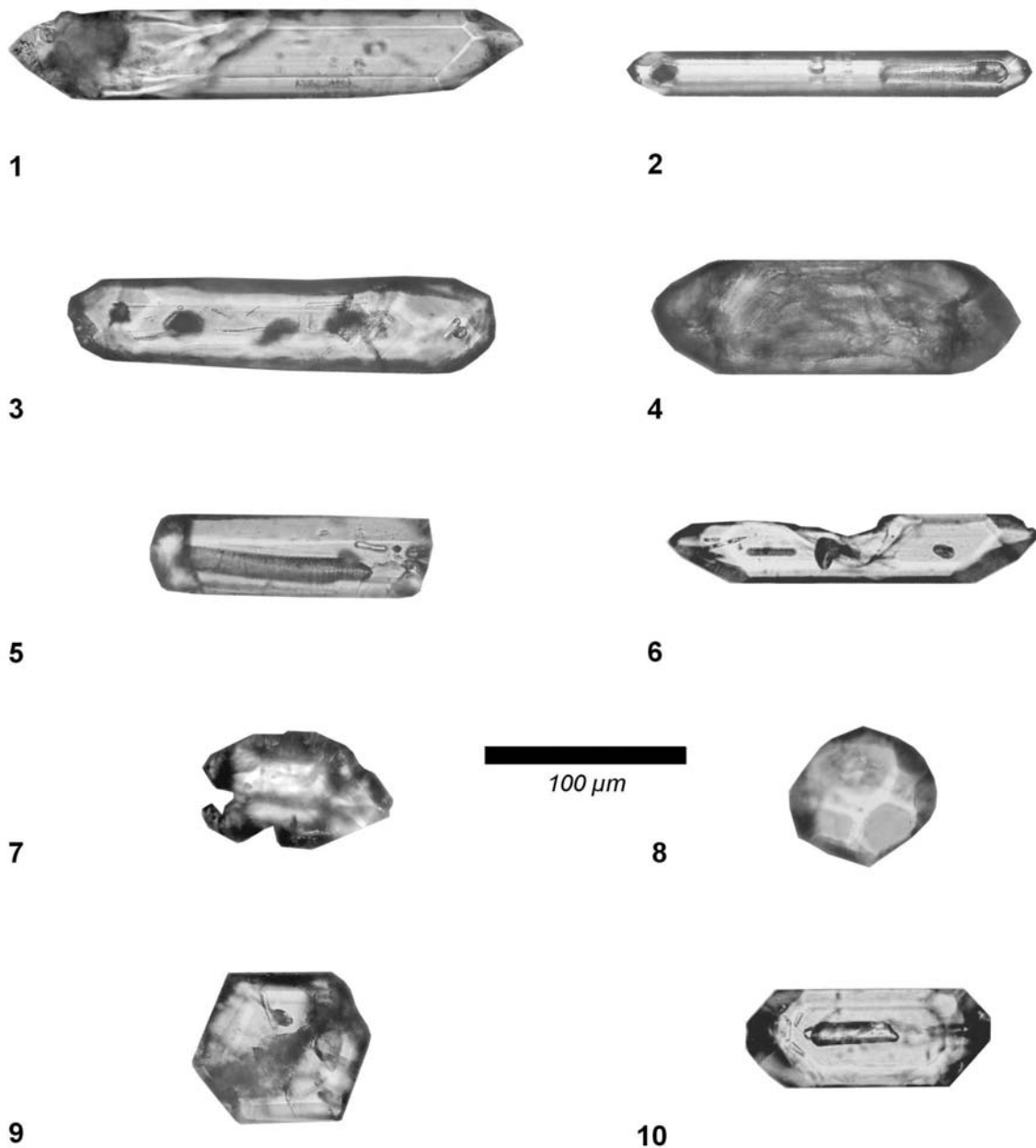


Plate 5: Juvenile zircons separated from the analysed tuff beds.

The elongation of all measured zircons varies between 1.13 and 8.67 but is mainly restricted to a smaller range in each bed. Average elongation varies between 1.89 and 3.44 with a bulk concentrated between 2.3 and 2.5 showing that most zircons are either stubby or normal-prismatic and only few are long-prismatic or even needle-prismatic. Fig. 95 and Fig. 96 show the elongation-frequency graphs of the tuff beds in which sufficient zircons were measurable. Many of them display two major peaks, one in the range of the stubby zircons and one in the range of

normal-prismatic zircons, minor peaks are found within the range of long-prismatic zircons and occasionally also within needle-like zircons, especially in samples of tuff bed IVb from the Aranos Basin of southern Namibia.

Euhedral two-sided zircon crystals from the Dwyka Group of southern Namibia are on average between 90 - 140 µm long including minimal lengths of 40 µm and maximum lengths of 264 µm. Their average width ranges between 40 - 57 µm varying between 20 and 80 µm.

Zircons from the Dwyka Group of South Africa show an average length between 105 - 116 μm including minimal lengths of 52 μm and maximum lengths of 328 μm . Their average width ranges between 44 - 53 μm varying between 24 and 76 μm . Finally, zircons from the

Ecce Group of South Africa display an average length of 101 - 122 μm with minimal lengths of 40 μm and maximum lengths of 208 μm . The average width ranges between 51 - 56 μm varying between 24 and 88 μm (Tab. 10).

Zircons		Grain size	measurements	Zircon grains	Zircon grains	Zircon grains	Zircon grains	max.	min.
#	Tuff Bed	μm		axial ratio <1.8	axial ratio 1.8 - 3.5	axial ratio 3.5 - 5.0	axial ratio >5.0	length	length
1	#2 T IIb	45-90	50	17	28	3	2	260	48
2	#23 T IIb	45-90	50	27	20	1	2	250	56
3	#28 T IIb	45-90	50	18	23	8	1	208	48
4	#32 IIb	45-90	no zircon measurements due to the low frequency of zircons						
5	#45 T IIb	45-90	50	12	33	4	1	224	56
6	#45 T IIb	90-180	50	9	34	6	1	240	72
	mean tuff IIb		50	17	28	4	1	236	56
7	#32 IIIb	45-90	no zircon measurements due to the low frequency of zircons						
8	#17 T IVa	45-90	no zircon measurements due to the low frequency of zircons						
9	#2 T IVb	45-90	no zircon measurements due to the low frequency of zircons						
10	#30 T IVb	45-90	50	5	23	12	10	224	64
11	#23 T IVb	45-90	50	11	25	7	7	264	72
	mean tuff IVb		50	8	24	9.5	8.5	244	68
12	#2 T V	45-90	18	2	14	2	0	164	80
13	#23 T V	45-90	no zircon measurements due to the low frequency of zircons						
14	#15 T VII	45-90	no zircon measurements due to the low frequency of zircons						
15	#27 T VIIIa	45-90	no zircon measurements due to the low frequency of zircons						
16	#9 T VIIIa	45-90	50	23	25	1	1	176	56
	mean Ganigobis							226.40	61.45
17	Zwart T IIIb	45-90	50	12	31	6	1	212	70
18	Zwart T XXIVa	45-90	50	16	32	1	1	200	40
19	OL 1/69: 378.00 m	45-90	50	20	22	5	3	200	52
20	OL 1/69: 396.36 m	45-90	19	3	14	2	0	184	72
21	Dwyka N Klaarstroom/RSA	45-90	50	13	33	4	0	328	72
22	Ecce N Ladismith/RSA	45-90	30	8	22	0	0	144	40
23	Ecce N Klaarstroom/RSA	45-90	50	9	40	1	0	208	80
Zircons		max.	min.	average	stdev	average	stdev	average	stdev
#	Tuff Bed	width	width	length	length	width	width	elongation	elongation
1	#2 T IIb	80	24	100.14	31.87	47.28	11.60	2.31	1.21
2	#23 T IIb	72	36	99.13	30.26	53.81	6.43	1.89	0.77
3	#28 T IIb	68	20	91.44	26.79	39.92	10.53	2.52	1.31
4	#32 IIb	no zircon measurements due to the low frequency of zircons							
5	#45 T IIb	80	28	109.12	30.60	49.74	9.07	2.30	0.99
6	#45 T IIb	80	36	138.80	39.43	56.60	11.37	2.52	0.85
	mean tuff IIb	76	29	107.73	31.79	49.47	9.80	2.31	1.03
7	#32 IIIb	no zircon measurements due to the low frequency of zircons							
8	#17 T IVa	no zircon measurements due to the low frequency of zircons							
9	#2 T IVb	no zircon measurements due to the low frequency of zircons							
10	#30 T IVb	68	24	126.56	39.62	40.36	11.21	3.44	1.56
11	#23 T IVb	64	24	124.40	43.48	44.72	11.35	3.07	1.69
	mean tuff IVb	66	24	125.48	41.55	42.54	11.28	3.26	1.63
12	#2 T V	80	36	117.11	27.33	52.44	10.77	2.32	0.78
13	#23 T V	no zircon measurements due to the low frequency of zircons							
14	#15 T VII	no zircon measurements due to the low frequency of zircons							
15	#27 T VIIIa	no zircon measurements due to the low frequency of zircons							
16	#9 T VIIIa	68	32	97.40	25.95	50.28	7.90	1.99	0.67
	mean Ganigobis	72.91	28.44	111.57	32.81	48.35	10.03	2.48	1.09
17	Zwart T IIIb	88	28	122.48	38.73	51.88	13.32	2.50	1.04
18	Zwart T XXIVa	64	16	93.28	26.81	44.32	10.50	2.17	0.64
19	OL 1/69: 378.00 m	68	24	105.28	35.70	46.72	9.92	2.43	1.26
20	OL 1/69: 396.36 m	64	28	107.58	25.95	43.79	9.28	2.53	0.66
21	Dwyka N Klaarstroom/RSA	76	28	116.08	38.60	52.88	11.55	2.25	0.69
22	Ecce N Ladismith/RSA	88	24	100.93	26.98	51.53	15.13	2.02	0.45
23	Ecce N Klaarstroom/RSA	80	40	122.16	26.74	56.16	8.66	2.21	0.51

Tab. 10: Crystal habit, length, width and elongation of zircons of the analysed tuff samples; see text for discussion.

Colour and inclusions

Almost all examined zircons are clear and colourless, only a few zircons show a pale yellow colour. Other crystals are mantled with yellow-

brown secondary coatings. Radioactive radiation of thorium and uranium within the zircons changed clear zircons into amorphous, metamictic zircons (malacons) which are generally dirty grey-brown and optically isotropic (Plate 5, Fig. 4).

Clear zircons show the characteristic bright high-order interference colours under cross-polarised light. The type and frequency of inclusions within the zircons varies between single tuff beds.

Following types of inclusions were observed:

Minute to small, colourless, clear to dirty inclusions which display normal- to long-prismatic, occasionally needle-like shape and are between 16 and 40 (80) μm long and up to 12 μm wide, they are disseminated rather randomly or orientated (sub)parallel to the crystal faces. They have no further inclusions and represent probably apatite or zircon (Armstrong, written comm.; Plate 5, Fig. 10).

Globular to oval with diameters of up to 8 μm but also elongate (up to 60 μm long), clear and colourless inclusions seem to be gas or fluid inclusions (Plate 5, Fig. 6).

Elongate, sometimes tube-like, dark inclusions with a length up to 80 μm and a width up to 10 μm showing a predominant orientation (sub)parallel to the c-axis appear to be altered volcanic glass (Plate 5, Fig. 5).

Brown-black and partly opaque substances, up to 40 μm long or up to 24 μm in diameter and of different shape comprise most likely ore minerals (Plate 5, Fig. 3).

In few cases small, round, red-brown rutiles up to 12 μm in diameter were enclosed within the zircons.

Magmatic zoning and growth obstruction

Especially cathodoluminescence imaging reveals prominent magmatic compositional zoning with occasional subordinate sector zoning (Plate 5, Fig. 9). In certain tuff beds a number of cores of inherited zircon were recognised which can be distinguished by their colour (brown, grey, sometimes opaque). Some crystals developed growth and penetration twins or show notches caused by growth obstruction in the melt which is typical of zircons of volcanic origin (Hoppe, 1963; Plate 5, Figs. 6 and 7). Few zircons show thin fissures which commonly grew from inclusions within the centre of the crystals. This

may be attributed to the internal radioactivity of the mineral (Hutton, 1950).

9.1.1.3 Monazite

Monazite ((Ce,La,Th)PO₄; Greek: to be rare; specific gravity 4.8 - 5.5 g/cm³) is a relative widely distributed accessory mineral in granitic rocks and often associated with zircon. This juvenile heavy mineral is quite resistant against weathering and diagenesis (Mange and Maurer, 1991) and thus often preserved within strongly altered rocks such as bentonites (Kubanek and Zimmerle, 1986). Only 12 out of 22 analysed tuff samples contain monazites of varying amounts between 1 % and 4.5 % averaging 1.1 % (Tab. 11).

The characteristic colour of the mostly small monazites is mainly pale yellow to occasionally yellow-brown distinguishing them from the mostly colourless zircons. Monazite shows a high relief with dark rims and a characteristic resin-like lustre. The crystals are mostly oval to spindle-shaped and well-rounded but also triangular. Crystal faces are mostly rounded and occasionally corroded possibly due to slight corrosion within the parent magma or minor reworking of the unconsolidated ash. Crystals often show rough surfaces with small etching pits or brown spots partly arranged in a mosaic-like pattern caused by acid susceptibility. Monazite shows high but blurred interference colours which are arranged in rounded grains as concentric rings contrasting the bright interference colours of zircon. Globular inclusions of opaque matter occasionally occur; a colourless, elongated, 72 x 16 μm large inclusion (glass?) was only found in one sample (Plate 6, Figs. 1 and 2).

Measured monazites in the heavy mineral separates are between 48 and 180 μm long (average: 108 μm , standard deviation: 33.83 μm) and between 40 and 152 μm wide (average: 81 μm , standard deviation: 28.05 μm). Of 19 measured monazite grains 17 are stubby-prismatic and only two are normal-prismatic (Fig. 92) using the elongation classification of the zircons.

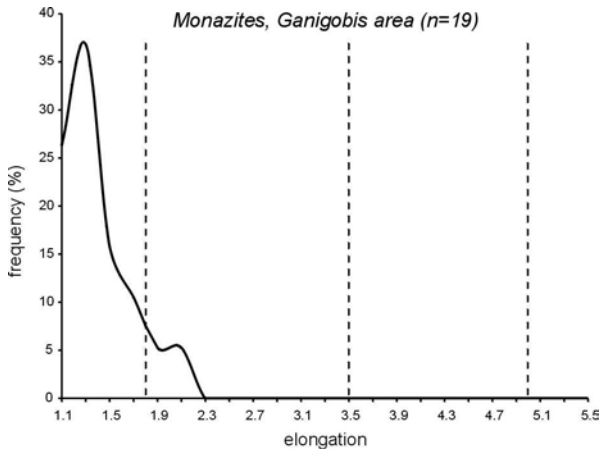


Fig. 92: Elongation-frequency graph of 19 selected monazites contained in tuff beds of the Ganigobis Shale Member near Ganigobis (Aranos Basin). Note the stubby crystal shape of the monazites; the subdivision of elongation values is adopted from the zircon measurements and indicated by the vertical, dashed lines.

The smaller grain size of monazite compared to other transparent heavy minerals is either due to an originally smaller size during crystal growth in the parent magma or is due to aeolian fractionation because of its high specific gravity and subsequently faster settling velocity compared to other heavy minerals (cf. Königer, 1999).

9.1.1.4 Sphene (titanite)

Sphene ($\text{CaTi}((\text{O},\text{OH},\text{F})\text{SiO}_4)$; Greek: wedge; gravity $3.30 - 3.55 \text{ g/cm}^3$) occurs in 8 of the 22 analysed tuff samples in amounts between 0.5 % and 1 % within the heavy mineral separates. Sample #27 tuff VIIIa (13 %) is an exception in which sphene is associated with green hornblende (cf. Tröger, 1967). Sphene is a relatively unstable juvenile component of the tuff beds compared to zircon and monazite and begins easily to disintegrate into other Ti-bearing minerals such as brookite or leucosene. Within acid to intermediate igneous rocks it is a frequent, accessory mineral of late-magmatic crystallisation and especially tuff deposits show an enrichment of sphene (Boenigk, 1983).

Sphene crystals show a high relief with dark rims and a resin-like lustre. Sphene is colourless to pale yellow or green. Intensive brass- to golden-yellow colours can be observed under

polarised light. Close to the extinction position anomalous blue interference colours are characteristic for sphene showing no total extinction (Plate 6, Figs. 3 and 4).

Eleven measured sphenes in the heavy mineral separates are between 80 and 160 μm (average: 109 μm , standard deviation: 26.06 μm) long and between 56 and 120 μm wide (average: 80 μm , standard deviation: 21.50 μm). 9 sphene crystals are rather stubby-prismatic and only two are normal-prismatic using the elongation classification of the zircons (Fig. 93).

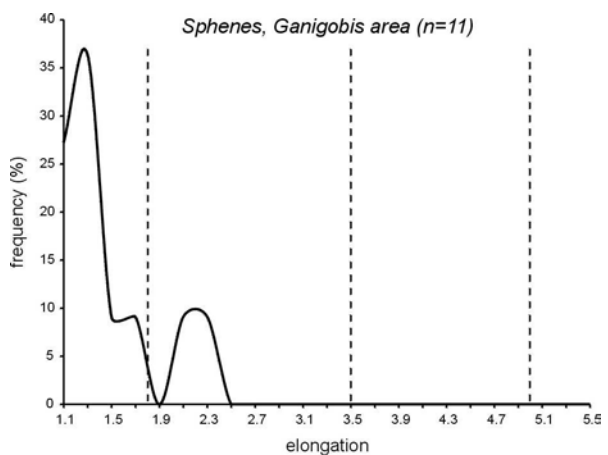


Fig. 93: Elongation-frequency graph of eleven selected sphenes contained in tuff beds of the Ganigobis Shale Member near Ganigobis (Aranos Basin). Note the mainly stubby crystal shape of the sphenes; the subdivision of elongation values is adopted from the zircon measurements and indicated by the vertical, dashed lines.

Euhedral sphenes mostly show an irregular to triangular form with crystal faces partly rounded or being corroded due to the high instability of the mineral. The surface of the grains occasionally displays etching pits and scars caused by corrosion.

Globular inclusions of opaque matter with a size of about 10 μm are the most frequent inclusions within the sphene crystals, others include red, globular inclusions of the same size. Single inclusions of 15 μm long apatite respectively 25 μm long zircon were recognised.

9.1.1.5 Rutile

In 12 of 22 analysed tuff samples rutile (TiO_2 ; Latin: rutilus: red-yellow; gravity $4.2 - 5.5 \text{ g/cm}^3$) occurs in amounts between 0.5 % and 4 % within the heavy mineral separates (Tab. 11). It is an ultrastable accessory mineral and widely distributed as trace component within metamorphic and less frequently in magmatic rocks (Mange and Maurer, 1991). It is the most stable and frequent of the three TiO_2 -modifications rutile, brookite, and anatase and crystallises primarily at relative high temperatures. Weaver (1963) assigned rutile to be mostly sedimentary in origin in bentonites. However, rutile occurred rarely as primary component within tonsteins (Bohor and Triplehorn, 1993) and is considered to be a juvenile component within the studied bentonites.

Rutiles have thick black rims due to their extremely high optical refraction and often show a slight pleochroism mostly varying from light golden-brown to middle- or darkbrown. Other varieties show an intense red colour. Varieties of rutile grains reach from mainly edge-rounded but euhedral crystals with prismatic terminations to well-rounded grains.

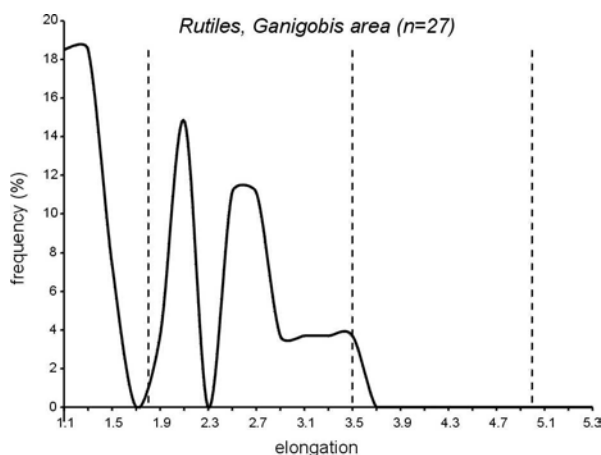


Fig. 94: Elongation-frequency graph of 27 selected rutiles contained in tuff beds of the Ganigobis Shale Member near Ganigobis (Aranos Basin). Note the stubby and normal-prismatic crystal shapes of the rutiles; the subdivision of elongation values is adopted from the zircon measurements and indicated by the vertical, dashed lines.

Rutile grains are often fragmented or show fracturing on one side of the crystal (Plate 6, Figs. 9 and 10). Measured rutiles in the heavy mineral separates are between 56 and 200 μm long (average: 126 μm , standard deviation: 37.21 μm) and between 40 and 144 μm wide (average: 69 μm , standard deviation: 21.54 μm). Of 27 measured rutile grains 12 are stubby-prismatic and 15 are normal-prismatic using the elongation classification of the zircons (Fig. 94).

9.1.1.6 Biotite

Biotite ($\text{K}(\text{Mg,Fe})_3((\text{OH})_2\text{Si}_3(\text{Al,Fe})\text{O}_{10})$; after J.B. Biot; specific gravity ranges between 2.7 and 3.3 g/cm^3) is a common juvenile component of silicic volcanic ashes (Weaver, 1963; Bohor and Triplehorn, 1993) but was only observed in tuff bed IVb of the Ganigobis area. Biotite also appears in heavy mineral separates of the South African Dwyka Group (OL 1/69: 378,00 m and 396,36 m, Tab. 11). If biotite is present within the separates, it generally dominates the heavy mineral suite (between 45 and 75 %).

Biotite flakes are principally aligned with their basal faces perpendicular to the c-axis being almost isotropic under crossed nicols. The flaky grains differ between euhedral pseudo-hexagonal (especially in the South African samples, Plate 6, Fig. 6) and anhedral, irregular forms with occasional lateral embayments (especially in #2 tuff IVb; Plate 6, Fig. 5). The biotites are slightly pleochroitic varying between light brown-green to darker brown. In cases, chloritisation starts at the margins of the crystals leading to the authigenic development of chlorites (Heim, 1960). Sizes of the biotite flakes of the sample #2 tuff IVb vary between 70 and 200 μm in length and 60 and 120 μm in width whereas flakes in the other samples reach lengths of up to 260 μm and width up to 140 μm . Biotite from the sample #2 tuff IVb are almost free of inclusions whereas the sample from borehole OL 1/69 from the Western Cape Province (South Africa) generally reveals a mesh of apatite inclusions which display a length of up to 25 μm , finely disseminated opaque minerals and globular inclusions of unidentified material.

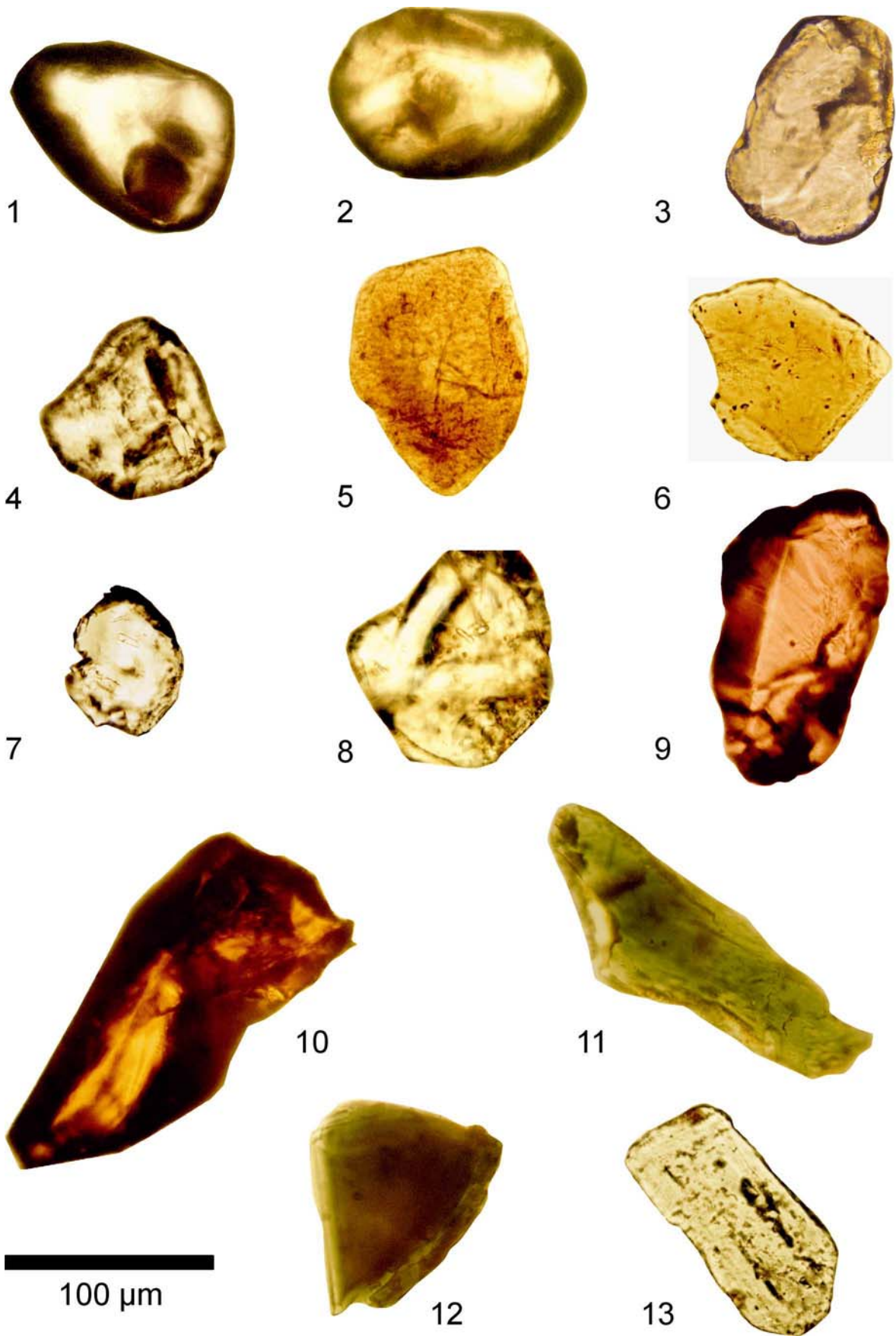


Plate 6: Juvenile and detrital heavy minerals separated from the analysed tuff beds.

Plate 6: Juvenile and detrital heavy minerals separated from the analysed tuff beds.

- Fig. 1:** euhedral, yellow-brown monazite with distinct crystal faces, note the dark-red inclusion in the lower right corner, #23 tuff IIb
Fig. 2: euhedral yellow monazite showing red dark inclusion, #2 tuff IIb
Fig. 3: irregular shaped, subhedral sphene with corroded edges, #23 tuff IIb
Fig. 4: irregular shaped, euhedral sphene with slightly rounded edges, #32 tuff IIIb
Fig. 5: subhedral to anhedral, brown biotite flake (detrital), #2 tuff IVb
Fig. 6: euhedral to subhedral, light brown biotite embodying single apatite crystals, OL 1/69: 378.00 m
Fig. 7: euhedral to subhedral, colourless, irregular jagged and partly corroded garnet embodying an inclusion of euhedral apatite, #27 tuff VIIIa
Fig. 8: euhedral to subhedral, colourless, slightly rounded garnet displaying small fluid inclusions, #27 tuff VIIIa
Fig. 9: golden-brown, slightly pleochroitic, euhedral rutile displaying well developed crystal faces, #23 tuff V
Fig. 10: red-brown, slightly pleochroitic, euhedral rutile with partly fractured crystal faces and terminations, #32 tuff IIa
Fig. 11: light green subhedral hornblende, #27 tuff VIIIa
Fig. 12: pleochroitic pink to dark green, triangular tourmaline grain, #27 tuff VIIIa
Fig. 13: euhedral colourless to light brown barite grain showing finely disseminated opaque minerals, #2 tuff IIb

9.1.1.7 Hornblende

Minerals of the hornblende group (e.g. hastingsite: $\text{NaCa}_2(\text{Mg,Fe}_4)\text{Fe}(\text{Si}_6\text{Al}_2\text{O}_{22})(\text{OH})_2$; after Hastings in Canada; gravity 3.0 - 3.6 g/cm³) occur mainly within intermediate to acidic and also alkalic magmatic rocks as well as in many metamorphic rocks (Mange and Maurer, 1991). In silicic volcanic ashes amphiboles are only present in traces but they are quite common in intermediate to basic ashes (Bohor and Triplehorn, 1993). Contrary, Weaver (1963) considered hornblende as the most common non-opaque heavy minerals in felsic ashes and tuffs. Similar to pyroxenes, amphiboles are considered to be one of the most unstable mineral groups (cf. Morton, 1985). They may survive alteration in older bentonites which have undergone only slight diagenesis or acid dissolution.

Hornblende was detected in two tuff beds (IVb and VIIIa) from the Aranos Basin of southern Namibia and in two tuff beds of the drill hole OL 1/69 from South Africa. In tuff bed IVb and the ones from South Africa green-brown hornblende is common whereas green hornblende occurs in tuff bed VIIIa (Plate 6, Fig. 11).

The green-brown variety separated from the tuff bed IVb shows a lightgreen-brown to middle-brown colour whereas the green variety of tuff VIIIa shows a stronger pleochroism from yellowbrown-green and olive-green to dark blue-green. The green-brown variety shows an almost

parallel but not complete extinction in combination with high interference colours. Green hornblende absorbs only minor contents of Ti and often occurs together with sphene (Tröger, 1967) which is also present in tuff VIIIa. Both varieties probably belong to hastingsite, an alkali-hornblende which is mainly derived from intermediate to acidic parent magmas.

Green-brown hornblende grains of tuff IVb are between 100 and 152 µm long and between 52 and 96 µm wide (7 measurements). Mainly distinct cleavaged after $\{110\}$, elongated, fibrous, edge-rounded, subhedral (stubby to normal-prismatic) to anhedral crystals were observed. Grains are occasionally marginally ragged by corrosion.

Few partly broken grains of subhedral green hornblende were recognised in tuff bed VIIIa displaying a length of 80 to 120 (250) µm and a width of 56 to 104 µm. A distinct cleavage after $\{110\}$ is again conspicuous. Minute, globular, clear inclusions and a larger, elongate and dark inclusion (length about 20 µm) were recognised.

Due to the solitary occurrence of hornblende, it is debatable if the green variety of tuff bed VIIIa is a juvenile component of the ash. The green-brown variety is thought to be magmatic in origin.

9.1.1.8 Garnet Group

The specific gravity of the garnet group (e.g. pyrope: $\text{Mg}_3\text{Al}_2(\text{SiO}_4)_3$; Latin: granatus =

granular) varies between 3.4 and 4.5 g/cm³ depending on their chemical composition. Mainly pale pink and also colourless, irregular formed, sharp-edged, sometimes edge-rounded fragments of garnet occur in tuff bed VIIIa (Plate 6, Figs. 7 and 8). Additional XRD analysis makes the variety pyrope likely (see Chapter 8.3.5). Splinters of garnet were also observed in the tuffaceous bed of the Dwyka Group north of Klaarstroom in the Western Cape Province (South Africa). The garnet grains are commonly irregular jagged and corroded displaying scarred surfaces and well-developed triangular etching pits. These features frequently develop by corrosion during diagenesis (Mange and Maurer, 1991). Splinters of garnet show typical conchoidal fracturing. Garnet is typically isotropic under crossed nicols. The size of the few determined crystals in tuff bed VIIIa varies between 80 and 160 µm in length and 64 and 112 µm in width. Most grains are free of inclusions but the largest grain with a length of 160 µm contains a brown, elongate inclusion with a size of 64 x 24 µm. Another one shows a 16 x 12 µm large inclusion of euhedral apatite.

According to Weaver (1963), garnet is a non-juvenile heavy mineral within bentonites indicating admixture of volcanic ash with non-volcanic material. However, occasional occurrence of pink garnet in rhyolitic lavas and pyroclastics might indicate a primary volcanic origin (Bohor and Triplehorn, 1993). Juvenile garnet (almandine) is for example known from acidic to intermediate Carboniferous-Permian subvolcanic rocks of the western Saar-Nahe Basin (Seckendorff, 1990). Garnet is quite susceptible to acid liquids, but it resists reworking and deep burial. It is found together with zircon, tourmaline, rutile and also apatite (Mange and Maurer, 1991) which fits to the observed spectrum of heavy minerals within the analysed tuff beds and is therefore regarded as being a juvenile component. It is assumed that the majority of garnets observed in the tuff beds are magmatic in origin.

9.1.1.9 Tourmaline

Tourmaline with specific gravity between 3.0 and 3.25 g/cm³ (Na(Al,Mg,Fe,Mn,Li)₃Al₆((OH)₄/

(BO₃)₃/Si₆O₁₈, after Turamali on Sri Lanka) occurs particularly in tuff bed VIIIa. It displays a characteristic strong pleochroism varying between pink or pale olive-grey and dark green-brown (Plate 6, Fig. 12). Tourmaline shows high interference colours which are arranged in thin strings parallel to the rims of the crystal. Euhedral, stubby to normal-prismatic tourmaline crystals have lengths between 88 and 130 µm and widths between 64 and 88 µm. Terminations are mostly fragmented and basal faces are triangular.

Tourmaline mainly occurs in granitic rocks but was also proved as euhedral tourmaline crystals in detritic volcanic rock fragments which indicate an occurrence in volcanic rocks (Zimmerle, 1976). Again, according to Weaver (1963), tourmaline is a non-juvenile heavy mineral within bentonites. However, published reports of rhyolitic lavas and pyroclastics containing tourmaline suggest that it can indicate a primary volcanic origin when found in bentonites or tonsteins, especially if they are euhedral and only occur in traces (Bohor and Triplehorn, 1993) which is the case in the studied tuff beds. Tourmaline is extremely stable against mechanical and chemical weathering. It is therefore one of the most widespread non-opaque accessory heavy mineral within sediments, belonging to ZTR-index (zircon-tourmaline-rutile).

9.1.2 Authigenic heavy minerals

Apart from the primary volcanic heavy minerals, the tuff beds contain varying amounts of authigenic heavy minerals caused by diagenesis and alteration. These are described shortly in the following but are not further mentioned within the descriptions of the heavy mineral content of the individual beds.

9.1.2.1 Barite

Barite (BaSO₄, Greek: heavy) has a specific gravity of 4.5 g/cm³ and occurs in almost all tuff beds, occasionally reaching 99 % of all separated heavy minerals (e.g. tuff Ib). The mostly colourless grains are sharp-edged, irregular and mostly anhedral, their rims are frequently corroded. Euhedral crystals are platy and occasionally rhombic.

Heavy Minerals		Grain size µm	absolute counted minerals	primary volcanic heavy minerals					
#	Locality & Tuff Bed			Zircon in %	Apatite in % with inclusions	Apatite in % without inclusions	Monazite in %	Sphene in %	Rutile in %
1	# 2 T IIb	45-90	200	97	0	0	2	0	1
2	# 23 T IIb	45-90	200	90	1.5	1	4	2	1.5
3	# 32 T IIb	45-90	15	7	0	0	53	7	33
4	# 28 T IIb	45-90	200	24.5	27.5	48	0	0	0
5	# 45 T IIb	45-90	200	15.5	12	66	4.5	1	1
6	# 45 T IIb	90-180	200	19	23	57	0	1	0
7	# 32 T IIIb	45-90	200	8	12	79	0	0	1
8	# 17 T IVa	45-90	200	8	12	76	0	2	2
9	# 2 T IVb	45-90	52	3	8	30	0	0	0
10	# 30 T IVb	45-90	200	16.5	28.5	55	0	0	0
11	# 23 T IVb	45-90	200	91	1	7	0	0.5	0.5
12	# 2 T V	45-90	200	14.5	17	67.5	0	0	1
13	# 23 T V	45-90	200	15	1	80	2	0	2
14	# 15 T VII	45-90	22	36	23	37	0	0	4
15	# 27 T VIIIa	45-90	300	6	3	68	3	13	1
16	# 9 T VIIIa	45-90	200	42	21	31.5	2	1	0
17	Zwart T IIIb	45-90	200	32	21	46	1	0	0
18	Zwart T XXIVa	45-90	200	98	0	1	1	0	0
19	OL 1/69: 378.00 m	45-90	200	6	6	9	0	0	0
20	OL 1/69: 396.36 m	45-90	200	16	9	25	0	1	0
21	Dwyka N Klarstroom/RSA	45-90	200	94.5	0	4	1	0	0
22	Ecca N Ladismith/RSA	45-90	200	30	29	40	1	0	0
23	Ecca N Klarstroom/RSA	45-90	200	46.5	26.5	25.5	1	0	0.5

Heavy Minerals		Grain size µm	absolute counted minerals	primary volcanic heavy minerals				authigenic minerals; estimated	
#	Locality & Tuff Bed			Hornblende in %	Garnet in %	Tourmaline in %	Biotite in %	Baryte in %	Opaque Minerals in %
1	# 2 T IIb	45-90	200	0	0	0	0	99	0
2	# 23 T IIb	45-90	200	0	0	0	0	95	0
3	# 32 T IIb	45-90	15	0	0	0	0	99	0
4	# 28 T IIb	45-90	200	0	0	0	0	95	0
5	# 45 T IIb	45-90	200	0	0	0	0	95	0
6	# 45 T IIb	90-180	200	0	0	0	0	1	0
7	# 32 T IIIb	45-90	200	0	0	0	0	95	0
8	# 17 T IVa	45-90	200	0	0	0	0	30	30
9	# 2 T IVb	45-90	52	5	0	0	54	2	61
10	# 30 T IVb	45-90	200	0	0	0	0	2	30
11	# 23 T IVb	45-90	200	0	0	0	0	10	30
12	# 2 T V	45-90	200	0	0	0	0	65	0
13	# 23 T V	45-90	200	0	0	0	0	95	0
14	# 15 T VII	45-90	22	0	0	0	0	99	0
15	# 27 T VIIIa	45-90	300	3	2	1	0	0	40
16	# 9 T VIIIa	45-90	200	1	1	0.5	0	50	40
17	Zwart T IIIb	45-90	200	0	0	0	0	5	1
18	Zwart T XXIVa	45-90	200	0	0	0	0	0	60
19	OL 1/69: 378.00 m	45-90	200	4	0	0	75	0	10
20	OL 1/69: 396.36 m	45-90	200	5	0	0	44	0	7
21	Dwyka N Klarstroom/RSA	45-90	200	0	0.5	0	0	5	0
22	Ecca N Ladismith/RSA	45-90	200	0	0	0	0	10	10
23	Ecca N Klarstroom/RSA	45-90	200	0	0	0	0	5	30

Tab. 11: Quantitative heavy mineral contents of analysed tuff samples. Separated grain sizes mostly comprise 45-90 µm with the exception of #45 tuff IIb; see text for discussion.

Thin grains generally show low interference colours (grey, pale yellow) but thicker grains display bright yellow, orange, red, and green-blue colours. Their extinction is occasionally incomplete. Sizes vary between 80 and 200 µm in length and 40 and 100 µm in width. Apart from abundant minute opaque inclusions the grains often contain elongated zones of bubble trains and banded colourless inclusions indicating the hydrothermal formation of barite (Plate 6, Fig. 13 and Plate 7, Fig. 8).

9.1.2.2 Opaque minerals

The main opaque heavy minerals are goethite (FeOOH, specific gravity: 4.0-4.4 g/cm³) and

hematite (Fe₂O₃, specific gravity: 5.2 g/cm³) which were identified by XRD analysis. Others include ulvospinel and iwakiite (see Chapter 8.3.5). These alteration products of iron-bearing minerals occur in most tuff beds but were easily eliminated using the Frantz magnetic separator. The opaque heavy minerals generally possess an irregular grain shape. Yellow-brown (goethite) and red-brown (hematite) colours were occasionally observed at the rims of very thin grains. Goethite forms thin crusts around other minerals (e.g. zircon).

9.1.2.3 *Leucoxene*

Leucoxene is a mixture of anatase, brookite, rutile and sphene which occurs in very fine aggregates. It is an alteration product of Ti-bearing minerals which formed on the expense of unstable Ti-bearing minerals like sphene or Ti-bearing biotite (Tröger, 1967; Mange and Maurer, 1991). Aggregates are yellow to light-brown with a slight pleochroism, edge-rounded with a very high relief; their length varies between 80 and 300 μm and their widths between 44 and 64 μm .

The anomalous interference colours of leucoxene are bright and of higher order with almost no extinction.

9.2 Heavy-mineral suites of the tuff beds from the Aranós Basin

In the following chapter the heavy-mineral suites of the individual tuff beds are described. Their stratigraphic position within the Ganigobis Shale Member is displayed in Fig. 14 and the heavy-mineral suites for each sample is recorded in Tab. 11. Zircon measurements of individual samples are quoted in Tab. 10. If heavy minerals are not further described, the general portraits from the previous chapter are valid.

9.2.1 *Tuff bed Ib*

Non-opaque, juvenile heavy minerals are *zircon* and *apatite*. Of 14 measured euhedral *zircon*s are 50 % stubby and 50 % normal-prismatic, elongation-values vary between 1.05 and 2.55 with an average of 1.77. Zircons are between 72 and 176 μm long (average: 100 μm) and between 44 and 88 μm wide (average: 57 μm). Euhedral zircons are mainly colourless with sharp and unrounded crystal faces, perfect crystals show the typical bipyramidal shape with partly complex tetragonal-bipyramidal terminations. Metamict zircons with rounded crystal faces are quite frequent, partly displaying delicate magmatic zoning. Inclusions are relatively rare within the zircons; a 20 μm long inclusion of apatite was detected.

Apatite crystals occur less frequent than zircons and are generally quite small and inconspicuous. They are up to 88 μm long and 64 μm wide, their

elongation values range between 1.37 and 2.5. Colourless, stubby to normal-prismatic, euhedral to subhedral crystals predominate. Globular, clear inclusions with diameters of 10 μm were the only detected inclusions within the apatite crystals. All heavy mineral separates of tuff bed Ib contain up to 99 % authigenic *barite*.

9.2.2 *Tuff bed IIb*

Tuff bed IIb has the greatest thickness (up to 2 cm) among the tuff beds of the Ganigobis Shale Member and was therefore most extensively sampled. Heavy mineral separates of outcrops #2, 23, 28, 32 and 45 yielded ubiquitous heavy minerals including abundant zircon crystals which were statistically analysed and were also used for SHRIMP-based age determinations (see Chapter 11.3.1).

Non-opaque heavy minerals include *zircon*, *apatite*, *monazite*, *sphene* and *rutile*. *Zircon* amounts vary largely between 16 and 97 % depending on the amounts of apatite crystals separated. Of 250 measured euhedral zircons from four samples 34 % show a stubby, 56 % a normal-prismatic, 8 % a long prismatic and 2 % a needle-like habit. Elongation-values vary between 1.14 and 8.67 with an average of 2.31 and an average standard deviation of 1.03. Elongation-frequency graphs (Fig. 95: 1-5) mostly show two major peaks at 1.3 or 1.5 and at 1.9 or 2.1 and a minor peak at 2.7. Zimmerle (1979) mentioned that elongation values depend on the studied grain-size fraction and slightly rises with larger grain size. This can be confirmed by the samples from #45 which show a higher average elongation value of the fraction 90-180 μm (2.52) than of the fraction 45-90 μm (2.30). Fraction 90-180 μm has especially higher elongation percentages between elongation values of 2.5 and 3.7.

The length of the zircons limits 48 and 260 μm (average: 108 μm , average standard deviation: 31.79 μm) and the width extents between 20 and 80 μm (average: 50 μm , average standard deviation: 9.80 μm). Euhedral zircons are mainly colourless with sharp and unrounded crystal faces. Ditetragonal-dipyramidal and tetragonal-bipyramidal terminations of the zircons counterbalance each other (Plate 5, Figs. 1 and 2).

One-ended zircons and splinters are quite

frequent. All types of inclusions described in the previous chapter are present – elongated apatite crystals with a size of 40 x 8 µm, globular to elongate (24 µm length) fluid inclusions and up to 88 µm long, opaque inclusions (Plate 5, Figs. 2, 3 and 6). Few malacons with slightly rounded crystal faces display magmatic zoning and cores of inherited zircon. These cores occasionally produce radially scattered fissures. Few other zircons show typical growth obstruction especially in the middle parts of long-prismatic zircons (Plate 5, Figs. 6 and 7).

Apatite crystals occur in varying contents between 0 % (outcrops #2 and 23) and 80 % (outcrop #45). Varying contents of apatite between the outcrops are attributed to a different amount of acid dissolution. 17 measured apatites of sample #45 (90-180 µm) reveal lengths between 104 and 264 µm (average: 178 µm, standard deviation: 49.07 µm) and widths between 32 and 80 µm (average: 57 µm, standard deviation: 13.87 µm), their elongation values range between 1.65 and 7.38. Of these measured euhedral apatite crystals 12 % show a stubby, 52 % a normal-prismatic, 18 % a long prismatic and 18 % a needle-like habit. Colourless, normal-prismatic, euhedral to subhedral crystals with only very minor rounding of the edges predominate the separates. Apatite crystals often contain axial tubular cavities that are either filled with a brown, magmatic material (Plate 4, Fig. 9) or seem to be hollow. Other types of inclusions are colourless long-prismatic and minute to small, globular gas / fluid-bearing inclusions (Plate 4, Figs. 5 and 7). Small, euhedral apatite or zircon crystals are also found as inclusions within larger apatite crystals, reaching a length of 60 respectively 80 µm and width of 5 respectively 10 µm (Plate 4, Fig. 9). Especially in samples from outcrop #45 20 % (fraction 45-90 µm) respectively 40 % (fraction 90-180 µm) of the apatite crystals contain inclusions.

Monazite occurs quite often within tuff bed IIb reaching an average of 3% of all transparent heavy minerals. The characteristic colour of the monazites is mainly pale grey or pale yellow to yellow-brown in cases. The crystals are oval to rounded and the crystal faces are mostly rounded and show rough surfaces with small etching pits.

Measured monazites within separates of tuff bed IIb are between 48 and 180 µm long and between 40 and 144 µm wide (Plate 6, Figs. 1 and 2 and Plate 7, Fig. 7).

Between 1% and 2% of all non-opaque heavy minerals are *sphenes* which are light-coloured, subhedral to anhedral minerals with rounded edges. The surfaces of most of the grains display etching pits and scars (Plate 6, Figs. 3 and 4).

Rutile grains make up about 1% of all transparent heavy minerals. The subhedral to anhedral grains are between 80 and 160 µm long and between 56 and 80 µm wide. If crystal faces are present, they are always rounded. The characteristic colour is red-brown.

With exception of sample #45 IIb (90-180 µm), *barite* was again the most frequent heavy mineral reaching values up to 99 %.

9.2.3 Tuff bed IIIb

Apatite crystals comprise 91% (#32) of the non-opaque heavy minerals. 12% of these contain small, globular inclusions, elongate inclusions of apatite and characteristic, up to 144 µm long axial, tubular cavities which are mostly filled with light grey to altered brown magmatic material.

Crystal faces are well-developed but occasionally corroded. Sizes vary between 96 and 230 µm in length and 40 and 68 µm in width. Less frequent *zircon* crystals range between 48 and 208 µm (average: 91 µm) in length and between 20 and 68 µm in width (average: 40 µm). Euhedral, bipyramidal zircons are mainly colourless and clear with sharp and unrounded crystal faces. They possess only few inclusions. A single zircon crystal with more than 12 minute, globular, clear inclusions has to be mentioned, another one with an elongation of almost 9 displays a dark-brown inclusion of 72 µm length and a width similar to the whole zircon crystal (24 µm).

Single grains of slightly rounded *monazite* with lengths of 64 - 104 µm and widths of 56 - 80 µm and slightly triangular *sphene* with rounded edges were especially detected in the separates of outcrop #32. More Ti-bearing phases resemble *rutiles*, which are subhedral showing crystal faces.

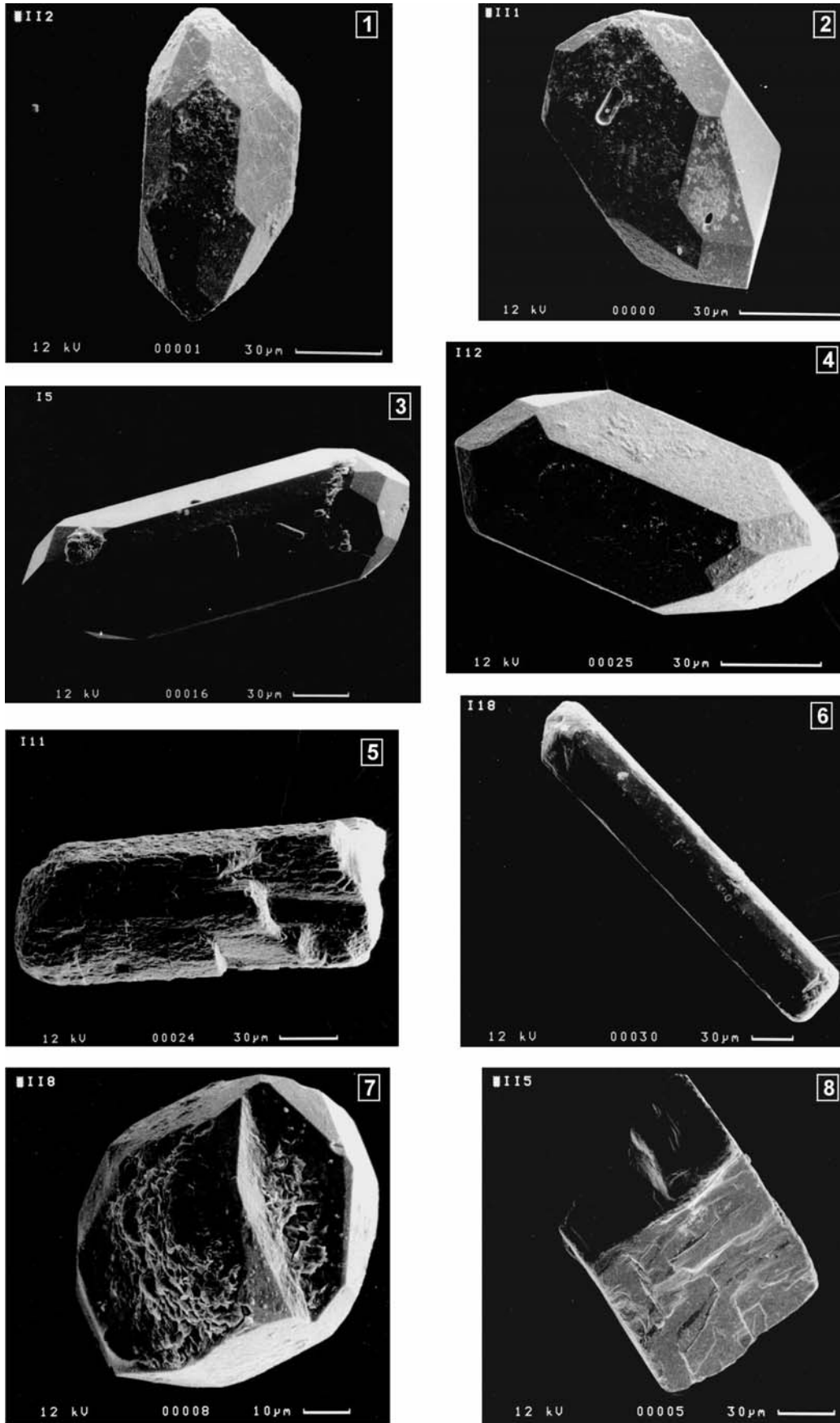


Plate 7: SEM photomicrographs of juvenile and detrital heavy minerals separated from the analysed tuff beds.

Plate 7: SEM photomicrographs of juvenile and detrital heavy minerals separated from the analysed tuff beds:

Fig. 1: Normal-prismatic zircon with bi-pyramidal, acicular terminations; #23 tuff IIb.

Fig. 2: Stubby, bi-pyramidal zircon showing one end acicular and one end blunt, note the 12 µm long imprint, probably of an apatite; #23 tuff IIb.

Fig. 3: Normal-prismatic zircon with short, pyramidal terminations, note the small imprints, probably of apatite; Ecça Group, north of Klaarstroom / South Africa.

Fig. 4: Normal-prismatic zircon with bi-pyramidal, complex terminations; Zwartbas, Namibia: tuff IIIb.

Fig. 5: Normal-prismatic, subhedral apatite displaying major corrosion probably due to the susceptibility to acid dissolution; Zwartbas, Namibia: tuff IIIb.

Fig. 6: Needle-like apatite with corroded terminations; Zwartbas, Namibia: tuff IIIb.

Fig. 7: Round, but euhedral monazite with distinct crystal faces; #45 tuff IIb.

Fig. 8: Euhedral crystal of barite; #23 tuff IIb.

Other Ti-bearing phases resemble in slightly pleochroitic, yellow-golden leucoxene aggregates with a high relief and a size of 130 x 64 µm.

The predominant heavy mineral phase within tuff bed IIIb is again authigenic *barite* which makes up to 95 % of the total heavy mineral content. It has a generally dirty brown appearance in this tuff bed due to ubiquitous, finely disseminated inclusions of opaque minerals.

9.2.4 Tuff bed IVa

Tuff bed IVa was sampled in outcrops #2, 17 and 30. Non-opaque heavy minerals were statistically analysed in separates of outcrop #17 showing that most heavy minerals are *apatites* (88%) and *zircon*s (8%); *sphene* and *rutile* only occur in minor portions (2%) (Fig. 97).

Euhedral *apatites* are generally very clear with the rims of the crystals only being slightly corroded, sizes vary between 88 and 192 µm in length (average: 130 µm, standard deviation: 32.19 µm) and 32 and 56 µm in width (average: 40 µm, standard deviation: 9.82 µm); of 9 measured *apatites* are 5 long-prismatic with a maximum elongation of 5.43 and only 4 are normal-prismatic. 15.8% of all counted *apatites* in samples from outcrop #17 show inclusions which comprise clear, globular inclusions with a diameter of 10 µm and clear elongate inclusions with a length of 96 µm. Characteristic, up to 44 µm long, axial, tubular cavities are mostly filled with altered brown, magmatic material. Up to 40 µm long, euhedral *apatite* and *zircon* crystals occur within the larger *apatite* crystals.

*Zircon*s mainly comprise splinters or rounded grains, partly also malacons, some with brown,

elongate inclusions and also with up to 40 µm long, euhedral *apatite* inclusions. *Rutiles* show subhedral and anhedral varieties with mostly middle-brown to red and slightly pleochroitic colours with lengths up to 150 µm. *Sphene* grains in separates of outcrop #30 are subhedral displaying rounded edges and red, globular inclusions as well as up to 15 µm long euhedral *apatite* inclusions.

9.2.5 Tuff bed IVb

Tuff bed IVb shows strongly varying percentages of *zircon* (3 - 91%) and *apatite* (8 - 83%) with only very minor portions of *sphene* and *rutile* (Fig. 97). Analysed samples originate from outcrops #2, 23 and 30. *Biotite* flakes dominate the heavy mineral suite of #2.

Of 100 measured euhedral *zircon*s from two samples of outcrops #23 and 30, 16 % show a stubby, 48 % a normal-prismatic, 19 % a long prismatic and 17 % a needle-like habit. Elongation-values vary between 1.29 and 8.50 with an average of 3.26 and an average standard deviation of 1.63. Elongation-frequency graphs (Fig. 95: 7-8) commonly show major peaks at 1.7 or 2.1 as well as at 2.5, 3.7 and 4.1 and minor peaks at 5.1, 5.7, 6.3 and 6.7. Habit and elongation values of *zircon*s from tuff bed IVb differ therefore largely from all other tuff beds allowing a correlation of tuff beds even if the correlation would not be known from the field work. The length of the *zircon*s ranges between 64 and 264 µm (average: 125 µm, average standard deviation: 41.55 µm) and the width varies between 24 and 68 µm (average: 43 µm, average standard deviation: 11.28 µm).

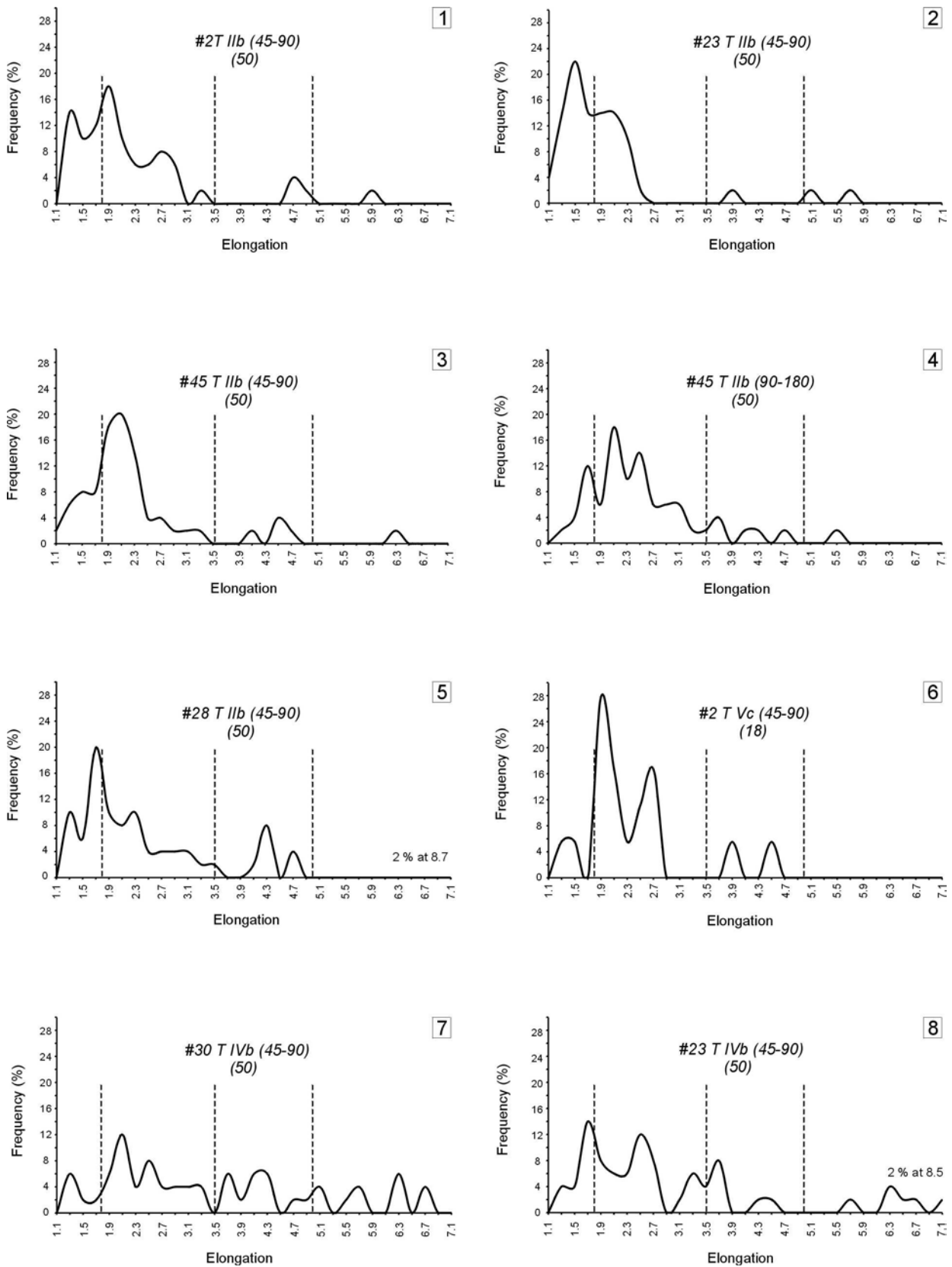


Fig. 95: Zircon elongation – frequency diagrams of analysed tuff samples from the Aranós Basin near Ganigobis. Zircons with elongation values below 1.8 are stubby, below 3.5 normal-prismatic, below 5.0 long-prismatic and above 5.0 needle-prismatic, numbers in brackets give the total numbers of the measured zircons. Note the different distribution of elongation values of tuff beds IVb compared to all other tuff beds, see text for discussion (cf. Chapter 9.7).

Euhedral zircons are mainly colourless and clear with sharp and unrounded crystal faces and occasionally show fissures. Ditetragonal-dipyramidal and tetragonal-bipyramidal terminations of the bipyramidal zircons counterbalance each other. One-ended zircons and especially splinters are frequent (Plate 5, Fig. 5). The following types of inclusions are present (cf. Chapter 9.1.1.2): elongated apatite and zircon crystals with maximum lengths of 20 μm , globular to elongate (up to 48 μm in length) fluid inclusions and elongate (up to 104 μm long) respectively globular opaque inclusions up to 25 μm in diameter. Elongate, unfilled cavities with lengths up to 120 μm and further cavities filled with dark magmatic material which probably represents altered glass are up to 160 μm long. Few zircons are devoid of inclusions, others show up to three types of inclusions in one zircon crystal. Malacons with slightly rounded crystal faces display magmatic zoning and cores of inherited zircon. Very few, other zircons show typical growth obstruction especially in the middle of long-prismatic zircons (Plate 5, Fig. 6).

Clear *apatites* are especially frequent (83 %) in separates of outcrop #30. *Apatites* displaying inclusions make up 27 % in outcrop #2 and 52 % in outcrop #30. Single, euhedral apatite crystals are up to 184 μm long and up to 48 μm wide reaching maximum elongation values of 6.6. Minute to small, globular and also elongated inclusions (Plate 4, Fig. 3) and the characteristic, up to 184 μm long and filled, axial, tubular cavities, which in cases extend over the whole length of the apatite crystal, are present within the *apatites* (Plate 4, Fig. 6).

Subhedral, dark-brown *rutile* grains and light-green to yellow sphene crystals occur as single specimen. Particularly the separates from outcrop #2 contain brown-green *hornblende* (5% of the non-opaque heavy minerals). Subhedral (stubby to normal-prismatic) to anhedral grains are up to 152 μm long and up to 96 μm wide. Mostly slightly rounded, green-brown *biotite* flakes dominate the separates of #2 (54 %). They have maximum sizes of 200 μm in length and 120 μm in width and are usually devoid of any inclusions (Plate 6, Fig. 5).

9.2.6 Tuff bed IVc

Heavy minerals of tuff bed IVc were only separated from outcrop #2 and yielded few non-opaque heavy minerals.

Slightly rounded *apatite* crystals with lengths of up to 160 μm and widths of up to 80 μm occasionally show fission tracks and minute, globular inclusions with diameters in the range of 5-10 μm . *Zircon* is mostly present in splinters and few euhedral, bipyramidal zircons show up to 40 μm large, dark inclusions. Most of the heavy minerals are dirty-grey, rounded, subhedral to anhedral *barite* grains.

9.2.7 Tuff bed V

Tuff bed V was sampled in outcrops #2 (Vc) and 23. Non-opaque heavy minerals were statistically analysed and show that *apatites* make up between 81 and 84%, *zircons* 15%; *monazite* and *rutile* only occur in minor portions (2%) (Fig. 97).

Apatites displaying inclusions make up 25% in outcrop #2 and 1% in outcrop #23. Single, euhedral apatite crystals (16 measurements) are between 72 and 172 μm long (average: 110.50 μm , standard deviation: 26.16 μm) and between 40 and 68 μm wide (average: 52.50 μm , standard deviation: 7.25 μm), elongation values vary between 1.50 and 3.58 (average: 2.13, standard deviation: 0.54). Minute, globular inclusions with sizes of 1-2 μm are partly aligned in rows, inclusions of euhedral *apatites* are quite frequent varying between 20 and 50 μm in length and 4 and 12 μm in width. The normally characteristic, filled, axial, tubular cavities were only detected in one apatite crystal (Plate 4, Fig. 1).

Of only 18 measured euhedral *zircons* from separates of outcrops #2, two grains are stubby, 14 are normal-prismatic and two grains are long prismatic (Tab. 10). Elongation-values vary between 1.25 and 4.56 with an average of 2.32 and a standard deviation of 0.78. The elongation-frequency graph (Fig. 95: 5) shows major peaks at 1.9 or 2.7 and minor peaks at 1.3, 3.9 and 4.5. The length of the zircons extends between 80 and 164 μm (average: 117 μm , standard deviation: 27.33 μm) and the width extends between 36 and 80 μm (average: 52 μm , standard deviation: 10.77

µm).

The few euhedral zircons are mainly colourless and clear with unrounded edges. In the samples of #23 rounded zircon grains and splinters predominate. Elongated apatite and zircon crystals with maximum lengths of 15 respectively 20 µm are especially conspicuous. They contain elongated or globular opaque inclusions, either up to 60 µm long or up to 24 µm in diameter. Malacons with slightly rounded crystal faces are quite frequent displaying magmatic zoning and cores of inherited zircon.

Single grains of slightly rounded, partly triangular *monazite* with lengths of 120 - 144 µm and widths of 80 - 92 µm and slightly rounded *sphene* with 25 µm large inclusions of zircon were detected in the heavy mineral separates. Other Ti-bearing phases resemble light golden-brown to middle-brown *rutiles*. They are subhedral to anhedral; their lengths vary between 96 and 200 µm and their widths between 48 and 80 µm. A 80 x 56 µm large fragment of a slightly pleochroitic, yellow-golden *leucoxene* aggregate was detected in separates of outcrop #23. However, the predominant heavy mineral phase within tuff bed V is authigenic *barite* which makes up to 95 % of all heavy minerals. It has a partly clear, partly dirty, brown appearance in this tuff bed.

9.2.8 Tuff bed VI

Tuff bed VI was only sampled in outcrop #2. Due to its poor quality only few heavy minerals could be separated including *zircon*, *apatite*, *monazite* and abundant *barite*. Most of the *zircons* are rounded splinters and only very few consist of euhedral zircons with rounded edges reaching a maximum size of 176 x 80 µm. Completely rounded malacons are also present within the separates which partly show delicate magmatic zoning. *Apatites* are mostly rounded fragments whereas a *monazite* crystal with a size of 100 x 80 µm is euhedral and displays a 24 µm large, rectangular inclusion.

9.2.9 Tuff bed VII

Tuff bed VII was only sampled in outcrop #15. Due to its poor quality (cf. Appendix B-1.1), 99% of the separated heavy minerals is authigenic

barite. Other heavy minerals include *apatite*, *zircon*, *rutile* and *sphene*.

Euhedral *apatites* are generally clear and sizes vary between 104 and 280 µm (average: 184 µm, standard deviation: 54.99 µm) in length and 40 and 66 µm in width (average: 47 µm, standard deviation: 9.46). Of 18 measured *apatites* 7 are normal-prismatic, 6 long-prismatic and 5 are even needle-prismatic with a maximum elongation of 7 giving an average elongation of 4.1 (long-prismatic, standard deviation: 1.66). 62% of all counted *apatites* show inclusions which comprise clear, elongate inclusions with a maximum length of 32 µm, characteristic, up to 25 µm long, axial, tubular cavities filled with altered brown, magmatic material and up to 32 µm long euhedral *apatite* crystals.

Apart from rounded fragments of *zircon*, very few euhedral, but partly fragmented zircon crystals with lengths of up to 176 µm and widths of up to 80 µm are present within the separates.

Rutiles are subhedral, up to 192 µm long and up to 80 µm wide, and show a pleochroitic dark yellow-red to middle-brown colour and partly rounded crystal faces. Single slightly rounded *sphene* crystals with dark inclusions and a 300 x 40 µm large, slightly pleochroitic, yellow-golden *leucoxene* aggregate were detected in the separates.

The predominant heavy mineral phase within tuff bed VII is authigenic *barite* which makes up to 99 % of all heavy minerals. It has a mostly dirty-brown appearance in tuff bed VII.

9.2.10 Tuff bed VIIIa

Tuff bed VIIIa was sampled in outcrops #9 and #27. It displays the highest variety of heavy minerals of all analysed tuff beds including *zircon*, *apatite*, *monazite*, *sphene*, *rutile*, *biotite*, *garnet*, *tourmaline* and *green hornblende* (Fig. 97).

Zircons were more frequent in samples from outcrop #9 than outcrop #27 (42% versus 6%). 50 euhedral zircons of #9 were measured, showing that 46 % are stubby, 50 % are normal-prismatic and only 2 % are long prismatic and needle-like. Elongation-values vary between 1.18 and 5.00 with an average of 1.99 and a standard deviation of 0.67.

Elongation-frequency graphs (Fig. 96: 1) show a dominant peak at 1.7 and minor peaks at 2.7, 3.7 and 5.1. The length of the zircons ranges between 56 and 176 μm (average: 97 μm , standard deviation: 25.95 μm) and the width extents between 32 and 68 μm (average: 50 μm , standard deviation: 7.90 μm). Euhedral zircons are mainly colourless and clear with sharp and unrounded crystal faces but splinters of zircon mainly predominate. Many zircons and zircon splinters are devoid of inclusions, one elongated 12 μm long apatite crystal and occasional globular to elongate opaque inclusions were noticed. Various zircon grains are slightly metamictised displaying magmatic zoning. Other crystals developed growth and penetration twins, up to 32 μm long, which grew perpendicular or oblique to the long axis of the main zircon crystal.

Contrary to zircon, *apatites* were more frequent in samples from outcrop #27 than outcrop #9 (71 % versus 53 %). The content of apatites with inclusions varies significantly between samples from the two outcrops making up 67 % of all apatites in outcrop #27 and only 4 % of all apatites in outcrop #9. Single, euhedral apatite crystals (7 measurements) are between 72 and 212 μm long (average: 118 μm , standard deviation: 47.60 μm) and between 36 and 60 μm wide (average: 47 μm , standard deviation: 13.41 μm) Elongation values vary between 1.57 and 3.5 (average: 2.56, standard deviation: 0.71). Up to 56 μm long and filled, axial, tubular cavities are characteristic of the apatites from tuff bed VIIIa (Plate 4, Fig. 2).

With up to 13%, *sphene* is especially frequent in samples from #27. The slightly pleochroitic, colourless to yellow-grey, partly green grains are rectangular to triangular with only slightly rounded edges. Minute, globular, opaque inclusions are quite numerous within up to 96 x 80 μm large crystals. *Monazite* grains show all, previously described features, their sizes vary between 48 and 152 μm in length and between 40 and 100 in width. A 72 x 16 μm large inclusion of brown, magmatic material in one of the monazite grains should be mentioned whereas many opaque inclusions are present in another grain. Golden-brown to dark-brown *rutile* grains with

rounded edges are subhedral to anhedral reaching sizes of up to 160 x 80 μm . *Hornblende* (also in tuff bed IVb), *garnet* and *tourmaline* only occur in tuff bed VIIIa (Plate 6, Figs. 7, 8, 11 and 12). All three heavy minerals were already described to further detail in chapters 9.1.1.6 to 9.1.1.9.

9.3 Analysed tuff beds from Zwartbas, southern Namibia

9.3.1 Tuff bed IIIb

The separates of tuff bed IIIb are dominated by *apatite* and *zircon*. 67 % of all counted grains are *apatites* (Plate 7, Figs. 5 and 6). 46 % of the apatites show the characteristic, up to 80 μm long, axial, tubular cavities filled with altered brown, magmatic material. *Zircons* make up about 32 % of all transparent heavy minerals. Of 50 euhedral zircons measured 24 % are stubby, 62 % are normal-prismatic, 12 % are long prismatic and 2 % are needle-like. Elongation-values vary between 1.13 and 6.63 with an average of 2.50 and a standard deviation of 1.04. The elongation-frequency graph (Fig. 96: 2) shows major peaks at 1.7, 2.1 and 2.7 and minor peaks at 3.5 and 4.3. The length of the zircons ranges between 70 and 212 μm (average: 122 μm , standard deviation: 38.73 μm) and the width extents between 28 and 88 μm (average: 52 μm , standard deviation: 13.32 μm). Bipyramidal, clear, colourless and euhedral zircons with sharp and unrounded crystal faces are relatively scarce but were used for SHRIMP-based age determinations (see Chapter 11.3.3; Plate 7, Fig. 4). Splinters of zircon predominate. Many zircons and zircon splinters are devoid of inclusions. Others show two or three types of inclusions within a single zircon crystal – for example up to 88 μm long inclusions of light grey, magmatic material, up to 40 μm long euhedral inclusions of apatite or globular opaque inclusions of similar size. Various zircons are slightly metamictised, display magmatic zoning and sporadically cores of inherited zircon. Ordinary *monazite* grains make up 1 % of all counted grains. They are euhedral to subhedral and show sizes which average 80 x 56 μm .

9.3.2 Tuff bed XXIVa

In tuff bed XXIVa *zircon* grains predominate the heavy mineral suite, *apatites* and *monazites* each make up 1 % (Fig. 97). Again, 50 euhedral *zircons* were measured of which 32 % are stubby, 64 % are normal-prismatic, 2 % are long prismatic and also needle-prismatic. Elongation-values vary between 1.50 and 5.00 with an average of 2.17 and a standard deviation of 0.64. The elongation-frequency graph (Fig. 96: 3) shows two dominant peaks at 1.7 and 2.1 and a minor peak at 2.7. The length of the zircons ranges between 40 and 200 μm (average: 93 μm , standard deviation: 26.81 μm) and the width extents between 16 and 64 μm (average: 44 μm , standard deviation: 10.50 μm). Bipyramidal, clear, colourless and euhedral zircons with sharp and unrounded crystal faces are quite frequent in contrary to tuff bed IIIb. Especially needle-like inclusions of apatite and globular opaque inclusions as well as thin fissures grown from inclusions within the centre of the crystals are conspicuous. *Apatite* crystals were rarely noticed. The mostly broken and rounded crystals are essentially devoid of inclusions. Euhedral, yellow *monazite* grains make up 1 % of all counted grains show sizes averaging 72 x 48 μm .

9.4 Analysed tuff beds from the Western Cape Province (South Africa)

9.4.1 OL 1/69: 378.00 m

Separates of this tuff bed are dominated by *biotite*, *zircon* and *apatite* (Fig. 97). The mostly yellow-brown *biotite* flakes constitute 75 % of all transparent grains (Plate 6, Fig. 6). They are pseudo-hexagonal, up to 300 x 200 μm large and were already described to detail in chapter 9.1.1.6. *Zircons* are mostly bipyramidal, clear and show very few inclusions. They constitute 6 % of all transparent heavy minerals. 50 euhedral *zircons* were measured exhibiting that 40 % are stubby, 44 % are normal-prismatic, 10 % are long prismatic and 6 % are needle-like. The length of the zircons varies between 52 and 200 μm (average: 105 μm , standard deviation: 35.70 μm) and the width extents between 24 and 68 μm wide (average: 47 μm , standard deviation: 9.92 μm).

Elongation-values range between 1.29 and 7.00 with an average of 2.43 and a standard deviation of 1.26. The elongation-frequency graph (Fig. 96: 5) shows two major peaks at 1.7 and 2.3 and minor peaks at 3.1, 3.5 and 4.1. *Apatite* crystals make up 15 % of all counted heavy minerals, they are mostly euhedral and 67 % of them contain up to 128 μm long tubular inclusions of magmatic material, up to 40 μm long, clear inclusions and minute, round inclusions. Green-brown *hornblende* grains are mainly elongated, fibrous and distinctly cleaved. The edge-rounded, subhedral (stubby to normal-prismatic) to anhedral crystals make up 4 % of all transparent heavy minerals.

9.4.2 OL 1/69: 396.36 m

The heavy mineral suite of this tuff bed consists of *biotite*, *apatite*, *zircon*, *sphene* and *hornblende* (Fig. 97). The mostly anhedral, light brown *biotite* flakes dominate the separates (44 %). They have irregular shapes and sizes of up to 150 x 80 μm . Some of them possess numerous small needles of apatite. *Apatites* make up 34 % of all transparent heavy minerals. They are mostly subhedral to anhedral with rounded and also corroded edges. 36 % of all counted apatites contain the characteristic, tubular inclusions of magmatic material with lengths of up to 100 μm . Small, elongate, colourless fluid inclusions are also present. Of 19 euhedral *zircons* measured 16 % are stubby, 74 % are normal-prismatic and 10 % are long prismatic. Elongation-values vary between 1.71 and 4.00 with an average of 2.53 and a standard deviation of 0.66. The elongation-frequency graph (Fig. 96: 6) displays major peaks at 1.7 and 2.5 and minor peaks at 3.1, 3.5 and 4.1. The length of the zircons ranges between 72 and 184 μm (average: 108 μm , standard deviation: 25.95 μm) and the width is between 28 and 64 μm (average: 44 μm , standard deviation: 9.28 μm). Bipyramidal, colourless and euhedral *zircons* with sharp and unrounded crystal faces are quite rare and splinters of zircon predominate. Some *zircons* and especially the zircon splinters are devoid of inclusions.

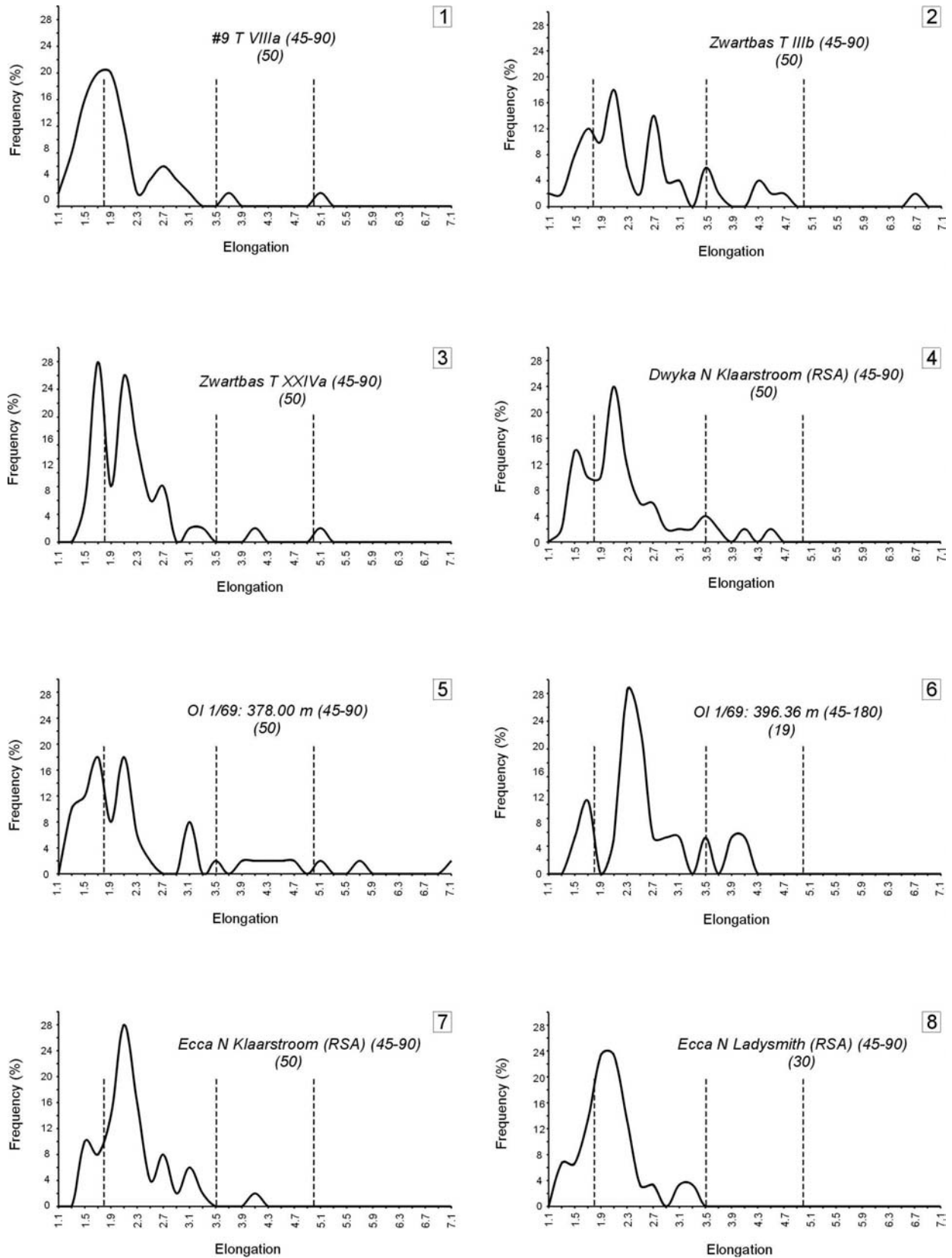


Fig. 96: Zircon elongation – frequency diagrams of analysed tuff samples from the Dwyka Group of southern Namibia and South Africa as well as from the Prince Albert Formation (Ecça Group) of South Africa; numbers in brackets give the total numbers of the measured zircons, the elongation classification is denoted in Fig. 95. Note the more stubby to normal-prismatic zircon population of the Ecça Group-equivalent tuff beds from South Africa compared to the other tuff beds from the Dwyka Group.

Other show up to 24 μm long, euhedral inclusions of apatite, minute, round and clear inclusions or globular, opaque inclusions of similar size. Occasionally zircons are slightly metamictised displaying magmatic zoning and thin fissures which grew from inclusions within the centre of the crystals. *Sphene* crystals are between 104 and 200 μm long and between 80 and 100 μm wide and represent 1 % of all transparent heavy minerals. The slightly yellow-green to grey grains are mostly rectangular and euhedral with only minor rounding or corrosion of the edges. One crystal shows growth obstruction on one side of the crystal. The pleochroitic, light green to brown *hornblende* crystals make up 5 % of all transparent heavy minerals. They are up to 120 μm long and 50 μm wide and exhibit a perfect cleavage.

Separates of tuff beds from the depths 390.59 m and 399.25 m contained only few transparent heavy minerals including euhedral *zircon* crystals as well as rounded fragments of *apatite*.

9.4.3 Tuffaceous bed from the Dwyka Group about 30 km north of Klaarstroom

Separates of this bed are dominated by *zircon* (94.5 %), minor portions are comprised of *apatite* (4 %), *monazite* and *garnet* splinters (Fig. 97). Colourless to slightly yellow *zircon* crystals are mostly bipyramidal with both terminations preserved, they are clear and their edges are not rounded. SHRIMP-based age determinations of these zircons resulted in age determinations with the lowest deviations (see Chapter 11.3.5). Zircons with needle-like inclusions of apatite and zircon, up to 36 μm respectively 20 μm long, with globular opaque inclusions and with up to 72 μm long inclusions of volcanic glass counterbalance zircons which are free of inclusions. Of 50 measured euhedral zircons 26 % show a stubby, 66 % a normal-prismatic and 8 % a long-prismatic habit. Elongation-values vary between 1.38 and 4.56 with an average of 2.25 and a standard deviation of 0.69. The elongation-frequency graph (Fig. 96: 4) shows two major peaks at 1.5 and 2.1 and minor peaks at 2.7 and 3.5. The length of the zircons ranges between 72 and 328 μm (average: 116 μm , standard

deviation: 38.60 μm) and the width extends between 28 and 76 μm (average: 53 μm , standard deviation: 11.55 μm). Few *apatite* crystals reach sizes between 84 and 128 μm in length and between 40 and 52 μm in width. They are mostly free of inclusions but one crystal with a 40 μm long, clear inclusion was also recognised. Two slightly rounded *monazite* grains with sizes of up to 104 x 64 μm are also present within the separates. Slightly yellow splinters of isotropic *garnet* show typical conchoidal fracturing.

9.4.4 Tuff bed from the Eccra Group about 30 km north of Klaarstroom

In this tuff bed the portions of *zircon* (46.5 %) and *apatite* grains (52 %) roughly counterbalance each other whereas monazites and rutiles only occur in traces (Fig. 97). 50 euhedral *zircons* were measured showing that 18 % are stubby, 80 % are normal-prismatic and 2 % are long prismatic. The elongation values vary between 1.41 and 4.00 with an average of 2.21 and a standard deviation of 0.51. The elongation-frequency graph (Fig. 96: 7) shows a dominant peak at 2.1 and minor peaks at 1.5, 2.7 and 3.1. The lengths of the zircons range between 80 and 208 μm (average: 122 μm , standard deviation: 26.74 μm) and the width extends between 40 and 80 μm (average: 56 μm , standard deviation: 8.66 μm). Bipyramidal, clear, colourless and euhedral zircons with sharp and unrounded crystal faces and many inclusions make up most of the zircons which were again used for SHRIMP-based age determinations (see chapter 11.3.7; Plate 7, Fig. 3). Inclusions comprise needle-like apatite with sizes up to 40 μm (Plate 5, Fig. 10) as well as globular opaque inclusions. Other zircons are devoid of any inclusions. Very few crystals show growth obstruction phenomena on the long side of the prism. More than 51 % of the euhedral, partly corroded *apatite* grains contain inclusions which involve mostly minute, globular, clear inclusions of gas or fluids with diameters less than 2 μm (Plate 4, Fig. 10) or the characteristic larger and mostly elongate, tubular cavities which are generally filled with grey to brown, magmatic material (Plate 4, Fig. 8).

Some of them also seem to be empty. The characteristic slightly rounded *monazite* grains are between 60 and 80 μm long and between 48 and 56 μm wide. Brown, subhedral, slightly rounded, rectangular *rutile* grains are between 64 and 128 μm long and between 40 and 64 μm wide.

9.4.5 Tuff bed from the Ecca Group north of Ladismith

Heavy mineral separates of this tuff bed are dominated by *apatite* (69 %) and *zircon* (30 %). Again *monazite* (1 %) occurs only in traces (Fig. 97). The euhedral *apatite* crystals are relatively clear but their edges are slightly corroded. Their size varies between 96 and 168 μm in length and 40 and 88 μm in width. 73 % of all *apatite* grains contain inclusions which mainly comprise minute to small, colourless inclusions of gas or fluids and only the large crystals show tubular cavities filled with the brown, magmatic material. Most of euhedral *zircons* are clear and were used for the SHRIMP-based age determinations (see Chapter 11.3.8). Only few show inclusions of *apatite* or dark, globular inclusions. The length of the *zircons* is between 40 and 144 μm (average: 101 μm , standard deviation: 26.98 μm) and the width varies between 24 and 88 μm (average: 52 μm , standard deviation: 15.13 μm). 30 euhedral *zircons* measured of which 27 % display a stubby and 73 % a normal-prismatic habit. Elongation-values vary between 1.25 and 3.33 with an average of 2.02 and the elongation-frequency graph (Fig. 96: 8) displays a broad major peak between 1.9 and 2.1 and very minor peaks at 1.3, 2.7 and 3.1.

9.4.6 Tuffaceous bed from the Dwyka Group of KwaZulu-Natal about 2 km east of Nondweni

Zircons vary between clear, euhedral and rounded, probably sedimentarily derived. The clear and euhedral *zircons* were examined with the SHRIMP II to gain an Dwyka Group-equivalent age (see Chapter 11.3.6). Malacons with sizes up to 160 x 76 μm and many fragments and splinters partly displaying a pinkish colour are present within the separates. The *apatites* are

clear and mostly rounded with lengths between 84 and 240 μm and widths between 60 and 72 μm . Only few possess small and clear inclusions. Slightly yellow to green crystals of *sphene* are quite frequent in one of the separates. They are subhedral with their edges being rounded and partly corroded and sizes reach up to 124 x 80 μm . The characteristically, slightly rounded *monazite* grains are between 76 and 88 μm long and between 48 and 64 μm wide. Pleochroitic light to dark brown, elongated *rutile* grains show rounded edges and are between 72 and 80 μm long and between 32 and 40 μm wide.

A quantitative summary of all occurring heavy minerals in the analysed tuff beds is found in Tab. 22 in Appendix E.

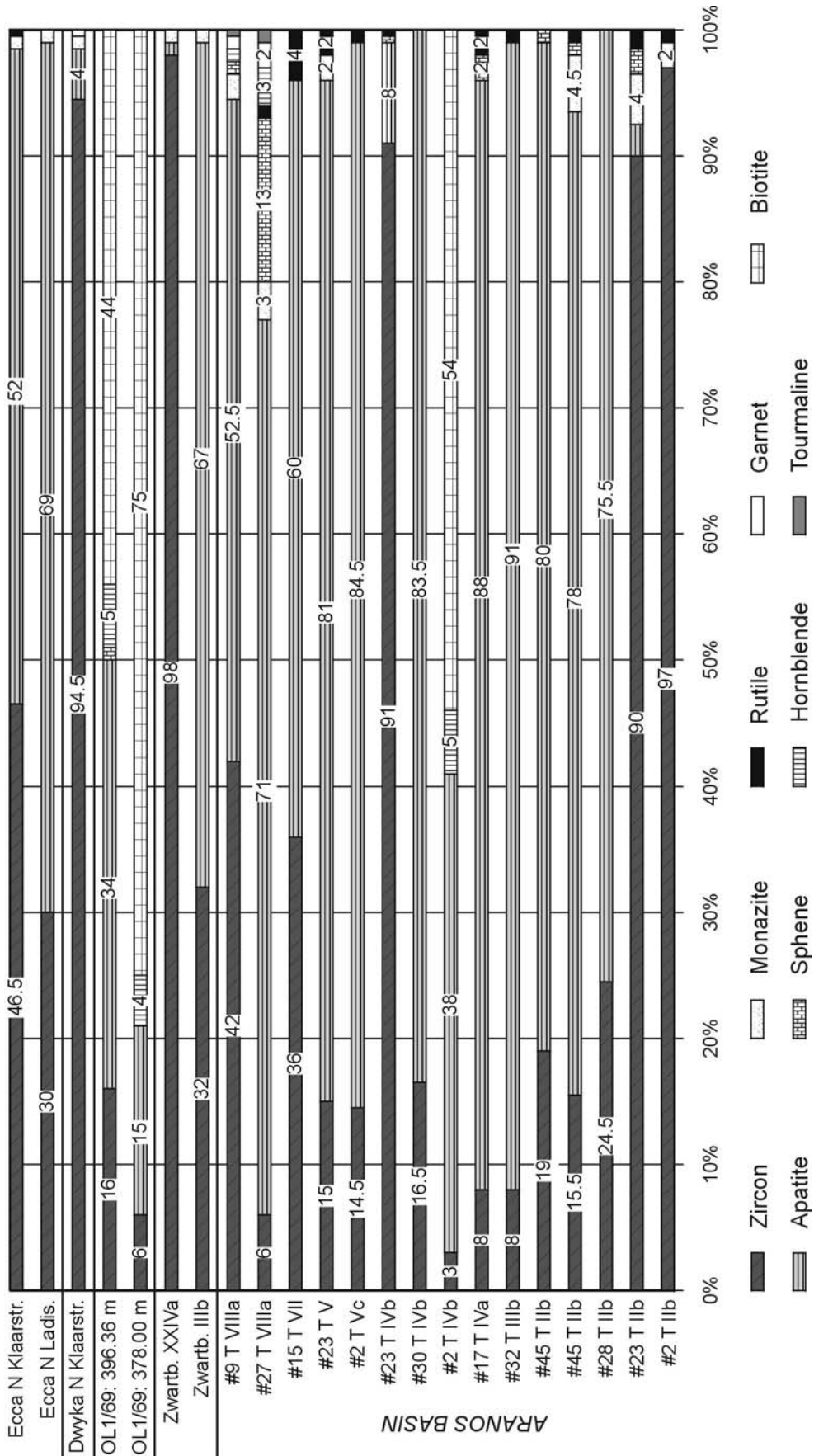


Fig. 97: Quantitative heavy-mineral composition of the analysed tuff beds, counted grains normally total 200 except #2 tuff IVb (52), #15 tuff VII (22) and #27 tuff VIIIa (300), see text for discussion.

9.5 Quantitative analysis of the main tuff beds

Grain counts of the transparent primary volcanic heavy minerals were performed in order to quantitatively compare single ash fall tuff beds. Zircon, apatite, monazite, sphene, rutile, tourmaline, garnet, hornblende and biotite were counted. Due to the small crystal and grain sizes

of the minerals, the 45-90 μm fraction was mostly analysed (except #45 I Ib). The accuracy of counting rises with the square root of counted grains ($V=Z \cdot (p \cdot q/n)^{1/2}$) which means that with a higher number of grains counted, the error of counting will be reduced. The following deviations have to be considered (Boenigk, 1983; Tab. 12):

counted grains n	portion of a mineral in % (p) within a separate, 95 % probability ($Z=2$, $q=100-p$)									
	1	2	5	10	20	30	40	50	60	80
100	2.00	2.80	4.40	6.00	8.00	9.20	9.80	10.00	9.80	8.00
200	1.40	2.00	3.10	4.20	5.70	6.50	6.90	7.10	6.90	5.70
300	1.10	1.60	2.50	3.50	4.60	5.30	5.70	5.80	5.70	4.60
600	0.80	1.10	1.80	2.50	3.30	3.70	4.00	4.10	4.00	3.30

Tab. 12: Possible inaccuracies of counting results in percent due to the relative frequency of grains, the probability and the number of counted grains (Boenigk, 1983).

For example: 200 grains are counted and the portion of a mineral is 30 %, the real portion of the mineral lies in 95 of 100 cases between 23.5 % and 36.5 % (cf. Boenigk, 1983). Henningsen (1967) states that with only few different mineral classes (3 - 5), the counting of 100 minerals is sufficient, otherwise 300-500 minerals should be counted.

Considering the restricted suite of heavy minerals within most of the analysed tuff beds, counting of 200 grains appeared to be sufficient. Due to the poor rock quality (cf. Appendix B-1.1) of some samples, separates of tuff beds #32 I Ib, #2 IVb and #15 VII revealed only few transparent heavy minerals. The counts of sample #32 I Ib were completely omitted as only 15 grains could be analysed. If only few grains are counted, amounts of less abundant minerals such as monazite or rutile can be overemphasised in comparison to generally more abundant minerals such as apatite or zircon. Because of the large variety of different heavy minerals, 300 grains were counted from tuff bed #27 VIIIa.

Fig. 97 shows the quantitative heavy-mineral composition of the main tuff beds. The exact values for individual samples and the number of counted grains per sample are quoted in Tab. 11.

Unfortunately, a clear trend could not be deduced from the quantitative analysis. *Apatites*

and *zircon*s dominate the heavy mineral suite. If *apatites* are obviously leached by dissolution of acids, *zircon* values are consequently higher than 90 % (#2 I Ib, #23 I Ib, #23 IVb and the tuffaceous bed of the Dwyka Group north Klaarstroom, South Africa). *Biotite* flakes predominate tuff beds #2 IVb and both analysed tuff beds from borehole OL 1/69. *Sphene* is quite frequent in #27 VIIIa. *Monazite*, *rutile*, *hornblende*, *garnet* and *tourmaline* only occur in traces (Fig. 97).

9.6 Heavy minerals in the adjacent mudstones

In order to check whether heavy minerals from the adjacent mudstones were admixed with the ones of the tephrostratigraphic beds, 7 mudstone samples of outcrop #2 were analysed. Sample #2/(-8) was taken close to tuff beds I, sample #2/(-1) close to tuff beds III, samples #2/7 and #2/8 close to tuff beds IV, samples #2/20 and #2/21 close to tuff bed Vc and #2/26 was taken close to tuff beds VIa and b.

Due to the restricted occurrence of transparent heavy minerals, the separates were only analysed qualitatively.

9.6.1 Qualitative analysis

The heavy-mineral suite of transparent grains comprises *zircon*, *apatite*, *sphene*, *rutile*, *tourmaline*, *garnet*, and *biotite*. Single grains of *topaz* and *xenotime* also occur. Secondary minerals comprise opaque minerals and barite.

Zircon grains are mainly subhedral to anhedral whereas euhedral crystals were rarely observed. Fragments of zircon are frequent, their edges are mostly rounded and corroded. Grains are colourless and quite large, their size varies between 136 and 232 μm in length and 88 and 170 μm in width as they were mostly observed in the fraction 90-180 μm . *Apatite* was commonly found as subhedral to anhedral grains. One euhedral crystal with two parallel, axial, tubular cavities filled with magmatic material was detected in sample #2/(-8). Other grains show minute, round fluid inclusions and up to 20 μm large, opaque inclusions. The length of the crystals and fragments varies between 56 and 180 μm and the width between 32 and 70 μm . Colourless or pale pinkish *garnet* grains are quite frequent in the separates and occur in 5 of 7 samples. Fragments or splinters are mostly angular but complete minerals are well-rounded. Garnet grains show the typical conchoidal fracturing; some of them show minute to small fluid inclusions. The grains were found in the fractions 45-90 μm and 90-180 μm , the length of the crystals, fragments and splinters varies between 76 and 360 μm and the width between 64 and 220 μm . *Sphene* grains are rectangular with rounded and corroded edges and occur in two samples in the fraction 90-180 μm . They display a maximum size of 184 x 136 μm .

Biotite is commonly bleached by weathering and has light brown colours or is even almost colourless. The irregular-shaped and rounded flakes show sizes of 120 to 144 μm in length and 80 to 112 μm in width. In #2/(-1) a single *rutile* grain was observed which displays completely rounded and corroded edges. A single grain of *tourmaline* was detected in #2/8. The rectangular and 184 x 88 μm large grain is pleochroitic changing between pink and black, it has rounded edges and shows up to 30 μm large inclusions of euhedral zircon and minute, round fluid inclusions.

Mostly colourless grains of *xenotime* and *topaz* were tentatively observed. *Xenotime* shows a irregular rounded to rectangular shape. It is colourless, has a high birefringence and displays narrow colour bands near to thin edges in polarised light. Opaque inclusions with sizes of 15 μm were also recognised. The grains only occur in the fraction 90–180 μm and are therefore large with maximum sizes of 256 x 160 μm . *Topaz* is also colourless but mostly angular and splintery. Rutile was observed as inclusion but most frequent are opaque inclusions. Topaz has a low birefringence with thicker grains showing typical red and blue colours of second order. Maximum sizes reach 160 x 128 μm .

Apart from an euhedral apatite grain with the characteristic, tubular cavities pointing to a volcanic origin, the heavy mineral suite of the mudstones of the Ganigobis Shale Member shows no correspondence with the heavy mineral suite of the analysed pyroclastic tuff beds. The heavy mineral suite of the mudstones is so different from the heavy mineral suite of the tuff beds that the juvenile character of apatite, zircon, monazite, sphene, rutile, biotite, hornblende, garnet and pink tourmaline within the tuff beds is most probable.

9.7 Discussion of the heavy-mineral suite

The mainly euhedral habit of *zircon* in the tuff beds indicates its volcanic origin and derivation from acid to intermediate melts. In contrast, zircon grains in the surrounding mudstones are always edge- to well-rounded. Published data suggest that elongation values of more than 3.0 are distinctive of pyroclastic rocks (Mange and Maurer, 1991) and confirm the pyroclastic nature of the bentonitic beds. The elongation-frequency graphs of almost all tuffs (Fig. 95 and Fig. 96) display a distinctive pattern with two or three major peaks between 1.3 and 2.7 showing that most zircons are stubby to normal-prismatic. Tuff bed IVb from the Aranós Basin is exceptional as elongation values are more or less evenly distributed from 1.3 to 6.7 indicating a higher proportion of long-prismatic to needle-like zircons. In many diagrams minor peaks at 3.1 and 3.5 are present.

Two to four preferred elongation values within the analysed zircon populations probably originate from contrasting magma composition and different crystal growth indicating a complex zircon population (Hoppe, 1963; Winter, 1981). Largest zircons are between 200 and 264 (328) μm long and 64 and 88 μm wide. Smaller zircons were only observed in the tuff beds Vc and VIIIa from southern Namibia as well as from the Dwyka Group of South Africa (OL 1/69: 396.36 m) and the Ecca Group north of Ladismith (South Africa).

Rounding of heavy minerals, especially of *zircons*, suggests that minerals are of detrital and not of primary volcanic origin. However, minor rounding of the edges of euhedral crystals or fragments can also originate from magmatic resorption within the parent magma (cf. Fisher and Schmincke, 1984). This is especially supposed for *monazite* but also *sphene*, *rutile* and *hornblende* mostly show minor rounding of the edges.

The following heavy minerals are considered to be detrital and were probably admixed into the volcanic ash from the siliciclastic background sedimentation due to reworking and secondary transport of the original ash or may be detrital xenocrysts of the ash. They mostly occur in minor contents in the tuff beds and only occasionally as single grains:

- Well-rounded metamictic *zircons* and also splinters with rounded crystal faces occur in tuff beds Ib, IIb, Vc, VI and VII of the Aranos Basin in southern Namibia as well as

in samples from the tuffaceous beds from the Dwyka Group of KwaZulu-Natal.

- Especially many rounded *sphene* grains from the tuffaceous beds of the Dwyka Group of KwaZulu-Natal but also sphenes from tuff beds IIb, IVa and VII
- Rounded, subhedral to anhedral *rutile* grains from tuff beds IIb, IVa, Vc, VII and VIIIa
- Rounded, subhedral to anhedral *biotite* flakes from tuff bed IVb and from the tuff beds of OL 1/69

Apatite crystals from the borehole OL 1/69 from the Western Cape Province (South Africa) often show corroded crystal faces due to their solubility in acids.

A zircon - apatite - monazite - biotite - tourmaline assemblage within the examined tuff beds indicates a rather acidic parent magma, whereas sphene and green hornblende rather suggest the participation of intermediate (to basic) magma (cf. Zimmerle, 1976). Sphene and hornblende only turn up in traces (except tuff bed VIIIa) within the analysed tephrostratigraphic beds leading to the conclusion that the overall type of parent magma from which the volcanic ash originated was mainly acidic with some minor participation of intermediate magma. This could be the case in tuff bed VIIIa where both sphene and green hornblende occur whereas sphene on its own turns up in various other tuff beds from the Aranos Basin (tuff beds IIb, IIIb, IVa, Vc and VII).

10 Geochemistry of the bentonitic tuff beds, Dwyka Group, southern Africa

10.1 Introduction

Bentonitic tuff beds have been increasingly investigated with geochemical methods in the past 20 years. Geochemical analyses are thus important with respect to rock identification and classification and with respect to the determination of the original magmatic composition and the tectonic setting of the source area.

Processes such as the admixture of ash-sized

wall rock components during eruption, aeolian fractionation within the wind-drifted ash cloud, resedimentation of the original volcanic ash, admixture of associated clastic sedimentary material, diagenetic alteration and growth of minerals as well as weathering processes affect the geochemical composition of the original tephra beds. Particularly in Palaeozoic tuff beds, volcanic glass, which is a major component of

ash fall tephra, has been devitrified and altered into clay minerals during compaction and diagenesis which significantly changes the chemical composition of the original tephra deposit. Determination of the major element chemistry of altered tuff beds has therefore little application in order to deduce the original composition of the tephra beds. However, immobile trace and rare-earth elements have been used by numerous workers to provide information on the original magmatic composition of the parent magma and the tectonic setting of the source volcanoes. It is thus possible to distinguish among altered tephra layers through immobile trace and rare-earth elements which are less affected by alteration.

Chemical fingerprinting has been successively used in tracing and correlating tephra layers. The relative immobile elements Ti and Al in European tuff beds were used to determine the composition of the original ash, and thus the type of source magma (Spears and Kanaris-Sotiriou, 1979; Spears *et al.*, 1999). Trace and rare-earth element chemistry of bulk rocks (Bergström *et al.*, 1997; Huff, 1983; Kolata *et al.*, 1986; Kolata *et al.*, 1996) and individual mineral species (Samson *et al.*, 1988) were used to distinguish individual Ordovician K-bentonites in North America and Europe, and to correlate them over several hundred kilometres. Groups of Silurian K-bentonite beds in Britain were identified on the basis of their chemical composition (Huff *et al.*, 1991; Huff *et al.*, 1996; Sarna-Wojcicki, 1976). Sarna-Wojcicki *et al.* (1984) correlated Cenozoic tuffs in California (U.S.A.) by means of trace and

rare-earth element chemistry of volcanic glass. Stable isotope geochemistry was used to discriminate volcanic ash layers on the island of Milos (Greece; Decher *et al.*, 1996). Statistical methods such as inter-element correlation coefficients and discriminant analysis provide powerful tools for the comparison between single tuff beds (e.g. Huff and Kolata, 1989). A comprehensive overview on the interpretation of geochemical data is provided by Rollinson, (1993).

The geochemistry of pyroclastic deposits which are exhibited in the lower Karoo Supergroup in southern Africa is mentioned in papers of Viljoen (1994, 1995: Dwyka to lower Beaufort Group); Keyser and Zawada (1988: Lower Beaufort Group), McLachlan and Jonker (1990: Ecca Group) and Karpeta (1996: Lower Beaufort Group).

For this study, whole rock analyses (major, trace and rare-earth elements) of individual tuff beds of the lower Karoo Supergroup in southern Africa were carried out to understand their present major element geochemistry with respect to the mineralogy deduced from XRD-measurements, to discriminate and possibly correlate between single tuff beds of a specified basin area as well as to deduce the original magmatic composition of the parent magma and the tectonic setting of the source area by immobile trace and rare earth elements. Sample selection, preparation and analytical methods are described in Appendix B-5. Results of all XRF- and ICP-MS measurements are listed in Tab. 24 in Appendix F-2.

10.2 The geochemistry of the present-day tuff beds: Major elements

All analyses are quoted in Appendix B-5.3. For the following interpretations of the major element contents, the data set was plotted not normalised and normalised to 100 % on a LOI and CO₂-free basis.

10.2.1 SiO₂

Euhedral quartz phenocrysts in high temperature modifications and light grey, glassy inclusions detected in juvenile zircons and apatites of the tuff beds suggest a rather

intermediate to acid character of the original ash. This character will be later ascertained by the analysis of mainly immobile trace elements. LOI and CO₂-normalised SiO₂- contents in the present tuff beds vary between 55 and 66 %. SiO₂ is therefore only slightly depleted in the present-day tuff beds. Retention of silica during alteration of the original ash is a function of clay mineral formation and, in turn, on porewater compositions and clay stability fields (Spears *et al.*, 1999). The marine mudstones of the Ganigobis Shale Member rather protected the tuff

beds as the mudstones probably created a slightly basic to circum-neutral environment in which only few silica was dissolved. SiO_2 is only soluble in very alkaline environments.

The SiO_2 - contents of the tuff beds from the Aranos Basin near Ganigobis are plotted in Fig. 98.

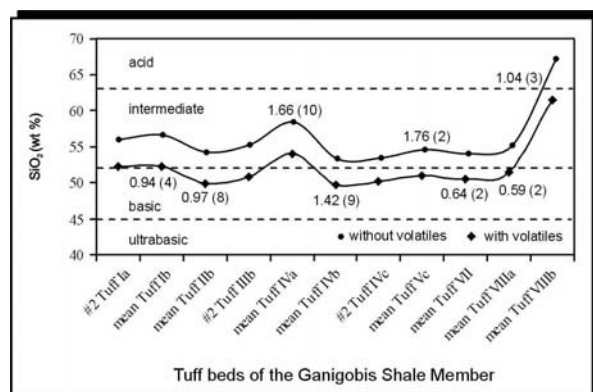


Fig. 98: SiO_2 - contents of tuff beds from the Ganigobis Shale Member calculated without and with volatiles (LOI and CO_2). Figures next to the data points denote the standard deviation of the measurements and the overall number of measurements which are also valid in the following figures.

Not normalised SiO_2 - contents respectively mean SiO_2 - contents suggest a basic character of the tuff beds. Normalised SiO_2 - contents, however, average 56.7 % and indicate a rather intermediate to acid character of the tuff beds. Figures next to the data points denote the standard deviation of the measurements and the overall number of measurements (in brackets). Standard deviations below 1.5 indicate a good sampling quality of the measured samples (cf. Appendix B-1.1) which indirectly provide a measure of the degree of weathering of the present-day tuff beds. The measurements of samples from tuff bed IVa and Vc are therefore the least reliable as they indicate the highest degree of weathering. Tuff bed VIIIb has significantly higher SiO_2 - contents with normalised values averaging 65.6 %.

Tuff beds of the Dwyka Group of the Karasburg Basin average 55.01 % SiO_2 . Normalised SiO_2 - contents of the Dwyka and Ecca Groups of the Western Cape Province in South Africa average 55.82 % respectively 56.00

%. These values are only slightly less than the average SiO_2 - contents of acid to intermediate igneous rocks containing 58,90 % (Wedepohl, 1978).

10.2.2 TiO_2

TiO_2 mainly occurs in heavy minerals such as rutile, anatase, brookite and sphene. Ti also replaces Al in the clay minerals and Fe-hydroxides (Friedl and Schwertmann, 1996). It is regarded as principally immobile in the course of devitrification of the original volcanic glass and the transformation into clay minerals and is regarded as resistant against weathering (Kolata *et al.*, 1996). Not normalised TiO_2 - values vary between 0.2 and 1.3 % (2.1 %) in the analysed tuff beds.

Especially in the highly altered tuff beds IIa, IIIb, IVa, Vc and VII from the Aranos Basin near Ganigobis, Ti seems to be concentrated due to weathering and is therefore enriched. Values range from 0.9 to 1.3 % in these beds. Highest standard deviations are found in tuff bed VIIIa which is due to the deviating analysis of #27 tuff VIIIa and also in tuff bed VIIIb (Fig. 99).

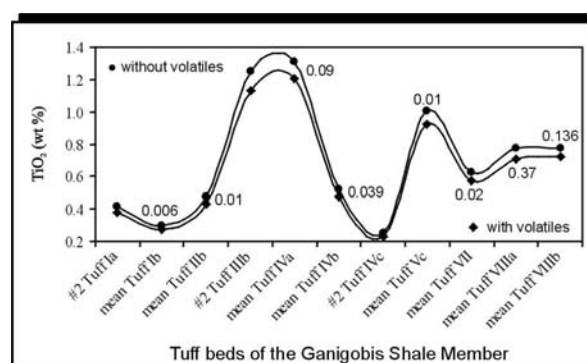


Fig. 99: TiO_2 - contents of tuff beds from the Ganigobis Shale Member; figures next to the data points denote the standard deviation of the measurements.

Tuff beds IIb and IVb, however, display values of 0.4 – 0.6 %. This concentration is regarded as the approximate value of the original ash composition of the tuff beds. Less altered tuff beds from Zwartbas (southern Namibia) show an average of 0.4 % TiO_2 which confirms the approximate value mentioned above. The tuff beds of the Dwyka Group from the Western Cape

Province, however, vary between 0.35 and 2.11 % whereas those of the Ecca Group from the Western Cape Province again average 0.42 %. Compared to common igneous rock types (Wedepohl, 1978) values of 0.4 – 0.6 % correspond to rhyodacitic to dacitic rocks which once more indicates the intermediate to acid character of the tuff beds.

10.2.3 Al_2O_3

The clay-rich nature of the bentonites is responsible for the high Al_2O_3 - contents and a low SiO_2/Al_2O_3 ratio compared with the mudstones of the Ganigobis Shale Member (cf. Fig. 118). The mobility of Al is low and Al is therefore relatively enriched in the analysed tuff beds. The tuff beds also have a higher Al_2O_3 concentration compared to possible parent volcanic ashes as a result of the net loss of other elements.

Tuff beds of the Ganigobis Shale Member from the Aranos Basin of southern Namibia comprise average values between 24 and 27 % Al_2O_3 (with volatiles) respectively 26 to 30 % (without volatiles). Highest standard deviations occur in tuff beds VIIIa and VIIIb (Fig. 100).

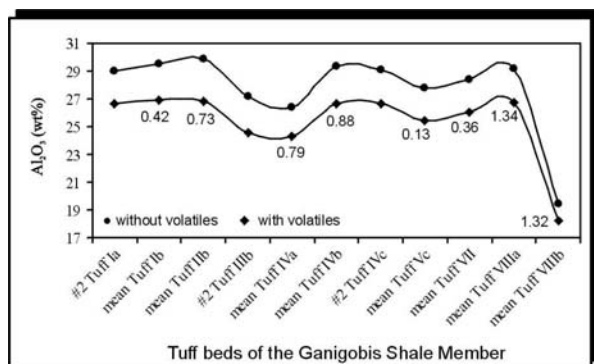


Fig. 100: Al_2O_3 - contents of tuff beds from the Ganigobis Shale Member displaying average Al_2O_3 - contents of 24 to 27 % (with volatiles) respectively 26 to 30 % (without volatiles); numbers next to the data points denote the standard deviation of the measurements.

Tuff bed VIIIb of the Ganigobis Shale Member only shows about 18-19 % Al_2O_3 on average. Tuff beds from Zwartbas (southern Namibia) average 28.5 % Al_2O_3 (not normalised) and 31.0 % (normalised). The tuff beds of the Dwyka Group from the Western Cape Province of South

Africa average 24.2 % Al_2O_3 (normalised: 25.9 %) whereas the ones of the Ecca Group reach up to 32 % (normalised). The Al_2O_3 -contents of the analysed tuff beds are therefore increased by a factor of 1.5 and 2 over that of comparable volcanic rocks which vary between 13 and 17 % Al_2O_3 (Wedepohl, 1978; cf. Chapter 10.6.1).

10.2.4 Fe_2O_3

Not normalised Fe_2O_3 - values range between 1.6 and 6.9 % (10.4 %) in the analysed tuff beds of the Ganigobis Shale Member near Ganigobis. Iron mainly occurs in secondary minerals such as goethite, ulvospinel, iwakiite and also jacobsite (cf. Chapter 8.3.5). The Fe_2O_3 - contents of the tuff beds of the Ganigobis Shale Member rise with their number and especially tuff beds IVc, V and VII and VIIIb show high values of Fe_2O_3 (Fig. 101).

The high value of Fe_2O_3 in tuff beds IVc, Vc and also VII is in accordance with the appearance of laminated mudstones close above tuff bed Vc which suggest a near-shore position and a higher influx of land-derived iron. The higher supply of iron probably led to a greater concentration of Fe_2O_3 in the tuff beds. Overall Fe_2O_3 -values of the tuff beds are nevertheless significantly lower than in the mudstones of the Ganigobis Shale Member (Fig. 118). The tuff beds from Zwartbas contain between 1.6 and 3.1 % Fe_2O_3 (not normalised).

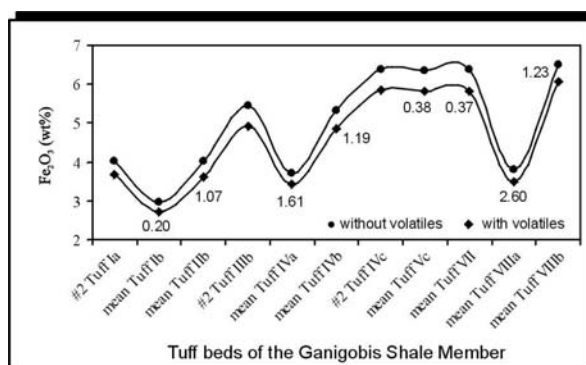


Fig. 101: Fe_2O_3 - contents of tuff beds (and their standard deviation) from the Ganigobis Shale Member. They generally rise up-section in the Ganigobis Shale Member.

Similar values are measured in the samples of the tuff beds from the Ecca Group, Western Cape

Province, South Africa whereas the tuff beds from the Dwyka Group of the same area show varying iron values between 2.2 and 8.1 %.

10.2.5 MnO

Not normalised MnO-values vary between 0.007 and 0.25 % in the analysed tuff beds. It occurs in secondary minerals such as iwakiite and jacobsite (cf. Chapter 8.3.5) but also in the clay minerals. The concentration of MnO correlates positively with the concentration of Fe₂O₃ in the tuff beds of the Ganigobis Shale Member and is highest in tuff beds IVc and VII (Fig. 102).

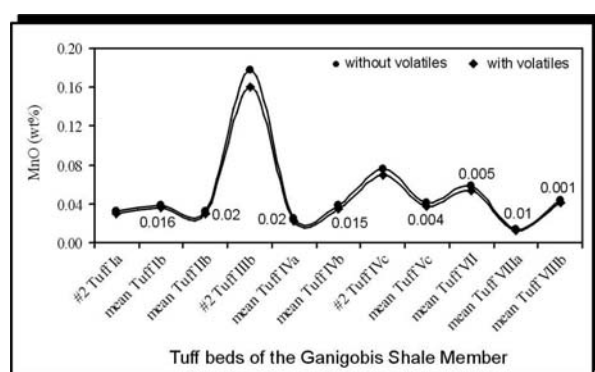


Fig. 102: MnO- contents of tuff beds from the Ganigobis Shale Member; figures next to the data points denote the standard deviation of the measurements. Tuff bed IIIb is statistically regarded as an outlier.

The sample of tuff bed IIIb is statistically regarded as an outlier and should not be incorporated in any calculations. The concentration of MnO is mostly lower than in the surrounding mudstones of the Ganigobis Shale Member (0.06 %) and also lower than in comparable igneous rocks such as dacites (0.12 % MnO, Wedepohl, 1978). The tuff beds from Zwartbas contain between 0.007 and 0.04 % MnO (not normalised). Similar values are measured in the samples of the tuff beds from the Ecca Group, Western Cape Province, South Africa whereas the tuff beds from the Dwyka Group of the same area show higher values between 0.04 and 0.17 % MnO (not normalised).

10.2.6 MgO

Magnesium is mainly concentrated in the clay minerals of the tuff beds as well as in secondary

mineral groups such as sulphates, borates and phosphates. Not normalised MgO concentrations vary between 0.6 to 0.9 % in the tuff beds from the Ecca Group, Western Cape Province, South Africa. Maximum values of 4.2 % are reached in samples of tuff beds from the Dwyka Group of the Western Cape Province, South Africa. Values of MgO in the tuff beds of the Aranos Basin near Ganigobis range between 1.56 % (tuff bed IVa) and 2.64 % (tuff bed IVb, Fig. 103). The Al/Mg-ratio is relatively constant at 10-11 (with the exception of tuff bed IVa) which points to a rather low degree of weathering.

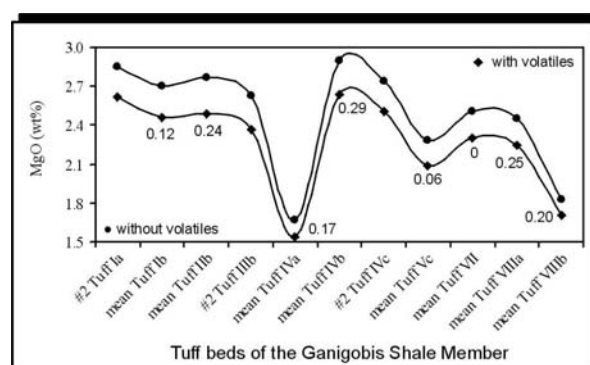


Fig. 103: MgO- contents of the tuff beds from the Ganigobis Shale Member; figures next to the data points denote the standard deviation of the measurements.

The tuff beds from Zwartbas interestingly show a continuous decrease in MgO from the lowest tuff beds IIIb (2.51 % MgO) to the highest tuff bed XXXIV (1.77 % MgO, all data given not normalised).

10.2.7 CaO

Calcium mostly occurs in secondarily formed calcite minerals but is also found in plagioclases, clay minerals or juvenile heavy minerals such as sphene.

The CaO-contents in the analysed tuff beds is mostly below 1.5 % which is thought to comprise the original composition of the tuff beds. Nevertheless, CaO-contents occasionally reach 7 - 8 % (not normalised). Samples of tuff bed IVa from the Ganigobis Shale Member near Ganigobis which were laterally taken in the same outcrop #2 vary in the CaO-contents between 0.19 and 6.98 % (not normalised).

High CaO values of 4.5 % of tuff bed VIIIa from the Ganigobis Shale Member originate from a directly overlying microbial limestone bed.

Calcium was dissolved from the limestone bed and then precipitated via the pore waters in the tuff bed (Fig. 104). Overall CaO-values of the tuff beds are significantly lower than average values of the mudstones of the Ganigobis Shale Member (cf. Fig. 118).

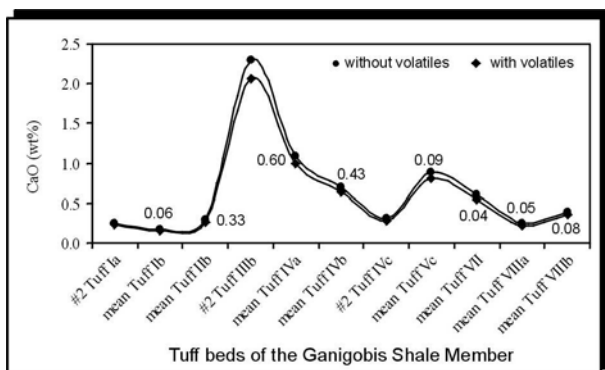


Fig. 104: CaO- contents of the tuff beds from the Ganigobis Shale Member; figures next to the data points denote the standard deviation of the measurements. Note the high contents of tuff bed V and VIIIa, see text for discussion.

10.2.8 Na₂O

Na₂O is highest in tuff bed IVa from the Ganigobis Shale Member near Ganigobis displaying concentrations between 2.2 and 4.2 % (not normalised, Fig. 105).

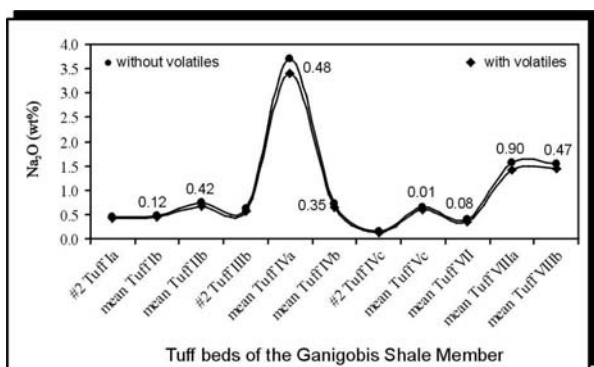


Fig. 105: Na₂O- contents of the tuff beds from the Ganigobis Shale Member; figures next to the data points denote the standard deviation of the measurements. Note the high Na₂O- contents of tuff bed IVa due to the abundance of plagioclase in this tuff bed.

Other tuff beds such as #27 tuff VIIIa and #45

tuff VIIIa reach 2% whereas the majority of the tuff beds show Na₂O concentrations of less than 1 % (not normalised). Sodium is a very mobile element and highly soluble. Most probably Na₂O was removed during the formation of the present-day tuff beds. In tuff bed IVa from the Ganigobis Shale Member it remained mostly stored in albite. Overall Na₂O- values of the tuff beds are therefore lower than average values of the mudstones of the Ganigobis Shale Member (Fig. 118).

Na₂O- contents in comparable intermediate to acid, igneous rocks are also higher and vary between 2.0 and 3.7 averaging 2.9 % (Wedepohl, 1978).

10.2.9 K₂O

The K₂O- contents of bentonitic tuff beds are generally proportional to the illite and the illite-smectite percentage of the tuff beds. Kaolinite does not contain K₂O whereas illite / smectite mixed layered minerals hold 7-9 % K₂O and K-feldspar up to 16.9 % K₂O (Kiipli *et al.*, 1997).

Tuff bed IVa and #23 tuff V of the Ganigobis Shale Member contain 3 % K₂O and show highest kaolinite peaks in XRD measurements (Fig. 87). They consequently show the highest kaolinite values of all measured tuff beds. These tuff beds show the highest degree of alteration as kaolinite is thought to form from illite or smectite as an end member in the process of degradation (Heim, 1990).

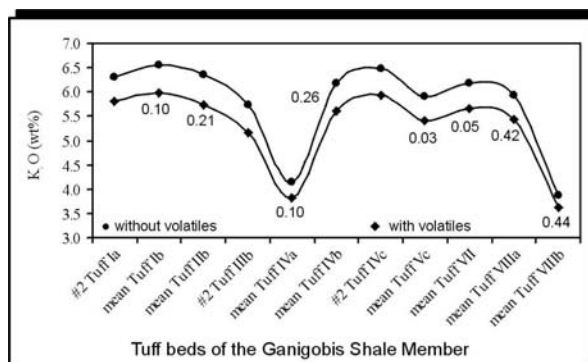


Fig. 106: K₂O- contents of the tuff beds from the Ganigobis Shale Member; figures next to the data points denote the standard deviation of the measurements. Note the low K₂O- contents of tuff bed IVa due to the abundance of kaolinite in this tuff bed.

All other tuff beds of the Ganigobis Shale Member contain 5-6 % K_2O and show less pronounced kaolinite peaks in the XRD-diagrams. They are therefore regarded as being more illite-smectite dominated and less altered. As the tuff beds from Zwartbas (southern Namibia) contain about 7% K_2O , they are mostly dominated by illite/smectite. Consequently, no kaolinite peaks were detected in XRD-measurements (Geiger, 2000b). The tuff beds of the Dwyka and Eccca Group of the Western Cape Province, South Africa, show 7-8 % K_2O respectively 5-6 % K_2O and are also illite/smectite dominated.

Average intermediate, igneous rocks contain about 3.2 % K_2O (Wedepohl, 1978). The bentonitic tuff beds analysed in this study thus contain about twice the K_2O -content. As potassium is required during illitization of the smectites, it was derived from associated igneous minerals within the tuff beds (feldspars) but additionally from the adjacent mudstones of the Ganigobis Shale Member via pore waters (cf. Spears *et al.*, 1999).

Overall K_2O -values of the tuff beds are also higher than average values of the mudstones of the Ganigobis Shale Member (cf. Fig. 118).

10.2.10 P_2O_5

P_2O_5 occurs in secondarily formed phosphates and Fe-hydroxides but is also found in heavy minerals such as apatite and monazite.

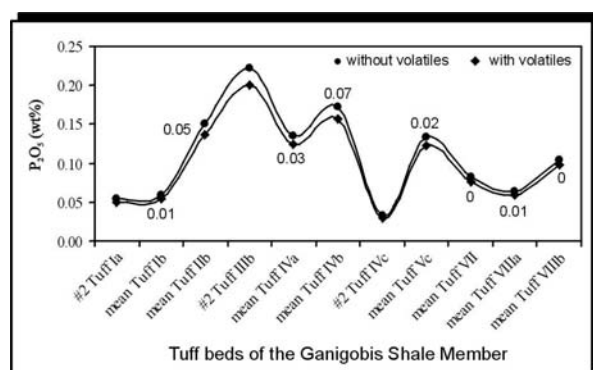


Fig. 107: P_2O_5 -contents of the tuff beds from the Ganigobis Shale Member; figures next to the data points denote the standard deviation of the measurements.

Not normalised values vary between 0.04 and 0.25 % in tuff beds from the Ganigobis Shale Member (Fig. 107). P_2O_5 - contents are similar to values of comparable, igneous rocks such as dacites (0.09-0.19 % P_2O_5 ; Wedepohl, 1978). P_2O_5 - values of the tuff beds from Zwartbas are lower and average 0.08. Values between 0.02 and 0.34 are measured in the samples of the tuff beds from the Dwyka Group, Western Cape Province, South Africa. Tuff beds from the Eccca Group of the same area show similar values between 0.05 and 0.37 % P_2O_5 . Overall P_2O_5 - values of the tuff beds are significantly lower than those of the mudstones of the Ganigobis Shale Member (cf. Fig. 118).

10.2.11 LOI

The intensity of alteration of the tuff beds is to some extent expressed by the loss on ignition (LOI), which is a measure of the volatile contents of a rock sample. H_2O is stored in the clay minerals and Fe-hydroxides whereas CO_2 is mainly retained in $CaCO_3$. The LOI-values of the 95 measured tuff samples turned out to be high compared to e.g. fresh basalts and vary between 4.23 % and 13.99 %. The values are nevertheless normal for bentonitic tuff beds. However, a high loss on ignition and therefore a high degree of alteration make geochemical analyses more unreliable.

Most element concentrations do not correlate with the LOI value. Only CaO and Fe_2O_3 and, to a lesser degree, MnO correlate positively with LOI (Fig. 108). This shows that alteration has led to input of iron, calcium and manganese from outside the system with pore waters, leading to an enrichment in these elements. Large carbonate- and iron-rich concretions as well as limestone bioherms are present in the surrounding mudstones, locally even concentrated below or above pyroclastic layers.

Nine of all in all 95 samples with more than 9 % LOI were omitted for the following geochemical interpretations.

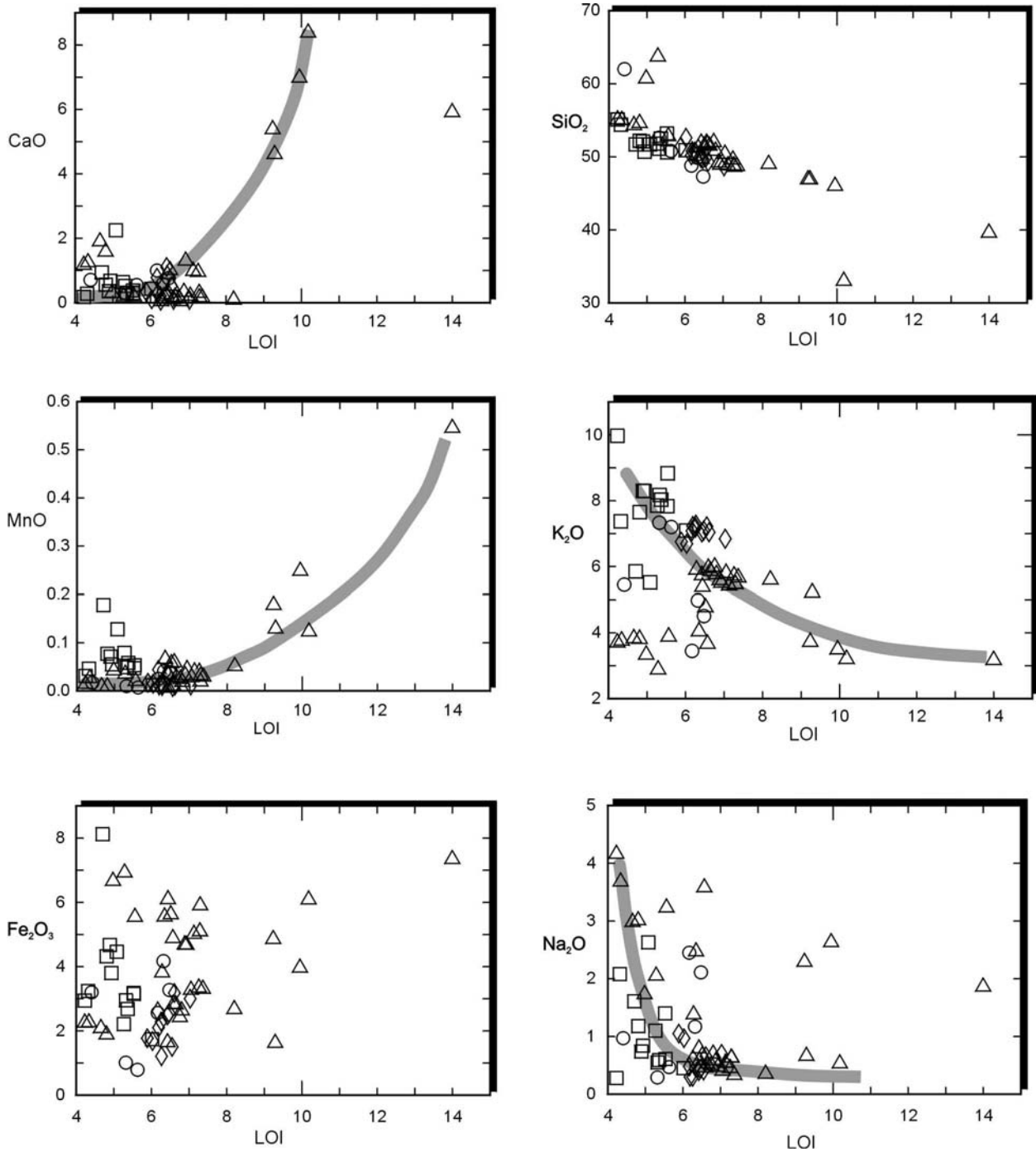


Fig. 108: Positive correlation of CaO- and MnO-contents respectively negative correlation of SiO₂, K₂O and Na₂O contents with increasing LOI-contents (all values in wt %). Fe₂O₃ contents show a rather scattered distribution. For legend see Fig. 118.

10.3 The geochemistry of the present-day tuff beds: Trace elements

Trace elements were compared to mean values of the mudstones of the Ganigobis Shale Member and mean values of acid to intermediate, igneous rocks in order to recognise the geochemical

influence of the surrounding mudstones on the tuff beds. They are also used to compare the geochemistry of the potential parent magma of the ash beds with the geochemistry of equivalent,

igneous rocks. They were further used to differentiate between tuff beds of the individual basin areas (Aranos Basin, Karasburg Basin and main Karoo Basin).

10.3.1 Niobium (Nb)

Nb is mainly contained in biotite and Ti-bearing minerals. During weathering processes Nb is either released due to the destruction of those minerals or remains behind within other more resistant minerals such as ilmenite, zircon or sphene.

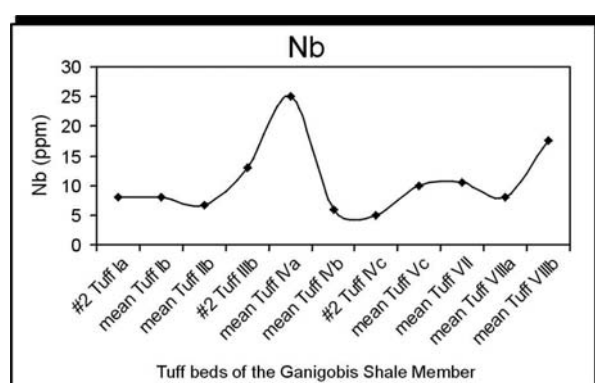


Fig. 109: Nb- contents of tuff beds from the Ganigobis Shale Member near Ganigobis, southern Namibia. Note the high Nb- contents of tuff bed IVa due to the high amount of Ti-bearing minerals within the tuff bed.

As tuff bed IVa of the Ganigobis Shale Member holds most Ti-bearing minerals, it displays the highest Nb- values (Fig. 109). Nb appears to be depleted in the tuff beds from Aranós Basin near Ganigobis and the Karasburg Basin near Zwartbas as average values comprise 14 and 8 ppm Nb. Tuff beds from South Africa (Dwyka and Ecca Groups) reveal average values of 29 ppm. The mudstones of the Ganigobis Shale Member contain 30 ppm Nb on average and did not geochemically influence the tuff beds (Fig. 118). With respect to the intermediate to acid character of the parent magma of the tuff beds, comparable igneous rocks contain similar values of Nb (15 ppm, Wedepohl, 1978).

10.3.2 Zirconium (Zr)

Most of the Zr is present in zircons but can also be incorporated in oxide minerals such as xenotime, ilmenite or rutile. Some Zr is also

incorporated into clay minerals and Fe-hydroxides. The relatively large size and high charge of the Zr^{4+} ion guarantee that Zr does not enter any of the main rock-forming minerals. Zircon is almost indestructible against weathering processes. As the highest numbers of the zircons could be extracted from tuff beds IIb and IVb, these tuff beds consequently show highest Zr-values (except tuff bed VIIIb, Fig. 110).

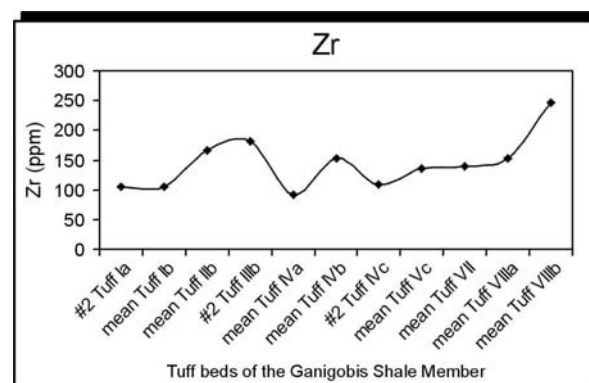


Fig. 110: Zr- contents of tuff beds from the Ganigobis Shale Member near Ganigobis, southern Namibia. Note the high Zr- contents of tuff beds IIb and IVb due to the high amount of zircons.

The tuff beds from near Ganigobis and Zwartbas contain 150 respectively 194 ppm Zr on average whereas the tuff beds from South Africa (Dwyka and Ecca Groups) embody higher amounts of zircons and thus reveal significantly higher average Zr- values of 544 and 415 ppm. Mudstones of the Ganigobis Shale Member and average mudstones (Wedepohl, 1978) contain 184 respectively 164 ppm Zr on average and are therefore not geochemically linked to the tuff beds (Fig. 118). With respect to the suggested, acid to intermediate character of the parent magma of the tuff beds, comparable igneous rocks contain 120 ppm Zr on average (Wedepohl, 1978).

10.3.3 Strontium (Sr)

The ionic radius of Sr^{2+} is intermediate in size between Ca^{2+} and K^+ . Sr therefore substitutes either Ca or K in its host minerals which mainly comprise plagioclase and alkali feldspar. In igneous rocks Sr is mostly incorporated in plagioclase replacing Ca.

Mobilisation of Sr during weathering is attributed to the decomposition of feldspar. Sr is a rather mobile element during weathering processes, although it is less mobile than Ca (Wedepohl, 1978).

Most feldspar is preserved in tuff IVa and also some samples of tuff IIb show high percentages of feldspar (cf. Chapter 9.2.6) which leads to the highest Sr- values of tuff beds from the Ganigobis Shale Member. High Sr- values cannot be explained with the presence of feldspar in tuff bed VII as this does not hold much feldspar (Fig. 111).

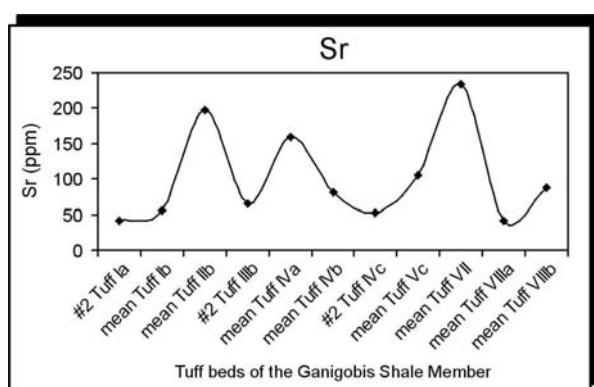


Fig. 111: Sr- contents of tuff beds from the Ganigobis Shale Member near Ganigobis, southern Namibia. Note the high Sr- contents of tuff beds IIb and IVa due to the high amount of feldspar.

Average Sr- values of the analysed tuff beds vary between 124 ppm (Aranos Basin near Ganigobis) and 139 ppm (Dwyka Group of the Western Cape Province, South Africa). Tuff beds from Zwartbas show 44 ppm on average as they only show traces of feldspar in XRD-measurements (Geiger, 2000b). Significantly higher Sr concentrations with an average of 364 ppm were detected in tuff beds of the lower Ecca Group in the north-western part of the main Karoo Basin in South Africa (McLachlan and Jonker, 1990). This value corresponds to average values of acid to intermediate, igneous rocks (cf. Wedepohl, 1978). The mudstones of the Ganigobis Shale Member have slightly higher Sr-values on average (Fig. 118). As fragments of mudstone were occasionally detected in tuff bed IVa of the Ganigobis Shale Member, Sr-contents might be slightly raised in this tuff bed.

10.3.4 Barium (Ba)

The ionic radius of Ba^{2+} is nearly identical to that of K^+ . Ba therefore replaces K in the mixed layered clay minerals. Biotite and K-feldspar are the most important Ba carriers. Ba is a highly mobile element during weathering, especially in connection with the destruction of biotite and K-feldspar.

The tuff beds from Zwartbas and the ones from the Western Cape Province, South Africa, show high average values of 900 – 1100 ppm Ba and seem to be enriched in Ba. Ba- contents in the tuff beds of the Ganigobis Shale Member are significantly lower and vary between 147 (tuff bed IVc) and 501 ppm Ba (tuff bed VII) averaging 374 ppm Ba (Fig. 112). The mudstones of the Ganigobis Shale Member show slightly higher Ba- values (376 – 602 ppm Ba) and might have affected the tuff beds as Ba is highly mobile (cf. Fig. 118).

With respect to the acid to intermediate character of the parent magma of the tuff beds, comparable igneous rocks contain similar values of Ba (666 ppm on average, Wedepohl, 1978).

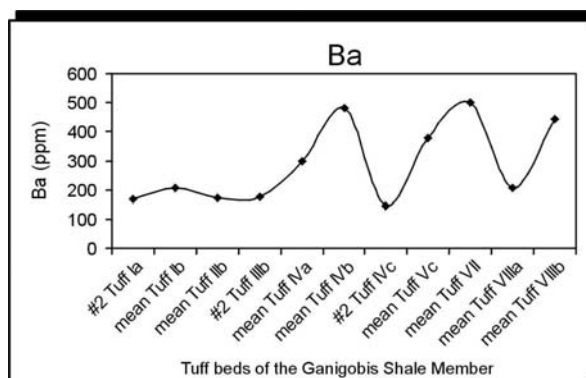


Fig. 112: Ba-contents of tuff beds from the Ganigobis Shale Member near Ganigobis, southern Namibia; see text for discussion.

10.3.5 Rubidium (Rb)

Rubidium corresponds very closely to potassium. Rb is therefore incorporated in K-bearing minerals such as biotite and K-feldspar. During weathering, Rb is again closely related to potassium but is retained more firmly than K (Wedepohl, 1978).

The tuff beds from the Ganigobis Shale Member, southern Namibia, contain between 170 and 190 ppm with the exception of the most intensively altered tuff bed IVa which only shows 120 ppm Rb on average (Fig. 113).

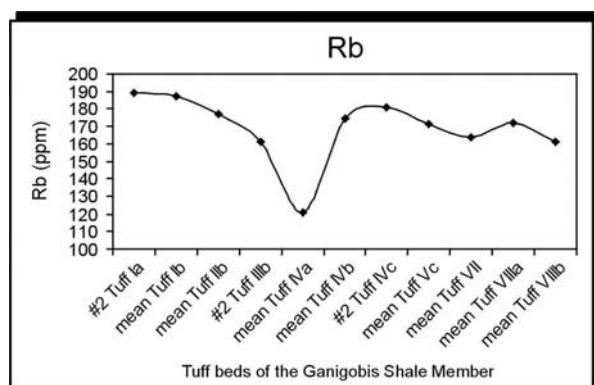


Fig. 113: Rb- contents of the tuff beds from the Ganigobis Shale Member near Ganigobis, southern Namibia. Note the Rb anomaly of the most altered tuff bed IVa.

The tuff beds of the Ganigobis Shale Member contain as much Rb as the mudstones but significantly more than comparable acid to intermediate igneous rocks (85 ppm on average). The K/Rb- ratio of almost 300 is lower than on average igneous rocks (K/Rb- ratio: 410). Tuff beds from Zwartbas contain 274 ppm Rb on average and especially the tuff beds from the Dwyka Group of South Africa show an average value of 437 ppm Rb.

10.3.6 Lead (Pb)

Lead has a similar ionic radius as potassium and replaces potassium in K-feldspar and biotite. It is also incorporated into the mixed layered clay minerals. Pb has a low rate of mobilisation during weathering.

Average values of tuff beds from the Aranos Basin and the main Karoo Basin (Dwyka and Ecca Groups) comprise 24 – 28 ppm whereas the tuff beds of the Karasburg Basin near Zwartbas only contain 13 ppm on average.

For comparison, marine shales of Precambrian to Triassic age from South Africa contain an average of 25 ppm Pb. Plutonic, intermediate rocks from the Coast Range in Oregon, U.S.A. hold about 10 ppm Pb on average (Wedepohl, 1978).

10.3.7 Gallium (Ga)

Ga^{3+} is similar in size to Al^{3+} and to a much lesser degree to Fe^{3+} . Ga (and also Sc) is therefore preferentially concentrated in the mixed layered clay minerals, feldspar and mica of the tuff beds. There is a tendency for Ga to be concentrated in residual materials during weathering. However, Ga is more mobile than Al, resulting in a decreasing Ga/Al ratio in the residual materials during weathering processes. The highly altered tuff IVa of the Ganigobis Shale Member has a Ga/Al ratio of 0.4 which is almost half of the ratio of tuff beds V, VII and VIII. Absolute values comprise 17 ppm Ga on average for the tuff beds from the Aranos Basin whereas the ones from Zwartbas reach 29 ppm Ga on average. The measured samples of tuff beds from South Africa contain 28 ppm Ga (Dwyka Group) and 23 ppm Ga (Ecca Group) on average. Palaeozoic, marine shales from the British Isles show average Ga-values of 22 ppm and also comparable acid to intermediate rocks show Ga- values of 20 – 30 ppm (Wedepohl, 1978).

10.3.8 Zinc (Zn)

The Zn^{2+} ion replaces ferrous Fe^{2+} and Mg^{2+} . Zn has only restricted mobility during weathering processes which is controlled by the adsorption from clay minerals, hydroxides, carbonates and phosphates rather than by its solubility.

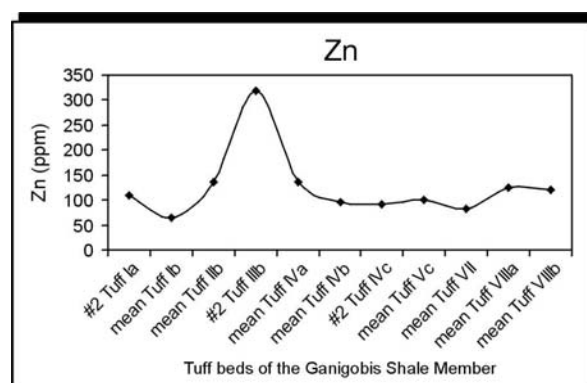


Fig. 114: Zn- contents of the tuff beds from the Ganigobis Shale Member near Ganigobis, southern Namibia. Note the rather uniform average contents with the two exceptions of tuff beds Ib and IIIb.

Zn- values vary between 91 and 136 ppm in the tuff beds of the Ganigobis Shale Member. Tuff bed Ib contains 66 ppm Zn on average whereas the single measurement of tuff bed IIIb reaches 318 ppm Zn (Fig. 114). The mudstones of the Ganigobis Shale Member contain only slightly more Zn on average (147 ppm, Fig. 118). With respect to the acid to intermediate character of the parent magma of the tuff beds, comparable igneous rocks only contain 66 ppm Zn on average (Wedepohl, 1978). Higher Zn- values in the tuff beds might originate from biotite. Zn can be used to discriminate between the tuff groups of the different study areas. Tuff beds from the Dwyka Group of South Africa and the ones from the Aranos Basin of southern Namibia contain 140 ppm respectively 120 ppm on average whereas the tuff beds from Zwartbas (Karasburg Basin, southern Namibia) and the ones from the Ecça Group of the Western Cape Province, South Africa, only hold 53 respectively 45 ppm Zn.

10.3.9 Copper (Cu)

Copper is predominantly incorporated in early-formed magmatic minerals such as olivine, pyroxene, biotite and amphibole. During weathering Cu will be extracted from these minerals due to their decomposition. In the tuff beds, Cu is probably incorporated into the mixed layered clay minerals. The tuff beds of the Dwyka Group of the Western Cape Province, South Africa, contain 97 ppm Cu on average whereas tuff beds of the other three groups only hold 12 – 17 ppm Cu on average. This is in accordance with Cu- values of intermediate, igneous rocks (10 – 20 ppm Cu, Wedepohl, 1978) and with Upper Carboniferous shales of the Donbas Basin in Russia which average 25 ppm Cu.

10.3.10 Nickel (Ni)

The ionic radius and charge of Ni^{2+} are identical with those of Mg^{2+} . Ni therefore replaces Mg in the mixed-layered clay minerals. During weathering Nickel is easily mobilised and is precipitated together with Fe- and Mg-hydroxides.

The tuff beds of the Ganigobis Shale Member contain 29 ppm Ni on average. Tuff beds IIb, IIIb and IVb hold up to 41 ppm (Fig. 115) which is

the average Ni- value of the mudstones of the Ganigobis Shale Member (cf. Fig. 118).

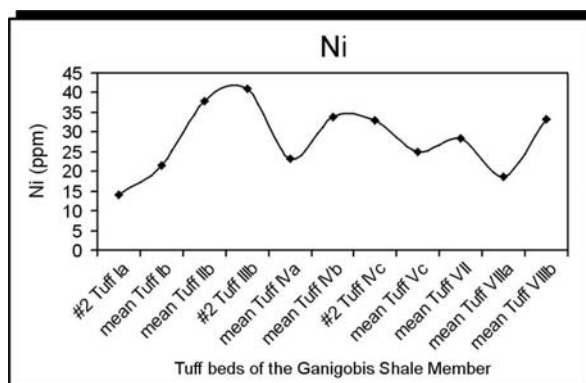


Fig. 115: Ni- contents of tuff beds from the Ganigobis Shale Member near Ganigobis, southern Namibia. Note the high Ni- contents of tuff beds IIb, IIIb and IVb.

Acid to intermediate igneous rocks contain about 18 ppm Ni on average which is the average value of the less altered tuff beds of the Karasburg Basin near Zwartbas. The tuff beds from the Dwyka and Ecça Group of the Western Cape Province, South Africa, hold 22 respectively 11 ppm Ni.

10.3.11 Cobalt (Co)

Cobalt behaves very similar to Ni. The major part of Co in a magma is fixed in early-formed Mg- minerals such as olivine, garnet, pyroxene, amphibole, magnetite and ilmenite. Co is very mobile during weathering and does not form residual silicate minerals like Ni.

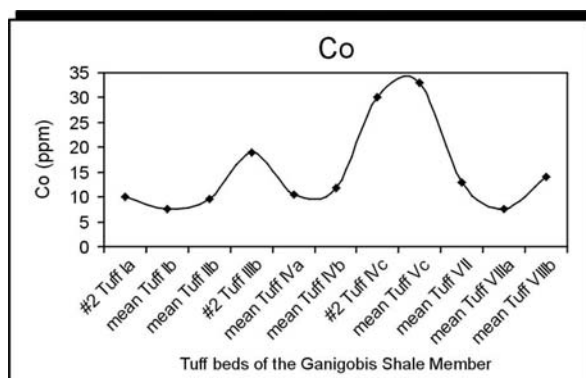


Fig. 116: Co- contents of the tuff beds from the Ganigobis Shale Member near Ganigobis, southern Namibia. Note the high Co- contents of tuff beds IVc and Vc.

The average value of Co is 12 ppm in the tuff beds of the Ganigobis Shale Member (Fig. 116). Highest values of Co are found in tuff beds IVc and Vc (33 ppm). The curves of Co and Ni do not fit although Co and Ni resemble closely each other. Especially Co but also Ni seems to be depleted in the tuff beds of the Ganigobis Shale Member.

Co- values are similar to average Co- values of the mudstones of the Ganigobis Shale Member (13 ppm, Fig. 118). With respect to the suggested, acid to intermediate character of the parent magma of the tuff beds, comparable igneous rocks contain 24 ppm on average (Wedepohl, 1978). Analysed tuff beds of the other three groups contain even less Co with average values between 5 and 8 ppm.

10.3.12 Chromium (Cr)

Cr³⁺ closely resembles Al³⁺ and Fe³⁺ and is incorporated in the mixed-layered clay minerals and hydroxides of the tuff beds. Generally, the Cr- contents are highest in ultramafic rocks and decreases continuously from basic to acid, igneous rocks. During alteration processes, Cr behaves similar to Al³⁺ and Fe³⁺ and is therefore concentrated in clay minerals (Wedepohl, 1978).

Cr-values vary in all measured tuff beds between 10 and 35 ppm, average values do not exceed 20 ppm Cr which is even less than in acid to intermediate, igneous rocks. The mudstones of the Ganigobis Shale Member in contrast contain 89 ppm Cr on average and thus do not seem to have affected the interlayered tuff beds (Fig. 118).

10.3.13 Vanadium (V)

Vanadium preferentially enters early-formed magnetite but also mica, amphibole, and clinopyroxene. During weathering V remains in the residual rock-forming and iron-bearing minerals and/or becomes incorporated into clay minerals.

The tuff beds of the Ganigobis Shale Member contain 92 ppm V on average and highest values are found in the most altered tuff beds Ia, IIIb and IVa (114 ppm, Fig. 117).

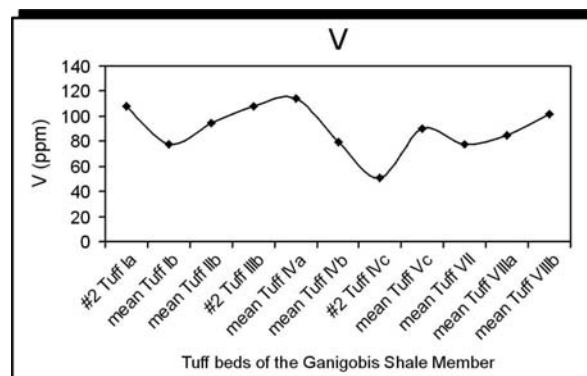


Fig. 117: V- contents of the tuff beds from the Ganigobis Shale Member near Ganigobis, southern Namibia. The most altered tuff beds Ia, IIIb and IVa show the highest V- values.

The mudstones of the Ganigobis Shale Member contain 123 ppm V on average and do not seem to have affected the tuff beds (cf. Fig. 118). Concerning the acid to intermediate origin of the tuff beds, they seem to be strongly depleted in V as comparable igneous rocks contain 231 ppm V on average. The tuff beds of the Dwyka Group in the Western Cape Province in South Africa hold 99 ppm V on average whereas the tuff beds of the Karasburg Basin near Zwartbas average 60 and the ones from the Ecca Group average only 40 ppm V.

10.3.14 Conclusions

Most values of major and trace elements changed from the original geochemical composition of the tuff beds which is suggested to have been acid to intermediate in character.

Characteristically, the bentonitic tuff beds show an enrichment in Al₂O₃ and K₂O. All other major elements are lower than in comparable acid to intermediate igneous rocks. Especially CaO and also MgO- values are very low. SiO₂, TiO₂, MnO, Na₂O and P₂O₅ are also lower than in comparable igneous rocks whereas Fe₂O₃ is ambivalent.

Of the 13 analysed trace elements only four are enriched compared to an acid to intermediate magma: Zr, Rb, Ba and Pb. Four elements are significantly lower (Sr, Co, Cr and V) whereas Nb and Ni are only slightly lower than comparable igneous rocks. Ga, Zn and Cu are ambivalent.

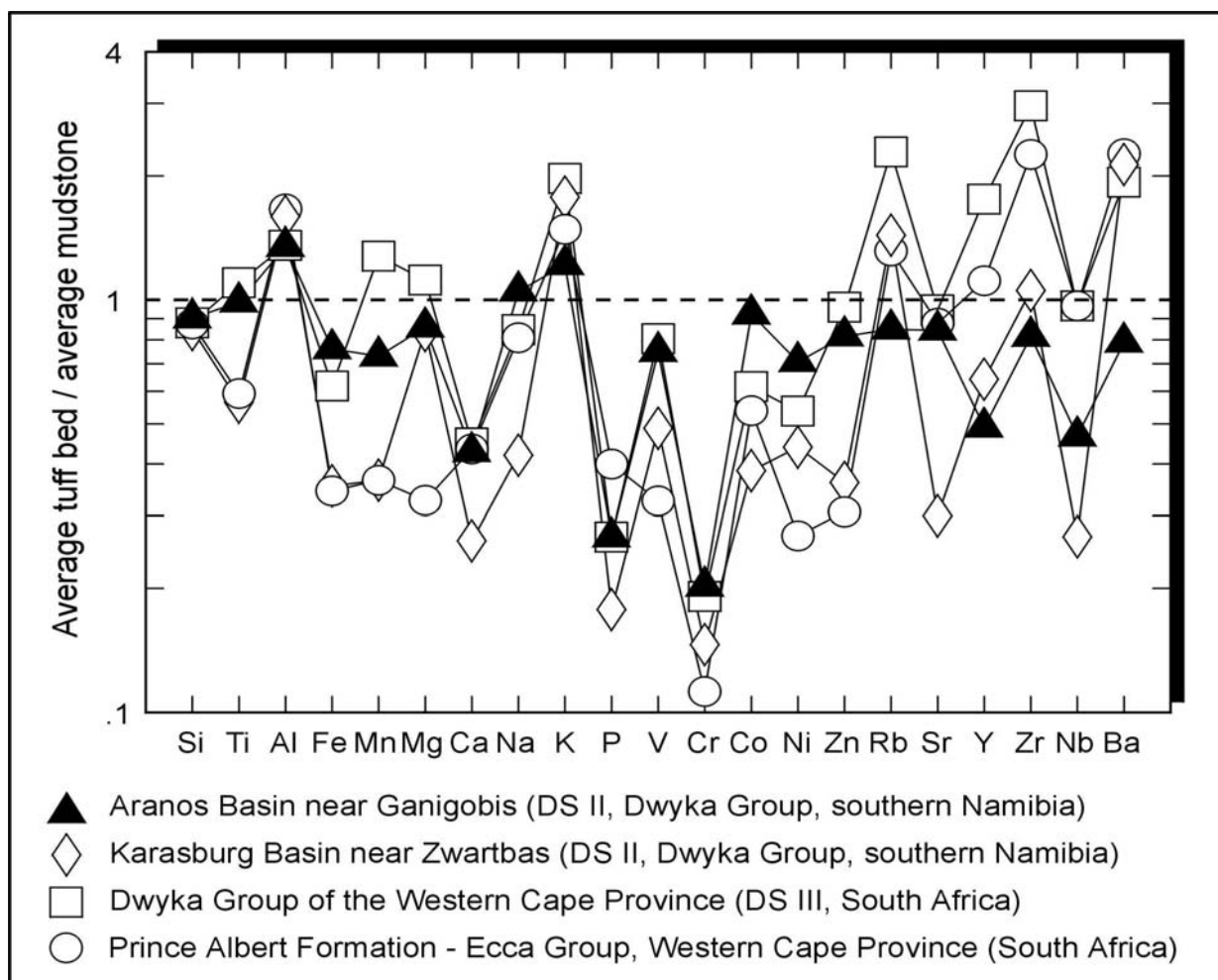


Fig. 118: Comparative average compositions of all analysed tuff beds from the Aranos (54 analyses) and Karasburg Basins (12 analyses) in southern Namibia and the main Karoo Basin in South Africa (Dwyka Group: 12 analyses and Ecca Group: 8 analyses) normalised on average values of the mudstones of the Ganigobis Shale Member (Dwyka Group, Aranos Basin, southern Namibia).

10.4 Major and trace element variations of the tuff beds

The general relationships between all determined major and trace elements may be examined in a first approach by calculating the inter-element correlation (cf. Rollinson, 1993). The correlation coefficient provides a numerical value for the correlation between paired elements. The sample correlation coefficient (r) may be calculated from the expression

$$r = \frac{\text{covariance}(x,y)}{\sqrt{[\text{variance}(x) \times \text{variance}(y)]}}$$

x, y are values for the elements x, y .

Values of r vary from -1 to $+1$. Values of $r < 1$ indicate negative and $r > 1$ positive correlations. A perfect positive or negative, linear relationship would be given for $r = +1$ or $r = -1$, respectively. If $r = 0$ there is no relationship between x and y at all. The advantage of this procedure is that the results which are presented in a correlation coefficient matrix allow the recognition of discernible linear trends without plotting them all in bivariate diagrams. Enrichment or depletion effects mentioned in the previous chapter do not affect the overall correlation trends.

Correlation coefficient matrices for samples from the tuff beds of the Dwyka Group in southern Namibia (Aranos and Karasburg Basins) and for samples of tuff beds of the Dwyka and Ecca Groups in South Africa (Western Cape

Province) are shown in Tab. 13 and Tab. 14. High correlation values of more than ± 0.8 are highlighted. Differences between samples of the tuff beds from southern Namibia and South Africa are obvious as only 12 (Aranos Basin) and 13 (Karasburg Basin) paired elements show good correlation. Tuff beds of the Dwyka Group of South Africa, however, show 24 paired elements with correlation values of more than ± 0.8 and tuff beds of the Ecca Group even display 38 paired elements with good correlation values. The parent magma of these tuff beds seems to be more

differentiated than the parent magma of the tuff beds from southern Namibia (cf. Rollinson, 1993).

As an example variations between Rb and TiO_2 , K_2O and Na_2O for the tuff beds of the Aranós Basin near Ganigobis are displayed in Fig. 119. As deduced from Tab. 13, TiO_2 and Na_2O mainly correlate negatively with Rb whereas K_2O correlates positively due to the close relationship between Rb and K_2O . This is in accordance with the r-values of -0.8 for Rb/TiO_2 , -0.8 for $\text{Rb}/\text{Na}_2\text{O}$ and $+0.9$ for $\text{Rb}/\text{K}_2\text{O}$.

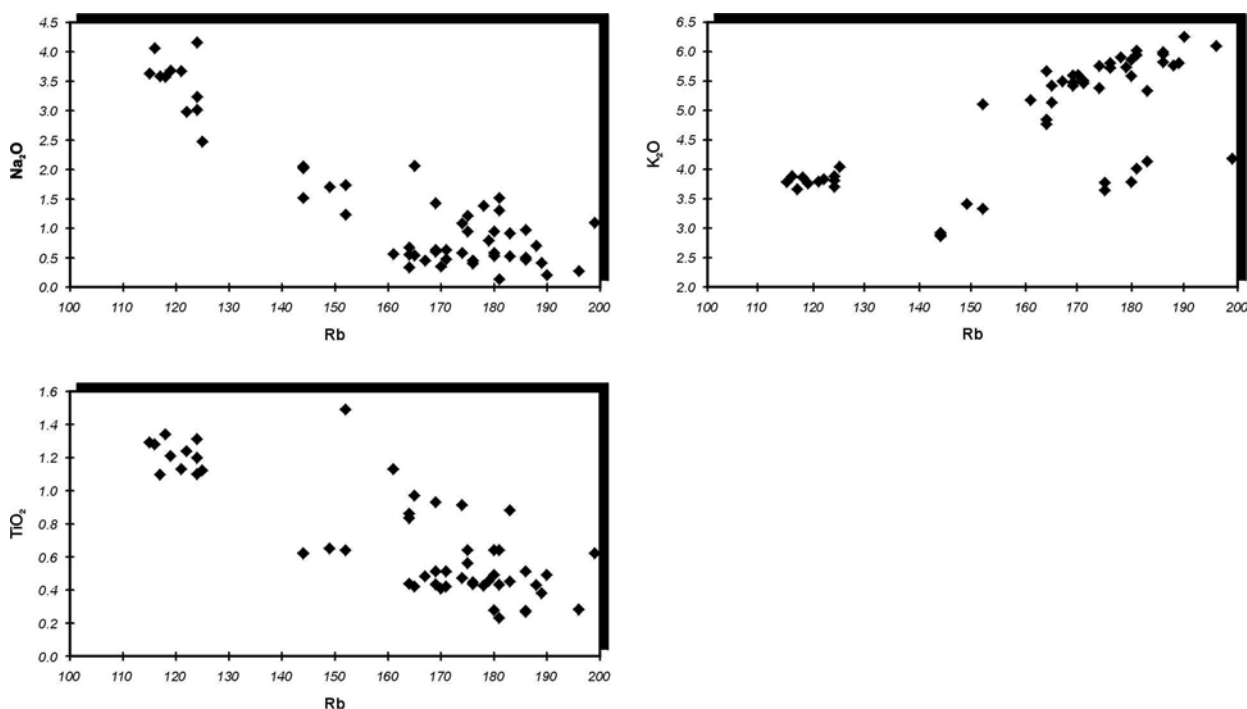


Fig. 119: Rb- contents of the tuff beds from the Ganigobis Shale Member near Ganigobis, southern Namibia plotted versus Na_2O , TiO_2 and K_2O . TiO_2 and Na_2O mainly correlate negatively with Rb whereas K_2O correlates positively. The element combinations were deduced from the determination of the correlation coefficient.

As a further example Sr-values of the tuff beds from the Ecca Group of the Western Cape Province, South Africa, show a negative

correlation with K_2O whereas CaO and especially Na_2O correlate positively with Sr due to the geochemically close relationship of Sr and Na_2O .

	TiO ₂	Al ₂ O ₃	Fe ₂ O ₃	MnO	MgO	CaO	Na ₂ O	K ₂ O	P ₂ O ₅	Nb	Zr	Y	Sr	Rb	Pb	Ga	Zn	Cu	Ni	Co	Cr	V	Ba	Sc	N = 12
	-0.5	-0.1	-0.7	-0.2	0.0	-0.1	0.4	-0.3	0.1	0.3	0.1	0.4	-0.1	0.0	-0.7	0.5	0.3	-0.5	-0.4	-0.5	0.5	-0.5	-0.3	-0.1	SiO ₂
		0.3	0.2	0.2	-0.2	0.0	0.4	-0.2	0.1	-0.7	-0.5	-0.7	0.1	-0.6	0.4	-0.7	0.1	0.4	0.3	0.3	-0.2	0.8	-0.3	0.1	TiO ₂
			-0.5	-0.7	-0.7	-0.4	0.1	0.3	-0.5	-0.2	-0.6	-0.3	0.3	-0.5	0.1	-0.2	0.1	-0.4	0.1	0.0	-0.2	0.2	-0.5	0.2	Al ₂ O ₃
				0.4	0.2	0.1	-0.1	-0.2	0.1	0.0	0.2	-0.2	-0.2	0.0	0.7	-0.2	0.1	0.8	0.4	0.4	0.0	0.4	0.2	0.1	Fe ₂ O ₃
TiO ₂	0.1				0.8	0.6	-0.2	0.0	0.6	0.3	0.2	-0.2	0.2	0.5	-0.2	-0.2	-0.4	0.5	-0.3	-0.2	-0.1	0.0	0.5	-0.2	MnO
Al ₂ O ₃	0.0	-0.4				0.3	-0.4	0.2	0.5	0.2	0.5	0.2	-0.1	0.7	-0.4	0.3	-0.4	0.2	-0.5	-0.4	0.0	-0.3	0.7	-0.4	MgO
Fe ₂ O ₃	-0.2	0.1	-0.6				-0.4	0.1	0.5	-0.2	0.2	-0.1	0.5	0.5	-0.3	-0.1	-0.6	0.3	-0.5	-0.3	-0.7	-0.2	0.4	0.0	CaO
MnO	-0.6	0.1	-0.5	0.4				-0.9	0.2	-0.4	-0.5	-0.3	-0.2	-0.8	0.2	-0.3	0.6	-0.2	0.4	0.2	0.4	0.4	-0.8	0.0	Na ₂ O
MgO	-0.4	-0.4	0.2	0.2	0.6				-0.3	0.3	0.3	0.3	0.2	0.6	-0.3	0.2	-0.4	0.0	-0.5	-0.3	-0.4	-0.2	0.6	0.2	K ₂ O
CaO	-0.7	0.4	-0.6	0.2	0.7	0.0				0.0	0.5	0.1	0.1	0.1	-0.3	0.0	-0.1	0.2	-0.3	-0.3	-0.2	-0.3	0.2	-0.4	P ₂ O ₅
Na ₂ O	0.3	0.9	-0.3	-0.1	0.1	-0.4	0.2				0.7	0.9	-0.4	0.5	-0.3	0.7	0.4	-0.1	-0.2	-0.4	0.3	-0.7	0.5	-0.1	Nb
K ₂ O	-0.1	-0.8	0.9	-0.4	-0.4	0.3	-0.6	-0.7				0.8	-0.2	0.7	-0.2	0.4	-0.1	0.1	-0.2	-0.2	0.0	-0.6	0.7	-0.1	Zr
P ₂ O ₅	-0.3	0.2	0.0	0.3	0.2	0.2	0.2	0.1	-0.1				-0.4	0.5	-0.3	0.6	0.2	-0.3	-0.1	-0.2	0.2	-0.7	0.5	-0.1	Y
Nb	0.4	0.8	-0.3	-0.2	0.0	-0.5	0.1	0.9	-0.7	0.0			0.1	-0.1	-0.4	-0.5	0.1	-0.3	-0.2	-0.5	0.0	-0.1	0.2	0.2	Sr
Zr	0.4	-0.5	0.0	0.2	-0.3	0.0	-0.4	-0.4	0.2	-0.1	-0.3			-0.5	0.5	-0.5	0.1	-0.6	-0.4	-0.2	-0.6	0.9	0.0	0.0	Rb
Y	0.1	0.1	-0.6	0.4	0.5	0.2	0.3	0.1	-0.5	0.1	0.0	0.3			-0.5	0.2	0.4	0.8	0.8	0.0	0.7	-0.3	0.4	0.4	Pb
Sr	-0.3	0.4	-0.2	0.0	0.1	-0.3	0.4	0.2	-0.3	0.2	0.3	-0.3	-0.2			0.2	-0.2	-0.5	-0.6	0.3	-0.7	0.4	0.0	0.0	Ga
Rb	0.2	-0.8	0.7	-0.2	-0.5	0.2	-0.6	-0.8	0.9	-0.3	-0.7	0.5	-0.3	-0.4			0.1	0.4	0.0	0.7	0.1	-0.5	0.1	0.1	Zn
Pb	-0.6	0.0	-0.3	0.5	0.8	0.7	0.4	-0.1	-0.2	0.4	-0.2	-0.3	0.2	0.1	-0.3			0.0	0.0	-0.2	0.4	0.2	0.3	0.3	Cu
Ga	0.6	-0.4	0.4	-0.3	-0.4	0.0	-0.6	-0.3	0.5	-0.4	-0.2	0.6	0.0	-0.4	0.6	-0.4			0.9	0.3	0.6	-0.4	0.0	0.0	Ni
Zn	-0.3	0.3	-0.4	0.4	0.5	0.1	0.5	0.3	-0.4	0.3	-0.1	-0.3	0.4	0.2	-0.5	0.2	-0.5			0.0	0.5	-0.3	0.1	0.1	Co
Cu	-0.1	0.4	-0.7	0.7	0.5	0.2	0.3	0.3	-0.7	0.1	0.2	-0.1	0.4	0.1	-0.6	0.5	-0.3	0.5			-0.1	-0.4	-0.1	0.1	Cr
Ni	-0.4	0.1	-0.3	0.5	0.8	0.7	0.3	0.1	-0.3	0.2	-0.1	-0.2	0.5	0.1	-0.4	0.8	-0.4	0.5	0.6			-0.5	0.4	0.4	V
Co	-0.6	0.3	-0.6	0.6	0.7	0.3	0.7	0.0	-0.5	0.3	0.0	-0.3	0.4	0.2	-0.5	0.6	-0.5	0.5	0.6	0.7			-0.2	0.4	Ba
Cr	0.6	0.0	-0.6	0.5	-0.1	-0.2	-0.1	0.1	-0.5	-0.2	0.2	0.5	0.5	-0.1	-0.1	-0.2	0.2	0.0	0.4	0.0	0.0				
V	-0.2	0.6	-0.6	0.3	0.2	-0.4	0.4	0.5	-0.7	0.2	0.4	-0.4	0.2	0.6	-0.7	0.1	-0.6	0.5	0.6	0.2	0.5	0.2			
Ba	-0.6	0.2	-0.5	0.2	0.1	-0.3	0.6	-0.1	-0.3	0.0	0.0	-0.1	-0.1	0.4	-0.3	0.1	-0.5	0.0	0.1	-0.1	0.5	0.0	0.5		
Sc	-0.4	0.4	-0.2	0.1	0.4	0.0	0.5	0.3	0.3	0.2	0.1	-0.4	0.2	0.3	-0.5	0.2	-0.5	0.7	0.4	0.4	0.5	-0.3	0.6	0.2	
N = 31	SiO ₂	TiO ₂	Al ₂ O ₃	Fe ₂ O ₃	MnO	MgO	CaO	Na ₂ O	K ₂ O	P ₂ O ₅	Nb	Zr	Y	Sr	Rb	Pb	Ga	Zn	Cu	Ni	Co	Cr	V	Ba	

Tab. 13: Correlation coefficient patterns for Dwyka Group-equivalent tuff beds from the Aranos Basin near Ganigobis, southern Namibia (lower triangle) and for the tuff beds from the Karasburg Basin near Zwartbas, southern Namibia (upper triangle). Shaded fields indicate r-values > +/- 0.8.

	TiO ₂	Al ₂ O ₃	Fe ₂ O ₃	MnO	MgO	CaO	Na ₂ O	K ₂ O	P ₂ O ₅	Nb	Zr	Y	Sr	Rb	Pb	Ga	Zn	Cu	Ni	Co	Cr	V	Ba	Sc	N = 6	
	-0.3	-1.0	0.0	-0.4	0.9	-0.2	-0.4	0.3	-0.3	-0.8	-0.9	-0.6	-0.6	0.0	-0.3	-0.7	-0.2	-0.2	0.1	-0.4	0.1	-0.7	-0.8	-0.6	SiO ₂	
		0.4	-0.8	-0.6	-0.7	-0.3	-0.2	0.3	0.3	0.2	0.6	0.5	-0.1	0.2	-0.6	0.2	-0.6	0.1	-0.7	-0.2	-0.4	0.3	0.1	0.1	0.1	TiO ₂
			-0.3	0.2	-1.0	0.0	0.2	0.0	0.3	0.6	0.9	0.7	0.4	0.2	0.1	0.8	-0.1	0.2	-0.2	0.3	-0.1	0.6	0.8	0.5	0.5	Al ₂ O ₃
				0.9	0.5	0.5	0.5	-0.7	-0.4	0.2	-0.2	-0.3	0.5	-0.6	0.8	-0.3	0.9	0.3	0.5	0.3	0.1	0.2	-0.1	0.1	0.2	Fe ₂ O ₃
TiO ₂	-0.4				0.0	0.4	0.7	-0.7	-0.3	0.5	0.2	-0.1	0.7	-0.5	0.9	0.1	0.9	0.3	0.4	0.5	0.0	0.5	0.3	0.2	0.2	MnO
Al ₂ O ₃	-0.3	-0.4				0.1	-0.2	-0.1	-0.4	-0.6	-0.9	-0.7	-0.3	-0.2	0.1	-0.7	0.3	-0.1	0.4	-0.2	0.2	-0.6	-0.7	-0.5	-0.5	MgO
Fe ₂ O ₃	-0.2	0.3	-0.8				0.9	-0.9	0.6	0.7	0.2	0.5	0.8	-0.9	0.0	-0.5	0.7	-0.4	0.2	0.2	-0.4	0.4	-0.4	0.1	0.1	CaO
MnO	-0.3	0.5	-0.6	0.8				-1.0	0.4	0.9	0.5	0.5	1.0	-0.9	0.3	-0.3	0.8	-0.2	0.2	0.5	-0.5	0.6	-0.4	0.1	0.1	Na ₂ O
MgO	-0.3	0.0	-0.5	0.9	0.7				-0.2	-0.7	-0.3	-0.3	-0.9	0.9	-0.4	0.4	-0.9	0.0	-0.2	-0.3	0.3	-0.6	0.2	-0.2	-0.2	K ₂ O
CaO	-0.4	0.9	-0.4	0.4	0.7	0.0				0.5	0.4	0.9	0.4	-0.3	-0.6	0.0	-0.1	-0.5	-0.3	-0.1	-0.2	0.2	-0.1	0.2	0.2	P ₂ O ₅
Na ₂ O	0.1	0.6	-0.6	0.4	0.6	0.1	0.7				0.8	0.8	0.9	-0.6	0.2	0.0	0.5	-0.2	0.0	0.5	-0.5	0.7	0.2	0.3	0.3	Nb
K ₂ O	0.3	-0.6	0.5	-0.6	-0.8	-0.4	-0.8	-0.9				0.8	0.6	-0.2	0.0	0.4	0.0	0.1	-0.3	0.3	-0.4	0.8	0.5	0.4	0.4	Zr
P ₂ O ₅	-0.1	0.9	-0.4	0.2	0.4	-0.2	0.9	0.7	-0.7				0.6	-0.3	-0.4	0.2	0.0	-0.2	-0.5	0.0	-0.3	0.6	0.2	0.5	0.5	Y
Nb	-0.2	0.3	-0.5	0.6	0.5	0.7	0.1	0.2	-0.4	0.1				-0.8	0.3	-0.1	0.8	-0.1	0.1	0.5	-0.4	0.7	0.1	0.3	0.3	Sr
Zr	-0.2	0.3	-0.5	0.6	0.5	0.7	0.1	0.2	-0.4	0.0	0.9				-0.1	0.7	-0.8	0.3	-0.2	-0.3	0.6	-0.4	0.5	0.1	0.2	Rb
Y	-0.4	0.3	-0.3	0.5	0.5	0.7	0.0	0.1	-0.3	0.2	0.9	0.9				0.2	0.7	0.4	0.6	0.6	0.1	0.2	0.5	0.0	0.0	Pb
Sr	-0.4	0.4	-0.4	0.6	0.6	0.6	0.3	0.3	-0.5	0.5	-0.2	-0.2	-0.1			-0.3	0.5	-0.3	0.0	0.5	0.3	0.9	0.6	0.6	0.6	Ga
Rb	0.2	0.5	-0.3	0.0	0.1	-0.3	0.5	0.6	-0.3	-0.6	-0.2	-0.1	-0.3	-0.2			0.1	0.4	0.4	-0.1	0.4	-0.1	0.4	0.1	0.2	Zn
Pb	0.2	-0.5	0.3	-0.4	-0.8	-0.3	-0.7	-0.7	0.9	-0.2	-0.1	-0.2	-0.2	-0.3	-0.2			-0.5	-0.4	0.5	0.5	0.4	0.7	0.7	0.7	Cu
Ga	-0.1	-0.4	0.1	0.2	0.1	0.3	-0.1	0.0	-0.2	-0.6	-0.6	-0.5	-0.6	-0.3	0.2	0.2			0.8	-0.2	-0.5	0.0	-0.6	-0.6	-0.6	Ni
Zn	0.0	-0.7	0.8	-0.6	-0.5	-0.4	-0.5	-0.6	0.6	-0.2	0.1	0.3	0.3	0.2	0.2	0.1	0.0			-0.5	0.0	0.3	-0.4	-0.4	-0.4	Co
Cu	-0.4	-0.1	0.2	-0.1	0.0	0.1	0.0	-0.1	0.1	-0.3	0.1	0.3	0.2	0.2	0.5	-0.1	0.0	0.8			-0.1	0.3	0.5	0.5	0.5	Cr
Ni	-0.4	0.0	0.3	-0.2	-0.2	0.0	-0.1	-0.2	0.3	0.1	0.4	0.3	0.4	0.2	-0.4	0.4	-0.5	0.3	0.1			0.3	0.7	0.7	0.7	V
Co	-0.1	0.2	-0.6	0.8	0.7	0.7	0.4	0.4	-0.5	-0.2	0.6	0.6	0.6	0.0	-0.2	0.2	-0.4	0.4	0.3	0.8			0.5	0.5	0.5	Ba
Cr	-0.2	0.0	-0.4	0.7	0.6	0.8	0.0	0.1	-0.3	0.7	0.3	0.3	0.5	0.4	-0.4	-0.4	-0.8	0.0	0.1	0.3	0.1					
V	-0.3	0.9	-0.5	0.4	0.4	0.1	0.7	0.6	-0.6	0.4	0.4	0.5	0.5	0.3	0.0	-0.2	-0.8	0.4	0.5	0.1	0.2	0.7				
Ba	-0.2	0.6	-0.4	0.2	0.1	0.1	0.3	0.5	-0.3	-0.3	0.1	-0.1	-0.1	0.1	0.3	-0										

10.5 Rare earth elements (REE)

The rare earth elements (REE) are important trace elements and REE studies have applications in igneous, sedimentary and metamorphic petrology (Rollinson, 1993). The 16 elements possess very similar chemical and physical properties because they form stable 3+ ions of similar size. In addition, the element Yttrium (Y) with an ionic radius similar to that of the REE Holmium (Ho) is included. Europium (Eu) is either trivalent or bivalent and Cerium (Ce) also exists as Ce⁴⁺, both depending on the redox state of the system. The size and the charge of the Eu²⁺ ion are almost identical to those of Ca²⁺. Eu substitutes for Ca in plagioclase and thus may behave as a compatible element. The other REE and Y are incompatible with respect to plagioclase. The negative Eu anomaly is characteristic of silicic volcanism and acid to intermediate tonsteins and bentonites (Bohor and Triplehorn, 1993). The REE are relatively insoluble during diagenesis and metamorphism. They can be mobilised over small distances under humid conditions at the earth's surface and are precipitated in that case in secondary alteration products (Wedepohl, 1978).

REE concentrations are usually normalised to values of chondritic meteorites. Chondritic meteorites were chosen because they are thought to be relatively unfractionated samples of the solar system.

La	Ce	Pr	Nd	Pm	Sm	Eu	Gd
0.237	0.612	0.095	0.467	1	0.153	0.058	0.2055

Tb	Dy	Ho	Er	Tm	Yb	Lu
0.037	0.254	0.057	0.166	0	0.17	0.025

Tab. 15: Normalisation values of C1-chondrites in ppm according to Sun and McDonough (1989).

Fig. 120 and Fig. 121 display the REE-patterns of tuff beds from the Ganigobis Shale Member (DS II, Dwyka Group, southern Namibia). Normalisation values of C1-chondrites by Sun and McDonough (1989) are listed in Tab. 15. The samples of the tuff beds are moderately to strongly enriched in light REE (LREE: La - Gd, atomic numbers: 57-64), show a strong Eu-

anomaly (except tuff IVa) and are moderately to strongly depleted in heavy REE (Tb - Lu, atomic numbers: 65 to 71). Tuff beds can be distinguished from each other by different enrichment in LREE. Biotite and especially apatite account for the enrichment of LREE in the bulk-rock samples. Highest values of La and Ce with an enrichment of up to 600 times the composition of the C1-chondrites are detected in tuff beds VII and VIIIa. These tuff beds show high portions of apatite in their heavy mineral spectrum (cf. Fig. 97). The majority of tuff beds show an La- and Ce- enrichment of 100 to 200 times the composition of the C1-chondrites. In contrast, tuff bed Ib and also tuff beds IVb and IVa display an La- enrichment of only 10 to 70 times compared to the C1- chondrites of Sun and McDonough (1989).

High amounts of garnet and especially zircon account for the depletion of HREE in the bulk-rock samples. Lowest values are particularly found in tuff beds Ib, Iib and IVb which partly contain a great number of zircon (cf. Fig. 97). Tuff beds VIIIb and VIIIc are the least depleted tuff beds concerning their HREE contents.

Average REE-contents of the tuff beds from the Dwyka Group of the Aranos Basin (23 measurements), of the Karasburg Basin (11 measurements) and of the main Karoo Basin of the Western Cape Province (South Africa, 12 measurements) are displayed in Fig. 122. All measurements show a moderate to high enrichment of the LREE compared to the composition of the C1- chondrites and a distinct negative Eu anomaly which is conspicuous in all tuff beds.

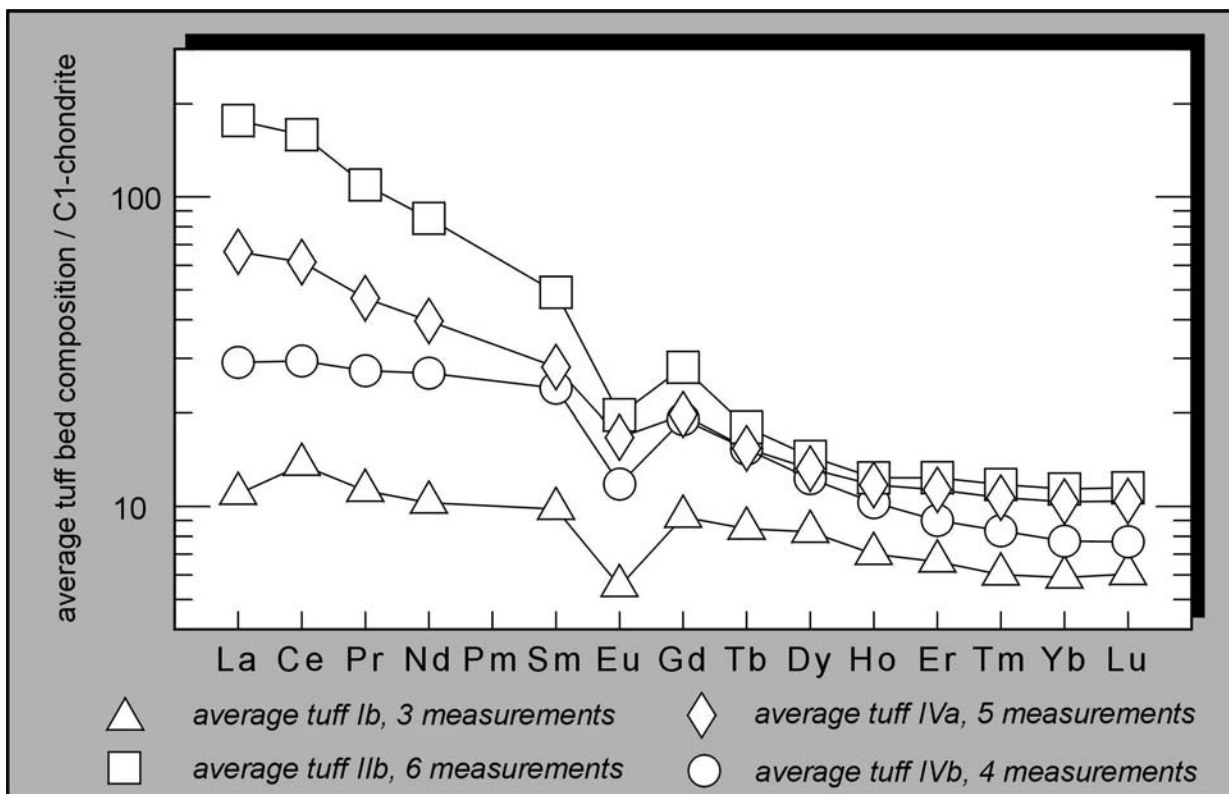


Fig. 120: REE spider diagram for tuff beds I – IV of the Aranos Basin near Ganigobis normalised on C1-chondrites according to Sun and McDonough (1989; cf. Tab. 15).

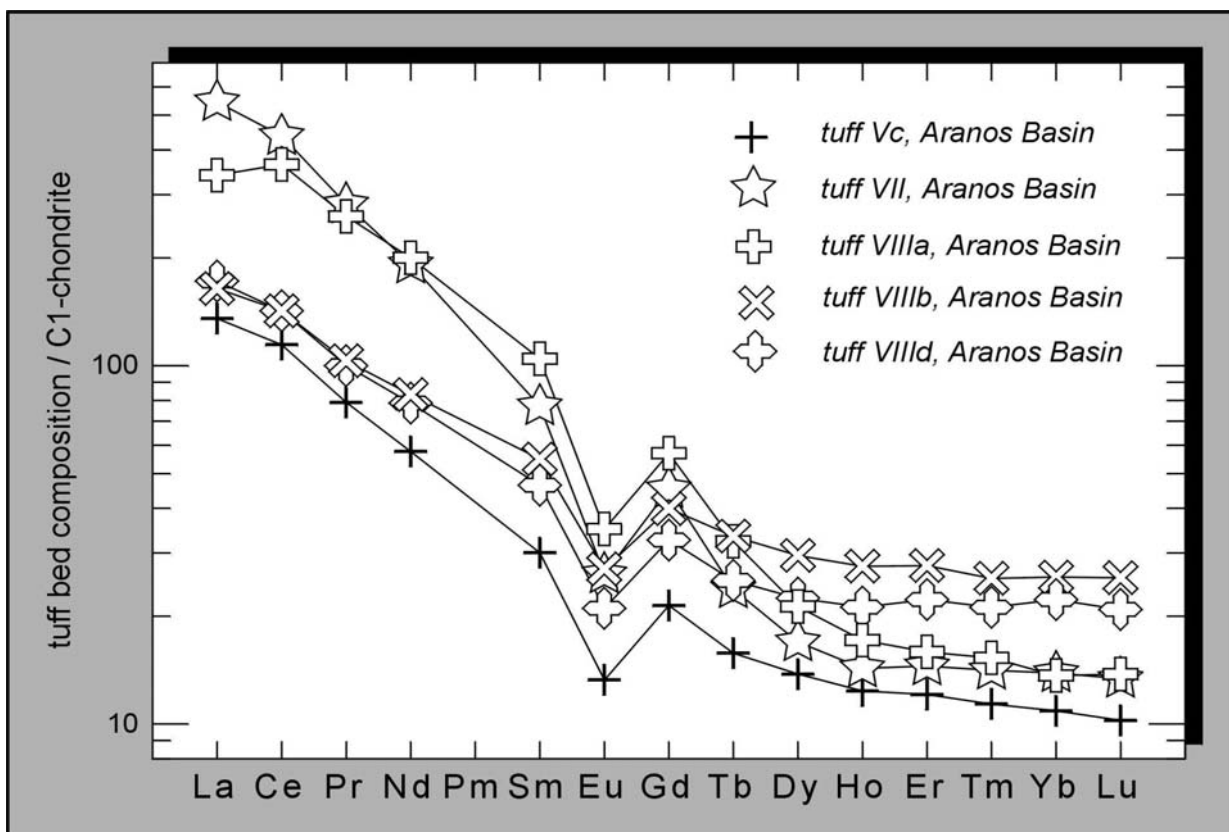


Fig. 121: REE spider diagram for tuff beds V – VIII of the Aranos Basin near Ganigobis normalised on C1-chondrites according to Sun and McDonough (1989; cf. Tab. 15).

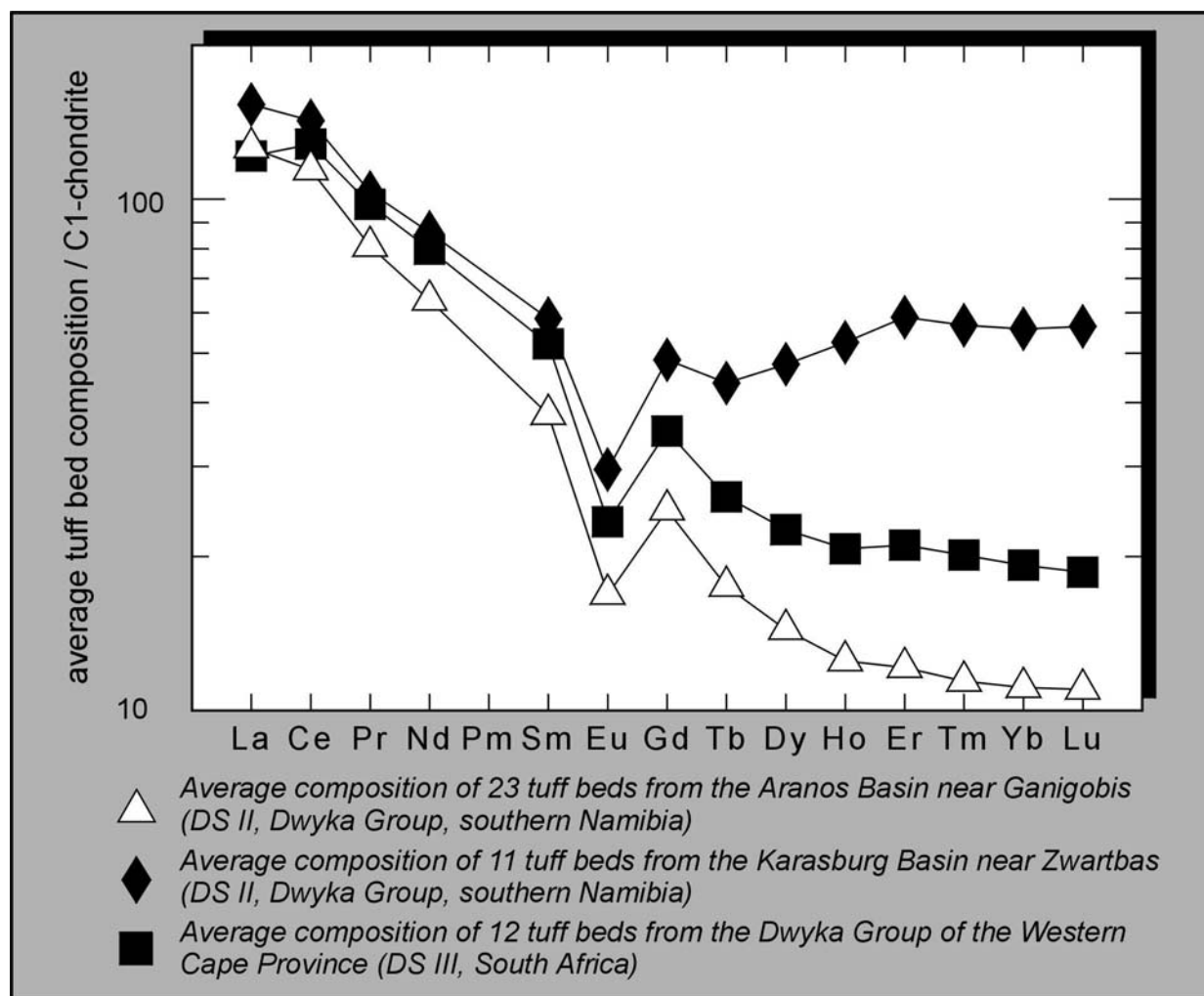


Fig. 122: REE spider diagram for average values of tuff beds from the Aranos Basin, Karasburg Basin and main Karoo Basin normalised on C1-chondrites according to Sun and McDonough (1989; cf. Tab. 15).

The HREE can be used to discriminate between the tuff beds of each basin. HREE are especially depleted in the samples of the Aranos Basin whereas the samples from the Karasburg Basin rather display an enrichment of HREE. The tuff samples from the main Karoo Basin are slightly to moderately depleted. The degree of fractionation between LREE and HREE may also be expressed by the ratios of chondrite-Normalised values for La and Yb (La_N/Yb_N). High values indicate a strong fractionation of LREE. Values of single tuff beds from the Ganigobis Shale Member (Dwyka Group, southern Namibia) vary considerably between 1.86 (average value of tuff Ib) and 39.21 for tuff VII. An La_N/Yb_N - average of all tuff beds from the Dwyka of the Karasburg Basin near Zwartbas is only 5.52 with a total range between 0.87 and

10.32. The tuff beds of the Dwyka Group from the Western Cape Province, South Africa reveal an average value of 2.85 and vary between 0.49 and 7.56.

The degree of REE fractionation with changing REE contents is displayed in a bivariate plot of La_N/Yb_N versus Yb_N (Fig. 123). Especially values of tuff beds Iib, Vc, VII and VIIIa of the Aranos Basin show a strong fractionation of the LREE relative to HREE. The average value of all measured tuff beds from the Aranos Basin shows fractionation of the LREE compared to the average value of all analysed tuff beds from the Karasburg Basin.

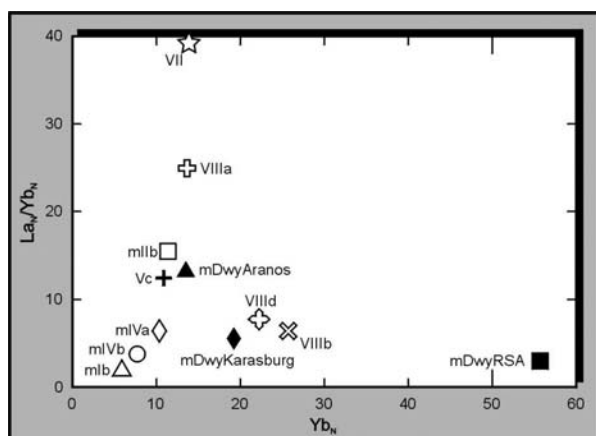


Fig. 123: Bivariate diagram of C1-chondrite normalised Yb vs. La/Yb values of single tuff beds from the Aranos Basin as well as average values of tuff beds from the three study areas. m: mean (average value); DwyAranos: average value for the tuff beds from the Aranos Basin; DwyKarasburg: average value for the tuff beds from the Karasburg Basin; DwyRSA: average value for the tuff beds from the Dwyka Group, Western Cape Province, South Africa.

However, the average value of all measured tuff beds from the Dwyka Group of the Western Cape Province, South Africa, displays high concentrations of HREE and almost no LREE fractionation (Fig. 123).

Fractionation within the LREE and the HREE group is commonly expressed by the ratios La_N/Sm_N and Gd_N/Yb_N . Average La_N/Sm_N -ratios are the highest in the tuff beds of the Aranos Basin (3.31) whereas the ones from the Karasburg Basin and the Western Cape Province show average ratios of 2.25 and 2.35, respectively. Average Gd_N/Yb_N -ratios are also the highest in the tuff beds of the Aranos Basin (2.32). Tuff beds from the Karasburg Basin and the Western Cape Province show average ratios of 1.67 and 0.90. LREE enrichment is characteristic of highly evolved, calc-alkaline magmas.

Eu anomalies may be quantified by comparing the measured Eu concentration with an expected concentration (Eu^*) obtained by the interpolation between the chondrite-normalised values of Sm and Gd. According to Taylor and McLennan (1985), the term Eu/Eu^* is calculated by:

$$Eu_N / \sqrt{Sm_N \times Gd_N}$$

Ratios of $Eu/Eu^* > 1.0$ indicate positive, $Eu/Eu^* < 1.0$ negative anomalies. Variations in Eu/Eu^* - ratios with changing LREE fractionation for all tuff beds are illustrated in Fig. 124.

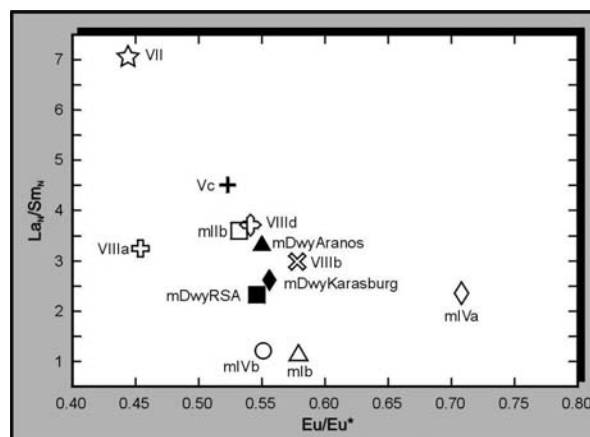


Fig. 124: Eu/Eu^* vs. La_N/Sm_N variations of single tuff beds from the Aranos Basin as well as average values of tuff beds from the three study areas. All values are C1-chondrite-normalised, for abbreviations see Fig. 123.

All tuff beds have negative Eu-anomalies which range between 0.44 and 0.71. The Eu deficiency depends on the composition of glass shards. In rhyolitic ashes large Eu deficiencies occur, whereas dacitic ashes have small Eu deficiencies and also lower Rb concentrations than the rhyolitic ashes (Izett, 1981). The Eu-anomalies show that the parent magma of the tuffs was a highly evolved calc-alkaline magma in which significant plagioclase fractionation occurred prior to the eruption or by winnowing during pyroclastic fallout (Bergström *et al.*, 1997). The Eu deficiency may also affirm reducing conditions during diagenesis of the volcanic ash layers, caused by removal (alteration) of plagioclase and possibly apatite (Kubaneck and Zimmerle, 1986).

La enrichment compared with Nb/U ratios supports the involvement of a dominantly crustal source. The Nb/U vs. Th/La plot compares mid-oceanic ridge basalts (MORB) and continental crust values (Kolata *et al.*, 1996). The bentonites correlate strongly with the continental values (Fig. 125).

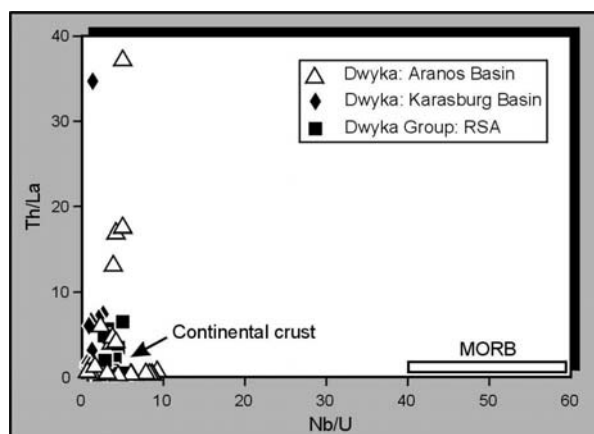


Fig. 125: Bivariate plot of Dwyka Group-equivalent tuff samples from southern Namibia (Aranos and Karasburg Basins) and from the Dwyka Group of the Western Cape Province, South Africa using Nb/U vs. Th/La. In contrast to MORB basalt samples, the tuff beds are similar to continental crustal rocks.

Further evidence for this phenomenon is derived from the comparison of Pb concentrations with Pb/Ce ratios. When compared with oceanic basalts and oceanic island basalts versus deep-sea sediments, the Pb and Ce values show a ratio similar to sediments and, by analogy, the continental crust. Most studies of arc systems indicate that the involvement of subducted sedimentary components is limited to a few percent. Addition of less than a few percent sediment to mantle or oceanic basalts leads to Pb/Ce ratios that are higher than any reported for fresh oceanic basalts (White, 1989). The close correlation of K-bentonite Pb/Ce values with oceanic sediments leads to the conclusion that melting of the continental crustal rocks played a dominant role in the generation of the parent magmas.

Conclusions: REE- values of the tuff beds from the Karasburg Basin and the Western Cape Province are thought to be similar to the ones of the parent magma. The partly abnormally increased La values of tuff beds IIb, Vc, VII and VIIIa from the Aranos Basin, southern Namibia, are not related to petrogenetic processes but seem to arise from secondary alteration processes. LREE enrichment and the Eu-anomalies show

that the parent magma of the tuff beds was a highly evolved calc-alkaline magma in which significant plagioclase fractionation took place. General La enrichment supports the involvement of a dominantly crustal source and also Pb and Ce values show a ratio similar to that of the continental crust.

10.6 The geochemical origin of the volcanic ash

Due to secondary enrichment or depletion, major elements are not directly indicative of the geochemical origin of the volcanic ash. However, some major elements provide clues of the original chemical nature of the tuff beds and the type of source rock if they are normalised adequately.

10.6.1 TiO_2/Al_2O_3

The TiO_2/Al_2O_3 - ratios mentioned in Fisher and Schmincke (1984) for example give hints to the chemical descent of tuff beds. Acid tuff beds have values <0.02 , intermediate tuff beds $0.02-0.14$, and basic tuff beds $0.14-0.18$. For Al_2O_3 , the average value of the tuff beds is normalised on an average value of acid to intermediate, igneous rocks which show a Al_2O_3 - value of 16.45 %. For TiO_2 a value of 0.4 % seems to be appropriate (cf. Chapter 10.2.2).

The Al_2O_3 -contents are thus increased between factors 1.46 to 1.8. Alteration increased the TiO_2 -contents in the tuff beds of the Ganigobis Shale Member by 1.75 and in tuff beds from the Ecca Group of the Western Cape Province, South Africa, by 1.95 whereas the tuff beds from the other two areas are not enriched in TiO_2 .

The average TiO_2/Al_2O_3 - ratio of the tuff beds from the Ganigobis Shale Member (southern Namibia) varies between 0.008 and 0.047. Values of the tuff beds from the Karasburg Basin near Zwartbas deviate less and range between 0.008 and 0.015. The tuff beds from the Dwyka Group of the Western Cape Province display values between 0.011 and 0.079 whereas tuff beds from the Ecca Group of the same area show values in the range of 0.008 and 0.017.

tuff beds	TiO ₂	Al ₂ O ₃	TiO ₂ /Al ₂ O ₃	chemical character
average Aranos Basin (54)	0.40	16.50	0.024	intermediate to acid
average Karasburg Basin (12)	0.23	19.51	0.012	acid
average Dwyka RSA (12)	0.44	16.61	0.027	intermediate to acid
average Ecça RSA (8)	0.24	20.35	0.012	acid

Tab. 16: Alteration corrected TiO₂- and Al₂O₃- values of tuff beds (see text for discussion), the TiO₂/Al₂O₃-ratio indicates their chemical character. Numbers in brackets denote the number of measured samples.

Tuff beds from the Ganigobis Shale Member and from the Dwyka Group of the Western Cape Province thus indicate a rather acid to intermediate character of the original ash whereas TiO₂/Al₂O₃- ratios of tuff beds from Zwartbas and from the Ecça Group are more uniform and suggest a solely acid character of the original ash (Tab. 16).

10.6.2 Zr/Ti-Nb/Y

The Zr/Ti-Nb/Y diagram of Winchester and Floyd (1977) is used to distinguish among different magma series and rock types. The Nb/Y ratio indicates the degree of alkalinity of the parent magma, because its concentration increases only slightly with increasing SiO₂-contents of the differentiation products. Due to a limiting value of 0.67 between basic and intermediate volcanic deposits, calc-alkaline eruptive rocks with low Nb/Y ratios can be distinguished from alkaline rocks with high Nb/Y values. The examined tuff beds predominantly have Nb/Y ratios <0.67, indicating a more calc-alkaline character.

Since both, the Nb/Y and the Zr/Ti ratio, are indices of alkalinity, only the Zr/Ti ratio acts as an index of differentiation. In the Zr/Ti-Nb/Y plot, the original ash principally shows an acid to intermediate composition which varies between rhyolitic and dacitic to slightly andesitic. The group of tuff beds IVa of the Aranos Basin in southern Namibia plots in the sector of alkaline basalt as they are secondarily enriched in TiO₂ and Nb (Fig. 126).

For comparison with the analysed tuff beds of this study, tuff beds of the Lower Karoo

Supergroup of the Western Cape Province, South Africa (Viljoen, 1995) are plotted in the Zr/Ti-Nb/Y diagram. They are subdivided in three groups due to their age. The group “older than Collingham Formation” comprises tuff beds of the Dwyka Group as well as from the Prince Albert and Whitehill Formations (Ecça Group). The group “younger than Collingham Formation” includes tuff beds from the upper Ecça and lower Beaufort Group. The distribution of the data principally confirms the acidic character of the ash which formed the original tuff beds. Tuff beds of the Dwyka and lower Ecça Group show a rhyolitic composition whereas tuff beds from the upper Ecça Group and lower Beaufort Group seem to be a little less differentiated (Fig. 127).

To show how variable these diagrams are, the data are plotted into the Zr/TiO₂-Ga diagram of Winchester and Floyd (1977). This is generally used to distinguish between alkaline and calc-alkaline original magma composition, because Ga concentrations are thought to be largely constant even within differentiated rocks of the calc-alkaline series, whereas in alkaline rocks Ga-contents distinctly increase with increasing differentiation. In contrast to the Zr/Ti-Nb/Y diagram, the original ash mainly plots into the alkaline sector and only the tuff beds of the Aranos Basin plot according to the original dacitic composition (Fig. 128). It appears to be likely that the tuff beds from the Karasburg Basin and the ones from South Africa (Dwyka and Ecça Group) are enriched in Ga by a factor of almost 2 (cf. Chapter 10.3.7).

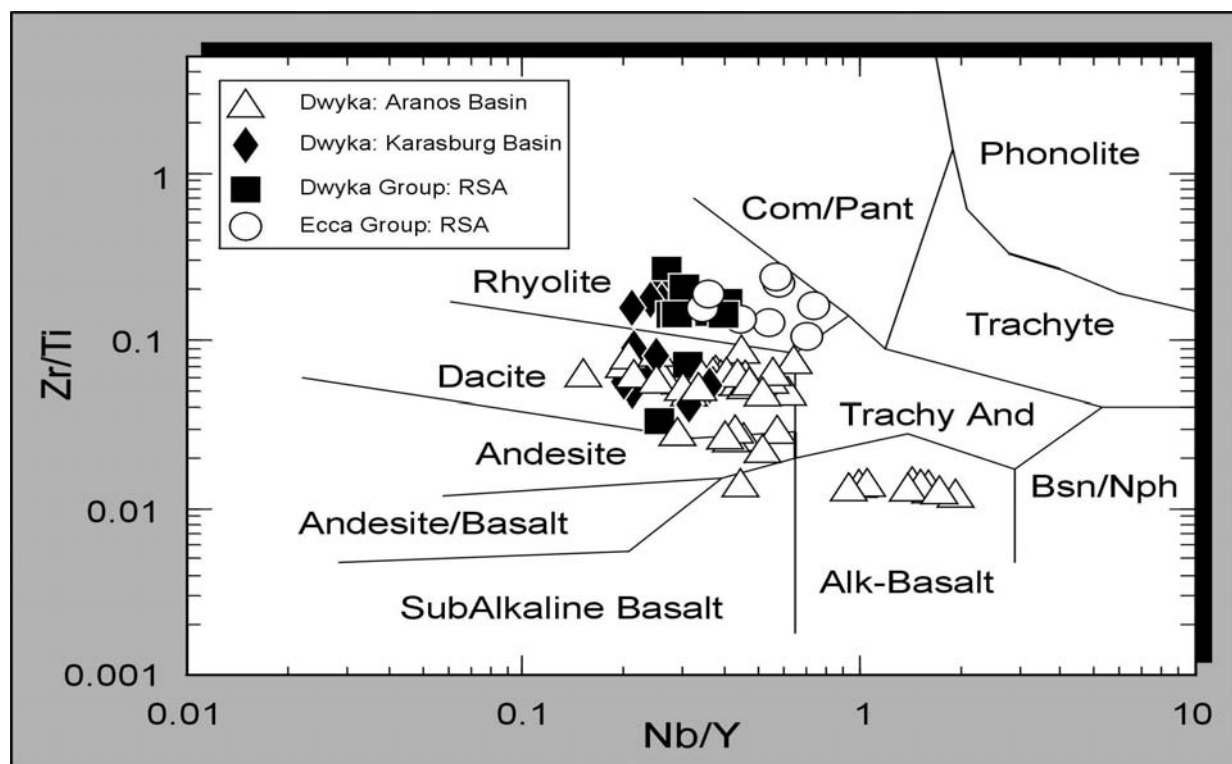


Fig. 126: Geochemical data of all tuff beds analysed in this study are plotted into the Nb/Y vs. Zi/Ti diagram of Winchester and Floyd (1977) illustrating the mainly intermediate to acidic composition of the tuff beds from the Dwyka Group of the Aranos Basin (54 analyses) and the Karasburg Basin (12 analyses) in southern Namibia versus the more acidic composition of the tuff beds from the Western Cape Province (Dwyka Group; 12 analyses and Prince Albert Formation, Ecce Group; 8 analyses).

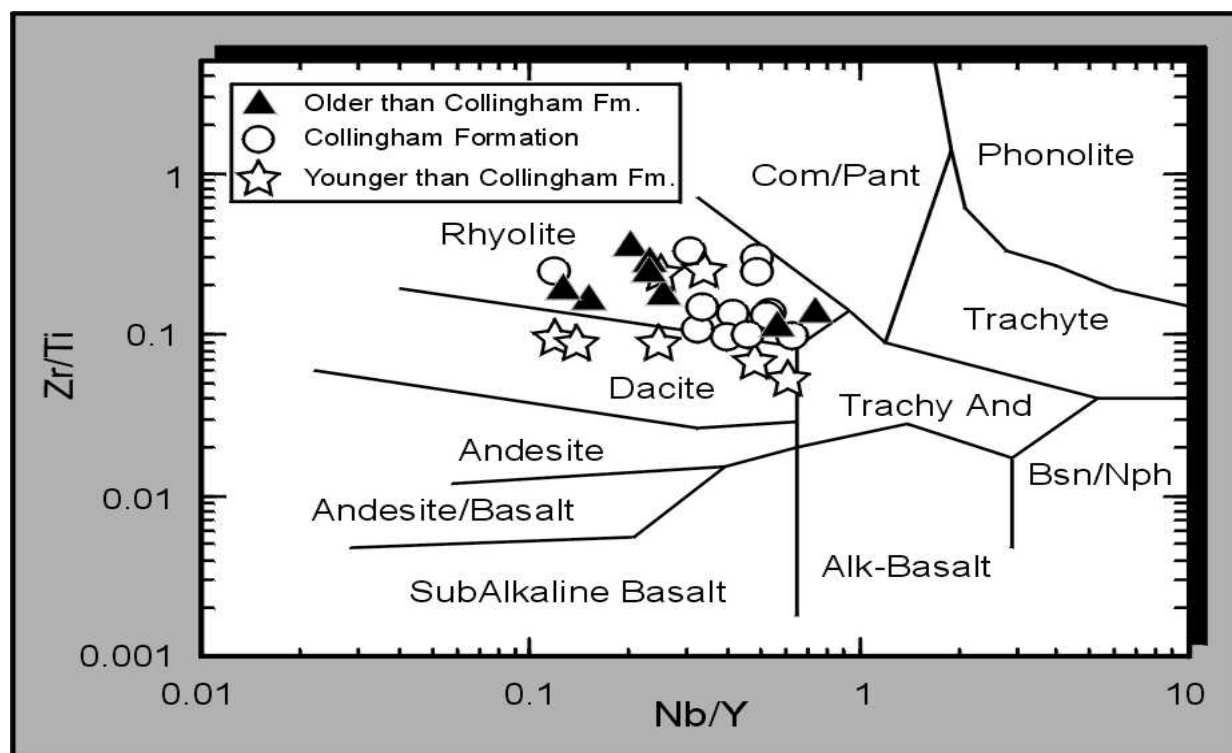


Fig. 127: Geochemical data of tuff beds from the Western Cape Province, South Africa (Viljoen, 1995) plotted into the Nb/Y vs. Zr/Ti diagram of Winchester and Floyd (1977) suggesting an acid composition of the original ash from the Late Carboniferous and Early Permian (Dwyka, Ecce and Beaufort Groups).

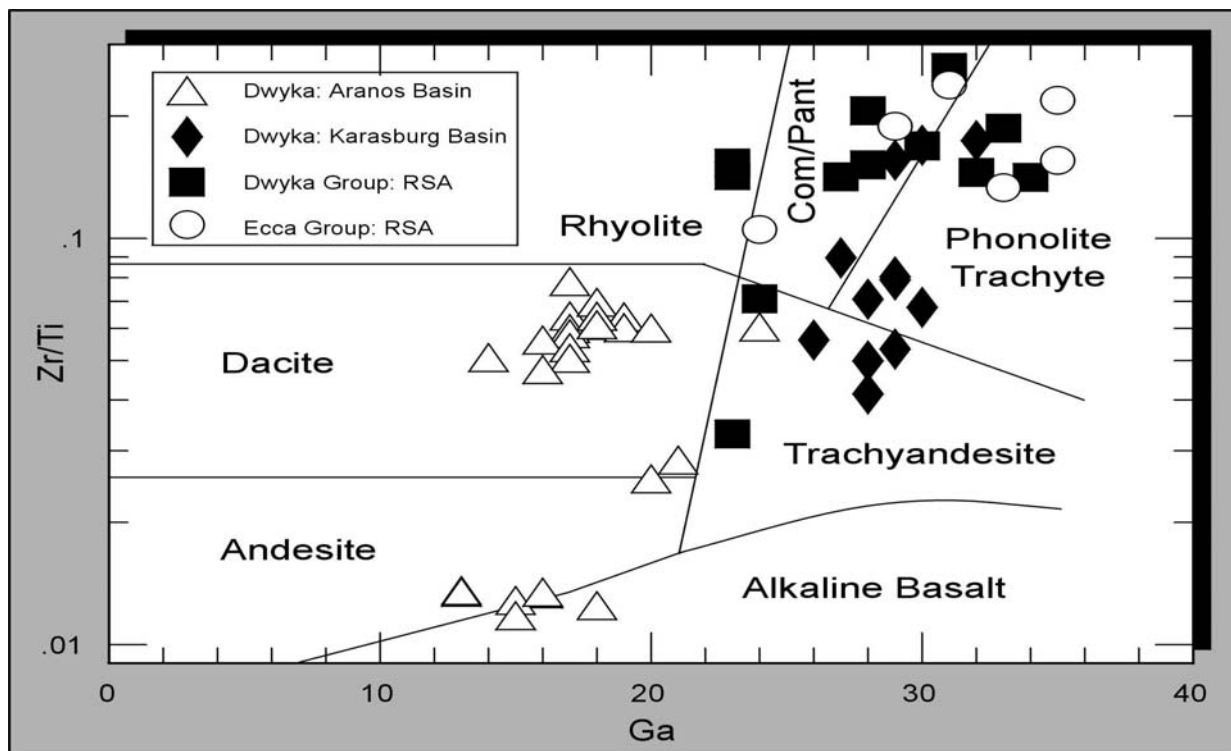


Fig. 128: Geochemical data of tuff beds analysed in this study are plotted into the Ga vs. Zi/Ti diagram of Winchester and Floyd (1977) illustrating the calc-alkaline composition of the tuff beds from the Dwyka Group of the Aranos Basin (26 analyses) whereas tuff beds of the Karasburg Basin (12 analyses) and of the Western Cape Province, South Africa (Dwyka Group: 12 analyses; Prince Albert Formation, Ecce Group: 6 analyses) appear to be more alkaline in composition.

10.7 The geotectonic origin of the tuff beds

Since the tuff beds of the Dwyka Group of southern Namibia and South Africa were classified as acid to intermediate in origin, tectonic discrimination diagrams of granites can be used to determine the tectonomagmatic derivation of the volcanic ashes. Granites are produced by partial melting of previously existing rocks. The source material is therefore reflected by the chemical composition of granites. As the tectonic setting also controls the type of source rocks at depth, the granite composition correlates with the tectonic setting which is the basis for tectonomagmatic discrimination diagrams.

Pearce *et al.* (1984) produced the first systematic study of the geochemistry of granites from known tectonic settings. They subdivided granitic rocks into four main groups according to their intrusive settings: ocean ridge granites (ORG), volcanic arc granites (VAG), within-plate granites (WPG), and (syn-, post-) collision

granites (Syn-, Post-COLG).

Tischendorf *et al.* (1995) tested the reliability of tectonomagmatic discrimination diagrams for silicic igneous rocks, especially of the most commonly used diagrams of Pearce *et al.* (1984), by compiling a data set of more than 5000 published analyses of granites from known tectonic settings. Tischendorf *et al.* (1995) stated that tectonic discrimination diagrams should be used with caution which applies not only to the diagrams and element parameters chosen by Pearce *et al.* (1984). Ambiguity and misclassification may result when magmatic differentiation or secondary alteration produce a shift in composition which crosses field boundaries.

According to Tischendorf *et al.* (1995), within-plate granites (WPG) are discriminated very well; there is almost no overlap of data with other fields regardless of the degree of differentiation.

Ocean ridge granites (ORG) that formed by

fractional crystallisation of basaltic magma plot correctly in the ORG field, but ORG formed by partial re-melting of basaltic rocks plot in the VAG field and would be misclassified. Volcanic arc granites (VAG) show considerable overlap into the WPG field. Granites emplaced in the main volcanic arc plot neatly in the VAG area, but granites of the back-arc area tend to be located in the WPG field. Continental arcs are more complicated and can overlap both the VAG and Syn-COLG fields. Syn-collision granites (Syn-COLG) can have a distinctive chemical signature (high Rb and Ta at relatively low HREE) because of mature sedimentary material in the source material. However, the range of compositions is large due to crustal heterogeneity,

and data points plot across the boundaries into the VAG and WPG fields. As noted originally by Pearce *et al.* (1984), this problem is acute in the case of post-collision granites, since their characteristics depend on the thickness and composition of the lithosphere involved in the collision event, and on the precise timing and location of magmatism.

Discriminating elements in the Pearce diagrams are Y, Nb and Rb. Compared to values of acid to intermediate, igneous rocks, Yttrium seems to be enriched in samples of the tuff beds from South Africa, especially in the ones from the Dwyka Group (93 ppm vs. 36 ppm Y on average acid to intermediate rocks (Wedepohl, 1978).

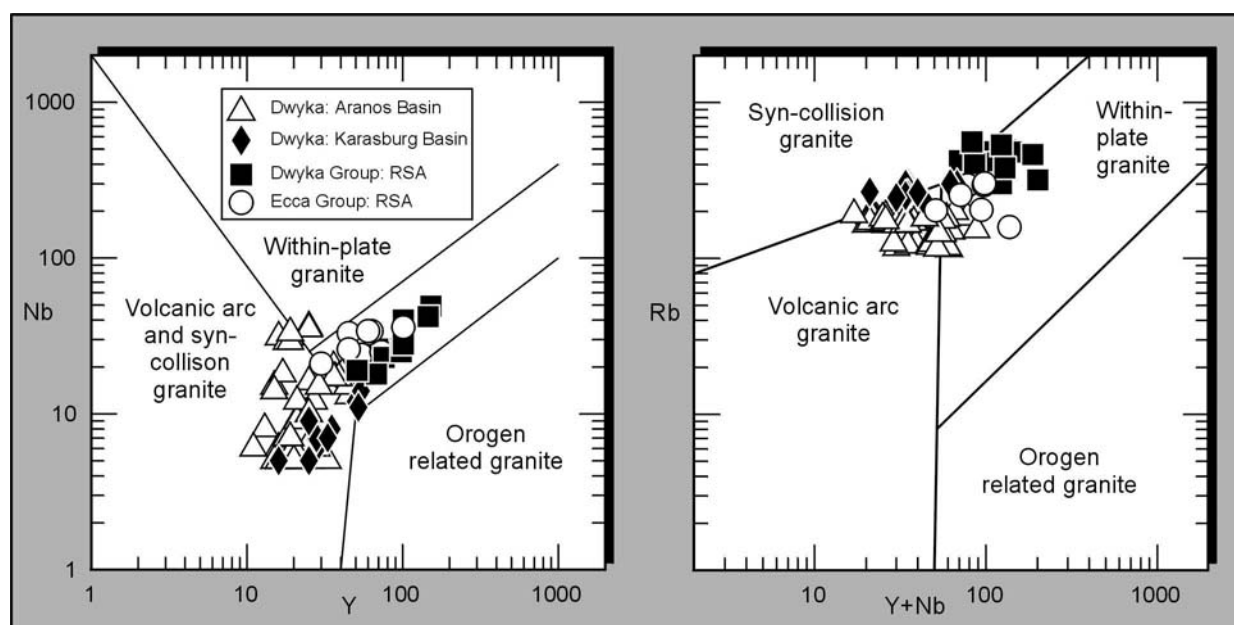


Fig. 129: Tectonomagmatic discrimination diagrams for granitic rocks (Pearce *et al.*, 1984) obviously showing the volcanic arc related composition of the Dwyka-equivalent tuff beds from southern Namibia and the within-plate related composition of the tuff beds from the Western Cape Province, South Africa (Dwyka Group and Prince Albert Formation, Ecça Group). See text for discussion.

Yttrium values of the tuff beds from southern Namibia are similar to the above mentioned values (26 and 34 ppm). Niob appears to be slightly depleted in tuff beds from southern Namibia and slightly to moderately enriched in tuff beds from South Africa (cf. Chapter 10.3.1). Rubidium is slightly to moderately enriched in all tuff beds, especially in samples from the Dwyka Group of South Africa (cf. Chapter 10.3.5).

In the Y vs. Nb and especially in the Y+Nb vs.

Rb-diagrams of Pearce *et al.* (1984; Fig. 129) analyses of the tuff beds from South Africa plot into the field of within-plate granites probably due to enrichment of Y and Nb. The original ash of these tuff beds therefore seems to have been more volcanic arc related than within-plate related. Taking an enrichment of Rb into consideration, the parent magma of all analysed tuff beds was not derived from collision induced processes.

Conclusions: All analysed tuff beds from southern Namibia and South Africa appear to have originated from a volcanic arc setting. Original ash of tuff beds especially from South Africa might plot in the WPG field but seem to be back-arc related (cf. Tischendorf *et al.*, 1995).

10.8 Potential source areas of the tuff beds

10.8.1 Previous studies and opinions

Pyroclastic beds are known from the whole lower Karoo sequence (Dwyka to lower Beaufort Group) within the main Karoo Basin. Published papers include Martini (1974), Elliot and Watts (1974), Lock and Johnson (1974), Lock and Wilson (1975), Ho Tun (1979), Keyser and Zawada (1988), Spears *et al.* (1988), McLachlan and Jonker (1990) and Viljoen (1987, 1990 and 1995) which confirm the widespread occurrence of pyroclastic beds in the main Karoo Basin. Lacking the knowledge about the exact location of the source of the tuff beds the authors split up into two groups of source area-interpretation.

(1) The majority of the authors (e.g. Viljoen) locate the source of the ash-fall tuffs to the south-west of the main Karoo Basin in a magmatic arc situated in present-day Patagonia (South America) as there is no clear evidence of magmatism of the appropriate age known from the Cape Fold Belt. Considering explosive magmatic activity to produce high eruptions columns affected by predominant south-westerly wind directions (cf. Kutzbach, 1994) during Early Permian times, fine ash particles could have been transported from South America to southern Africa over distances of up to 2000 km.

(2) A more local source with respect to the main Karoo Basin is inferred by McLachlan and Jonker (1990) and Keyser and Zawada (1988). McLachlan and Jonker (1990) describe ash-fall tuffs from the Ecca and lower Beaufort Group of the north-western main Karoo Basin. Comparing the sizes of the glass shards contained in the tuff beds with published grain size versus transport distance relationships (Fisher and Schmincke, 1984), they suggest a maximum transport distance in the order of 100 - 300 km. Keyser and Zawada (1988) report two occurrences of ash-

flow tuffs from the Lower Beaufort Group of the north-western part of the main Karoo Basin which led them to postulate a local source towards the north of the basin (Bangert *et al.*, 1999).

10.8.2 Own considerations

The generally small and uniform grain size of the tuff beds suggests ash-fall from a distant source area. The key question is how far the source area was located from the site of deposition which can be indirectly determined by the thickness of the tuff beds and the juvenile components preserved in the tuff beds.

Grain sizes of particles generally decrease downwind from a vent. It has therefore to be considered that transport distances of glass particles and juvenile crystals largely depend on the height of the eruption column. Powerful eruptions are less susceptible to wind shear than weak eruptions. Transport distances of particles of a certain grain size are further influenced by the wind velocity. A median diameter-distance plot for tephra samples is useful to infer broad limits for travel distance when the source is unknown, but it cannot be used to determine exact limits because of wide scatter (cf. Fisher and Schmincke, 1984). Maximum transport distances of fine-grained particles like zircon are very difficult to evaluate due to convective and thermal transport processes which affect these components within ash clouds. Larger particles presumably fall out earlier from an ash cloud whereas smaller ones drift farther downwind.

Pyroclasts up to 100 μm in size were detected by (Heiken and Wohletz, 1985) in samples of the Bandelier Tuff (U.S.A.), taken 528 km away from its source, and in samples of the Mazama tephra (U.S.A.), taken 600 km downwind from the vent.

During the much smaller eruption of Mount St. Helens, U.S.A. in 1980 cumulative weight-percent curves of ash show that in a distance of 241 km downwind of the source, samples contain on average only 5 wt % grains of the size 200-350 μm . No grains larger than 130 μm and 90 μm occur at distances of 308 km and 416 km, respectively (Sarna-Wojcicki *et al.*, 1981; Königer, 1999).

The following maximum and average grain

sizes of juvenile constituents of the tuff beds were observed: Quartz splinters (up to 340 μm , average 58 μm), relic structures of glass shards (up to 220 μm , average 70 μm), zircon (up to 328 μm , average: 90 – 140 μm), apatite (up to 280 μm , average: 157 μm), monazite (up to 180 μm , average: 108 μm), biotite (up to 240 μm , average 100 μm) and feldspar (100 μm). Juvenile components thus display average sizes of 100 –

150 μm but may reach sizes of 350 μm in single cases.

Considering the theory of Viljoen and others who postulate the source area of the ash-fall tuffs in a magmatic arc situated in present-day Patagonia (South America), the minimum distance between the source and the depositional areas of the ash was 1000 km (cf. Kay *et al.*, 1989).

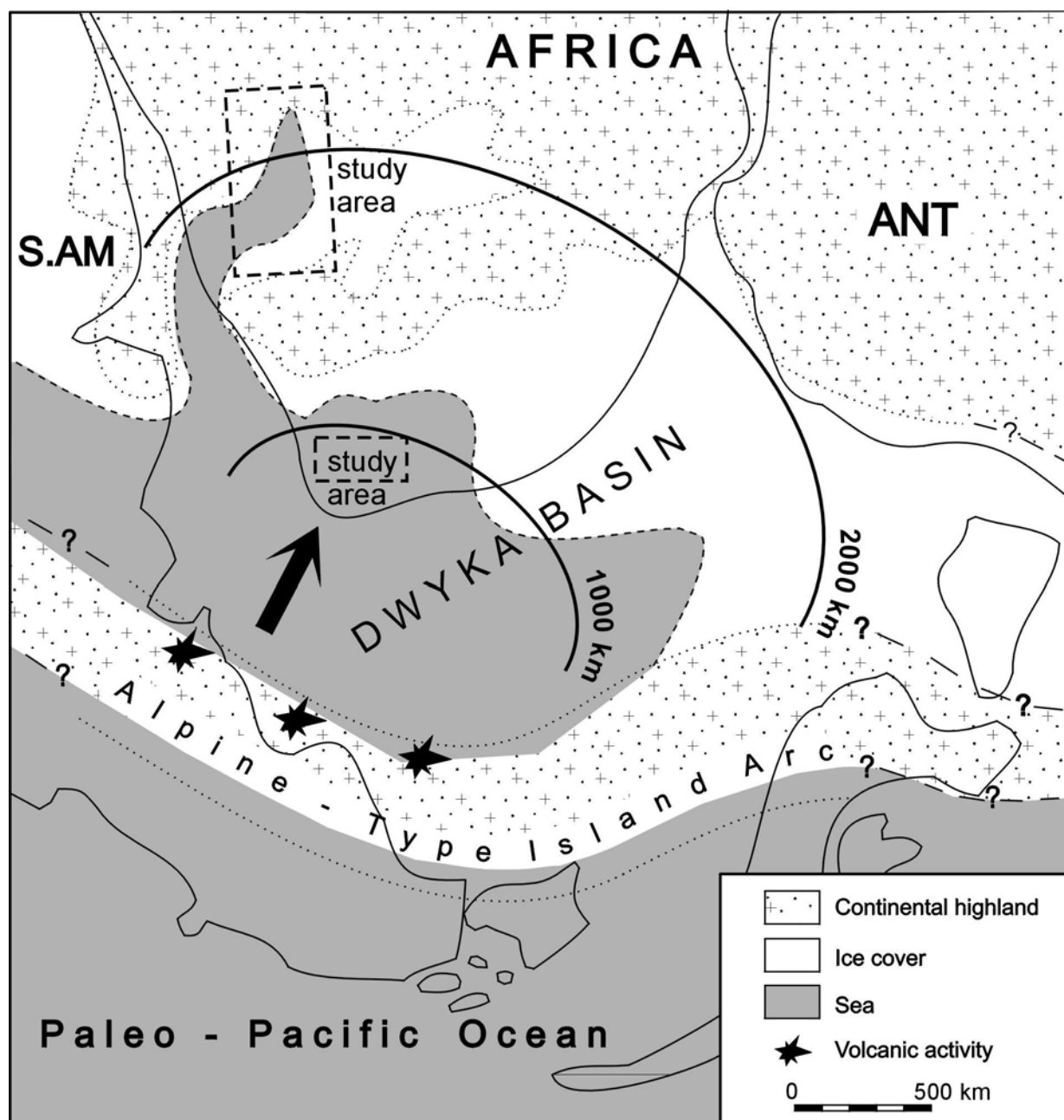


Fig. 130: Palaeogeographic map of south-western Gondwana in the Late Carboniferous showing distribution of continental highland and marine areas as well as postulated ice cover (adapted from Visser, 1989 and Grill, 1997). An alpine-type island arc suggested from subduction processes at the outer margin of south-western Gondwana is thought to be the main source area for the studied tuff beds in southern Africa (cf. Viljoen, 1995).

The measured sizes of the juvenile components of the tuff beds from southern Namibia and South Africa as well as the maximum thickness of 4 cm near Zwartbas (Karasburg Basin, southern Namibia) leads to the conclusion that the eruptions which produced the tuff beds of the Dwyka Group in southern Namibia and South Africa should have been much larger than the ones recorded in historical times. For example, the recorded thickness of the Mazama tephra was on average 0.5 cm at a distance of about 1000 km from the vent (Fisher and Schmincke, 1984).

Nevertheless, the general source area of the studied tuff beds from southern Namibia and South Africa is thought to have been located in an active magmatic arc associated with the Samfrau subducting margin of southern South America, Antarctica and Australia (c.f. Veevers *et al.* (1994). The closest sites of this magmatic arc in the Carboniferous-Permian in south-western Gondwana are known from Patagonia (e.g. Caminos *et al.*, 1988). Acidic magmatism is known from the Choiyoi rhyolite province and the Somuncura batholiths in the North Patagonian Massif. The Choiyoi province consists of ignimbrites with interbedded acidic, pyroclastic rocks (Caminos *et al.*, 1988). Viljoen (1995) states that the thickness and frequency of the tuff beds in the Lower Karoo Supergroup of the Western Cape Province, South Africa, generally decrease from southwest to north-east. Thus, the fall-out ashes contained within the Namibian and South African Dwyka Group sediments could have originated from Patagonia and potentially been transported by prevailing westerly to south-westerly winds (cf. Kutzbach, 1994, Fig. 130).

The following characteristics of the tuff beds support the general derivation of all studied tuff beds from an active magmatic arc associated with the Samfrau subducting margin of southern South America:

- (1) REE patterns show a fractionation of the LREE and distinct Eu-anomalies which indicate that the parent magma of the tuff beds was a highly evolved calc-alkaline magma. La enrichment and Pb and Ce values support the involvement of a dominantly crustal source.
- (2) Trace element ratios such as Zr/Ti and Nb/Y

as well as the grey, magmatic material preserved in inclusions of zircons and apatites suggest an acid to intermediate character of the original ash.

- (3) Tectonic discrimination plots reveal a concentration of data points in a field transitional between that of typical volcanic arc and within plate granites. However, taking the effects of enrichment and depletion of the discriminating elements into consideration, the overall tectonic setting of the source area appears to have been a composite volcanic arc (cf. Fig. 129).

However, a second possibility for the existence of a more local source is indicated by the presence of basaltic Permian *in situ* volcanics and subvolcanics in the Western Cape Province of South Africa (Rowsell and De Swardt, 1976) and the presence of mainly andesitic ash-flow tuffs in the northern part of the main Karoo Basin of South Africa. Keyser and Zawada (1988) suggest that more proximal volcanic activity existed as early as during the Permian.

The following characteristics of the tuff beds support a more proximal source area of the tuff beds from the Western Cape Province, South Africa:

- (1) Th and U values of juvenile zircons measured by SHRIMP of reveal different Th/U ratios between tuff beds from southern Namibia and South Africa (Fig. 131). The Th-values of all zircons from two measured tuff beds from southern Namibia are distinctly higher than the values derived from zircons of tuff beds from the Western Cape Province (South Africa) which invokes different crystallisation environments and potentially different source areas.
- (2) Trace element ratios such as Zr/Ti and Nb/Y (Fig. 126) suggest that the tuff beds from South Africa are more acid in character as the tuff beds from southern Namibia.
- (3) Tectonic discrimination diagrams point to a possibly more within-plate related geochemistry of the tuff beds from South Africa than those from southern Namibia.

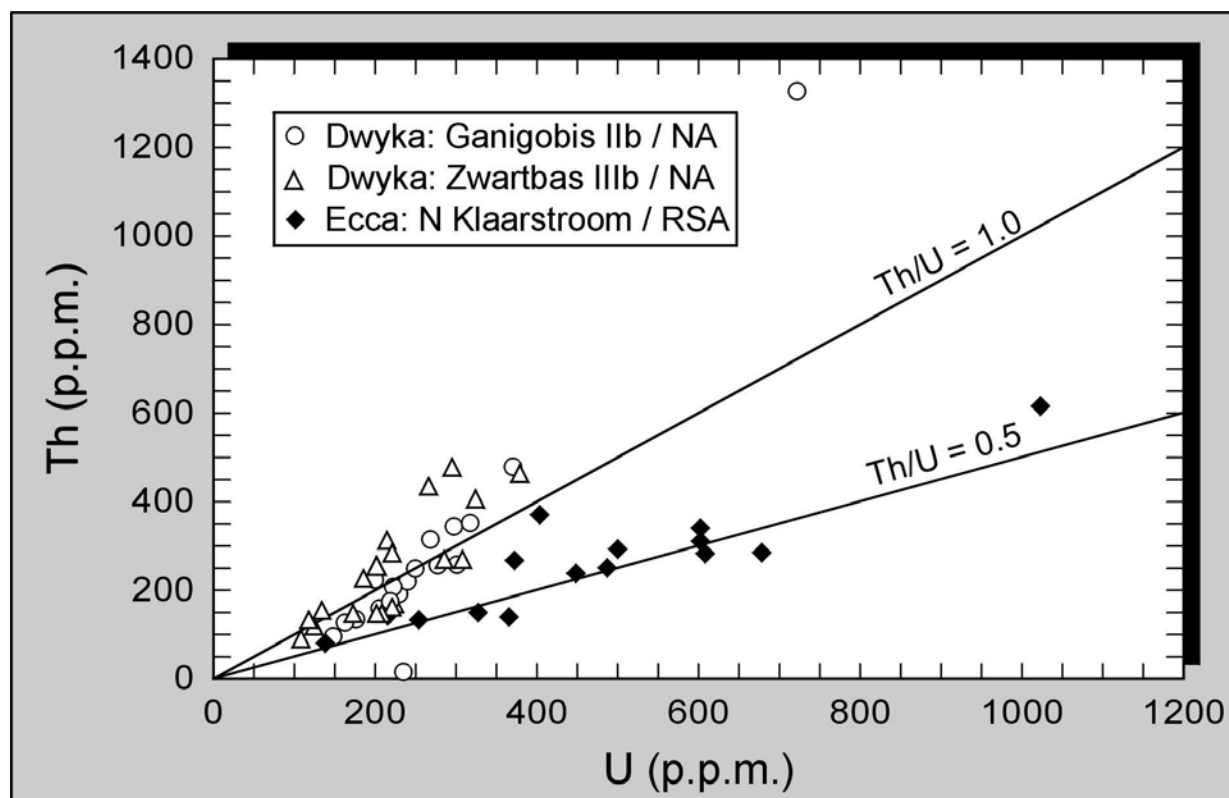


Fig. 131: Th/U-plot of juvenile zircons from southern Namibia (17 zircons of tuff IIb from the Aranos Basin and 19 zircons of tuff IIIb from the Karasburg Basin) and the Western Cape Province (15 zircons) showing different Th-concentration of zircons which invokes different crystallisation environments and potentially different source areas.

Stollhofen *et al.* (in press) speculated about a potential site of proximal volcanism which could have been located in an intracontinental rift zone along the western margin of southern Africa which hosted a marine seaway during Carboniferous-Permian times. They concluded that the distribution of Dwyka-equivalent marine deposits suggest a rift basin structure that was later used by the Whitehill sea (Ecça Group). In its maximum extent, it spanned from the Falklands through the Paraná Basin as far as Northern Brazil and Guyana (cf. Williams, 1995), almost entirely across the Gondwanan supercontinent. The NW-SE trending rift axis became one of the most pronounced extensional features in southern Gondwana with the climax recorded by the extrusion of the extensive Paraná-Etendeka flood basalts during the Early Cretaceous. However, oceanic onset to the north of Namibia then used more northerly trending zones of lithospheric weakness and the previously active NW-SE trending axis of extension through

the Paraná basin became an aborted rift branch (Stollhofen *et al.*, in press).

The author does not want to decide which possibility of the two mentioned is correct or not. Transportation of the ash from South America sounds possible especially concerning the lack of volcanic rocks in Lower Karoo strata, the south-westerly wind directions and the fact that the frequency and thickness of the tuff beds decrease to the north-west in South Africa and southern Namibia. The geochemistry of the tuff beds suggests an arc-related, calc-alkaline magmatism which makes a South-American source area likely. The main point which points to a more near-by source area is the size of the juvenile minerals which, with regard to recent literature, cannot be transported over distances of 2000 km. However, higher eruption plumes of volcanoes or stronger westerly winds than previously known may increase transport widths to the required distance.

10.9 Volcanic clasts

Undeformed volcanic clasts of the Dwyka Group within the Aranos Basin clasts which appear in the same stratigraphic levels as the tuff beds may also confirm a more proximal source of the tuff beds if they would have the same age as the tuff beds. They are found as single dropstones on top of deglaciation sequence II between the uppermost diamictites and dropstone-bearing siltstones just below the Ganigobis Shale Member and reach into the Ganigobis Shale Member as far as up to the tuff beds I. They thus occur in a rather thin zone of less than 10 m thickness coinciding almost exactly with the earliest occurrences of the tuff beds. It was therefore

speculated that the undeformed volcanic clasts and the tuff beds might belong to the same volcanic events.

The mostly well-rounded clasts are occasionally concentrated in horizons within the diamictites and the dropstone-bearing siltstones (Fig. 132: left) whereas they appear randomly distributed in the overlying Ganigobis Shale Member (Fig. 132: right). They vary between porphyritic, amygdaloidal or vesicle-free basalt dropstones with diameters up to 50 cm and andesitic to rhyolitic clasts with diameters ranging from 3 to 60 cm.



Fig. 132: left: large basaltic block below tuff beds I in # 23, 5 km south of Ganigobis; right: large rhyolitic block in stratified diamictite in the upper part of DS II; # 42, 4 km west of Ganigobis (cf. Grill, 1997)

10.9.1 Thin-section petrography

Thin-sections of the undeformed volcanic clasts reveal a basic and intermediate to acid composition. Most basic to intermediate are rocks

are to a certain degree propylitic. The cryptocrystalline to microcrystalline *tholeiitic basalt* clasts show the typical intersertal texture with plagioclase laths, glass, which is mostly altered to clay minerals.

Plate 8: Photomicrographs of analysed volcanic dropstones.

Fig. 1: propylitic andesite clast showing up to 1.5 mm large alkali feldspar laths (AF) and up to 0.5 mm large plagioclases. The matrix consists of feldspar laths (sanidine?), probably quartz, chlorite (Ch) and opaque minerals (BB 25)

Fig. 2: intermediate, dacitic clast with up to 1.5 mm large, heavily altered plagioclases (P) in a crypto- to microcrystalline quartz-feldspar matrix with few opaque minerals (BB 23)

Fig. 3: porphyritic rhyolitic clast with 2.5 mm large euhedral (high) quartz phenocrysts (Q), subhedral, kaolinised alkali feldspars (up to 3.0 mm, AF) and completely chloritized basaltic xenoliths (BX) (90-2/1)

Fig. 4: porphyritic rhyolitic clast with 0.8 - 1.5 mm large, heavily altered plagioclases (P) and green amphibole (A, 1 mm) in a crypto- to microcrystalline quartz-feldspar matrix (81-4)

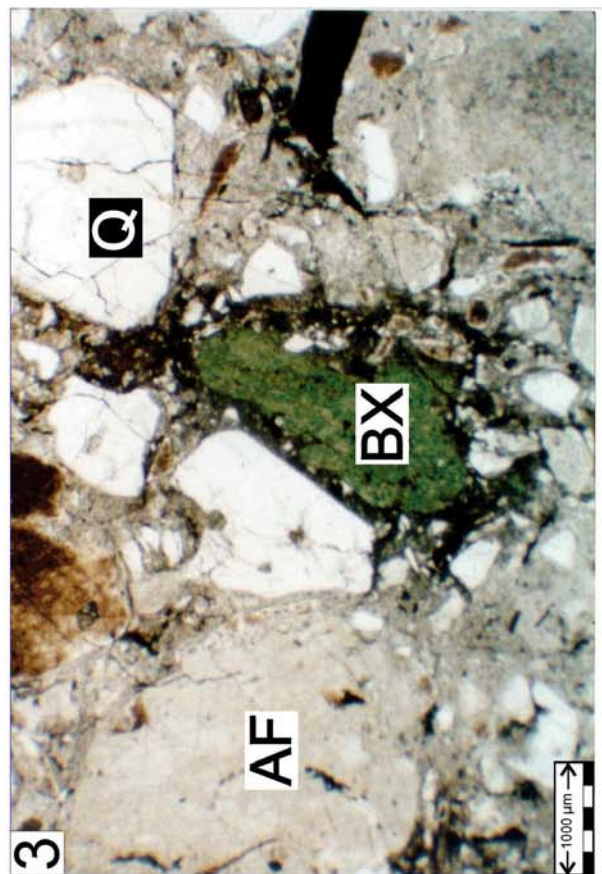
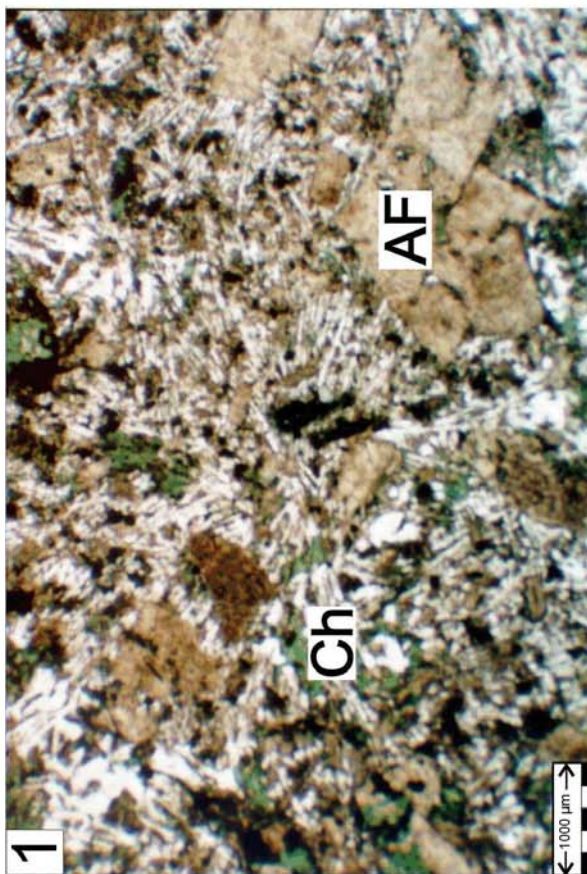
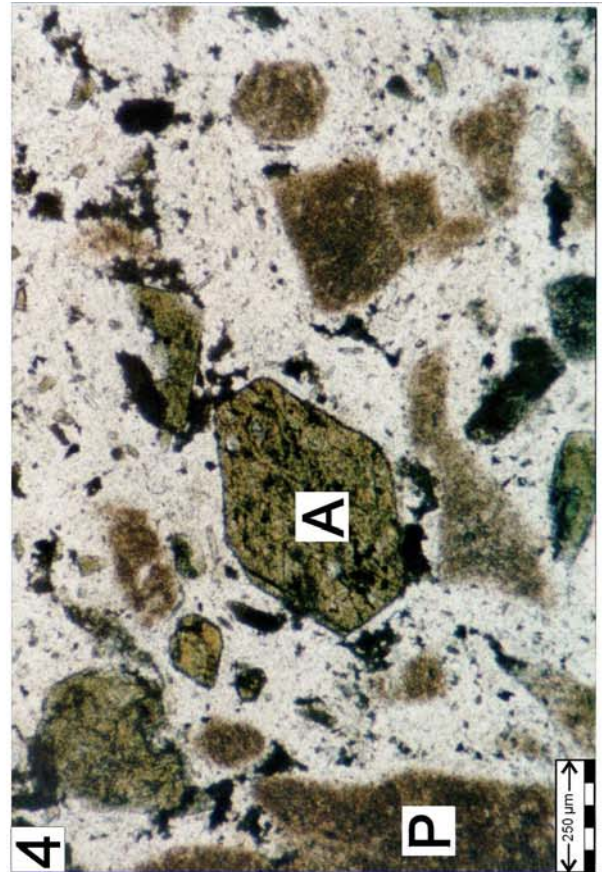
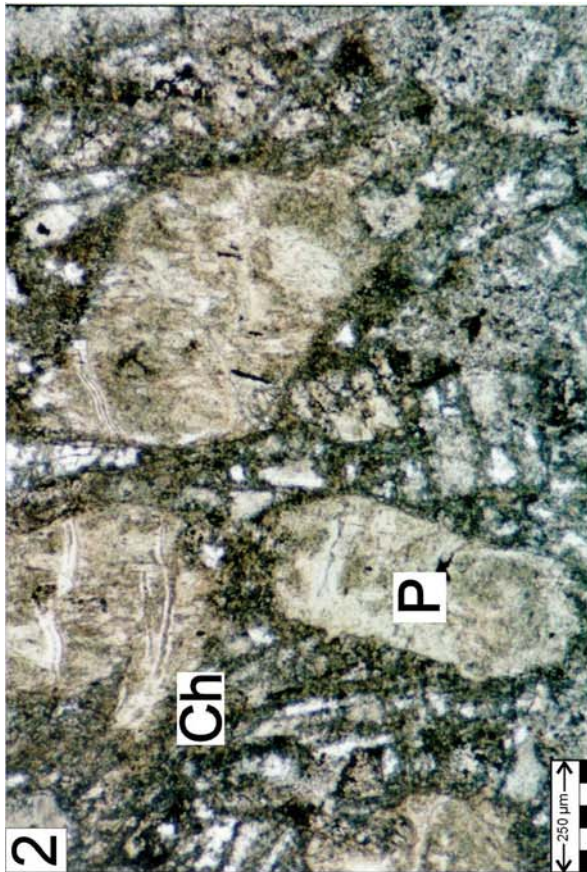


Plate 8: Photomicrographs of analysed volcanic dropstones.

Pyroxenes are mostly replaced by secondary chlorite and opaque minerals. Calcite-filled vesicles are surrounded by thin veneers of chlorite. Accessoric minerals are euhedral zircons and sphenes with a size less than 100 μm (thin-sections # 84-3 and 98-7). Thin-sections of *olivine basalts* show up to 8 mm large euhedral, but heavily altered plagioclases, contours of completely altered olivines with iddingsitic rims and epidote which occurs in the matrix (thin-section # 81-2). A thin-section of a retrogressive, superimposed, propylitic *andesite* displays up to 0.5 mm long plagioclases and few simply twinned alkali-feldspars (up to 1.5 mm long). The matrix consists of feldspar laths (sanidine?), probably quartz, chlorite and opaque minerals (Plate 8, Fig. 1). Accessoric minerals comprise up to 200 μm long, euhedral, normal- to longprismatic zircons and few six-sided apatites (thin-section # BB 25). The texture of the intermediate, *dacitic* clasts is dominated by 0.8 – 1.5 mm large, zoned, kaolinised plagioclases and occasional green biotite (0.3 mm). The crypto- to microcrystalline matrix consists of a quartz-feldspar-mixture with secondary chlorite and opaque minerals. Zircon was determined as the main accessory mineral (Plate 8, Fig. 2; thin-section # BB 23).

The acidic suite of the clasts ranges from rhyodacitic to rhyolitic. The porphyric *rhyodacitic* clasts are dominated by up to 3.7 mm large quartz phenocrysts in β -form and up to 2.3 mm large euhedral plagioclases. The cryptocrystalline and recrystallized matrix consists of quartz, opaque minerals and volcanic glass showing spherulitic devitrification. Basaltic xenoliths point to a bimodal composition of the parent magma (thin-section # 90-1). Porphyric *alkali rhyolitic* clasts show up to 10 mm long alkali feldspars and up to 6 mm large, secondary calcite crystals. Plagioclase-phenocrysts of a second generation, up to 0.3 mm large, appear concentrated in clusters. The crypto- to microcrystalline matrix is composed of quartz, secondary chlorite, opaque minerals and zircon (thin-section # 90-2/2). The porphyric *rhyolitic* clasts are dominated by up to 2.5 mm large euhedral quartz phenocrysts in β -form and

subhedral, kaolinised alkali feldspars (up to 3.0 mm) as well as few plagioclase and biotite phenocrysts. Completely chloritized xenoliths, probably basaltic in origin, again suggest a bimodal composition of the parent magma (Plate 8, Fig. 3; thin-section # 90-2/1). The matrix consists of a microcrystalline mixture of opaque minerals, quartz and feldspar which is partly altered into carbonate. Another sample shows phenocrysts of plagioclase (max. 1.2 mm), quartz (max. 0.4 mm) and nice basal faces of hornblende (Plate 8, Fig. 4; thin-section # 81-4). This thin-section contains a porphyric xenolith with plagioclases and amphiboles in a microcrystalline, greenish matrix. The chloritized matrix of this sample is mainly made up by quartz and feldspars. The porphyric *rhyolite* clast (thin-section # SA 1) which was radiometrically dated (cf. Chapter 10.9.3) displays up to 1.2 mm large euhedral quartz phenocrysts in β -form and euhedral to subhedral, kaolinised alkali feldspars (up to 4.0 mm). Few biotite phenocrysts (up to 0.5 mm) which are opaque at their edges and completely chloritized as well as very few plagioclase phenocrysts with multiple twinning (up to 0.3 mm) were observed in the thin-section. The matrix consists of a microcrystalline mixture of opaque minerals, quartz and feldspar laths.

10.9.2 Geochemical rock classification of the volcanic clasts

The geochemical character of the volcanic clasts varies between basic and intermediate to acidic. Geochemical data plotted into the alkali-silica diagram after Le Bas *et al.* (1986) show that three of the analysed clasts plot within basaltic fields, one within the andesitic field, two within the dacitic field and five within the field of the rhyolites (Fig. 133). Slightly different results are visible in the Zr/TiO_2 vs. Nb/Y discrimination diagram after Winchester and Floyd (1977). Contrary to the diagram of Le Bas *et al.* (1986), samples 90-1 and 90-2 move to the field of the dacites (rhyodacites) in the diagram of Winchester and Floyd (1977). All geochemical data of the volcanic clasts is found in Tab. 25 in Appendix F-3.

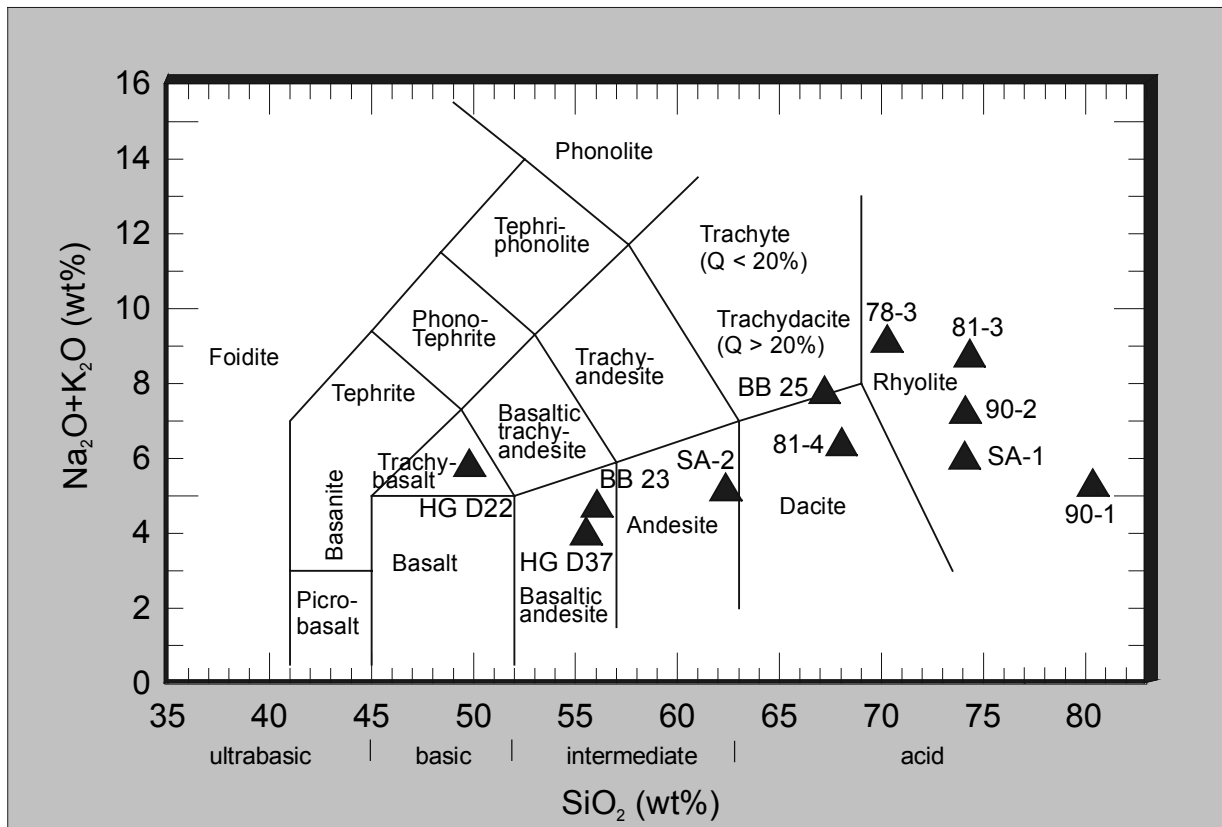


Fig. 133: Total alkali-silica discrimination diagram for the analysed volcanic clasts after Le Bas *et al.* (1986)

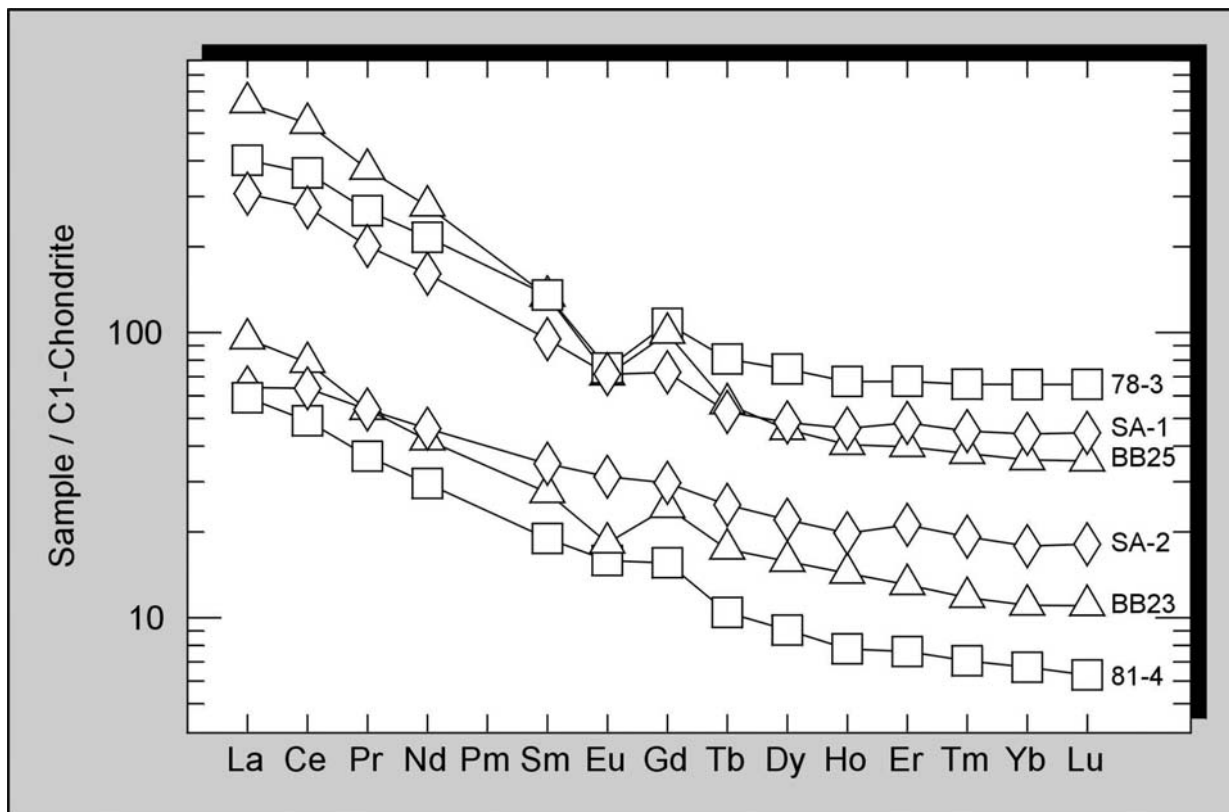


Fig. 134: REE-distribution of volcanic clasts from the Dwyka Group of the Aranos Basin in southern Namibia normalised to C1-chondrite composition of Sun and McDonough (1989).

10.9.3 REE - discrimination of the volcanic clasts

Rare earth elements (REE) are very similar in terms of their chemical and physical properties. They are relative immobile during diagenesis, low-grade metamorphism, weathering or hydrothermal alteration (Michard, 1989). REE patterns of 5 measured volcanic clasts are displayed in Fig. 134. They are characterized by a fractionation of the light rare earth elements and mostly weak Eu-anomalies. Samples SA 1, SA 2 and 81-4 show no Eu-anomalies.

10.9.4 Radiometric age of the volcanic clasts

The major uncertainty in speculating, that the described volcanic clasts could have been coupled volcanologically with the tuff beds, was the unknown age of the volcanic clasts. In order

to test their radiometric age, a quartz-bearing acid volcanic clast which is shown in Fig. 132 and petrographically described in Chapter 10.9.1 was chosen for U/Pb-determinations of zircons by ion-microprobe (SHRIMP). The methodology is described in Chapter 11.2 together with the results of the radiometric age determinations of the tuff beds.

The first two zircons analysed from this sample were Proterozoic in age (Fig. 135 and Tab. 17), giving a weighted mean $^{207}\text{Pb}/^{206}\text{Pb}$ age of 2047 ± 12 Ma. Since the zircon population was uniform in appearance, it was concluded that these zircons were representative of the host rock. As this volcanic clast was therefore not related to any magmatism coeval with the tuff beds of the Dwyka Group, no further analyses were conducted in order to save funds.

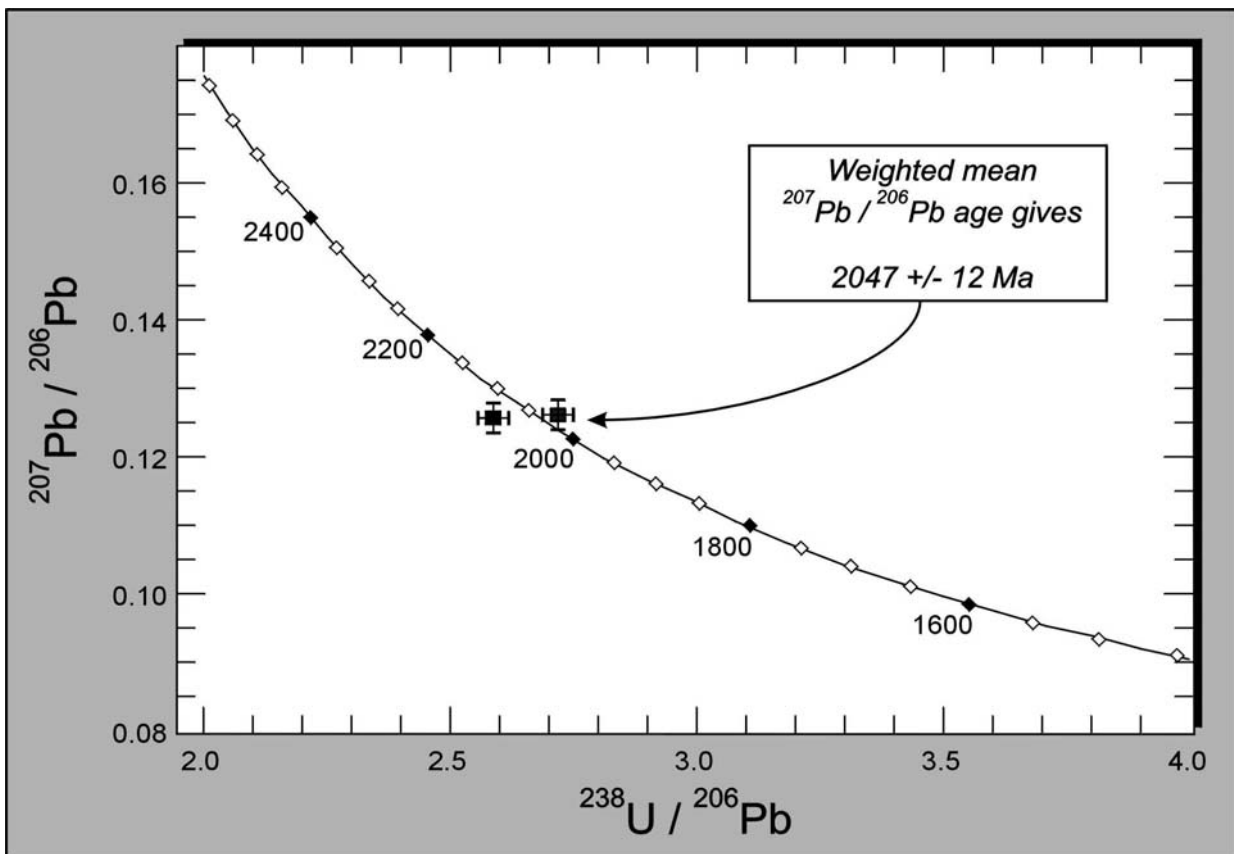


Fig. 135: SHRIMP U-Pb analyses of two zircons from a volcanic dropstone sampled on top of DS II, Dwyka Group, southern Namibia. Note that data are plotted corrected for common Pb, using the measured $^{204}\text{Pb}/^{206}\text{Pb}$.

Grain. spot	Radiogenic Ratios										Age (Ma)				Conc %				
	U (ppm)	Th (ppm)	Th/U	Pb* (ppm)	²⁰⁴ Pb/ ²⁰⁶ Pb	f ₂₀₆ %	²⁰⁶ Pb/ ²³⁸ U	²⁰⁷ Pb/ ±	²⁰⁷ Pb/ ²³⁵ U	²⁰⁷ Pb/ ±	²⁰⁶ Pb/ ±	²⁰⁷ Pb/ ²³⁵ U	²⁰⁷ Pb/ ±	²⁰⁷ Pb/ ²⁰⁶ Pb		±			
1.1	167	74	0.44	69	0.00000	0.01	0.3866	0.0050	6.721	0.096	0.1261	0.0006	2107	23	2075	13	2044	9	103
2.1	216	96	0.44	86	0.00001	0.02	0.3678	0.0042	6.411	0.082	0.1264	0.0006	2019	20	2034	11	2049	8	99

Tab. 17: SHRIMP U-Th-Pb zircon results for two zircon from a volcanic clast, DS II, Dwyka Group, southern Namibia. Note that uncertainties are given at the one σ level, f_{206} % denotes the percentage of ²⁰⁶Pb that is common Pb, correction for common Pb is designed using the measured ²³⁸U/²⁰⁶Pb and ²⁰⁷Pb/²⁰⁶Pb ratios following Tera and Wasserburg (1972) as outlined in Compston (1992).

Volcanic rocks of this age are commonly associated with the Bushveld Complex on the Kaapvaal Craton towards the east of the study area. General ice-flow directions in Dwyka Group times were directed westwards (Grill, 1997). Glaciers might have transported the clasts subsequently to the west into the study area

where they were accidentally deposited together with the tuff beds.

As only one volcanic dropstone was analysed, others still may hold a Dwyka Group-equivalent age. With respect to other Dwyka Group-aged dropstones, a more proximal source of the tuff beds is not generally ruled out.

11 New radiometric age determinations of tuff beds from the Dwyka and Ecca Groups, southern Africa

Ash-fall derived tuff beds are exact chronostratigraphic horizons due to their short duration of sedimentation and their potential large lateral extent. Consequently, ash layers are regarded to be isochronous and their dating allows to establish a tephrochronology of a specific sequence. Radiometric age determinations of tuff beds provide the means for the correlation of potential source areas or for the correlation of sediment strata of other basins.

To obtain radiometric ages from tuff beds, mostly juvenile, igneous minerals are used such as zircon, apatite, hornblende, plagioclase, sanidine and biotite. Whole-rock ages for tuff beds are less useful because tuff beds usually form in open systems where elements can be introduced or removed by percolating solutions (Bohor and Triplehorn, 1993).

Until present, the age of the sediments of the Dwyka Group in southern Africa has been rather weakly determined. Available age determinations mainly depended on palaeontological data from palynology and macrofossils, which most of times assigned a Late Carboniferous to Early

Permian age for the Dwyka Group in southern Africa. So far, a minimum age for the Dwyka Group has been indirectly provided by ⁴⁰Ar/³⁹Ar-whole rock dating of the Swartberg deformation event at 278±2 Ma which, according to Hålbich *et al.* (1983), affected the Dwyka Group but not the overlying Ecca Group sediments in the vicinity of the northerly advancing Cape Fold Belt in the Western Cape Province, South Africa.

In this study however, radiometrically determined ages of the Dwyka Group of southern Africa are specified for the first time. U/Pb ages of zircons from tuff beds of the Dwyka Group in southern Namibia and South Africa as well as of the basal Ecca Group in South Africa were determined (1) to identify the crystallisation age of the zircons and approximately the age of the eruption of the volcanic ash, (2) to correlate deposits of the Dwyka Group between single basins or parts of basins and (3) to estimate the duration of the Dwyka Group respectively the duration of the single deglaciation sequences of the Dwyka Group in southern Africa.

Heavy mineral separates of seven tuff beds of the Dwyka and Ecca Groups of southern Namibia and South Africa were chosen for radiometric age dating.

11.1 Sample selection

Aranos Basin (Namibia): In order to obtain the duration of the Ganigobis Shale Member (DS II, Dwyka Group), samples of the lowermost and uppermost tuff beds were selected for radiometric dating. Unfortunately, it turned out that only few of the analysed tuff beds contained enough dateable zircons. Finally, two comparable ages of tuff bed IIIb were achieved. The exact sample locations are given in Chapter 2.3 and Fig. 13.

Karasburg Basin (Namibia): Again samples of the lowermost and uppermost tuff beds within the outcrops of the Dwyka Group were chosen to avoid overlapping of the margins of error but only the sample of tuff IIIb contained qualitatively and quantitatively enough zircons to obtain an excellent age. The heavy mineral concentrate of tuff bed XXXIV revealed only two measurable zircons giving a rather imprecise age. The exact sample locations are supplied in Chapter 5.1.

Western Cape Province (South Africa): Heavy mineral concentrates of a tuffaceous bed within the Dwyka Group north of Klaarstroom revealed many juvenile zircons, measurements of these resulted in an exceptionally well-constrained age.

Tuff beds of the Ecca Group north of Klaarstroom and south of Laingsburg contained adequate zircons again leading to excellent ages. The exact sample locations are given in Chapter 7.2.

KwaZulu-Natal (South Africa): Tuffaceous beds of the Dwyka Group carried perfectly preserved magmatic zircons as well as rounded, detrital zircons. Two measured magmatic zircons, however, revealed Proterozoic ages. The exact sample location is supplied in Chapter 7.4.

11.2 Analytical procedures

Heavy mineral concentrates of the selected tuff

beds were produced at the Institut für Geologie in Würzburg, Germany and were sent to **PRISE Laboratories (Precise Radiogenic Isotope SErvices)** located at the Research School of Earth Sciences, Australian National University, Canberra, Australia. Dr. R. Armstrong coordinated and supervised the entire analytical procedure. The radiometric age determinations were carried out by ion microprobe U/Pb zircon dating on the **SHRIMP II (Secondary High Resolution Ion Micro Probe)**.

Zircon grains were handpicked under a binocular microscope and were mounted in epoxy together with the zircon standard AS3 (Duluth Complex gabbroic anorthosite; Paces and Miller, 1993) and the standard SL13. The grains were sectioned approximately in half, polished, and photographed. All zircons were then examined by cathodoluminescence imaging on a SEM, a procedure which greatly enhances the quality of data produced in the subsequent ion microprobe sessions. Through cathodoluminescence imaging of the zircons, hidden and complex internal structures can be determined more accurately than under normal reflected or transmitted light and consequently the target area can be more reliably selected for analysis.

The SHRIMP data have been reduced in a manner similar to that described by Williams and Claesson (1987) and Compston *et al.* (1992). U/Pb in the unknown zircons were normalised to a $^{206}\text{Pb}/^{238}\text{U}$ value of 0.1859 (equivalent to an age of 1099.1 Ma) for AS3 using an empirical power law calibration. The U and Th concentrations were determined relative to those measured in the SL13 standard. Ages calculated for Proterozoic zircons (e.g. the analyses of the detrital zircons from the tuffaceous beds east of Nondweni and the volcanic clast sample reported in Chapters 11.3.6 and 10.9.3, respectively) are given as $^{207}\text{Pb}/^{206}\text{Pb}$ ages. They are corrected for any common Pb component using the measured $^{204}\text{Pb}/^{206}\text{Pb}$ ratio, the appropriate Cumming and Richards (1975) model of Pb composition, using the decay constants recommended by Steiger and Jäger (1977). U/Pb ages of Palaeozoic zircons were calculated using the $^{206}\text{Pb}/^{238}\text{U}$ ratios, with the correction for common Pb made using the measured $^{207}\text{Pb}/^{206}\text{Pb}$ and $^{206}\text{Pb}/^{238}\text{U}$ values

following Tera and Wasserburg (1972) and as described in Compston *et al.* (1992). In the following Tera-Wasserburg concordia plots the data are, however, plotted uncorrected for common Pb. This shows the dispersion of data relative to the common Pb-contents (the lower the common Pb, the closer the data points plot to the concordia curve).

Uncertainties in the isotopic ratios and ages in the data tables (and in the error bars in the plotted data) are reported at the 1σ level, but final ages on pooled data are reported as weighted means with 95% confidence limits or $t\sigma$, where t is the "Fisher's t " value. All age calculations and statistical assessments of the data have been done utilising the geochronological statistical software package Isoplot/Ex (version 2.00) of Ludwig (1999). Both inheritance and radiogenic Pb loss – the latter resulting in younger apparent U/Pb ages, can complicate U-Pb zircon dating of tuffs. Inheritance can be difficult to detect if the xenocrystic zircons are not much older than the particular ash bed under investigation. The zircons might have very similar morphological and geochemical characteristics as the magmatic zircons deposited from the eruption, which produced the ash bed. For this study zircons which have ages with high common Pb-contents or unusually high U (or Th) contents were rejected, as were analyses which were identified as outliers via a modified 2σ set of criteria.

11.3 Dating results

11.3.1 Dwyka Group (top DS II) of the Aranos Basin (southern Namibia): tuff bed #23 IIb

The zircons extracted from this tuff bed are euhedral and of variable shape but are generally equant and stubby. Cathodoluminescence imaging reveals some prominent magmatic, compositional zoning with occasional subordinate sector zoning.

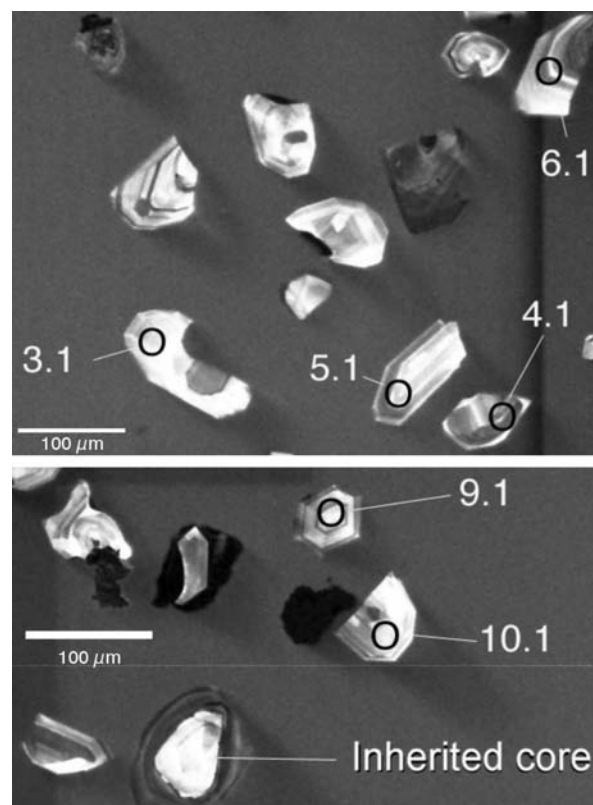


Fig. 136: Cathodoluminescence (CL) images of zircons from tuff bed #23 IIb showing morphology, internal structure and SHRIMP spot analyses. Note the sharp edges and the partly well-developed, magmatic, compositional zoning of the zircons.

A number of rounded, detrital grains were also present in the separate, as were a number of cores of inherited zircon which were not analysed in this study. U-Th-Pb SHRIMP analyses were done on seventeen different zircons, with spot positions selected using both transmitted and reflected light microphotographs and CL images (Tab. 26, Appendix G; Fig. 136).

The U-Pb data are plotted *uncorrected for common Pb* on a Tera-Wasserburg U-Pb concordia diagram (Fig. 137). Note that the data lie on a mixing line between the radiogenic Pb composition (on the concordia) and a common Pb component in this diagram. The data from these zircons plot very close to the concordia diagram and have little of the common Pb component in the total Pb measured. The Pb-loss trend for recent Pb-loss is also shown as an arrow in this figure, as this would appear to be the major cause of scatter in this data set.

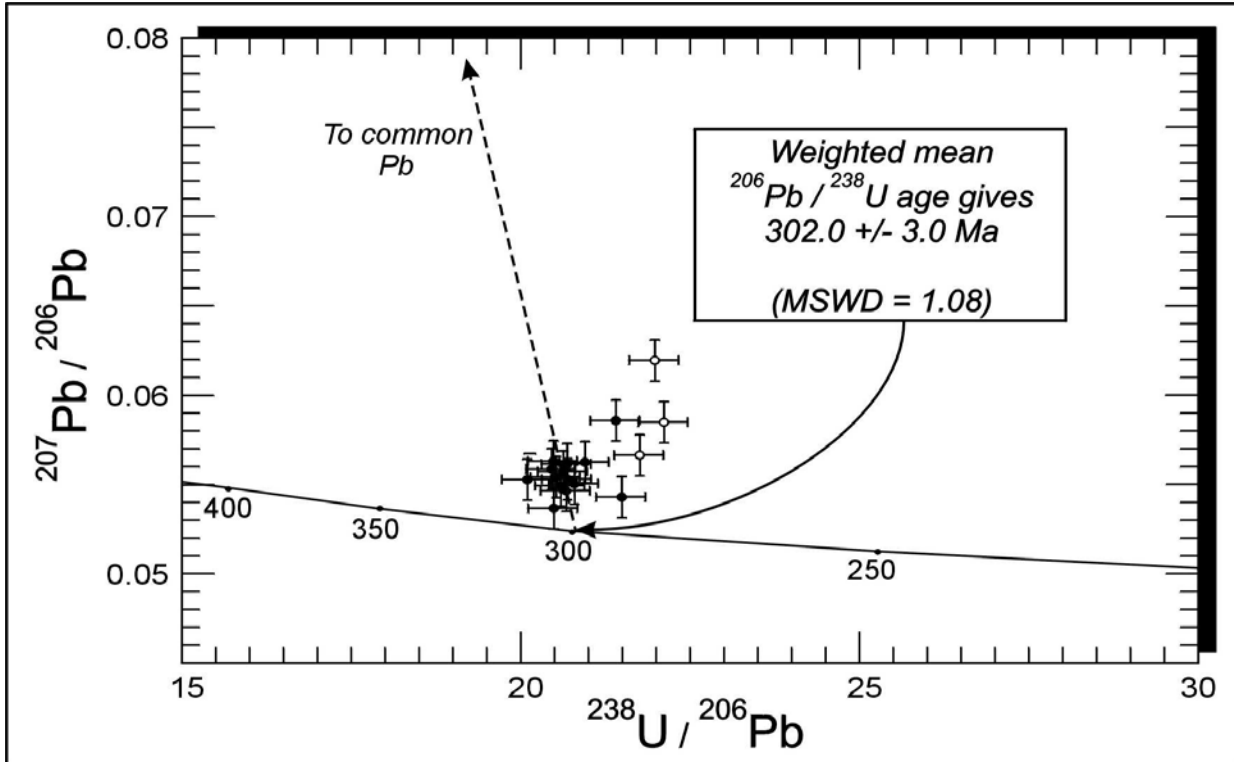


Fig. 137: Tera-Wasserburg U-Pb concordia plot of SHRIMP data of zircons separated from the tuff bed #23 IIb; plotted uncorrected for common Pb. The unfilled data points are excluded from the main group due to statistical reasons and have probably suffered Pb-loss. The dashed arrow shows the vector defining a mixing line between the common Pb composition and the radiogenic composition (on the concordia curve).

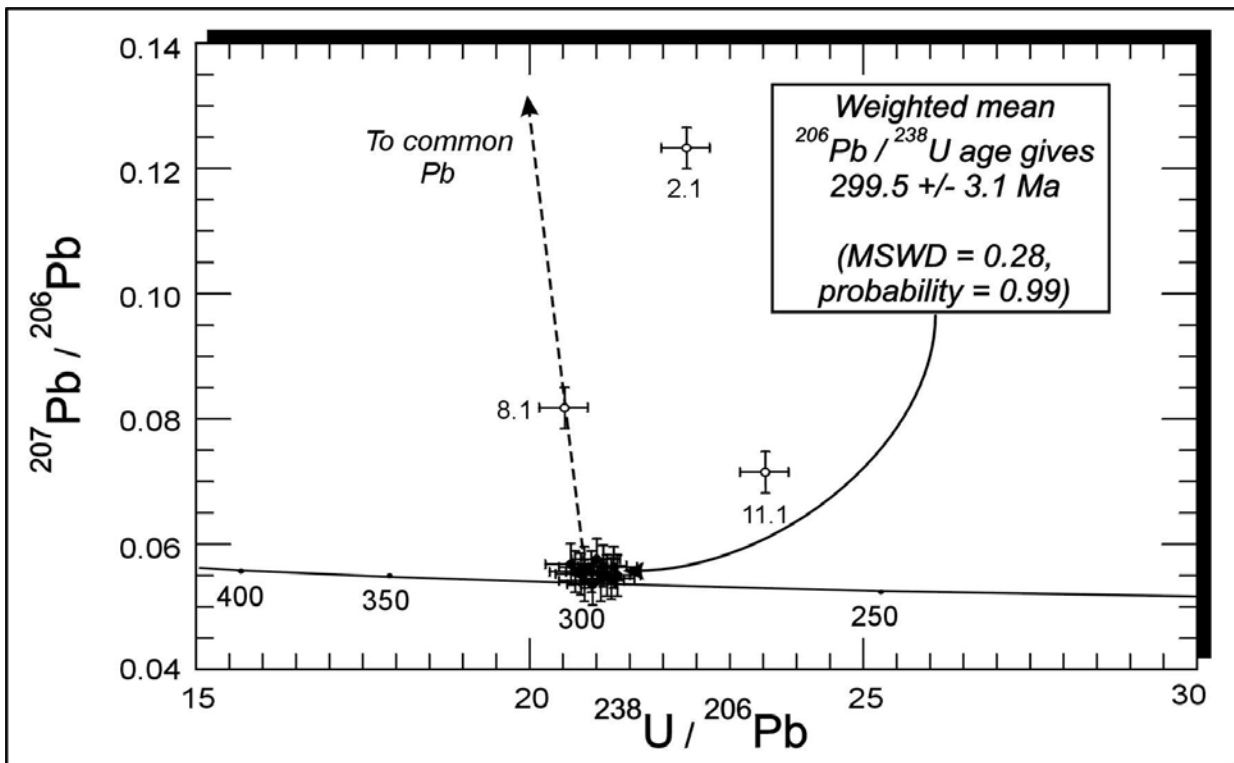


Fig. 138: Tera-Wasserburg U-Pb concordia plot of SHRIMP data of zircons separated from the tuff bed #45 IIb, plotted uncorrected for common Pb. Analyses that were excluded from the age calculation are shown as unfilled circles.

The analyses, plotted as filled circles, all conform to a single population giving a weighted mean $^{206}\text{Pb}/^{238}\text{U}$ age of **302.0. \pm 3.0 Ma** (n=14; Mean Sum of the Weighted Deviates (MSWD) = 1.08). Three analyses which fall outside this group appear to have suffered Pb loss and have not been included in the calculation.

11.3.2 Dwyka Group (top DS II) of the Aranos Basin (Namibia): tuff bed #45 IIB

The zircons of this sample are light pink and clear, and are generally euhedral, but many are broken. All zircons show strong compositional zoning with occasional sector zoning (Fig. 139)

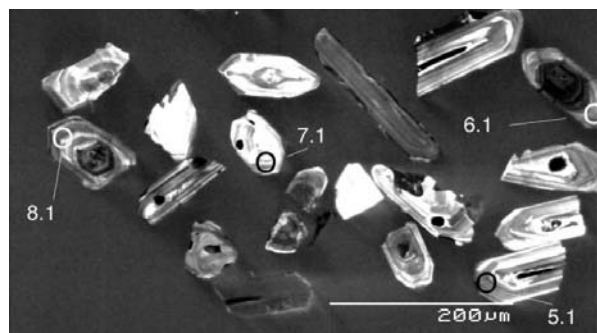


Fig. 139: CL-images of zircons from tuff bed #45 IIB showing morphology, internal structure and SHRIMP spot analyses. Note the variety of zircons shapes and the inherited cores of spotted zircons 6.1 and 8.1.

The U-Pb analyses of the zircons from this tuff bed present a relatively simple picture (Fig. 138; Tab. 27, Appendix G), with thirteen of the fifteen analyses plotting in a group near the concordia curve. These analyses show minimal common Pb and combine to give a weighted mean $^{206}\text{Pb}/^{238}\text{U}$ age of **299.5 \pm 3.1 Ma** (MSWD = 0.28; probability = 0.99). Three analyses, viz. 2.1, 8.1 & 11.1 were not considered in this age calculation, as they had relatively high common Pb-contents, and in the case of 2.1 and 11.1, had suffered Pb-loss. No inheritance was detected.

11.3.3 Dwyka Group (DS II) near Zwartbas, Karasburg Basin (southern Namibia): tuff bed IIIb

The zircons from this sample are light brown, with variable shapes from elongate to somewhat squat shapes with dominant pyramidal faces.

Irregular gas bubble inclusions and holes are common (Fig. 140).

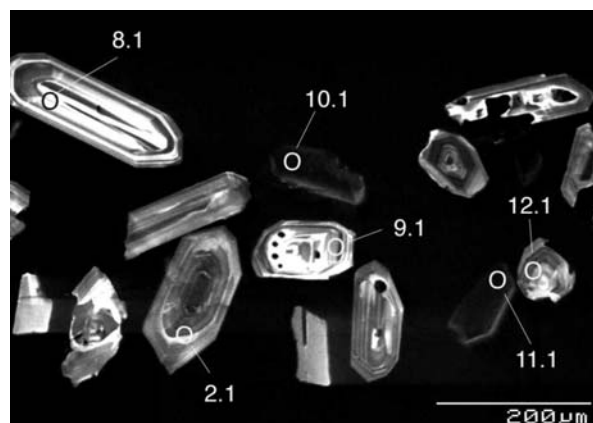


Fig. 140: CL-images of zircons from tuff bed IIIb near Zwartbas showing morphology, internal structure and SHRIMP spot analyses. Note the sharp edges and the well-developed magmatic, compositional zoning of the zircons.

A total of nineteen analyses were performed on nineteen different grains in order to determine their U-Th-Pb isotopic compositions and concentrations. The data are plotted in Fig. 141 and are listed in Tab. 28, Appendix G. It is obvious in Fig. 141 that the data points cluster near the concordia with the majority showing minimal Pb-loss and common Pb-contents. Analyses 1.1 and 13.1 have very high common Pb-contents and were therefore excluded from any age calculation. The only other analysis excluded is 8.1 which appears to have suffered Pb-loss and also has a slightly elevated common Pb-contents.

The remaining seventeen analyses are statistically part of a single age-group for which a weighted mean $^{206}\text{Pb}/^{238}\text{U}$ age of **302.3 \pm 2.1 Ma** is calculated (n=17; MSWD = 0.56, probability = 0.92). This age is interpreted to be the age of the magmatic event that produced the tuff bed.

11.3.4 Dwyka Group (DS II) near Zwartbas, Karasburg Basin (southern Namibia): tuff bed XXXIV

The heavy mineral concentrate provided for this sample was dominated by barite and Fe-oxides. Careful handpicking produced only three zircons or zircon fragments, one of which was too altered to be useful.

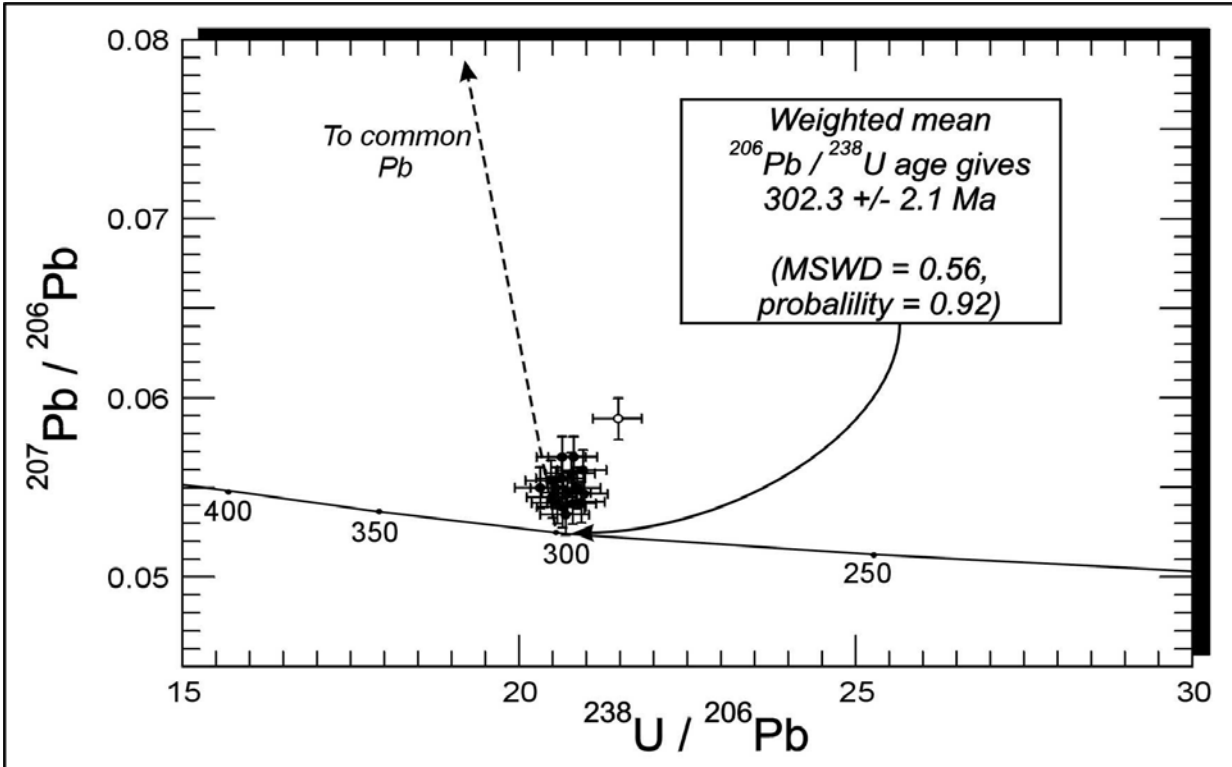


Fig. 141: Tera-Wasserburg U-Pb concordia plot of SHRIMP data of zircons separated from the tuff sample IIIb (near Zwartbas, southern Namibia); plotted uncorrected for common Pb. The unfilled data point is excluded from the main group for the reasons described in the text. Analyses 1.1 and 13.1 plot off-scale, with very high common Pb-contents.

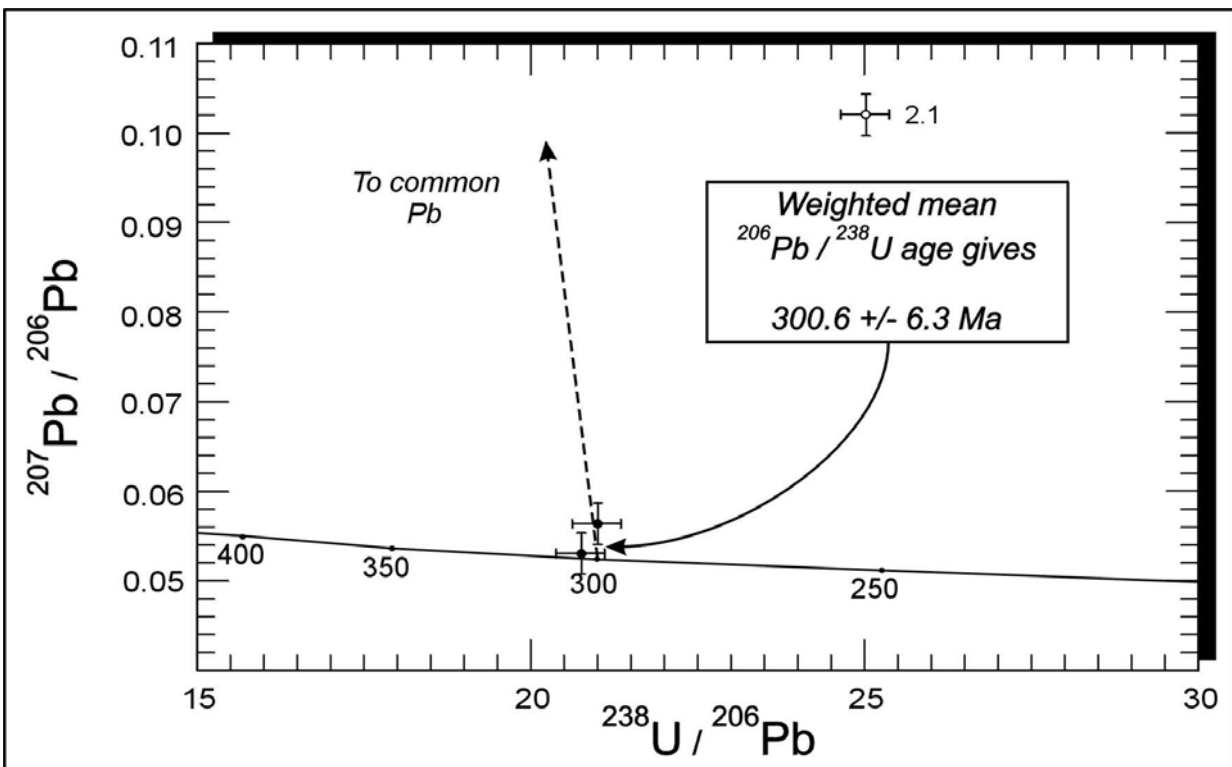


Fig. 142: Tera-Wasserburg U-Pb concordia plot of SHRIMP data from zircons separated from the tuff sample XXXIV (near Zwartbas, southern Namibia), plotted uncorrected for common Pb. The age was calculated from the two analyses displayed as filled circles.

The other two zircons show well-defined magmatic zoning and no signs of mechanical abrasion.

Only three analyses were performed on two zircons grains, with the data reported in Tab. 29, Appendix G and plotted on a Tera-Wasserburg U-Pb diagram (Fig. 142). The two analyses on grain #1 are statistically indistinguishable and give a weighted mean $^{206}\text{Pb}/^{238}\text{U}$ age of 300.3 ± 6.3 Ma. A single analysis on the second zircon revealed unexpectedly high Th and U concentrations. The relatively poor precision of the age calculated on the pooled data set is a consequence of the small number of analyses possible, but is statistically within error of the other Dwyka Group ages reported here.

11.3.5 Dwyka Group (top DS III), 30 km north of Klaarstroom, Western Cape Province, South Africa

This tuff contains numerous 72-328 μm large zircons (cf. Tab. 10) which are generally clear, only lightly coloured and euhedral. Acicular apatite and other inclusions are common.

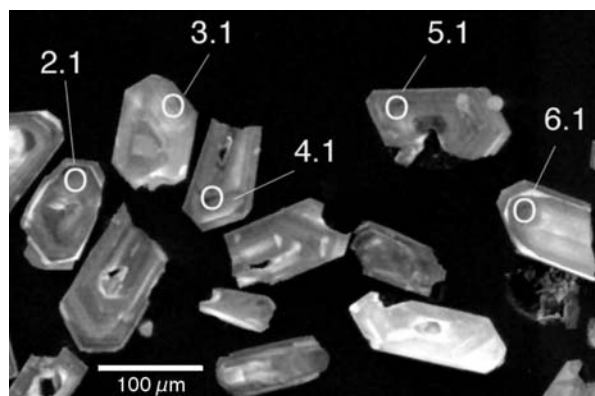


Fig. 143: CL-images of zircons from the tuffaceous bed north of Klaarstroom (Dwyka Group, South Africa) showing morphology, internal structure and SHRIMP spot analyses. Note the generally, well-developed magmatic, compositional zoning of the zircons and the growth obstruction in spotted zircon 5.1.

Cathodoluminescence images of sectioned grains clearly show the compositional zoning typically seen in zircons from felsic volcanic rocks (Fig. 143).

Nineteen U-Th-Pb SHRIMP analyses were done on nineteen different zircons. The data are reported in Tab. 30, Appendix G and are plotted on a Tera-Wasserburg U-Pb concordia diagram (Fig. 144). Most of the analyses plot as a group near concordia indicating that only minimal corrections for common Pb are required for this data set. As far as can be ascertained (by the errors on individual data points), the zircons have not suffered significant Pb-loss and with the exception of one analysis (15.1), the data set defines a single population for which a weighted mean $^{206}\text{Pb}/^{238}\text{U}$ age of 297.1 ± 1.8 Ma ($n=18$; MSWD = 0.73, probability = 0.77) is calculated. Analysis 15.1 is significantly older than the remainder of the group and this zircon is thus interpreted to be inherited. Inclusion of this analysis into the age calculation changes the weighted mean $^{206}\text{Pb}/^{238}\text{U}$ age to 297.6 ± 1.8 Ma ($n=19$; MSWD = 0.96, probability = 0.50).

11.3.6 Dwyka Group, 2 km east of Nondweni, KwaZulu-Natal, South Africa

The sample originates from a yellow, fine-grained, tuffaceous bed in an outcrop of the Dwyka Group. Zircons extracted from this sample are of variable quality and appearance, from rounded and clearly detrital zircons to clear, magmatic zircons with perfectly preserved pyramidal facets. Only the latter zircons were selected for analysis. Two analyses of the magmatic zircons yielded Proterozoic ages (Tab. 33, Appendix G) that were within error of each other and clearly came from the same source. A weighted mean $^{207}\text{Pb}/^{206}\text{Pb}$ age of 2054 ± 31 Ma can be calculated from these two analyses (Fig. 145). No further analyses were undertaken, as it appeared that this sample was unlikely to contain any Dwyka Group-aged zircons.

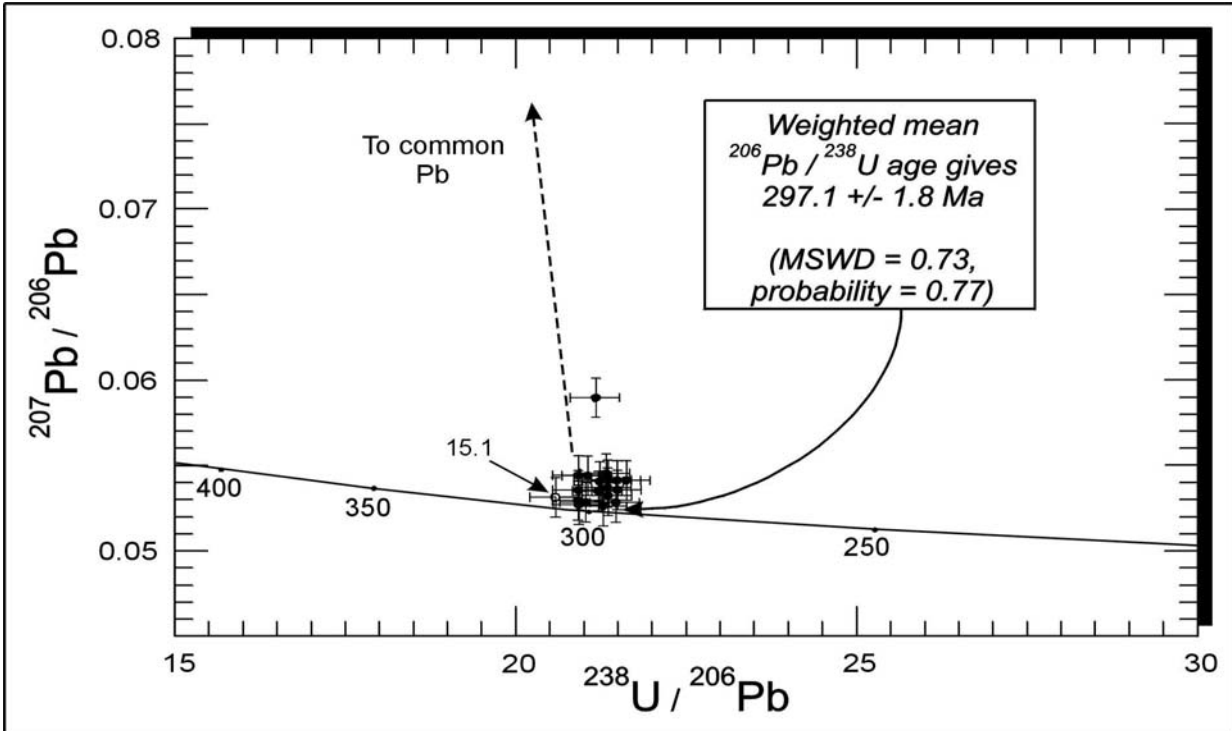


Fig. 144: Tera-Wasserburg U-Pb concordia plot of all data from zircons separated from the tuffaceous bed, 30 km north of Klaarstroom, Dwyka Group, South Africa. The data are plotted as measured ratios, i.e. uncorrected for common Pb. The unfilled data point 15.1 is excluded from the age calculation as it appears to be too old and is interpreted to be xenocrystic. The dashed arrow shows the vector defining a mixing line between the common Pb composition and the radiogenic composition (on the concordia curve).

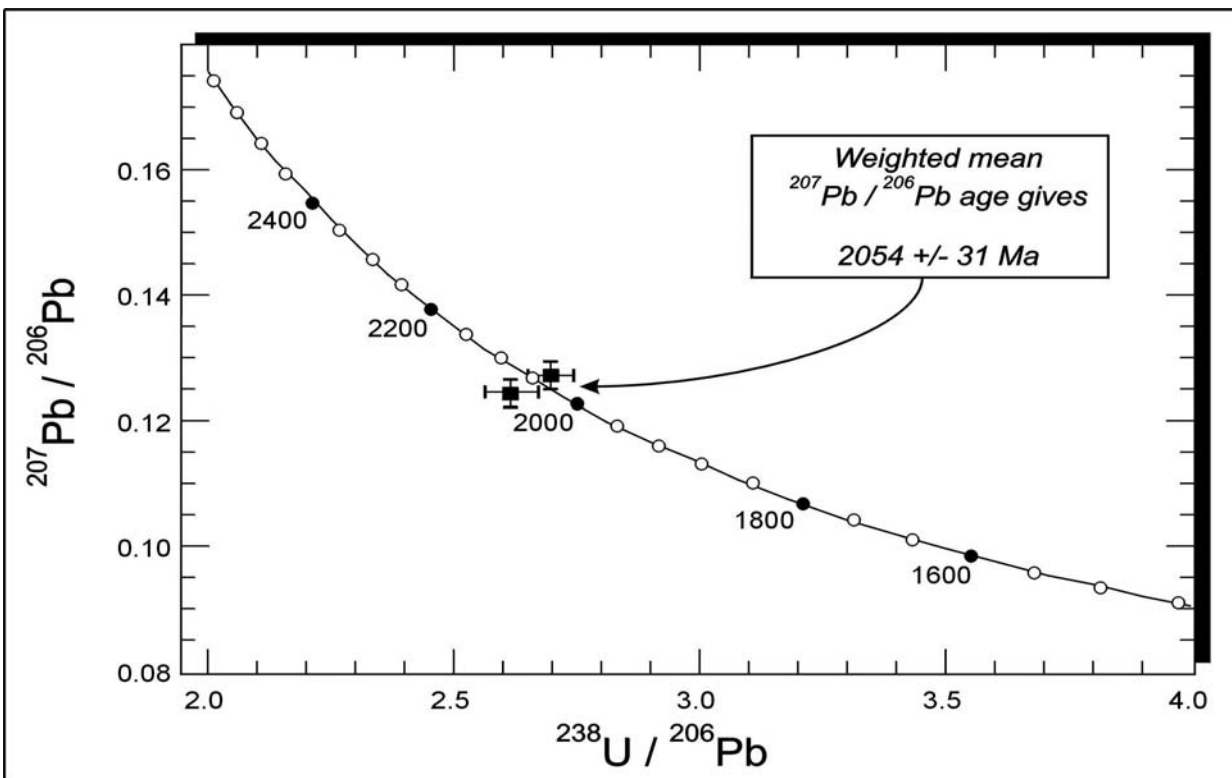


Fig. 145: SHRIMP U-Pb analyses of zircons from a volcano-sedimentary deposit 2 km east of Nondweni, Dwyka Group, KwaZulu-Natal, South Africa. Note that the data are plotted corrected for common Pb in this instance, using the measured $^{204}\text{Pb}/^{206}\text{Pb}$.

11.3.7 *Ecca Group (basal Prince Albert Formation), 30 km north of Klaarstroom, Western Cape Province, South Africa: tuff bed VIb*

The zircons from this sample are euhedral and approximately 80-208 μm in size (cf. Tab. 10). They are variable in form from elongate grains to grains which are more squat and rectangular in shape. Acicular inclusions of apatite are common. Almost all grains have well-developed magmatic compositional zoning (Fig. 146).

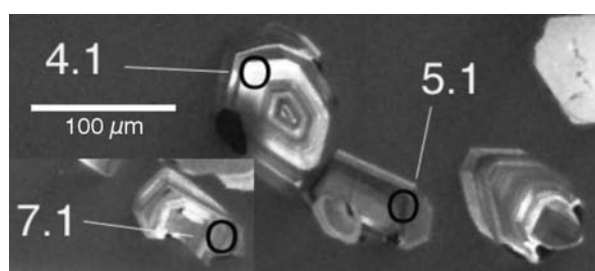


Fig. 146: Selected CL-images of zircons from tuff bed VIb north of Klaarstroom (*Ecca Group*, South Africa) showing morphology, internal structure and SHRIMP spot analyses. Note the generally, well-developed magmatic, compositional zoning of the zircons.

From this sample fifteen different zircons were analysed for their U-Th-Pb isotope compositions. The data are presented in Tab. 31, Appendix G and are plotted on a Tera-Wasserburg concordia plot (Fig. 148). Apart from one analysis (grain #8) all the data plot close to the concordia curve and thus have minimum common Pb-contents. Statistically, two of the analyses are identified as outliers and the fact that these plot to the right of the main group of data suggests that they have suffered significant recent Pb loss. The remainder of the analyses (n=12) plot as a coherent group for which a weighted mean $^{206}\text{Pb}/^{238}\text{U}$ age of **288.0 \pm 3.0 Ma** can be calculated (95% confidence limits; MSWD=1.03).

11.3.8 *Ecca Group (basal Prince Albert Formation), south of Laingsburg, Western Cape Province, South Africa*

This sample was collected from a bentonitic tuff bed of the lowermost Prince Albert Shale Formation, exposed in a road-cutting between Laingsburg and Ladismith, 13.2 km south of Laingsburg and west of Floriskraaldam. The zircons are euhedral to subhedral and of variable quality. Magmatic compositional and sector zoning is present in most zircons (Fig. 147).

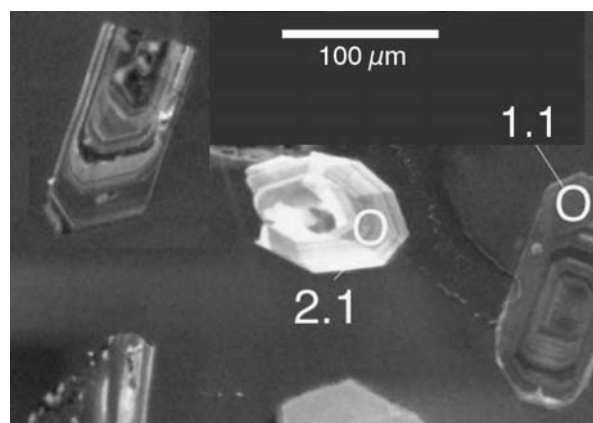


Fig. 147: Selected CL-images of zircons from a bentonitic tuff bed south of Laingsburg (*Ecca Group*, South Africa) showing morphology, internal structure and SHRIMP spot analyses. Note the well-developed magmatic, compositional zoning of all zircons making it difficult to pick out the true Dwyka Group-age magmatic component. Spotted zircon 1.1 was omitted from the age calculation as it revealed an age of 460.5 ± 5.6 whereas zircon 2.1 showed an age of 290.1 ± 5.0 Ma.

Analysis of this sample was complicated due to the heterogeneous nature of the zircon population. All zircons show well-developed sector and / or compositional zoning and have well-developed euhedral forms, making it difficult to pick out the true Dwyka Group-equivalent, magmatic component from the inherited zircons. As a result, it was necessary to perform 20 analyses on 19 different grains, resulting in a bimodal age distribution shown in Fig. 149 and Tab.32 (Appendix G). Seven of the eight analyses of the older zircons combine to yield a weighted mean $^{206}\text{Pb}/^{238}\text{U}$ age of 464 ± 5 Ma (MSWD = 1.00; probability = 0.43).

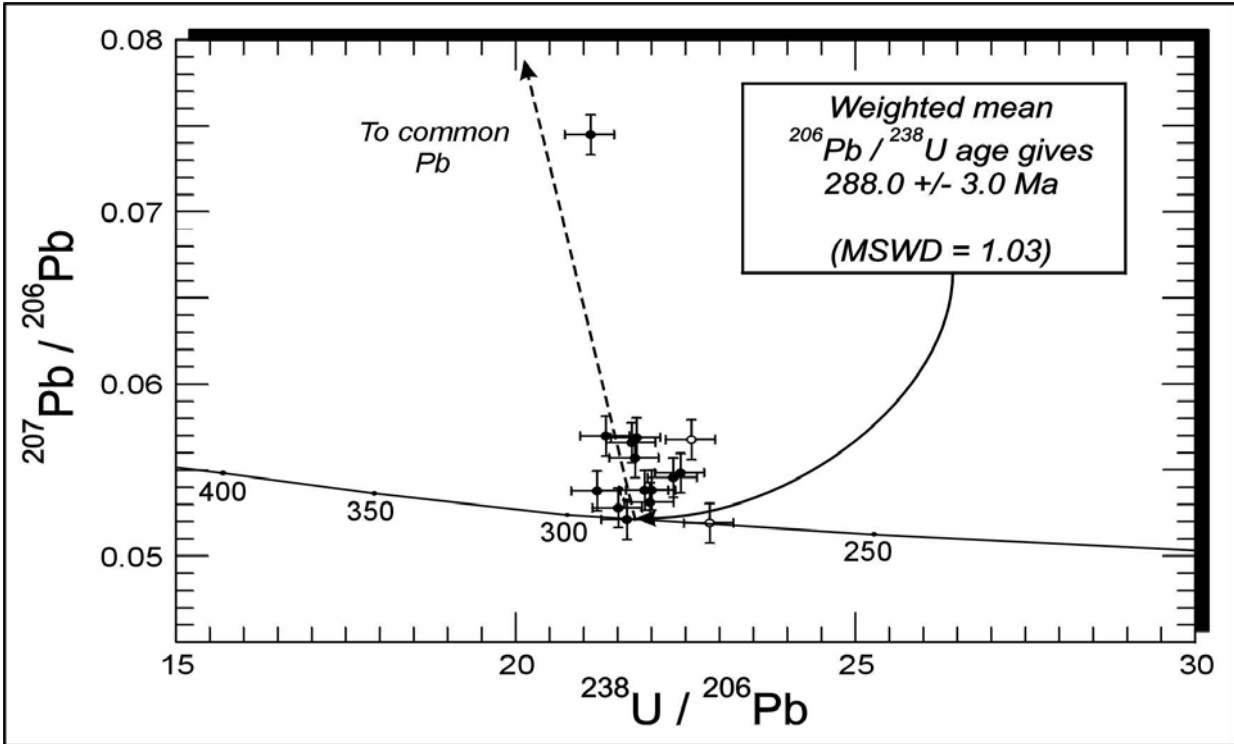


Fig. 148: Tera-Wasserburg U-Pb concordia plot of SHRIMP data of zircons separated from tuff bed VIb of the lowermost Ecca Group sampled north of Klaarstroom in the main Karoo Basin, Western Cape Province, South Africa; plotted uncorrected for common Pb. The unfilled data points are excluded from the main group due to statistical reasons and have probably suffered Pb-loss.

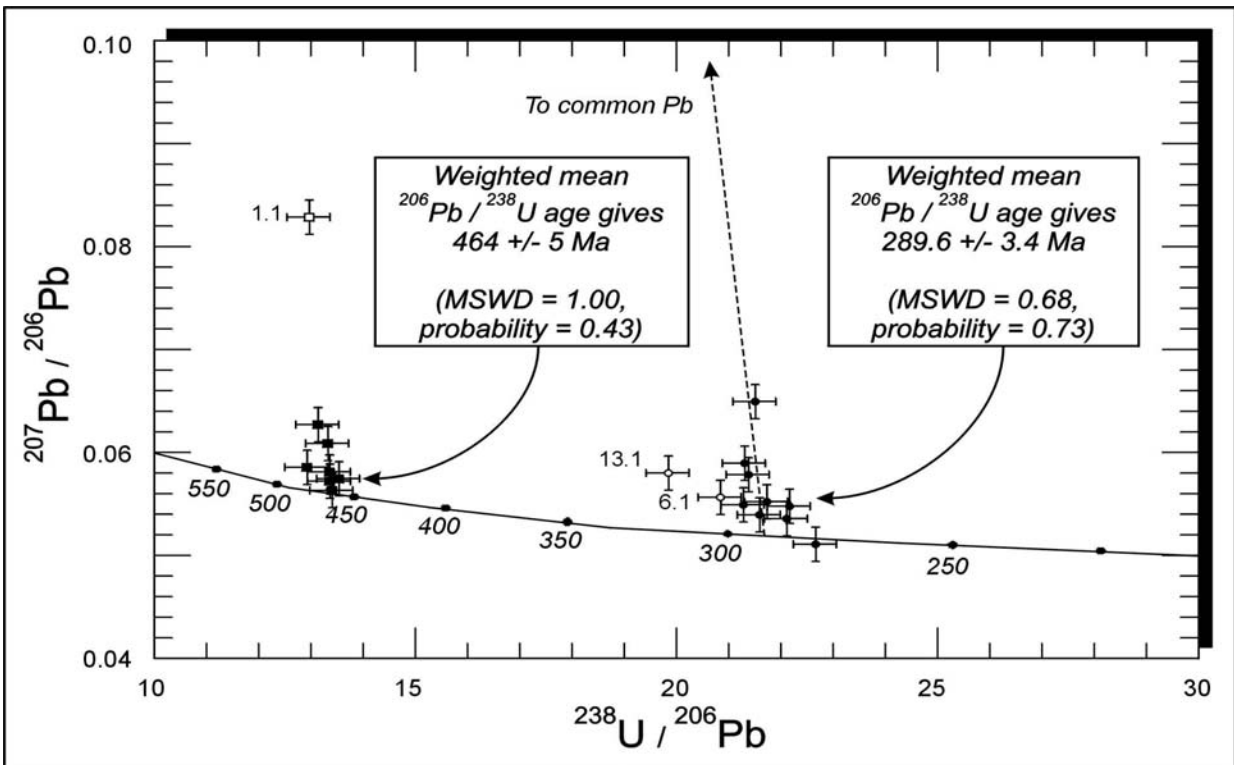


Fig. 149: Tera-Wasserburg U-Pb concordia plot of SHRIMP data of zircons separated from a tuff bed of the lowermost Ecca Group sampled south of Laingsburg, Western Cape Province, South Africa; plotted uncorrected for common Pb. Analyses that were excluded from the age calculation are shown as unfilled circles.

Analysis 1.1 was excluded from this age calculation on the basis of its elevated common Pb-contents. The younger group which comprises mainly the zircons relating to the volcanism which produced the tuff bed, is also not strictly uniform in age. Two analyses (6.1 & 13.1) appear to be inherited. The remainder of the analyses are combined to assign a weighted mean $^{206}\text{Pb}/^{238}\text{U}$ age of **289.6 ± 3.4 Ma** (MSWD = 0.68; probability = 0.73). The relatively poor precision on this age is a consequence of the complexity of the data, including possible unresolvable and subtle effects of Pb loss and inheritance within the group identified here as the relevant magmatic population.

11.4 Discussion of the new dating results

11.4.1 Aranos Basin (Namibia)

Although separated from the same tuff bed IIb which was sampled only about 8 km apart, the zircons reveal crystallisation ages ranging from a maximum of 305 Ma to a minimum of 296 Ma. As the margin of errors interfere with each other, an approximate age of 299-302 Ma is assumed. Furthermore, as the analysed zircons from #45 display a more coherent group (MSWD = 0.28) than the ones from #23 (MSWD = 1.08), the age may be situated closer to the calculated age of 299.5 Ma. All ages, however, settle within the Late Carboniferous (Stephanian respectively Kasimovian or Gzelian; Fig. 150).

11.4.2 Karasburg Basin (Namibia)

The calculated age of the zircons from tuff bed IIIb near Zwartbas is more precise than the two results from tuff bed IIb from the Aranos Basin displaying a margin of error of about 2 Ma and a MSWD of 0.56. It is similar to the determined ages from tuff bed IIb of the Aranos Basin,

especially if compared to #23 tuff IIb (302.3 vs. 302.0 Ma). It is therefore inferred that the Carboniferous, glaciomarine deposits cropping out near Zwartbas are stratigraphically located on top of DS II as the deposits of the Ganigobis Shale Member are. The age from zircons of tuff bed XXXIV was determined from only two zircons and is therefore rather imprecise. Taking the determined age of 300.6 Ma into account and considering that tuff bed XXXIV is located about 64 m above tuff bed IIIb, the mainly mud- and siltstone dominated sediment package was deposited within 1.6 Ma.

11.4.3 Western Cape Province (South Africa)

Zircons separated from the tuffaceous bed sampled about 30 km north of Klaarstroom located on top of DS III revealed an exceptional well-constrained age with the smallest margin of error (1.8 Ma) and a MSWD of 0.77. As the Carboniferous-Permian boundary is presently defined at 296 Ma (Menning *et al.*, 1997), the Carboniferous-Permian boundary is located near the tuffaceous bed within the surrounding sediments on top of DS III (Dwyka Group).

Zircons separated from two tuff beds of the basal Prince Albert Formation (Ecca Group) reveal an Early Sakmarian age (cf. Menning *et al.*, 1997). 12 measured zircons of a tuff bed from north of Klaarstroom plot as a coherent group revealing a well-constrained age with a margin of error of 3 Ma and a MSWD of 1.03 Ma. Measured zircons from a tuff bed south of Laingsburg show two groups of ages. The older ones give a weighted mean age of middle Ordovician time (464 Ma) whereas the younger ones plot as a coherent group giving an Early Sakmarian age which is identified as the relevant age of the juvenile zircon population (Fig. 150).

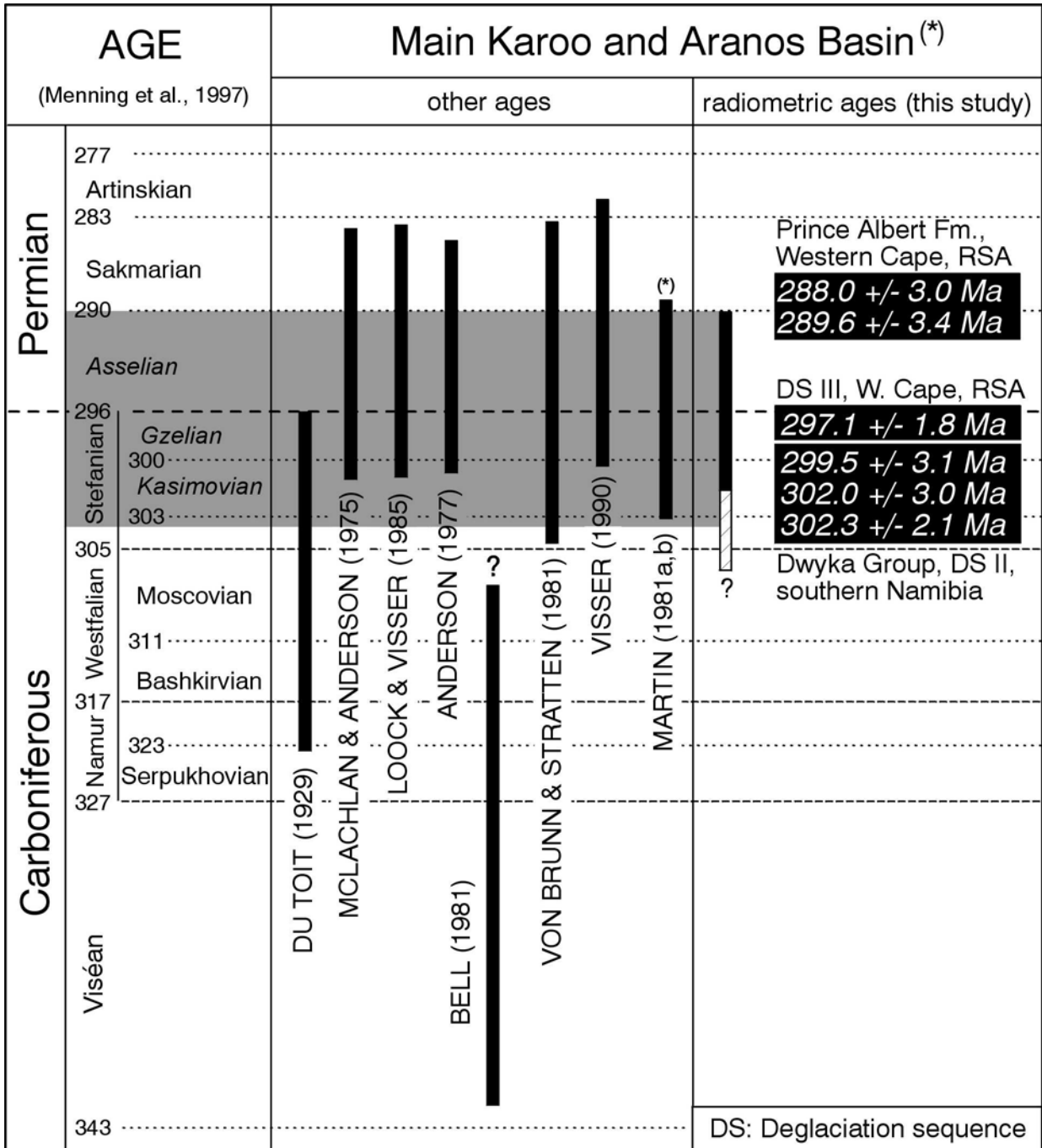


Fig. 150: Duration of the Dwyka Group in the main Karoo Basin and in the Aranos Basin from published data in comparison with radiometric ages determined in this study which reveal that the Dwyka Group lasted approximately from the Late Westphalian to Late Asselian. Used time scale according to Menning *et al.* (1997).

11.4.4 KwaZulu-Natal (South Africa)

The Proterozoic ages revealed from euhedral zircons within these beds do not coincide with any Dwyka Group-aged magmatism. The age of the zircons (2054 ± 31 Ma) rather coincides with the intrusion of the Bushveld Complex in South

Africa. The Bushveld Complex includes one of the world's largest anorogenic alkaline granite intrusions (66,000 km²) which forms a composite laccolith, of 350 x 250 km in area and about 2 km in thickness. It was emplaced at about 5 km depth into sediments overlying the Kaapvaal Craton at 2054 Ma (Ferre *et al.*, 1999).

11.6 The duration of the deglaciation sequences of the Dwyka Group

Visser (1997) estimated without having a proper age control that the duration of each of the deglaciation sequences comprises 9-11 Ma supposing that the Dwyka Group lasted a maximum of 36 Ma (Fig. 151).

The new age constraints, however, are the base for an age controlled arrangement of the deglaciation sequences assigning for the first time a precise time frame for the entire Dwyka Group of southern Africa. Taking the new age determinations into account, the duration of each of the deglaciation sequences can be estimated to last about 5-7 Ma (third-order) (Fig. 151).

The start of the deposition of the Dwyka Group will stay uncertain as basal deposits of DS I are not preserved and deposits of the upper parts of DS I are rarely known (e.g. in the vicinity of Wolwefontein, Eastern Cape Province; Visser, 1997). As glaciers or larger ice-shields have migrated back and forth, only few sediment was preserved which gives way to speculation that DS I lasted very much longer than the other deglaciation sequences. If sediment structures found in the Waaiport Formation (Witteberg Group, Western Cape Province, South Africa) are clearly of glacial origin, it may indicate the start of the Dwyka Group in that specific area. Bell (1981) reports soft sediment deformation in the uppermost Witteberg Group. It was therefore speculated that the Dwyka Group started as early as 342 Ma ago. Glacial deposition in North America started about 327 Ma but older, poorly dated glacial deposits are also known (Langhorne and Read, 2000). As the top of DS I has an approximate age of 306 Ma (Moskovich), the first deglaciation sequence could have lasted for a maximum of 36 Ma whereas DS II-IV could have lasted only for approximately 16 Ma.

The topmost part of DS II is dated with 300-302 Ma (Kasimovich) from zircons of the tuff beds in southern Namibia giving DS II a duration of 4-6 Ma. The uppermost part of DS III has an approximate age of 297-298 Ma (Gzelian/Asselian) revealed from zircons of the tuffaceous bed in the Western Cape Province

(South Africa). DS III therefore lasted for approximately 2-5 Ma.

The new SHRIMP-based age determinations (288.0 ± 3.0 Ma and 289.6 ± 3.4 Ma) of zircons separated from the tuff beds of the basal Prince Albert Formation (Ecca Group) are used for a new calibration of the Dwyka/Ecca Group boundary. As the dated tuff beds were sampled immediately above the lithostratigraphic Dwyka/Ecca Group boundary in the basal part of the Prince Albert Formation, the age of the Dwyka/Ecca Group boundary in the Western Cape Province (South Africa) can be estimated at approximately 290 Ma. This implies that the boundary approximately coincides with the Asselian/Sakmarian boundary (cf. Menning *et al.*, 1997). Consequently, DS IV lasted approximately 7-8 Ma finally leading to the complete deglaciation of southern Africa. (Fig. 152).

11.7 Eustatic sea-level changes within the lower Karoo Supergroup of southern Africa

The deglaciation sequences were controlled by four major fluctuations in the relative position of the ice margin within the basins. These fluctuations (third-order) may have been controlled by tectono-eustatic events with lowstands resulting in basinward advance of ice sheets and non-deposition. During the stillstand or slow retreat of the glaciers or ice margin, a basal diamictite was deposited. As the sea-level continued to rise, glacial retreat accelerated, causing the deposition of stratified diamictite and meltwater deposits. During the highstand, muddy sediments were deposited, but once sea-level dropped again, the ice advanced and caused the reworking of the underlying sediments, marking the top of the preceding deglaciation sequence. The presence of boulder beds and large mudstone lenses within the deglaciation sequences suggests shorter-term fluctuations superimposed on the major deglaciation (Visser, 1997).

In the following third-order sea-level changes in the Aranos Basin of southern Namibia (cf. Grill, 1997) and the main Karoo Basin (cf. Visser, 1993) will be compared with global sea-level fluctuations (Ross and Ross, 1988).

Sea-level started to rise globally with the beginning of the Westphalian (about 315 Ma) which is recorded in both basin areas (Fig. 153). The climax was reached on top of DS I (Moscovian transgression). After a short retreat, sea-level started to rise again leading to the

deposition of marine glacial deposits. The peak of this sea-level rise was reached with the top of DS II (Kasimovian transgression) where especially in southern Namibia more than 40 m thick marine mudstones (Ganigobis Shale Member) were deposited.

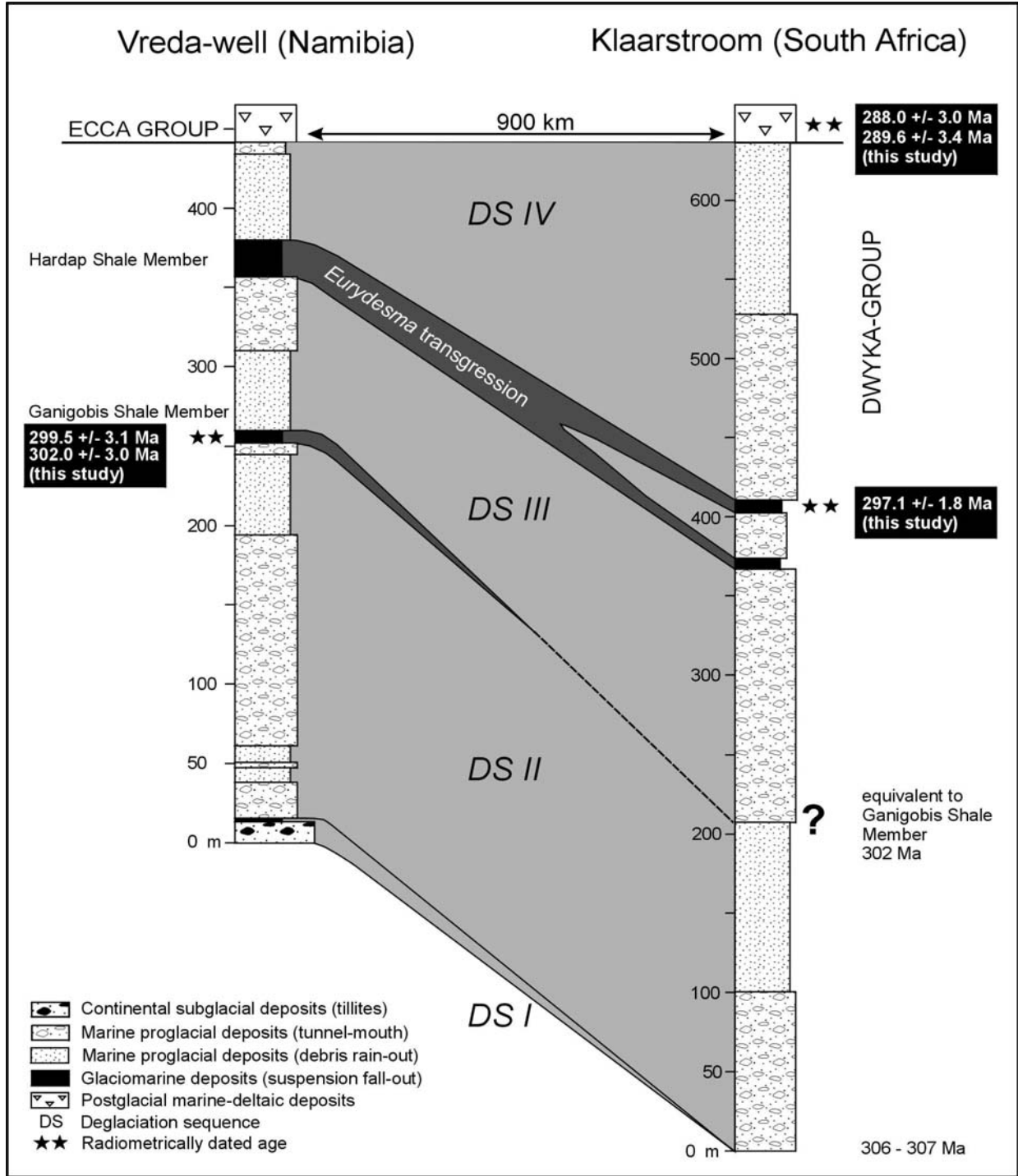


Fig. 152: Stratigraphic correlation diagram between the Dwyka Group in southern Namibia (Vreda-well) and South Africa (Klaarstroom). Deglaciation sequences (DS I - DS IV) and postulated age estimates are indicated. The new SHRIMP-based age data of zircons separated from the tuff beds of this study are marked by asterisks (Bangert *et al.*, 1999).

This transgression was also recognized globally in the sea-level curve of Ross and Ross (1988). In DS III the sea-level dropped not significantly which resulted in the deposition of clast-poor diamictites in southern Namibia, capped by the 75 m thick Hardap Shale Member (Gzelian transgression). The latter is characterised by occurrences of the marine bivalve *Eurydesma mytiloides* (Heath, 1972) and has been related to the Gondwana-wide *Eurydesma*-transgression (Dickins, 1984). DS IV shows no significant sea-level change. Sea-level probably rose to some extent at the end of DS IV due to the complete deglaciation. The transition into the Prince Albert Shale Formation (Ecca Group) in the main Karoo Basin south of Laingsburg is gradual whereas in the Aranos Basin of southern Namibia the boundary is marked by a sharp regression of the sea-level which is recorded by the turbiditic sandstones of the Nossob Member. This regression corresponds to the global sea-level fluctuations.

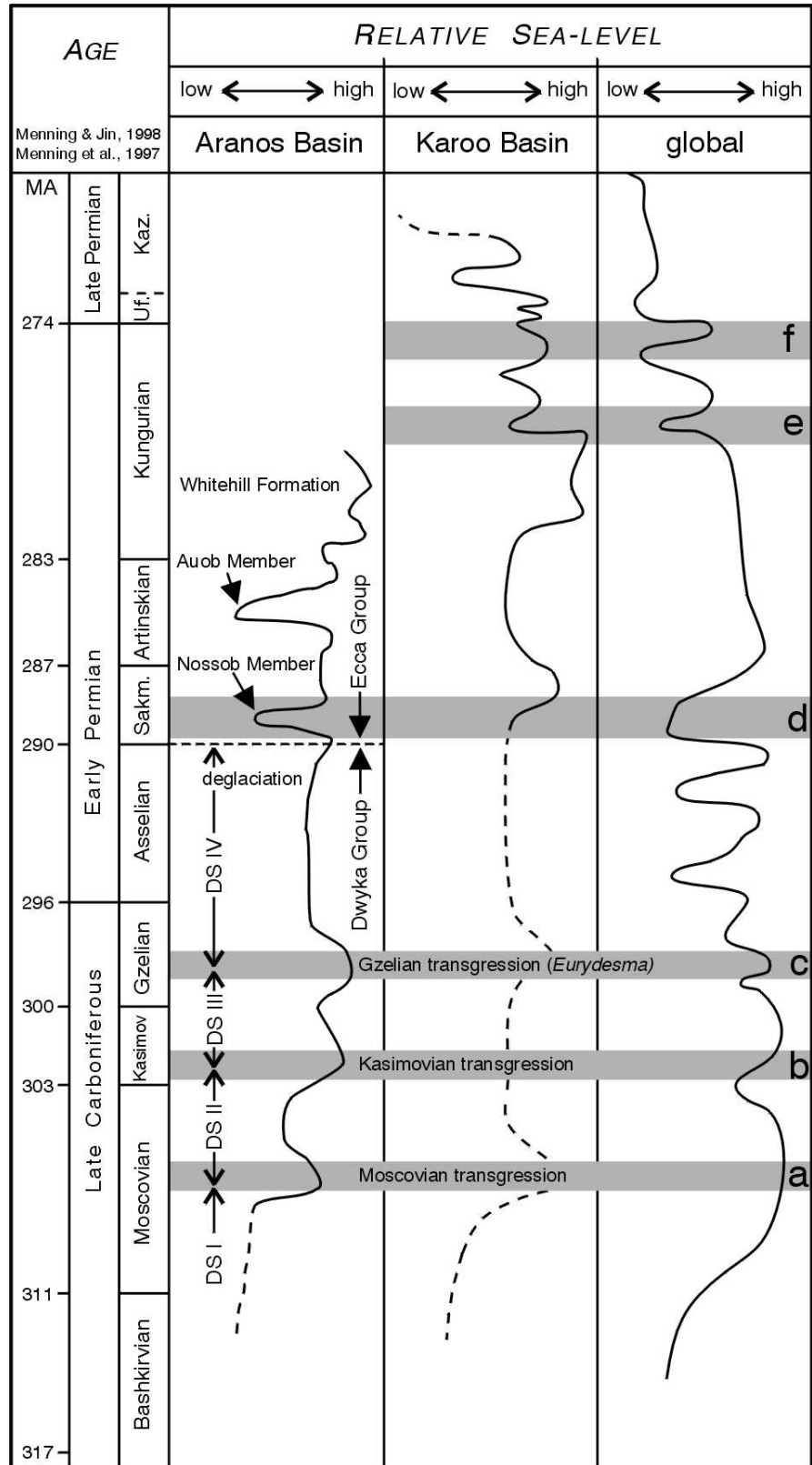


Fig. 153: Relative sea-level fluctuations during the Late Carboniferous and Early to Late Permian of the Aranos Basin (modified and revised after Grill (1997), main Karoo Basin (modified and revised after Visser (1993) and inferred global fluctuations (from Visser, 1993, after Ross and Ross, 1988). Time scale from Menning and Jin (1998) for the Permian and Menning *et al.* (1997) for the Carboniferous. A, b, c, d, e and f represent possible synchronous events, DS: deglaciation sequences (Dwyka Group), dashed lines represent uncertain data.

Contrary, the Auob Member (Ecca Group) has no counterpart in the sea-level curves of the main Karoo Basin and the global sea-level fluctuations. Transgression-regression patterns in the Kungurian coincide remarkably between the main Karoo Basin and global sea-level fluctuations. Deposits of this age are not present in the Aranos Basin of southern Namibia (Fig. 153).

The four major fluctuations of sea-level are not only preserved in the Karoo basins of southern

Africa, they are also present in the Itararé Group in Brazil. Soares *et al.* (1994) recognized four glacial sedimentary cycles which can be transformed into four stacked deglaciation sequences (Visser, 1997). Bearing in mind that these glacial deposits have the same age as the Dwyka-Group deposits in the Karoo basins, it seems likely that the four major sea-level fluctuations had been controlled by the same tectono-eustatic events.

References

- ADAMS, J. A. S. & WEAVER, C. E. (1958) Thorium-to-uranium ratios as indicators of sedimentary processes: example of concept of geochemical facies. *Bulletin of the American Association of Petroleum Geologists*, **42**(2), 387-430.
- ANDERSON, J. M. & MCLACHLAN, I. R. (1976) The plant record in the Dwyka and Ecca Series (Permian) of the south-western half of the Great Karoo Basin. *Palaeontologia africana*, **19**, 31-42.
- BANFIELD, J. F. & EGGLETON, R. A. (1990) Analytical transmission electron microprobe studies of plagioclase, muscovite, and K-feldspar weathering. *Clay and clay minerals*, **38**, 77-89.
- BANGERT, B., LORENZ, V. & ARMSTRONG, R. (1998) Bentonitic tuff horizons of the Permo-Carboniferous Dwyka-Group in Southern Africa - Volcaniclastic deposits as ideal time markers. *Journal of African Earth Sciences*, **27**(1A), 18-19.
- BANGERT, B., STOLLHOFEN, H., LORENZ, V. & ARMSTRONG, R. (1999) The geochronology and significance of ash-fallout tuffs in the glaciogenic Carboniferous-Permian Dwyka Group of Namibia and South Africa. *Journal of African Earth Sciences*, **29**(1), 33-49.
- BANGERT, B., STOLLHOFEN, H., GEIGER, M. & LORENZ, V. (2000) High resolution tephrostratigraphy, fossil record and age of Carboniferous-Permian glaciomarine mudstones within the Dwyka Group of southern Namibia. *Communications of the Geological Survey of Namibia*, **12**, 235-245.
- BANGERT, B. & BAMFORD, M. (2001) Carboniferous pycnoxylic woods from the Dwyka Group of southern Namibia. *Palaeontologia africana*, **37**, 13 - 23. BPI Paleontology, University of the Witwatersrand, Johannesburg, South Africa.
- BELL, C. M. (1981) Soft sediment deformation of sandstone related to the Dwyka glaciation in South Africa. *Sedimentology*, **28**, 321-329.
- BENDER, P. A., RUBIDGE, B. S., GARDINER, B. G., LOOCK, J. C. & BREMNER, A. T. (1991) The stratigraphic range of the paleonioscoid fish *Namaichthys digitata* in rocks of the Karoo Sequence and its palaeoenvironmental significance. *South African Journal of Science*, **87**, 468-470.
- BERGSTRÖM, S. M., HUFF, W. D., KOLATA, D. R. & MELCHIN, M. J. (1997) Occurrence and significance of Silurian K-bentonite beds at Arisaig, Nova Scotia, eastern Canada. *Canadian Journal of Earth Sciences*, **34**, 1630-1643.
- BERNER, R. A. & RAISWELL, R. (1984) C/S method for distinguishing freshwater from marine sedimentary rocks. *Geology*, **12**, 365-368.
- BLATT, H., MIDDELTON, G. & MURRAY, R. (1980) *Origin of Sedimentary Rocks*. Prentice - Hall Inc., Englewood Cliffs, N.J., U.S.A., 782 pp.
- BOENIGK, W. (1983) *Schwermineralanalyse*. Enke, Stuttgart, 152 pp.
- BOHOR, B. F. & TRIPLEHORN, D. M. (1993) Tonsteins: Altered volcanic-ash layers in coal-bearing sequences. *Geological Society of America Special Publication*, **285**, 44 pp.
- BRIME, C. (1985) The accuracy of X-ray diffraction methods for determining mineral mixtures. *Mineralogical Magazine*, **49**, 531-538.
- BRODZIKOWSKI, K. & VAN LOON, A. J. (1991) *Glacigenic sediments*. Elsevier, Amsterdam, 674 pp.
- CAMINOS, R., LLAMBIANS, E. J., RAPELA, C. W. & PARCIA, C. A. (1988) Late Palaeozoic - Early Triassic magmatic activity of Argentina and the significance of new Rb-Sr ages from northern Patagonia. *Journal of South American Earth Sciences*, **1**, 137-145.
- CHUNG, F. H. (1974a) Quantitative interpretation of X-ray patterns of mixtures. I. Matrix flushing method for quantitative multi-component analysis. *Journal of Applied Crystallography*, **7**, 519-525.

- CHUNG, F. H. (1974b) Quantitative interpretation of X-ray patterns of mixtures. II. Adiabatic principle of X-ray diffraction analysis of mixtures. *Journal of Applied Crystallography*, **7**, 526-531.
- COLE, D. I. & WICKENS, H. DE. V. (1998) Lower Karoo Supergroup: glacial, basinal and terrestrial environments in the south-western part of the main Karoo basin. In: *Guidebook 10 th Gondwana Conference*, pp. 77, University of Cape Town, South Africa.
- COLLINSON, J. W., ISBELL, J. L., ELLIOT, D. H., MILLER, M. F. & MILLER, J. M. G. (1994) Permian-Triassic Transantarctic basin. In: *Permian - Triassic Pangaeon Basins and Foldbelts along the Panthalassan Margin of Gondwanaland.*, Vol. 184 (Ed. by J. J. Veivers and C. M. Powell), pp. 173-222. Geological Society of America Memoir, Boulder, Colorado, USA.
- COMPSTON, W., WILLIAMS, I. S., KIRSCHVINK, J. L., ZHANG, Z. & MA, G. (1992) Zircon U-Pb ages for the Early Cambrian time-scale. *Journal of the Geological Society, London*, **149**, 171-184.
- CROWELL, J. C. & FRAKES, L. A. (1975) The Late Palaeozoic glaciation. In: *International Gondwana Symposium 3* (Ed. by E. S. W. Campbell), pp. 313-331. University Press, Canberra.
- CUMMING, G. L. & RICHARDS, J. R. (1975) Ore lead isotope ratios in a continuously changing Earth. *Earth Planetary Science Letter*, **28**, 155-171.
- DAVIES, S. J. & ELLIOTT, T. (1996) Spectral gamma ray characterisation of high resolution sequence stratigraphy: examples from the Clare Basin, western Ireland. In: *High Resolution Sequence Stratigraphy: Innovations and Applications*, Vol. 140 (Ed. by J. A. Howell and J. F. Aitken), pp. 25-35. Geological Society Special Publications, London.
- DECHER, A., BECHTEL, A., ECHLE, W., FRIEDRICH, G. & HOERNES, S. (1996) Stable isotope geochemistry of bentonites from the island of Milos (Greece). *Chemical Geology*, **129**, 101-113.
- DEER, W. A., HOWIE, R. A. & ZUSSMAN, J. (1992) *An introduction to the rock-forming minerals*. Longman, Scientific & Technical, Harlow, England, 696 pp.
- DICKINS, J. M. (1961) *Eurydesma* and *Peruvispira* from the Dwyka beds of South Africa. *Paleontology*, **4**(1), 138-148.
- DICKINS, J. M. (1984) Late Palaeozoic glaciation. *BMR J. Austr. Geol. Geophys*, **9**, 163-169.
- DICKINS, J. M. (1996) Problems of a Late Palaeozoic glaciation in Australia and subsequent climate in the Permian. *Palaeogeography, Palaeoclimatology, Palaeoecology*, **125**, 185-197.
- DIEKMANN, B. (1993) Paläoklima und glazigene Karoo-Sedimente des späten Paläozoikums in SW-Tansania., Dissertation, Universität Köln, 183 pp.
- DONALDSON, C. H. & HENDERSON, C. M. B. (1980) A new interpretation of round embayments in quartz crystals. *Mineralogical Magazine*, **52**, 27-33.
- DOS SANTOS, P. R., ROCHA-CAMPOS, A. C. & CANUTO, J. R. (1996) Patterns of Late Palaeozoic deglaciation in the Paraná Basin, Brazil. *Palaeogeography, Palaeoclimatology, Palaeoecology*, **125**, 165-184.
- EBERL, D. D., SRODON, J., KRALIK, M., TAYLOR, B. E. & PETERMAN, Z. E. (1990) Ostwald ripening of clays and metamorphic minerals. *Science*, **248**, 474-475.
- ELDHOLM, O. & THOMAS, E. (1993) Environmental impact of volcanic margin formation. *Earth and Planetary Science Letters*, **117**, 319-329.
- ELLIOT, D. H. & WATTS, D. R. (1974) The nature and origin of volcanoclastic material in some Karoo and Beacon rocks. *Transactions of the Geological Society South Africa*, **77**, 109-111.
- EVANS, F. J. (1998) Taphonomy of some Upper Palaeozoic actinopterygian fish from southern Africa. *Journal of African Earth Sciences*, **27**(1A), 69-70.
- EYLES, N. & EYLES, C. H. (1993) Glacial geological confirmation of an interplate boundary in the Paraná basin of Brazil. *Geology*, **21**, 459-

462.

- FERRE, E. C., WILSON, J. & GLEIZES, G. (1999) Magnetic susceptibility and AMS of the Bushveld alkaline granites, South Africa. *Tectonophysics*, **307**(1-2), 113-133.
- FISHER, I. S. & HUDSON, J. D. (1987) Pyrite formation in Jurassic shales of contrasting biofacies. In: *Marine geological source rocks*, Vol. 26 (Ed. by J. Brooks and K. W. Glennie), pp. 69-78. Geological Society Special Publication, London, U.K.
- FISHER, R. V. & SCHMINCKE, H. U. (1984) *Pyroclastic Rocks*. Springer, Berlin, 472 pp.
- FRAKES, L. A. & CROWELL, J. C. (1969) Late Palaeozoic Glaciation, I, South America. *Bulletin of the Geological Society of America*, **80**, 1007-1042.
- FRANÇA, A. B. & POTTER, P. E. (1988) Estratigrafia, ambiente deposicional e análise de reservatório do Grupo Itararé (Permo-Carbonífero), Bacia do Paraná (Parte 1). *Boletim de Geociências da Petrobras*, **2**, 147-191.
- FREY, R. W. & COWLES, J. (1969) New observations on Tisoa, a trace fossil from Lincoln Creek Formation (mid-Tertiary) of Washington. *Compass of Sigma Gamma Epsilon*, **47**(1), 10-22.
- FRIEDL, J. & SCHWERTMANN, U. (1996) Aluminium influence on iron oxides; XVIII, The effect of Al substitution and crystal size on magnetic hyperfine fields of natural goethites. *Clay Minerals*, **31**(4), 455-464.
- FROMMHERZ, B. (1998) Palaeoecology of Westphalian and Stephanian fluvio-lacustrine strata in the Saar Basin (SW Germany): a synthesis of the macro- and microflora. Dissertation, Würzburg, 309 pp.
- GARDINER, B. G. (1962) *Namaichthys schroederi* Gürich and other Palaeozoic fishes from South Africa. *Palaeontology*, **5**, 9-21.
- GEIGER, M. (2000a) An explanation of the Geological Map 1:10 000 of the Namibian borderland along the Orange River at Zwartbas - Warmbad District - Karas Region - Namibia. Diploma Thesis, Universität Würzburg, 80 pp.
- GEIGER, M. (2000b) The geology of the southern Warmbad Basin margin - tephrostratigraphy, age, fossil record and sedimentary environment of Carboniferous-Permian glaciogenic deposits of the Dwyka Group, Zwartbas, southern Namibia. Diploma Thesis, Universität Würzburg, 79 pp.
- GERSCHÜTZ, S. (1996) Geology, volcanology, and petrogenesis of the Kalkrand Basalt Formation and the Keetmanshoop dolerite complex, southern Namibia. Dissertation, Universität Würzburg, 186 pp.
- GOULD, R. E. & DELEVORYAS, T. (1977) The biology of *Glossopteris*: evidence from petrified seed-bearing and pollen-bearing organs. *Alcheringa*, **1**, 387-399.
- GOVINDARAJU, K. (1995) 1995 working values with confidence limits for twenty-six CRPG, ANRT and IWG-GIT geostandards. *Geostandards Newsletter*, **19** (Special Issue), 1-32.
- GRABAU, A. W. (1936) Revised classification of the Palaeozoic systems in the light of the pulsation theory. *Geological Society of China*, **15**(1), 23-51.
- GRESSE, B. G. & GERMS, G. J. B. (1993) The Nama foreland basin; sedimentation, major unconformity bounded sequences and multisided active margin advance. *Precambrian Research*, **63**(3-4), 247-272.
- GRILL, H. (1997) The Permo-Carboniferous glacial to marine Karoo record in southern Namibia: sedimentary facies and sequence stratigraphy. *Beringeria*, **19**, 98 pp.; Würzburg
- GUNTORPE, R. J. (1987) Final report, Samoa and Tevrede prospecting grants (M46/3/1240 and 1241), Otjiwarongo District, South West Africa/Namibia., Tsumeb Corp. Ltd., 14 pp, Tsumeb, Namibia.
- GÜRICH, G. (1923) Acrolepis lotzi und andere Ganoiden aus den Dwyka Schichten von Ganikobis, Südwestafrika. *Beiträge zur geologischen Erforschung der Deutschen Schutzgebiete*, **19**, 26-74.

- HÄLBICH, I. W., FITCH, F. J. & MILLER, J. A. (1983) Dating the Cape orogeny. In: *Geodynamics of the Cape Fold Belt., Vol. 12* (Ed. by A. P. G. Söhnge and I. W. Hälbich), pp. 149-164. Geological Society of South Africa Special Publications.
- HARTMANN, G. (1994) Late-medieval glass manufacture in the Eichsfeld region (Thuringia, Germany). *Chemie der Erde*, **54**, 103-124.
- HAUGHTON, S. H. & FROMMURZE, H. F. (1927) The Karroo Beds of the Warmbad District, South West Africa. *Transactions of the Geological Society South Africa*, **30**, 133-142.
- HEATH, D. C. (1972) Die geologie van die Sisteem Karoo in die gebied Mariental-Asab, Suidwes-Afrika. *Memoir of the Geological Survey of South Africa*, **61**, 36 pp.
- HEIKEN, G. (1974) An atlas of volcanic ash. *Smithsonian Contribution to Earth Sciences*, **12**, 101 pp.
- HEIKEN, G. & WOHLLETZ, K. (1985) Volcanic ash. University of California Press, Berkeley, California, U.S.A., 246 pp.
- HEIM, D. (1960) Über die Petrographie und Genese der Tonsteine aus dem Rotliegend des Saar-Nahe-Beckens. *Beiträge zur Mineralogie und Petrographie*, **7**, 281-317.
- HEIM, D. (1970) Die Tonsteine im Unterrot-liegend des Saar-Nahe-Gebietes. *Zeitschrift der deutschen geologischen Gesellschaft*, **120**, 297-307.
- HEIM, D. (1971) Über den 'Hygrophyllit' im Rotliegenden des Saar-Nahe-Gebietes, ein Beitrag zur Diagenese pyroklastischer Gesteine. *Contributions to Mineralogy and Petrology*, **32**, 149-164.
- HEIM, D. (1990) Tone und Tonminerale. Enke, Stuttgart, Germany, 157 pp.
- HEINRICH, H. (1988) Origin and consequences of cyclic ice rafting in the Northeast Atlantic ocean during the past 130 000 years. *Quaternary Research*, **29**(2), 142-152.
- HENNINGSEN, D. (1967) Crushing of sedimentary rock samples and its effect on shape and number of heavy minerals. *Sedimentology*, **7**, 253-255.
- HO TUN, E. (1979) Volcaniclastic material in the Lower Beaufort Group, Karoo Rocks. In: *Geocongress 1979*, Vol. 79, pp. 197-199. Geological Society of South Africa, Port Elizabeth.
- HOLZFÖRSTER, F. & STOLLHOFEN, H. (in press) Early Permian deposits of the Huab Area, NW Namibia: a continental to marine transition. (Ed. by the Geological Survey of Namibia), Windhoek, Namibia.
- HOPPE, G. (1963) Die Verwendbarkeit morphologischer Erscheinungen an akzessorischen Zirkonen für petrogenetische Auswertungen. Akademie-Verlag, Berlin, 130 pp.
- HORSTHEMKE, E., LEDENDECKER, S. & PORADA, H. (1990) Depositional environments and stratigraphic correlations of the Karoo Sequence in north-western Damaraland. *Communications Geological Survey of Namibia*, **6**, 63-73.
- HUFF, W. D. (1983) Correlation of Middle Ordovician K-bentonites based on chemical fingerprinting. *Journal of Geology*, **91**, 657-669.
- HUFF, W. D., ANDERSON, T. B., RUNDLE, C. C. & ODIN, G. S. (1991) Chemostratigraphy, K-Ar ages and illitization of Silurian K-bentonites from the Central Belt of the Southern Uplands-Down-Long-ford terrane, British Isles. *Journal of the Geological Society London*, **148**, 861-868.
- HUFF, W. D. & KOLATA, D. R. (1989) Correlation of K-bentonite beds by chemical fingerprinting using multivariate statistics. In: *Quantitative Dynamic Stratigraphy*. (Ed. by T. A. Cross), pp. 567-577. Prentice Hall, London, UK.
- HUFF, W. D., MORGAN, D. J. & RUNDLE, C. C. (1996) Silurian K-bentonites of the Welsh Borderlands: Geochemistry, mineralogy and K-Ar ages of illitization. In: *Technical Report, Vol. WG/96/45* (Ed. by the British Geological Survey), 25 pp., Keyworth, Nottingham, UK.
- HUTTON, C. O. (1950) Studies of heavy detrital minerals. *Geological Society of America Bulletin*, **61**, 635-710.

- IJIMA, A. (1978) Geological occurrences in marine environments. In: *Natural zeolites: occurrence, properties, use*. (Ed. by L. B. Sand and S. A. Mumpton), pp. 175-198. Pergamon Press, Oxford, England.
- IZETT, G. A. (1981) Volcanic ash beds: Records of Upper Cenozoic silicic pyroclastic volcanism in the Western United States. *Journal of Geophysical Research*, **86**, 10200-10222.
- JCPDS (1974) Selected powder diffraction data for minerals. JCPDS, Pennsylvania, USA.
- JEYASINGH, D. E. P. & KUMARASAMY, D. (1995) An unusual pyncnoxylic wood from the upper Gondwana locality in Tamil Nadu, India. *Review of Palaeobotany and Palynology*, **85**(3-4), 341-350.
- JOHNSON, M. R., VAN VUUREN, C. J., HEGENBERGER, W. F., KEY, R. & SHOKO, U. (1996) Stratigraphy of the Karoo Supergroup in southern Africa: an overview. *Journal of African Earth Sciences*, **23**(1), 3-15.
- JOHNSTON, M. R. & STEVENS, G. R. (1985) Fossil evidence of the age of Brook Street Volcanics Group, Nelson. *New Zealand Journal of Geology and Geophysics*, **28**(4), 743-750.
- JUBB, R. A. & GARDINER, B. G. (1975) A preliminary catalogue of identifiable fossil fish material from southern Africa. *Annales South African Museum*, **76**, 381-440.
- KARPETA, W. P. (1996) Tuffs from the Permian Teekloof Formation (Beaufort Group) from Murraysburg and Aberdeen, Cape Province - Their origin and alteration. *South African Journal of Geology*, **99**, 51-67.
- KAY, S. M., RAMOS, V. A., MPODOZIS, C. & SRUOGA, P. (1989) Late Palaeozoic to Jurassic silicic magmatism at the Gondwana margin: Analogy to the Middle Proterozoic in North America. *Geology*, **17**, 324-328.
- KEY, R. M., TIDI, J., MCGEORGE, I., AITKEN, G., CADMAN, A. & ANSCOMBE, J. (1998) The Lower Karoo Supergroup geology of the southeastern part of the Gemsbok Sub-basin of the Kalahari Basin, Botswana. *South African Journal of Geology*, **101**(3), 225-236.
- KEYSER, N. & ZAWADA, P. K. (1988) Two occurrences of ash-flow tuff from the lower Beaufort Group in the Heilbron-Frankfort area, northern Orange Free State. *South African Journal of Geology*, **91**(4), 509-521.
- KIIPLI, T., KIIPLI, E. & KALLASTE, T. (1997) Metabentonite composition related to sedimentary facies in the lower Silurian of Estonia. *Proceedings of the Estonian Academy of Sciences*, **46**(2), 93-104.
- KOLATA, D. R., FROST, J. K. & HUFF, W. D. (1986) K-bentonites of the Ordovician Decorah Subgroup, Upper Mississippi Valley: Correlation by chemical fingerprinting. Illinois State Geological Survey, Circular **537**, 30 pp., Champaign, Illinois, USA.
- KOLATA, D. R., HUFF, W. D. & BERGSTRÖM, S. M. (1996) Ordovician K-bentonites of eastern North America. *Geological Society of America Special Paper*, **313**, 84 pp.
- KÖNIGER, S. (1999) Distal ash tuffs in the lowermost Permian of the Saar-Nahe Basin (SW-Germany): Distribution, sedimentology, volcanology, petrography, geochemistry, and zircon ages. Dissertation, Universität Würzburg, 269 pp.
- KRÄUSEL, R. (1956a) Hölzer aus dem südlichen Gebiet der Karru-Schichten Südwest-Afrikas. *Senckenbergiana lethaea*, **37**, 447-453.
- KRÄUSEL, R. (1956b) Der "Versteinerte Wald" im Kaokoveld, Südwest-Afrika. *Senckenbergiana lethaea*, **37**, 411-426.
- KUBANEK, F. & ZIMMERLE, W. (1986) Tuffe und kieselige Tonschiefer aus dem tieferen Unterkarbon der Bohrung Adlersberg (West-Harz). *Geologisches Jahrbuch*, **D 78**, 207-268.
- KUTZBACH, J. E. (1994) Idealised Pangean climates: sensitivity to orbital change. In: *Pangea: palaeoclimate, tectonics and sedimentation during accretion, zenith, and breakup of a supercontinent.*, Vol. 288 (Ed. by G. Klein), pp. 41-55. Geological Society America, Special Publications, Boulder, Colorado, U.S.A.

- LANE, N. G. & FRAKES, L. A. (1970) A Permian starfish from South West Africa. *Journal of Palaeontology*, **44**, 1135-1136.
- LANGHORNE, B. S. J. & READ, J. F. (2000) Rapid onset of Late Palaeozoic glaciation on Gondwana: Evidence from Upper Mississippian strata of the Midcontinent, United States. *Geology*, **28**(3), 279-282.
- LE BAS, M. J., LE MAITRE, R. W., STRECKEISEN, A. & ZANETTIN, A. (1986) A chemical classification of volcanic rocks based on the total alkali-silica diagram. *Journal of Petrology*, **27**, 745-750.
- LOCK, B. E. & JOHNSON, M. R. (1974) A crystal tuff from the Ecca near Lake Mentz, Eastern Cape Province. *Transactions Geological Society South Africa*, **77**, 373-374.
- LOCK, B. E. & WILSON, J. D. (1975) Discussion on "The nature and origin of volcanoclastic material in some Karoo and Beacon rocks". *Transactions Geological Society of South Africa*, **78**, 171.
- LUDWIG, K. R. (1999) Isoplot/Ex version 2.00: A Geochronological Toolkit for Microsoft Excel. *Berkeley Geochronology Center Special Publication*, **1a**, 46 pp.
- MANGE, M. A. & MAURER, H. F. W. (1991) *Schwerminerale in Farbe*. Enke, Stuttgart, 148 pp.
- MARTIN, H. (1953) Notes on the Dwyka succession and on some pre-Dwyka valleys in South West Africa. *Transactions of the Geological Society of South Africa*, **56**, 37-41.
- MARTIN, H. (1975) Structural and palaeogeographical evidence for an Upper Palaeozoic sea between southern Africa and South America. In: *International Gondwana Symposium 3* (Ed. by E. S. W. Campbell), pp. 37-51. University Press, Canberra, Australia.
- MARTIN, H. (1981a) The Late Palaeozoic Dwyka Group of the South Kalahari Basin in Namibia and Botswana and the subglacial valleys of the Kaokoveld in Namibia. In: *Earth's pre-Pleistocene glacial record, Vol. A8* (Ed. by M. J. Hambrey and W. B. Harland), pp. 61-66. Cambridge University Press, New York.
- MARTIN, H., WALLISER, O. H. & WILCZEWSKI, N. (1970) A goniatite from the glaciomarine Dwyka beds near Schlip, South West Africa. In: *Gondwana 2* (Ed. by S. H. Haughton), pp. 621-626. Preceding Paper IUGS 2nd Gondwana Symposium (South Africa), Pretoria.
- MARTIN, H. & WILCZEWSKI, N. (1970) Palaeoecology, conditions of deposition and the paleogeography of the marine Dwyka Beds of South West Africa. In: *Gondwana 2* (Ed. by S. H. Haughton), pp. 225-232. Preceding Paper IUGS 2nd Gondwana Symposium (South Africa), Pretoria.
- MARTINI, J. E. J. (1974) On the presence of ash beds and volcanic fragments in the greywackes of the Karoo system in the southern Cape Province (South Africa). *Transactions Geological Society of South Africa*, **77**, 113-116.
- MCLACHLAN, I. R. & ANDERSON, A. (1973) A review of the evidence for marine conditions in southern Africa during Dwyka times. *Palaeontologica africana*, **15**, 37-64.
- MCLACHLAN, I. R. & JONKER, J. P. (1990) Tuff beds in the north-western part of the Karoo Basin. *South African Journal of Geology*, **93**(2), 329-338.
- MENNING, M. & JIN, Y. G. (1998) Comment on 'Permo-Triassic magnetostratigraphy in China: the type section near Taiyuan, Shanxi Province, North China' by B.J.J. Embleton, M.W. McElhinny, X.Ma, Z.Zhang and Z.X.I. Li. *Geophys. J. Int.*, **133**, 213-216.
- MENNING, M., WEYER, D., DROZDZEWSKI, G. & VAN AMEROM, H. W. J. (1997) Carboniferous time scales revised 1997. *Carboniferous Newsletter*, **15**, 26-28.
- MICHARD, A. (1989) Rare earth systematics in hydrothermal fluids. *Geochim. Cosmochim. Acta*, **53**, 745-750.
- MILLER, R. M. & SCHALK, K. E. L. (1980) Geological Map of Namibia 1:1 000 000. Geological Survey of Namibia, Windhoek, Namibia.

- MISHRA, H. K. (1996) Comparative petrological analysis between the Permian coals of India and Western Australia: palaeoenvironments and thermal history. *Palaeogeography, Palaeoclimatology, Palaeoecology*, **125**, 199-216.
- MORTON, A. C. (1985) Heavy minerals in provenance studies. In: *Provenance of Arenites*. (Ed. by G. G. Zuffa), pp. 249-277. NATO ASI, Dordrecht, The Netherlands.
- MYERS, K. J. & BRISTOW, C. S. (1989) Detailed sedimentology and gamma-ray log characteristics of a Namurian deltaic succession II: Gamma ray logging. In: *Deltas: Sites and traps for fossil fuels, Vol. 41* (Ed. by M. K. G. Whateley and K. T. Pickering), pp. 81-88. Geological Society Special Publication, London, U.K.
- MYERS, K. J. & WIGNALL, P. B. (1987) Understanding Jurassic organic-rich mudrocks - new concepts using gamma-ray spectrometry and palaeoecology: examples from the Kimmeridge Clay of Dorset and the Jet Rock of Yorkshire. In: *Marine clastic sedimentology: developments and case studies* (Ed. by J. K. Leggett and G. G. Zuffa), pp. 172-189. Graham & Trotman, London.
- NEISH, P. G., DRINNAN, A. P. & CANTRILL, D. J. (1993) Structure and ontogeny of Vertebraria from silicified Permian sediments in East Antarctica. *Review of Palaeobotany and Palynology*, **79**(3-4), 221-244.
- NESBITT, H. W. & YOUNG, G. M. (1982) Early Proterozoic climates and plate motions inferred from major element chemistry of lutites. *Nature*, **299**, 715-717.
- NIEDERBUDE, E. A. (1975) Veränderungen von Dreischicht-Tomineralen durch natives Kalium in mitteldeutschen und niederbayerischen holozänen Lößböden. *Zeitschrift der Pflanzenernährung und Bodenkunde*, 217-234.
- NORTH, F. K. (1985) *Petroleum Geology*. Allen & Unwin, Boston, U.S.A., 607 pp.
- OESTERLEN, P. M. (1990) A new occurrence of the Dwyka Formation in western Zimbabwe. *South African Journal of Geology*, **93**(2), 382-388.
- PACES, J. B. & MILLER, J. D. (1993) Precise U-Pb ages of Duluth Complex and related mafic intrusions, Northeastern Minnesota: Geochronological insights to physical, petrogenic, paleomagnetic and tectono-magmatic processes associated with the 1.1 Ga midcontinent rift system. *Journal of Geophysical Research*, **98**(B8), 13997-14013.
- PEARCE, J. A., HARRIS, N. B. W. & TINDLE, A. G. (1984) Trace element discrimination diagrams for the tectonic interpretation of granitic rocks. *Journal of Petrology*, **25**, 956-983.
- PEARSON, M. & SMALL, S. (1988) Illite-smectite diagenesis and palaeotemperatures in northern North Sea Quaternary to Mesozoic shales sequences. *Clay mineralogy*, **23**, 109-132.
- PICKFORD, M. (1995) Karoo Supergroup palaeontology of Namibia and brief description of a thecodont from Omingonde. *Palaeontology africana*, **32**, 51-66.
- PICOTRACE (1997) PicoTrace digestion system. Manual. Bovenden, 21 + Appendix.
- POLDERVAART, A. (1956) Zircon in rocks. 2. Igneous rocks. *American Journal of Science*, **254**, 521-554.
- RANGE, P. (1912) Geologie des Deutschen Namalandes. *Beiträge zur geologischen Erforschung deutscher Schutzgebiete.*, **2**, 104 pp., Berlin, Germany.
- RANGE, P. (1920) Geologische Spezialaufnahmen in Südwestafrika. *Beiträge zur geologischen Erforschung der Deutschen Schutzgebiete*, **18**, 33-42.
- RANGE, P. (1928) Die geologischen Verhältnisse der Karruformation Deutsch-Südwestafrikas. *Beiträge zur geologischen Erforschung der Deutschen Schutzgebiete*, **20**, 1-16.
- REUNIG, E. & MARTIN, H. (1957) Die Prä-Karoo-Landschaft, die Karroo-Sedimente und Karroo-Eruptiva des südlichen Kaokoveldes in Südwestafrika. *Neues Jahrbuch für mineralogische Abhandlungen*, **91**, 193-212.
- REYNOLDS, R. C. (1980) Interstratified clay minerals. In: *Crystal structures of clay minerals*

- and their x-ray identification. (Ed. by G. W. Brindley and G. Brown), pp. 249-303. Mineralogical Society, London, U.K.
- RING, U. (1995) Tectonic and lithological constraints on the evolution of the Karoo graben of northern Malawi (East Africa). *Geologische Rundschau*, **84**, 607-625.
- ROCHA-CAMPOS, A. C. (1970) Upper Palaeozoic bivalves and gastropods of Brazil and Argentina; a review. In: *International Gondwana Symposium 2* (Ed. by S. H. Haughton), pp. 605-612. Preceding Paper IUGS 2nd Gondwana Symposium (South Africa), Pretoria.
- ROLLINSON, H. R. (1993) Using geochemical data: Evaluation, presentation, interpretation. Longman Scientific and Technical, 352 pp., Harlow, Essex, U.K.
- ROSS, C. A. & ROSS, J. R. P. (1988) Late Palaeozoic transgressive-regressive deposition. In: *Sea-level changes: An Integrated Approach*, Vol. 42 (Ed. by C. K. Wilgus, B. S. Hastings, H. W. Posamentier, J. van Wagoner, C. A. Ross and C. G. S. C. Kendall), pp. 227-247. SEPM Special Publications, Tulsa, U.S.A.
- ROWSELL, D. M. & DE SWARDT, A. M. J. (1976) Diagenesis in Cape and Karoo sediments, South Africa, and its bearing on their hydrocarbon potential. *Transactions of the Geological Society of South Africa*, **79**, 81-145.
- SAMSON, S. D., KYLE, P. R. & ALEXANDER, E. C. J. (1988) Correlation of North American Ordovician bentonites by using apatite chemistry. *Geology*, **16**, 444-447.
- SANTOS, P. R. DOS., ROCHA-CAMPOS, A. C. & CANUTO, J. R. (1996) Patterns of Late Palaeozoic deglaciation in the Paraná Basin, Brazil. *Palaeogeography, Palaeoclimatology, Palaeoecology*, **125**, 165-184.
- SARNA-WOJCICKI, A. M. (1976) Correlation of Late Cenozoic tuffs in the central Coast Ranges of California by means of trace- and minor-element chemistry. In: *Professional Paper, Vol. 972* (Ed. by United States Geological Survey), 30 pp.
- SARNA-WOJCICKI, A. M., BOWMAN, H. R., MEYER, C. E., RUSSELL, P. C., WOODWARD, M. J., MCCOY, G., ROWE JR., J. J., BAEDECKER, P. A., ASARO, F. & MICHAEL, H. (1984) Chemical analyses, correlations, and ages of Upper Pliocene and Pleistocene ash layers of east-central and southern California. In: *Professional Paper, Vol. 1293* (Ed. by U. S. G. Survey), 40 pp.
- SARNA-WOJCICKI, A. M., SHIPLEY, S., WAITT, R. B. J., DZURISIN, D. & WOOD, S. H. (1981) Areal distribution, thickness, mass, volume, and grain size of air-fall ash from the six major eruptions of 1980. In: *The 1980 eruptions of Mount St. Helens, Washington*, Vol. 1250 (Ed. by P. W. Lioman and D. R. Mullineaux), pp. 577-600. U. S. Geological Survey Special Paper.
- SCHLEICHER, H. & LIPPOLT, H. J. (1981) Magmatic muscovite in felsitic parts of rhyolites from southwest Germany. *Contributions to Mineralogy and Petrology*, **78**, 220-224.
- SCHMID, R. (1981) Descriptive nomenclature and classification of pyroclastic deposits and fragments. *Geologische Rundschau*, **70**(2), 794-799.
- SCHMIDT-RÖHL, A. (1999) Hochauflösende geochemische Untersuchungen im Posidonien-schiefer von SW-Deutschland. *Tübinger Geowissenschaftliche Arbeiten, Reihe A, Band 48*, Tübingen, 189 pp.
- SCHROEDER, H. (1908) Marine Fossilien in Verbindung mit permischen Glazial-konglomerat in Deutsch-Südwestafrika. *Jahrbuch königliche Preussische geologische Landesanstalt*, **29**, 694-697.
- SECKENDORFF, V. V. (1990) Geologische, petrographische und geochemische Untersuchungen an permischen Magmatiten im Saarland (Blatt 6507 Lebach). *Berichte des Geologischen Paläontologischen Instituts und des Museums, Universität Kiel*, **39**, 232 pp.
- SEIDOV, D. & MASLIN, M. (1999) North Atlantic deep water circulation collapse during Heinrich events. *Geology*, **27**(1), 23-26.
- SINGER, A. & STOFFERS, P. (1980) Clay mineral diagenesis in two East African lake sediments.

- Clay mineralogy*, **15**, 291-307.
- SMITH, R. M. H., ERIKSSON, P. G. & BOTHA, W. J. (1993) A review of the stratigraphy and sedimentary environments of the Karoo-aged basins of Southern Africa. *Journal of African Earth Sciences*, **16**(1/2), 143-169.
- SOARES, P. C., ASSINE, M. L., ROSTIROLLA, S. P., FERREIRA, F. J. F. & QUINTAS, M. C. I. (1994) Cyclicity, episodocity and sequenciality during the evolution of the Paraná intracratonic basin, Brazil. In: *14 th International Congress Sedimentology*, pp. E27-E28, Recife, Brazil.
- SOUTH AFRICAN COMMITTEE FOR STRATIGRAPHY (SACS) (1980) Stratigraphy of South Africa. Part 1: Lithostratigraphy of the Republic of South Africa, South West Africa/Namibia and the Republics of Bophuthatswana, Transkei and Venda. Government Printer, Pretoria, 690 pp.
- SPEARS, D. A., DUFF, P. & CAINE, P. M. (1988) The west Waterberg tonstein, South Africa. *International Journal of Coal Geology*, **9**, 221-223.
- SPEARS, D. A. & KANARIS-SOTIRIOU, R. (1979) A geochemical and mineralogical investigation of some British and other European tonsteins. *Sedimentology*, **26**, 407-425.
- SPEARS, D. A., KANARIS-SOTIRIOU, R., RILEY, N. & KRAUSE, P. (1999) Namurian bentonites in the Pennine Basin, UK - origin and magmatic affinities. *Sedimentology*, **46**, 385-401.
- STEIGER, R. H. & JÄGER, E. (1977) Sub-commission on geochronology: convention on the use of decay constants in geo- and cosmochronology. *Earth Planetary Science Letter*, **36**, 359-362.
- STOLLHOFEN, H. (1991) Die basalen Vulkaniklastika des Oberrotliegend im Saar-Nahe-Becken (SW-Deutschland). Dissertation, Universität Würzburg, 413 pp.
- STOLLHOFEN, H. (1999) Karoo Synrift-Sedimentation und ihre tektonische Kontrolle am entstehenden Kontinentalrand Namibias. *Zeitschrift der Deutschen Geologischen Gesellschaft*, **149**(4), 519-632.
- STOLLHOFEN, H., STANISTREET, I. G., BANGERT, B. & GRILL, H. (2000) Tuffs, tectonism and glacially related sea-level changes, Carboniferous-Permian, southern Namibia. *Palaeogeography, Palaeoclimatology, Palaeoecology*, **161**, 127 - 150.
- STRATTEN, T. (1967) A preliminary report on a direction study of the Dwyka tillite in the Karroo basin of South Africa. In: *Proceedings 1st IUGS Gondwana Symposium, Vol. 2*, pp. 741-762, Buenos Aires, Argentina.
- STRATTEN, T. (1977) Conflicting directions of Dwyka ice flow in the Western Cape Province and southern South West Africa. *Transactions of the Geological Society of South Africa*, **80**, 79-86.
- SUN, S. S. & MCDONOUGH, W. F. (1989) Chemical and isotopic systematics of oceanic basalts; implications for mantle composition and processes. In: *Magmatism in the ocean basins. Vol. 42* (Ed. by A. D. Saunders and M. J. Norry), pp. 313-345. Geological Society Special Publications London, U.K.
- TAYLOR, J. H. (1937) A contribution to the study of accessory minerals of igneous rocks. *American Mineralogist*, **22**, 686-700.
- TAYLOR, S. R. & MCLENNAN, S. M. (1985) The continental crust: its composition and evolution. *Blackwell Scientific Publications*, Oxford, UK.
- TERA, F. & WASSERBURG, G. J. (1972) U-Th-Pb systematics in three Apollo 14 basalts and the problem of initial Pb in lunar rocks. *Earth Planetary Science Letter*, **14**, 281-304.
- THERON, J. N. & BLIGNAULT, H. J. (1975) A model for the sedimentation of the Dwyka glacials in the Southwestern Cape. In: *International Gondwana Symposium 3* (Ed. by E. S. W. Campbell), pp. 347-356. University Press, Canberra, Australia.
- TISCHENDORF, G., FÖRSTER, H.-J. & TRUMBULL, R. B. (1995) Evaluation of trace element tectonic discrimination diagrams for silicic igneous rocks. *Terra Nostra*, **7**, 137-140.
- TRIVETT, M. L. & ROTHWELL, G. W. (1991) Diversity among Palaeozoic Cordaitales. *Neues*

- Jahrbuch für Geologie und Paläontologie Abhandlungen*, **183**, 289-305.
- TRÖGER, W. E. (1967) *Optische Bestimmung der gesteinsbildenden Minerale*. Schweizerbart, Stuttgart, 822 pp.
- VEEVERS, J. J. & POWELL, MC CA (1987) Late Palaeozoic glacial episodes in Gondwanaland reflected in transgressive-regressive depositional sequences in Euramerica. *GSA Bulletin*, **98**, 475-487.
- VEEVERS, J. J., COLE, D. I. & COWAN, E. J. (1994) Southern Africa: Karoo Basin and Cape Fold Belt. In: *Permian-Triassic Pangean basins and foldbelts along the Panthalassan margin of Gondwanaland.*, Vol. 184 (Ed. by J. J. Veivers and C. M. Powell), pp. 223-280. Geological Society of America Memoir, Boulder, Colorado, USA.
- VERSFELD, J. A. (1988) The geology of the Nondweni Greenstone Belt, Natal. Dissertation, University of Natal at Pietermaritzburg, 298 pp.
- VILJOEN, J. H. A. (1987) Subaqueous fallout tuffs of the Ecca Group in the southern Cape Province. In: *Workshop on Pyroclastic Volcanism and Associated Deposits*. (Ed. by G. Brown and V. A. Preston), pp. 45-48. University of Natal, Pietermaritzburg, South Africa.
- VILJOEN, J. H. A. (1990) K-Bentonites in the Ecca Group of the south and central Karoo Basin. In: *23rd Geocongress 1990*, pp. 576-579. Geological Society of South Africa, Cape Town, South Africa.
- VILJOEN, J. H. A. (1994) Sedimentology of the Collingham Formation, Karoo Supergroup. *South African Journal of Geology*, **97**, 167-183.
- VILJOEN, J. H. A. (1995) Piroklastiese afsettings van Perm-ouderdom in die Hoof-Karookom. PhD-thesis, 274 pp., University of Stellenbosch, South Africa.
- VISSER, J. N. J. (1983a) Glacial-marine sedimentation in the Late Palaeozoic Karoo Basin, Southern Africa. In: *Glacial-Marine Sedimentation*. (Ed. by B. F. Molnia), pp. 667-701. Plenum Press, New York, U.S.A.
- VISSER, J. N. J. (1983b) An analysis of the Permo-Carboniferous glaciation in the marine Kalahari Basin, southern Africa. *Palaeogeography, Palaeoclimatology, Palaeoecology*, **44**, 295-315.
- VISSER, J. N. J. (1986) Lateral lithofacies relationships in the glacial Dwyka Formation in the western and central parts of the Karoo Basin. *Transactions of the Geological Society of South Africa*, **89**, 373-383.
- VISSER, J. N. J. (1989) The Permo-Carboniferous Dwyka Formation of southern Africa: Deposition by a predominantly subpolar ice sheet. *Palaeogeography, Palaeoclimatology, Palaeoecology*, **70**, 377-391.
- VISSER, J. N. J. (1992) The Dwyka Group in the western half of the Karoo Basin, South Africa. In: *24th Geocongress of the Geological Society of South Africa*, pp. 27, Geological Society of South Africa, Bloemfontein, South Africa.
- VISSER, J. N. J. (1993) Sea-level changes in a back-arc-foreland transition: the Late Carboniferous-Permian Karoo Basin of South Africa. *Sedimentary Geology*, **83**, 115-131.
- VISSER, J. N. J. (1994) The interpretation of massive rain-out and debris-flow diamictites from glacial marine environment. In: *Earth's Glacial Record*. (Ed. by M. Deynoux, J. M. G. Miller, E. W. Domack, N. Eyles, I. J. Fairchild and G. M. Young), pp. 193-203. University Press, Cambridge, U.K.
- VISSER, J. N. J. (1996) Controls on Early Permian shelf deglaciation in the Karoo Basin of South Africa. *Palaeogeography, Palaeoclimatology, Palaeoecology*, **125**, 129-139.
- VISSER, J. N. J. (1997) Deglaciation sequences in the Permo-Carboniferous Karoo and Kalahari Basins of southern Africa: a tool in the analysis of cyclic glaciomarine basin fills. *Sedimentology*, **44**, 507-521.
- VISSER, J. N. J., LOOCK, J. C. & COLLISTON, W. P. (1987) Subaqueous Outwash Fan and Esker Sandstones in the Permo-Carboniferous Dwyka Formation of South Africa. *Journal Sedimentary Petrology*, **57**(3), 467-478.

- VISSER, J. N. J., VAN NIEKERK, B. N. & VAN DER MERWE, S. W. (1997) Sediment transport of the Late Palaeozoic glacial Dwyka Group in the south-western Karoo Basin. *South African Journal of Geology*, **100**(3), 223-236.
- VISSER, J. N. J. & YOUNG, G. M. (1990) Major element geochemistry and paleoclimatology of the Permo-Carboniferous glaciogene Dwyka Formation and postglacial mudrocks in southern Africa. *Palaeogeography, Palaeo-climatology, Palaeoecology*, **81**, 49-57.
- VON BRUNN, V. (1977) A furrowed intratillite pavement in the Dwyka Group of northern Natal. *Transactions of the Geological Society of South Africa*, **80**, 125-130.
- VON BRUNN, V. (1996) The Dwyka Group in the northern part of KwaZulu/Natal, South Africa: sedimentation during Late Palaeozoic glaciation. *Palaeogeography, Palaeoclimatology, Palaeoecology*, **125**, 141-163.
- WAGNER, P. A. (1915) The Dwyka Series in South-West Africa. *Transactions of the Geological Society of South Africa*, **18**, 102-117.
- WANG, S. (1997) Discovery of *Tisoa* in the Middle Triassic Bianyang Formation in Guizhou. *Regional Geology of China*, **16**(1 (60)), 104-107.
- WASS, R. E. (1970) Bryozoa from the Dwyka Series and their palaeogeographic significance. *Annales Geological Survey of South Africa*, **8**, 95-97.
- WEAVER, C. E. (1963) Interpretative value of heavy minerals from bentonites. *Journal of Sedimentary Petrology*, **33**, 343-349.
- WEDEPOHL, K. H. (1978) *Handbook of Geochemistry*. Vol. II - 1-5, Springer, Berlin, Germany.
- WHITE, W. H. (1989) Geochemical evidence for crust-to-mantle recycling in subduction zones. In: *Crust / mantle recycling at convergence zones*. (Ed. by S. R. Hart and S. Gulen), pp. 43-58. Kluwer, Amsterdam, The Netherlands.
- WILLIAMS, I. S. & CLAEISSON, S. (1987) Isotopic evidence for the Precambrian provenance and Caledonian metamorphism of high grade paragneisses from the Seve Nappes, Scandinavian Caledonides. II. Ion microprobe zircon U-Th-Pb ages. *Contributions to Mineralogy and Petrology*, **97**, 205-217.
- WILLIAMS, K. E. (1995) Tectonic subsidence analysis and Palaeozoic palaeogeography of Gondwana. In: *Petroleum basins of South America.*, Vol. 62 (Ed. by A. J. Tankard, R. Suárez Soruco and H. J. Welsink), Memoir American Association Petroleum Geology, pp. 79-100.
- WILSON, M. J. (1987) A handbook of determinative methods in clay mineralogy. Blackie & Son Limited, London, 308 pp.
- WINCHESTER, J. H. & FLOYD, P. A. (1977) Geochemical discrimination of different magma series and their differentiation products using immobile elements. *Chemical Geology*, **20**, 325-343.
- WINTER, J. (1981) Exakte tephrostratigraphische Korrelation mit morphologisch differenzierten Zirkonpopulationen (Grenzbereich Unter-/Mitteldevon, Eifel-Ardennen). *Neues Jahrbuch für Geologie und Paläontologie Abhandlungen*, **162**, 97-136.
- WOPFNER, H. (1998) The Early Permian euxinic deglaciation event between East Africa and north-west Australia. *Journal of African Earth Sciences*, **27**(1A), 212-213.
- ZIMMERLE, W. (1976) Die Tiefbohrung Saar 1: Petrographische Beschreibung und Deutung der erbohrten Schichten. *Geologisches Jahrbuch*, **A 27**, 91-305.
- ZIMMERLE, W. (1979) Accessory Zircon from a Rhyolite, Yellowstone National Park (Wyoming, U.S.A.). *Zeitschrift der deutschen geologischen Gesellschaft*, **130**, 361-369.
- ZIMMERLE, W. (1995) *Petroleum Sedimentology*. Enke, Stuttgart, Germany, 413 pp.

Appendices

Table of Contents

Appendix A-1: Outcrop locations within the Aranos Basin of southern Namibia	210
Appendix A-2: Summary of all noticed features within the Ganigobis Shale Member	212
Appendix A-3: Summary of all tuff beds of the Ganigobis Shale Member, their thickness and the vertical distance to the underlying tuff bed.....	218
Appendix B: Analytical methods and techniques.....	221
B-1 Sampling techniques and denominations	221
B-1.1 Tuff beds	221
B-1.2 Mudstones	221
B-1.3 Sample denominations	221
B-2 Thin-section analysis	221
B-3 X-ray diffraction analysis	222
B-3.1 Methods	222
B-3.1.1 Separation of the fraction < 2 µm	222
B-3.1.2 Sample preparation	222
B-4 Separation of heavy minerals	223
B-5 Geochemistry	223
B-5.1 Sample preparation	223
B-5.2 Loss On Ignition (LOI)	223
B-5.3 Whole-rock major and trace elements analysis by XRF	223
B-5.4 Trace elements and REE-analysis by ICP-MS	224
Appendix C: Summary of all gamma-ray measurements in the Aranos Basin.....	226
Appendix D-1: XRF-results of mudstones sampled from the Ganigobis Shale Member, Aranos Basin, southern Namibia.	230
Appendix D-2: ICP-MS standards used at IGDL Göttingen.	231
Appendix D-3: XRF- and ICP-MS results of all analysed tuff beds.....	232
Appendix D-4: XRF-results of volcanic clasts sampled from the Ganigobis Shale Member, Aranos Basin, southern Namibia.	238
Appendix E: Results of all SHRIMP U-Th-Pb zircon measurements	239

Appendix A-1 (Tab. 18): Outcrop locations within the Aranos Basin of southern Namibia

# BB	# HG	Locality	Outcrop type	Tuff beds, others	Co-ordinates
1	72	4 km SE of Hardap dam	Escarpment	Hardap Shale Member (DS III), no tuff beds	24°31'35" S, 17°54'20" E
2	40	Fish and Khomb River, N of Ganigobis	Eroded river banks	Ganigobis Shale Member (l.p., DS II), Tuff beds I-VI, permineralised wood, fish remains	25°48'52" S, 18°00'40" E
3		Schlip	Eroded river banks	Hardap Shale Member (DS III), tuffaceous beds	24°02'49" S, 17°07'05" E
4		2.5 km W Falkenhorst	Eroded river banks	Hardap Shale Member (DS III), no tuff beds	25°03'02" S, 17°51'02" E
5		6 km S Falkenhorst, 150 m W of B1 to Windhoek	Eroded river banks	Hardap Shale Member (DS III), no tuff beds	25°05'41" S, 17°51'47" E
6		C19 Mariental-Maltahöhe, 200 m S bridge crossing Fish River	Eroded river banks	Hardap Shale Member (DS III), no tuff beds	24°39'32" S, 17°55'59" E
9		Brukkaros River, 150 m E of B1	Eroded river banks	Ganigobis Shale Member (u.p., DS II), Tuff beds VIII, fossils	25°40'16" S, 18°02'36" E
12		contributory to Brukkaros River, 50 m W of B1	Eroded river banks	Ganigobis Shale Member (u.p., DS II), no tuff beds, black, massive mudstones	25°40'52" S, 18°02'35" E
13		Huam River	Eroded river banks	Ganigobis Shale Member (m.p., DS II), pyritic, concretionary horizons	25°48'17" S, 18°01'43" E
15		Huam River, 0.3 km S of Haams	Eroded river banks	Ganigobis Shale Member (m.p., DS II), tuff bed VII, pyritic concretions	25°47'11" S, 18°00'37" E
16		Asab River, 0.2 km W of Haams	Eroded river banks	Ganigobis Shale Member (m.p., DS II), tuff beds VI, pyritic concretions	25°46'56" S, 18°00'21" E
17		Asab River, 0.8 km SW of Haams	Eroded river banks	Ganigobis Shale Member (l.p., DS II), Tuff beds IV-V	25°47'28" S, 18°00'08" E
19		Asab River, 1.5 km N of Haams	Eroded river banks	Ganigobis Shale Member (m.p., DS II), no tuff beds, large pyritic concretions	25°45'47" S, 18°00'23" E
20		Brukkaros River, 0.5 km NE of confluence with Asab River	Eroded river banks	Ganigobis Shale Member (m.p., DS II), tuff bed VII, permineralised tree log	25°44'15" S, 18°00'10" E
22		9.5 km W of Tses, road to Berseba, 200 m N of bridge	Eroded river banks	Ganigobis Shale Member (l.p., DS II), Tuff beds IV-V, fish remains	25°54'44" S, 18°01'08" E
23		Tses River, 0.3 km NE of farm Waterval	Eroded river banks	Ganigobis Shale Member (l.p., DS II): tuff beds I-V, fish remains, shales with dropstones at base	25°53'35" S, 18°00'51" E

# BB	# HG	Locality	Outcrop type	Tuff beds, others	Co-ordinates
24	51	Snyfontein, 33 km WNW of Keetmanshoop	Escarpment	4 tuff beds in marine shales with dropstones, 1 fish remains-bearing mudstone concretion	26°33'49" S, 17°47'03" E
25	85	Tsaraxa, 22 km SW of Tses	Eroded river banks	3 tuff beds in Ganigobis Shale Member (l.p., DS II)	26°04'16" S, 17°57'29" E
26	94	Wasser, 19 km S of Tses	Eroded river banks	No tuff beds, Hardap Shale Member (DS III)	26°05'03" S, 18°08'07" E
27		Brukkaros River, 2 km NE of Nauchas	Eroded river banks	Ganigobis Shale Member (u.p., DS II), tuff bed VIII, gastropod shells, 5 carbonatite dykes	25°41'24" S, 18°01'54" E
28		Asab River, 4 km WSW of Nauchas	Eroded river banks	Ganigobis Shale Member (l.p., DS II), tuff beds I-IV, faults, 2 carbonatite dykes	25°43'04" S, 17°59'08" E
29		Asab River, 4.5 km WNW of Nauchas	Eroded river banks	Ganigobis Shale Member (l.p., DS II), Tuff beds I-IV	25°41'48" S, 17°58'21" E
30		1.5 km W of farm Aretitis	Eroded river banks	Ganigobis Shale Member (l.p., DS II), Tuff beds III-IV	25°39'42" S, 17°58'21" E
31		Contributory of the Asab River from the W, 4.5 km WNW of Nauchas	Eroded river banks	Ganigobis Shale Member (l.p., DS II), Tuff beds I-IV, shales with dropstones at base	25°41'48" S, 17°58'18" E
32		Asab River, 3 km SW of farm Aretitis	Eroded river banks	Ganigobis Shale Member (l.p., DS II), Tuff beds I-V	25°40'33" S, 17°58'24" E
33		3 km NW of farm Aretitis	Eroded river banks	Ganigobis Shale Member (l.p., DS II), Tuff beds III-IV	25°39'01" S, 17°57'52" E
34		3.5 km NW of farm Aretitis	Eroded river banks	No tuff beds, black, massive mudstones pass into greenish siltstones (DS II)	25°38'46" S, 17°57'51" E
35		Asab River, 1.3 km WNW of confluence with Brukkaros River	Eroded river banks	Ganigobis Shale Member (m.p., DS II), tuff bed VII	25°44'12" S, 17°59'32" E
36		Ganigobes River, 2.5 km W of B1 to Windhoek	Eroded river banks	Greenish shales with quartzitic dropstones and mudstone concretions (DS III)	25°49'16" S, 18°03'57" E
37		Ganigobes River, 3.2 km W of B1 to Windhoek	Eroded river banks	2 tuff beds in shales with dropstones (DS III)	25°49'23" S, 18°03'39" E
38		Ganigobes River, directly N of Ganigobis	Eroded river banks	Ganigobis Shale Member (l.p., DS II), Tuff beds I-IV, shales with dropstones at base	25°49'34" S, 18°00'38" E
39		Ganigobes River, 6.0 km W of B1 to Windhoek	Eroded river banks	Ganigobis Shale Member (u.p., DS II), no tuff beds, black, massive mudstones, gastropod shell	25°49'11" S, 18°01'54" E
40		Ganigobes River, 4.5 km W of B1 to Windhoek	Eroded river banks	Ganigobis Shale Member (u.p., DS II), tuff bed VIIIa, microbial limestone mats and mounds	25°48'56" S, 18°02'36" E
41		Asab River, 3.5 km NW of Ganigobis	Eroded river banks	Diamictites & shales with dropstones, tuff beds I (DS - II)	25°48'20" S, 17°59'45" E

# BB	# HG	Locality	Outcrop type	Tuff beds, others	Co-ordinates
42	42	Fish River, 2 km NW of Ganigobis	River bed	Diamictites with few undeformed volcanic clasts (DS II)	25°49'26" S, 17°59'40" E
43	43	Ganigobes River, 4.2 km W of B1 to Windhoek	Eroded river banks	Ganigobis Shale Member (u.p., DS II), tuff beds VIII, microbial bioherms (Grill, 1997)	25°48'55" S, 18°02'45" E
44		Brukkaros River, 1 km W of Nauchas	Eroded river banks	Ganigobis Shale Member (m.p., DS II), no tuff beds	25°42'32" S, 18°00'45" E
45	2	Road D 98 Tses to Berseba E of the Fish River Bridge, 20 km W of Tses	Road gully	Ganigobis Shale Member (l.p., DS II), tuff beds I-IV, shales with dropstones	25°53'22" S, 17°56'48" E

Abbreviations: BB: outcrop numbers by Berthold Bangert; HG: outcrop numbers by Hermann Grill; l.p.: lower part of the Ganigobis Shale Member; m.p.: middle part; u.p.: upper part; DS: deglaciation sequence

Appendix A-2 (Tab. 19): Summary of all noticed features within the Ganigobis Shale Member

Locality 2				
DROPSTONES: lithology	tephrostratigraphic classification	size	remarks	other remarks
quartzites, plutonites, dolerites and mica shists	0.70 m and more below tuff bed Ia, EACS: 1 cm	variable, up to 60 cm in diameter	to the bottom increasing number of dropstones	
mica schist	0.45 m below tuff bed Ia	26x12x5 cm		
quartzite	0.55 m below tuff bed Ia	60x50x20 cm	striae	
quartzites and	0.45 m below tuff bed Ia	< 5 cm	well-rounded to	concretionary horizon I
plutonites	0.25 m below tuff bed Ia	< 5 cm	rounded	concretionary horizon II
quartzite	0.15 m above tuff bed Ic	20x16x8 cm	angular	
quartzite	0.50 m below tuff bed IIIb	8x6x3 cm	angular	
fine-grained sandstone	0.29 m below tuff bed IVa	3x2.5x1 cm	angular	
quartzite	2.50 m below tuff bed Vc	24x20x>15 cm	subangular to subrounded	
CONCRETIONS	tephrostratigraphic classification	size and shape	remarks	
concretion horizon I	0.45 m below tuff bed Ia	lobate, thickness 12 cm, length and width in m-range	siliceous-phospatic	
concretion horizon II	0.25 m below tuff bed Ia	lobate, thickness 18 cm, length and width in m-range	siliceous-phospatic	
many fish remains bearing	between tuff beds I and II	max. 12x5 cm, oval	siliceous-phospatic	
fish bones bearing	55 cm above tuff bed IIIb	11x8x3 cm, oval	siliceous-phospatic	
few nonfossiliferous	between tuff beds II and IV	max. 40x8 cm, oval	siliceous-phospatic	
some fish remains bearing	between tuff beds IV and V	max. 10x4 cm, oval	siliceous-phospatic	

cone-in-cone concretions	from 4 m below tuff bed Vc to the top	max. 6 m in length and 1.5 m in height	sandy-calcareous	
COPROLITES	tephrostratigraphic classification	size of coprolite	size of concretion	orientation
spiral coprolite	just below tuff bed Ib	7.0x1.8 cm	8x2x1 cm	135°
coprolite	between tuff beds I and II	10.0x2.5 cm	12x6.5x5 cm	thinsection
spiral coprolite	just below tuff bed IIb	8x2 cm	without concretion	
coprolite	between tuff beds II and III	6x1.4 cm	9x5.5x4 cm	
coprolite	0.65 m below tuff bed IIIb	6.5x1.2 cm	9x6x4 cm	
spiral coprolite	0.50 m below tuff bed IIIb	5.5x2.0 cm	8.5x5x3.5 cm	
spiral coprolite	0.25 m below tuff bed IIIb	6.0x1.2 cm	11x5x4.5 cm	130°
coprolite	between tuff beds III and IV	6.0x1.5 cm	8x4x3.5 cm	
spiral coprolite	1.35 m below tuff bed IVa			
coprolite	1.0 m below tuff bed IVa			
coprolite and fish remains	4.0 m below tuff bed Vc			
coprolite and fish remains	2.2 m below tuff bed Vc			
spiral coprolite	1.2 m below tuff bed Vc			
coprolite	0.4 m above tuff bed Vc	7x0.8 cm	10x6x4 cm	
PERMINERALISED WOOD	tephrostratigraphic classification	size of wood	shape	all uncorrected for declination
coalified wood	0.75 m above tuff bed Ic	190x38x3 cm	flattened down	135°
coalified wood particles	0.57 m above tuff bed Ic	8x8x1 cm		80°
coalified wood	0.30 m above tuff bed IIb	>20x15x7xcm	flattened down	131°
coalified wood	0.45 m above tuff bed IIb	25x10x4 cm	flattened down	100°
permineralised wood	0.45 m above tuff bed IIb	15x8x3 cm		73°
permineralised wood	0.25 m below tuff bed IIIb	2.6x1.8x>4 cm		80°
permineralised wood	0.30 m above tuff bed IIIb	5x3x>4 cm		70°
permineralised wood	0.30 m above tuff bed IIIb	>9x3.5x3 cm	almost round	100°
permineralised wood	0.30 m above tuff bed IIIb	diameter 1.5 cm	almost round, in concretion	108°
permineralised wood	5.0 m above tuff bed IVc	>40x30x3 cm	flattened down	82°
permineralised wood	1.35 m below tuff bed Vc	25x3x3 cm		135°
permineralised wood	>1.20 m below tuff bed Vc	>20x2.7x1.3 cm		14°
permineralised wood	1.10 m below tuff bed Vc	15x8.5x6 cm		53°
Locality 23				
DROPSTONES: lithology	tephrostratigraphic classification	size	remarks	
quartzites and plutonites	2.5 m and more below tuff bed Ia, EACS: 1 cm	variable, up to 50 cm in diameter	to the bottom increasing number of dropstones	
quartzite, reddish	1.45 m below tuff bed Ia	36x25x12 cm		

quartzite, greyish	1.3 m below tuff bed Ia	28x15x9 cm		
granite	1.2 m below tuff bed Ia	5x2.5x2 cm		
andesite	1.2 m below tuff bed Ia	50x30x25 cm	thin-section BB 23	
granite	1.1 m below tuff bed Ia	12x12x7 cm		
quartzite, reddish	0.95 m below tuff bed Ia	10x6x4.5 cm		
quartzite, reddish	0.9 m below tuff bed Ia	5x4x3 cm	photograph (with finger pointing)	
CONCRETIONS: shape	tephrostratigraphic classification	size	all are siliceous-phospatic	
flat	2.2 m below tuff bed Ia	9x9x7 cm		
	1.4 m below tuff bed Ia	65x27x15 cm		
round	1.25 m below tuff bed Ia	28x28x15 cm		
flat and elongate	1.0 m below tuff bed Ia	58x38x20 cm	comparable to concretion horizon I (#2)	
flat and elongate	0.55 m below tuff bed Ia	250x65x15 cm	comparable to concretion horizon II (#2)	
flat	0.75 m below tuff bed IIa	max. 30x15x7 cm	partly fish scales bearing	
flat, round	0.45 m above tuff bed IIIb	max. 20x12x5 cm	fish remains bearing: scales, fins and bones	
flat, round	below and above tuff bed Va	max. 12x10x5 cm	fish remains bearing: scales, fins and bones	
	0.5 m above tuff bed VI	max. 100x30x13 cm		
COPROLITES	tephrostratigraphic classification	max. size of coprolite	max. size of concretion	
spiral coprolite	between tuff beds I and II	5.5x1.8 cm	12x8x7 cm	
spiral coprolite	below and above tuff bed IVa	7.0x1.8 cm	9x6x5 cm	
PLANT DEBRIS	tephrostratigraphic classification			
organic matter on bedding and joint planes	about 1 m below tuff bed Ia			
organic matter on bedding and joint planes	about 0.8 m above tuff bed Id			
organic matter finely disseminated	about 1 m below tuff bed IVa			
Locality 45				
DROPSTONES: lithology	tephrostratigraphic classification	size	shape	
quartzites and plutonites	> 2.0 m below tuff bed Ia		subangular to subrounded	
quartzites and plutonites	1.6 m below tuff bed Ia	EACS: 5 cm	subangular to subrounded	
greyish quartzite	1.4 m below tuff bed Ia	70x50x40 cm	subangular to subrounded	
greyish quartzite	0.7 m above tuff bed Ic	12x10x7 cm	subrounded	
CONCRETIONS: shape	tephrostratigraphic classification	size	remarks	
flat and elongate	1.2 m below tuff bed Ia	100x50x20 cm	comparable to concretion horizon I (# 2)	
flat and elongate	0.8 m below tuff bed Ia	thickness: 15 cm	comparable to concretion horizon II (# 2)	
PERMINERALISED WOOD	tephrostratigraphic classification	size	remarks	

permineralised wood	between tuff bed IV and V	size of wood: 50x5 cm		
Locality 31				
DROPSTONES: lithology	tephrostratigraphic classification	size	remarks	
greyish quartzite	below tuff bed I	10x8x4 cm		
CONCRETIONS: shape	tephrostratigraphic classification	size	remarks	
flat and elongate	0.55 m below tuff beds I	104x35x11 cm	comparable to concretion horizon II (# 2)	
flat	0.4 m below tuff beds II	9x7x4.5 cm	fish scales bearing	
flat	0.35 m above tuff beds II	11x8.5x5 cm		
Locality 32				
COPROLITES	tephrostratigraphic classification	max. size of coprolite	max. size of concretion	
spiral coprolite	10 cm below tuff bed IVa	5.5x1.4 cm	10x6x5 cm	
REEF-LIKE STRUCTURES	tephrostratigraphic classification	size of reef structure	remarks	
microbial limestones	above tuff bed I	95x20 cm high	downstream	
microbial limestones	above tuff bed I	45x20 cm high	downstream	
microbial limestones	above tuff bed I	70x15 cm high	downstream	
microbial limestones	above tuff bed I	90x18 cm high	upstream	
Locality 30				
CONCRETIONS: shape	tephrostratigraphic classification	size	remarks	
elongate	below tuff bed IIIb	max. 90x60x20 cm		
elongate	0.6 m below tuff bed IVa	max. 15x5 cm		
amalgamated	0.4 m above tuff bed IVc	thickness: 5 cm		
Localities 15 and 16				
CONCRETIONS	tephrostratigraphic classification	size and shape	remarks	
fish scales - bearing	0.6 m below tuff bed VIa	9x7x3 cm, oval	siliceous-pyritic	
fish scales and jaws -bearing	0.35 m above tuff bed VIa	11x10x4.5 cm, oval	siliceous-pyritic	
pyritic	1.4 m above tuff bed VIa	30x8 cm	yellowish-weathered	
sandy-calcareous	1.9 m above tuff bed VIa	max. 50 cm	with cone-in-cone structures	
pyritic	2.2 m above tuff bed VIa	15x3 cm	2 x elongate	
pyritic	3.0 m above tuff bed VIa	max. 8x3 cm, oval	8 horizons	
pyritic	0.3 m above tuff bed VII	max. 6x2 cm, oval	2 horizons	
sandy-calcareous	0.45 m above tuff bed VII	max. 40 cm	bed-like with cone-in-cone structures	

Locality 20				
CONCRETIONS	tephrostratigraphic classification	size and shape	remarks	
pyritic	below tuff bed VII	max. 6x2.5 cm, oval	2 horizons	
sandy-calcareous	0.7 m above tuff bed VII	max. 35 cm	bed-like with cone-in-cone structures	
sandy-calcareous	2.0 m above tuff bed VII	max. 15 cm	few cone-in-cone structures	
REEF-LIKE STRUCTURES	tephrostratigraphic classification	size of reef structure	remarks	
microbial limestones	below tuff bed VII	20 cm high	bottom of the outcrop	
microbial limestones	below tuff bed VII	15 cm high	0.6 m high mounds within the Brukkaros River	
PERMINERALISED WOOD	tephrostratigraphic classification	size of wood	shape	uncorrected for declination
permineralised tree log	above tuff bed VII	1160x10-26 cm	almost round	80°
Locality 13				
CONCRETIONS	tephrostratigraphic classification	size and shape	remarks	
pyritic	no tuff bed	max. 14x5 cm	orange-red	funnel-shaped coprolites
pyritic zone A	no tuff bed	4-20 cm	light greyish to orange-red	in the centre
pyritic zone B	no tuff bed	4-12 cm	light greyish to orange-red	
sandy-calcareous	no tuff bed	height max. 1 m	cone-in-cone structures	continue in thin calcareous sandstone beds
Locality 44				
CONCRETIONS	tephrostratigraphic classification	size and shape	remarks	
pyritic	no tuff bed	max. 10x5 cm	orange-red	large funnel-shaped
sandy-calcareous	no tuff bed	max. 22 cm	passes into a mm-thick bed of calcareous sandstone bed	coprolites in the centre
Locality 40				
CONCRETIONS	tephrostratigraphic classification	size and shape	remarks	
siliceous concretions	below and above tuff bed VIIIa	length max. 70 cm	lobate, merge into each other	
REEF-LIKE STRUCTURES	tephrostratigraphic classification	size of reef structure	remarks	
microbial limestones	directly above tuff bed VIIIa	max. 30 cm high	greyish	
Locality 43				
REEF-LIKE STRUCTURES	tephrostratigraphic classification	size of reef structure	remarks	
microbial limestones	1 m above tuff bed VIIIa	max. 30 cm high	grey, flat	
algae-serpulid bioherms	from above tuff bed VIIIa to above VIIId	max. 250 cm high and 150 cm wide	grey, sack-shaped	

Locality 27				
CONCRETIONS	tephrostratigraphic classification	size and shape	remarks	
sandy-calcareous	below tuff bed VIIIa	max. 300 cm long and 60 cm high	cone-in-cone structures, some with trace fossils on bedding planes	
siliceous concretions	below tuff bed VIIIa	max. 18x10x6 cm	contain anvil-like coprolites	
siliceous concretions	below tuff bed VIIIa	max. 11x7x3 cm	contain spiral coprolites	
PERMINERALISED WOOD	tephrostratigraphic classification	size of wood	shape	uncorrected for declination
permineralised wood	above tuff bed VIIIa	>50x12 cm	round	110°
permineralised wood	above tuff bed VIIIa	8x4 cm	with wide annual growth rings	disrupted
permineralised wood	above tuff bed VIIIa	10x8 cm	with wide annual growth rings	disrupted
FOSSILS	tephrostratigraphic classification	size and shape	remarks	
Conularia	below tuff bed VIIIa	max. 3 cm and 1.5 cm in diameter	stick in the lowermost exposed mudstones, rarely found	
Crinoids	above tuff bed VIIIa	length of 0.2-1.0 cm and diameter of 0.1 to 0.5 cm	2 samples next to mounds	
Gastropods	above tuff bed VIIIa	length of up to 1.0 cm	numerous in in irregular, partly branching mudstone concretions	
REEF-LIKE STRUCTURES	tephrostratigraphic classification	size of reef structure	remarks	
microbial biostroms	below tuff bed VIIIa	80x12 cm	brownish, knoblike, similar to #9	
CARBONATITE DYKES	tephrostratigraphic classification	thickness	distance to next carbonatite dyke	uncorrected for declination
greyish, with vesicles	perpendicular to tuff beds	80 cm		64°
greyish, with vesicles		60 cm	250 cm	parallel
greyish, with vesicles		45 cm	350 cm	parallel
greyish, without vesicles		12 cm	300 cm	parallel
greyish, without vesicles		15 cm	50 cm	parallel
Locality 9				
CONCRETIONS	tephrostratigraphic classification	size and shape	remarks	
siliceous concretions	0.7 m above tuff bed VIIIa	max. 80x22 cm	oval shape	
FOSSILS	tephrostratigraphic classification	size and shape	remarks	
single gastropod shell of <i>Omphalonema</i>	2 m below tuff bed VIIIa	base: 4.3x3.2 cm and height: 2.5 cm	turbiniform	
bivalve shells of <i>Myonia</i>	55 cm above tuff bed VIIIa	1x0.4 cm in concretion	thin, elongate, concentric	
PERMINERALISED WOOD	tephrostratigraphic classification	size of wood	shape	uncorrected for declination
permineralised wood	2 m below tuff bed VIIIa	>40x4.5x2 cm	flattened	
permineralised wood	0.7m above tuff bed VIIIa	35x15x8 cm	in mudstone concretion	171°
REEF-LIKE STRUCTURES	tephrostratigraphic classification	size of reef structure	remarks	
microbial biostroms	directly above tuff bed VIIIa	80x12 cm	brownish, knoblike, similar to #27	
microbial bioherm	directly above tuff bed VIIIa	95x75 cm	grey, sack-shaped, similar to #27	

Appendix A-3 (Tab. 20): Summary of all tuff beds of the Ganigobis Shale Member, their thickness and the vertical distance to the underlying tuff bed

Tuff Beds	True Thickness (thickness after contact with water)	Distance to underlying tuff bed	Remarks
Locality 2			
Ia	2 mm (5 mm)		occasionally gypsum substituted
Ib	5 mm (10 mm)	8 cm	bentonitic, flaky
Ic	4 mm (8 mm)	3.5 cm	occasionally gypsum substituted
IIa	2 mm (4 mm)	140 cm	occasionally gypsum substituted
IIb	10 mm (20-25 mm)	23 cm	thickest tuff horizon
IIIa	1 mm (3 mm)	128 cm	mostly as gypsum layer
IIIb	5 mm (15 mm)	20 cm	occasionally gypsum substituted
IVa	4 mm (6 mm)	305 cm	occasionally greyish
IVb	7 mm (12 mm)	15 cm	bentonitic, flaky
IVc	2 mm (4 mm)	23 cm	bentonitic, flaky
Va	1 mm (2 mm)	310 cm	occasionally gypsum substituted
Vb	2 mm (3 mm)	100 cm	occasionally gypsum substituted
Vc	8 mm (15 mm)	300 cm	bentonitic, flaky
VIa	2 mm (10-30 mm)	270 cm	occasionally gypsum substituted
VIb	3 mm (5-25 mm)	20 cm	occasionally gypsum substituted
Locality 23			
Ia	3 mm (10-180 mm)		gypsum substituted
Ib	4 mm (10-40 mm)	30 cm	occasionally gypsum substituted
Ic	2 mm (10-20 mm)	20 cm	occasionally gypsum substituted
Id	1 mm (5-10 mm)	7 cm	bentonitic, flaky
IIa	3 mm (10-20 mm)	230 cm	bentonitic, flaky
IIb	8 mm (20-30 mm)	30 cm	thickest tuff horizon
IIIa	1 mm (3 mm)	65 cm	mostly as gypsum layer
IIIb	2 mm (4 mm)	13 cm	gypsum substituted
IVa	2 mm (4-8 mm)	195 cm	gypsum substituted
IVb	5 mm (10-15 mm)	8 cm	gypsum substituted
IVc	4 mm (8-15 mm)	12 cm	mostly as gypsum layer
Va	1 mm (2 mm)	215 cm	only occasionally exposed
Vb	5 mm (10 mm)	55 cm	occasionally gypsum substituted
VI	3 mm (8 mm)	575 cm	occasionally gypsum substituted, passes into a micritic horizon

Tuff Beds	True Thickness (thickness after contact with water)	Distance to underlying tuff bed	Remarks
Locality 45			
Ia	2 mm (3 mm)		
Ib	3 mm (5 mm)	2 cm	
Ic	2 mm (5-25 mm)	12 cm	gypsum substituted
Id	2 mm (4-18 mm)	3.5 cm	gypsum substituted
IIa	1 mm (5 mm)	distance between tuff horizon groups not measurable due to faulting	bentonitic, flaky
IIb	10 mm (20-25 mm)	15 cm	thickest tuff horizon
IIIa	1 mm (2 mm)	distance between tuff horizon groups not measurable due to faulting	mostly as gypsum layer
IIIb	3 mm (5 mm)	13 cm	
IVa	3 mm (5 mm)	distance between tuff horizon groups not measurable due to faulting	gypsum substituted
IVb	5 mm (8 mm)	5 cm	gypsum substituted
IVc	2 mm (4 mm)	8 cm	mostly as gypsum layer
Locality 31			
I	2 mm (3-5 mm)		gypsum substituted
IIa	1 mm (5 mm)	150 cm	bentonitic, flaky
IIb	10 mm (20-25 mm)	12 cm	gypsum substituted
IIIa	1 mm (3 mm)	200 cm	gypsum substituted
IIIb	3 mm (5 mm)	90 cm	bentonitic, flaky
IVa	3 mm (10 mm)	110 cm	gypsum substituted
IVb	5 mm (10 mm)	50 cm	gypsum substituted
IVc	2 mm (5 mm)	15 cm	mostly as gypsum layer
Locality 32			
I	up to 120 mm		mostly as gypsum layer
IIa	2 mm (5 mm)	250 cm	gypsum substituted
IIb	5 mm (10-15 mm)	80 cm	gypsum substituted
IIIa	2 mm (10-40 mm)	110 cm	gypsum substituted
IIIb	3 mm (10-20 mm)	100 cm	gypsum substituted
IVa	3 mm (10 mm)	120 cm	bentonitic, flaky
IVb	2 mm (up to 800 mm)	40 cm	mostly as gypsum layer
IVc	2 mm (10-30 mm)	80 cm	mostly as gypsum layer
V	1 mm (10 mm)	40 cm	gypsum substituted

Tuff Beds	True Thickness (thickness after contact with water)	Distance to underlying tuff bed	Remarks
Locality 30			
IIIb	3 mm (20-40 mm)		gypsum substituted
IVa	8 mm (10 mm)	130 cm	bentonitic, flaky
IVb	3 mm (10-80 mm)	40 cm	mostly as gypsum layer
IVc	3 mm (10-150 mm)	70 cm	mostly as gypsum layer
Localities 15 and 16			
VIb	3 mm (5 mm)		gypsum substituted
VII	5 mm (10-20 mm)	480 cm	bentonitic, flaky
Locality 20			
VII	4 mm		bentonitic, flaky
Locality 35			
VII	3-4 mm		bentonitic, flaky
Locality 40			
VIIIa	3-4 mm		gypsum substituted
Locality 43			
VIIIa	3-4 mm		gypsum substituted
VIIIb	2-3 mm	195 cm	gypsum substituted
VIIIc	8-10 mm	38 cm	gypsum substituted
VIII d	2 mm	25 cm	gypsum substituted
Locality 27			
VIIIa	2-3 mm		gypsum substituted
Locality 9			
VIIIa	15-20 mm		calcite substituted
VIIIb	2-5 mm	155 cm	gypsum substituted

B. Analytical methods and techniques

B-1 Sampling techniques and denominations

B-1.1 Tuff beds

Samples were generally taken in situ. As the generally softer tuff beds are interbedded in the more resistant mudstones, the outermost, weathered centimetres of the tuff bed were excavated. Pieces displaying a length of more than 5 cm were only rarely extracted, most of the pieces were below 1 cm in length. The clay material of the bentonitic tuff beds is often replaced by gypsum or also by carbonates such as calcite (e.g. #9: tuff bed VIIIa from the Aranos Basin). It was therefore most important during the course of sampling that gypsum and other secondary minerals were separated from the bentonitic material which formed from the originally deposited tuff bed.

Tuff beds of „good quality“ were only rarely replaced by gypsum (e.g. tuff bed IIb from the Aranos Basin of southern Namibia) whereas other tuff beds such as VI and VII from the Aranos Basin were mostly substituted by gypsum. The sampled material from these tuff beds therefore yielded only few, juvenile minerals whereas other tuff beds of good quality revealed many juvenile heavy minerals.

Samples were enumerated as follows: outcrop - tuff bed (e.g.: #2, tuff bed IVa). Numbers after tuff samples indicate laterally taken samples, e.g. #2, tuff bed IVa-2 indicate the second sample of tuff bed IVa.

B-1.2 Mudstones

Mudstones of the Ganigobis Shale Member were sampled in association with the gamma-ray measurements about every 0.5 metres in each outcrop. The mudstones become softer with increased duration of exposure. As river banks are sporadically excavated by floods, samples of the lower parts of the eroded river banks are generally less weathered than samples of the upper parts. Samples in the uppermost parts of the outcrops were most of times taken in large cavities which were also used for the gamma-ray

measurements.

B-1.3 Sample denominations

Mudstone samples were taken approximately in vertical distances of 0.5 m and were therefore enumerated as follows: Number of outcrop - sample. For example, sample 9/5 was taken 0.5 m above 9/4. In outcrop locality #2, samples were obtained from divers river banks. As samples were taken from stratigraphically higher outcrops at first, later samples which were taken from stratigraphically lower outcrops were enumerated as follows: outcrop - (-sample). Sample 2/(-10) was therefore obtained about 0.5 m above sample 2(-11).

B-2 Thin-section analysis

In order to study the matrix, main phenocrysts, structural and textural features of the tuff horizons, thin-sections were analysed with a LEITZ Laborlux 12 Pol S polarisation microscope. In total 72 thin sections were examined. About half of the thin sections were prepared at the Institute of Geology by Rupert Wassermann, the other half at MIEKINIA in Krakow (Poland). The preparation of thin-sections from bentonitic tuff horizons is problematic due to (1) the shattering of samples because of the high degree of alteration, (2) the occasional removal of larger components (e.g. quartz splinters) from the matrix and (3) the occurrence of smectitic clay minerals which rapidly swell with contact of water. This required a careful preparation with dry sawing and polishing or with an oil immersion. Nevertheless, the rock displayed in the thin-sections is generally distorted or occurs in pieces. The sorting and the phenocryst content of the rocks were determined by visual estimation and grain sizes were measured with an internal scale within the ocular.

B-3 X-ray diffraction analysis

B-3.1 Methods

B-3.1.1 Separation of the fraction < 2 µm

The bentonitic material was pulverised to a grain size < 50 µm in an agate grinding vessel on a swing mill. For the determination of the clay minerals the fraction < 2 µm had to be separated. The pulverised sample was given into approximately 1 litre of distilled water, elutriated and shaken for complete dispersion on a shake table for five hours. 5 ml of 0,125 mol Sodiumpyrophosphate (Na₄P₂O₇) in aqueous solution was added to avoid flocculation of the material. The resulting disaggregated suspension was transferred to a settling column in an Atterberg measuring cylinder. Applying Stoke's law the fraction > 2 µm settled out in a 25 cm high settling column in approximately 20 hours depending on the room temperature. The remaining suspension with the fraction < 2 µm was drained into a bottle. 10 ml of a 0,5 mol MgCl₂-solution was added for a rapid flocculation of the suspended material. The water was drained off and further separated in a centrifuge (10 min at 3000 r.p.m.). The clay material was filled into

glass containers against desiccation.

B-3.1.2 Sample preparation

Measurements were carried out in three different ways:

a, as a whole rock powder sample (at the Geologisches Landesamt Rheinland-Pfalz in Mainz)

b, as a non treated textured specimen on a smear slide (at the Mineralogisches Institut, Universität Würzburg)

c, as a textured specimen on a smear slide, treated with glycerol (at the Mineralogisches Institut, Universität Würzburg)

a, the rock powder was filled into a stainless steel sample holder and pressed for an even surface

b, the clay material was smeared on a microscopic glass slide, mixed with a few droplets of distilled water and stirred until a homogeneous suspension developed, the specimen was dried for 30 minutes in an oven heated to 50°C

c, the clay material was smeared on a microscopic glass slide, mixed with a few droplets of glycerol and stirred until a homogeneous suspension developed, the specimen was dried for two hours in an oven heated to 50°C.

	Mainz	Würzburg
Instrument type	Phillips PW 3710	Phillips PW 1170
Radiation	CuKα	CuKα
Accelerating voltage (kV)	45	40
Amperage (mA)	40	30
Divergence slit	Automatic	1°
Steptime of measurement (sec)	1	2
Degree/steptime	0.02	0.04
Measuring range (2-Theta)	3.00 - 79.98	2.50 - 60.02

Tab. C-1.2: Comparison of diffractometer settings in Mainz and Würzburg

Arising problems

a, Due to their high content, peaks of quartz and feldspars dominate the spectrum and reduce the intensity of the clay mineral peaks which impedes their detection.

b, The intensities of the clay mineral peaks are

enhanced through the described separation if the platy clay minerals come to lie parallel to the plane surface of the diffractometer. This is achieved by smearing the material on the slides, disadvantages of this technique may arise by thickness variations and uneven surfaces.

c, Glycerol widens the diagnostic basal reflections of swelling clay minerals and moves them to higher Å-values.

B-4 Separation of heavy minerals

If necessary, the rock samples were crushed with a jaw breaker to 5 mm large particles. Most of the samples were only mechanically milled for about 15-20 seconds. The milled sample material of the tuffs was divided by dry sieving into three grain-size fractions (45-90 µm, 90-180 µm, 180-250 µm). At a late stage of the thesis, samples were simply dissolved in water and detergent which helped to disintegrate the samples due to reduced surface tensions. The milled and dry-sieved samples as well as the dissolved samples were then rinsed with water within the sieves of 45, 90 and 180 µm. While washing, the sieves were placed in an ultrasonic basin which enhanced the removal of dust of the dry-sieved material. The clay fraction of the dissolved samples and also the clay coatings which occasionally cover the heavy minerals were removed by the combined washing and ultrasonic treatment. After drying, the fractions were further separated with a Frantz magnetic separator in a non-magnetic and a magnetic fraction. An amperage of 0.8 A and a 20° degree angle of inclination were used as standard values. The non-magnetic fraction was finally divided with the help of a Sodumpolytungstate-gravity solution ($3\text{Na}_2 - \text{WO}_4 \times 9\text{WO}_2 \times \text{H}_2\text{O}$, density $2.90 \pm 0.02 \text{ g/cm}^3$ at 200 C) within separatory funnels over four hours. It turned out that within the fraction 45-90 µm most non-opaque heavy minerals were concentrated whereas the larger grain size fractions mostly contained secondary opaque minerals such as goethite or secondary non-opaque minerals such as barite. The isolated heavy minerals were embedded into the permanent mount Lakeside C 70 ($n = 1.54$) on object carriers for optical identification. The optical identification of the heavy minerals was carried out with a LEITZ Laborlux 12 Pol S polarisation microscope. The heavy minerals were counted in quadrants. The quadrants were drawn on the object carrier by a water-resistant pen. However, minerals below the lines were occasionally difficult to determine.

B-5 Geochemistry

B-5.1 Sample preparation

Criteria for sample selection have already been described in Chapter A-1. Sample preparation was carried out at the Institut für Geologie, Universität Würzburg. About 100 g of rock material were pulverised using a swing mill with agate grinding vessel. The sample material was manually homogenised and separated into 4 equal portions. The procedure was always repeated twice.

B-5.2 Loss On Ignition (LOI)

Loss On Ignition (LOI) was determined for each sample. The sample powder was dried over night at 105-110 °C. About 1 g of sample powder was then weighed in a porcelain beaker and heated for 4 hours at 1000 °C. The LOI was then calculated from the weight difference between dried and heated sample material.

B-5.3 Whole-rock major and trace elements analysis by X-ray Fluorescence Spectrometry (XRF)

The XRF-determination of major and trace elements was performed at the Mineralogisches Institut, Universität Würzburg (1996 and 1997) and at the Institut für Geologie und Dynamik der Lithosphäre, Universität Göttingen (1998).

Mudstone and tuff beds sampled in 1996 and 1997 were analysed in Würzburg. Following elements were analysed: SiO_2 , TiO_2 , Al_2O_3 , Fe_2O_3 , MnO , MgO , CaO , Na_2O , K_2O , P_2O_5 , S, V, Cr, Co, Ni, Zn, Rb, Sr, Y, Zr, Nb, Ba.

All elements were determined from fusion disks. 0.6 g of dried sample powder was mixed with 3.6 g of lithium tetraborate and lithium metaborate (MERCK SPEKTROMELT A 12). 1.5 g of ammonium nitrate (NH_4NO_3) was added to guarantee total conversion of Fe^{2+} to Fe^{3+} , since total iron was determined as total Fe_2O_3 . The mixture was melted in a platinum crucible in four steps until it reached a temperature of about 1000° C, poured into a platinum disk mould and cooled in an air stream.

All disks were analysed in a Philips PW 1480 XRF spectrometer with a Rh target tube (Philips X 40 software, measuring program GEO-1). Additionally, corrections were based on a calibration using the international rock standards W-2 (basalt), BE-N (basalt), GSS-6 (sediment), and GH (granite). The analytical error of the major elements is 1-3 % depending on the proximity to the detection limits. Detection limits of the trace elements range from 5 to 10 ppm. The precision errors are usually 10 % but they increase to 50 % if the concentrations are close to their limits.

Tuff beds and volcanic clasts sampled in 1998 were analysed in Göttingen. Following elements were analysed: SiO₂, TiO₂, Al₂O₃, Fe₂O₃, MnO, MgO, CaO, Na₂O, K₂O, P₂O₅, Nb, Zr, Y, Sr, Rb, Pb, Ga, Zn, Cu, Ni, Co, Cr, V, Ba and Sc. The XRF-technique used in Göttingen is extensively described in Hartmann (1994). Thus, preparation and analytical procedures will be discussed just briefly.

Glass disks were used for the measurements. They were prepared by mixtures of prefused lithium tetraborate, lithium metaborate, and LiF. For the dilution, 6.0 g of this flux and 1.0 g of the ground glass sample were weighted in platinum-gold crucibles and fused for 25 min at 1100° C. The melt was poured into pre-heated, polished 40 mm-diameter molds. All elements were analysed by a Philips PW 1480 automated sequential spectrometer using a 3 kilowatt rhodium target X-ray tube for sample excitation. Data processing was controlled by a Philips X40 software package.

B-5.4 Trace elements and REE-analysis by inductively coupled plasma-mass spectrometry (ICP-MS)

The trace elements Li, Be, Rb, Sr, Y, Zr, Nb, Mo, Cs, Ba, Hf, Ta, W, Tl, Pb, Bi, Th and U as well as the rare earth elements (REE) La, Ce, Pr, Nd, Sm, Eu, Gd, Tb, Dy, Ho, Er, Tm, Yb and Lu were measured by ICP-MS (inductively coupled plasma-mass spectrometry) at the Institut für Geologie und Dynamik der Lithosphäre (IGDL), Universität Göttingen.

About 100 mg of sample powder were mixed with 4 ml HF (48%) and 4 ml HClO₄ (70%) in a teflon crucible. The samples were heated for 12 hours at 170 °C under pressure (Pico Trace, 1997). Subsequently the solutions were almost completely condensed. The residue was dissolved in 4 ml concentrated HNO₃ (65%) and 1.2 ml 6n HCl. The solution was filled up with H₂O to 200 ml and stored in polyethylene bottles. All solutions were clear and without residues. Element concentrations were determined from the solutions.

The REE analyses were performed using the ICP-MS PQ2+ made by Fisons with 20 µg/l as interior standard. Every sample series was monitored by the international standard DR-N (diorite; Govindaraju, 1995) and by the internal standard BB 46 (basalt) of the IGDL Göttingen (cf. Appendix F-2, Tab 24).

Most elements correspond very well with each other which confirms that the measurements are overall highly reliable. Values of W should not be used as measurements of W differ from the standard DR-N by the factor 15. Zircon was easily dissolved and correlates with the basic standard BB 46 but not with DR-N. Lower Hf-values in comparison with the DR-N standard are therefore reasonable.

Ta varies a lot and should be used with great care. Varying values might be due to stability problems of the solutions. Sr, Rb, Nb, Zr, Y, Ba and Pb were measured with XRF and ICP-MS. Values correspond very well with each other. Zr-values also fit very well apart from an analysis of a volcanic clast sample. This means that all elements contained in the zircons were completely dissolved. It is therefore very likely that the REE-analyses are correct. According to the IGDL Göttingen, the values of the XRF-measurements should be used for the elements Zr, Sr, Ba and Rb whereas for Nb, Pb (<50 ppm) and Y (<50 ppm) the values of the ICP-MS measurements seem to be more appropriate.

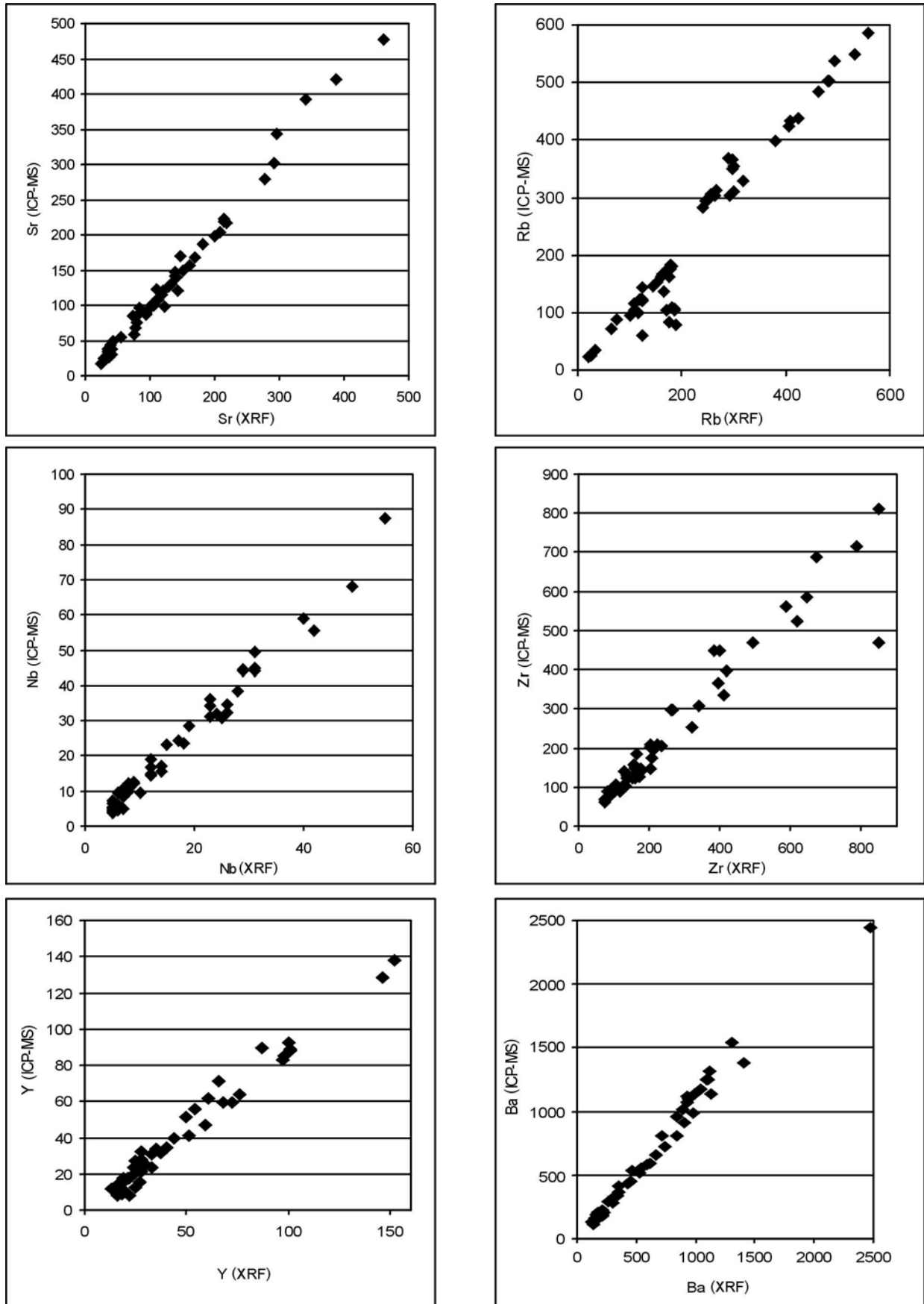


Fig. 154: Comparison of trace element concentrations measured both by XRF and ICP-MS.

Appendix C (Tab. 21): Summary of all gamma-ray measurements in the Aranos Basin, southern Namibia.

Outcrop/Sample #	Gamma-ray #	Total	ppm	K (%)	ppm	U	ppm	Th	ppm	Spectro-meter	Remarks
# 1-6	29	165.8	11158	5.4	1397	5.7	272	31.2	234	cv1	darkgrey shales
# 1-7	30	167.4	11266	5.6	1466	6.9	293	29.9	225	cv2	darkgrey shales
# 1-8	31	162.7	10949	4.4	1145	4.2	230	28.7	216	cv2	darkgrey shales
# 1-9	32	161.8	10887	5.2	1324	5.4	246	27.0	202	cv1	
# 1-10	33	162.4	10930	5.0	1284	4.4	225	27.3	204	cv1	4 km SW HARDAP DAMM
# 1-11	34	164.6	11074	4.7	1211	4.5	228	27.3	205	cv1	
# 1-12	35	160.2	10780	4.0	1064	5.2	230	24.4	184	cv1	
# 1-13	36	161.3	10856	4.2	1096	5.7	232	22.6	170	cv1 / vp	
# 1-14	37	161.4	10865	4.8	1228	4.6	231	27.2	204	vp	
# 1-15	38	167.1	11247	4.5	1206	7.0	269	24.5	185	dp	
# 1-16	39	162.3	10919	4.9	1278	5.8	262	28.7	216	cv1	
# 1-17	40	161.2	10847	4.8	1243	5.3	234	25.0	187	vp / cv1	
# 1-18	41	165.4	11132	4.4	1157	5.3	235	25.0	188	cv1	
# 1-19	42	161.6	10872	4.7	1234	6.7	254	23.1	173	cv1	
# 1-20	43	162.4	10972	4.9	1264	4.7	230	26.9	201	cv1	
# 1-21	44	161.0	10888	4.8	1231	5.0	234	26.4	198	cv1	
# 1-22	45	162.2	10917	4.9	1271	7.6	263	21.1	158	vp	
# 1-23	46	164.3	11060	4.7	1264	8.5	296	23.5	177	cv1	
# 1-24	47	161.4	10863	5.0	1282	6.0	244	23.9	178	dp	
# 1-25	48	165.2	11120	4.8	1266	6.1	264	27.5	207	dp	
# 1-26	49	161.3	10858	4.5	1194	6.2	249	24.2	182	cv1	
# 1-27	50	158.2	10649	3.9	1019	4.6	204	21.7	163	dp	
# 1-28	51	160.3	10790	3.5	950	5.8	244	24.7	188	dp	0,1 m below brown sandstone bed
# 1-29	52	168.3	11326	5.0	1294	6.7	259	24.2	181	vp / cv1	0,4 m above brown sandstone bed
# 1-29 + 0,5 m	66	157.8	10617	3.2	869	5.6	209	18.4	139	vp / cv1	
# 1-30	53	162.4	10931	4.7	1251	6.8	286	29.1	220	cv1-2	
# 1-30 + 0,5 m	67	165.0	11102	4.0	1034	3.4	190	24.0	181	vp	
# 1-31	54	161.9	10839	4.5	1165	4.3	227	27.6	208	cv1	
# 1-31 + 0,5 m	68	163.9	11032	4.9	1272	6.4	261	25.9	194	cv1	
# 1-32	55	167.2	11254	4.2	1124	5.0	240	27.2	205	cv1	
# 1-32 + 0,5 m	69	158.4	10661	3.9	995	4.4	178	17.8	132	dp / vp	
# 1-33	56	158.3	10656	4.1	1051	4.8	204	20.9	157	vp / cv1	
# 1-33 + 0,5 m	70	159.3	10719	4.2	1062	3.4	175	21.5	161	dp	
# 1-34	57	166.1	11176	4.1	1027	2.8	170	22.7	169	cv1	
# 1-34 + 0,5 m	71	159.4	10729	3.6	948	4.3	193	20.8	157	dp	
# 1-34 + 1m	58	169.4	10727	3.3	863	2.9	181	24.4	185	cv1	no sample
# 2(-12)	168	161.8	10885	4.2	1121	5.7	236	23.5	177	vp	3rd outcrop
# 2(-11)	167	160.1	10775	3.9	1016	5.2	210	20.3	153	vp	FISH RIVER
# 2(-10)	166	158.4	10662	3.5	905	3.4	177	21.2	160	vp	10 cm below concretionary horizon 1
# 2(-9)	165	161.9	10892	4.8	1229	4.8	220	24.5	183	hp	30 cm below concretionary horizon 2
# 2(-8)	164	166.1	11180	4.6	1240	7.7	298	27.5	208	vp	directly below tuff bed Ia
# 2(-7)	163	167.6	11279	5.1	1374	8.6	315	27.1	204	vp	
# 2(-6)	162	165.3	11122	4.7	1271	8.1	299	26.1	197	vp	2nd outcrop
# 2(-5)	161	162.9	10965	4.1	1084	6.0	227	20.2	151	cv1	10 cm below tuff bed IIa
# 2(-4)	160	170.3	11463	5.0	1333	8.5	306	25.9	194	vp / cv1	10 cm above tuff bed IIb
# 2(-3)	159	164.9	11095	4.4	1174	7.8	264	20.3	152	vp	
# 2(-2)	158	165.9	11165	4.7	1245	6.9	265	24.2	182	cv1	1st outcrop
# 2(-1)	157	163.5	11003	4.9	1289	7.4	274	24.0	180	cv1	10 cm below tuff bed IIIb
# 2-1	122	164.4	11065	4.7	1262	8.3	296	24.4	184	dp	KHOMAB / FISH RIVER
# 2-2	123	167.5	11272	4.8	1283	8.8	291	21.4	160	cv1	
# 2-3	124	163.9	11031	5.5	1402	5.2	244	27.7	207	vp / cv1	
# 2-4	125	164.4	10997	5.1	1299	4.9	241	28.4	213	vp / cv1	
# 2-5	126	168.1	11312	5.1	1336	7.1	273	25.1	188	vp	
# 2-6	127	166.0	11170	4.9	1254	5.1	226	24.3	181	vp	
# 2-7	128	164.5	11068	5.2	1374	7.3	300	29.6	223	vp	
# 2-8	129	167.6	11281	5.3	1355	5.3	253	29.1	218	vp	
# 2-9	130	169.0	11374	5.1	1299	4.4	237	29.8	224	vp	gypsum coatings
# 2-10	131	171.9	11566	5.4	1442	7.1	312	33.2	250	vp	gypsum coatings
# 2-11	132	168.3	11325	4.9	1286	5.1	272	33.5	253	vp	gypsum coatings
# 2-12	133	162.7	10952	3.9	1072	5.1	273	33.6	256	hp	gypsum coatings
# 2-13	134	164.8	11090	5.1	1352	6.2	286	31.8	240	cv1	
# 2-14	135	163.6	11008	5.0	1304	5.5	269	31.1	234	hp	10 cm below tuff bed Vb
# 2-15	136	161.9	10894	4.3	1169	6.2	280	30.4	231	vp	
# 2-16	137	166.7	11218	4.7	1255	6.4	280	29.6	223	vp	lamination, gypsum layers
# 2-17	138	165.9	11254	4.2	1156	6.6	285	29.2	222	vp	lamination, microturbidites
# 2-18	139	165.9	11168	4.4	1151	3.3	232	32.8	248	vp	
# 2-19	140	166.6	11214	4.4	1168	5.5	257	28.8	218	vp	measurement on joint plane
# 2-20	141	163.0	10971	4.5	1222	5.9	280	31.5	238	vp	35 cm above tuff bed Vc
# 2-21	142	167.4	11263	5.0	1298	5.2	257	29.9	225	vp	lamination

Outcrop/Sample #	Gamma ray #	Total	ppm	K (%)	ppm	U	ppm	Th	ppm	Spectrometer	Remarks
# 2-23	144	161.9	10897	4.4	1192	6.2	279	30.1	228	vp	massive shales
# 2-24	145	162.1	10906	4.5	1196	5.9	269	29.2	221	vp	lamination, microturbidites
# 2-25	146	163.3	10987	4.4	1171	4.5	246	30.6	231	vp	laminated shales
# 2-26	147	165.8	11156	4.3	1148	4.5	243	30.4	230	vp	laminated shales
# 2-27	148	161.6	10878	4.0	1066	5.8	242	24.4	187	vp	laminated shales
# 2-28	149	163.9	11031	4.9	1260	4.0	244	32.7	247	vp / cx	faintly laminated shales
# 2-29	150	165.8	11156	4.5	1196	5.2	257	30	227	cx	massive shales
# 2-30	151	166.1	11178	3.9	1088	5.6	279	32.5	247	vp	massive shales
# 2-31	152	163.2	10982	4.1	1142	7.4	292	27.4	208	vp	slightly laminated shales
# 2-32	153	163.7	11015	4.7	1267	7.8	310	29.2	223	vp	massive shales
# 2-33	154	162.8	10959	3.8	1033	5.7	255	27.1	206	vp	zone of soil development
# 2-34	155	170.0	11439	4.2	1224	9.6	368	32.8	250	vp / cv1	soil, gypsum layers
# 2-35	156	170.4	11467	4.3	1292	11.7	410	32.5	249	cv1	10 cm below river gravel
# 3-1	1	157.6	10604	3.8	972	3.0	173	22.4	168	dp / cv1	SCHLIP
# 3-1 + 0.5 m	13	155.6	10471	3.2	840	4.0	165	16.7	125	dp	
# 3-2	2	157.0	10568	3.7	939	4.6	174	16.0	119	dp / cv1	
# 3-2 + 0.5 m	14	157.2	10581	4.3	1063	2.5	157	21.5	160	cv1	
# 3-3	3	157.5	10602	3.5	920	4.5	180	17.4	130	dp / cv1	
# 3-3 + 0.5 m	15	158.2	10647	4.1	1048	4.4	195	20.9	156	cv1-2	
# 3-4	4	157.0	10565	3.7	974	5.2	196	17.4	130	dp / cv1	
# 3-4 + 0.5 m	16	158.5	10667	4.3	1087	3.6	189	23.0	172	cv1	
# 3-5	5	161.3	10577	3.7	976	4.1	198	22.5	170	dp / cv1	
# 3-5 + 0.5 m	17	161.3	10852	4.3	1070	4.4	178	17.4	129	cv1	
# 3-6	6	162.3	10919	4.4	1143	4.8	221	24.3	183	cv1	
# 3-6 + 0.5 m	18	154.4	10387	3.1	820	4.0	185	16.9	127	cv1	
# 3-7	7	158.6	10672	3.5	905	4.0	185	20.6	155	dp / cv1	
# 3-10	10	161.7	10880	4.6	1226	6.4	262	26.1	196	dp / cv1	
# 3-8	8	159.9	10760	4.9	1203	3.7	176	20.4	150	vp	
# 3-11	11	162.3	10922	4.3	1085	4.3	195	25.5	161	vp	
# 3-9	9	164.7	11082	4.8	1198	5.2	203	19.3	143	vp	
# 3-12	12	162.3	10926	5.1	1250	2.6	170	23.8	176	vp	20 cm below calcrete
# 4-1	20	159.5	10733	3.9	999	4.0	187	21.1	158	Basis	2.5 km W FALKENHORST
# 4-2	21	158.3	10652	3.5	925	3.8	194	23.1	174	Top	soil development, roots
# 4-3	22	161.6	10873	4.4	1166	6.5	257	24.4	184	Basis	
# 4-4	23	160.7	10816	4.0	1065	5.0	223	24.0	181		
# 4-5	24	160.4	10793	4.3	1116	4.2	210	25.0	188	Top	
# 4-6	25	161.1	10841	4.7	1184	4.4	205	23.3	174	Basis	
# 4-7	26	161.1	10839	4.2	1127	5.5	246	26.3	199	Top	
# 4-8	27	161.0	10835	3.9	1046	4.8	233	26.9	204		
# 4-9	28	160.7	10817	3.7	979	4.5	215	24.4	185		
# 5-1	77	164.1	11041	4.8	1266	6.8	272	26.3	197	cv1	
# 5-2	78	166.2	11183	4.7	1249	6.7	267	25.6	192	vp / cv1	
# 5-3	79	163.5	11006	3.8	1047	6.6	251	22.7	171	vp	soil development, gypsum layers
# 5-4	80	163.2	10984	4.3	1168	8.2	286	22.8	172	cv1	soil development, gypsum layers
# 5-5	81	164.4	11067	3.4	981	7.6	278	23.8	181	cv1	soil development, gypsum layers
# 6-3	59	163.5	11003	5.2	1317	5.1	230	25.4	189	dp	
# 6-4	60	165.7	11150	5.4	1424	7.6	301	28.8	216	cv1	
# 6-5	61	165.8	11161	5.1	1341	5.9	277	30.9	232	dp / cv1	
# 6-6	62	163.3	10989	5.3	1342	4.4	228	27.6	206	cv1	
# 6-7	63	164.4	11066	4.4	1131	3.9	208	25.7	193	dp / cv1	
# 6-8	64	168.1	11315	4.8	1218	4.0	222	28.1	211	cv1-2	30 cm below sandstone bed
sandstone bed	65	157.2	10576	2.5	652	4.4	137	9.1	68	vp	
# 7-1	72	153.3	10313	2.7	677	2.6	117	12.6	94	hp	diamictite, silty matrix
# 7-2	73	154.8	10420	2.5	660	4.1	145	11.9	90	dp	diamictite, silty matrix
# 7-3	74	155.3	10451	3.0	758	3.3	135	13.3	99	dp	diamictite, silty matrix
# 7-4	75	154.8	10414	3.2	813	2.8	134	15.4	115	vp	diamictite, silty matrix
sandy diamictite	76	152.9	10289	2.2	571	2.0	99	11.9	89	vp	diamictite, sandy matrix
# 8-1	82	160.5	10799	3.9	1049	6.6	251	22.7	171	dp	
# 8-2	83	161.6	10873	3.8	1018	5.8	231	21.9	165	vp	
# 9-13	96	160.6	10806	3.5	964	4.9	229	25.3	192	vp / cv1	unweathered rock
# 9-12	95	159.8	10756	4.3	1130	5.8	231	22.0	165	vp	unweathered rock
# 9-11	94	158.9	10691	3.7	950	3.1	185	24.4	184	vp	0.5 m below 9-10
# 9-10	93	162.7	10946	3.4	926	5.4	218	21.1	160	vp	0.5 m below 9-9
# 9-9	92	160.5	10804	3.4	925	4.9	217	23.1	175	vp	0.5 m below 9-1
# 9-1	84	159.9	10764	3.4	932	6.0	234	21.6	164	hp	unweathered, hard
# 9-2	85	159.4	10730	3.1	855	5.6	213	19.3	143	hp	unweathered, hard
# 9-3	86	165.7	11150	3.6	957	5.1	217	22.4	169	vp	weathered rock
# 9-4	87	160.5	10800	3.6	979	5.4	234	24.4	185	vp / cv1	weathered rock
# 9-5	88	161.5	10872	3.8	1045	5.8	252	26.1	197	cv1	weathered rock
# 9-6	89	161.2	10850	3.5	941	5.0	217	22.6	171	vp	weathered rock
# 9-7	90	164.6	11079	3.9	1016	5.0	213	22.1	166	cv1	weathered rock
# 9-8	91	162.2	10917	3.3	873	4.2	185	19.8	149	vp	weathered rock, soil development

Outcrop/Sample #	Gamma ray #	Total	ppm	K (%)	ppm	U	ppm	Th	ppm	Spectro-meter	Remarks
# 12-2	102	164.4	11063	4.0	1093	7.4	262	21.6	163	vp	
# 12-3	103	167.4	11263	4.1	1107	7.4	264	22.0	166	vp / cv1	gypsum layers: 3 mm
# 12-4	104	166.1	11181	4.3	1153	6.5	253	23.6	178	vp	gypsum layers: 2-5 mm
# 12-5	105	166.7	11221	3.6	1028	8.9	286	19.7	149	vp	10 cm below fault
# 13-4	106	163.1	10979	4.1	1085	4.7	239	28.4	215	vp	5 cm below cone-in-cone layers
# 13-5	107	166.9	11231	4.7	1249	5.5	269	31.3	236	vp	30 cm below pyritic zone A
# 13-6	108	162.9	10962	5.0	1314	4.4	259	33.9	256	vp	15 cm above pyritic zone A
# 13-7	109	164.3	11054	4.7	1248	6.6	280	28.7	217	dp	
# 13-8	110	161.9	10895	4.5	1207	5.3	263	30.8	233	vp	
# 13-9	111	161.2	10846	4.3	1126	5.2	237	25.7	194	vp	10 cm below pyritic zone B
# 13-10	112	164.1	11042	4.5	1157	3.5	224	30.5	230	vp / cv1	
# 13-11	113	158.2	10647	3.7	971	3.3	189	24.3	183	cv1	heavily weathered
96/13: pyritic zone B	114	162.0	10901	3.7	975	3.8	197	23.9	180	vp	red zentral zone
96/13: pyritic zone A	115	160.9	10829	4.0	1063	4.0	223	28.2	213	vp	grey mudstone layers
# 14-1	116	157.7	10616	3.1	836	3.3	180	22.3	169	hp	unweathered rock
# 14-2	117	158.8	10690	3.5	938	3.7	207	26.3	199	dp	unweathered rock
# 14-3	118	160.2	10782	3.8	998	3.8	204	25.3	191	cv1	weathered rock
# 14-4	119	163.7	11019	4.0	1034	4.2	203	23.5	176	cv1	weathered rock, gypsum layers
# 14-5	120	160.8	10822	3.7	1010	5.2	237	26.1	197	cv1	weathered rock, gypsum layers
# 14-6	121	167.3	11261	4.2	1126	5.6	255	28.1	212	vp / cv1	weathered rock, soil development
# 15-1	169	160.1	10773	3.6	984	4.7	239	28.4	216	vp	unweathered rock
# 15-2	170	162.2	10919	3.6	967	4.4	228	27.4	208	vp / cv1	
# 15-3	171	164.8	11092	3.8	1017	4.8	237	27.6	209	vp	
# 15-4	172	163.2	10985	3.9	1038	4.5	233	28.2	214	vp / cv1	
# 15-5	173	160.9	10829	3.7	994	4.5	227	26.9	204	hp	18 cm below tuff bed VII
# 15-6	174	163.3	10991	4.4	1165	5.1	254	29.7	224	cv1	0,6 m below top of outcrop
# 18-1	175	159.3	10720	3.3	911	4.9	218	23.0	175	hp	unweathered rock
# 18-2	176	164.1	11046	3.5	938	4.3	212	24.6	186	vp	
# 18-3	177	162.1	10911	3.7	996	4.2	221	27.0	204	vp	
# 18-4	178	161.9	10895	3.9	1006	3.1	198	27.1	205	vp	
# 18-5	179	161.6	10874	4.1	1064	3.8	215	27.5	208	vp	soil development, roots
# 23(-6)	220	160.2	10781	3.8	1007	4.2	207	24.1	182	vp / cv1	Mud-/Siltstones with
# 23(-5)	219	159.6	10739	4.1	1054	4.4	195	20.7	155	dp	dropstones, pyritic concretions
# 23(-4)	218	162.2	10915	4.3	1128	4.4	228	27.3	205	vp	tuff bed "0"
# 23(-3)	217	164.9	11099	4.7	1225	5.1	244	27.6	208	vp	
# 23(-2)	216	168.0	11307	4.9	1264	4.4	248	31.8	239	vp / cv1	outcrop 30 m towards the west
# 23(-1)	215	164.7	11087	5.4	1373	5.1	247	28.5	213	vp	
# 23-1	180	165.0	11107	4.5	1163	4.8	231	26.6	200	vp	Farm Waterval
# 23-2	181	162.9	10963	4.6	1218	5.0	253	29.9	225	vp	
# 23-3	182	164.9	11100	4.6	1210	5.3	246	27.2	205	vp	
# 23-4	183	159.6	10738	3.9	1061	7.4	252	19.7	148	vp	tuff bed I
# 23-5	184	169.5	11406	5.0	1334	8.8	296	22.7	170	vp	
# 23-6	185	164.5	11072	4.6	1244	8.1	298	25.7	194	vp	
# 23-7	186	169.3	11394	5.1	1353	7.8	288	25.1	188	vp	
# 23-8	187	165.1	11110	5.4	1413	7.8	285	24.7	184	vp	25 cm below tuff bed IIa
# 23-9	188	171.8	11563	5.0	1377	9.9	344	27.3	206	vp	Tuff bed IIb
# 23-10	189	166.0	11172	5.3	1400	7.8	306	28.5	215	vp	
# 23-11	190	163.4	10994	4.6	1229	5.8	261	28.3	213	vp	15 cm below tuff bed III
# 23-12	191	166.2	11185	5.0	1286	5.5	246	26.4	197	vp	
# 23-13	192	166.4	11195	4.9	1241	4.0	209	25.4	190	vp	
# 23-14	193	162.6	10940	5.4	1362	5.0	227	25.0	186	vp	10 cm below tuff beds IV
# 23-15	194	164.7	11086	5.3	1370	5.7	259	28.6	214	vp	
# 23-16	195	166.5	11202	4.6	1256	8.0	298	26.3	199	vp	red hematite coatings
# 23-17	196	163.1	10978	5.2	1361	6.9	280	27.3	205	vp	red hematite coatings
# 23-18	197	164.2	11047	5.0	1342	7.3	299	29.7	224	vp	
# 23-19	198	165.5	11136	4.7	1314	7.7	338	35.5	270	vp	
# 23-20	199	164.6	11074	4.5	1226	6.6	290	30.7	233	vp	10 cm below tuff bed V
# 23-21	200	161.6	10876	4.1	1138	6.0	286	32.3	245	vp	begin of lamination
# 23-22	201	160.6	10811	3.8	1025	3.4	224	31.2	237	vp	well laminated
# 23-23	202	168.3	11327	4.2	1117	5.2	248	28.1	212	vp	well laminated
# 23-24	203	161.8	10887	4.2	1116	5.2	238	26.3	198	vp	lamination
# 23-25	204	164.8	11079	4.6	1204	3.4	241	34.4	260	vp	faint lamination
# 23-26	205	163.5	11001	4.1	1133	5.5	276	32.4	246	vp	massive shales, with microturbidites
# 23-27	206	167.2	11255	4.4	1177	5.6	268	30.4	230	vp / cv1	massive shales, with microturbidites
# 23-28	207	167.5	11275	4.5	1238	7.3	206	31.0	235	vp / cv1	massive shales, with microturbidites
# 23-29	208	166.5	11206	4.0	1078	4.6	239	28.8	218	vp	massive shales, with microturbidites
# 23-30	209	163.7	11018	3.8	1042	5.0	248	28.9	219	vp	massive shales, with microturbidites
# 23-31	210	167.1	11243	3.7	1009	6.0	247	24.5	186	vp / cv1	lamination, with microturbidites
# 23-32	211	166.5	11208	4.4	1211	7.6	307	29.5	224	vp / cv1	microturbidites
# 23-33	212	169.0	11372	4.7	1289	8.1	318	29.8	226	cv1	weathered zone, with gypsum (1 cm)
# 23-34	213	166.0	11172	4.1	1137	6.2	287	31.7	241	cv1	
# 23-35	214	167.7	11288	4.0	1099	6.3	269	27.6	209	cv1	20 cm below river gravel

Outcrop/Sample #	Gamma ray #	Total	ppm	K (%)	ppm	U	ppm	Th	ppm	Spectrometer	Remarks
# 24-2	221	165.8	11156	4.0	1072	6.6	254	23.1	174	cv1	
# 24-3	222	161.1	10842	3.7	999	5.0	229	25.1	190	dp / cv1	dropstones up to tuff bed II
# 24-4	223	160.9	10828	3.5	978	7.2	264	22.8	173	cv1	
# 24-5	224	163.6	11009	4.0	1045	4.3	214	25.1	189	cv1	
# 24-6	225	168.5	11341	4.2	1152	7.8	281	23.6	178	cv1-2	# 24-4 to 24-10:
# 24-7	226	161.2	10851	4.0	1067	5.4	225	22.8	171	cv1-2	rocks generally weathered
# 24-8	227	161.6	10874	3.7	1010	6.0	239	23.1	175	cv1	no lamination
# 24-9	230	164.1	11042	3.7	1006	6.3	243	22.1	167	cv1	
# 24-10	231	166.2	11188	4.2	1091	4.8	205	21.1	158	cv1-2	
# 24-11	232	166.6	11212	4.1	1107	6.2	252	24.7	186	cv2	10 cm above tuff bed III
# 24-12	233	160.5	10801	3.5	955	6.0	229	20.7	157	cv1	
# 24-13	234	158.9	10693	3.1	824	3.9	180	19.7	148	dp	siltstones, tuff bed IV
# 24-14	235	158.8	10689	3.4	907	4.8	201	20.1	151	vp	massive, silty mudstones
# 24-15	236	161.4	10859	3.6	983	5.5	234	24.1	183	vp / cv1	massive, silty mudstones
# 24-16	237	159.6	10738	3.5	906	4.3	175	17.2	128	vp	siltstone
# 24-17	238	157.1	10575	3.1	822	3.1	175	22.2	168	dp	hard, silicified mud-/siltstones
# 24-18	239	165.4	11133	3.4	959	7.1	257	21.9	166	vp / cv1	black, massive mudstones
# 24-19	240	160.1	10775	3.4	936	6.0	233	21.4	162	cv1	black, friable mudstones
# 24-20	241	158.0	10633	3.6	931	3.7	184	21.8	164	dp	black, friable mudstones
# 24-21	242	161.8	10889	3.7	1018	5.1	239	26.2	202	dp / cv1	10 cm below fine-grained sandstone bed
# 24-22	243	158.6	10671	3.2	852	3.6	187	22.7	172	vp	hard, silicified mud-/siltstones
# 24-23	244	160.7	10792	3.7	990	4.9	224	24.3	184	cv1	black, friable mudstones
# 24-24	245	160.7	10812	3.8	1030	5.8	234	22.7	171	dp / cv1	black, friable mudstones
# 24-25	246	162.5	10939	4.3	1165	6.5	267	26.2	198	cv1 / cv2	25 cm below diamictitic, fine-grained sandstone
# 25-1	247	166.3	11190	4.3	1196	7.3	302	30.0	228	vp / cv1	massive, black shales with dropstones
# 25-2	248	163.5	11002	4.6	1226	5.9	271	29.8	225	vp	
# 25-3	249	165.6	11142	4.3	1139	5.6	251	26.8	203	vp	15 cm below tuff bed
# 25-4	250	167.8	11291	4.4	1223	8.9	327	28.0	212	vp / cv1	weathered zone, soil development
# 26-1	251	160.0	10769	4.0	1065	5.7	241	24.2	183	dp	WASSER-RIVER
# 26-2	252	160.8	10824	3.8	1021	7.8	248	16.7	125	dp	coarse siltstones
# 26-3	253	158.6	10675	3.3	926	6.7	241	20.1	152	dp	very well laminated siltstones
# 26-4	254	159.2	10713	3.4	917	5.7	217	19.7	148	hp	well laminated siltstones
# 26-5	255	158.5	10669	3.5	936	5.7	219	20.2	152	dp	faintly laminated siltstones
# 26-6	256	158.9	10693	3.3	923	6.9	248	20.8	158	dp / vp	well laminated siltstones
# 26-7	257	159.3	10723	3.3	878	5.2	204	19.2	145	vp	well laminated mud-/siltstones
# 26-8	258	159.2	10717	3.3	883	5.0	205	20.3	153	vp	massive mud-/siltstones
# 26-9	259	160.6	10805	3.5	987	7.8	261	19.6	148	vp	massive mud-/siltstones
# 26-10	260	162.9	10965	3.8	1031	7.0	254	21.7	164	vp	26-10 to 26-12: black,
# 26-11	261	166.3	11190	3.6	968	4.9	228	25.2	191	vp	massive mudstones,
# 26-12	262	160.8	10821	3.7	999	4.9	222	24.0	182	vp	pyritic concretionary zones
# 26-13	263	160.7	10812	3.5	962	5.8	235	22.8	173	vp / cv1	black, massive mud-/siltstones
# 26-14	264	162.6	10919	4.2	1092	4.3	212	25.0	188	vp / cv1	black, massive mud-/siltstones
# 26-15	265	160.7	10816	3.7	1005	6.5	235	19.7	148	cv1	black, massive mud-/siltstones
# 26-16	266	160.0	10771	3.5	950	5.1	224	23.5	178	cv1	black, massive mud-/siltstones
# 26-17	267	167.8	11295	4.2	1124	5.8	244	24.8	187	cv2	black, massive mud-/siltstones
# 26-18	268	163.1	10975	4.0	1104	7.5	270	22.7	171	cv2	weathered zone, soil development
# 27-1	269	162.5	10934	4.1	1130	6.1	272	29.2	222	cv1	
# 27-2	270	163.2	10980	4.5	1218	6.5	279	28.9	219	vp / cv1	
# 27-3	271	161.3	10854	4.0	1063	3.7	225	30.0	227	vp	grey-black, flaky shales
# 27-4	272	162.3	10921	3.8	1029	5.3	229	23.8	180	vp	grey-black, flaky shales
# 27-5	273	163.6	11009	3.8	998	2.8	202	29.0	219	vp	grey-black, flaky shales
# 27-6	274	160.4	10797	3.7	995	5.9	234	22.3	168	vp	green-grey shales with clay intraclasts
# 27-7	275	163.1	10973	3.3	911	5.4	219	21.3	161	vp	green-grey mud-/siltstones
# 27-8	276	158.4	10661	3.5	930	4.7	207	22.1	167	vp	green-grey mud-/siltstones
# 27-9	277	160.2	10738	3.5	953	6.1	241	22.5	170	dp	35 cm below tuff bed VIIIa

Abbreviations:

- Vp: measurement on a vertical plane
Dp: measurement on a diagonal plane
Cv1: measurement in a cavity (grade 1)
Cv2: measurement in a cavity (grade 2)
Cx: measurement on a convex side

Appendix D-1 (Tab. 22): XRF-results of mudstones sampled from the Ganigobis Shale Member, Aranos Basin, southern Namibia

sample	SiO ₂ in %	TiO ₂	Al ₂ O ₃	Fe ₂ O ₃	MnO	MgO	CaO	Na ₂ O	K ₂ O	P ₂ O ₅	S	LOI	Total
# 2(-12)	61.12	0.78	18.03	6.13	0.19	2.72	0.72	1.44	4.25	0.13	0.04	5.32	100.87
# 2(-10)	60.06	0.68	15.62	5.97	0.12	2.31	3.52	1.52	3.57	2.18	0.02	4.47	100.04
# 2(-8)	56.55	0.82	18.95	7.75	0.04	2.94	0.40	1.47	4.42	0.14	0.95	6.50	100.93
# 2(-6)	59.20	0.71	19.52	4.64	0.03	2.10	0.15	0.82	4.75	0.11	0.56	8.51	101.10
# 2(-4)	58.98	0.74	18.76	5.96	0.04	2.24	0.22	0.73	4.55	0.11	1.00	7.88	101.21
# 2(-2)	60.39	0.72	18.77	5.42	0.02	2.16	0.29	0.71	4.41	0.12	0.52	7.39	100.92
# 2(-1)	60.06	0.73	18.28	5.53	0.03	2.22	0.15	0.72	4.28	0.09	0.93	8.18	101.20
# 2(1)	59.45	0.71	18.44	5.75	0.05	2.32	0.56	0.72	4.31	0.12	1.16	6.93	100.52
# 2(3)	59.66	0.69	18.34	5.75	0.05	2.36	0.44	0.69	4.22	0.11	0.56	7.24	100.11
# 2(5)	60.33	0.69	18.14	5.87	0.04	2.41	0.54	0.76	4.19	0.11	0.74	6.73	100.55
# 2(7)	61.25	0.63	18.47	5.06	0.03	2.45	0.70	0.69	4.27	0.10	0.31	6.39	100.35
# 2(9)	60.12	0.70	18.21	5.78	0.03	2.35	0.21	0.77	4.14	0.08	0.51	7.65	100.55
# 2(11)	59.57	0.69	18.10	7.03	0.03	2.67	0.42	1.69	3.79	0.10	0.68	6.38	101.15
# 2(13)	60.74	0.67	17.46	6.00	0.04	2.46	1.11	1.49	3.84	0.10	0.58	5.92	100.41
# 2(15)	60.66	0.70	17.73	6.00	0.04	2.59	0.96	1.34	3.91	0.10	0.41	5.85	100.29
# 2(17)	61.58	0.66	17.47	6.20	0.04	2.36	1.05	1.56	3.71	0.11	0.02	5.43	100.19
# 2(19)	45.80	0.51	13.07	5.29	0.16	1.86	13.68	1.40	2.53	6.14	0.02	8.11	98.55
# 2(21)	60.92	0.69	17.93	6.40	0.04	2.47	1.11	1.66	3.74	0.13	0.02	5.21	100.32
# 2(23)	61.16	0.71	17.81	6.35	0.04	2.51	1.16	1.60	3.74	0.12	0.02	5.26	100.48
# 2(25)	61.22	0.74	17.69	6.45	0.04	2.69	1.03	1.71	3.71	0.13	0.02	4.98	100.41
# 2(27)	61.19	0.70	17.21	6.31	0.05	2.55	1.73	1.79	3.62	0.17	0.02	5.36	100.70
# 2(29)	60.72	0.73	17.81	6.61	0.05	2.65	1.06	1.78	3.76	0.16	0.02	5.36	100.71
# 2(31)	59.16	0.77	18.31	7.31	0.04	2.87	0.97	1.94	3.79	0.17	0.02	5.04	100.39
# 2(33)	58.44	0.73	18.09	7.16	0.07	2.85	1.57	2.05	3.69	0.21	0.02	5.49	100.37
# 2(35)	58.29	0.82	18.72	7.46	0.06	2.93	0.76	2.31	3.88	0.22	0.02	4.80	100.27

sample	ppm V	Cr	Co	Ni	Zn	Rb	Sr	Y	Zr	Nb	Ba
# 2(-12)	132	97	16	36	115	198	98	42	190	29	497
# 2(-10)	128	92	11	44	125	163	174	148	182	26	592
# 2(-8)	151	102	35	61	180	203	111	42	170	29	566
# 2(-6)	153	109	26	42	205	228	117	50	198	27	450
# 2(-4)	166	97	24	53	259	221	105	46	200	32	439
# 2(-2)	131	79	<10	25	124	214	93	38	196	29	393
# 2(-1)	142	99	<10	37	173	214	104	43	212	30	409
# 2(1)	138	89	16	43	172	215	129	43	200	29	408
# 2(3)	114	76	12	38	142	212	114	43	190	32	376
# 2(5)	120	75	23	37	156	217	132	43	190	29	407
# 2(7)	101	69	13	29	155	213	118	44	192	32	372
# 2(9)	122	95	14	41	141	215	116	37	174	30	445
# 2(11)	125	117	14	46	162	183	128	30	136	28	495
# 2(13)	106	90	21	40	145	184	131	36	152	30	458
# 2(15)	106	86	14	42	140	186	126	45	177	32	471
# 2(17)	107	76	<10	38	118	176	136	44	182	33	474
# 2(19)	102	62	<10	30	88	122	386	224	365	25	516
# 2(21)	107	86	12	42	109	174	154	41	180	31	531
# 2(23)	120	75	<10	42	119	172	166	45	179	32	480
# 2(25)	123	84	<10	42	114	173	154	42	174	32	498
# 2(27)	107	75	11	33	107	169	156	38	165	29	470
# 2(29)	112	90	14	42	122	179	176	41	163	30	497
# 2(31)	126	102	15	41	245	180	178	36	152	32	515
# 2(33)	118	89	15	49	118	172	185	39	146	31	479
# 2(35)	128	113	19	54	146	180	190	40	131	32	602

Appendix D-2 (Tab. 23): ICP-MS standard reference rocks used at IGDL Göttingen

Isotop	BB (basic reference rock)				Ref.wert	Diorit DR-N (international reference rock)								Ref.wert
	BB46-1	BB46-1	BB46-2	BB46-2	BB46	DR-N1	DR-N2	DR-N2	DR-N1	DR-N2	DR-N1	DR-N2	DR-N	
Li 6	12.0	11.9	12.2	12.2	13.0	40.8	40.9	40.8	40.2	40.4	40.9	39.7	40.0	
Be 9	1.49	1.54	1.51	1.56	1.4	1.59	1.66	1.60	1.59	1.60	1.59	1.56	1.8	
Sc 45	18.2	18.4	17.8	19.2	18.0	26.6	28.6	28.8	27.0	28.1	26.7	29.1	28.0	
Rb 85	45.2	45.7	45.7	47.3	44.0	74.1	76.9	76.7	72.4	72.4	71.8	72.1	73.0	
Sr 88	916	925	920	947	930	396	401	399	384	383	385	385	400	
Y 89	20.8	20.8	20.8	21.2	21.0	23.3	23.9	23.4	22.9	23.1	23.1	23.2	26.0	
Zr 91	183	183	181	189	185	56.1	61.7	61.1	54.7	60.6	55.3	59.9	125	
Nb 93	57	57	57	61	60.0	8.4	7.5	7.5	6.6	7.0	6.7	7.0	7.0	
Mo 95			1.58	1.66	1.5	0.94	0.97	1.04	1.13	0.90	0.94	0.87	0.9	
Cs 133	1.02	1.00	0.94	0.99	0.90	6.3	6.4	6.5	6.4	6.4	6.4	6.4	6.30	
Ba 137	655	651	650	656	650	377	377	378	377	377	378	379	400	
La 139	46.6	46.5	46.4	47.5	49.0	20.8	20.7	20.5	20.7	20.7	20.7	20.4	21.5	
Ce 140	93.5	93.8	93.7	95.0	88	46.4	46.7	46.3	46.3	46.2	46.7	46.3	46	
Pr 141	10.5	10.6	10.5	10.6	11.00	5.5	5.5	5.4	5.5	5.5	5.6	5.6	5.70	
Nd 143	41.6	42.2	42.0	41.8	49.0	23.1	23.4	23.3	22.9	22.6	23.0	22.9	23.5	
Sm 147	7.88	7.88	8.00	8.23	8.70	5.09	5.11	5.37	4.92	4.94	5.03	4.89	5.40	
Eu 151	2.58	2.59	2.60	2.57	2.70	1.50	1.50	1.44	1.52	1.56	1.51	1.52	1.45	
Gd 157	7.53	7.82	7.68	7.67	7.30	5.18	5.36	5.37	5.37	5.40	5.43	5.20	4.70	
Tb 159	0.91	0.96	0.91	0.90	1.00	0.75	0.73	0.71	0.72	0.74	0.74	0.73	0.77	
Dy 163	4.8	4.7	4.5	4.5	5.10	4.4	4.5	4.4	4.5	4.4	4.5	4.3	4.60	
Ho 165	0.81	0.83	0.82	0.82	0.93	0.88	0.91	0.89	0.89	0.89	0.86	0.87	1.00	
Er 167	2.12	2.10	2.14	2.01	2.10	2.59	2.61	2.46	2.61	2.54	2.52	2.59	2.50	
Tm 169	0.27	0.27	0.27	0.26	0.33	0.35	0.37	0.36	0.37	0.36	0.36	0.35	0.39	
Yb 172	1.71	1.61	1.63	1.56	1.70	2.34	2.33	2.37	2.26	2.27	2.31	2.24	2.50	
Lu 175	0.23	0.24	0.23	0.22	0.26	0.36	0.34	0.37	0.36	0.34	0.35	0.34	0.40	
Hf 178	4.5	4.5	4.5	4.4	4.50	1.78	1.87	1.95	1.82	1.90	1.83	1.84	3.50	
Ta 181	3.1	3.2	3.7	4.0	3.50				0.52	0.64	0.58	0.62	0.60	
W 184	0.47	0.50	0.49	0.46	0.48	157	129	127	163	119	149	116	130	
Tl 205	0.06	0.06	0.06	0.06	0.06	0.66	0.64	0.60	0.65	0.64	0.64	0.61	0.70	
Pb 208	4.9	5.4	5.0	4.7	4.20	53.6	53.8	53.3	54.2	53.8	54.3	53.4	55.0	
Bi 209	0.03	0.04	0.04	0.04	0.03	0.44	0.50	0.48	0.48	0.47	0.43	0.48	0.50	
Th 232	6.6	6.7	6.8	6.6	6.30	4.9	5.1	5.2	4.9	5.1	4.8	4.8	5.00	
U 238	1.56	1.60	1.58	1.60	1.60	1.59			1.60		1.59		1.50	

Appendix D-3 (Tab. 24): XRF- and ICP-MS results of all analysed tuff beds

Aranos Basin, southern Namibia																
Sample	#2 Tuff Ia	#2 Tuff Ib -1	#2 Tuff Ib -2	#2 Tuff Ib -3	#2 Tuff Ib	#2 Tuff IIb -2	#2 Tuff IIb -3	#2 Tuff IIb -4	#2 Tuff IIb -5	#2 Tuff IIb	#23 Tuff IIb	#23 Tuff IIb	#45 Tuff IIb	#45 Tuff IIb	#2 Tuff IIIb	#2 Tuff IVa -1
Analysis	WÜ	GÖ	GÖ	GÖ	WÜ	GÖ	GÖ	GÖ	GÖ	WÜ	GÖ	WÜ	GÖ	WÜ	WÜ	GÖ
SiO ₂	52.22	51.50	51.70	52.00	53.57	50.80	50.40	49.60	49.00	48.84	48.70	51.25	50.10	51.32	50.77	46.0
TiO ₂	0.380	0.276	0.272	0.267	0.280	0.427	0.434	0.445	0.406	0.450	0.435	0.460	0.424	0.430	1.130	0.959
Al ₂ O ₃	26.69	26.60	26.70	26.80	27.52	27.00	26.70	26.40	26.40	25.74	26.90	28.25	27.50	28.14	24.57	20.5
Fe ₂ O ₃	3.69	2.82	2.83	2.42	2.78	2.63	3.27	3.34	2.67	6.02	3.30	3.45	3.81	3.89	4.91	3.96
MnO	0.03	0.03	0.06	0.03	0.03	0.02	0.03	0.04	0.05	0.05	0.03	0.03	0.01	<0.01	0.16	0.248
MgO	2.62	2.34	2.48	2.41	2.61	2.32	2.52	2.53	2.85	2.79	2.47	2.58	2.21	2.23	2.37	1.65
CaO	0.23	0.18	0.10	0.13	0.23	0.04	0.21	0.95	0.09	0.56	0.16	0.20	0.04	0.07	2.07	6.98
Na ₂ O	0.41	0.53	0.46	0.50	0.27	0.70	0.40	0.45	0.35	0.52	0.33	0.15	1.38	1.30	0.56	2.63
K ₂ O	5.80	5.86	5.95	5.99	6.09	5.76	5.80	5.72	5.60	5.33	5.66	5.92	5.90	6.01	5.17	3.49
P ₂ O ₅	0.050	0.070	0.040	0.050	0.060	0.050	0.160	0.180	0.150	0.180	0.160	0.170	0.100	0.100	0.200	0.161
LOI	7.61	6.65	6.59	6.76	7.26	6.81	7.05	7.26	8.20	9.15	7.37	7.55	6.28	6.29	8.62	9.95
SUM	99.73	96.85	97.18	97.35	100.70	96.55	96.98	96.92	95.77	99.63	95.52	100.01	97.76	99.79	100.53	96.53
Nb	8	<5	6	<5	16	<5	<5	6	<5	17	<5	5	<5	5	13	14
Zr	106	103	102	95	120	160	176	203	145	222	152	163	133	139	181	76
Y	13	18	16	16	25	22	25	29	33	38	21	24	16	17	45	37
Sr	42	123	40	28	29	25	36	94	143	31	278	306	461	506	66	219
Rb	189	180	186	186	196	188	176	176	170	183	164	173	178	181	161	108
Pb	-	18	31	27	-	<10	16	37	13	-	58	-	35	-	-	32
Ga	-	19	17	18	-	18	18	17	18	-	17	-	17	-	-	12
Zn	109	54	60	60	89	72	67	143	138	153	106	135	183	218	318	419
Cu	-	10	10	10	-	10	10	10	10	-	25	-	14	-	-	25
Ni	14	19	26	23	18	20	19	21	55	38	37	33	60	52	41	48
Co	<10	3	7	6	14	8	7	5	18	14	9	10	6	<10	19	25
Cr	-	19	17	19	<10	12	12	15	13	16	22	17	15	<10	-	25
V	108	88	73	73	77	84	83	81	87	92	122	104	109	98	108	119
Ba	168	212	296	176	149	134	144	156	141	141	192	298	174	280	174	195
Sc	-	16	11	11	-	14	19	13	12	-	17	-	15	-	-	21
Li 6	-	11	15	13	-	14	14	20	30	-	32	-	58	-	-	25
Be 9	-	1.50	1.62	1.63	-	1.00	1.21	1.41	1.52	-	1.60	-	1.40	-	-	0.87
Rb 85	-	109	104	106	-	79	84	163	105	-	166	-	183	-	-	104
Sr 88	-	98	31	20	-	18	26	87	120	-	279	-	478	-	-	216
Y 89	-	9.1	7.7	8.5	-	8.0	12.5	24.9	23.2	-	17.7	-	13.0	-	-	31.2
Zr 91	-	89	89	85	-	135	141	147	125	-	122	-	103	-	-	67
Nb 93	-	7.2	6.1	5.2	-	5.5	5.3	4.6	4.3	-	4.9	-	4.0	-	-	15.7
Mo 95	-	4.4	1.7	2.4	-	0.8	1.4	1.3	2.5	-	16.1	-	1.9	-	-	1.9
Cs 133	-	27	30	30	-	23	22	24	20	-	25	-	41	-	-	11
Ba 137	-	181	279	161	-	115	131	156	138	-	181	-	203	-	-	196
La 139	-	2.4	2.1	3.3	-	3.5	5.0	23.9	55.0	-	88.3	-	75.1	-	-	19.3
Ce 140	-	7	7	11	-	10	15	58	130	-	201	-	169	-	-	52
Pr 141	-	0.9	0.9	1.4	-	1.1	1.9	6.7	13.3	-	21.4	-	17.8	-	-	7.1
Nd 143	-	4.3	4.0	6.1	-	4.5	8.4	26.5	50.3	-	82.7	-	66.0	-	-	33.5
Sm 147	-	1.4	1.3	1.8	-	1.2	2.3	5.6	9.6	-	15.0	-	11.3	-	-	9.9
Eu 151	-	0.30	0.30	0.36	-	0.26	0.46	1.00	1.46	-	2.03	-	1.65	-	-	2.04
Gd 157	-	1.9	1.7	2.1	-	1.4	2.6	5.7	8.0	-	9.7	-	7.2	-	-	10.0
Tb 159	-	0.32	0.30	0.33	-	0.26	0.45	0.83	0.93	-	0.92	-	0.65	-	-	1.40
Dy 163	-	2.2	1.9	2.2	-	1.9	3.1	5.1	5.1	-	4.0	-	2.9	-	-	7.1
Ho 165	-	0.42	0.37	0.40	-	0.41	0.61	0.95	0.96	-	0.73	-	0.54	-	-	1.20
Er 167	-	1.13	1.00	1.16	-	1.31	1.91	2.89	2.72	-	1.92	-	1.54	-	-	2.97
Tm 169	-	0.16	0.14	0.16	-	0.21	0.29	0.41	0.39	-	0.26	-	0.24	-	-	0.37
Yb 172	-	1.04	0.91	1.05	-	1.42	1.83	2.68	2.44	-	1.72	-	1.52	-	-	2.33
Lu 175	-	0.16	0.14	0.16	-	0.22	0.29	0.39	0.37	-	0.26	-	0.22	-	-	0.35
Hf 178	-	2.5	2.4	2.4	-	3.2	3.5	3.5	3.0	-	2.8	-	2.4	-	-	1.3
Ta 181	-	6.3	6.7	6.5	-	4.6	4.9	4.3	4.5	-	5.0	-	5.2	-	-	1.6
W 184	-	2.5	2.3	3.0	-	2.5	2.7	2.2	3.7	-	1.3	-	1.5	-	-	8.6
Tl 205	-	0.99	1.10	1.13	-	1.23	0.89	1.00	1.09	-	0.94	-	1.04	-	-	0.61
Pb 208	-	19.4	34.7	28.7	-	9.0	17.1	28.0	19.9	-	38.8	-	42.5	-	-	39.0
Bi 209	-	1.35	1.38	1.38	-	0.75	0.85	0.88	0.80	-	0.86	-	0.89	-	-	0.25
Th 232	-	40.4	36.7	43.1	-	17.5	29.6	40.7	34.8	-	42.1	-	34.2	-	-	4.6
U 238	-	1.2	1.2	1.3	-	1.6	2.2	5.3	2.1	-	4.2	-	4.6	-	-	2.3

Appendix D-3 (Tab. 24): XRF- and ICP-MS results of all analysed tuff beds

Aranos Basin, southern Namibia															
Sample	#2 Tuff IVa -2	#2 Tuff IVa -3	#2 Tuff IVa -4	#17 Tuff IVa	#17 Tuff IVa	#38 Tuff IVa	#30 Tuff IVa -1	#30 Tuff IVa -2	#32 Tuff IVa	#97/30 Tuff IVa	#97/33 Tuff IVa	#30 Tuff IVa	#2 Tuff IVb -1	#2 Tuff IVb -2	#2 Tuff IVb -3
Analysis	GÖ	GÖ	GÖ	WÜ	WÜ	GÖ	GÖ	GÖ	WÜ	GÖ	GÖ	WÜ	GÖ	GÖ	GÖ
SiO ₂	46.9	52.80	39.6	51.90	53.80	51.20	54.30	54.60	56.05	55.00	55.10	56.08	48.80	48.60	48.90
TiO ₂	1.011	1.099	0.829	1.096	1.130	1.122	1.238	1.311	1.290	1.209	1.198	1.340	0.420	0.510	0.419
Al ₂ O ₃	21.5	23.30	18.5	23.00	23.64	23.90	24.70	25.00	25.39	24.60	24.20	24.89	26.00	26.10	26.00
Fe ₂ O ₃	4.85	5.54	7.34	4.88	5.10	5.55	2.08	1.88	2.15	2.26	2.25	2.46	5.01	5.90	4.67
MnO	0.178	0.02	0.545	0.01	<0.01	0.07	0.01	0.01	0.05	0.03	0.01	0.01	0.04	0.03	0.05
MgO	1.73	1.75	5.42	1.49	1.57	1.90	1.39	1.49	1.52	1.41	1.38	1.49	2.78	2.66	2.67
CaO	5.38	0.19	5.91	0.52	0.57	0.20	1.90	1.58	1.07	1.25	1.17	1.56	0.98	0.16	1.30
Na ₂ O	2.29	3.23	1.86	3.58	3.67	2.47	2.98	3.01	3.63	3.68	4.16	3.57	0.54	0.63	0.47
K ₂ O	3.72	3.88	3.17	3.66	3.79	4.04	3.83	3.81	3.78	3.76	3.70	3.86	5.42	5.46	5.50
P ₂ O ₅	0.158	0.130	0.159	0.090	0.090	0.130	0.130	0.100	0.150	0.100	0.150	0.160	0.190	0.090	0.180
LOI	9.24	5.56	13.99	6.57	6.52	6.35	4.66	4.81	5.05	4.34	4.23	4.65	7.13	7.30	6.93
SUM	96.95	97.50	97.33	96.80	99.89	96.93	97.22	97.60	100.13	97.64	97.55	100.07	97.32	97.43	97.08
Nb	12	12	12	15	18	14	31	31	36	29	29	35	<5	<5	<5
Zr	76	87	73	86	90	84	90	90	105	94	94	100	124	173	116
Y	30	27	40	15	17	15	19	16	25	18	19	25	15	19	16
Sr	209	76	112	140	150	62	291	214	138	181	139	196	77	32	106
Rb	117	124	102	117	121	125	122	124	115	119	124	118	165	171	171
Pb	38	29	181	26	-	34	17	17	-	15	<10	-	66	28	59
Ga	15	13	13	13	-	15	18	15	-	16	16	-	17	17	16
Zn	373	315	244	200	233	270	43	52	95	58	40	53	27	142	24
Cu	22	36	44	22	-	33	11	22	-	12	11	-	10	19	10
Ni	65	47	193	27	23	47	16	13	13	17	13	16	17	58	21
Co	40	13	63	5	<10	27	7	5	16	6	6	10	6	14	5
Cr	24	24	25	-	-	28	21	19	-	25	21	-	14	13	14
V	119	138	107	122	111	142	112	112	101	106	100	100	76	80	74
Ba	209	213	181	217	270	194	356	320	332	334	341	386	126	226	156
Sc	20	20	19	15	-	18	14	16	-	16	12	-	10	15	8
Li 6	25	19	38	-	-	-	29	30	-	38	34	-	26	49	28
Be 9	0.99	1.35	1.12	-	-	-	1.30	1.31	-	1.37	1.25	-	1.00	1.61	1.23
Rb 85	99	60	95	-	-	-	123	124	-	123	121	-	136	104	170
Sr 88	203	59	108	-	-	-	301	222	-	186	141	-	68	25	101
Y 89	25.1	15.4	34.2	-	-	-	17.0	13.3	-	14.9	16.9	-	11.8	10.9	12.2
Zr 91	68	76	63	-	-	-	86	83	-	85	85	-	101	127	91
Nb 93	19.0	14.6	14.8	-	-	-	45.0	49.5	-	44.0	44.4	-	4.7	5.3	3.8
Mo 95	2.5	2.2	8.2	-	-	-	0.9	0.8	-	1.4	1.5	-	1.0	0.9	0.7
Cs 133	11	11	5	-	-	-	10	11	-	11	9	-	16	23	22
Ba 137	204	189	176	-	-	-	368	330	-	342	339	-	128	203	152
La 139	15.5	5.8	23.7	-	-	-	19.3	22.4	-	17.0	14.1	-	8.3	0.9	9.6
Ce 140	42	18	57	-	-	-	43	48	-	44	35	-	21	3	24
Pr 141	5.5	2.3	7.5	-	-	-	5.0	5.1	-	5.7	4.2	-	2.7	0.7	2.9
Nd 143	25.6	10.9	33.8	-	-	-	19.8	17.8	-	26.1	17.9	-	11.3	4.4	12.0
Sm 147	7.5	3.2	9.1	-	-	-	4.4	3.2	-	6.2	4.5	-	2.6	2.0	2.7
Eu 151	1.65	0.68	1.76	-	-	-	1.06	0.80	-	1.23	1.07	-	0.54	0.43	0.53
Gd 157	7.8	3.8	9.3	-	-	-	4.5	3.0	-	4.7	4.3	-	2.8	2.6	2.8
Tb 159	1.04	0.60	1.26	-	-	-	0.63	0.41	-	0.63	0.61	-	0.44	0.43	0.42
Dy 163	5.6	3.7	6.7	-	-	-	3.6	2.6	-	3.3	3.6	-	2.4	2.6	2.5
Ho 165	0.96	0.71	1.18	-	-	-	0.71	0.56	-	0.64	0.70	-	0.46	0.53	0.49
Er 167	2.46	1.92	3.02	-	-	-	1.87	1.68	-	1.79	2.10	-	1.27	1.40	1.27
Tm 169	0.32	0.28	0.39	-	-	-	0.29	0.25	-	0.25	0.29	-	0.18	0.20	0.19
Yb 172	2.11	1.76	2.44	-	-	-	1.76	1.73	-	1.66	1.89	-	1.17	1.26	1.11
Lu 175	0.30	0.27	0.36	-	-	-	0.26	0.26	-	0.25	0.28	-	0.17	0.19	0.18
Hf 178	1.3	1.5	1.2	-	-	-	1.6	1.5	-	1.6	1.7	-	2.6	3.1	2.5
Ta 181	1.5	1.5	1.2	-	-	-	1.5	1.8	-	1.3	1.5	-	4.6	4.7	4.2
W 184	10.1	11.5	7.4	-	-	-	14.9	14.8	-	12.7	13.4	-	2.5	2.1	2.2
Ti 205	0.73	0.72	1.17	-	-	-	0.65	0.78	-	0.85	0.65	-	0.96	1.07	1.39
Pb 208	46.0	28.7	200.4	-	-	-	22.4	16.5	-	18.5	14.3	-	77.6	30.3	70.4
Bi 209	0.24	0.29	0.24	-	-	-	0.25	0.25	-	0.24	0.24	-	0.80	0.88	0.86
Th 232	4.1	3.6	4.0	-	-	-	5.6	5.3	-	5.1	5.2	-	33.7	33.4	37.1
U 238	2.0	1.3	2.7	-	-	-	3.6	3.6	-	3.5	3.7	-	1.2	1.0	1.4

Appendix D-3 (Tab. 24): XRF- and ICP-MS results of all analysed tuff beds

Aranos Basin, southern Namibia															
Sample	#2 Tuff IVb -4	#2 Tuff IVb	#38 Tuff IVb	#23 Tuff IVb	#30 Tuff IVb	#45 Tuff IVb	#2 Tuff IVc	#2 Tuff Vc	#23 Tuff V	#2 Tuff Vc	#15 Tuff VII	#15 Tuff VII	#97/9 Tuff VIIIa	#98/9 Tuff VIIIa	#27 Tuff VIIIa
Analysis	GÖ	WÜ	GÖ	WÜ	WÜ	WÜ	WÜ	GÖ	GÖ	WÜ	GÖ	WÜ	GÖ	GÖ	WÜ
SiO ₂	49.20	49.37	48.80	52.86	51.15	49.25	50.20	49.70	33.0	52.19	51.50	52.41	46.9	51.90	51.07
TiO ₂	0.489	0.480	0.432	0.490	0.510	0.510	0.230	0.912	0.898	0.930	0.832	0.860	0.396	0.451	0.970
Al ₂ O ₃	26.40	26.27	26.20	28.69	27.21	26.99	26.65	25.30	16.1	25.49	23.70	24.21	25.4	27.70	25.81
Fe ₂ O ₃	4.68	5.99	5.09	1.98	4.67	5.62	5.84	6.09	6.08	5.55	5.62	6.15	1.62	1.64	5.32
MnO	0.03	0.03	0.02	<0.01	0.05	0.06	0.07	0.03	0.123	0.04	0.06	0.05	0.129	0.01	0.02
MgO	2.83	2.88	2.87	1.95	2.53	2.56	2.51	2.04	1.26	2.13	2.28	2.28	2.23	2.43	2.07
CaO	0.33	1.13	0.30	0.69	0.64	0.17	0.28	0.88	8.38	0.75	1.01	1.07	4.61	0.26	0.19
Na ₂ O	0.58	0.45	0.63	0.20	1.42	0.97	0.13	0.58	0.53	0.60	0.67	0.55	0.66	0.79	2.06
K ₂ O	5.58	5.49	5.47	6.25	5.59	5.82	5.94	5.38	3.20	5.42	4.77	4.84	5.21	5.73	5.13
P ₂ O ₅	0.170	0.250	0.140	0.020	0.250	0.120	0.030	0.130	0.122	0.110	0.120	0.120	0.062	0.070	0.050
LOI	6.89	7.97	7.29	6.99	6.19	7.52	8.16	6.44	10.18	6.97	6.52	7.21	9.29	6.43	7.30
SUM	97.18	100.31	97.24	100.13	100.21	99.59	100.04	97.49	79.87	100.18	97.07	99.75	96.51	97.40	99.99
Nb	6	7	6	6	7	7	<5	10	8	10	9	12	7	6	10
Zr	160	169	128	160	185	162	109	136	102	137	138	142	176	159	148
Y	24	18	20	11	19	19	20	22	19	24	21	21	27	28	25
Sr	29	84	23	81	56	247	52	105	387	106	215	252	56	41	41
Rb	180	167	169	190	169	186	181	174	109	169	164	164	161	179	165
Pb	25	-	22	-	-	-	-	38	54	-	67	-	10	11	-
Ga	16	-	14	-	-	-	-	20	9	-	21	-	20	24	-
Zn	134	72	103	63	76	219	91	97	125	102	70	95	53	57	193
Cu	14	-	10	-	-	-	-	24	23	-	24	-	<10	10	-
Ni	47	19	27	13	19	83	33	22	24	28	27	30	10	9	28
Co	7	13	5	<10	<10	37	30	44	51	22	16	10	<5	5	<10
Cr	17	-	15	-	-	-	-	23	21	-	35	-	13	12	-
V	80	65	77	101	56	104	51	93	149	87	79	76	52	73	96
Ba	172	200	137	150	229	2938	147	174	12758	582	457	545	213	179	235
Sc	12	-	15	-	-	-	-	18	18	-	14	-	14	12	-
Li 6	44	-	-	-	-	-	-	18	17	-	31	-	12	14	-
Be 9	1.54	-	-	-	-	-	-	2.26	1.52	-	2.29	-	1.91	2.03	-
Rb 85	182	-	-	-	-	-	-	176	117	-	167	-	161	175	-
Sr 88	25	-	-	-	-	-	-	102	420	-	219	-	55	38	-
Y 89	20.2	-	-	-	-	-	-	17.7	18.0	-	17.8	-	24.8	25.7	-
Zr 91	125	-	-	-	-	-	-	122	97	-	132	-	148	152	-
Nb 93	5.2	-	-	-	-	-	-	9.4	12.3	-	12.1	-	4.8	6.2	-
Mo 95	1.1	-	-	-	-	-	-	2.8	2.8	-	2.1	-	1.4	1.2	-
Cs 133	27	-	-	-	-	-	-	32	22	-	13	-	14	15	-
Ba 137	164	-	-	-	-	-	-	170	13308	-	455	-	221	163	-
La 139	8.8	-	-	-	-	-	-	32.1	40.2	-	129.0	-	31.5	80.6	-
Ce 140	24	-	-	-	-	-	-	70	108	-	268	-	74	223	-
Pr 141	4.1	-	-	-	-	-	-	7.5	10.9	-	26.8	-	8.6	24.8	-
Nd 143	22.5	-	-	-	-	-	-	26.9	39.9	-	89.5	-	32.8	93.4	-
Sm 147	7.4	-	-	-	-	-	-	4.6	6.7	-	11.8	-	6.0	16.0	-
Eu 151	1.24	-	-	-	-	-	-	0.77	3.54	-	1.52	-	1.00	2.03	-
Gd 157	7.5	-	-	-	-	-	-	4.4	12.3	-	9.3	-	5.5	11.7	-
Tb 159	1.00	-	-	-	-	-	-	0.59	0.73	-	0.89	-	0.77	1.21	-
Dy 163	5.0	-	-	-	-	-	-	3.5	3.8	-	4.3	-	4.4	5.4	-
Ho 165	0.85	-	-	-	-	-	-	0.70	0.76	-	0.81	-	0.92	0.97	-
Er 167	2.02	-	-	-	-	-	-	2.00	2.11	-	2.40	-	2.60	2.63	-
Tm 169	0.28	-	-	-	-	-	-	0.29	0.30	-	0.36	-	0.38	0.39	-
Yb 172	1.71	-	-	-	-	-	-	1.85	1.95	-	2.36	-	2.46	2.32	-
Lu 175	0.24	-	-	-	-	-	-	0.26	0.30	-	0.34	-	0.35	0.35	-
Hf 178	2.9	-	-	-	-	-	-	4.2	2.3	-	4.1	-	4.9	5.0	-
Ta 181	4.8	-	-	-	-	-	-	3.7	3.8	-	3.9	-	4.9	5.8	-
W 184	1.8	-	-	-	-	-	-	4.4	8.1	-	5.2	-	3.5	2.7	-
Tl 205	1.00	-	-	-	-	-	-	1.06	1.38	-	0.93	-	0.91	0.97	-
Pb 208	32.7	-	-	-	-	-	-	44.0	79.3	-	227.5	-	14.8	16.1	-
Bi 209	0.88	-	-	-	-	-	-	0.49	0.55	-	0.51	-	1.10	1.19	-
Th 232	40.4	-	-	-	-	-	-	18.4	20.6	-	24.9	-	36.9	44.8	-
U 238	1.6	-	-	-	-	-	-	3.0	4.5	-	5.1	-	4.4	8.9	-

Appendix D-3 (Tab. 24): XRF- and ICP-MS results of all analysed tuff beds

Sample	Karasburg Basin, southern Namibia											M. Karoo Basin: Dwyka			
	MG 3b - 3	MG 3b - 3	MG Tuff 7 - 1	MG Tuff 7 - M	MG Tuff 8b	MG Tuff 13	MG Tuff 19	MG Tuff 24a - 2	MG Tuff 24a - 3	MG Tuff 24a - 5	MG Tuff 34	E.W. 879.95 m	E.W. 879.75 m	E.W. 798.79 m	E.W. 798.39 m
Analysis	GÖ	GÖ	GÖ	GÖ	GÖ	GÖ	GÖ	GÖ	GÖ	GÖ	GÖ	GÖ	GÖ	GÖ	GÖ
SiO ₂	49.80	50.20	50.80	50.70	50.90	52.60	51.40	49.30	50.70	48.70	49.90	50.70	52.10	51.70	52.20
TiO ₂	0.429	0.436	0.257	0.259	0.272	0.316	0.481	0.497	0.518	0.478	0.387	1.580	0.401	0.926	0.759
Al ₂ O ₃	27.60	27.70	28.20	28.10	28.40	28.10	28.70	29.00	29.80	28.50	30.10	24.70	23.90	20.90	23.60
Fe ₂ O ₃	2.48	2.61	2.10	2.29	1.74	1.68	1.77	3.18	1.21	3.00	1.50	3.80	4.67	8.12	4.32
MnO	0.03	0.04	0.01	0.02	0.01	0.02	0.02	0.01	0.01	0.01	0.01	0.06	0.07	0.18	0.08
MgO	2.27	2.35	2.19	2.18	2.07	1.96	1.98	1.83	1.92	1.69	1.77	2.73	2.99	4.23	2.98
CaO	1.11	0.78	0.29	0.21	0.43	0.11	0.33	0.09	0.06	0.09	0.51	0.68	0.36	0.94	0.56
Na ₂ O	0.40	0.48	0.30	0.30	0.45	0.97	1.05	0.66	0.60	0.70	0.41	0.84	0.74	1.61	1.18
K ₂ O	7.04	7.08	7.23	7.18	7.09	6.69	6.75	7.04	7.27	6.84	7.22	8.29	8.30	5.85	7.65
P ₂ O ₅	0.110	0.130	0.070	0.070	0.080	0.050	0.170	0.070	0.030	0.030	0.040	0.160	0.060	0.120	0.110
LOI	6.43	6.17	6.19	6.26	6.02	6.03	5.89	6.61	6.27	7.03	6.55	4.94	4.90	4.71	4.81
SUM	97.70	97.98	97.64	97.56	97.47	98.52	98.55	98.28	98.39	97.07	98.40	98.48	98.49	99.28	98.24
Nb	7	6	12	14	11	7	8	9	7	<5	<5	31	23	49	40
Zr	203	234	268	263	254	128	204	159	155	161	96	672	495	850	644
Y	28	28	50	54	52	28	35	25	33	25	16	100	76	152	101
Sr	39	74	38	34	44	37	43	39	35	36	79	139	113	129	118
Rb	290	298	301	298	290	255	241	252	264	245	267	495	483	318	481
Pb	10	14	10	10	10	10	10	23	10	30	10	10	25	37	37
Ga	29	27	32	30	29	30	28	29	28	26	28	24	28	23	27
Zn	14	17	44	101	15	96	101	122	57	52	1	40	40	152	57
Cu	15	17	10	12	10	10	10	18	10	12	10	226	35	13	54
Ni	10	13	13	20	10	17	22	19	18	47	10	17	20	39	22
Co	5	5	5	5	5	5	5	5	5	8	5	7	5	19	6
Cr	9	12	13	17	11	19	14	14	13	13	10	21	16	18	16
V	63	73	30	28	25	61	51	92	87	102	55	142	94	98	109
Ba	1123	1040	1105	1098	1087	840	889	946	993	926	934	541	910	1407	669
Sc	13	16	16	11	13	14	11	16	15	14	13	23	16	20	25
Li 6	27	29	17	17	-	20	20	13	15	13	15	37	42	68	39
Be 9	4.58	4.99	3.49	3.27	-	2.70	2.34	2.61	2.29	2.43	2.96	5.85	5.09	4.50	5.43
Rb 85	368	350	356	365	-	306	282	295	303	295	312	538	503	328	503
Sr 88	43	85	40	37	-	37	49	40	35	36	84	146	110	127	115
Y 89	26.0	25.8	51.0	55.5	-	27.7	33.5	27.5	30.9	23.5	14.0	92.7	63.7	138.0	88.1
Zr 91	208	207	296	297	-	141	203	155	158	146	98	686	470	812	587
Nb 93	10.2	9.6	16.8	17.0	-	8.3	9.7	12.5	9.4	7.3	3.9	44.2	31.3	68.1	59.0
Mo 95	0.3	0.2	4.6	8.9	-	0.6	1.5	14.7	4.1	37.4	0.7	0.2	0.2	0.3	0.2
Cs 133	20	17	18	19	-	17	14	17	17	19	14	28	23	16	30
Ba 137	1318	1178	1253	1251	-	957	1013	1098	1134	1116	1069	552	908	1379	661
La 139	11.8	12.4	63.1	73.0	-	11.4	40.1	16.2	47.9	29.0	1.9	7.7	9.6	16.9	9.0
Ce 140	30	34	179	203	-	26	89	45	143	83	5	23	25	45	24
Pr 141	3.8	4.1	21.9	25.1	-	3.2	9.6	5.2	16.3	9.4	0.6	2.7	2.7	5.4	3.0
Nd 143	15.5	16.2	89.1	104.2	-	13.8	35.3	21.0	63.9	36.4	2.4	12.7	11.5	25.1	14.1
Sm 147	3.3	3.8	18.4	21.9	-	3.9	7.2	4.9	13.0	7.5	0.9	3.9	3.4	9.1	4.2
Eu 151	0.92	0.89	2.13	2.53	-	1.07	1.63	1.18	1.96	1.37	0.53	0.83	0.85	2.03	0.81
Gd 157	3.8	4.0	15.4	17.6	-	4.5	7.1	5.2	10.6	6.5	1.6	5.7	5.2	13.7	6.3
Tb 159	0.63	0.67	1.91	2.14	-	0.77	1.02	0.77	1.17	0.78	0.32	1.26	1.02	2.68	1.24
Dy 163	4.4	4.5	10.1	11.0	-	5.0	5.9	5.0	6.2	4.6	2.6	11.1	8.5	20.6	10.8
Ho 165	0.97	0.99	2.02	2.18	-	1.03	1.21	1.01	1.19	0.90	0.56	3.28	2.24	4.80	2.99
Er 167	2.86	3.00	5.98	6.01	-	3.00	3.75	3.03	3.60	2.80	1.76	11.45	7.62	14.94	10.93
Tm 169	0.45	0.43	0.84	0.88	-	0.45	0.58	0.45	0.53	0.42	0.24	1.68	1.07	2.11	1.62
Yb 172	2.70	2.94	5.50	5.67	-	2.86	3.61	2.82	3.31	2.59	1.69	11.31	7.54	14.04	10.99
Lu 175	0.39	0.43	0.79	0.77	-	0.40	0.51	0.42	0.49	0.40	0.24	1.69	1.12	2.09	1.72
Hf 178	4.7	4.8	6.2	6.0	-	3.8	4.7	5.3	5.7	5.3	3.2	9.8	8.4	12.0	9.2
Ta 181	16.0	15.7	15.1	14.7	-	14.8	10.6	6.5	5.9	5.0	4.2	7.6	9.3	10.3	9.5
W 184	1.2	2.4	1.6	6.3	-	2.4	2.5	2.6	2.8	4.6	2.8	6.3	3.1	6.8	5.8
Tl 205	1.67	1.70	1.92	1.95	-	1.88	1.78	1.85	1.98	1.96	2.34	2.77	2.62	1.86	2.61
Pb 208	6.4	17.4	10.8	8.0	-	2.0	6.2	26.4	7.3	40.4	2.2	9.7	23.3	43.5	39.6
Bi 209	0.63	1.31	2.07	2.16	-	0.46	0.89	1.55	1.46	1.39	0.11	0.04	0.10	0.20	0.17
Th 232	81.4	81.4	60.1	57.4	-	68.6	55.3	50.3	57.8	47.0	65.9	43.3	46.3	35.4	31.0
U 238	3.4	5.4	12.9	12.9	-	8.2	8.5	7.3	12.6	8.2	3.8	9.8	8.4	14.6	9.0

Appendix D-3 (Tab. 24): XRF- and ICP-MS results of all analysed tuff beds

Main Karoo Basin: Dwyka Group								Main Karoo Basin: Eccca Group								
Sample	KL 1/65: 1616.54 m	QU 1/65: 2244.50 m	QU 1/65: 2239.31 m	OL 1/69: 591.09 m	OL 1/69: 588.46 m	OL 1/69: 394.59 m	OL 1/69: 392.29 m	RSA N12 Dwyka	RSA N12 Eccca -1	RSA N12 Eccca -2	RSA N12 Eccca -3	RSA N12 Eccca -4	RSA S Laings. Eccca -1	RSA S Laings. Eccca -2	RSA S Laings. Eccca -3	RSA S Laings. Eccca -4
Analysis	GÖ	GÖ	GÖ	GÖ	GÖ	GÖ	GÖ	GÖ	GÖ	GÖ	GÖ	GÖ	GÖ	GÖ	GÖ	GÖ
SiO ₂	54.40	51.10	51.70	50.60	53.20	52.50	51.80	55.10	52.95	52.60	50.80	62.00	51.24	49.90	47.30	48.80
TiO ₂	0.351	0.470	2.108	0.372	0.920	0.355	0.729	0.336	0.470	0.622	0.445	0.311	0.350	0.299	0.372	0.526
Al ₂ O ₃	23.90	26.80	22.30	26.00	23.50	26.30	26.00	23.10	30.51	30.20	31.40	19.90	32.87	29.50	32.30	31.00
Fe ₂ O ₃	3.24	2.95	4.46	3.15	3.18	2.68	2.21	2.94	1.09	1.01	0.79	3.20	0.86	4.17	3.27	2.56
MnO	0.05	0.05	0.13	0.05	0.05	0.06	0.08	0.03	0.01	0.01	0.01	0.02	0.01	0.04	0.04	0.03
MgO	2.53	2.53	2.27	2.80	2.71	2.71	2.47	2.28	0.66	0.64	0.70	1.46	0.69	0.94	0.73	0.63
CaO	0.28	0.52	2.25	0.38	0.30	0.31	0.64	0.18	0.55	0.31	0.55	0.71	0.34	0.58	0.76	1.00
Na ₂ O	2.08	0.55	2.63	0.61	1.40	0.59	1.10	0.28	0.31	0.29	0.47	0.97	0.84	1.17	2.11	2.45
K ₂ O	7.37	8.17	5.52	8.83	7.83	8.03	7.85	9.97	7.19	7.33	7.20	5.45	6.91	4.98	4.51	3.45
P ₂ O ₅	0.130	0.150	0.340	0.020	0.150	0.060	0.100	0.070	0.230	0.100	0.330	0.140	0.050	0.080	0.160	0.370
LOI	4.32	5.33	5.08	5.54	5.53	5.37	5.27	4.23	5.40	5.32	5.63	4.41	5.67	6.32	6.48	6.17
SUM	98.64	98.62	98.79	98.35	98.76	98.96	98.24	98.52	99.37	98.43	98.32	98.56	99.83	97.98	98.03	96.98
Nb	19	26	25	26	42	18	28	24	34	24	25	21	33	26	34	36
Zr	319	409	417	587	786	397	617	340	358	497	415	196	337	392	532	595
Y	51	72	98	97	146	68	101	59	63	54	73	30	45	45	60	101
Sr	169	93	199	162	133	121	140	152	60	38	64	72	114	152	242	291
Rb	423	408	301	533	463	405	380	558	295	293	303	203	295	255	205	159
Pb	42	47	19	32	10	32	10	12	-	22	11	25	-	56	58	16
Ga	28	32	23	31	23	33	34	30	-	33	35	24	-	35	31	29
Zn	76	165	134	571	272	71	75	35	40	5	5	57	25	82	77	71
Cu	30	10	38	531	175	10	28	11	-	33	10	10	-	47	10	19
Ni	21	16	28	27	18	24	11	20	10	10	11	12	10	11	13	10
Co	7	5	5	12	9	7	5	6	10	5	5	5	10	5	7	5
Cr	14	13	24	14	20	16	13	13	-	12	16	13	-	18	10	11
V	112	66	136	120	174	40	54	48	19	47	29	20	36	57	44	71
Ba	745	531	589	621	845	662	986	2469	1177	1013	1057	786	1472	1090	1073	917
Sc	11	15	31	14	20	14	14	14	-	13	16	5	-	24	8	21
Li 6	29	16	24	39	36	25	22	16	-	-	-	-	-	-	-	-
Be 9	4.65	3.87	3.33	8.39	6.87	5.00	5.25	4.96	-	-	-	-	-	-	-	-
Rb 85	439	434	310	550	483	424	398	586	-	-	-	-	-	-	-	-
Sr 88	167	88	198	157	130	120	140	149	-	-	-	-	-	-	-	-
Y 89	40.7	59.4	85.3	82.9	128.4	59.6	88.8	47.2	-	-	-	-	-	-	-	-
Zr 91	254	334	398	562	715	368	524	309	-	-	-	-	-	-	-	-
Nb 93	28.6	34.8	30.7	32.2	55.3	23.7	38.4	32.1	-	-	-	-	-	-	-	-
Mo 95	0.1	0.2	0.4	0.2	0.5	0.4	2.1	0.3	-	-	-	-	-	-	-	-
Cs 133	18	24	15	30	24	19	22	14	-	-	-	-	-	-	-	-
Ba 137	720	513	583	591	807	654	984	2447	-	-	-	-	-	-	-	-
La 139	16.6	71.0	24.8	13.5	87.5	54.5	103.9	20.5	-	-	-	-	-	-	-	-
Ce 140	41	158	61	31	206	168	235	27	-	-	-	-	-	-	-	-
Pr 141	4.7	16.8	7.9	3.3	20.0	20.0	25.8	5.4	-	-	-	-	-	-	-	-
Nd 143	19.7	66.7	38.4	13.0	76.2	83.2	100.4	21.4	-	-	-	-	-	-	-	-
Sm 147	4.6	12.6	10.8	3.2	13.9	17.4	19.3	4.7	-	-	-	-	-	-	-	-
Eu 151	0.84	2.15	2.13	1.31	2.64	2.58	3.23	1.20	-	-	-	-	-	-	-	-
Gd 157	5.3	11.8	13.1	5.2	14.8	15.1	18.0	5.4	-	-	-	-	-	-	-	-
Tb 159	0.88	1.52	2.20	1.30	2.41	1.84	2.35	0.90	-	-	-	-	-	-	-	-
Dy 163	6.4	9.9	15.1	12.0	18.7	10.6	14.4	6.8	-	-	-	-	-	-	-	-
Ho 165	1.56	2.28	3.28	3.00	4.75	2.38	3.30	1.77	-	-	-	-	-	-	-	-
Er 167	5.37	7.53	9.93	9.75	15.80	7.27	10.47	5.62	-	-	-	-	-	-	-	-
Tm 169	0.86	1.12	1.38	1.49	2.45	1.14	1.56	0.87	-	-	-	-	-	-	-	-
Yb 172	5.74	7.66	8.54	9.48	15.35	7.40	9.86	5.78	-	-	-	-	-	-	-	-
Lu 175	0.89	1.15	1.26	1.40	2.34	1.13	1.49	0.88	-	-	-	-	-	-	-	-
Hf 178	4.9	6.0	5.7	9.5	11.2	6.8	7.9	5.3	-	-	-	-	-	-	-	-
Ta 181	7.3	8.2	4.3	15.9	12.2	8.8	8.2	6.7	-	-	-	-	-	-	-	-
W 184	4.2	4.0	11.1	3.6	9.0	3.9	5.3	3.2	-	-	-	-	-	-	-	-
Tl 205	2.41	2.41	1.77	2.74	2.44	2.40	2.36	3.32	-	-	-	-	-	-	-	-
Pb 208	43.0	52.3	22.7	32.6	10.5	34.5	3.1	15.8	-	-	-	-	-	-	-	-
Bi 209	0.26	0.56	0.09	0.15	0.06	0.61	0.18	0.57	-	-	-	-	-	-	-	-
Th 232	34.6	39.2	12.7	87.4	39.5	40.6	39.7	39.6	-	-	-	-	-	-	-	-
U 238	4.7	6.2	6.4	5.2	7.9	5.0	7.8	8.5	-	-	-	-	-	-	-	-

GÖ: Analyses performed in Göttingen; WÜ: Analyses performed in Würzburg; - or n.a.: not analysed

Appendix D-4 (Tab. 25): XRF-results of volcanic clasts sampled from the Ganigobis Shale Member, Aranos Basin, southern Namibia

Pr.Nr.	SiO ₂	TiO ₂	Al ₂ O ₃	Fe ₂ O ₃	MnO	MgO	CaO	Na ₂ O	K ₂ O	P ₂ O ₅	S	LOI	SUM
BB 23	49.3	0.566	13.0	7.75	0.365	5.31	8.48	1.82	2.30	0.120	n.a.	n.a.	89.09
BB 25	64.0	1.148	13.4	5.33	0.102	1.80	2.07	4.28	2.92	0.435	n.a.	n.a.	95.55
78-3	68.6	0.841	12.9	5.38	0.033	0.32	0.98	4.86	3.86	0.202	n.a.	n.a.	97.97
81-4	66.5	0.411	14.9	4.18	0.078	2.70	3.20	5.26	0.64	0.092	n.a.	n.a.	97.96
SA-1	71.6	0.572	12.0	4.34	0.057	0.74	1.77	4.73	1.01	0.155	n.a.	n.a.	97.00
SA-2	58.1	0.779	14.6	7.66	0.139	3.68	3.94	4.09	0.65	0.168	n.a.	n.a.	93.78
HG D22	43.03	0.94	13.41	6.13	0.64	1.93	15.78	2.82	2.15	0.10	n.a.	14.07	101.00
HG D37	53.01	0.99	15.85	17.16	0.15	5.48	0.54	3.63	0.11	0.21	n.a.	4.16	101.29
81-3	73.62	0.40	12.69	2.76	0.05	0.72	0.42	3.19	5.41	0.06	< 0.02	0.81	100.13
90-1	80.35	0.27	10.18	1.80	0.03	0.89	0.41	4.91	0.32	0.05	0.03	0.94	100.18
90-2	73.05	0.29	13.97	1.79	0.03	0.49	1.95	2.74	4.33	0.08	< 0.02	1.14	99.86

Pr.Nr.	Nb	Zr	Y	Sr	Rb	Pb	Ga	Zn	Cu	Ni	Co	Cr	V
BB 23	7	84	24	111	64	23	9	61	75	154	35	638	80
BB 25	23	400	61	296	76	80	18	43	<10	18	10	22	103
78-3	55	851	87	37	123	16	20	52	20	10	<5	10	22
81-4	5	106	13	340	21	13	18	49	<10	93	11	129	65
SA-1	23	383	66	147	33	25	13	133	<10	10	<5	13	14
SA-2	8	166	28	84	25	12	9	63	53	109	24	183	87
HG D22	7	112	12	162	94	n.a.	10.9	111	n.a.	45	26	53	104
HG D37	7	140	25	37	3	n.a.	23.3	90	n.a.	127	51	108	177
81-3	13	261	37	100	222	15	12	48	n.a.	5	<10	14	30
90-1	6	138	31	69	7	73	9	<5	n.a.	<5	<10	15	25
90-2	7	161	38	94	191	31	15	32	n.a.	<5	<10	18	21

Pr.Nr.	Ba	Sc	Mo	Sn	Li 6	Be 9	Rb 85	Sr 88	Y 89	Zr 91	Nb 93	Mo 95	Cs 133
BB 23	469	10	n.a.	n.a.	93	0.48	72	123	23.2	88	10.6	1.3	5.2
BB 25	1310	11	n.a.	n.a.	42	1.22	87	343	61.7	447	34.3	3.7	1.4
78-3	720	10	n.a.	n.a.	8	1.05	145	37	89.6	467	87.6	0.8	0.5
81-4	264	7	n.a.	n.a.	22	1.37	24	392	11.6	104	6.4	0.8	0.5
SA-1	353	8	n.a.	n.a.	55	2.02	36	170	71.0	450	36.0	1.2	0.7
SA-2	162	13	n.a.	n.a.	61	0.74	24	97	31.9	183	10.6	1.3	1.6
HG D22	472	n.a.	n.a.	n.a.	n.a.	n.a.	n.a.	n.a.	n.a.	n.a.	n.a.	n.a.	n.a.
HG D37	78	n.a.	n.a.	n.a.	n.a.	n.a.	n.a.	n.a.	n.a.	n.a.	n.a.	n.a.	n.a.
81-3	798	<10	<5	<15	n.a.	n.a.	n.a.	n.a.	n.a.	n.a.	n.a.	n.a.	n.a.
90-1	71	11	<5	<15	n.a.	n.a.	n.a.	n.a.	n.a.	n.a.	n.a.	n.a.	n.a.
90-2	527	<10	<5	<15	n.a.	n.a.	n.a.	n.a.	n.a.	n.a.	n.a.	n.a.	n.a.

Pr.Nr.	Ba 137	La 139	Ce 140	Pr 141	Nd 143	Sm 147	Eu 151	Gd 157	Tb 159	Dy 163	Ho 165	Er 167	Tm 169
BB 23	535	22.5	48	5.1	19.6	4.2	1.06	5.0	0.65	4.0	0.81	2.16	0.30
BB 25	1541	151.3	331	35.5	129.5	20.5	4.11	20.4	2.10	11.6	2.29	6.58	0.96
78-3	806	95.2	222	25.4	100.7	20.7	4.35	22.1	3.02	18.9	3.81	11.16	1.68
81-4	291	14.0	30	3.5	13.8	2.9	0.92	3.2	0.39	2.3	0.44	1.26	0.18
SA-1	413	72.7	168	19.1	75.0	14.5	4.14	14.9	1.97	12.3	2.61	7.98	1.15
SA-2	187	15.2	39	5.1	21.5	5.3	1.81	6.1	0.93	5.6	1.12	3.50	0.49
HG D22	n.a.	n.a.	n.a.	n.a.	n.a.	n.a.	n.a.	n.a.	n.a.	n.a.	n.a.	n.a.	n.a.
HG D37	n.a.	n.a.	n.a.	n.a.	n.a.	n.a.	n.a.	n.a.	n.a.	n.a.	n.a.	n.a.	n.a.
81-3	n.a.	n.a.	n.a.	n.a.	n.a.	n.a.	n.a.	n.a.	n.a.	n.a.	n.a.	n.a.	n.a.
90-1	n.a.	n.a.	n.a.	n.a.	n.a.	n.a.	n.a.	n.a.	n.a.	n.a.	n.a.	n.a.	n.a.
90-2	n.a.	n.a.	n.a.	n.a.	n.a.	n.a.	n.a.	n.a.	n.a.	n.a.	n.a.	n.a.	n.a.

Pr.Nr.	Yb 172	Lu 175	Hf 178	Ta 181	W 184	Tl 205	Pb 208	Bi 209	Th 232	U 238
BB 23	1.88	0.28	1.1	1.3	4.8	0.35	95.8	0.08	8.0	3.0
BB 25	6.08	0.90	5.7	3.1	6.3	0.76	106.5	0.09	13.9	2.7
78-3	11.17	1.67	6.9	9.2	1.9	0.44	25.3	0.02	28.9	5.1
81-4	1.14	0.16	1.6	1.0	1.0	0.16	15.0	0.07	4.0	1.5
SA-1	7.50	1.13	6.3	4.1	6.3	0.22	28.4	0.06	20.3	6.1
SA-2	3.03	0.46	2.5	1.4	5.5	0.16	18.0	0.07	4.3	1.4
HG D22	n.a.	n.a.	n.a.	n.a.	n.a.	n.a.	n.a.	n.a.	n.a.	n.a.
HG D37	n.a.	n.a.	n.a.	n.a.	n.a.	n.a.	n.a.	n.a.	n.a.	n.a.
81-3	n.a.	n.a.	n.a.	n.a.	n.a.	n.a.	n.a.	n.a.	32	<5
90-1	n.a.	n.a.	n.a.	n.a.	n.a.	n.a.	n.a.	n.a.	<5	<5
90-2	n.a.	n.a.	n.a.	n.a.	n.a.	n.a.	n.a.	n.a.	10	<5

Appendix E (Tab. 26 - 33): Results of all SHRIMP U-Th-Pb zircon measurements

Table 26: Summary of SHRIMP U-Th-Pb zircon results for tuff bed #23 Iib

Grain. spot	U (ppm)	Th (ppm)	Th/U	Pb* (ppm)	²⁰⁴ Pb/ ²⁰⁶ Pb	f ₂₀₆ %	Radiogenic		Age (Ma)	
							²⁰⁶ Pb/ ²³⁸ U	±	²⁰⁶ Pb/ ²³⁸ U	±
1.1	199	229	1.15	11	0.000172		0.0470	0.0008	296	5
2.1	320	357	1.12	19	0.000010		0.0486	0.0009	306	5
3.1	168	135	0.80	9	0.000010		0.0483	0.0011	304	6
4.1	270	320	1.18	16	0.000010		0.0479	0.0009	302	5
5.1	280	264	0.94	15	0.000010		0.0466	0.0007	294	5
6.1	207	165	0.80	11	0.000010		0.0485	0.0009	306	6
7.1	223	216	0.97	12	0.000010		0.0478	0.0008	301	5
8.1	250	254	1.02	15	0.000400		0.0495	0.0010	311	6
9.1	241	225	0.93	13	0.000130		0.0458	0.0009	289	6
10.1	180	143	0.79	9	0.000010		0.0466	0.0011	294	6
11.1	224	184	0.82	11	0.000010		0.0449	0.0008	283	5
12.1	152	103	0.67	8	0.000056		0.0464	0.0009	292	6
13.1	724	1328	1.83	49	0.000053		0.0484	0.0007	304	4
14.1	232	208	0.90	13	0.000237		0.0485	0.0008	305	5
15.1	304	263	0.86	17	0.000010		0.0481	0.0008	303	5
16.1	301	349	1.16	16	0.000153		0.0449	0.0007	283	4
17.1	375	484	1.29	23	0.000010		0.0483	0.0008	304	5

Table 27: Summary of SHRIMP U-Th-Pb zircon results for tuff bed #45 Iib

Grain. spot	U (ppm)	Th (ppm)	Th/U	Pb* (ppm)	²⁰⁴ Pb/ ²⁰⁶ Pb	f ₂₀₆ %	Radiogenic		Age (Ma)	
							²⁰⁶ Pb/ ²³⁸ U	±	²⁰⁶ Pb/ ²³⁸ U	±
1.1	382	514	1.35	23	0.000290	-	0.0479	0.0007	301.42	4.31
2.1	305	685	2.25	15	0.004907	8.62	0.0408	0.0011	257.92	6.49
3.1	144	167	1.16	8	0.001494	0.48	0.0473	0.0010	297.73	5.98
4.1	337	410	1.22	20	0.000066	0.07	0.0478	0.0007	300.99	4.37
5.1	526	607	1.16	31	0.000354	0.46	0.0479	0.0007	301.88	3.98
6.1	529	511	0.97	28	0.000123	0.39	0.0466	0.0011	293.37	6.85
7.1	259	309	1.19	15	0.000243	0.20	0.0473	0.0013	298.02	7.92
8.1	591	765	1.29	32	0.001710	3.51	0.0469	0.0009	295.44	5.25
9.1	263	225	0.86	14	0.000659	0.47	0.0470	0.0010	296.01	6.35
10.1	236	269	1.14	14	0.000540	0.43	0.0481	0.0016	302.64	9.82
11.1	277	419	1.51	14	0.001507	2.23	0.0415	0.0009	261.91	5.33
12.1	252	222	0.88	14	0.000426	0.40	0.0474	0.0008	298.36	4.88
13.1	190	157	0.83	10	0.000233	0.35	0.0476	0.0008	299.51	4.85
14.1	459	401	0.87	25	0.000001	0.07	0.0482	0.0010	303.26	6.13
15.1	498	542	1.09	28	0.000207	0.28	0.0465	0.0013	293.09	7.71

Table 28: Summary of SHRIMP U-Th-Pb zircon results for tuff bed IIIb from Zwartbas, southern Namibia

Grain. spot	U (ppm)	Th (ppm)	Th/U	Pb* (ppm)	²⁰⁴ Pb/ ²⁰⁶ Pb	f ₂₀₆ %	Radiogenic		Age (Ma)	
							²⁰⁶ Pb/ ²³⁸ U	±	²⁰⁶ Pb/ ²³⁸ U	±
1.1	324	405	1.25	19	0.022534	43.83	0.0490	0.0191	308.3	118.6
2.1	307	270	0.88	17	0.000366	0.25	0.0488	0.0007	307.0	4.6
3.1	125	114	0.91	7	0.000424	0.34	0.0485	0.0007	305.5	4.4
4.1	200	144	0.72	11	0.000037	0.22	0.0482	0.0008	303.5	4.6
5.1	214	313	1.46	13	0.000323	0.48	0.0476	0.0007	299.5	4.5
6.1	267	431	1.62	17	0.000096	0.15	0.0482	0.0006	303.2	3.9
7.1	201	255	1.27	12	0.000010	0.38	0.0478	0.0008	301.2	4.7
8.1	115	128	1.11	6	0.000010	0.75	0.0463	0.0008	292.0	4.7
9.1	134	152	1.13	8	0.000134	0.51	0.0479	0.0008	301.9	4.6
10.1	285	266	0.93	16	0.000126	0.31	0.0489	0.0007	307.8	4.5
11.1	172	145	0.84	9	0.000448	0.42	0.0474	0.0007	298.4	4.2
12.1	107	90	0.84	6	0.000322	0.26	0.0477	0.0008	300.6	4.7
13.1	221	280	1.27	12	0.002856	5.65	0.0468	0.0007	295.0	4.4
14.1	185	225	1.22	11	0.000000	0.27	0.0477	0.0007	300.5	4.2
15.1	294	477	1.62	19	0.000102	0.23	0.0485	0.0007	305.4	4.0
16.1	219	157	0.72	12	0.000010	0.20	0.0484	0.0008	304.7	4.7
17.1	225	167	0.74	12	0.000222	0.18	0.0482	0.0008	303.7	4.7
18.1	380	464	1.22	23	0.000010	0.22	0.0476	0.0007	299.4	4.0
19.1	206	144	0.70	11	0.000360	0.26	0.0480	0.0008	302.4	4.8

Table 29: Summary of SHRIMP U-Th-Pb zircon results for tuff bed XXXIV from Zwartbas, southern Namibia

Grain. spot	U (ppm)	Th (ppm)	Th/U	Pb* (ppm)	²⁰⁴ Pb/ ²⁰⁶ Pb	f ₂₀₆ %	Radiogenic		Age (Ma)	
							²⁰⁶ Pb/ ²³⁸ U	±	²⁰⁶ Pb/ ²³⁸ U	±
1.1	374	220	0.59	19	0.000055	0.07	0.0481	0.0007	302.87	4.31
1.2	135	61	0.45	7	0.000127	0.49	0.0472	0.0008	297.28	4.74
2.1	979	2480	2.53	41	0.003532	6.24	0.0378	0.0005	239.19	3.06

Table 30: Summary of SHRIMP U-Th-Pb results from the tuffaceous bed of the Dwyka Group, 30 km north of Klaarstroom, South Africa

Grain. spot	U (ppm)	Th (ppm)	Th/U	Pb* (ppm)	²⁰⁴ Pb/ ²⁰⁶ Pb	f ₂₀₆ %	Radiogenic		Age (Ma)	
							²⁰⁶ Pb/ ²³⁸ U	±	²⁰⁶ Pb/ ²³⁸ U	±
1.1	465	172	0.37	22	0.000010	0.06	0.0480	0.0007	302.2	4.1
2.1	538	255	0.47	26	0.000272	0.29	0.0468	0.0006	294.8	3.8
3.1	209	107	0.51	10	0.000168	0.37	0.0476	0.0008	299.6	4.7
4.1	389	248	0.64	19	0.000004	0.19	0.0466	0.0006	293.5	3.7
5.1	396	219	0.55	19	0.000244	0.23	0.0463	0.0006	291.9	3.7
6.1	334	259	0.78	18	0.000245	0.18	0.0472	0.0006	297.2	3.9
7.1	370	133	0.36	17	0.000176	0.19	0.0470	0.0006	296.2	3.9
8.1	587	496	0.84	31	0.000061	0.09	0.0468	0.0006	294.7	3.9
9.1	360	168	0.47	18	0.000079	0.20	0.0472	0.0007	297.0	4.2
10.1	360	140	0.39	17	0.000410	0.84	0.0469	0.0006	295.6	3.8
11.1	411	188	0.46	20	0.000065	0.09	0.0467	0.0007	294.3	4.0
12.1	422	174	0.41	20	0.000025	0.24	0.0468	0.0006	294.6	3.9
13.1	458	317	0.69	24	0.000127	0.38	0.0480	0.0006	302.2	3.9
14.1	392	145	0.37	19	0.000010	0.10	0.0480	0.0007	302.3	4.0
15.1	362	165	0.46	18	0.000108	0.10	0.0487	0.0007	306.4	4.1
16.1	438	234	0.53	22	0.000054	0.07	0.0477	0.0006	300.3	3.8
17.1	335	161	0.48	16	0.000081	0.04	0.0472	0.0007	297.1	4.1
18.1	275	120	0.44	14	0.000013	0.22	0.0481	0.0007	302.7	4.4
19.1	469	259	0.55	23	0.000089	0.20	0.0469	0.0007	295.3	4.1

Table 31: Summary of SHRIMP U-Th-Pb results from tuff bed VIb, Eccca Group 30km north of Klaarstroom, South Africa

Grain. spot	U (ppm)	Th (ppm)	Th/U	Pb* (ppm)	²⁰⁴ Pb/ ²⁰⁶ Pb	f ₂₀₆ %	Radiogenic		Age (Ma)	
							²⁰⁶ Pb/ ²³⁸ U	±	²⁰⁶ Pb/ ²³⁸ U	±
1.1	610	292	0.48	29	0.000010		0.0453	0.0007	286	4
2.1	491	260	0.53	24	0.000103		0.0470	0.0008	296	5
3.1	331	159	0.48	16	0.000010		0.0458	0.0008	289	5
4.1	405	377	0.93	21	0.000090		0.0439	0.0007	277	4
5.1	1024	618	0.60	50	0.000046		0.0453	0.0007	285	4
6.1	604	321	0.53	29	0.000010		0.0464	0.0007	292	4
7.1	375	274	0.73	19	0.000211		0.0461	0.0007	291	4
8.1	141	91	0.65	7	0.000200		0.0465	0.0010	293	6
9.1	679	291	0.43	30	0.000010		0.0435	0.0007	275	4
10.1	218	152	0.70	11	0.000010		0.0457	0.0008	288	5
11.1	451	247	0.55	21	0.000103		0.0444	0.0008	280	5
12.1	502	301	0.60	24	0.000079		0.0455	0.0007	287	4
13.1	255	143	0.56	12	0.000010		0.0457	0.0007	288	5
14.1	369	151	0.41	17	0.000167		0.0443	0.0007	279	4
15.1	604	346	0.57	30	0.000010		0.0461	0.0007	291	4

Table 32: Summary of SHRIMP U-Th-Pb results for zircons from a tuff bed south of Laingsburg, Ecca Group, South Africa.

Grain. spot	U (ppm)	Th (ppm)	Th/U	Pb* (ppm)	²⁰⁴ Pb/ ²⁰⁶ Pb	f ₂₀₆ %	Radiogenic		Age (Ma)	
							²⁰⁶ Pb/ ²³⁸ U	±	²⁰⁶ Pb/ ²³⁸ U	±
1.1	1204	763	0.63	92	0.001784	3.85	0.0741	0.0009	460.5	5.6
2.1	233	203	0.87	12	0.000361	0.32	0.0460	0.0008	290.1	5.0
3.1	125	117	0.93	7	0.000281	0.41	0.0458	0.0008	288.9	4.7
4.1	253	217	0.86	13	0.000573	0.85	0.0466	0.0007	293.4	4.4
5.1	988	647	0.65	79	0.000370	1.33	0.0751	0.0010	466.5	6.1
6.1	163	115	0.71	9	0.000018	0.46	0.0478	0.0007	301.0	4.2
7.1	434	316	0.73	35	0.000032	0.62	0.0742	0.0010	461.5	6.0
8.1	283	137	0.48	22	0.000267	0.81	0.0767	0.0011	476.5	6.6
9.1	539	415	0.77	44	0.000000	0.53	0.0742	0.0012	461.3	7.0
10.1	420	170	0.40	31	0.000349	1.11	0.0740	0.0012	460.3	7.2
11.1	164	140	0.85	9	0.000698	0.72	0.0464	0.0010	292.6	6.0
12.1	367	216	0.59	29	0.000087	0.74	0.0740	0.0016	460.3	9.4
13.1	262	223	0.85	15	0.000723	0.76	0.0500	0.0008	314.7	4.8
14.1	776	311	0.40	57	0.000050	0.67	0.0733	0.0011	456.0	6.5
15.1	248	212	0.86	13	0.000195	0.20	0.0451	0.0009	284.2	5.8
16.1	146	115	0.79	8	0.001056	1.61	0.0457	0.0009	288.1	5.4
17.1	259	243	0.94	13	0.000001	-	0.0442	0.0012	278.7	7.3
17.2	201	168	0.84	10	0.000204	0.34	0.0449	0.0013	283.3	8.1
18.1	163	133	0.82	9	0.000511	0.36	0.0468	0.0008	295.0	5.0
19.1	375	325	0.87	20	0.000084	0.25	0.0462	0.0010	291.2	5.9

Table 33: Summary of SHRIMP U-Th-Pb results for zircons from tuffaceous beds 2 km east of Nondweni, KwaZulu-Natal, South Africa

Grain. spot	U (ppm)	Th (ppm)	Th/ U	Pb* (ppm)	²⁰⁴ Pb/ ²⁰⁶ Pb	f ₂₀₆ %	²⁰⁶ Pb/ ²³⁸ U	±
1.1	160	81	0.51	65	0.00006	0.12	0.3702	0.0062
1.2	76	32	0.42	31	0.0001	0.18	0.3822	0.0080

Radiogenic Ratios					Age (Ma)					Conc
²⁰⁷ Pb/ ²³⁵ U	±	²⁰⁷ Pb/ ²⁰⁶ Pb	±	²⁰⁶ Pb/ ²³⁸ U	±	²⁰⁷ Pb/ ²³⁵ U	±	²⁰⁷ Pb/ ²⁰⁶ Pb	±	%
6.503	0.132	0.1274	0.0013	2030	29	2046	18	2063	17	98
6.564	0.194	0.1246	0.0023	2087	37	2055	26	2023	33	103